QA: NA

June 2004

Technical Basis Document No. 4: Mechanical Degradation and Seismic Effects

Revision 1

Prepared for:
U.S. Department of Energy
Office of Civilian Radioactive Waste Management
Office of Repository Development
1551 Hillshire Drive
Las Vegas, Nevada 89134-6321

Prepared by:
Bechtel SAIC Company, LLC
1180 Town Center Drive
Las Vegas, Nevada 89144

Under Contract Number
DE-AC28-01RW12101

CONTENTS

Page

ACRONYMS xv

1. INTRODUCTION 1-1
   1.1 OBJECTIVE AND SCOPE 1-3
   1.2 SUMMARY OF CURRENT UNDERSTANDING 1-4
      1.2.1 General Description of the Repository Layout and Waste Emplacement 1-4
      1.2.2 General Degradation Processes 1-9
      1.2.3 Summary of Approach to Addressing Preclosure and Postclosure Issues 1-13
   1.3 ORGANIZATION OF THE REPORT 1-18
   1.4 NOTE REGARDING THE STATUS OF SUPPORTING TECHNICAL INFORMATION 1-19

2. GEOLOGIC CHARACTERISTICS OF THE REPOSITORY HOST HORIZON RELEVANT TO MECHANICAL DEGRADATION 2-1
   2.1 GENERAL GEOLOGY OF REPOSITORY HOST HORIZON 2-1
   2.2 UNDERGROUND REPOSITORY LAYOUT AND LITHOLOGIC INTERSECTIONS 2-3
   2.3 ENGINEERING CHARACTERISTICS OF THE ROCK MASS IMPORTANT TO MECHANICAL PERFORMANCE OF REPOSITORY EXCAVATIONS 2-4
      2.3.1 Characterization of Fractures 2-5
      2.3.2 Characteristics of Lithophysae 2-11
      2.3.3 In Situ Stress State 2-15
   2.4 SUMMARY 2-15

3. THERMAL-MECHANICAL ROCK PROPERTIES DATABASE— REVIEW OF LABORATORY AND IN SITU TESTING FOR THE NONLITHOPHYSAL AND LITHOPHYSAL ROCK MASSES 3-1
   3.1 INTRODUCTION 3-1
   3.2 GEOMECHANICAL PROPERTIES OF YUCCA MOUNTAIN ROCK 3-3
      3.2.1 Mechanical Intact Rock Properties of Nonlithophysal and Lithophysal Rocks 3-3
      3.2.2 Summary of Laboratory Testing of Lithophysal and Nonlithophysal Cores 3-14
      3.2.3 In Situ Mechanical Testing of Nonlithophysal and Lithophysal Rocks 3-15
      3.2.4 Mechanical Properties of Fractures 3-18
      3.2.5 Thermal Properties of the Repository Host Rocks 3-21

4. DEVELOPMENT OF ROCK MASS MATERIAL MODELING APPROACHES FOR NONLITHOPHYSAL AND LITHOPHYSAL ROCKS 4-1
   4.1 MECHANICAL DEGRADATION MODELING APPROACH FOR NONLITHOPHYSAL ROCK 4-1
      4.1.1 Development of Fracture Geometries for Nonlithophysal Rock 4-3

CONTENTS (Continued)

Page

4.1.2 Example—Fracture Geometry Generation for the Middle Nonlithophysal Unit 4-4
4.2 MECHANICAL DEGRADATION MODELING APPROACH FOR LITHOPHYSAL ROCK 4-6
4.2.1 Material Model Requirements 4-6
4.2.2 Mechanical Material Model and Numerical Analysis Approach Development for Lithophysal Rocks 4-8
4.2.3 Validation of the Particle Flow Code–A Micromechanical Model Representation of the Mechanical Behavior of Lithophysal Rock 4-15
4.2.4 Extrapolated Triaxial Behavior of Lithophysal Rock and Estimation of Rock Mass Constitutive Response 4-21
4.2.5 Estimation of Linear and Nonlinear Failure Envelopes 4-23
4.2.6 Summary of Material Model Development 4-25
4.2.7 Development and Validation of a Drift-Scale Modeling Method for Lithophysal Rock Using the UDEC Program 4-25
4.3 ROCK MASS MODELING APPROACH FOR GROUND SUPPORT ASSESSMENT AND DESIGN 4-31

5. ANALYSIS OF PRECLOSURE AND POSTCLOSURE DRIFT DEGRADATION UNDER GRAVITATIONAL, THERMAL, AND SEISMIC LOADING 5-1
5.1 INTRODUCTION 5-1
5.2 PRECLOSURE GROUND SUPPORT ISSUES 5-1
5.3 ANALYSIS OF PRECLOSURE AND POSTCLOSURE DRIFT DEGRADATION. 5-2
5.3.1 Emplacement Drift Degradation from In Situ and Thermal Stressing Effects 5-2
5.3.2 Analysis of Drift Degradation from Combined In Situ, Thermal, and Seismic Loading 5-12
5.4 SUMMARY OF OUTPUT FROM THE DRIFT DEGRADATION ANALYSIS TO OTHER DISCIPLINES 5-84

6. SUMMARY AND INTERACTIONS WITH ENGINEERED AND NATURAL SYSTEMS 6-1
6.1 SUMMARY 6-1
6.2 CLOSURE 6-4

7. REFERENCES 7-1
7.1 DOCUMENTS CITED 7-1
7.2 CODES, STANDARDS, AND REGULATIONS 7-7
7.3 DATA, LISTED BY DATA TRACKING NUMBER 7-7

CONTENTS (Continued)

Page

APPENDIX A ROCK-MASS CLASSIFICATION FOR LITHOPHYSAL ROCK (RESPONSE TO RDTME 3.05)..... A-1

APPENDIX B SCOPING ANALYSIS OF INPUT DATA AND SENSITIVITY AND UNCERTAINTY ANALYSIS OF EMPLACEMENT DRIFT STABILITY (RESPONSE TO RDTME 3.06) B-1

APPENDIX C ROCKFALL IN EMPLACEMENT DRIFTS (RESPONSE TO RDTME 3.15, RDTME 3.16, RDTME 3.17, RDTME 3.19, AND GEN 1.01 (COMMENT 3)).....C-1

APPENDIX D ANALYSIS OF LOAD COMBINATION AND MODELING APPROACH RELATED TO EVALUATION OF EMPLACEMENT DRIFT STABILITY (RESPONSE TO RDTME 3.02, RDTME 3.10, AND RDTME 3.13)..... D-1

APPENDIX E SITE-SPECIFIC PROPERTIES OF THE HOST ROCK (RESPONSE TO RDTME 3.04).....E-1

APPENDIX F DESIGN SENSITIVITY AND UNCERTAINTY ANALYSES OF THE FRACTURE PATTERNS WITH DISCONTINUUM APPROACH (RESPONSE TO RDTME 3.08 AND RDTME 3.12)..... F-1

APPENDIX G ANALYSIS OF ROCK MOVEMENT IN INVERT (RESPONSE TO RDTME 3.09)..... G-1

APPENDIX H CONTINUUM AND DISCONTINUUM ANALYSES OF GROUND SUPPORT SYSTEM PERFORMANCE (RESPONSE TO RDTME 3.11)..... H-1

INTENTIONALLY LEFT BLANK

FIGURES

Page

1-1. Components of the Postclosure Technical Basis for the License Application 1-1
1-2. Repository Layout in Plan View Showing Ramps, Access Intake and Exhaust Mains, Emplacement Drifts, Shafts, and Existing Excavations (as Dashed Lines)..... 1-6
1-3. Plan View and Cross-Sectional Views of Primary Repository Excavations 1-7
1-4. Ground Support Method for Emplacement Drifts Showing Drip Shield 1-8
1-5. Shielded Waste Transporter at Docking Bay Showing Waste Package, Waste Emplacement Gantry, and Locomotive 1-9
1-6. Potential Postclosure Performance Impacts of Rockfall on Engineered Barriers, In-Drift Environment, and Groundwater Seepage into Drifts 1-12
1-7. General Approach to Resolution of the Repository Design and Thermal-Mechanical Effects Key Technical Issues 1-15

2-1. Geologic Cross Section at the Location of the Enhanced Characterization of the Repository Block Cross-Drift 2-2
2-2. Structure of the Topopah Spring Tuff Showing the Relative Relationship between Fracturing and Lithophysae in the Major Flow Subunits 2-3
2-3. Overlay of the Lithostratigraphic Units on the Planned Repository Layout 2-4
2-4. Composite Plot of Fracture Frequency and Lithophysal Porosity as a Function of Distance along the Enhanced Characterization of the Repository Block Cross-Drift 2-5
2-5. Fracture Trace Length as a Function of Depth in the Enhanced Characterization of the Repository Block Cross-Drift and by Subunit of the Tptp from Detailed Line Surveys 2-7
2-6. Fractures in Wall of the Enhanced Characterization of the Repository Block Cross-Drift in the Tptpmn 2-7
2-7. Low-Angle Vapor-Phase Partings in Tptpmn 2-8
2-8. Comparison of Lithophysae and Fracturing in the Tptpul and Tptpll 2-10
2-9. Lithophysae, Spots, and Clasts of Tptpll (as Discussed Below) in Panel Map 1493 Located on the Right Rib from Station 14+93 to 14+96 2-11
2-10. Calculated Porosity of Lithophysal Cavities, Rims, Spots, Matrix-Groundmass, and the Total Porosity in the Tptpll Exposed along the ECRB Cross-Drift 2-13
2-11 Illustration of the Process of Sampling and Modeling Spatial Variability Using Lithophysal Porosity 2-14

3-1. Development Strategy for Rock Properties Database and Modeling Strategy for Nonlithophysal Rocks 3-2
3-2. Development Strategy for Rock Properties Database and Modeling Strategy for Lithophysal Rocks 3-3
3-3. Intact Unconfined Compressive Strength (a) and Young's Modulus (b) for Topopah Spring Subunits as a Function of Effective Porosity 3-5
3-4. Photograph of Busted Butte Sample from the Upper Lithophysal Zone 3-6
3-5. Plot of Axial (σ_1) Versus Confining (σ_3) Stress for 50.8 mm Diameter Specimens of the Tptpmn: Room Dry and Room Temperature (top), Saturated at 150°C (bottom)..... 3-7

FIGURES (Continued)

Page

3-6. Effect of Sample Size on the Unconfined Compressive Strength of Welded Tuff from the Middle Nonlithophysal Zone 3-8
3-7. Development of Rectangular Specimens for Matrix Size Effect and Anisotropy Study 3-8
3-8. Results of Size Effect Study Showing Variation in Sample Unconfined Compressive Strength as a Function of Sample Volume 3-10
3-9. Anisotropy in Young's Modulus of Nonlithophysal Tptpll Matrix for Three Mutually Perpendicular Coring Directions 3-10
3-10. Photographs of Large Lithophysal Core Samples (290 mm/11.5″ diameter) from the Tptpll and Tptpul (a) and a Sample in Unconfined Compression (b) 3-12
3-11. Unconfined Compressive Strength (a) and Young's Modulus (b) as Functions of Estimated Lithophysal Porosity from Large Core (290 mm diameter) Compression Tests from Lithophysal Rocks 3-13
3-12. Unconfined Compressive Strength as a Function of Young's Modulus from Large Core (290 mm and 267 mm diameter) Compression Tests from Lithophysal Rocks ... 3-14
3-13. Photographs of (a) Preparation of Slot Test 3 in the Floor of the Enhanced Characterization of the Repository Block, Tptpll Unit, Lowering of Flatjack into Place in Sawcut Slot and (b) Slot Test 2 Showing Central Instrumentation Hole and Parallel Slots 3-16
3-14. Composite of Flatjack Pressure versus Central Hole Diametral Strain for the Three Pressurized Slot Tests 3-17
3-15. Photographs of Direct Shear Samples from Rough Vapor Phase Partings (a) and Smooth Cooling Joints (b) 3-18

4-1. Evidence of Key-Block Occurrence in the Enhanced Characterization of the Repository Block Cross-Drift, Station 11+55 4-2
4-2. Comparison of Full Periphery Geologic Maps from the Tptpmn in the Exploratory Studies Facility (a) with Simulated Full Periphery Geologic Maps from the FracMan Cube (b) 4-5
4-3. Large (290 mm) Diameter Core from Tptpll 4-7
4-4. Relationship of Unconfined Compressive Strength to Young's Modulus from Large Core Testing of Lithophysal Rock (Figure 3-11) and Assignment of Five Average Quality Categories 4-9
4-5. Distribution of Lithophysal Porosity and Estimated Rock Properties Categories for the Tptpll in the Enhanced Characterization of the Repository Block Cross-Drift 4-11
4-6. Continuum (Left) and Discontinuum (Right) Approaches to Modeling Drift Stability 4-12
4-7. General Approach for Estimation of Lithophysal Rock Property Bounds 4-14
4-8. Particle Flow Code Calibration Compression Experiment "Samples" and Their Respective Uniaxial Stress-Strain Curves for (a) Nonlithophysal and (b) Lithophysal Rock 4-17

FIGURES (Continued)

Page

4-9. Plots Showing Data from Large Core Compression Testing of Tptpul and Tptpll Compared to Particle Flow Code Simulations Using Circular Shaped Lithophysae as well as Actual "Stenciled" Shapes from Enhanced Characterization of the Repository Block Panel Maps 4-18
4-10. Examples of Particle Flow Code Compression Tests Using Simulated Rock Specimens Developed by "Stenciling" Field Panel Maps in the Enhanced Characterization of the Repository Block 4-19
4-11. Estimated Upper and Lower Bounds of Unconfined Compressive Strength and Young's Modulus for Lithophysal Rock 4-21
4-12. Stress-Strain Response and Failure Mechanisms for Lithophysal Porosity of 17.8% as Predicted by the UDEC Model 4-23
4-13. Hoek-Brown Failure Envelopes Based on UDEC Simulations for Various Lithophysal Porosities 4-24
4-14. General Approach to Validation of Mechanical Material Model for Lithophysal Rocks 4-26
4-15. UDEC Lithophysal Rock Specimen Composed of Many Irregular Blocks with Roughly Equal Side Lengths 4-27
4-16. Validation of the UDEC Numerical Approach for Lithophysal Rock against Observation of Springline Wall-Parallel Fracturing in the Exploratory Studies Facility and Enhanced Characterization of the Repository Block 4-29
4-17. Results from Heated Drift Analysis with Temperature Conditions after 3 Years of Heating 4-30

5-1. Aerial View of the Yucca Mountain Site and Digital Elevation Calculation Created from Topographic Information (a) and View of the Regional-Scale FLAC3D Thermal-Mechanical Model Constructed from the Digital Elevation Calculation and Available Geologic Information (b) 5-4
5-2. Heat Decay Curves for Thermal Calculations 5-5
5-3. Temperature History at the Drift Crown Due to the Linear Heat Load Presented in Figure 5-2 5-6
5-4. Comparison of Temperatures, Major and Minor Principal Stress Trajectories at 80 (Peak Temperature) and 10,000 Years for Lithophysal Rock, Lowest Quality, Category 1 5-8
5-5. Elastic Principal Stress Path Histories for Points at Increasing Depth from Emplacement Drift Crown (a) and Springline (b) for Lithophysal Rock, Modulus from Lowest Quality Category 1 5-9
5-6. Elastic Principal Stress Path Histories for Points at Increasing Depth from Emplacement Drift Crown (a) and Springline (b) for Lithophysal Rock, Modulus from Highest Quality Category 5 5-10
5-7. Elastic Principal Stress Path Histories for Points at Increasing Depth from Emplacement Drift Crown (a) and Springline (b) for Nonlithophysal Rock, Strength Category 3 5-11

FIGURES (Continued)

Page

5-8. Approach to Analysis of Drift Degradation and Rockfall from Combined In Situ, Thermal, and Seismic Loading 5-12
5-9. 3DEC Model Geometry and Cross Sections 5-14
5-10. Examples of Ground Velocity Time Histories (H1) with Truncated Duration for Analysis 5-16
5-11. Simulation of Rockfall Impact to the Drip Shield 5-20
5-12. Histogram for Block Mass (10^{-6} Annual Probability of Exceedance Hazard) 5-21
5-13. Histogram for Relative Impact Velocity (10^{-6} Annual Probability of Exceedance Hazard) 5-22
5-14. Histogram for Impact Angle (10^{-6} Annual Probability of Exceedance Hazard) 5-22
5-15. Histogram for Impact Momentum (10^{-6} Annual Probability of Exceedance Hazard) 5-23
5-16. Histogram for Impact Energy (10^{-6} Annual Probability of Exceedance Hazard) 5-23
5-17. Comparison of Histograms of Block Mass from All Postclosure and Preclosure Ground Motion 5-25
5-18. Drift Profile Showing Blocks That Become Detached from Drift Wall during Simulation for 10^{-6} Hazard Level, Case with Greatest Amount of Rockfall of 50 Total Realizations 5-26
5-19. Drift Profile Showing Blocks that Become Detached from Drift Wall During Simulation for 10^{-6} Hazard Level, 50th Percentile Case 5-27
5-20. Geometry and Initial Conditions of the UDEC Model 5-33
5-21. Dynamic Model, Initial and Boundary Conditions: Initial Static Simulation 5-34
5-22. Dynamic Model Boundary Conditions for Dynamic Simulation 5-35
5-23. Geometry of the Model after Simulation for Preclosure Ground Motion (Probability 10^{-4}): Rock Mass Category 1 5-36
5-24. Example of Comparison of Damage Levels for Lower End of Peak Ground Velocity (104 cm/s) for 10^{-5} Annual Exceedance Level 5-38
5-25. Example of Comparison of Damage Levels for Peak Ground Velocity of 152 cm/s for 10^{-5} Annual Exceedance Level 5-39
5-26. Example of Comparison of Damage Levels for Upper End of Peak Ground Velocity (333 cm/s) for 10^{-5} m/s 5-40
5-27. Estimate 10^{-5} Damage Level, Expressed as m^3/m of Emplacement Drift Length for Rock Strength Categories 1 (Top), 3 (Center), and 5 (Bottom) for All 15 Ground Motion Data. 5-41
5-28. Rockfall Damage as a Function of the Energy Associated with the Vertical Velocity Time History 5-42
5-29. Contours of Lithophysal Porosity Contoured on the UDEC Spatial Variability Model (Top) and a Histogram Showing the Percentage of Lithophysal Porosity within the Model (Bottom) 5-44
5-30. Schematic Representation of Two Cases of Drip Shield Loading Showing (a) Rigid Rectangular Geometry and (b) Deformable Arched Geometry 5-45
5-31. Example of Dynamic Impact Loading to the Right Wall (Top) and Roof (Bottom) of Deformable Drip Shield with Arched Roof 5-46

FIGURES (Continued)

Page

5-32 Typical Geometry of the Model after Simulations for Postclosure Ground Motion (Probability 10^{-6}) 5-47
5-33. Rockfall and Fractures Induced around a Drift by 1×10^{-4} Preclosure Ground Motion after the Peak Thermal Condition Occurring at 80 Years of Heating (30 Years after Closure) in Rock Mass Categories 1 and 5 5-49
5-34. Static-Fatigue Data for Welded Tuff and Lac du Bonnet Granite 5-53
5-35. PFC2D Specimens of Tuff Material for Static Fatigue Testing 5-55
5-36. Creep Curve and Damage in mS50 Material for Static-Fatigue Test (0.1 MPa Confinement) at Driving-Stress Ratio of 0.8 5-57
5-37. Effect of Void Porosity on Static-Fatigue Curves (0.1 MPa Confinement) for Lithophysal Tuff Material (0% to 20% Void Porosity) 5-57
5-38. Time Evolution of Damage Due to Strength Degradation Coefficient for Nonlithophysal Tuff Material during Static-Fatigue Tests (0.1 MPa Confinement) at Driving-Stress Ratios Ranging from 0.2 to 0.8 5-58
5-39. Static-Fatigue Curves Used as Input to the UDEC Analyses 5-59
5-40. Damage Curves Used as Input to the UDEC Tuff Best-Fit Analyses 5-60
5-41. Predicted Evolution of Damage Due to Strength Degradation for Category 1–Tuff Best-Fit Static-Fatigue Curve, Applied In Situ Stress Only 5-62
5-42. Predicted Evolution of Damage Due to Strength Degradation for Category 2–Tuff Best-Fit Static-Fatigue Curve, Applied In Situ Stress Only 5-63
5-43. Predicted Evolution of Damage Due to Strength Degradation for Category 3–Tuff Best-Fit Static-Fatigue Curve, Applied In Situ Stress Only 5-64
5-44. Predicted Evolution of Damage Due to Strength Degradation for Category 5–Tuff Best-Fit Static-Fatigue Curve, Applied In Situ Stress Only 5-65
5-45. Predicted Evolution of Damage Due to Strength Degradation for Category 2–Tuff Best-Fit Static-Fatigue Fit, Combined In Situ and Thermal Stresses 5-67
5-46. Predicted Evolution of Damage Due to Strength Degradation for Category 3–Tuff Best-Fit Static-Fatigue Curve, Combined In Situ and Thermal Stresses 5-68
5-47. Predicted Evolution of Damage Due to Strength Degradation for Category 5–Tuff Best-Fit Static-Fatigue Curve, Combined In Situ and Thermal Stresses 5-69
5-48. Effect of 10^{-4} Ground Motion after 80 Years of Heating in Category 2 before Seismic Shaking (Left) and after Seismic Shaking (Right): Blocks Colored by Contours of Displacement Magnitude 5-71
5-49. Effect of 10^{-4} Ground Motion after 80 Years of Heating in Category 5 before Seismic Shaking (Left) and after Seismic Shaking (Right): Blocks Colored by Contours of Displacement Magnitude 5-72
5-50. Effect of 10^{-4} Ground Motion after 10,000 Years of Heating in Category 2 before Seismic Shaking (Left) and after Seismic Shaking (Right) Contours of Displacement Magnitude 5-72
5-51. Effect of 10^{-4} Ground Motion after 10,000 Years of Heating in Category 5, before Seismic Shaking (Left) and after Seismic Shaking (Right): Blocks Colored by Contours of Displacement Magnitude 5-73
5-52. Piping Type of Caving Mechanism 5-77

FIGURES (Continued)

Page

5-53. Terzaghi-Type Caving Mechanism 5-77
5-54. Failure Mechanism of a Deep Tunnel in Cohesionless Material 5-79
5-55. Quasi-Static Drift Degradation, 0.2 m Block Size: Equilibrium State for Deformable Drip Shield with Arched Top, Footings Free to Slide or Detach from the Invert 5-81
5-56. Quasi-Static Drift Degradation, 0.2 m Block Size: Contours of Displacement Magnitude for Deformable Drip Shield Showing Approximate Collapse Height of 7 m (about 6 m above Top of Drip Shield Crown) 5-82
5-57. Quasi-Static Pressure on Drip Shield Segments for Six Realizations for Random, 0.2 m Block Geometries 5-83
5-58. Summary of Average Vertical Pressure on the Drip Shield as a Function of Bulking Factor for Analytical and Numerical Analysis 5-84

TABLES

Page

1-1. Key Technical Issue Agreements–Relevant Section Supporting Documents 1-10

2-1. General Characteristics of Fracture Sets in the Middle Nonlithophysal Unit 2-6
2-2. In Situ Stress Estimates at Yucca Mountain Site 2-15

3-1. Impact of Moisture Conditions on Unconfined Compressive Strength of Nonlithophysal Tptpll Samples 3-11
3-2. Summary of In Situ Slot Compression Tests in Lithophysal Rock Units 3-16
3-3. Summary of Mechanical Properties Results from the Pressurized Slot Tests 3-17
3-4. Direct Shear Test Summary of Tptpmn Fractures 3-19
3-5. Summary Statistics of Direct Shear Tests of Fracture Peak Strength 3-19
3-6. Summary Statistics of Direct Shear Fracture Degraded Strength 3-19
3-7. Summary Statistics of Fracture Strength Using Rotary Shear 3-20
3-8. Estimate of Peak Dilation Angles for Topopah Spring Formation Fracture Sets 3-21
3-9. Intact Rock Thermal Conductivities for Repository Units 3-22
3-10. Rock Mass Thermal Conductivities from Field Measurements 3-23
3-11. Rock Mass Thermal Conductivities for Repository Units 3-23
3-12. Rock Grain Heat Capacities for Repository Units 3-24
3-13. Rock Mass Heat Capacities for Repository Units 3-24
3-14. Intact Rock Coefficients of Thermal Expansion for Repository Units 3-26
3-15. Rock Mass Coefficients of Thermal Expansion for Repository Units 3-27

4-1. Comparison of Data from Detailed Line Survey, Full-Periphery Geologic Maps, and FracMan Output for the Tptpmn 4-4
4-2. Suggested Range of Mechanical Properties Selected for Base-Case Design and Performance Analyses 4-9
4-3. Summary of Average Strength and Modulus for Variation In Lithophysal Porosity and Mohr-Coulomb (Linear) and Hoek-Brown (Nonlinear) Yield Criteria Parameters as Derived from UDEC Simulations 4-24
4-4. Rock Mass Mechanical Properties Estimates for the Tptpmn 4-32

5-1. Peak Ground-Motion Parameters 5-17
5-2. Base-Case Material Properties for 3DEC Analysis 5-18
5-3. Summary of 3DEC Rockfall Prediction for 10^{-6} Annual Probability of Exceedance Hazard 5-19
5-4. Statistical Summary of the Rockfall Impact Parameters, 10^{-6} Annual Probability of Exceedance Hazard, Variability in Fracture Geometry and Ground Motion 5-21
5-5. Comparison of Rockfall Statistics for Preclosure and Postclosure Events 5-24
5-6. Three Categories of Joint Properties Used in the Sensitivity Study 5-28
5-7. Impact of Thermal Loading on Rockfall for 10^{-5} Ground Motion, Nonlithophysal Rock 5-31
5-8. Static-Fatigue Data for Busted Butte Specimens 5-53

INTENTIONALLY LEFT BLANK

ACRONYMS

AIN	Additional Information Needed
CT	computerized tomography
CTE	coefficient of thermal expansion
DOE	U.S. Department of Energy
DST	Drift Scale Test
ECRB	Enhanced Characterization of the Repository Block
ESF	Exploratory Studies Facility
GSI	geologic strength index
KTI	key technical issue
NRC	U.S. Nuclear Regulatory Commission
PST	pressurized slot test
RDTME	Repository Design and Thermal-Mechanical Effects
RMR	rock mass rating
TBM	tunnel boring machine
VPP	vapor-phase parting

INTENTIONALLY LEFT BLANK

1. INTRODUCTION

This technical basis document provides a summary of the stability of repository excavations and potential mechanical degradation under the action of in situ, thermal, and seismic stresses during the preclosure and postclosure time periods. The document further identifies the interactions of the mechanical degradation of the emplacement drifts with the engineered barriers, in-drift environment, and water seepage into emplacement drifts. This document is one in a series of technical basis documents prepared for each component of the Yucca Mountain repository system relevant to predicting the likely postclosure performance of the repository. The relationship of mechanical degradation and seismic effects to the other components of the repository system is illustrated in Figure 1-1.

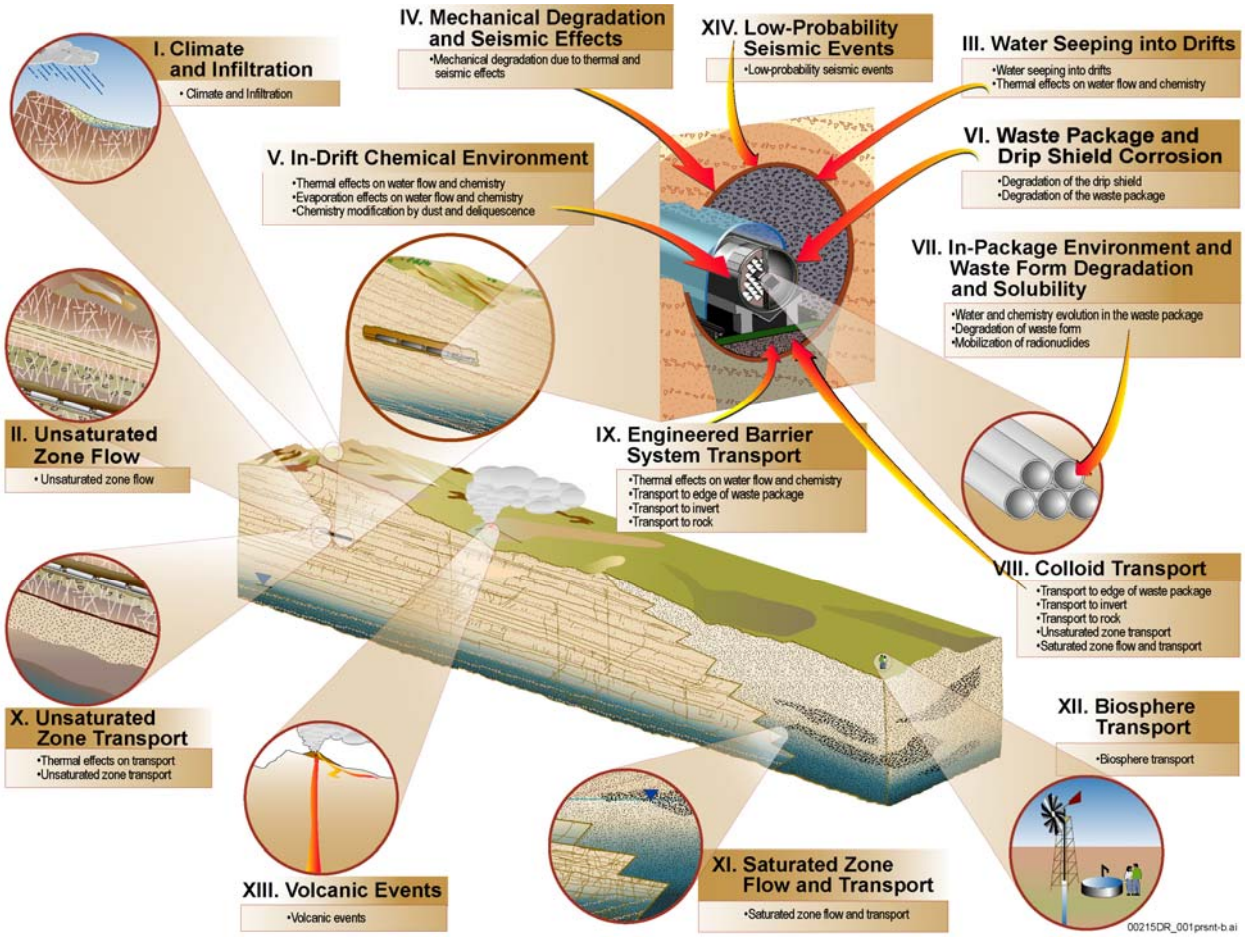

Figure 1-1. Components of the Postclosure Technical Basis for the License Application

The information presented in this document, and the associated references, is part of the ongoing development of the postclosure safety analysis that will be included in the license application. This information is also used to respond to open Key Technical Issue (KTI) agreements made between the U.S. Nuclear Regulatory Commission (NRC) and the U.S. Department of Energy (DOE). Placing the DOE responses to individual KTI and NRC Additional Information Needed (AIN) requests within the context of the overall mechanical degradation analyses, as it relates to

postclosure safety analyses, allows for a more direct discussion of the relevance of the agreements.

Appendices to this document are designed to allow for a transparent and direct response to each KTI agreement and AIN requests. Each appendix addresses one or more of the agreements. If agreements apply to similar aspects of the mechanical drift degradation issue, they were grouped in a single appendix. In some cases, appendices provide detailed discussions of data, analyses, or information related to the further conceptual understanding presented in this technical basis document. In other cases, the appendices provide information that is related to the technical basis document information but at a level of detail that relates more to the uncertainty in a particular data set or feature, event, or process that is less relevant to the overall technical basis. In these cases, the appendices reference the relevant section of the technical basis document to put the particular KTI agreement into context, but the technical basis document does not reference the appendices.

This technical basis document provides a summary-level synthesis of many relevant aspects of the mechanical drift degradation and ground support design studies. This document describes the development of an understanding of the thermal-mechanical behavior of Yucca Mountain tuffs and the development of suitable models to represent this behavior when subjected to static and transient loading. The analyses described here are applied primarily to estimating the stability and rockfall potential of the excavations, and less to the design of ground support, which is primarily a preclosure design issue. However, the techniques described here are applicable to both the design and performance studies.

This document presents a summary and synthesis of the detailed technical information presented in the analyses and model reports and other technical products that are used as the basis for the description of the mechanical degradation analysis and the incorporation of this work into the postclosure performance assessment. Several analyses, model reports, and other technical products support this summary:

- *Drift Degradation Analysis* (BSC 2004a)
- *Subsurface Geotechnical Parameters Report* (BSC 2003a)
- *Longevity of Emplacement Drift Ground Support Materials for LA* (BSC 2003b)
- *Ground Control for Emplacement Drifts for the LA* (BSC 2003c)
- *Scoping Analysis on Sensitivity and Uncertainty of Emplacement Drift Stability* (BSC 2003d)
- *Ground Control for Non-Emplacement Drifts for LA* (BSC 2004b)
- *Development of Earthquake Ground Motion Input for Preclosure Seismic Design and Postclosure Performance Assessment of a Geologic Repository at Yucca Mountain, NV* (BSC 2004c)
- *Geology of the ECRB Cross Drift—Exploratory Studies Facility, Yucca Mountain Project, Yucca Mountain, Nevada* (Mongano et al. 1999)

- *Resolution Strategy for Geomechanically-Related Repository Design and Thermal-Mechanical Effects (RDTME)* (Board 2003).

The basic approach used in this document is to review the relevant portions of these reports to provide a comprehensive overview of the data and analyses that describe the process of mechanical degradation and to provide a context for the attached KTI resolution documents. The details of the data and analyses can be found in the above reports.

1.1 OBJECTIVE AND SCOPE

The objectives of this technical basis document are to:

- Provide an overview of the anticipated mechanical degradation processes in the emplacement drifts and the boundary conditions this degradation provides to the engineered barrier system and drift seepage
- Present an overview of the KTI agreements, how they relate to this process, and the strategy employed to resolve these issues
- Present a summary of the relevant geomechanical rock mass properties database developed for lithophysal and nonlithophysal rocks
- Describe the numerical modeling and analysis techniques used for ground support and drift degradation analysis
- Present the analysis of postclosure mechanical degradation under the action of in situ, thermal, and seismic stresses, as well as time-dependent strength changes.

The purpose of the mechanical degradation analyses is to provide an estimate of the temporal evolution of the stability of the emplacement drifts under the action of in situ, thermal, and seismic loading, as well as time-dependent changes in rock mass strength. In particular, the model(s) provide an estimate of:

- The yield of the rock mass around the emplacement drifts, and the associated rockfall once the ground support function is lost due to postclosure corrosion
- The temporal change in emplacement drift shape and size
- The temporal evolution of rockfall, including the rockfall particle size distribution and total amount
- The temporal evolution of rockfall loading (both dynamic and quasi-static[1]) on the drip shield.

[1] Quasi-static refers here to the development of loading on the drip shield, which slowly evolves over time but is more-or-less in static equilibrium.

Due to the distinctly different mechanical characteristics of the major rock units that comprise the repository host horizon (lithophysal and nonlithophysal rocks), the above estimates will vary with location within the repository.

For the postclosure period, 10 CFR 63.114 requires that DOE conduct a performance assessment that considers only events that have at least one chance in 10,000 of occurring over 10,000 years. Seismic events that have this probability of occurrence have been analyzed and are discussed in this technical basis document. In addition, 10 CFR 63.102(j) provides that, for the postclosure period, the event classes analyzed in the performance assessment should consist of all possible specific initiating events that are caused by a common natural process (e.g., the event class for seismicity includes the range of credible earthquakes for the Yucca Mountain site). Additional sensitivity studies are currently being conducted to ascertain the range of credible ground motions, and those studies are not discussed in this document. The additional studies do not affect the technical bases or conclusions described in this document. The results of those sensitivity studies will be included in the license application, as appropriate.

1.2 SUMMARY OF CURRENT UNDERSTANDING

1.2.1 General Description of the Repository Layout and Waste Emplacement

A general description of the design and layout of the repository can be found in *Underground Layout Configuration* (BSC 2003e). The repository is located at approximately 300 m below ground surface within the Topopah Spring Tuff—a densely welded tuff unit comprised of a number of subunits that dip approximately 15° from west to east. These subunits can be divided into two broad, mechanical categories: nonlithophysal and lithophysal[2] welded tuffs. The basic matrix material of these two subunits is similar in mineralogical, textural, and mechanical properties. However, due to varying cooling histories and as a result of position within the formation, they are structurally and thermal-mechanically significantly different in character. The nonlithophysal rocks are hard, mechanically strong, fine-grained and fractured volcanic rocks whose mechanical behavior is strongly controlled by the geometry and surface characteristics of its fracturing. The lithophysal rock is composed of the same strong, hard matrix material, but has porosity in the form of lithophysal cavities ranging from about 10% to 30% by volume. The presence of these cavities results in significantly different deformability and strength of the rock mass. The current repository layout places approximately 85% of the emplacement drifts within the lithophysal rocks (BSC 2003e, Table I-2).

The repository (Figure 1-2) is accessed from ground surface on the east side of Yucca Mountain by three 7.62 m diameter entry ramps (the north and south ramps currently exist and are part of the Exploratory Studies Facility (ESF) and are driven at 2.5% grade). Once these ramps achieve the depth of the Topopah Spring Tuff, they join a number of subhorizontal, 7.62-m diameter access mains. These access mains define the outer perimeter of four panels that are composed of 5.5 m nominal diameter waste emplacement drifts (BSC 2003e). The emplacement drifts are accessed at one end from the fresh air intake main via a turnout (Figure 1-3) and intersect the exhaust main at the opposite end. The excavations, with the exception of the turnouts, are driven

[2] Lithophysae: hollow, bubblelike cavities in a volcanic rock surrounded by porous rims formed by fine-grained alkali feldspar, quartz, and other minerals. Lithophysae are typically a few centimeters to a few decimeters in diameter; however, they can be as small as 1 mm in diameter or less to as large as 1 m or more in diameter.

by tunnel boring machines (TBMs). The access mains are supported with rock bolts and heavy wire mesh, the turnout-access mains intersections with rock bolts and shotcrete, and the emplacement drifts with thin (2 to 3 mm), perforated, stainless steel sheeting held tight to the drift walls using stainless steel, friction-type rock bolts (Figure 1-4). All of the ground support is placed over a 240° arc on roof and walls. The general ventilation method employed is to draw fresh air into the repository via the ramps and a number of intake shafts, distribute it down the intake mains, through the emplacement drifts, and out through a series of exhaust shafts (BSC 2003e, Table I-2).

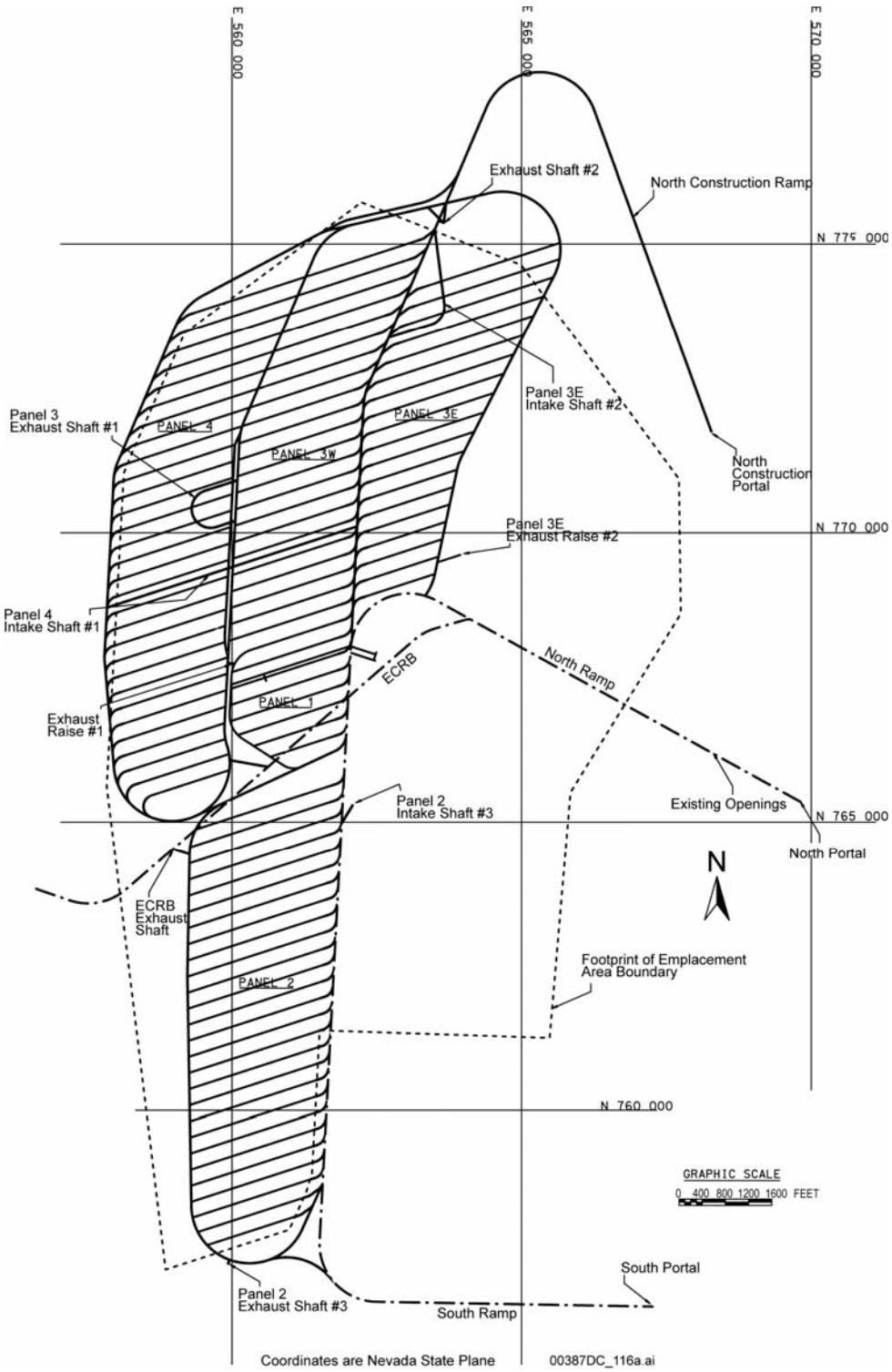

Source: BSC 2003e.

NOTE: Footprint of emplacement area boundary is shown as a dashed line. This footprint represents the currently characterized area in which emplacement drifts can be located.

Figure 1-2. Repository Layout in Plan View Showing Ramps, Access Intake and Exhaust Mains, Emplacement Drifts, Shafts, and Existing Excavations (as Dashed Lines)

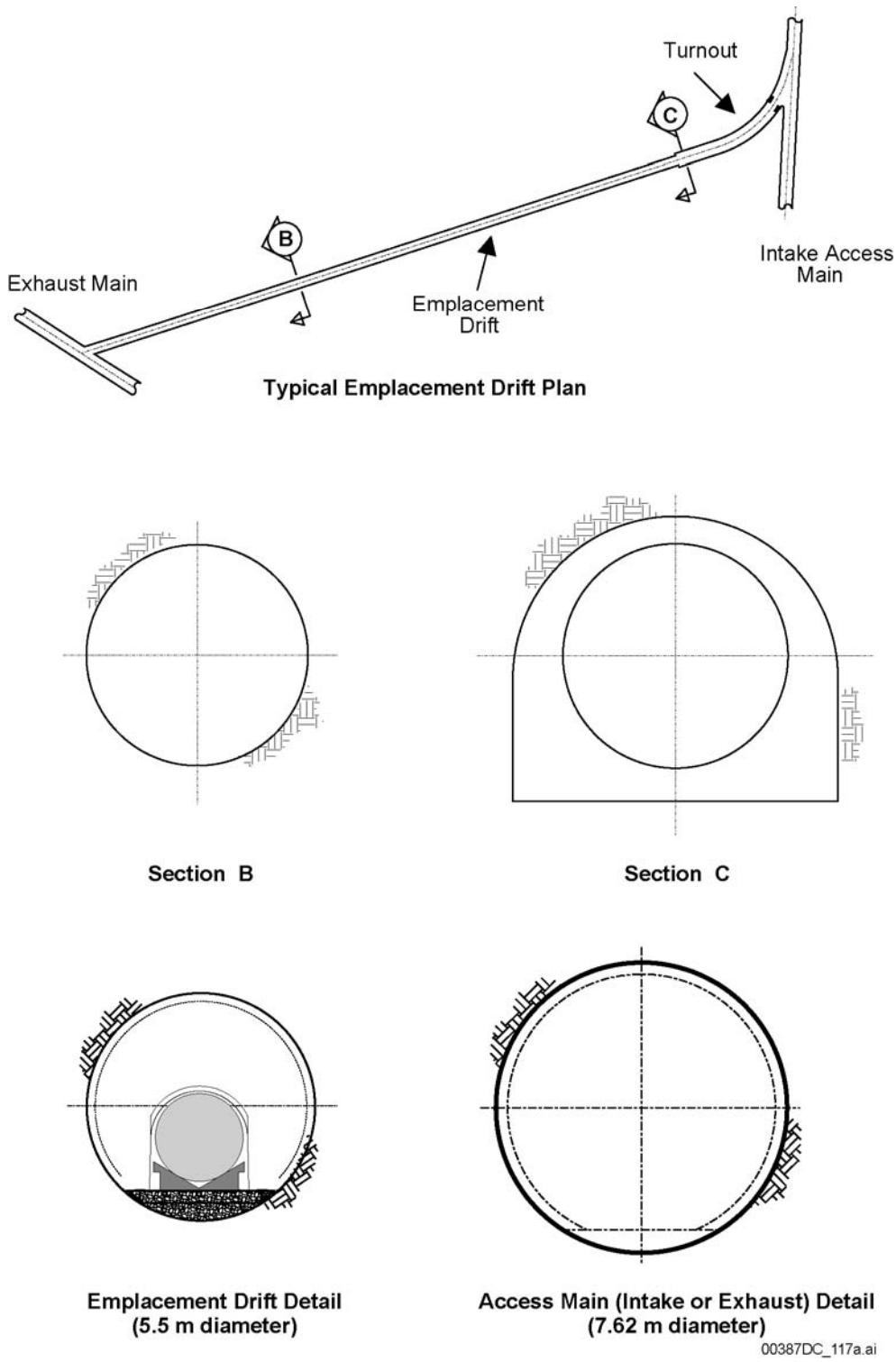

Figure 1-3. Plan View and Cross-Sectional Views of Primary Repository Excavations

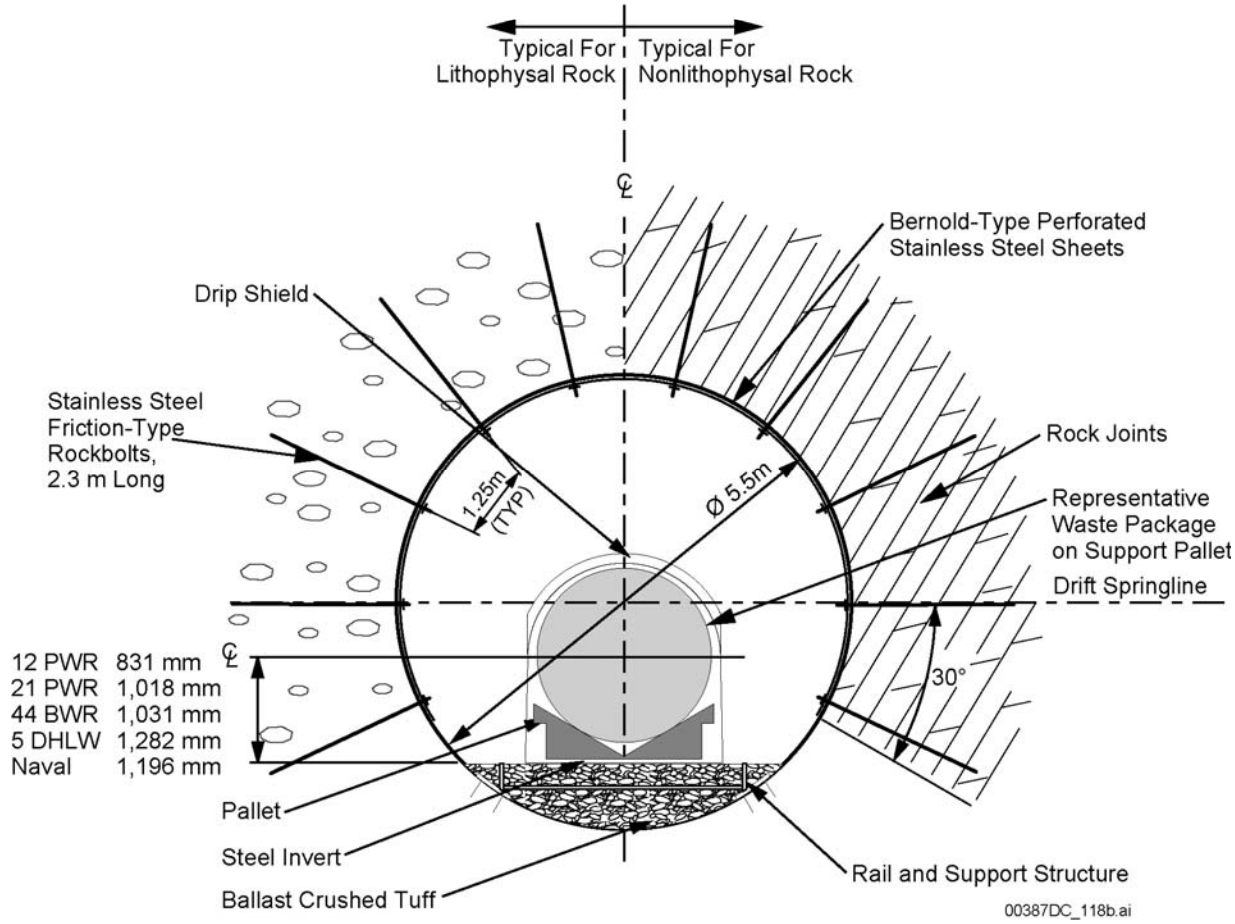

Source: BSC 2003c and BSC 2004d.

NOTE: Ground support coverage using Bernold-Type stainless steel sheets (240° of circumference above invert) and stainless steel friction bolts.

Figure 1-4. Ground Support Method for Emplacement Drifts Showing Drip Shield

A rail-based waste emplacement transporter, drawn by electric locomotives, will leave the surface waste handling facilities with a waste package on the emplacement pallet loaded within a shielded rail car. The transporter will deliver the waste package, via the access mains, to the emplacement drift turnout. In the turnout, the waste package will be transferred, in an automated mode, by pushing the waste package and pallet from the transporter onto a docking bay at the end of the emplacement drift. The waste package will then be picked up from the loading dock and transported into the emplacement drift by an emplacement gantry crane (Figure 1-5). The emplacement gantry will deliver the waste package and pallet to their resting location on the drift invert structure, and will return to the docking bay. Normal retrieval operations, if required, will involve a reversal of the emplacement sequence. At closure, a titanium drip shield will be placed over the top of the waste packages (Figure 1-4), and all nonemplacement drifts will be backfilled with crushed tuff from the TBM operations.

1.2.2 General Degradation Processes

The general process of mechanical degradation of emplacement drifts during the preclosure and postclosure time frames involves interactions with several engineered and natural barrier systems. A general description of the impact or interaction of the mechanical degradation of the emplacement drifts is given here.

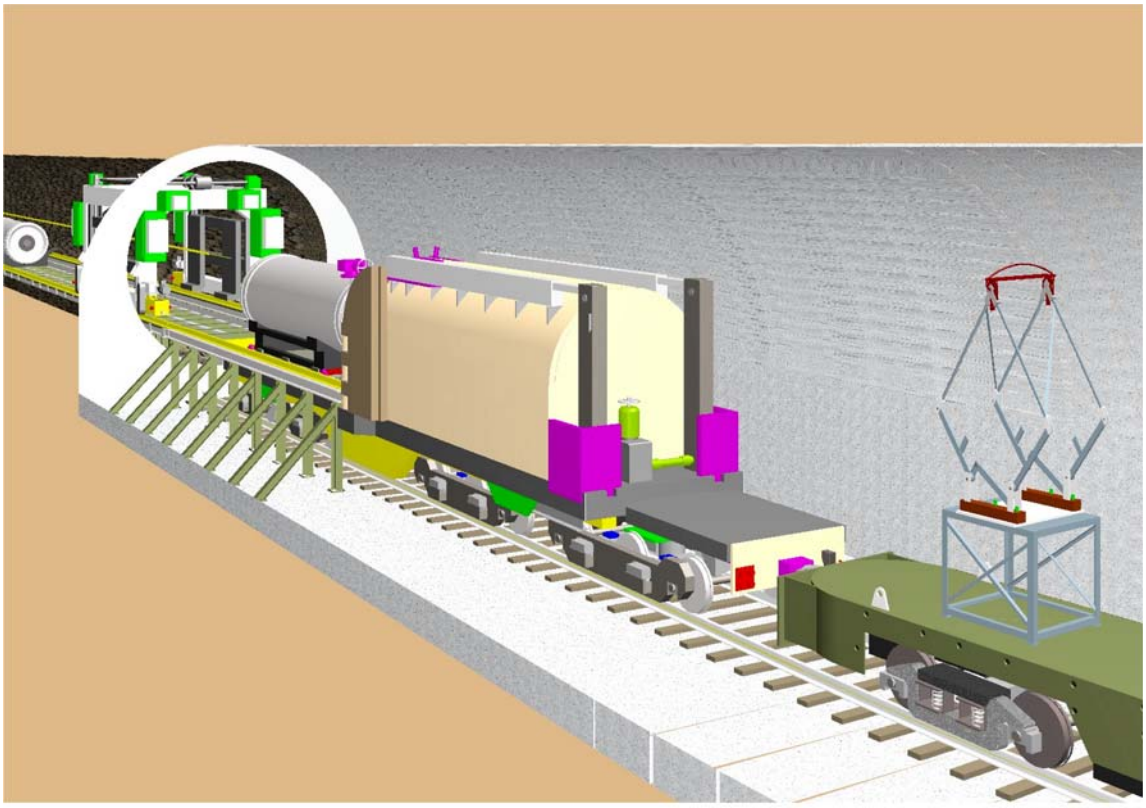

Figure 1-5. Shielded Waste Transporter at Docking Bay Showing Waste Package, Waste Emplacement Gantry, and Locomotive

1.2.2.1 Preclosure Effects

Excavation of the repository drifts will result in concentration of in situ stresses around the openings. Because the in situ stresses are relatively small in comparison to the rock mass strength, little, if any, yield of the rock mass is expected. Thus, the openings will undergo primarily elastic deformation, which equilibrates within a short distance (about two tunnel diameters) behind the advancing TBM. Light, temporary ground support is placed directly behind the TBM for worker protection purposes. Permanent ground support is placed after the emplacement drift is completed and the TBM withdrawn, therefore, it will be subjected only to deformation and loading that may occur from transient effects such as thermal and seismic loading.

During the preclosure time period, approximately 100 years from initial excavation of the emplacement drifts, forced ventilation will be used to remove approximately 90% of the heat generated by the waste packages. This heat removal will keep drift wall temperatures cooler

(BSC 2004a, Section 6.2) and will result in small thermally related rock mass stress changes (see Section 5.3.1). The emplacement drifts will be supported by rock bolts and slotted stainless steel sheeting, thus minimizing, if not eliminating, mechanical degradation of the excavations.

Although this technical basis document is concerned primarily with the postclosure mechanical and seismic degradation effects, a number of the Repository Design and Thermal-Mechanical Effects (RDTME) KTI agreements either relate specifically to preclosure ground support performance or are concerned with rock mass characterization and modeling issues that are common to both preclosure and postclosure performance. Since a detailed review of preclosure design issues is not given in this document, Table 1-1 is provided to give a cross-reference between the KTI agreement resolution summaries found in the appendices and the specific source document that provides greater details of the analyses that support the agreement.

Table 1-1. Key Technical Issue Agreements–Relevant Section Supporting Documents

Appendix	KTI Agreement	Description	Where Addressed
A	RDTME 3.05	Technical basis for accounting for effects of lithophysae	Sections 3.2 and 4.2
B	RDTME 3.06	Design sensitivity and uncertainty analyses of the rock support system	Sections 3.2, 4.1, 4.2, and 5.3 Document A
C	RDTME 3.15 RDTME 3.16 RDTME 3.17 RDTME 3.19	Data and analysis of rock bridges between joints Modeling joint planes as circular discs, small trace length fractures Technical basis for effective max rock size Determine whether rockfall can be screened from PA abstractions	Sections 3.2, 4.1, and 5.3
D	RDTME 3.02 RDTME 3.10 RDTME 3.13	Critical combinations of in situ, thermal, and seismic stresses Two-dimensional modeling of emplacement drifts Boundary conditions, discontinuum versus continuum modeling	Sections 4.1, 4.2, and 5.3 Documents A and B
E	RDTME 3.04	Site-specific properties of the host rock	Section 3.2 Document D
F	RDTME 3.08 RDTME 3.12	Design sensitivity and uncertainty analyses of fracture patterns Dynamic analyses of ground support performance	Section 3.2, 4.1, and 5.3 Documents A, B, C, and D
G	RDTME 3.09	Rock movements in the invert	Sections 3.2, 4.2, and 5.3 Document A
H	RDTME 3.11	Continuum and discontinuum analyses of ground support system performance	Section 4.1, 4.2 Document A

NOTE: Document A is BSC 2003d. Document B is BSC 2003c. Document C is BSC 2004b. Document D is BSC 2003a.

1.2.2.2 Postclosure Effects

Repository closure will involve installation of titanium drip shields over the waste packages, backfilling of access mains and shafts, and the cessation of forced ventilation. This will result in a rapid rise in temperature of the drift walls, reaching approximately 140°C to 165°C within

about 20 years after closure. The temperature then slowly decreases over time, with the emplacement drift remaining above 96°C for approximately 1,000 years (BSC 2004a).

After closure, the ground support will corrode and lose its function over the period of perhaps decades to centuries, resulting in unsupported emplacement drifts through the large majority of the postclosure period.

During the postclosure period, the emplacement drifts will be subjected to the following loading conditions (Figure 1-6): the in situ gravitational/tectonic stress state, transient thermally induced stresses due to expansion of the rock mass[3], and seismic stresses due to potential earthquake shaking. Additionally, the rock mass strength, particularly in lithophysal rock, will exhibit a degree of time-dependency as a result of typical stress corrosion mechanisms[4]. The impact of these in situ and induced stress components is the potential for rock mass yield in the immediate region around the tunnels and some degree of rockfall. The rockfall has potential performance impacts on the following systems (BSC 2004e):

- Mechanical Effects on Engineered Barriers
  - Effects include possible rock particle impacts and dynamic loading of the drip shield, either under gravitational or earthquake-induced accelerations.
  - Quasi-static loading and contact from rock particles resting on the drip shield following rockfall.
  - Dynamic loading of the drip shield could occur from seismic ground motions applied to a previously collapsed drift.
- Mechanical Effects on In-Drift Environment
  - Rockfall of sufficient volume could result in an “insulating” blanket surrounding drip shields, impairing heat transfer to the rock mass and increasing waste package temperatures.
  - Rock particles within the drift will potentially alter the in-drift moisture and chemical environment around and upon the engineered barrier system components, and therefore need to be accounted for in drip shield and waste package corrosion.
- Mechanical Effects on Seepage of Groundwater Into the Drift
  - Rockfall will result in changes to the size and shape of the emplacement drifts as a function of time, thus altering the seepage flow to the drift.

[3] A large portion of the thermally induced strains and stress are recoverable as the rock mass cools over time.

[4] “Stress corrosion” is a term commonly used in the field of rock mechanics (and metals) that represents time-dependent, subcritical crack growth that occurs when existing material flaws in the rock are subjected to stresses that are near the failure state of the material. This process, which occurs at a more rapid rate in the presence of moisture, may result in damage and yield at applied stresses that are less than the short-term strength. Corrosion here does not refer to corrosion of metals.

– Rock particles within the drift will have impacts on the drift capillary strength and seepage transport mechanisms and travel paths within the drift depending on particle size distribution.

– Damage around the drift itself will affect the rock mass hydraulic characteristics that affect the capillary barrier in the periphery of the drift.

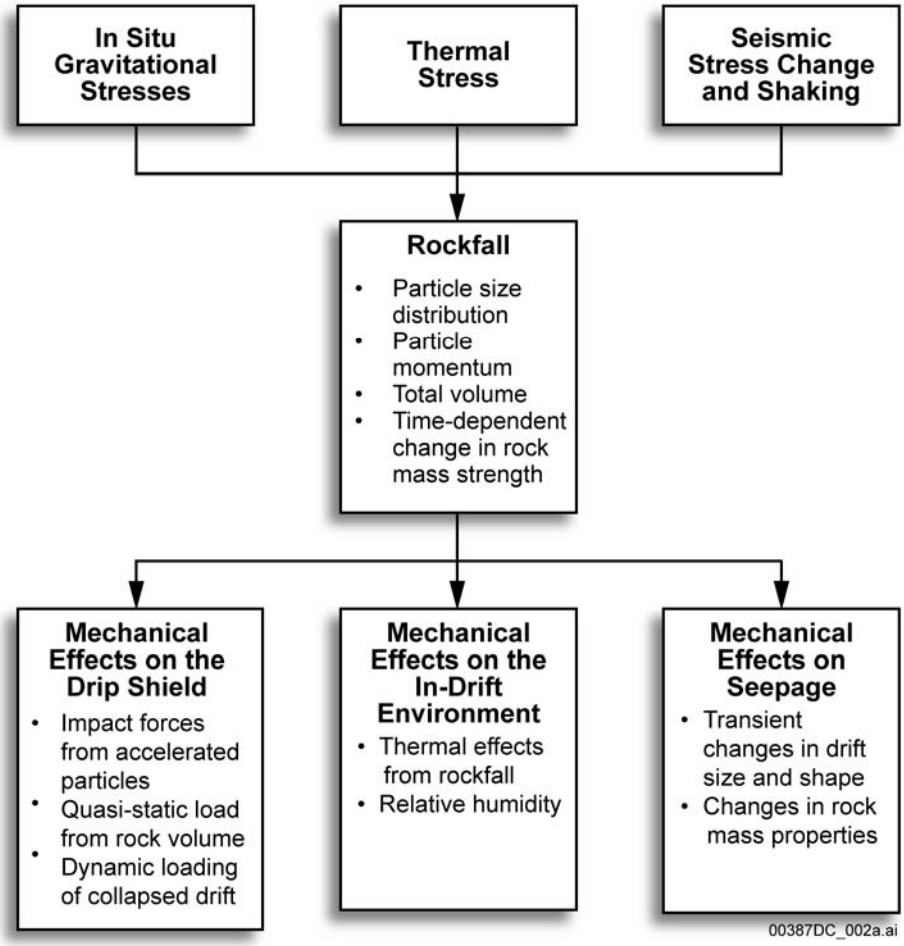

Figure 1-6. Potential Postclosure Performance Impacts of Rockfall on Engineered Barriers, In-Drift Environment, and Groundwater Seepage into Drifts

A series of NRC KTI agreements deal specifically with the methodology for analysis of and estimation of rockfall size distribution and volume as a function of the variability of rock mass properties, loading conditions and strength time-dependency. A number of KTI agreements in other areas (waste package, drip shield, seepage) address the impacts of rockfall as these performance issues.

1.2.3 Summary of Approach to Addressing Preclosure and Postclosure Issues

The primary technical issues that have formed the basis for the mechanical degradation resolution strategy can be summarized in three categories: (1) geotechnical characterization and rock mass property definition, (2) development and validation of numerical modeling tools, and (3) design and performance analyses.

1. Geotechnical Characterization and Rock Mass Property Definition

   - Development of laboratory and in situ testing database of thermal-mechanical and time-dependent material properties for intact rock and fractures

   - Development of a relationship between geologic structure (fractures in the nonlithophysal rocks and lithophysae in the lithophysal rocks) and rock mass material response

   - Determination of the impact of the variability of geologic structure on rock mass property size effect, variability, and uncertainty.

2. Development and Validation of Numerical Modeling Tools (determination or development of appropriate models for sensitivity studies of excavation stability and rockfall under in situ, thermal, and seismic loading)

   - Continuum versus discontinuum modeling

     – Discontinuum modeling required for representing rockfall

     – Continuum modeling suitable for parameter studies

   - Two- versus three-dimensional models

     – Three-dimensional models required in joint-controlled nonlithophysal rock, where response to seismic load is generally anisotropic

     – Two-dimensional models sufficient in generally isotropic lithophysal rock

3. Design and Performance Analyses

   - Design studies

     – Verification, via empirical and numerical analyses, of the functional and operational requirements and specification of ground support

     – Develop initial ground support designs and specifications based on requirements

     – Verify design concepts via analysis of rock mass stability in lithophysal and nonlithophysal rock for in situ stress and preclosure thermal and seismic loading

  - Development of observation and maintenance plans for ground support

- Performance analyses
  - Stability analysis and rockfall estimate under in situ, thermal, and seismic loading
  - Assessment of long-term stability of tunnels under quasi-static loading and time-dependent rock mass strength degradation

The approach taken to address these issues (Figure 1-7) is based on development of a progressively more detailed understanding of the mechanical behavior of the lithophysal and nonlithophysal rock masses, starting with basic geologic characterization to understand rock mass variability, followed by laboratory and in situ testing with closely coupled numerical model development and validation. The process was developed from laboratory to field scale, allowing testing of the models and development of confidence in their ability to predict complex degradation modes. Next, the validated site-specific models were used to conduct sensitivity studies to examine thermal and mechanical drift degradation for variation in rock mass structure (and properties) under static and transient loading. The KTI agreements that have been addressed at each stage in this process are also given in this figure.

The process was composed of six major program work elements. The approach initially involved developing a detailed understanding of the thermal-mechanical properties and variability of lithophysal and nonlithophysal rocks, and developing validated numerical models that can be used for design and performance assessment. The outcome of this process was a set of material models and properties and their ranges that were used as input to sensitivity studies of drift degradation in response to seismic events and to time-dependent processes.

As described in Section 3, the mechanical and thermal properties of the lithophysal rocks are sensitive primarily to the lithophysal porosity. Because the lithophysal cavities range in size from millimeters to over a meter, and are of widely different shape and distribution within the rock mass, sampling and mechanical testing of sufficiently large samples presents a challenge, and thus characterization of properties and property variability is an issue.

To overcome this issue, mechanical testing at increasing scales was used to understand porosity and size effects. Calibrated numerical modeling using discontinuum methods were used as a means of exploring the variability of lithophysal porosity, size, shape, and distribution on failure mechanisms and mechanical property variations. Thus, testing was used to define the basic lithophysal rock mass properties and was supplemented by modeling to explore variability ranges.

The sensitivity modeling was aimed at estimating tunnel stability in the preclosure and postclosure time frames. In the preclosure period, the primary issue was the verification of ground support methods. In the postclosure period, the primary issues were estimation of mechanical degradation of emplacement drifts from thermal and seismic loading, or time-dependent degradation response of the rock mass.

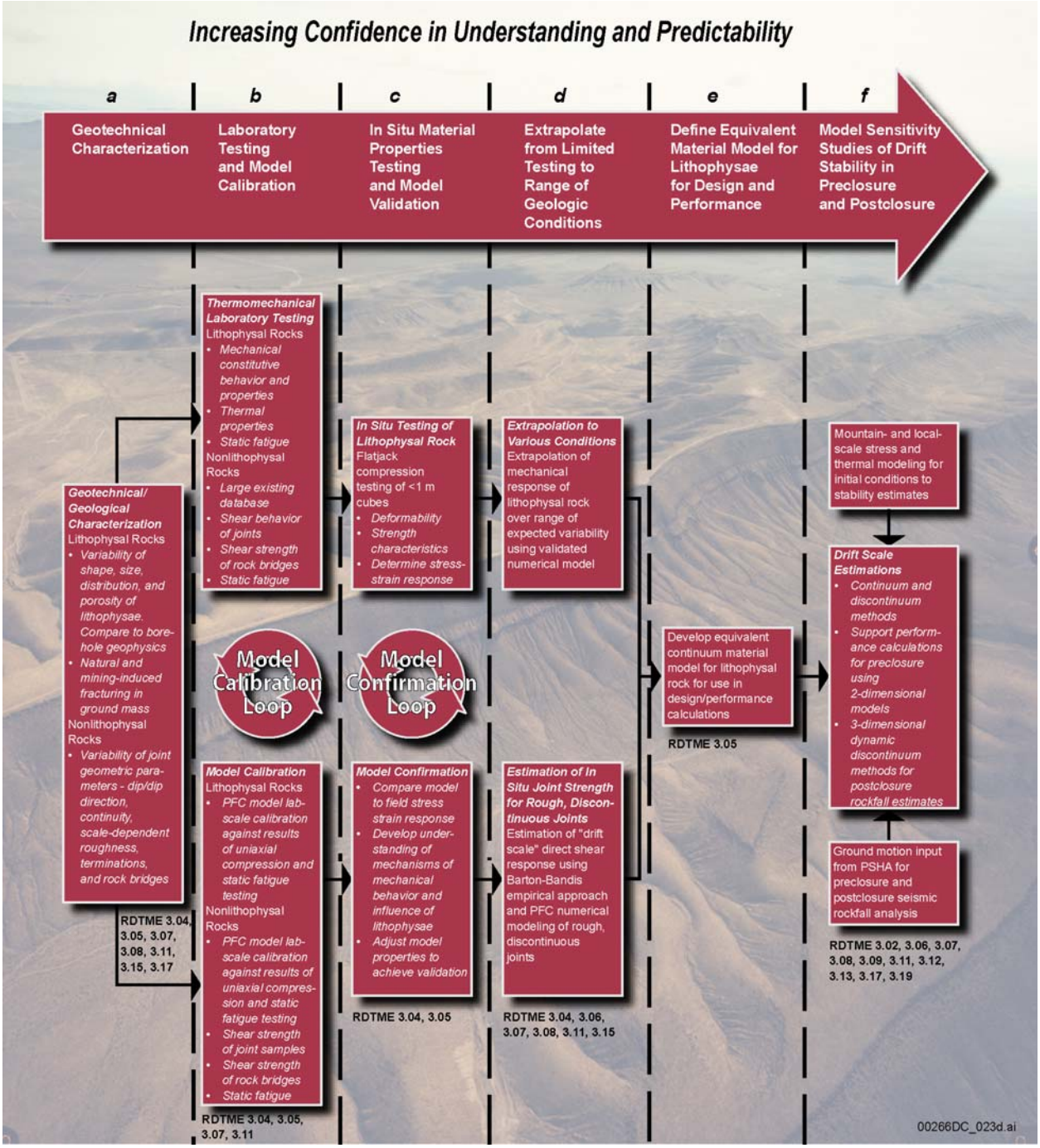

NOTE: Process starts with compilation and analysis of basic geotechnical mapping, followed by laboratory and field testing and model validation to develop rock mass property estimates for design and performance sensitivity studies. PSHA = probabilistic seismic hazard analysis.

Figure 1-7. General Approach to Resolution of the Repository Design and Thermal-Mechanical Effects Key Technical Issues

A review of the six major program work elements is as follows:

1. **Geotechnical Characterization**–Further analysis of the extensive, existing rock mass geologic and geotechnical characterization data from the ESF and the Enhanced

Characterization of the Repository Block (ECRB) Cross-Drift, as well as surface outcrops and boreholes, to estimate the geometrical variability of rock mass fracturing and lithophysae. These data are supplemented by new detailed panel mapping of lithophysae in the ECRB Cross-Drift. Detailed statistical analysis of the fracture geometry in the middle nonlithophysal unit of the Topopah Spring Tuff (Tptpmn) and the lithophysae geometry in lower lithophysal unit of the Topopah Spring Tuff (Tptpll) is performed to provide the basic rock mass structural input and its variability to the modeling and analysis activities (see Section 2.3).

2. **Laboratory Testing and Model Calibration**–A large amount of data for thermal and mechanical rock properties exists for nonlithophysal rocks. These data have been supplemented with laboratory direct shear testing of representative fracture samples. Additional compression tests on nonlithophysal samples with varying size and saturation levels, as well as static fatigue testing to derive time-dependent strength properties, have been conducted. Laboratory tests on lithophysal rock cores with a large diameter (290 mm) have been conducted to determine mechanical and thermal properties as a function of porosity, temperature, and saturation level. These laboratory tests, combined with in situ testing and previous large diameter (267-mm) cores, are used to establish the basic engineering properties of the lithophysal and nonlithophysal rock masses and their variability with porosity (see Sections 3.2.1, 4.2.2, and 4.2.3).

   The lithophysal laboratory data (i.e., strength, modulus, and variation with porosity) and observations of failure mechanisms are used as the basis for initial calibration of discontinuum numerical models[5]. Two discontinuum numerical approaches are used to back-analyze laboratory data and to provide an understanding of the impact of lithophysal cavities on deformability and yield mechanisms. These approaches can represent the presence of voids as well as the physical reality of complex failure mechanisms involving interlithophysae fracturing and compaction of void space. PFC2D and PFC3D, which use a “micromechanical” discontinuum approach for representing rock, and UDEC, a standard discontinuum modeling program, are used to reproduce stress-strain behavior and failure mechanisms observed from the laboratory experiments. The models are also calibrated against static fatigue testing, which determines a relationship between the “time-to-failure” and applied stress level for nonlithophysal cores. These data are used to develop a basic mechanistic approach for predicting time dependency that is based on a standard stress corrosion crack growth model.

3. **In Situ Material Properties Testing and Model Validation**–In situ mechanical and thermal testing of lithophysal rocks is performed to determine the size effect (porosity and fracture) on rock mass constitutive behavior. These tests are further used for

[5] Discontinuum numerical models simulate rock masses as actual blocks of solid material separated by fracture surfaces that have cohesive tensile and frictional strength. When the rock mass yields, the fractures may physically break in shear or tension, creating individual blocks that are free to detach from the surrounding rock mass. Continuum numerical models represent the rock mass as a continuous body in which the stiffness and yielding effects of fractures are represented via material stress-strain relationships. The rock mass cannot represent detachment of individual blocks from the parent rock mass.

validation of the numerical modeling approaches at increasing size scales. This results in numerical modeling approaches that can be used with confidence for extrapolating the mechanical response of lithophysal rocks (see Sections 3.2.3 and 4.2.7).

4. **Model Extrapolation for Establishing Property Variability**–Due to the size effect on thermal and mechanical properties introduced by lithophysae, it is necessary to test large sample sizes (for lithophysal units) to obtain realistic in situ rock mass properties. It is impractical to perform a statistically large number of in situ tests to determine strength and deformability variability. However, the numerical models, suitably calibrated against the laboratory and field data, provide the capability of exploring the impact of lithophysal variations such as porosity, lithophysal shape, size distribution, and spacing on strength and deformability variation. These models have been used to provide an understanding of the basic mechanics of the lithophysal rock mass and to define the resulting input property ranges for subsequent design and performance calculations. The models are also used as a means of understanding the impact of lithophysal porosity on stress redistribution within the rock mass and thus its impact on stress-related time dependency (see Section 4.2.3.3).

5. **Best-Estimate Constitutive Models and Property Ranges for Sensitivity Studies**–The testing data and numerical extrapolations are used to define the constitutive[6] models and property ranges for the lithophysal rock mass. The lithophysal rock mass properties are subdivided into five categories. These categories are based on lithophysal porosity level and are indicative of the in situ rock mass strength and moduli variation. Laboratory data from direct shear testing and field characterization of joints are used to define property ranges for modeling of nonlithophysal rocks (see Section 4.2.4).

6. **Design and Performance Assessment Sensitivity Studies**–Sensitivity studies of excavation stability under in situ, thermal, and seismic loads in the preclosure and postclosure time frames have been performed. Numerical model sensitivity studies are performed using the range and distribution of rock mass properties determined from testing and model extrapolation. The deformation and yield of the rock mass around the openings in preclosure time are used to define ground support requirements and appropriate support methods. These models are supplemented with practical empirical ground support specification methods, where applicable, to determine ground support methods and materials that will require minimal or no maintenance over the preclosure period. Extensive discontinuum modeling studies are used to examine thermal and seismic loading effects on mechanical degradation of the emplacement drifts in the postclosure. In nonlithophysal rocks, analysis of the jointing is used to generate a large number of three-dimensional, stochastically defined fracture geometries that realistically represent the rock mass fracturing documented from field mapping. These jointing realizations and associated emplacement drifts are subjected to postclosure

[6] A constitutive model in this case is a set of mathematical equations that describe the relationship of applied stress to strain for the rock mass. These equations include a description of the elastic and failure characteristics of the rock mass. Typically, rock is described by yield criteria that account for the strength of the fracture fabric of the rock mass. A typical form of yield criteria for rock is the Mohr-Coulomb or Hoek-Brown criteria (e.g., Hoek 2000).

rock mass temperature levels and ground motions representative of seismic events with 10^{-5}, 10^{-6}, and 10^{-7} annual exceedance frequencies. The rock mass is also subjected to predicted postclosure temperature distribution. Two-dimensional models representing the range of strength categories of the lithophysal rocks are subjected to similar thermal and seismic loading. The rockfall generated by these simulations is presented in a number of ways, including the size distribution of the particles, the peak velocities of each particle and the total mass of rock dislodged from the surrounding mass. This information is used to define dynamic and quasi-static loads applied to the drip shield as well as the resulting shape of the tunnels (see Section 5.3).

Finally, the models are used to predict the time-related degradation in the lithophysal rocks resulting from quasi-static loading and time-dependent strength reduction. Sensitivity studies for the range of rock mass strength categories are used to predict the change in shape of the emplacement drifts and the total dislodged rock volume as a function of time. This information provides a basis for the estimation of in-drift and seepage effects due to mechanical degradation (see Section 5.3.2.2.4).

A detailed discussion of the methodology for inclusion of drift degradation estimates into the total system performance assessment is given in *Seismic Consequence Abstraction* (BSC 2004e). The drift degradation estimates, including rockfall and drift size and shape, are considered in both "nominal" and "seismic" performance scenario classes[7]. The nominal scenario class considers the estimated time-dependant change in drift shape, and the volume of associated rockfall on and around the drip shield is considered. The mechanical damage to the drip shield resulting from quasi-static loading of dislodged rock is considered, as well as the impacts of the rockfall on heat transfer mechanisms. The seismic scenario class takes into account the rockfall induced by possible seismic events. Here, the estimates of rockfall onto the drip shield as a function of the annual exceedance frequencies are used to estimate the drip shield damage level and the subsequent effects on seepage of ground water through it. Additionally, dynamic loading of the drip shield due to seismic shaking of a previously failed, rubble-filled drift are also considered. Although not specifically part of the drift degradation effects, the seismic scenario also includes estimation of performance consequences of vibratory motion on waste package damage resulting from waste package impacts with the pallet, adjacent waste packages, and the drip shield.

1.3 ORGANIZATION OF THE REPORT

The report format is as follows:

- **Introduction (Section 1)**–The objectives and scope of this technical basis document, and a summary of the mechanical degradation issues and issue resolution strategy.

[7] The TSPA model takes into account "nominal" and "disruptive events" scenario classes. The disruptive events scenario class includes both seismic and igneous scenarios. The nominal scenario class includes FEPs expected to occur over the life of the repository, including seismic events with annual probabilities in the range of 10^{-4} and 10^{-5} per year. The seismic scenario class includes higher consequence, lower probability events with annual probabilities in the range of 10^{-6} to 10^{-8} per year.

- **Geologic Characteristics of the Repository Host Horizon Relevant to Mechanical Degradation (Section 2)**–The geology of the Topopah Spring Tuff as it relates to understanding of the thermal-mechanical rock mass properties and the variability introduced by fracturing and lithophysae.

- **Thermal-Mechanic Rock Properties Database—Review of Laboratory and In Situ Testing for the Nonlithophysal and Lithophysal Rock Masses (Section 3)**–A review of the results from nearly 20 years of laboratory and field testing programs for lithophysal and nonlithophysal rocks.

- **Development of Rock Mass Material Modeling Approaches for Nonlithophysal and Lithophysal Rocks (Section 4)**–The development of appropriate mechanical material models for lithophysal and nonlithophysal rocks. The generalization of these data into modeling approaches for mechanical degradation studies in lithophysal rocks. Calibration and validation of discontinuum numerical models against these data and extrapolation studies using these models to establish variability in mechanical properties of the lithophysal rocks.

- **Analysis of Preclosure and Postclosure Drift Mechanical Degradation under Gravitational, Thermal, and Seismic Loading (Section 5)**–The details of numerical parameter studies of mechanical degradation under various loading conditions and time-dependent strength loss. The output from these studies to other disciplines.

- **Summary and Interactions with Engineered and Natural Systems (Section 6)**–A summary of the conclusions and information feeds to other postclosure performance systems.

- **References (Section 7)**–Sources of information used in this document.

- **Appendices–**Address specific RDTME KTI agreements.

1.4 NOTE REGARDING THE STATUS OF SUPPORTING TECHNICAL INFORMATION

This document was prepared using the most current information available at the time of its development. This technical basis document and its appendices providing KTI agreement responses that were prepared using preliminary or draft information reflect the status of the Yucca Mountain Project's scientific and design bases at the time of submittal. In some cases this involved the use of draft analysis and model reports and other draft references whose contents may change with time. Information that evolves through subsequent revisions of the analysis and model reports and other references will be reflected in the license application as the approved analyses of record at the time of license application submittal. Consequently, the Yucca Mountain Project will not routinely update either this technical basis document or its KTI agreement appendices to reflect changes in the supporting references prior to submittal of the license application.

INTENTIONALLY LEFT BLANK

2. GEOLOGIC CHARACTERISTICS OF THE REPOSITORY HOST HORIZON RELEVANT TO MECHANICAL DEGRADATION

2.1 GENERAL GEOLOGY OF REPOSITORY HOST HORIZON

The lithostratigraphy and geologic evolution of the Yucca Mountain site is described in *Yucca Mountain Site Description* (BSC 2004f). This section gives a summary of the geologic characteristics of the repository host horizon relevant to the analysis of mechanical degradation response of the repository excavations.

Site-specific characteristics of the rock units of the Topopah Spring Tuff that constitute the host rock at the repository horizon are found in the geologic mapping of those units in both the main drift and ramps of the ESF and the ECRB Cross-Drift.

The locations of the ESF and ECRB Cross-Drift, and the lithostratigraphic units exposed by the tunnels, are illustrated in the geologic cross section (Figure 2-1). The units that comprise the host rocks of the repository horizon are zones of the crystal-poor member (Tptp) of the Topopah Spring Tuff. The host rocks are shown schematically in Figure 2-2. In descending order (by depth), the host rocks consist of the lower part of the upper lithophysal zone (Tptpul), the middle nonlithophysal zone (Tptpmn), the lower lithophysal zone (Tptpll), and the lower nonlithophysal zone (Tptpln).

The repository host rock units can be categorized into two general engineering classifications: nonlithophysal units (Tptpmn and Tptpln) and lithophysal units (Tptpul and Tptpll), based on the relative proportion of lithophysal cavities.

The nonlithophysal units are generally hard, strong, fractured rocks with matrix porosities of 10% or less. Fractures that formed during the cooling process are the primary structural features found in these units. In contrast, the lithophysal units have significantly fewer fractures of significant continuous length (i.e., trace length greater than 1 m), but have relatively uniformly distributed porosity in the form of lithophysal cavities. Lithophysal porosity in the Tptpul and Tptpll is generally on the order of less than 10% to about 30% by volume. The groundmass that makes up the rock matrix in the lithophysal units is mineralogically the same as the matrix of the nonlithophysal units, but is heavily fractured with small scale (lengths of less than 1 m) interlithophysal fractures in the Tptpll; however, it is relatively fracture-free in the Tptpul.

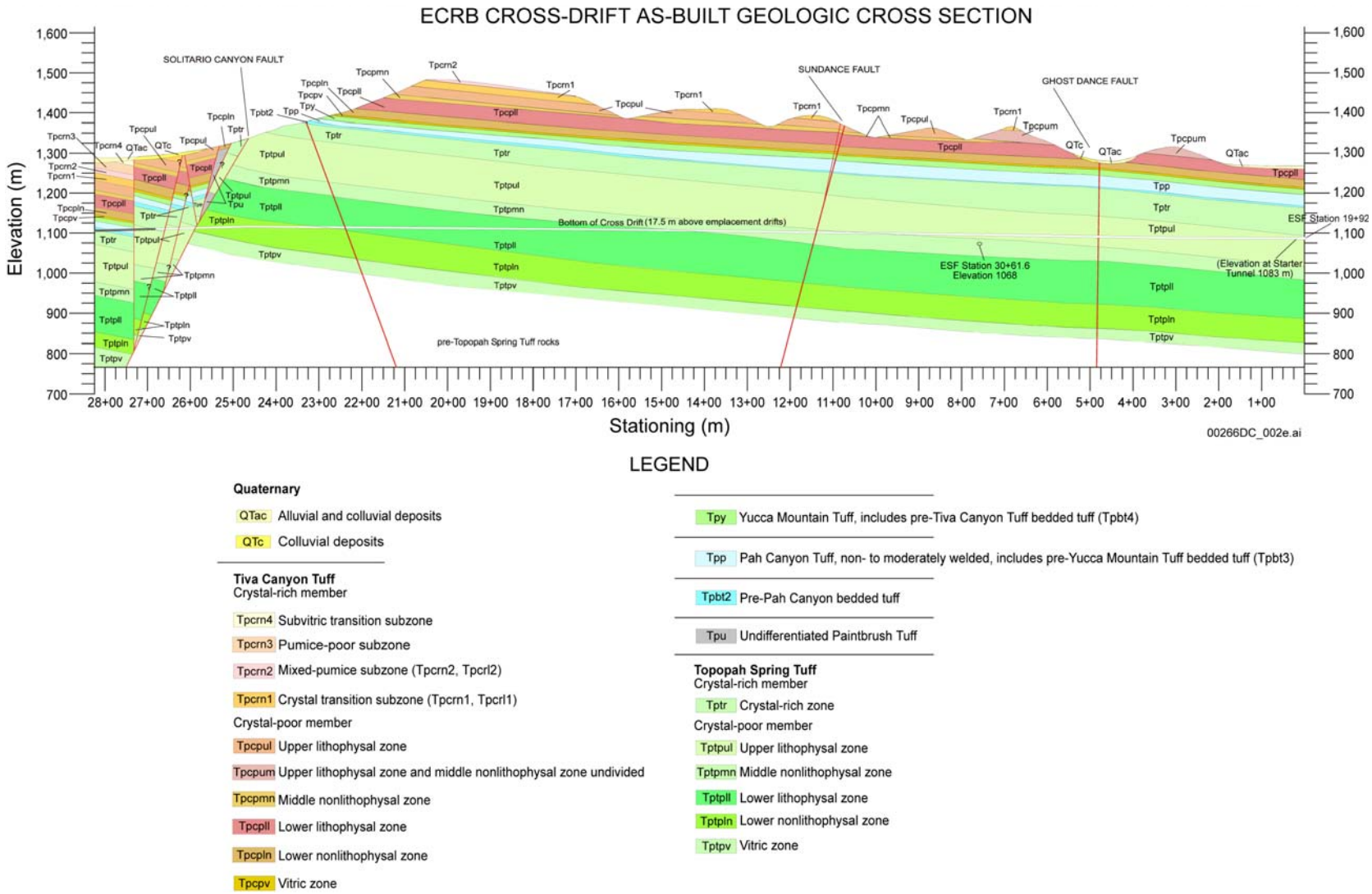

Source: Mongano et al. 1999, Drawing 06-46-345 and 0A-46-345.

NOTE: Repository host horizon includes the major subunits of the Topopah Spring Formation, designated the Tptpul (upper lithophysal), Tptpmn (middle nonlithophysal), Tptpll (lower lithophysal), and Tptpln (lower nonlithophysal).

Figure 2-1. Geologic Cross Section at the Location of the Enhanced Characterization of the Repository Block Cross-Drift

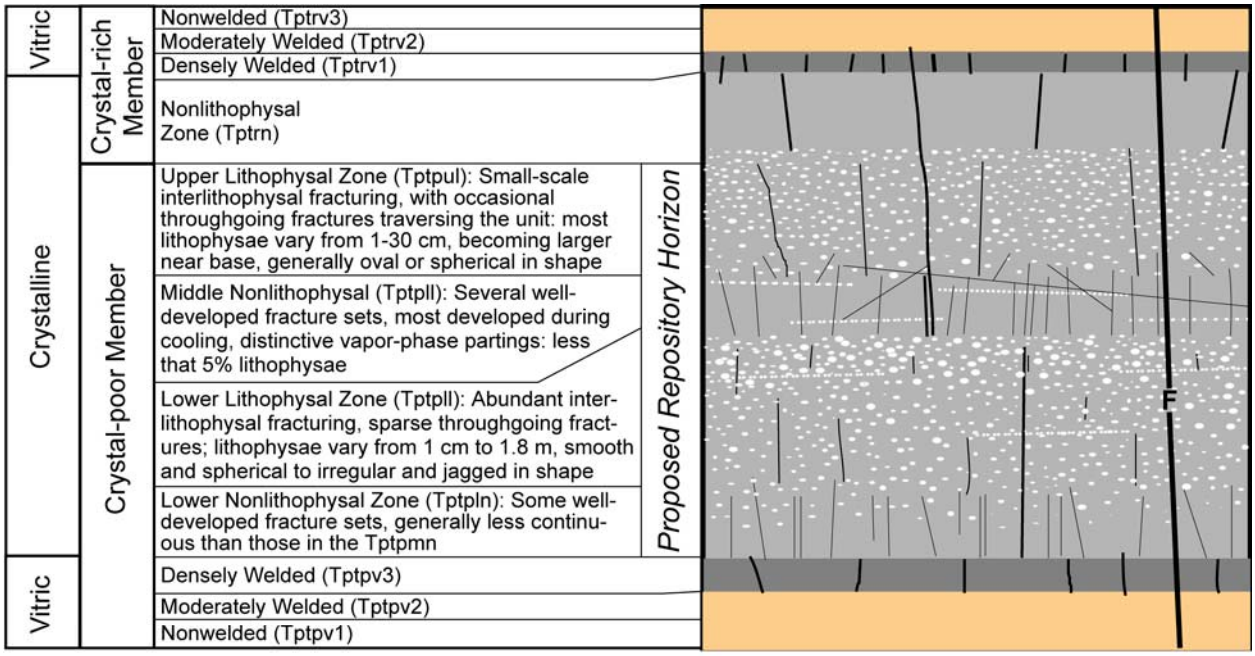

Diagrammatic Cross-Section of the Topopah Spring Tuff Illustrating Relative Discontinuity Densities and Orientations: This figure indicates how fractures, faults, and lithophysae are typically distributed through the ignimbrite.

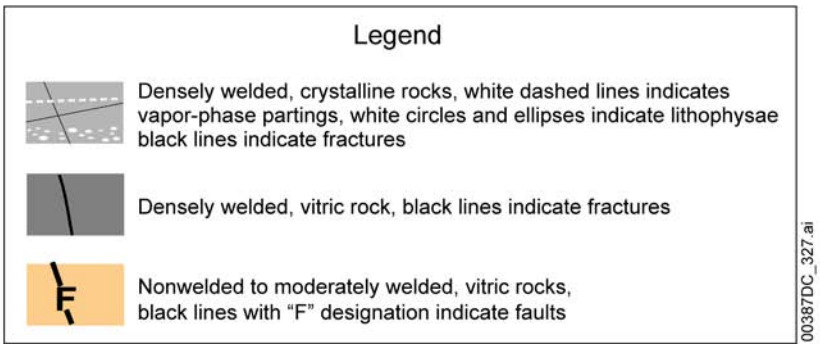

Source: Buesch et al. 1996, Appendix 2; Mongano et al. 1999, pp. 12 to 43.

Figure 2-2. Structure of the Topopah Spring Tuff Showing the Relative Relationship between Fracturing and Lithophysae in the Major Flow Subunits

2.2 UNDERGROUND REPOSITORY LAYOUT AND LITHOLOGIC INTERSECTIONS

The repository consists of four panels that will cover about 5 km^2 within the Topopah Spring Tuff (Figure 2-3). The repository layout extends about 5 km in length (north–south) with the widest part being about 2 km (east–west). The total length of all excavated openings including the drifts, turnouts, exhaust mains, exhaust shafts and raises and other miscellaneous openings is about 110 km. The emplacement drifts comprise about 66 km of tunnels contained primarily within the Tptpll (less than or equal to 81%) and the Tptpmn (less than or equal to 12%). The remaining geologic units comprise roughly 7% (Tptpul about 4% and Tptpln about 3%) of the emplacement drift area. Overall, the nonlithophysal rocks comprise roughly 15% of the

emplacement area, whereas the lithophysal rocks comprise approximately 85% (BSC 2003e, Table I-2).

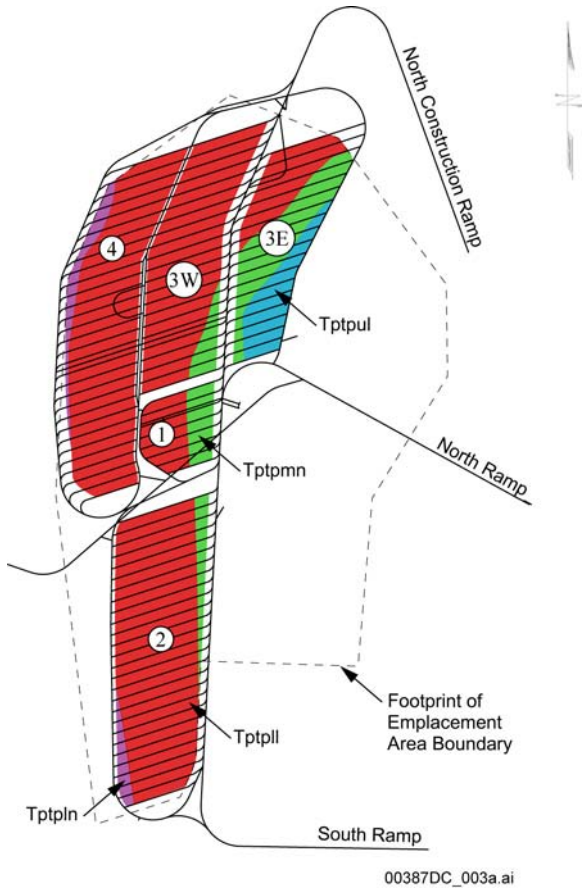

Source: BSC 2004g.

Figure 2-3. Overlay of the Lithostratigraphic Units on the Planned Repository Layout

2.3 ENGINEERING CHARACTERISTICS OF THE ROCK MASS IMPORTANT TO MECHANICAL PERFORMANCE OF REPOSITORY EXCAVATIONS

The rock matrix material is a typical fine-grained volcanic rock of silica content. The structure of the rock mass defines the properties and overall mechanical response of the rock mass to thermal and mechanical loading. The fracture geometry and properties in the nonlithophysal rocks and the degree of porosity (total and lithophysal) in the lithophysal subunits are the primary geologic structural features that impact rock mass behavior.

Geotechnical mapping of fractures has been performed in the ESF and the ECRB Cross-Drift (CRWMS M&O 1998a; Mongano et al. 1999). Figure 2-2 presents a schematic of the Topopah Spring Formation illustrating the general occurrence of fracturing and lithophysae in the various subunits of the repository host horizon. The occurrence of fractures and lithophysae are roughly inversely proportional as demonstrated quantitatively in Figure 2-4, where the fracture density (fractures with trace length greater than 1 m), determined from detailed line mapping, and the approximate percentage of lithophysal porosity in the ECRB Cross-Drift are shown. The density

of fractures with trace length greater than 1 m is significantly larger in the Tptpmn and Tptpln (20 to 35 fractures/10 m), as compared to 5 fractures/10 m or less in the Tptpul and Tptpll. Lithophysae, on the other hand, are sparse in the Tptpmn and Tptpln.

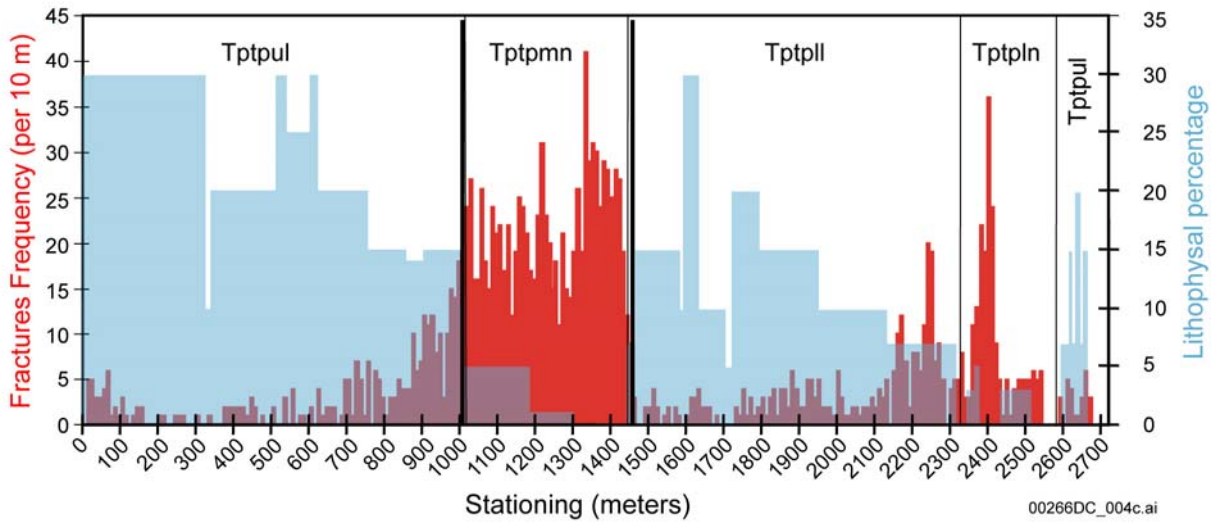

Source: Mongano et al. 1999, Figure 13.

NOTE: There is an inverse relationship between fracture density and lithophysal porosity.

Figure 2-4. Composite Plot of Fracture Frequency and Lithophysal Porosity as a Function of Distance along the Enhanced Characterization of the Repository Block Cross-Drift

2.3.1 Characterization of Fractures

Fracturing in the Tptpmn–The field fracture database, constructed from mapping in the ESF and ECRB Cross-Drift during tunneling operations, consists of full-periphery maps and detailed line surveys of all fractures with length of one meter or greater. The full periphery maps consist of traced fracture lengths drawn directly on invert-to-invert surface maps of the tunnels and include the dip and dip direction of the feature and any intersections with other fractures. Detailed line surveys consist of mapping the detail geometry and surface characteristics of every fracture crossing a line hung along the springline of the tunnel. The details of this mapping are provided by Mongano et al. (1999). In total, a database of more than 35,000 fracture descriptions is available. Additionally, a small-scale fracture-mapping program was conducted to document the characteristics of fractures of less than 1-m length in the nonlithophysal and lithophysal rocks.

In summary, there are four sets of fractures in the Tptpmn with the geometrical and surface characteristics provided in Table 2-1.

Table 2-1. General Characteristics of Fracture Sets in the Middle Nonlithophysal Unit

Set	Mean Azimuth/Dip	Mean Spacing (m)	Trace Length Median from Full Periphery Geologic Maps (m)	Comment
1	120°/84°	0.48	3.3	Rough to smooth, planar
2	215°/88°	1.08	3.1	Smooth but curved
3	302°/38°	3.40	3.6	Random fractures with generally flat to moderate dip
VPP	329°/14°	2.46	3.4	Random fractures with generally flat to moderate dip

Source: DTNs for tunnel mapping include: GS960908314224.020, GS000608314224.006, GS960908314224.015, GS960908314224.016, GS971108314224.025, GS960708314224.008, GS000608314224.004, and GS960708314224.010.

NOTE: Trace length medians are taken from a compilation of tunnel mapping and synthetic tunnel samples from FracMan. VPP = vapor phase parting.

The fractures, particularly the high angle sets (sets 1 and 2), have mean trace lengths less than the diameter of the emplacement drifts (Figure 2-5), with ends that sometimes terminate either against other fractures or in solid rock. Thus, rather than having continuous joint sets, there is often a solid rock bridge between joint tracks. A photograph of a typical wall in the ECRB Cross-Drift (Figure 2-6), demonstrates an important aspect of the fracturing in the Tptpmn. The fracture traces were painted during the detailed line survey, as seen in this photo, and each fracture termination was logged as being against another fracture, within solid rock, or continuous. The photo shows the common occurrence of fractures that terminate in solid rock (T-junctions) as opposed to continuous structures (arrowheads). The subvertical fractures have smooth surfaces but often have curved surfaces with large-amplitude (dozens of centimeters) asperities and wavelength of meters (Mongano et al. 1999).

Figure 2-7 shows that low angle vapor phase partings are relatively continuous structures seen throughout the Tptpmn. These continuous, but anastomosing fractures are subparallel to the dip of the rock unit, and are filled with concentrations of vapor-phase mineralization (primarily tridymite and cristobalite). The surfaces are rough on a small scale and, unlike the subvertical fractures, have cohesion as a result of the mineral filling.

The nature of the fracture geometry governs the estimates of the stability and degradation of the nonlithophysal rock mass, particularly under the action of seismic shaking, as well as estimates of the support function and level of required ground support. Most rock mass classification schemes are based on experience of rock masses with continuous joint sets that create regular, blocky masses (e.g., Hoek 2000). In the Tptpmn, the relatively short trace lengths and nonpersistent joints create relatively few kinematically removable blocks. This is evidenced by the fact that only a small number of rock blocks have actually been dislodged in the ECRB Cross-Drift (BSC 2004a, Appendix F). They were either dislodged under the action of the TBM or were scaled out of the drift back and walls immediately after mining. There have been no reported keyblock failures in the ECRB Cross-Drift since excavation, even though only light bolting and meshing is used for ground support.

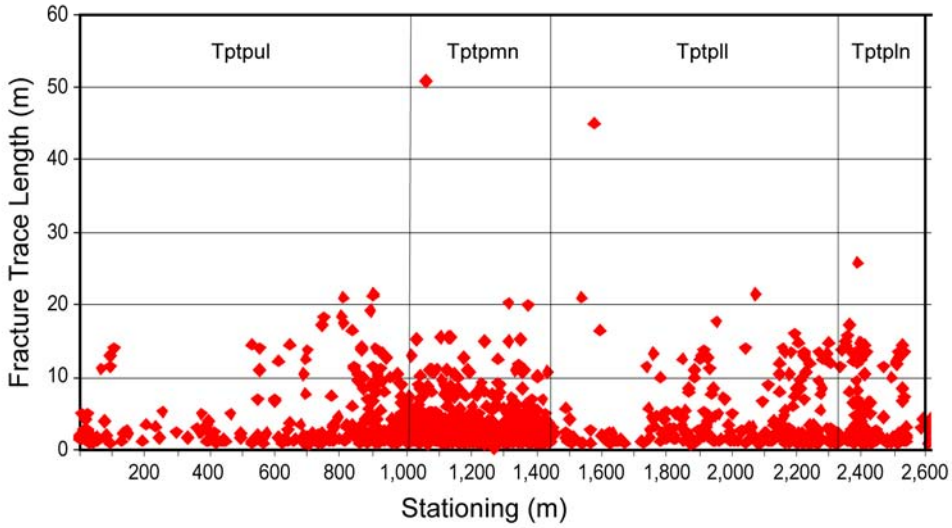

Source: Mongano et al. 1999, Figure 14.

Figure 2-5. Fracture Trace Length as a Function of Depth in the Enhanced Characterization of the Repository Block Cross-Drift and by Subunit of the Tptp from Detailed Line Surveys

00266DC_007.ai

NOTE: T-junctions on fractures indicate terminations; arrowheads show continuous features.

Figure 2-6. Fractures in Wall of the Enhanced Characterization of the Repository Block Cross-Drift in the Tptpmn

00266DC_008.ai

Figure 2-7. Low-Angle Vapor-Phase Partings in Tptpmn

Fracture geometry and surface characteristics are required for numerical analysis of mechanical degradation of emplacement drifts. Three-dimensional discontinuum numerical methods are used to simulate the degradation of the drifts under the action of in situ, thermal, and seismic stressing. These models require geometric input of fracture distributions that are statistically similar to those observed in the ESF and ECRB Cross-Drift. The mapping data (both full periphery and detail line surveys) are used as the basis for generation of a synthetic rock mass fracture distribution developed stochastically using the FracMan fracture generation program (USGS 1999). Section 4.1.1 discusses the use of FracMan for generation of a statistically equivalent fracture domain and the subsequent discontinuum modeling.

Fracturing in the Tptpll–Short-length fractures (less than 1-m trace length), coupled with the lithophysae, are the most important features that govern stability in the Tptpll. Whereas the Tptpul tends to have sparse, small-scale, interlithophysal fracturing (Figure 2-8a), the Tptpll has abundant fracturing (Figure 2-8b). The fractures, existing throughout the Tptpll, have a primary vertical orientation and have spacing of a few centimeters.

Thin-section analyses of the fracturing in the Tptpll and the Tptpmn show vapor phase alterations on most of the fracture surfaces within the rock mass away from the tunnel wall, indicating they are natural fractures (i.e., not mining-induced) that were formed during the cooling process (BSC 2004a, Section 6.1.4.1). Near the tunnel wall, it is clear that some of the fractures have been disturbed by mining, and that at a small number of locations, new, stress-induced, wall-parallel fractures have been created in the immediate springline of the tunnel. These stress-induced fractures are observed to a depth of about 0.5 m in some of the large diameter (290 mm) core holes drilled in the springline area for rock mechanics testing purposes.

No matter the origin of the fracturing, it is clear that the Tptpll has a ubiquitous fracture fabric that is evident in panel mapping or when large diameter core is removed from boreholes (Figure 2-9). The matrix material, although strong and similar to the Tptpmn, has numerous fracture surfaces that tend to separate during the drilling process. The result is breakage into small blocks, making removal of large lengths of core (and thus laboratory testing of sufficiently large samples) very difficult. These fractures, which interconnect the lithophysae, tend to create blocks with dimensions on the order of about 10 cm or less on a side. Longer length fractures that cut the entire drift are widely separated and have been found to be incapable of producing kinematically possible wedges (BSC 2004a). Therefore, the potential mode of failure within the Tptpll under seismic or time-dependent yield will be in a raveling mode that creates small block sizes.

Emplacement drift ground support for preclosure in this type of rock mass requires a more-or-less continuous surface confinement that prevents any loosening of these small blocks. The design solution developed for support of this rock mass is a thin, continuous, perforated steel sheeting that is bolted directly to the emplacement drift surface (see Figure 1-4). Calculations indicate that large blocks do not form in the Tptpll (BSC 2004a, Section 6.4.3). The combination of lithophysae and fractures in this zone tend to create small blocks with dimensions on the order of about 10 cm or less on a side (BSC 2004a, Section 6.1.4.1). Blocks of this size are not capable of breaching the drip shield or waste package under dynamic loading.

(a)

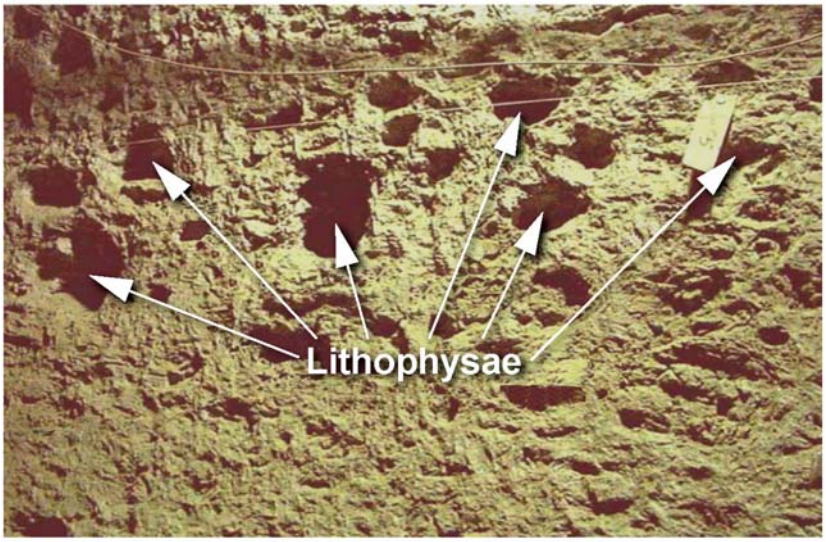

(b)

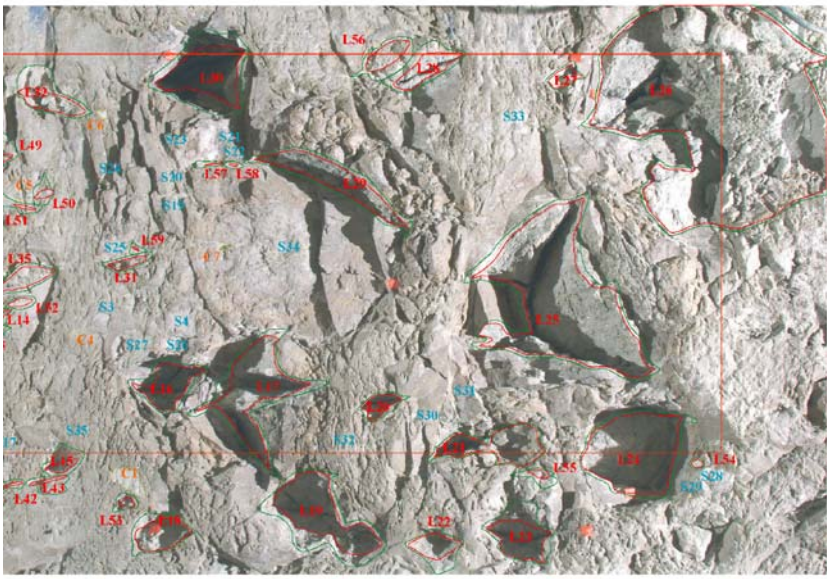

00387DC_004b.ai

NOTE: The Tptpul (a) is characterized by a relatively unfractured matrix between lithophysae, whereas the Tptpll (b) is abundant in natural, short-length fractures that interconnect lithophysae. Spacing of the fractures is generally less than 5 cm. Hackly surface in (a) is a result of TBM cutting process.

Figure 2-8. Comparison of Lithophysae and Fracturing in the Tptpul and Tptpll

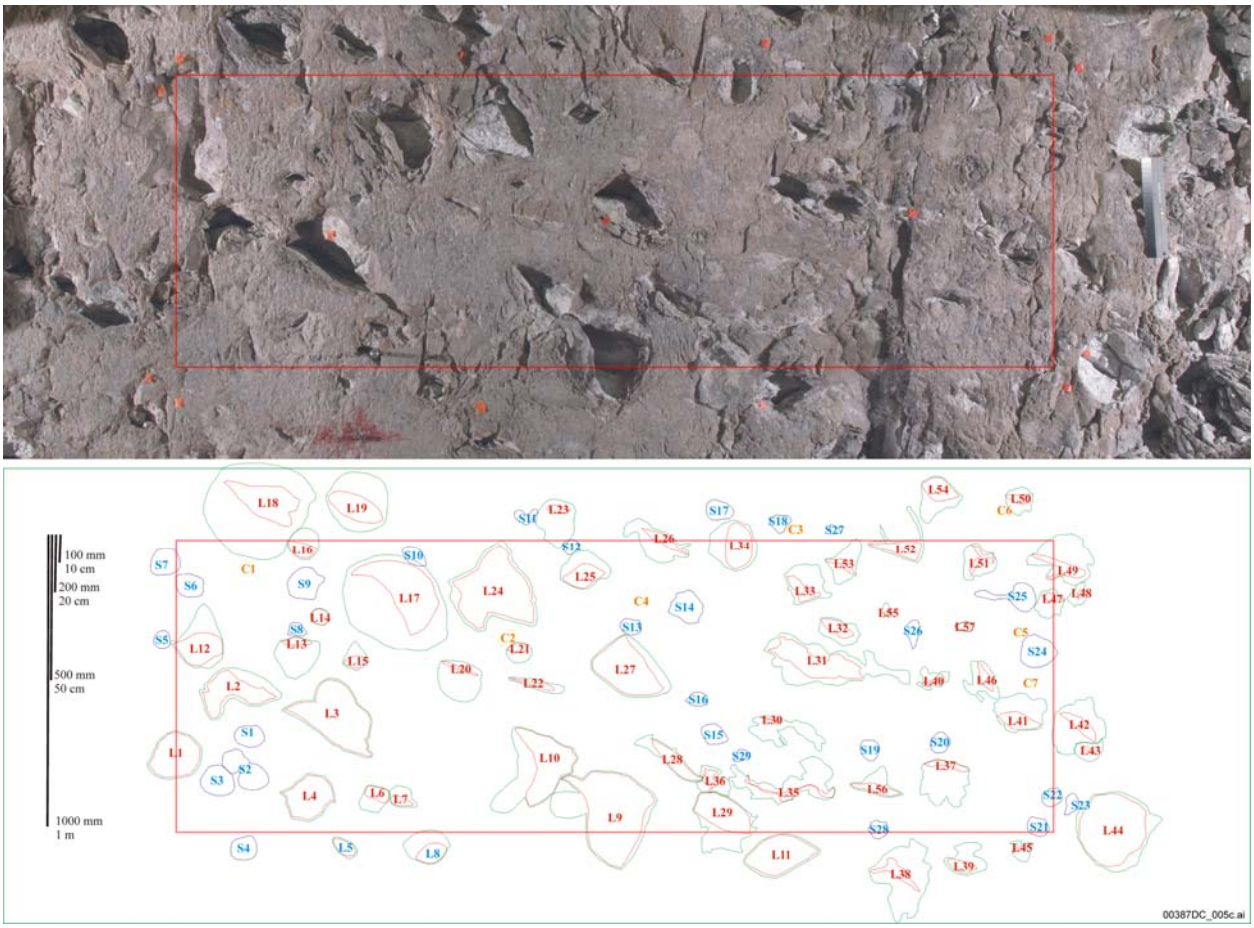

Source: BSC 2004a, Figure O-3.

NOTE: Lithophysae have red "L" identifiers with cavities outlined in red and rims in green. Spots have blue "S" identifiers with cyan outlines. Lithic clasts have orange "C" identifiers with gold outlines. The panel shown is 1 × 3 m. Geometry of lithophysae, rims, and spots are scaled from the photographs and used to determine porosity, size, and shape distributions. Lithophysal porosity averages about 20% within the Tptpll.

Figure 2-9. Lithophysae, Spots, and Clasts of Tptpll (as Discussed Below) in Panel Map 1493 Located on the Right Rib from Station 14+93 to 14+96

2.3.2 Characteristics of Lithophysae

Although the character of the lithophysae varies between the Tptpul and Tptpll, the mineralogy of the matrix material within both of these units is the same as in the nonlithophysal units.

The lithophysae in the Tptpul (BSC 2004a):

- Tend to be smaller (roughly 1 to 10 cm in diameter)
- Are more uniform in size and distribution within the unit
- Vary in infilling and rim thicknesses
- Have a volume percentage that varies consistently with stratigraphic position
- Are stratigraphically predictable.

In contrast, the lithophysae in the Tptpll tend to be highly variable in size, ranging from roughly 1 cm to 1.8 m in diameter (BSC 2004a). They also:

- Have shapes that are highly variable from smooth and spherical to irregular and sharp boundaries
- Have infilling and rim thickness that vary widely with vertical and horizontal spacing
- Have volume percentages that vary consistently with stratigraphic position
- Are stratigraphically predictable.

A detailed study of the lithostratigraphic features in the lower lithophysal zone exposed in the ECRB Cross-Drift has recently been completed. These data are summarized in *Drift Degradation Analysis* (BSC 2004a), and a representative plot is given in Figure 2-9. The data package documents the distributions of size, shape, and abundance of lithophysal cavities, rims, spots, and lithic clasts, and these data can be displayed and analyzed as (1) local variations, (2) along the tunnel (a critical type of variation), and (3) as values for the total zone.

In addition to the variation in the abundance of features, such as lithophysae along the ECRB Cross-Drift, there are variations in the size, shape, and distance between features. These types of variations are most easily observed with panel map data[8] (Figure 2-9), which have been converted into porosity variations as functions of distance along the ECRB Cross-Drift, through the entire Tptpll subunit (Figure 2-10). This information provides direct input to mechanical degradation studies in the following ways:

- The panel maps and porosity, size, and shape variations of lithophysae provide the basis for numerical estimation of impact of lithophysae on rock mass properties.
- Rock mass properties in the lithophysal rocks are primarily a function of porosity, and the variation in porosity provided by the direct panel mapping allow the variation in rock mass properties to be estimated.

[8] A total of 18 1-by-3-m panel maps were developed in the ECRB Cross-Drift from top to bottom of the Tptpll.

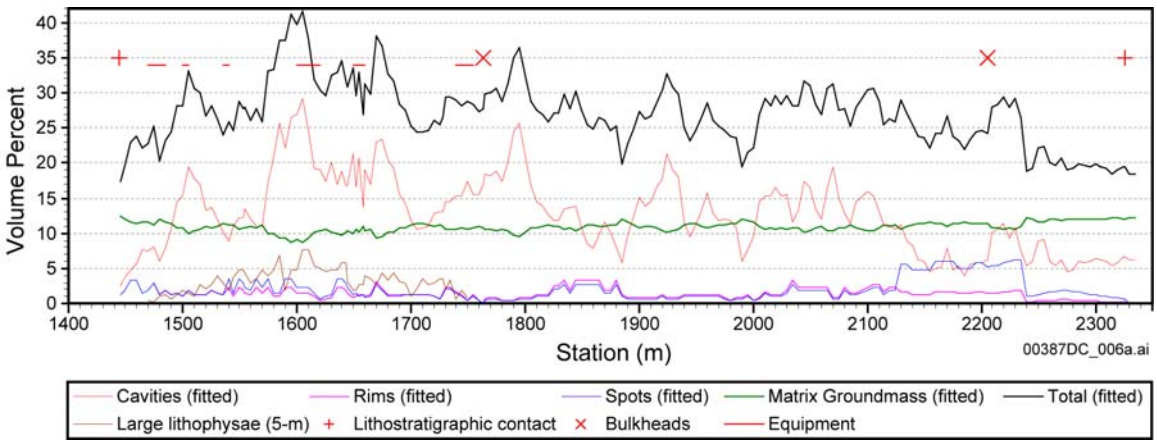

Source: BSC 2004a, Figure O-15.

NOTE: Porosity of the 5-m averaged large-lithophysae inventory is not included in the total.

Figure 2-10. Calculated Porosity of Lithophysal Cavities, Rims, Spots, Matrix-Groundmass, and the Total Porosity in the Tptpll Exposed along the ECRB Cross-Drift

This information has been used to develop a model for simulation of the spatial variability of lithophysal porosity within the Tptpll (BSC 2004a, Appendix T). The lithophysal porosity within the Tptpll follows a general stratiform geometry in a fashion similar to the occurrence of lithostratigraphic contacts within the overall Topopah Spring Tuff (i.e., the Tptpmn, Tptpll, etc.). The ECRB Cross-Drift transects the entire Tptpll unit, allowing determination of the stratiform nature of laterally continuous subzones of lithophysal porosity within the Tptpll. The lateral continuity of lithostratigraphic features and the projection of these features along the apparent dip of the ECRB Cross-Drift has been used to develop a vertical cross section of the distribution of lithophysal porosity within the Tptpll. Figure 2-11 presents two simulated vertical projections of lithophysal porosity for 50-m-tall vertical cross sections through the top and lower portions of the Tptpll. Each of the "cells" of these cross sections represent a volume of the Tptpll and have a lithophysal porosity associated with it. As seen in these cross sections, the lithophysal porosity occurs as stratiform subzones, with the highest values (i.e., 20% or higher) occurring in thin bands near the top of the subzone. The lowest lithophysal porosities occur in the lower portions of the subzone near the contact with the Tptpln. These simulated cross sections are used in Section 5.3 of this report as a basis for examination of the impact of spatial variability on rock mass mechanical response.

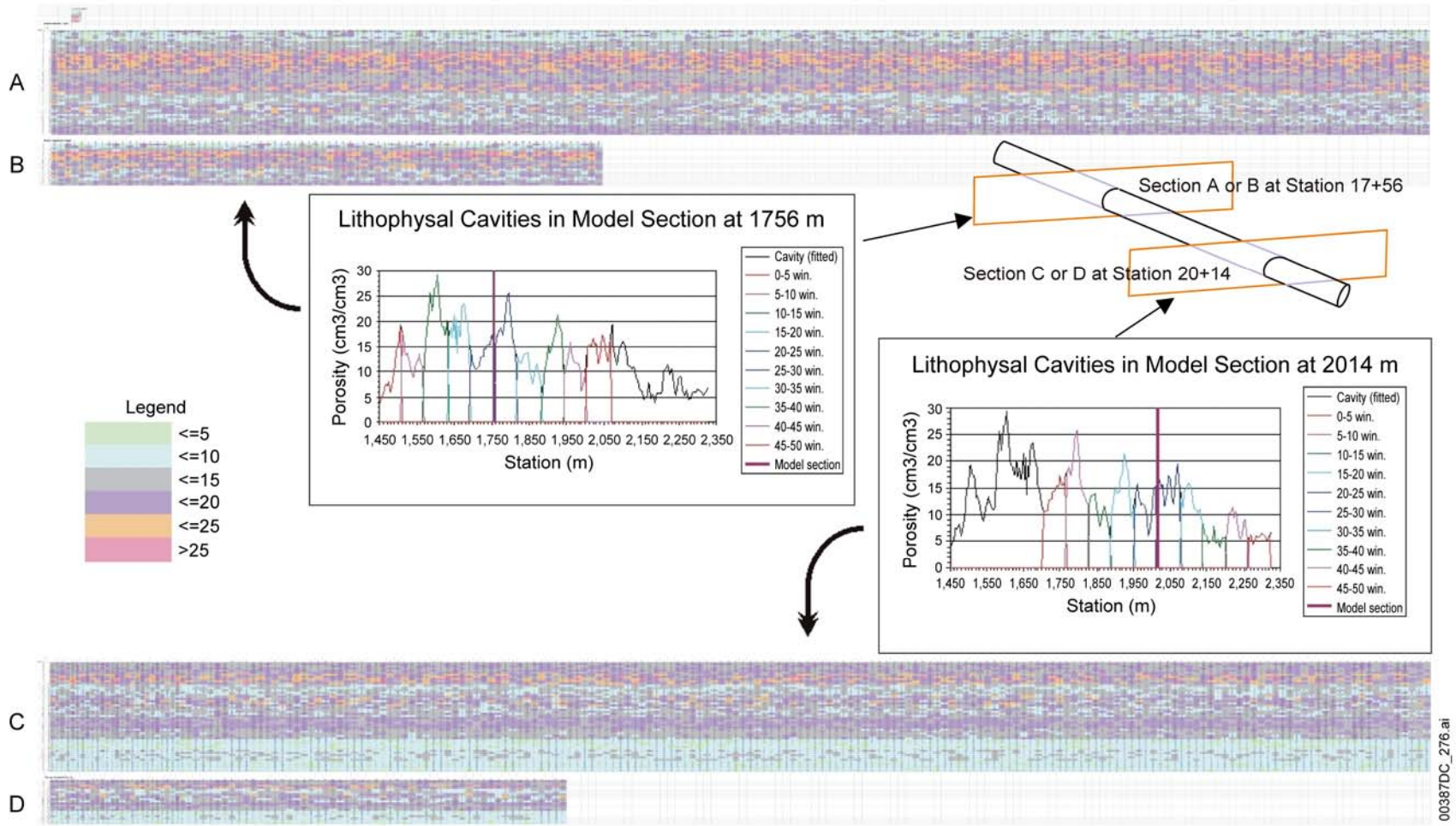

Source: BSC 2004a, Figure T-5.

NOTE: Cross section A is a 50 x 200-cell table representing a 1 x 1-m grid, and cross section B is a 20 x 80-cell table representing a 2.5 x 2.5-m grid for the simulated section at 17+56 in the ECRB Cross-Drift. Cross sections C and D represent simulated section at 20+14 in the ECRB Cross-Drift. Two 50 x 200-m Simulated Cross Sections (Aspect Ratio is not 1:1) at Upper (A/B) and Lower (C/D) Sections of the Tptpll.

Figure 2-11 Illustration of the Process of Sampling and Modeling Spatial Variability Using Lithophysal Porosity

2.3.3 In Situ Stress State

The in situ stress state at and in the vicinity of the Yucca Mountain site has been determined by hydraulic fracturing by Sandia National Laboratories (CRWMS M&O 1997a) and by Stock et al. (1985). A summary of the measurements is given in Table 2-2.

Table 2-2. In Situ Stress Estimates at Yucca Mountain Site

Stress Component	Magnitude (MPa)	Direction
σ_1	~0.023 × depth (m)	Vertical
σ_2	0.617 × σ_1	N15°E
σ_3	0.362 × σ_1	N105°E

Source: DTN: SNF37100195002.001.

2.4 SUMMARY

The rock mass that comprises the repository host horizon consists of a number of subunits of the Topopah Spring Tuff. From an engineering and mechanical degradation standpoint, these subunits can be divided into two broad classifications: lithophysal and nonlithophysal rocks. The matrix material of both is similar mineralogically and mechanically, with the distinguishing characteristics, from a geomechanics standpoint, being their structural features (i.e., the fractures and lithophysae). Due to the importance of these structural features in the mechanical response of the rock, it has been necessary to perform detailed geologic and statistical descriptions of the geometric characteristics of the fractures and lithophysae. This information has been used to provide the basis for input to engineering design and performance modeling of these units, as described in Section 5.3.

INTENTIONALLY LEFT BLANK

3. THERMAL-MECHANICAL ROCK PROPERTIES DATABASE—REVIEW OF LABORATORY AND IN SITU TESTING FOR THE NONLITHOPHYSAL AND LITHOPHYSAL ROCK MASSES

3.1 INTRODUCTION

This section of the report reviews the rock mass properties database for repository host horizon units. Two documents provide a detailed review and analysis of this information: *Yucca Mountain Site Geotechnical Report* (CRWMS M&O 1997b) and *Subsurface Geotechnical Parameters Report* (BSC 2003a). The former presents field and laboratory test data available through June 1996, while the latter presents the geomechanical data acquired since that time. The original report presents data primarily from small-diameter cores and thus provided little information on more representatively sized samples of lithophysal rock. A major laboratory and field testing effort to obtain data on lithophysal rocks was conducted in 2002 and 2003. This section presents an overview of the geomechanical database, and is organized in terms of rock type.

To perform estimates of the mechanical degradation of emplacement drifts subject to stresses and time dependent material property changes, it is necessary to determine the basic thermal and mechanical properties of intact rock and the rock mass and to estimate their variability within the repository host horizon. The properties and geotechnical characteristics that need to be determined are:

- Mechanical Properties of Intact Rock
  - Elastic moduli (E) and Poisson's ratio (ν)
  - Strength properties (T_o) (from uniaxial, triaxial compression, and tensile testing).

- Mechanical Properties of Joints
  - Normal (K_n) and Shear (K_s) stiffness
  - Shear strength (σ_s)
  - Surface roughness (J_r) and dilation angle.

- Thermal Properties
  - Conductivity (k)
  - Heat capacity (C_p)
  - Expansion coefficient (α).

- Geotechnical Characterization
  - Fracture geometry statistics (dip, dip direction, spacing, length)
  - Fracture surface characteristics (roughness, planarity)
  - Classification indices (Q', RMR, GSI).

Figures 3-1 and 3-2 illustrate the approaches taken to defining rock mass thermal-mechanical constitutive models and properties for design and performance assessment studies. Laboratory testing of small cores from surface-based boreholes (diameter of 50 mm) and large cores from drilling within the ESF and ECRB Cross-Drift and Busted Butte (diameter of 305 mm and 267 mm, respectively), as well as field geotechnical characterization, form the bases for initial

properties estimates and materials model definition. For nonlithophysal rocks (Figure 3-1), which are typically strong and fractured volcanic materials, a standard geomechanical approach to rock properties estimation and numerical model definition is taken (e.g., Hoek 2000). Laboratory testing and ESF and ECRB Cross-Drift field mapping, using geotechnical characterization methods, are used to perform estimates of the in situ rock mass properties for use in ground support design parameter studies. Rockfall analyses require that the rock mass be modeled as a discontinuum material with explicitly defined fractures; therefore, for these studies, a detailed, statistical description of the rock mass fracturing and fracture properties is required for direct input to three-dimensional numerical models. The FracMan program (USGS 1999) is used for the fracture geometric modeling and field estimates, and direct shear testing of large joints in the laboratory is used for estimating surface properties.

Definition of the material properties of, and mechanical constitutive modeling approach for, lithophysal rocks requires a different approach (Figure 3-2). The use of empirical techniques for estimating rock mass properties is not particularly applicable to these rock masses since there is little available experience in excavating similar rock types. Due to the presence of the lithophysal cavities, the rock mass properties are also both porosity- and size-dependent. In other words, the properties of the material are a function of both the size of the sample being tested, and the size, shape and degree of lithophysal cavities that the sample contains.

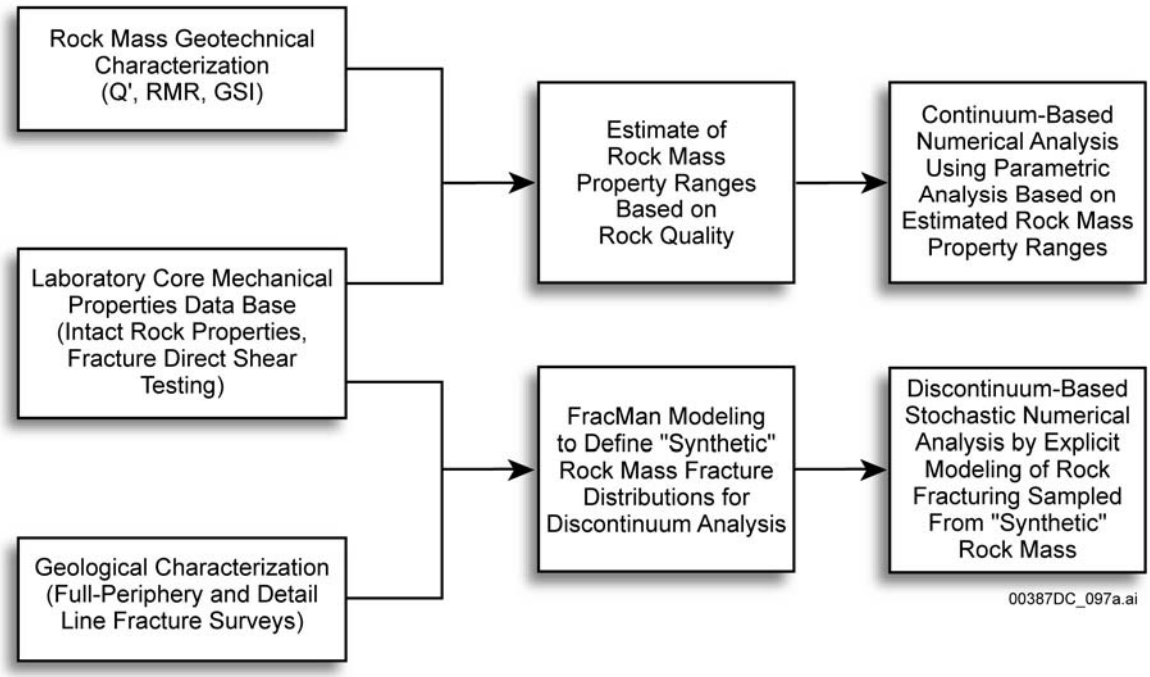

Figure 3-1. Development Strategy for Rock Properties Database and Modeling Strategy for Nonlithophysal Rocks

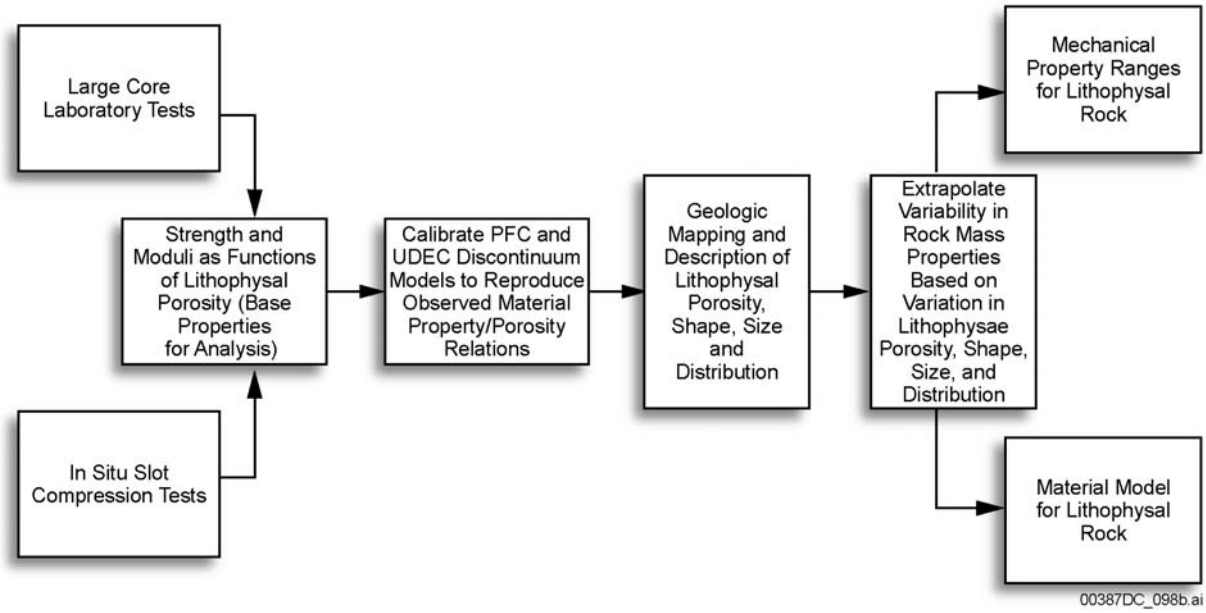

Figure 3-2. Development Strategy for Rock Properties Database and Modeling Strategy for Lithophysal Rocks

To address these issues, an approach is taken based on laboratory and field-scale testing at increasingly larger scales to define the size effect and to provide data for model calibration and validation. An integral aspect of this approach is the comparison and validation of discontinuum numerical models that can simulate the basic mechanical response of the lithophysal tuff to applied stresses.

Once it is demonstrated that the model can account for the observed response, it is used for conducting parametric compression testing studies on simulated "samples" of lithophysal tuff to investigate the impact of variability of lithophysae shape, size, and porosity on the range of expected mechanical properties. In this manner, the numerical models are used to extend the field and laboratory testing and establish the range of material properties for design and performance studies. This technique, combined with the laboratory testing, is used to establish the upper and lower bounds of lithophysal rock properties. In addition, the rock mass properties of large-scale samples of Tptpll, taking into account the impact of spatial variability of lithophysal porosity, are examined numerically. Comparison of the mechanical properties ranges to in situ ESF and ECRB Cross-Drift fracturing observations and thermal stress-induced spalling in the Drift Scale Test (DST) are used as validation tests of the model and properties ranges (see Section 4.2.7). All of these studies are used to define the base set and range of rock mass properties for use in performance assessment.

3.2 GEOMECHANICAL PROPERTIES OF YUCCA MOUNTAIN ROCK

3.2.1 Mechanical Intact Rock Properties of Nonlithophysal and Lithophysal Rocks

In the late 1970s and through the mid-1980s, many samples were tested, from units extending from the upper-most parts of the Paintbrush Tuff down through the lower regions of the Crater Flat Tuff. From the beginning, an approach was adopted to assign a baseline set of conditions

and then study the effects of other conditions (i.e., sample related, environmental, and inherent rock characteristics) relative to that baseline.

Initially, samples were difficult to obtain, so the baseline conditions were defined as: each test specimen was machined as a right-circular-cylinder, with a nominal diameter of 25 mm (1 in) and a 2:1 length: diameter ratio, and tested in a water-saturated state at room temperature, atmospheric pressure, and a nominal axial strain rate of 10^{-5}/s. The results from these test series (Olsson and Jones 1980; Nimick et al. 1985; Price and Jones 1982; Price, Jones, and Nimick 1982; Price and Nimick 1982; Price, Nimick, and Zirzow 1982; Price, Spence, and Jones 1984) revealed that there is some lateral (i.e., within a unit) and vertical (i.e., unit to unit) variability. However, the variabilities in the elastic and strength properties of the tuffs (all having similar chemical constituents) are predominantly a function of the tuff porosity (Figure 3-3; Price 1983; Price and Bauer 1985). Figure 3-3 shows a compilation of the unconfined compressive strength and Young's modulus as a function of total porosity for test samples with a diameter of 50.8 mm. To account for the impact of lithophysae on strength and deformability, cores with a diameter of 254 mm (Figure 3-4) were sampled (Price et al. 1985). These cores were extracted from the Tptpul from Busted Butte, which is adjacent to Yucca Mountain. These results, combined with testing of Tptpul and Tptpll cores with diameters of 305 and 267 mm, are discussed further in Section 4.2.

Confined (triaxial) compression testing has been conducted on 25.4 and 50.8 mm samples taken from surface boreholes from the various welded and nonwelded tuff units (Figure 3-5). Environmental parameters used during the testing, in addition to confining pressure, include temperature and saturation (either room dry, heated dry, or vacuum saturated). A detailed description of the test data can be found in *Subsurface Geotechnical Parameters Report* (BSC 2003a). The results show significant variability, presumably due to the variability in porosity of samples within the Tptpmn. Sample temperatures of 150°C resulted in a slight decrease in strength compared to those samples tested at room temperature.

Indirect tensile strength testing was conducted on 50.8 mm diameter core samples from the Tptpmn and Tptpll under saturated conditions. The results show mean values of 10.8 MPa ±4.02 MPa (14 samples) in the Tptpmn and 8.33 MPa ±2.93 MPa (24 samples) in the Tptpll (BSC 2003a, Table 8-35).

The next key study (Price 1986) examined the effect of sample size on the elastic and strength properties of the middle nonlithophysal zone of the Topopah Spring tuff (Figure 3-6).[9] Sometime later, a model relating strength, sample size, and functional porosity was developed from these data (Price et al. 1993) in combination with the early fits of strength versus functional porosity.

To further explore the effect of sample size for nonlithophysal material, a single large block of material from the nonlithophysal section of the Tptpll near its lower boundary with the Tptpln was obtained from Busted Butte (outcropping adjacent to Yucca Mountain, Figure 3-7).

[9] As seen in Figure 3-8, this original work on sample size influence on properties of the Tptpmn has been recently supplemented by additional size-effect studies on nonlithophysal rock from the base of the Tptpll subunit.

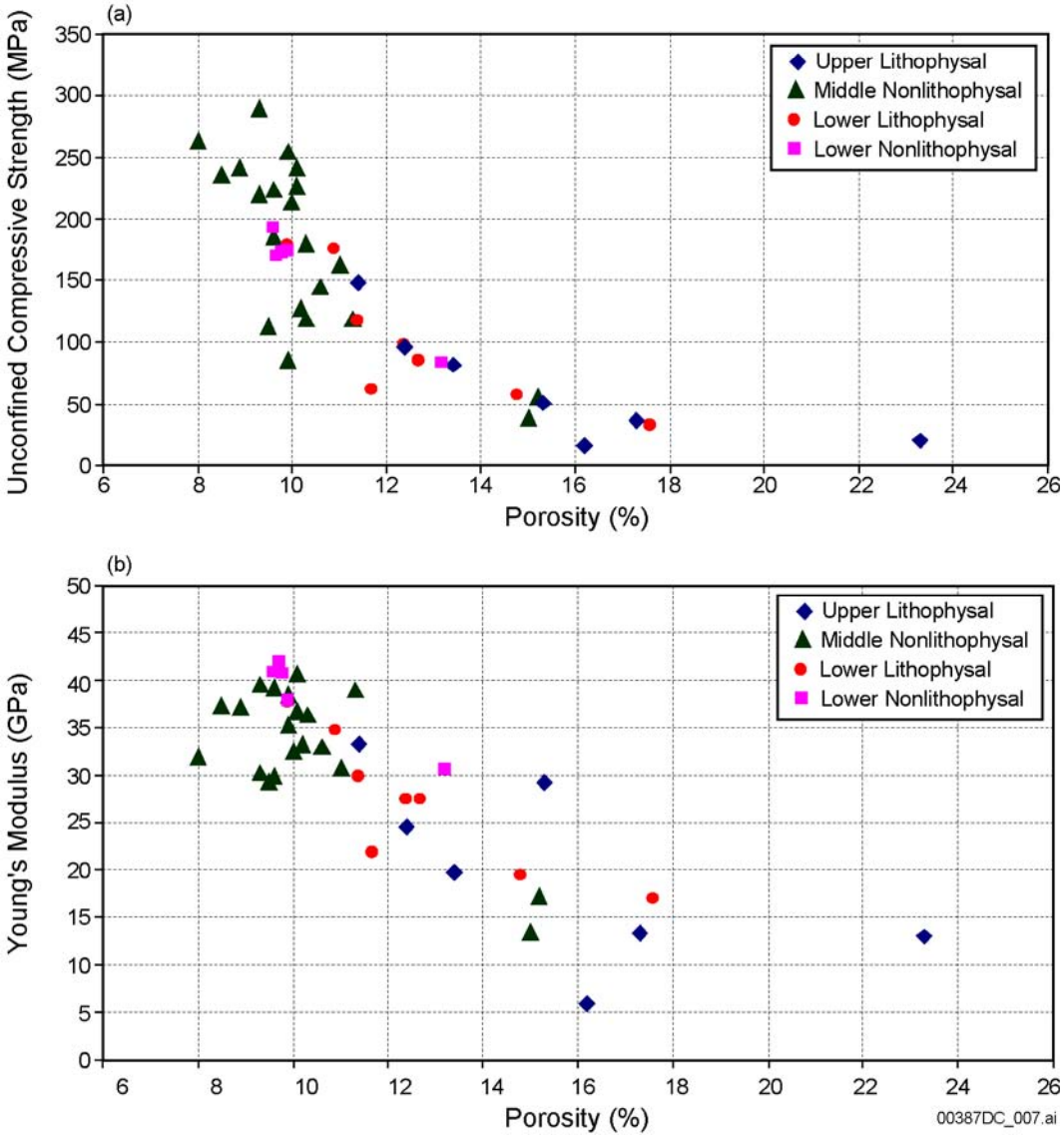

Source: BSC 2003a, Figures 8-22 and 8-11.

NOTE: Porosity is composed of matrix and lithophysal porosity. All measurements are from a 50.8 mm diameter core that is saturated and at room temperature with a length to diameter ratio of 2:1 and a strain rate of 10^{-5}. Small cores from lithophysal zones generally contain only small amounts of lithophysal porosity, and thus the above tests are not indicative, in general, of properties of the lower and upper lithophysal units.

Figure 3-3. Intact Unconfined Compressive Strength (a) and Young's Modulus (b) for Topopah Spring Subunits as a Function of Effective Porosity

00266DC_018 Pt 2.ai

Figure 3-4. Photograph of Busted Butte Sample from the Upper Lithophysal Zone

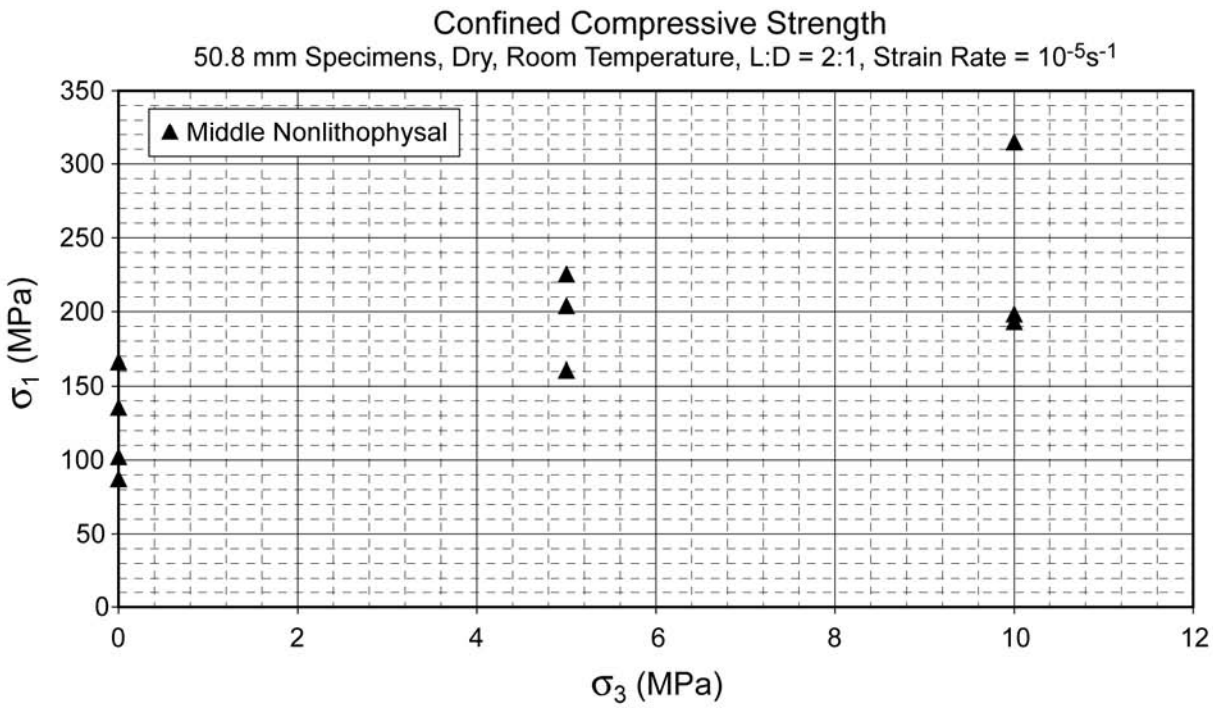

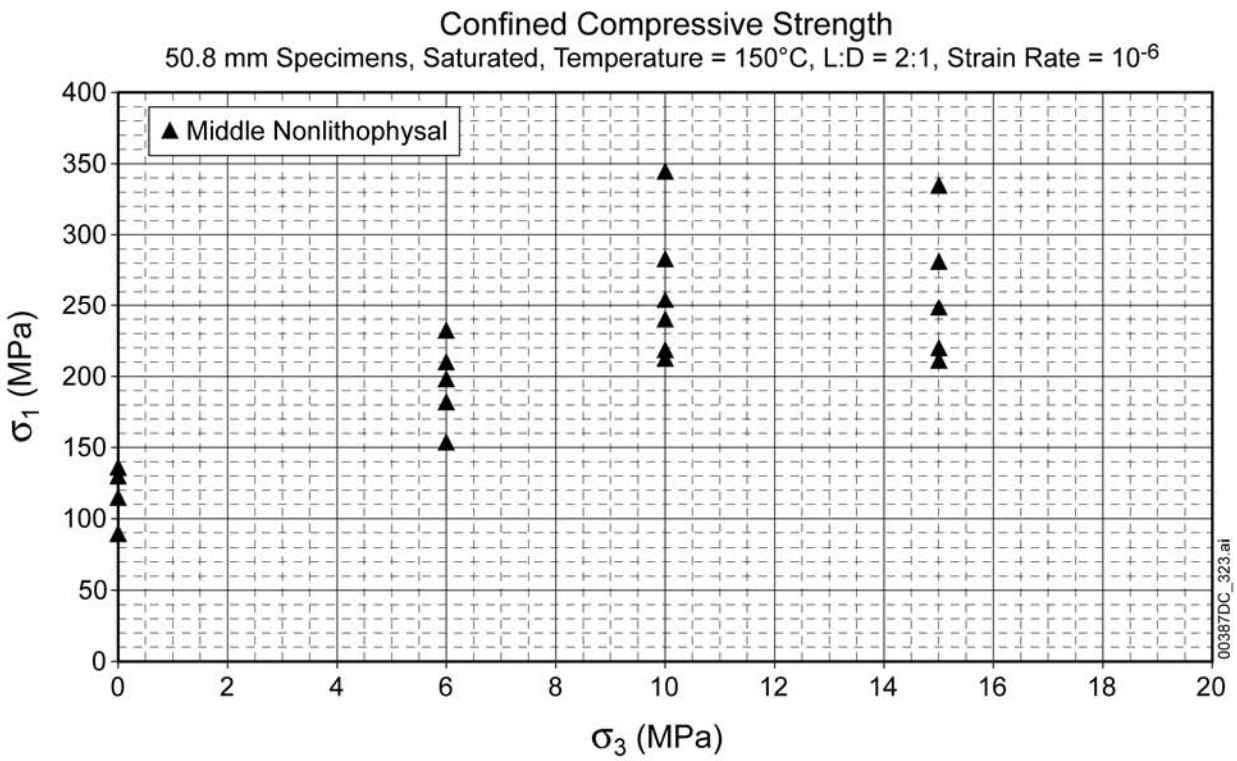

Source: BSC 2003a, pp. 8-106 and 8-107.

Figure 3-5. Plot of Axial (σ_1) Versus Confining (σ_3) Stress for 50.8 mm Diameter Specimens of the Tptpmn: Room Dry and Room Temperature (top), Saturated at 150°C (bottom).

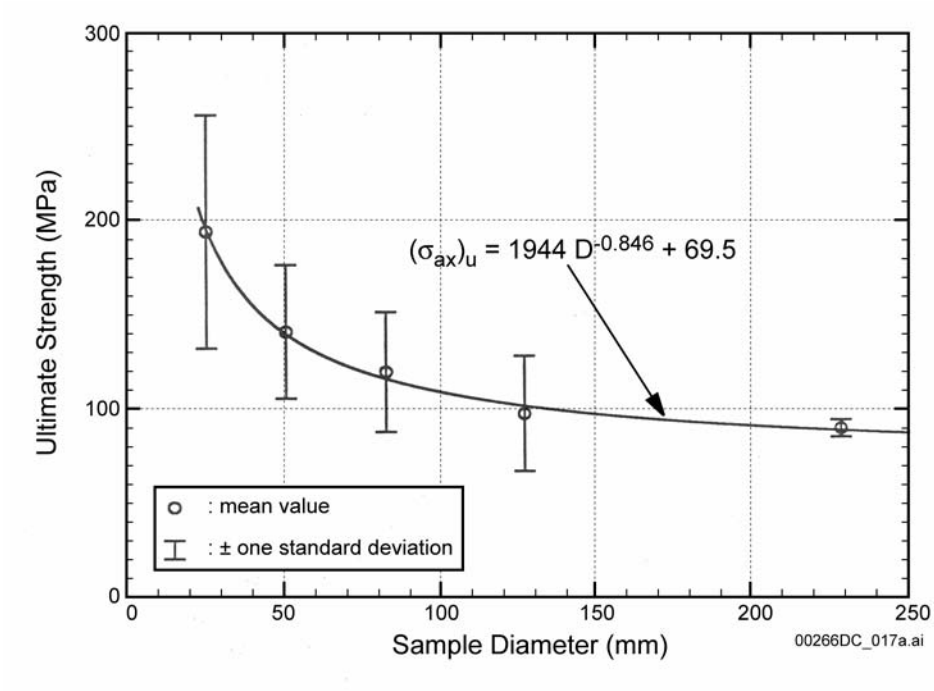

Source: Price 1986, Figure 11.

Figure 3-6. Effect of Sample Size on the Unconfined Compressive Strength of Welded Tuff from the Middle Nonlithophysal Zone

00387DC_009.ai

NOTE: The block shown was obtained from the nonlithophysal portion of the Tptpll near its lower boundary with the Tptpln, Busted Butte.

Figure 3-7. Development of Rectangular Specimens for Matrix Size Effect and Anisotropy Study

Several studies (Martin et al. 1993a; Martin et al. 1993b; Martin et al. 1995; Martin et al. 1997a; Martin et al. 1997b) have produced indications that the strength properties of the tuffs are somewhat time-dependent. A total of nine nonlithophysal rock samples obtained from the Tptpmn at Busted Butte were used to conduct static fatigue experiments with saturated rock conditions at 150°C. Except at very fast rates of deformation (i.e., an axial strain rate of 10^{-3}/s), the strengths of the tuffs were found to decrease with decreasing strain rate (from 10^{-5}/s to 10^{-9}/s), although the average change was relatively minor (about a 10% decrease in strength per decade change in strain rate). In addition, constant stress (creep) experiments at fairly high stresses (most tests at 100 MPa and higher) resulted in very little strain accumulating after several million seconds. The existing test data are described in Section 5.3.3.2.4 (Table 5-8) and in detail in *Drift Degradation Analysis* (BSC 2004a, Appendix S).

A total of 110 samples with size ranging from 26 to 223 mm diameter were cut and tested to examine both size effect and mechanical anisotropy. The mechanical anisotropy studies included testing of 62 to 51 mm samples drilled at three mutually perpendicular directions from the same block of material.

The results of the sample size on unconfined compressive strength are shown in Figure 3-8, where the unconfined compressive strength is plotted as a function of the sample volume (as a log-log plot), and is compared to the data given in Figure 3-6 for the Tptpmn. The vertical offset of the two lines is indicative of the slightly different average strength of the Tptpll and Tptpmn matrix material, although the size effects for the two are virtually identical. The mechanical anisotropy is demonstrated in terms of the average values for the Young's moduli from each of the perpendicular orientations. As seen in Figure 3-9, there is a maximum anisotropy of approximately 10.5% in the average matrix moduli, which is considered to be a second order effect in comparison to lithophysal and fracturing effects.

A series of tests were run on 50.8-mm nonlithophysal Tptpll samples from the same outcrop boulder to examine the impact of saturation level on unconfined compressive strength. It is impossible to accurately control moisture content at specific levels of saturation for a rock sample, so a number of tests were performed to fully dry and saturate the samples before allowing them to equilibrate at room humidity conditions (Table 3-1). As seen in this table, the presence of moisture has a significant effect on unconfined compressive strength, particularly whether the samples are under heated-dry or exposed to humid air conditions. Complete drying of samples increases the mean strength of the samples tested by approximately 20%.

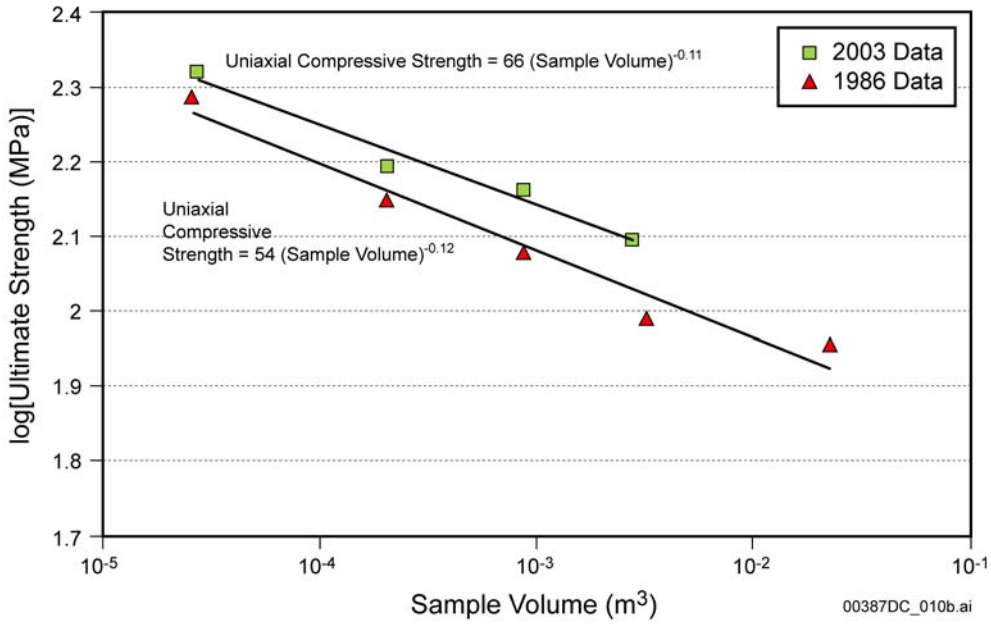

Source: BSC 2004a, Figure E-20.

NOTE: Results from the 2003 testing of Tptpln/Tptpll samples (DTN: SN0306L0207502.008) are compared to previous testing of samples from the Tptpmn (Price 1986). The 2003 data, although from the Tptpll, are composed of matrix material and contain no observed lithophysae.

Figure 3-8. Results of Size Effect Study Showing Variation in Sample Unconfined Compressive Strength as a Function of Sample Volume

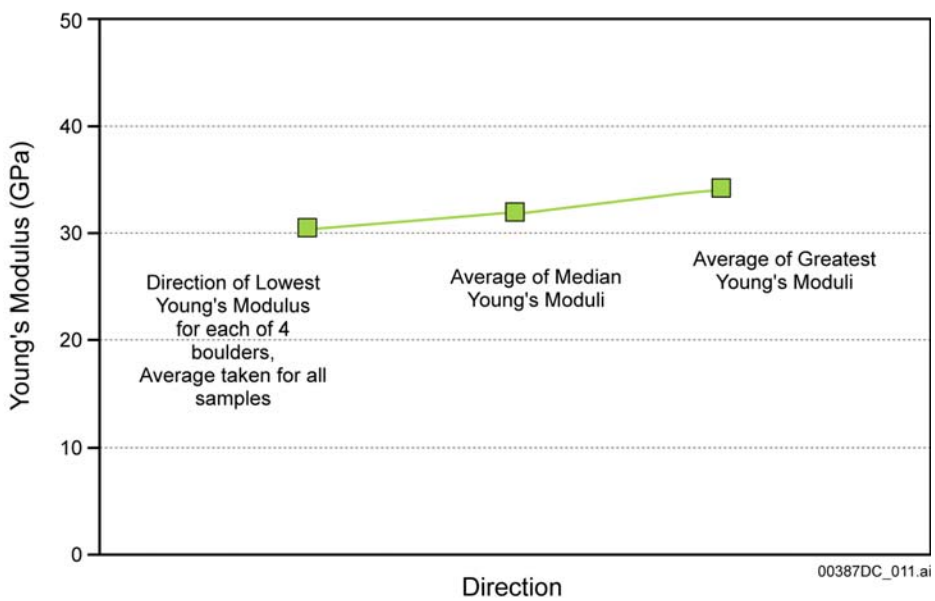

Source: BSC 2004a, Figure E-21.

NOTE: Averages of values from 62 samples shows maximum of 10.5% anisotropy in the average modulus.

Figure 3-9. Anisotropy in Young's Modulus of Nonlithophysal Tptpll Matrix for Three Mutually Perpendicular Coring Directions

Table 3-1. Impact of Moisture Conditions on Unconfined Compressive Strength of Nonlithophysal Tptpll Samples

Test Condition	Moisture Condition	Mean Strength (MPa)
1	Samples dried by slow heating to 200°C, tested at 200°C	213
2	Samples dried by slow heating to 200°C, then slowly cooled in dry environment, exposed to room humidity for about 30 minutes, and tested at room temperature	176
3	Samples allowed to equilibrate with room humidity, tested at room temperature	158
4	Samples water saturated, tested at room temperature	149

Source: BSC 2004a, Table E-12.

NOTE: Strengths are mean values from testing of 51-mm diameter samples at each moisture condition.

This strength decrease in the presence of moisture is consistent with other testing of silicic rocks and is a typical stress-corrosion mechanism involving chemical alterations due to moisture in flaws within the samples. The compression test data reported here is, unless otherwise noted, all at room humidity conditions.

Following a conservative design approach, performance calculations performed for ground support or postclosure effects assume average strength conditions from room temperature testing, with data ranges to cover fully saturated conditions.

Large Core Laboratory Testing of Lithophysal Rocks–In an attempt to obtain more representative samples of lithophysal rocks, a series of large core (305-mm diameter) samplings of the Tptpul and Tptpll were taken in the ESF and ECRB Cross-Drift. The objective of the drilling was to obtain samples that had a number (approximately 3 to 5) of lithophysae across a sample diameter. Drilling of such large core in this material is quite difficult due to the tendency of the core to break in shear when a large or poorly placed lithophysae is encountered. Figure 3-10 shows a series of these samples as prepared for laboratory compression testing.

Approximately 20 samples were tested at varying environmental conditions, including air dry, saturated under vacuum, and at 200°C. Plots of the unconfined compressive strength and Young's modulus as functions of the approximate levels of lithophysal porosity[10] are given in Figure 3-11. In these results, the unconfined compressive strength and Young's Modulus are relatively insensitive to lithophysal porosity above approximately 20%, with rapid increase in both for lithophysal porosities below about 15%. This trend fits the general exponential relationship between these parameters and porosity as seen in Figure 3-3, and can generally be viewed as an extension of this response at higher porosity levels. As was shown previously via field measurement in the ECRB Cross-Drift (Figure 2-10), lithophysal porosity through the Tptpll averages approximately 15%, with a range from about 10% to 25%. The laboratory-scale unconfined compressive strength of the Tptpll can vary from as high as about 25 to 30 MPa to as low as about 10 MPa, while the Young's modulus can vary from 20 to 5 GPa.

[10] Lithophysal porosity is approximate, as it was estimated from core surface measurements.

(a)

(b)

00387DC_012.ai

Figure 3-10. Photographs of Large Lithophysal Core Samples (290 mm/11.5″ diameter) from the Tptpll and Tptpul (a) and a Sample in Unconfined Compression (b)

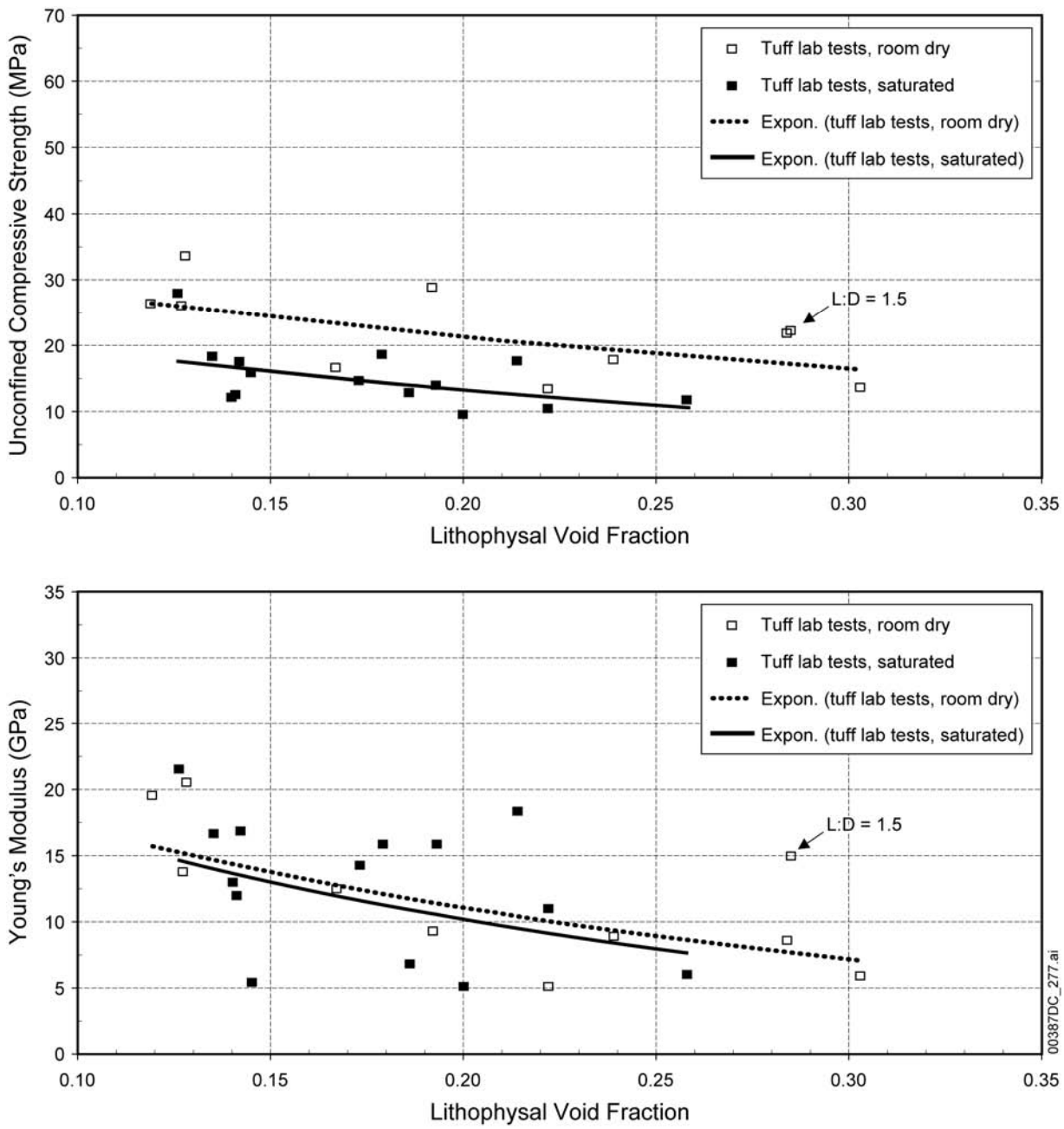

Source: DTNs: SN0208L0207502.001; SN0211L0207502.002; SN0305L0207502.006 (for laboratory data).

Figure 3-11. Unconfined Compressive Strength (a) and Young's Modulus (b) as Functions of Estimated Lithophysal Porosity from Large Core (290 mm diameter) Compression Tests from Lithophysal Rocks

A convenient way of presenting these data for design purposes is in terms of the relationship between the unconfined compressive strength and Young's modulus (Figure 3-12). Some of the primary mechanical properties that are input data to numerical models are the unconfined compressive strength and Young's modulus. Figure 3-12 illustrates the interrelationship of these parameters, the total range of their variation, and that they vary in a generally linear fashion,

irrespective of the lithophysal porosity values. As will be discussed later, this entire range of data is subdivided into a series of categories for design parameter studies. Discontinuum numerical models, calibrated to this data, are used to examine the impact of variability of lithophysal porosity, shape, size and distribution on the variability of these parameters for design purposes.

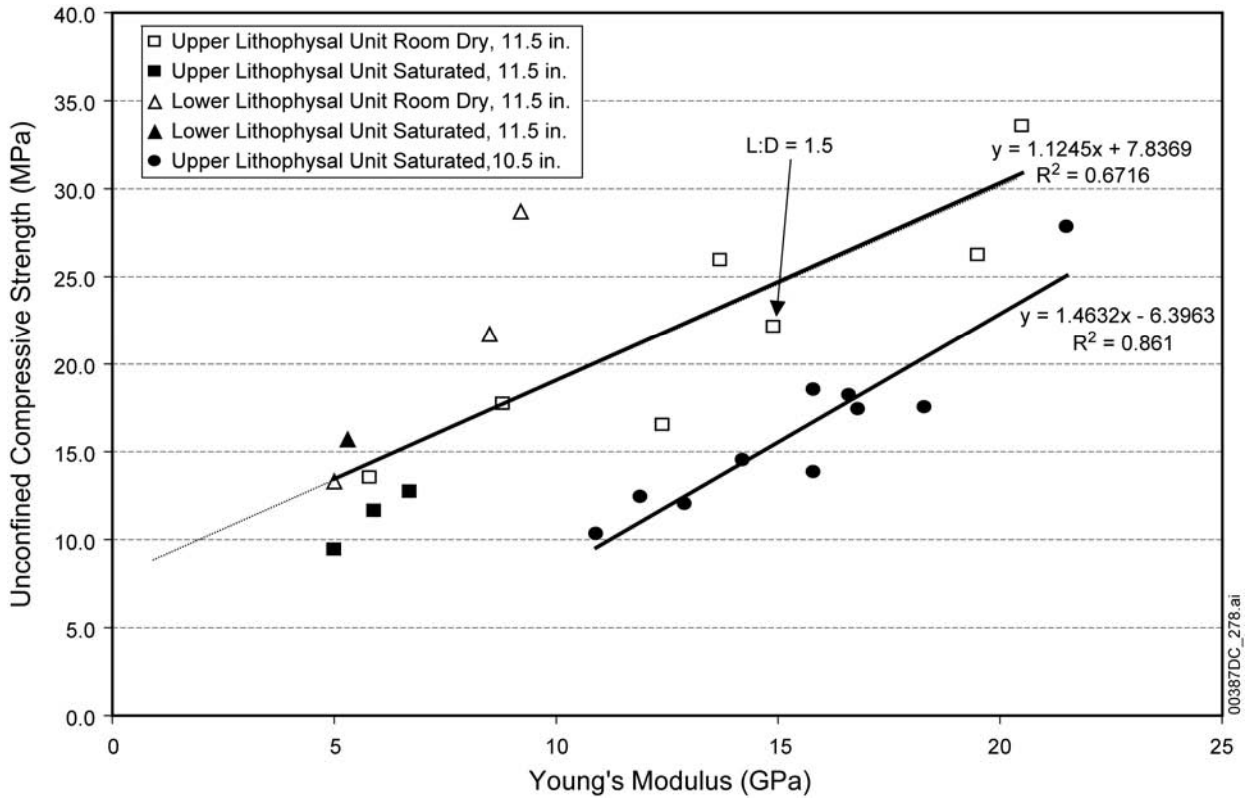

Source: DTNs: SN0208L0207502.001; SN0211L0207502.002; SN0305L0207502.006 (for laboratory data).

NOTE: Linear fits made to 11.5-in. and 10.5-in. core tests.

Figure 3-12. Unconfined Compressive Strength as a Function of Young's Modulus from Large Core (290 mm and 267 mm diameter) Compression Tests from Lithophysal Rocks

3.2.2 Summary of Laboratory Testing of Lithophysal and Nonlithophysal Cores

In summary, a large amount of data has been collected to date on tuffaceous samples from Yucca Mountain at a baseline set of conditions. These data have shown that the variabilities in elastic and strength properties are not random functions of lateral or vertical position, but primarily a function of porosity and its spatial distribution.

Though there are obvious trends in the Young's modulus and strength data when plotted against porosity, the data have a significant scatter, based on sample porosity variability. The secondary effect that creates the scatter is the distribution of the porosity within the sample. Other investigations have examined the effects of many other conditions (i.e., sample related, environmental and inherent rock characteristics); for example, sample size, saturation, pressure, temperature, deformation rate, attenuation, anisotropy have all been studied.

In Section 4, the development of mechanical material models and numerical modeling techniques are described for both lithophysal and nonlithophysal units. In lithophysal rocks, the trends observed in the relationship of mechanical properties to porosity are used as a basis for development of the models. In situ measurements of the variability of lithophysal porosity are used as the basis for establishing a linkage between the measured mechanical properties and the estimated field properties ranges. For nonlithophysal rocks, discontinuum modeling approaches are used in which intact blocks and fractures are modeled explicitly. The intact core testing data described in this section is used to assign the mechanical properties of intact blocks, whereas fracture shear strength properties (described in Section 3.2.4) define the fracture response. In conclusion, the intact and large core rock mechanical property information collected over the last two decades has provided adequate characterization and property values for design and analysis of the behavior of Yucca Mountain tuffs.

3.2.3 In Situ Mechanical Testing of Nonlithophysal and Lithophysal Rocks

In situ testing provides data on the mechanical characteristics of the rock mass at a scale commensurate with the excavation dimension. Field compression testing has been performed in both the nonlithophysal and lithophysal rocks. For nonlithophysal rocks (Tptpmn), field testing is restricted to measuring the deformation modulus, as the rock mass strength is too large to conduct strength measurements. However, in the lithophysal rocks, the in situ rock mass strength is sufficiently low that both the deformation modulus and unconfined compressive strength can be measured.

The Plate Loading Test, conducted as part of the larger DST, was used to apply load to the drift wall adjacent to the DST in the Tptpmn unit. The results of the testing show an estimated rock mass modulus from 11.4 GPa to 29.5 GPa for ambient and thermally perturbed fractured tuffs, respectively (George et al. 1999).

A series of three pressurized slot tests (PSTs) were conducted to perform deformation modulus and strength measurements in lithophysal rock units (Table 3-2). PST#1 was conducted in the poorest quality Tptpll material characterized by large lithophysae and heavily fractured matrix at the transition between the Tptpmn and the Tptpll. PST#2 was conducted in good quality Tptpul in the ESF and PST#3 was conducted in what was considered to be average Tptpll repository conditions in the ECRB Cross-Drift. All three tests included compressions at ambient temperature and one test included compressions at elevated temperature.

Table 3-2. Summary of In Situ Slot Compression Tests in Lithophysal Rock Units

Test	Location	Thermal-Mechanical Unit	Temperature	Location
PST#1	ESF 57+77	Tptpll	ambient	Wall
PST#2	ESF 63+83 ESF 63+83	Tptpul Tptpul	ambient temperature–90°C	Wall Wall
PST#3	ECRB 21+25	Tptpll	ambient	Floor

Source: Sobolik 2002a, Table 1; Sobolik 2002b, Table 1; Schuhen and Sobolik 2003, Table 1.

NOTE: Metric stationing is used throughout the ESF, so that Station 57+77 is located 5,777 m from the start of the tunnel.

The flatjack slot test first involves placing steel flatjack bladders into parallel, thin, sawcut excavations in the sidewall or floor of a tunnel (Figure 3-13). The parallel sawcuts isolate an approximately 1-m^3 rock specimen between them, which is subsequently compressed by pressurizing the flatjacks within the slots. Typically, an instrumentation borehole (305 mm in this case) is drilled midway between the slots to allow observation of the interior of the rock sample and to monitor deformations during the flatjack pressurization. The flatjack slots are excavated larger than the flatjacks to minimize end effects due to block attachment to the surrounding solid rock. The flatjacks' pressure is raised in a series of pressure cycles to monitor hysteresis effects and time-dependent strain at increasing levels of applied stress.

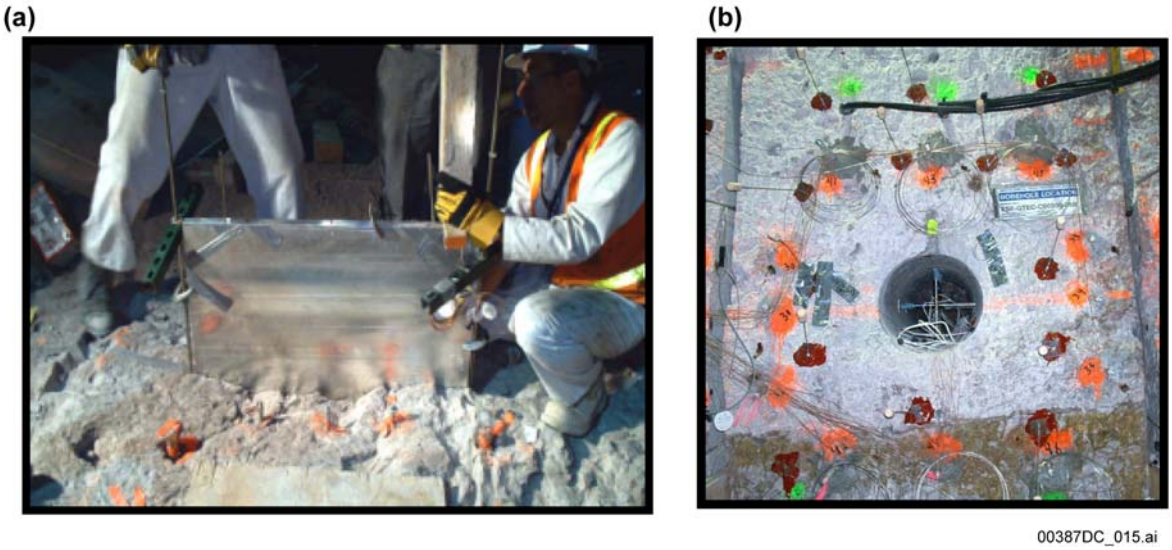

Figure 3-13. Photographs of (a) Preparation of Slot Test 3 in the Floor of the Enhanced Characterization of the Repository Block, Tptpll Unit, Lowering of Flatjack into Place in Sawcut Slot and (b) Slot Test 2 Showing Central Instrumentation Hole and Parallel Slots

Figure 3-14 shows flatjack pressure versus instrumentation hole diametral deformation for the tests. The loading results show a typical elastic-plastic response in which a linear loading slope is followed by yield and plastic deformation. Yielding of the rock was typically in shear, emanating from the central borehole, and resulting in rockfall in the form of small rock particles in the central borehole during yield. The results, summarized in Table 3-3, show that the rock mass has deformation modulus and strength that lie at the lower end of the design range given in

Figure 3-12, but consistent with the same general relationship of strength to modulus as observed in the large core laboratory tests. However, the results illustrate the difficulties with performing large in situ slot tests. PST#1 was located in the poorest quality lithophysal rock immediately adjacent to the contact of the Tptpmn. The low value of modulus obtained indicates that the skin of rock surrounding the tunnels at this particular sidewall locations, is likely in a preyielded state due to mining-induced stress and excavation effects induced by the TBM. PST#2 resulted in shear along a preexisting fracture outside the block (without failing the block itself), and PST#3 resulted in spalling of the tunnel floor prior to actually failing the rock block between the flatjacks.

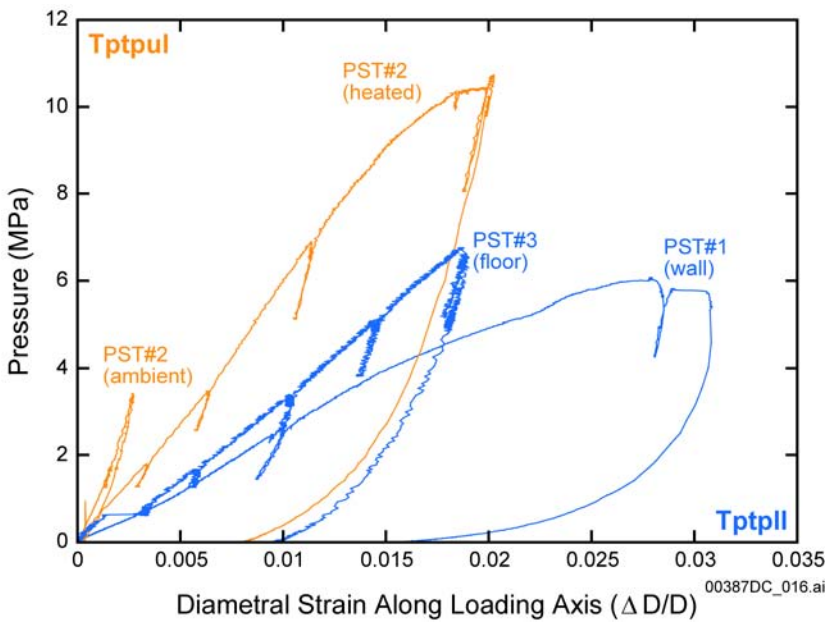

Source: Sobolik 2002a, Figure 7; Sobolik 2002b, Figures 7 and 9; Schuhen and Sobolik 2003, Figure 7.

Figure 3-14. Composite of Flatjack Pressure versus Central Hole Diametral Strain for the Three Pressurized Slot Tests

Table 3-3. Summary of Mechanical Properties Results from the Pressurized Slot Tests

Test	Location	Condition	Tuff Unit	E (GPa)	Strength (MPa)
PST#1	ESF	Ambient	Tptpll	0.5 ±0.3	6[a]
PST#2	ESF	Ambient	Tptpul	3.0 ±0.5	NA
PST#2	ESF	Heated, >80°C	Tptpul	1.5 ±0.5	11[a]
PST#3	ECRB Cross-Drift	Ambient	Tptpll	1.0 ±0.3	7[a]

Source: Sobolik 2002a, Table 1; Sobolik 2002b, Table 1; Schuhen and Sobolik 2003, Table 1.

NOTE: PST#1 in poorest quality Tptpll, PST#2 in good quality Tptpul, and PST#3 in typical repository Tptpll. Strength here is the peak flatjack pressure reached during the test. PST#2 failed on the fracture outside block, and PST#3 spalled the tunnel floor above flatjacks.
[a] Results do not account for presence of central hole in failure load.

3.2.4 Mechanical Properties of Fractures

3.2.4.1 Direct Shear Test Results

Five direct shear tests were performed on core samples with a diameter of 305 mm and with internal fracture surfaces from the Tptpmn unit. Photographs of the direct shear samples are shown in Figure 3-15. Two tests were performed on subvertical cooling joints, and three tests were conducted on more or less horizontal vapor-phase partings (VPPs). The two fracture types have a physically distinct appearance, and testing of these fractures resulted in equally distinct fracture behaviors (Table 3-4).

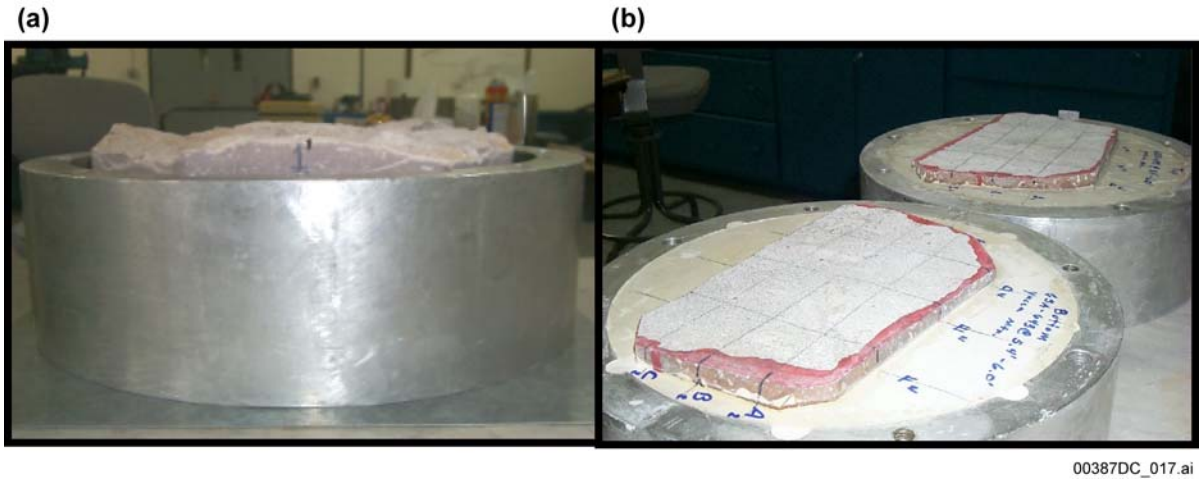

Figure 3-15. Photographs of Direct Shear Samples from Rough Vapor Phase Partings (a) and Smooth Cooling Joints (b)

Cohesion and friction angle parameters were determined from repeated tests on the same fracture surface (Table 3-4). The advantage of this is that the same fracture is being tested in the same equipment setup. The disadvantage is that because of repeated tests on the same fracture surface, degradation of the asperities changes the fracture behavior on subsequent loading tests.

Table 3-4. Direct Shear Test Summary of Tptpmn Fractures

Joint Type	Test ID	Length (mm)	Area (m^2)	JRC	Cohesion (MPa)	Friction Angle (°)	CC
Cooling	65A-643	238.76	0.04	2.00	−0.01	33.7	1.00
Cooling	65A-657	142.24	0.02	1.00	0.08	33.1	1.00
VPP	65A-642	241.30	0.06	15.00	0.72	45.7	0.99
VPP	65A-646	226.06	0.03	16.00	0.66	41.9	1.00
VPP	65A-647	246.38	0.05	10.00	0.84	44.5	0.99

Source: DTN: GS030283114222.001.

NOTE: JRC = the measured value of joint roughness coefficient; CC = the correlation coefficient of a linear fit through the data.

Table 3-5 illustrates that cooling fractures have lower cohesion, lower peak friction angle, and much lower peak dilation angle than the VPP fractures.

Table 3-5. Summary Statistics of Direct Shear Tests of Fracture Peak Strength

Joint	Unit	Count	Mean	Standard Error	Standard Deviation	Deviation / Mean	Median	Minimum	Maximum
Direct Shear Rock Peak Cohesion (MPa)									
Cooling	Tptpmn	2	0.32	0.04	0.06	1.97	0.03	−0.01	0.08
VPP	Tptpmn	3	0.74	0.05	0.09	0.12	0.72	0.66	0.84
Direct Shear Rock Peak Friction Angle (°)									
Cooling	Tptpmn	2	33.4	0.3	0.4	0.01	33.0	33.1	33.7
VPP	Tptpmn	3	44.0	1.1	1.9	0.04	44.5	41.9	45.7
Direct Shear Rock Joint Dilation Angle at Peak Stress									
Cooling	Tptpmn	2	1.6	2.55	3.61	2.33	1.6	−1.0	4.1
VPP	Tptpmn	3	14.0	1.22	2.12	0.15	13.7	12.1	16.3

Source: DTN: GS030283114222.001.

The final normal stress and shear stress measured in the last shearing for each fracture was used to determine the degraded friction angle values assuming the cohesion was zero. These degraded shear results are shown in Table 3-6. The peak and degraded friction angles are roughly the same for the smooth subvertical cooling fracture, whereas the degraded friction angle for VPP fractures was slightly higher than the peak value.

Table 3-6. Summary Statistics of Direct Shear Fracture Degraded Strength

Direct Shear Rock Degraded Friction Angle (°)									
Joint	**Unit**	**Count**	**Mean**	**Standard Error**	**Standard Deviation**	**Deviation / Mean**	**Median**	**Minimum**	**Maximum**
Cooling	Tptpmn	2	33.4	1.9	2.7	0.08	33.4	31.5	35.3
VPP	Tptpmn	3	46.9	1.7	3.0	0.06	46.5	44.1	50.0

Source: DTN: GS030283114222.001.

3.2.4.2 Rotary Shear Tests

A series of 22 rotary shear tests have been conducted on natural rock fractures from core samples in the repository host units. The samples ranged in size to 76 mm and tests were conducted at room dry, room temperature and at 175°C. Rotary tests involve application of constant normal stress and torque to undercored samples (undercoring creates a pipe-like sample with an inner and outer radius). The shear stress induced on the surfaces of the joint result in slip and dilation of the surfaces can be determined with continued displacement. Table 3-7 provides summary statistics of the results of this testing; further discussion can be found in *Subsurface Geotechnical Parameters Report* (BSC 2003a).

Table 3-7. Summary Statistics of Fracture Strength Using Rotary Shear

Rock Unit	Temperature (°C)	Count	Peak Cohesion (MPa)	Peak Friction Angle	Peak CC*	Ultimate Cohesion (MPa)	Ultimate Friction Angle	Ultimate CC*
Tptpul/ll	Room	6	1.48	40°	0.92	1.51	32°	0.76
Tptpmn/ln	Room	8	0.79	42°	0.85	0.60	39°	0.90
Tptpmn/ln	175	8	1.38	44°	0.96	0.24	44°	0.91

Source: DTNs: SNL02112293001.001; SNL02112293001.003; SNL02112293001.005; SNL02112293001.006; SNL02112293001.007.

NOTE: CC* refers to the correlation coefficient of a linear fit through the data.

3.2.4.3 Empirical Estimate of Peak Dilation Angle

Barton (in Duan 2003, p. 40) used the following equation to empirically estimate peak dilation angles[11], ψ_{peak}, for Yucca Mountain joint sets:

$$\psi_{peak} = \frac{1}{2} JRC \log\left(\frac{JCS}{\sigma_n}\right) \qquad \text{(Eq. 3-1)}$$

where *JRC* is joint roughness coefficient, *JCS* is joint wall compressive strength, and σ_n is the effective normal stress. A range of laboratory scale *JRC* values for joint sets is estimated (Table 3-4) by making *JRC* measurements from roughness traces of the rotary shear and direct shear laboratory fractures, making field *JRC* measurements of fractures in the ESF, and correlating *JRC* values to U.S. Bureau of Reclamation field roughness statistics (R1 to R6). Adopting a "common" value of joint wall normal strength (*JCS*) of 100 MPa, a normal stress (σ_n) range of 4 to 8 MPa, and the joint roughness coefficient (*JRC*) range shown in Table 3-8, the range of peak dilation angles is derived. The empirically derived field dilation angle estimates are consistent with those determined from the laboratory testing (Table 3-5).

[11] Dilation angle is defined as the ratio of the displacements perpendicular and parallel to the fracture surface when subjected to shear. This value provides an indication of the roughness of the joint surface.

Table 3-8. Estimate of Peak Dilation Angles for Topopah Spring Formation Fracture Sets

		Joint Roughness Coefficient Range	Peak Dilation Angle Range
Nonlithophysal Rock	Cooling Joint Sets 1 and 4	2 to 4	1.4 to 2.2
	Cooling Joint Set 2	4 to 8	2.8 to 4.4
	VPP Joint Set 3	12 to 16	8.4 to 8.8
Lithophysal Rock	Lithophysal Fractures	12 to 20	8.4 to 11.0

NOTE: Peak dilation angles calculated from Equation 3-1 for *JCS* = 100 MPa and σ_n = 4 to 8 MPa.

3.2.5 Thermal Properties of the Repository Host Rocks

Thermal properties (i.e., thermal conductivity, heat capacity or specific heat, and coefficient of thermal expansion) of lithostratigraphic rock units at the repository host horizon are important parameters used in the design and performance assessment because they are used in calculating the transient rock mass temperature and thermally induced stress. Their values are estimated primarily based on laboratory and field measurements. These measurements are essential in providing not only the site-specific values of thermal properties but also the information of their spatial variability and dependencies on temperature, porosity and fracture, and moisture content. Additionally, these testing efforts have also assisted in development of theoretical models that describe spatial variation of thermal properties and correlation between rock mass thermal properties, intact rock thermal properties, and other rock properties such as porosity.

Numerous laboratory tests using small specimens containing few voids and/or fractures show that intact rock thermal characteristics of lithophysal and nonlithophysal of rocks are similar (CRWMS M&O 1997b, Tables 5-11, 5-13, 5-15, and 5-16), indicating that similar methods may be used for acquiring intact rock thermal properties. However, rock mass characteristics of these rocks are quite different due to their different dominant features. These impacting factors are reflected in the difference in their rock mass thermal properties, suggesting, for example, the use of different methods of acquiring rock mass thermal properties for the lithophysal rocks versus those for the nonlithophysal rocks. Due to the associated relatively high cost and logistics involved, only a limited number of field thermal tests have been conducted (BSC 2002a, Sections 6.2.3.5, 6.3.1.4, and 6.3.3.6.5). Thus, estimation of rock mass thermal properties and their spatial variations based solely on the available field testing data may not be sufficient. This points to the desirability of using theoretical models to aid in describing the correlation between intact rock and rock mass thermal properties and the spatial variations.

Factors that may affect thermal properties include temperature, porosity, fracture, moisture content, specimen size or scale, mineral content, and loading condition. The effects of these factors on thermal properties have been a primary focus of investigation in the characterization of Yucca Mountain host rocks.

3.2.5.1 Thermal Conductivity

Thermal conductivity is a proportionality constant that relates the heat transfer (conduction) rate per unit area in a material to the normal temperature gradient. Thermal conductivity of rock is used in predicting temperature changes in the rock mass after waste emplacement.

Due to the heterogeneity and discontinuities in the rock units that will host the repository, thermal conductivity of the rock of interest is both scale- and direction-dependent. When increasing the size of testing specimens, the degree of heterogeneity and the impact of discontinuities increase, thus affecting the thermal conductivity of the rock specimen. It is important to understand the effect of scale on the rock thermal conductivity and the difference between the intact rock and the rock mass, so a correct value of thermal conductivity can be used in the design.

Intact Rock Thermal Conductivity–Thermal conductivity of intact rock was estimated based on laboratory thermal conductivity measurements using small specimens. These specimens had nominal dimensions of 50.8 mm in diameter and 12.7 mm in length (Brodsky et al. 1997, Section 2.1, Table 2-1), and contained few voids or fractures. The effects of these discontinuities on the measurements were considered minimal. A large number of laboratory thermal conductivity measurements have been conducted since the late 1990s. The results are summarized in Table 3-9 for the four rock units at the repository host horizon.

Table 3-9. Intact Rock Thermal Conductivities for Repository Units

Rock Units	Below 100°C (W/m·K)						Above 100°C (W/m·K)	
	Saturated		Air Dry		Dry		Dry	
	Mean	Standard Deviation	Mean	Standard Deviation	Mean	Standard Deviation	Mean	Standard Deviation
Tptpul	1.97	0.11	1.20	0.21	1.07	0.12	1.06	0.22
Tptpmn	2.33	0.45	1.68	0.12	1.51	0.49	1.60	0.11
Tptpll	2.13	0.13	1.65	0.08	1.45	0.03	1.54	0.04
Tptpln	N/A	N/A	N/A	N/A	N/A	N/A	N/A	N/A

Source: CRWMS M&O 1997b, Tables 5-11 and 5-13; DTN: SNL01A05059301.005.

Rock Mass Thermal Conductivity–Thermal conductivity of the rock mass is the effective value of thermal conductivity that relates the heat conduction rate to the normal temperature gradient in a rock mass. It accounts for the effects of voids, fractures, and any heterogeneity or discontinuity on thermal conductivity. Correlations between intact rock or rock matrix thermal conductivity, porosity (both matrix and lithophysae), and rock mass thermal conductivity are developed in *Subsurface Geotechnical Parameters Report* (BSC 2003a, Section 8.3.3.2). These efforts included both conducting experimental tests and developing theoretical approaches.

A limited number of experimental tests have been conducted to estimate rock mass thermal conductivity. They included laboratory measurements using large specimens and field measurements in the DST and the ECRB Cross-Drift. The DST measurements were of the Tptpmn unit, while the ECRB Cross-Drift measurements were of the Tptpll unit. Table 3-10 provides a range of rock mass thermal conductivity for the Tptpmn and Tptpll units obtained from the field measurements. Compared to those listed in Table 3-9, it is seen that the in situ values are within the ranges observed in the laboratory measurements on small specimens.

Table 3-10. Rock Mass Thermal Conductivities from Field Measurements

Rock Unit	Range of Thermal Conductivity (W/m·K)
Tptpmn[a]	1.69 to 1.95
Tptpll[b]	1.73 to 2.18

Source: [a] DTNs: LL980411104244.061; LL980902104244.070; UN0106SPA013GD.004; UN0201SPA013GD.007.
[b] DTNs: SN0206F3504502.012; SN0206F3504502.013; SN0208F3504502.019.

Alternative analytical approaches have also been developed to estimate rock mass thermal conductivity (BSC 2002b). The rock mass thermal conductivity, estimated from analytical correlations for the various repository host horizons, is summarized in Table 3-11. The analytical approaches, which account for matrix void volume, compares well to field measurements in Table 3-10. Compared to those listed in Table 3-9 for the intact rock, it is obvious that porosity and moisture content have significant effect on the rock mass thermal conductivity. For conservatism, ranges of thermal properties that encompass the rock mass thermal conductivity are used in design and performance assessment.

Table 3-11. Rock Mass Thermal Conductivities for Repository Units

Rock Units	Dry (W/m·K)		Saturated (W/m·K)	
	Mean	Standard Deviation	Mean	Standard Deviation
Tptpul	1.18	0.24	1.77	0.25
Tptpmn	1.42	0.27	2.07	0.25
Tptpll	1.28	0.25	1.89	0.25
Tptpln	1.49	0.28	2.13	0.27

Source: DTN: SN0208T0503102.007.

The thermal conductivity ranges provided in Table 3-11 are used as the basis for parametric analysis of rock mass temperature distributions in the postclosure period (see Section 5.3.1).

3.2.5.2 Heat Capacity

Heat capacity of a substance is defined as the amount of energy required to raise the temperature of a unit mass of the substance by one-degree (Nimick and Connolly 1991, p. 5). It is an important parameter used in thermal analysis to evaluate temperature changes in rock after waste emplacement. For solid materials, heat capacity is strongly dependent on temperature. For the temperature range of interest in the design and performance assessment, heat capacity for the repository rock units is estimated for three temperature ranges, 25°C to 94°C, 95°C to 114°C, and 115°C to 325°C, corresponding to the preboiling, transboiling, and postboiling regimes, respectively.

Only a limited number of laboratory and field measurements have been made to estimate rock heat capacitance (product of heat capacity and density). These measurements covered only a few rock units. Instead, the heat capacity values used in the design and performance assessment are

largely based on the calculated values obtained from analytical methods. The estimates have been compared with laboratory and field measurements and correlate sufficiently well as to validate the estimate model and the resulting values. These methods are presented in *Heat Capacity and Thermal Expansion Coefficients Analysis Report* (BSC 2003f).

Rock Grain Heat Capacity–The calculated average values of rock grain heat capacity for the four repository rock units are presented in Table 3-12. These values were estimated based on available data on mineral abundance and mineral heat capacity.

Table 3-12. Rock Grain Heat Capacities for Repository Units

Rock Units	T = 25°C to 94°C		T = 95°C to 114°C		T = 114°C to 325°C	
	Average	Standard Deviation	Average	Standard Deviation	Average	Standard Deviation
Tptpul	780	90	870	90	990	110
Tptpmn	780	110	870	110	990	130
Tptpll	780	100	870	100	990	120
Tptpln	780	70	870	70	990	90

Source: DTN: SN0307T0510902.003.

NOTE: All measurements are in (J/kg·K).

Rock Mass Heat Capacity–Rock mass heat capacity is the effective value of heat capacity that accounts for the effect of air-filled voids and of water that exists in the voids.

Efforts to measure the rock mass heat capacity were made. Rock mass volumetric heat capacity or heat capacitance of the Tptpll unit was estimated from the thermal measurements in the ECRB Cross-Drift. The estimated rock mass volumetric heat capacity values range from 1.96×10^6 to 2.30×10^6 J/m^3·K (DTNs: SN0206F3504502.012; SN0206F3504502.013; SN0208F3504502.019). Given a bulk density value of 2,360 kg/m^3 for the Tptpll unit, the rock mass heat capacity is estimated to range from 831 to 975 J/kg·K.

The calculated values of rock mass heat capacity for the four repository rock units using the analytical methods are summarized in Table 3-13. These values were estimated for the preboiling, transboiling, and postboiling regimes, based on the available data on rock matrix porosity and saturation, lithophysal porosity, rock grain heat capacity, and density.

Table 3-13. Rock Mass Heat Capacities for Repository Units

Rock Units	T = 25°C to 94°C		T = 95°C to 114°C		T = 114°C to 325°C	
	Average	Standard Deviation	Average	Standard Deviation	Average	Standard Deviation
Tptpul	940	300	3600	1000	990	300
Tptpmn	910	300	3000	900	990	300
Tptpll	930	300	3300	1000	990	300
Tptpln	900	300	2800	800	990	300

Source: DTN: SN0307T0510902.003.

NOTE: All measurements in (J/kg·K).

It is appropriate to use the rock mass heat capacity in the design and performance assessment if the phase change over the transboiling regime cannot be accounted for in the analysis. Otherwise, the rock grain heat capacity should be used because the modeling accounts for the heat capacity effects in boiling of pore water. The estimates have been compared with laboratory and field measurements and sufficient correlation is found to validate the estimate model and the resulting values.

3.2.5.3 Coefficient of Thermal Expansion

Thermal expansion is a mechanical response in the form of strain because of the change of temperature. The coefficient of thermal expansion (CTE) of rock is strongly dependent on temperature. It is an important parameter in thermal-mechanical analysis to predict thermally induced rock displacements and stresses and to evaluate stability of repository openings and performance of installed ground support during heating.

Intact Rock CTE–Intact rock CTE was estimated based on laboratory thermal expansion measurements using small specimens. A large number of thermal expansion measurements have been made on specimens taken from the rock units at the repository host horizon. Most of the measurements were conducted on dry or saturated specimens over a temperature range of 25°C to over 300°C. Table 3-14 summarizes the measured intact rock CTE for the four repository rock units.

Rock Mass CTE–Rock mass CTE is the effective thermal expansion that rock mass experiences when subjected to a change in temperature. It accounts for the effects of voids, fractures, moisture content, and any heterogeneity or discontinuity that affect the thermal expansion. Estimation of rock mass CTE is based on field or large core (diameter of 305 mm) thermal expansion measurements. Two major field tests, which involved the measurements of rock mass CTE, are the Single Heater Test and the DST. Both tests are located in the Tptpmn unit. The results from these measurements are summarized in Table 3-15.

There are no field thermal expansion measurements available in the Tptpll unit. The best data available on rock mass CTE for this rock unit are those from laboratory thermal expansion measurements on specimens with a nominal diameter of 305 mm (12 in.). The results from these laboratory measurements are also presented in Table 3-15.

After comparing the rock mass CTEs presented in Table 3-15 to those listed in Table 3-14 for the intact rock, it is apparent that the former are lower than the latter. The difference decreases as temperature increases, which indicates that the effect of fractures or voids on CTEs diminishes as more fractures or voids are closed by rock deformation as a result of temperature increase. From the perspective of ground support design, use of the intact rock CTE is conservative.

Table 3-14. Intact Rock Coefficients of Thermal Expansion for Repository Units

CTE on Heat-Up (10^{-6}/°C)													
Rock Units	**Temperature Range**		**25–50°C**	**50–75°C**	**75–100°C**	**100–125°C**	**125–150°C**	**150–175°C**	**175–200°C**	**200–225°C**	**225–250°C**	**250–275°C**	**275–300°C**
Tptpul	Saturated	Mean	7.59	7.00	7.91	10.22	10.76	12.95	16.73	25.60	32.83	43.98	53.94
		Std. Dev.	0.01	0.33	0.65	0.69	0.32	1.76	3.19	7.08	3.35	8.99	3.49
	Dry	Mean	7.41	8.43	8.89	9.52	10.86	13.51	19.38	29.34	32.35	40.16	48.83
		Std. Dev.	0.42	0.36	0.39	0.52	1.34	2.57	6.89	10.73	8.56	17.22	18.41
Tptpmn	Saturated	Mean	7.20	7.78	7.93	8.73	10.11	11.74	12.96	15.53	20.60	31.23	50.39
		Std. Dev.	0.84	1.90	0.94	2.04	0.87	0.47	0.70	1.02	2.04	3.75	7.55
	Dry	Mean	6.89	8.45	8.95	9.50	10.12	10.95	12.09	14.57	19.45	27.24	41.56
		Std. Dev.	1.45	0.30	0.24	0.27	0.36	0.52	1.01	2.04	3.47	6.23	7.92
Tptpll	Saturated	Mean	7.09	7.20	7.03	9.37	9.87	11.73	13.20	15.42	17.80	20.65	26.93
		Std. Dev.	0.45	1.09	1.31	2.78	0.69	1.76	1.85	2.22	3.29	4.80	8.26
	Dry	Mean	6.41	8.15	8.77	9.12	9.87	10.75	12.55	15.14	25.19	26.15	33.40
		Std. Dev.	0.75	0.47	0.54	0.57	0.68	1.01	1.80	3.26	27.61	13.65	17.99
Tptpln	Saturated	Mean	N/A	N/A	N/A	N/A	N/A	N/A	N/A	N/A	N/A	N/A	N/A
		Std. Dev.	N/A	N/A	N/A	N/A	N/A	N/A	N/A	N/A	N/A	N/A	N/A
	Dry	Mean	6.55	8.24	8.79	9.58	10.65	11.56	11.90	12.78	13.87	15.28	17.78
		Std. Dev.	1.29	0.57	0.47	1.07	2.17	2.75	2.35	1.53	1.11	1.94	4.38
CTE on Cool-Down (10^{-6}/°C)													
Rock Units	**Temperature Range**		**275–300°C**	**250–275°C**	**225–250°C**	**200–225°C**	**175–200°C**	**150–175°C**	**125–150°C**	**100–125°C**	**75–100°C**	**50–75°C**	**35–50°C**
Tptpul	Saturated	Mean	19.87	28.46	34.81	33.46	35.28	23.61	17.14	13.93	11.91	10.84	9.84
		Std. Dev.	2.44	1.92	3.38	2.90	5.21	5.79	2.61	1.30	0.41	0.26	0.01
	Dry	Mean	21.56	29.24	34.20	30.06	30.33	22.27	16.63	13.40	10.82	9.68	6.95
		Std. Dev.	3.32	9.61	15.44	8.76	11.03	7.57	4.29	2.41	0.91	0.81	1.80
Tptpmn	Saturated	Mean	27.79	38.28	36.20	25.84	17.93	14.51	12.75	11.48	10.65	9.83	9.14
		Std. Dev.	1.45	2.14	5.05	4.41	3.02	1.32	0.84	0.63	0.47	0.40	0.52
	Dry	Mean	24.82	30.08	28.39	22.55	17.20	13.72	11.88	10.73	9.93	9.34	8.38
		Std. Dev.	2.25	5.33	6.30	4.27	5.10	3.42	2.78	1.86	1.07	0.45	1.25
Tptpll	Saturated	Mean	17.30	19.71	19.05	17.91	16.75	13.66	12.26	11.56	9.92	9.16	8.50
		Std. Dev.	3.93	5.31	4.90	3.92	3.16	1.38	1.65	2.77	0.54	0.64	0.57
	Dry	Mean	17.15	20.16	22.11	21.69	22.06	15.80	11.47	10.10	8.88	8.12	7.03
		Std. Dev.	2.71	4.78	8.25	8.17	14.24	5.54	3.63	2.87	2.50	2.33	2.39
Tptpln	Saturated	Mean	N/A	N/A	N/A	N/A	N/A	N/A	N/A	N/A	N/A	N/A	N/A
		Std. Dev.	N/A	N/A	N/A	N/A	N/A	N/A	N/A	N/A	N/A	N/A	N/A
	Dry	Mean	15.02	15.52	15.38	15.07	14.08	13.03	11.98	10.85	9.95	9.20	5.24
		Std. Dev.	2.70	2.89	2.28	1.63	2.06	2.61	2.56	1.87	1.09	0.63	0.23

Source: CRWMS M&O 1997b, Tables 5-15 and 5-16; DTN: SNL01B05059301.006.

Table 3-15. Rock Mass Coefficients of Thermal Expansion for Repository Units

Rock Unit	Specimen Source	Temperature	Mean	Standard Deviation
Tptpmn	Single Heater Test[a]	70°C	4.14	N/A
		117°C	2.36	N/A
		160°C	5.88	N/A
	Drift Scale Test[b]	50°C	2.03	1.29
		75°C	2.41	0.93
		100°C	4.19	2.07
		125°C	4.40	1.96
		150°C	7.44	0.45
		175°C	9.81	0.80
		200°C	12.55	N/A
Tptpll	12” Specimens[c]	80°C	6.50	1.49
		120°C	6.60	1.73
		160°C	10.04	1.69
		200°C	15.34	5.58

Source: [a] BSC 2002a, Table 6.2.3.5-1.
[b] BSC 2002a, Table 6.3.3.6-5.
[c] DTNs: SN0208L01B8102.001; SN0211L01B8102.002.

INTENTIONALLY LEFT BLANK

4. DEVELOPMENT OF ROCK MASS MATERIAL MODELING APPROACHES FOR NONLITHOPHYSAL AND LITHOPHYSAL ROCKS

Section 3 reviewed the basic laboratory and in situ thermal and mechanical testing data that have been generated by the Yucca Mountain Project for the repository host horizon units. These data, typically on small-scale samples, need to be generated to provide input properties and property ranges for design and performance analyses. This section describes the integration of geologic mapping and geotechnical characterization studies with the laboratory and field testing to produce field-scale rock mass properties. Constitutive modeling approaches are also described.

4.1 MECHANICAL DEGRADATION MODELING APPROACH FOR NONLITHOPHYSAL ROCK

The nonlithophysal rocks are strong, hard materials. The degradation behavior of tunnels in these rock units is controlled by the occurrence of "keyblocks," or kinematically removable wedges, which can dislodge and fall under the action of external loading. Dislodging of these keyblocks does not necessarily lead to extensive failure and may simply result in isolated rock falls. Thus, isolated blocks may become dislodged, yet the excavation remains stable.

Keyblocks in the 5-m-diameter ECRB Cross-Drift are first evident in the crown at about Station 10+50 in the Tptpmn unit. Most of the keyblocks in this region are of minor size and have typically been forcibly removed by scaling operations immediately after excavation, but prior to ground support installation. Keyblocks are possible in this area because of the increased presence of planes of weakness (i.e., a vapor-phase parting) in the near horizontal orientation that intersects with two opposing near vertical joint planes. The largest resultant void is approximately 0.5 m^3 at approximately Station 11+55 as shown in Figure 4-1. No unstable keyblocks (i.e., those that have fallen out at a later time due to gravity) have been observed in the field (BSC 2004a).

The approach taken here to represent the degradation response of nonlithophysal rocks is to explicitly model the fractured, blocky response of the material to allow a direct calculation of rockfall and opening shape change as a function of loading. This approach requires that the stochastic nature of the fracturing be captured in the modeling. Two items are required to successfully implement this approach: a tool for producing representative fractured volumes of rock, and numerical models that can simulate the physical, three-dimensional collapse modes of a blocky rock mass subjected to seismic and other loadings. A sufficient number of mechanical simulations[12] using representative fracture realizations are necessary to adequately describe the full range of stochastic response of the rock mass. Uncertainty in the estimate of rockfall arises from three sources:

1. The uncertainty in the knowledge of the fracture geometry
2. The uncertainty in mechanical properties of the fractures
3. Uncertainty in the applied loadings.

[12] A sufficient number of fracture realizations is described in Section 5.3.

00387DC_019.ai

Figure 4-1. Evidence of Key-Block Occurrence in the Enhanced Characterization of the Repository Block Cross-Drift, Station 11+55

Uncertainty in the fracture geometry is inherently accounted for through stochastic representation of fracture geometries using the FracMan fracture simulation model and by conducting a sufficiently large number of analyses with randomly selected fracture patterns. Uncertainty in fracture mechanical properties is investigated by varying the properties over their expected ranges. Uncertainty in the applied loading is accounted for by the use of measured in situ stresses, inclusion of thermal loading histories, and use of 15 sets of probabilistically defined ground motions that account for the range of uncertainties in the ground motion (BSC 2004c).

This section describes the development of the stochastic fracture geometry model that provides the input for the three-dimensional discontinuum stability model. The model and modeling approach is described in Section 5.3.

4.1.1 Development of Fracture Geometries for Nonlithophysal Rock

Analysis of seismic response and rockfall in emplacement drifts in fractured, nonlithophysal rock is, in general, a three-dimensional problem requiring the rock mass to be represented as an explicitly fractured assemblage. To achieve this objective, the 3DEC, three-dimensional discontinuum program (BSC 2002c) is used to model the mechanical response of a rock block assemblage subjected to in situ, thermal, and seismic loads. The 3DEC program allows direct input of the fracture geometry in creation of a “synthetic” rock mass composed of an assemblage of blocks within which emplacement drifts may be simulated. The details of the 3DEC model are described in Section 5.3.

The blocks of nonlithophysal rock are significantly stronger than the in situ and thermally induced stresses, and thus the problem of modeling this material is essentially one of elastic blocks separated by fracture surfaces. Therefore, in modeling of the stability of the tunnels and the rockfall that may occur from the applied load, the fracture geometry and surface properties become of primary importance. A methodology for defining statistically representative fractures is therefore required as a direct input to the 3DEC program. In particular, the input fracture geometry must provide an adequate representation of the orientation, length, spacing and continuity of fractures and their variability, as this controls the size and number of removable blocks that surround the tunnel. Additionally, the surface characteristics, including roughness, planarity, and alteration/infilling define the shearing and tensile resistance of the fractures under load.

The development of a stochastically defined fracture system, representative of the actual rock mass is accomplished using the FracMan program (USGS 1999). The existing fracture mapping database, described in Section 2.3.1, provides the basic input to the FracMan program, which develops sets of planar, circular fractures that conform to the statistical variability of the geometric characteristics of the input data. Statistical models are fitted to the various geometric characteristics of each fracture set in the database, followed by generation of representative fracture sets. These representative fractures are then back-checked against the statistical variability and geologic realism of the original sets (i.e., field data) to achieve an acceptable facsimile. Details of this process are described in *Drift Degradation Analysis* (BSC 2004a).

A three-dimensional representative rock mass cube, 100 m on a side, is generated using FracMan for each Topopah Spring subunit. Each fracture is described by its centroid coordinate, dip, dip

direction, and radius. These geometric properties are used as direct inputs to the 3DEC program for development of a block geometry within which emplacement drifts can be randomly excavated.

4.1.2 Example—Fracture Geometry Generation for the Middle Nonlithophysal Unit

Because the large-scale fracture control of block geometry is most prevalent in the nonlithophysal rock, and in the Tptpmn in particular, an example of the FracMan methodology for construction of an equivalent fracture model for this unit is given. The analysis for the Tptpmn uses a classical approach to identify sets based on orientation only (Mongano et al. 1999; CRWMS M&O 2000).

The detailed line survey data are used to condition FracMan to develop representative fracture trace lengths and spacings. Table 4-1 displays the mean orientation of the sets, a comparison of average fracture radius converted to diameter and average trace length, and intensity (average spacing) from FracMan and average spacing from the detailed line surveys.

Table 4-1. Comparison of Data from Detailed Line Survey, Full-Periphery Geologic Maps, and FracMan Output for the Tptpmn

Set Number	Observed Orientation (Strike/Dip)	FracMan Orientation (Strike/Dip)	Inter-Fracture Distance (m)		Trace Length Median from Full Periphery Geologic Maps (m)	Trace Length Median from FracMan (m)
			Observed	FracMan		
Set 1	120/84 (210/06)	125/84	0.48	0.79	3.3	2.8
Set 2	215/88 (305/02)	214/86	1.08	1.29	3.1	2.9
Set 3	302/38 (212/52)	299/43	3.40	3.16	3.6	3.7
Vapor-Phase Parting	329/14 (239/76)	327/08	2.46	1.48	3.4	3.5

Source: DTNs for tunnel mapping include GS960908314224.020, GS000608314224.006, GS960908314224.015, GS960908314224.016, GS971108314224.025, GS960708314224.008, GS000608314224.004, and GS960708314224.010.

NOTE: Trace length medians are taken from a compilation of tunnel mapping and synthetic tunnel samples from FracMan.

A direct comparison between actual full periphery geologic maps from the ESF to synthetic full periphery geologic maps from FracMan is given in Figure 4-2. This comparison ensures that the synthetic fracture geometries are not only quantitatively validated, but similar from a geological perspective as well. Details of the quantitative comparison of FracMan results to the full periphery and detailed line surveys is given in *Drift Degradation Analysis* (BSC 2004a).

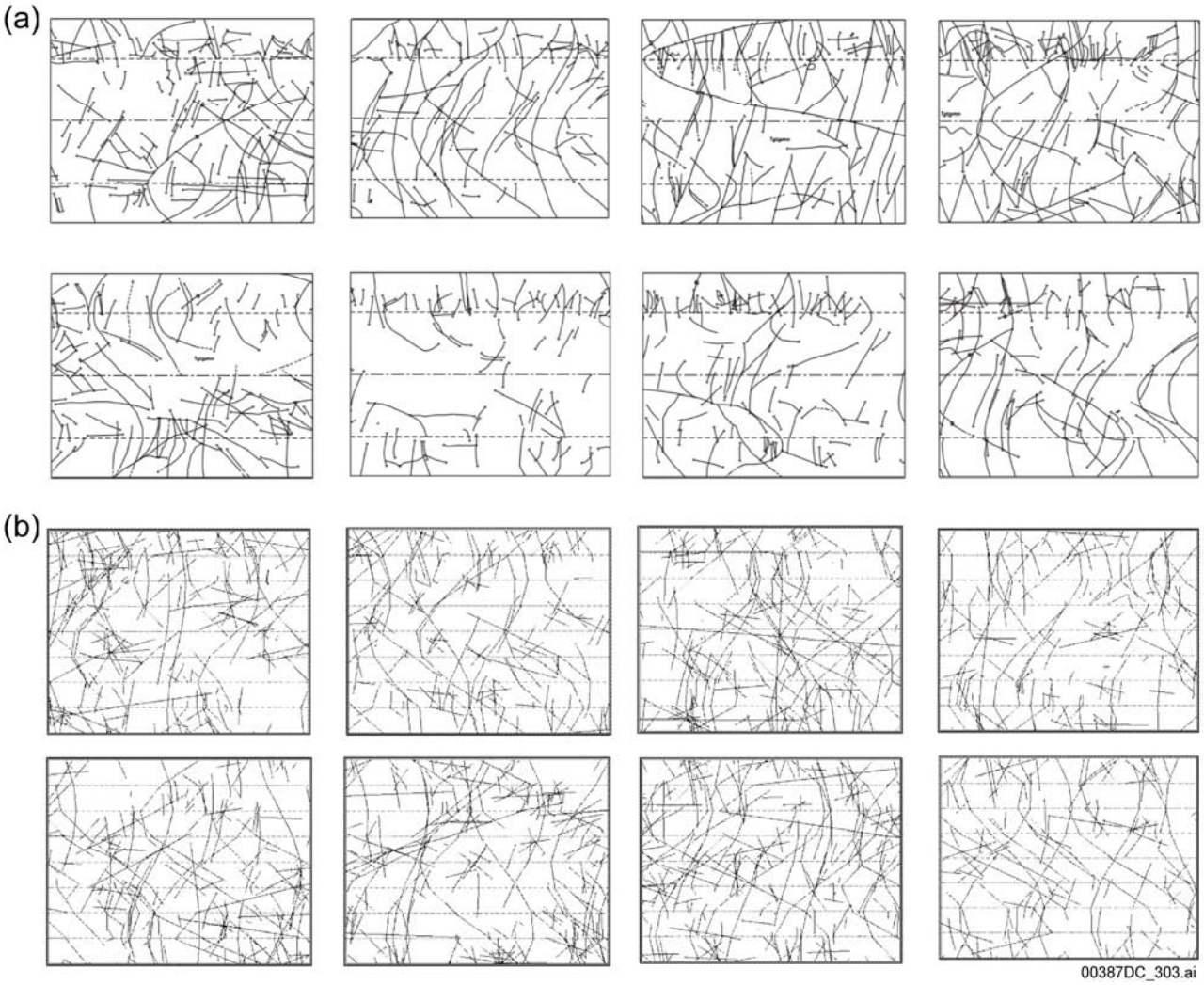

Source: (a) DTNs: GS990408314224.004; GS000608314224.006; GS960908314224.015; GS960908314224.016; (b) BSC 2004a.

NOTE: The purpose of this figure is to illustrate the geologic structure contained on a full periphery geologic map. The annotated information on this figure is not intended to be legible.

Figure 4-2. Comparison of Full Periphery Geologic Maps from the Tptpmn in the Exploratory Studies Facility (a) with Simulated Full Periphery Geologic Maps from the FracMan Cube (b)

4.2 MECHANICAL DEGRADATION MODELING APPROACH FOR LITHOPHYSAL ROCK

4.2.1 Material Model Requirements

The lower lithophysal unit (Tptpll)[13] is characterized by intense, small-scale fracturing. Joint sets are not as clearly defined as in the middle nonlithophysal (Tptpmn) unit. Average joint spacing is less than 1 m, and at certain locations this spacing is much smaller, on the order of 0.1 m. In addition to fracturing on different scales, the lithophysal rock mass is characterized by the presence of almost uniformly distributed holes (lithophysae) of varying size (from less than 1 cm to greater than 1 m in diameter). The lithophysae account for up to 30% of the rock mass volume. The size of the internal lithophysae structure and fracture spacing is much smaller than the drift size (i.e., 5.5-m diameter). Since the lithophysae size is small in comparison to the drift diameter, the impact of lithophysae on mechanical effects on drift stability can be represented numerically using average properties for the rock mass that take into account the porosity without actual modeling of individual lithophysae. Based on the fracture and lithophysae network, it is possible to empirically deduce that failure of this material will produce constituent block sizes that are controlled by the spacing of these features (i.e., blocks on the order of tens of centimeters on a side).

Figure 4-3 is a core sample from the Tptpll with a diameter of 290 mm that has been removed from the core barrel and is still moist from drilling water. The moisture highlights the intensive fracture system that exists in the rock mass. These fractures are largely of a cooling origin, as evidenced by vapor phase alteration along the fracture faces (i.e., they are not of a mining origin). Drilling of core in this material without special techniques is problematic due to stresses placed on the core by the rotating barrel, which tend to pull it apart along these very rough fracture surfaces. This photograph clearly shows the ultimate small rock block sizes that would be created in the event that failure occurs in the lithophysal rock. Therefore, it is not the goal of the degradation modeling effort to attempt to predict block size (as was the case in the nonlithophysal rocks), but to predict the ultimate volume of detached rock, the shape of the excavation, and the quasi-static loading applied to the drip shield.

[13] Although the Tptpll is emphasized in this document since a majority of the repository is located in this unit, the results also apply to the Tptpul, which exhibits similar rock mechanical properties.

00387DC_025.ai

NOTE: Moisture on core surface clearly shows intensive internal fracture and lithophysae network.

Figure 4-3. Large (290 mm) Diameter Core from Tptpll

There is no preferred direction in the orientation of fracturing or lithophysae distribution that would justify the necessity of inclusion of anisotropy in analysis of the mechanical response of excavations within the Tptpll (BSC 2004a). Heterogeneity in rock mass properties resulting from spatial variability of the lithophysal porosity is considered in two ways in stability analyses. First, a series of base case parameter studies are conducted on the drift scale in which homogenous rock properties are assumed for a given drift cross section, but using properties that cover the range of potential mechanical properties. Second, analyses are also conducted in which the spatial variability of lithophysal porosity is accounted for by explicitly representing nonhomogenous distributions of rock mass properties. These analyses take into account the stochastic variability of rock properties but require a larger number of realizations to cover extreme cases. With homogeneous properties, using a range of mechanical property categories, conservative results can be obtained with fewer analyses. Therefore, the simple, bounding range approach with constant properties (method 1 above) is used for the majority of calculations, and explicit modeling of the estimated spatial variability (method 2) is used in a checking mode to verify the conservative nature of the bounding range approach. Use of a two-dimensional modeling approach is justified for lithophysal rocks based on the lack of anisotropy in the rock mass and the fact that the block sizes created upon failure are very small (essentially granular in nature) with respect to the size of the emplacement drift. Finally, since a two-dimensional modeling approach is used, the initial, in situ horizontal stress component is projected into the plane perpendicular to the axis of the emplacement drifts. This stress component is approximately 0.5 times the vertical component.

To represent drift degradation mechanisms and rockfall in lithophysal rock, the mechanical model and the numerical method in which it is embedded must have the following capabilities:

- The model must provide a general capability of modeling in situ stress, thermal, and seismic loading of the rock mass.
- The model must represent the effects of porosity and matrix preexisting fracturing on the elastic and strength properties of the material.
- The model must allow internal fracturing and detachment of the rock mass (i.e., rockfall) to occur in response to gravity, thermal effects, and seismic shaking.

These requirements imply the necessity of a discontinuum approach to represent the rock mass.

4.2.2 Mechanical Material Model and Numerical Analysis Approach Development for Lithophysal Rocks

4.2.2.1 Generalization of Lithophysal Rock Mass Properties into a Number of Rock Quality Categories

In the lithophysal units, lithophysal porosity is the primary physical feature impacting rock quality conditions (and therefore rock mass strength and stiffness). As seen in Figure 4-4, the laboratory data shows a range in unconfined compressive strength from approximately 10 to 30 MPa with a corresponding range in Young's modulus from approximately 5 to 20 GPa. The estimated sample lithophysal porosity varies from approximately 10% to 30% over this range, or is roughly comparable to the range of in situ values defined from mapping in the ECRB Cross-Drift (Figure 2-10). Thus, the core sampling used for the laboratory testing spans roughly the same range of lithophysal porosity (if not lithophysae size and shape) as observed throughout the ECRB Cross-Drift.

For convenience of analysis, the mechanical rock properties range, as shown in Figure 4-4, is subdivided into five rock strength "categories" that cover the entire range of large-core laboratory testing and in situ testing results. Table 4-2 presents these strength and moduli ranges derived by subdividing the laboratory data into five categories with an unconfined compressive strength increment of 5 MPa. The associated Young's modulus for each unconfined compressive strength is derived from the linear data fit to the 290-mm core data given in Figure 4-4. The approximate equivalent lithophysal porosity for each of these ranges is given in Table 4-2 (BSC 2004a, Section E.4).

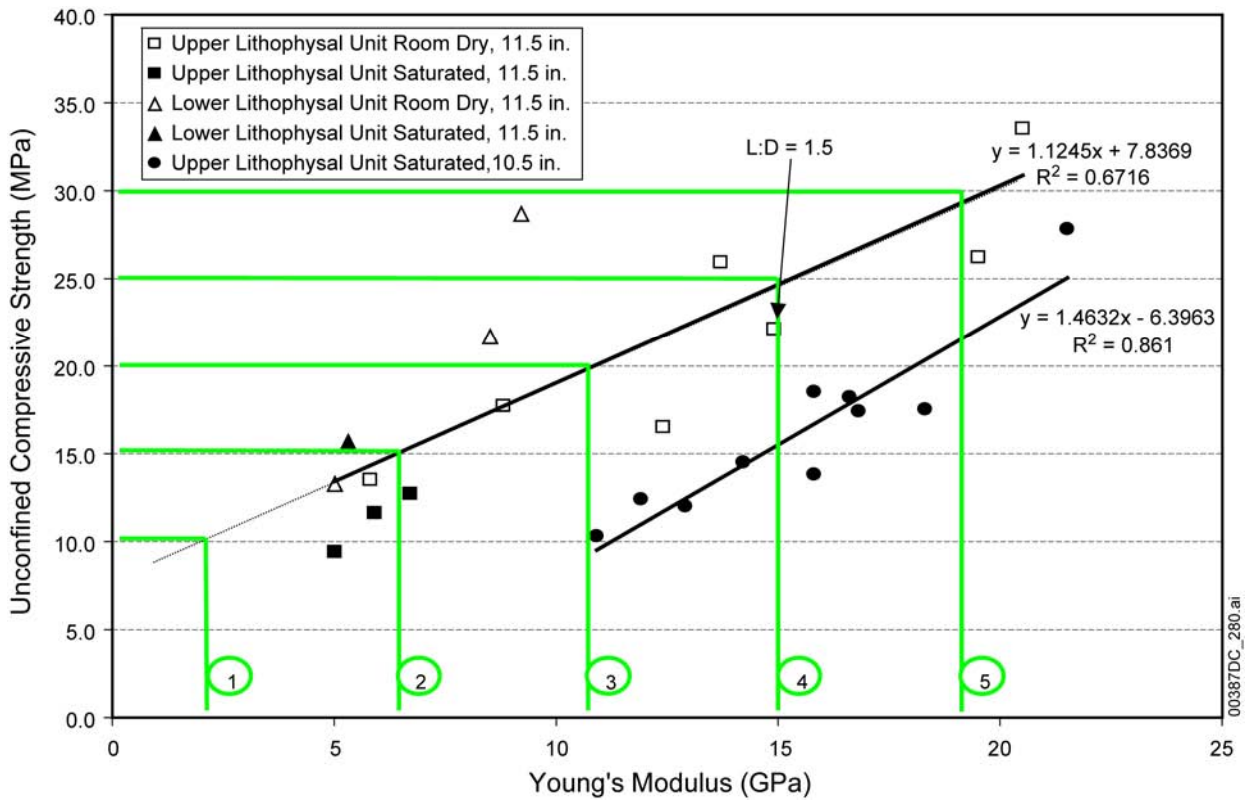

Source: DTNs: SN0208L0207502.001; SN0211L0207502.002; SN0305L0207502.006.

NOTE: Base case strength and modulus based on fit to 11.5-in. (290-mm) core data. Data for this plot are from Figure 3-11.

Figure 4-4. Relationship of Unconfined Compressive Strength to Young's Modulus from Large Core Testing of Lithophysal Rock (Figure 3-11) and Assignment of Five Average Quality Categories

Table 4-2. Suggested Range of Mechanical Properties Selected for Base-Case Design and Performance Analyses

Category	Unconfined Compressive Strength (MPa)	Estimated Young's Modulus[a] (GPa)	Approximate Lithophysal Porosity From Laboratory Tests[b] (%)
1	10	1.9	35 +/- 8
2	15	6.4	28 +/- 6
3	20	10.8	21 +/- 4
4	25	15.3	13 +/- 5
5	30	19.7	7 +/- 7

Source: BSC 2004a, Table E-10.

NOTE: [a]The calculation of Young's modulus values is documented in BSC 2004a, Section E.4.1.
[b]Approximate lithophysal porosity estimates provided in BSC 2004a, Section E.4.1.

It is considered that, by conducting numerical analyses with this entire range of data, that all levels of rock quality and rock mass response from lowest to highest porosity ranges and size effects can be covered. A histogram constructed to provide the information on the percentage of each rock category in the Tptpll as a whole is shown in Figure 4-5. The distribution of lithophysal porosity is based on the lithophysal mapping data in the ECRB Cross-Drift (BSC 2004a, Appendix O). It is shown that approximately 90% of the mapped rock quality is equal or better than the Category 3 rock. Categories 1 and 2 are related to localized, stratiform, high porosity zones that occur particularly near the top of the Tptpll. Although of low abundance, Categories 1 and 2 are included in the range of rock properties for analysis to test the conservative bounds of rock strength. Figure 4-5 also shows photographs of example panel maps that illustrate lithophysal porosity levels characteristic of Categories 3, 4, and 5.

The rock strength categories that form the basis for parametric stability calculations are based on a linear fit to the strength-modulus data from 305-mm diameter core testing. Properties are given in Section 4.2.3.3.

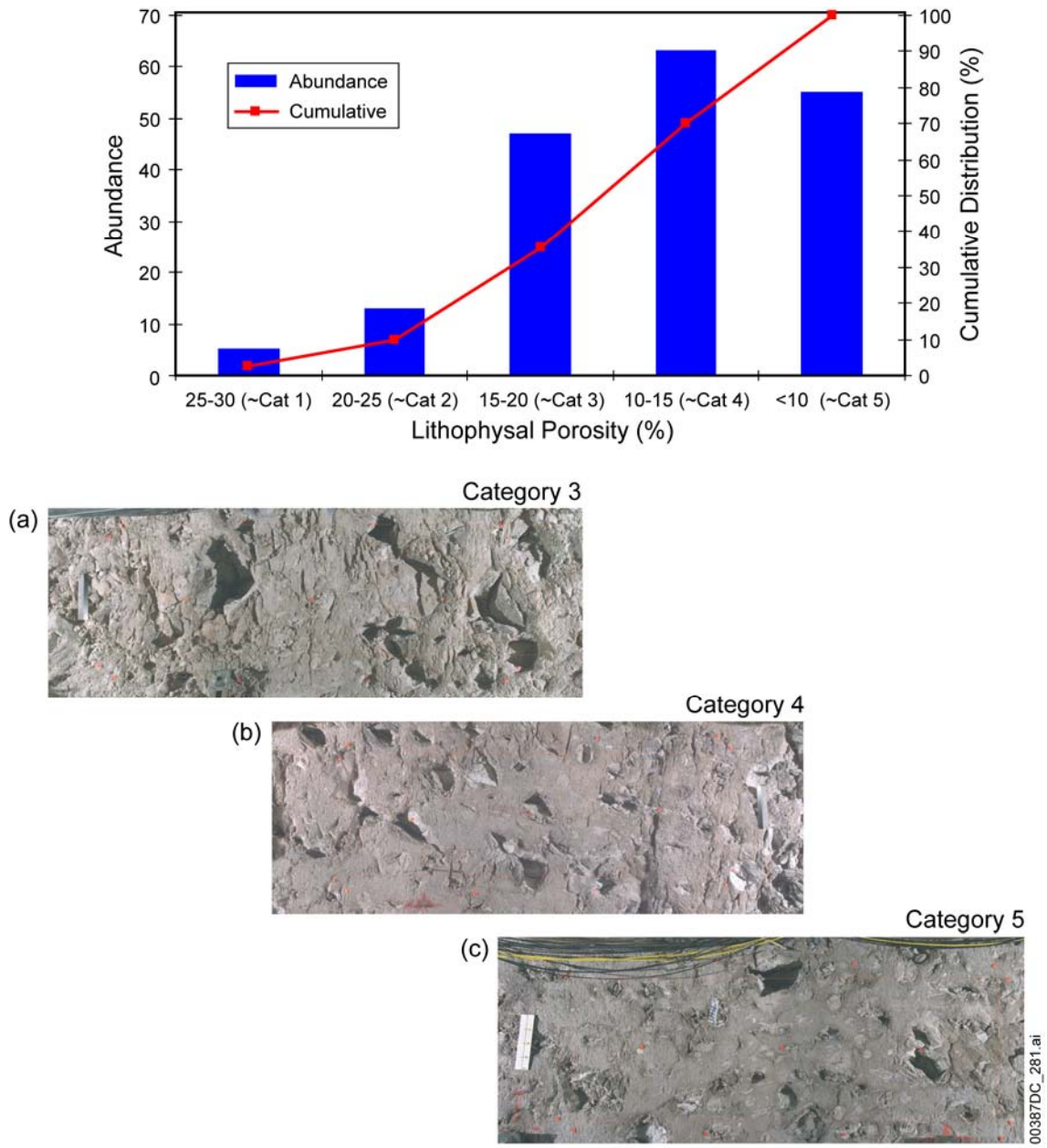

Source: (a) BSC 2004a, Appendix O, Section O.6.6.

NOTE: Lithophysal porosity data are based on 183 5-m traverse locations from the ECRB Cross-Drift between stations 14+44 and 23+26. Examples of approximate rock strength category levels taken from 1-by-3-m panel maps: Category 3 (a) with lithophysal porosity of approximately 19%; Category 4 (b) with lithophysal porosity of 13.3%; and Category 5 (c) with lithophysal porosity of 8.5%.

Figure 4-5. Distribution of Lithophysal Porosity and Estimated Rock Properties Categories for the Tptpll in the Enhanced Characterization of the Repository Block Cross-Drift

4.2.2.2 Continuum- and Discontinuum-Based Approaches to Representing Rock Masses

A standard approach for solving excavation stability problems in geotechnical engineering is the use of numerical models based on continuum mechanics assumptions (Figure 4-6). Such an approach is quite effective if the rock mass, in response to stressing, eventually arrives at a state of mechanical stability and where the primary purpose of the modeling is the computation of stress redistribution around an opening or determination of the final displacement profiles. However, difficulties are encountered if a continuum model is used for prediction of a mechanical system (i.e., a tunnel) that does not arrive at a stable condition upon excavation.

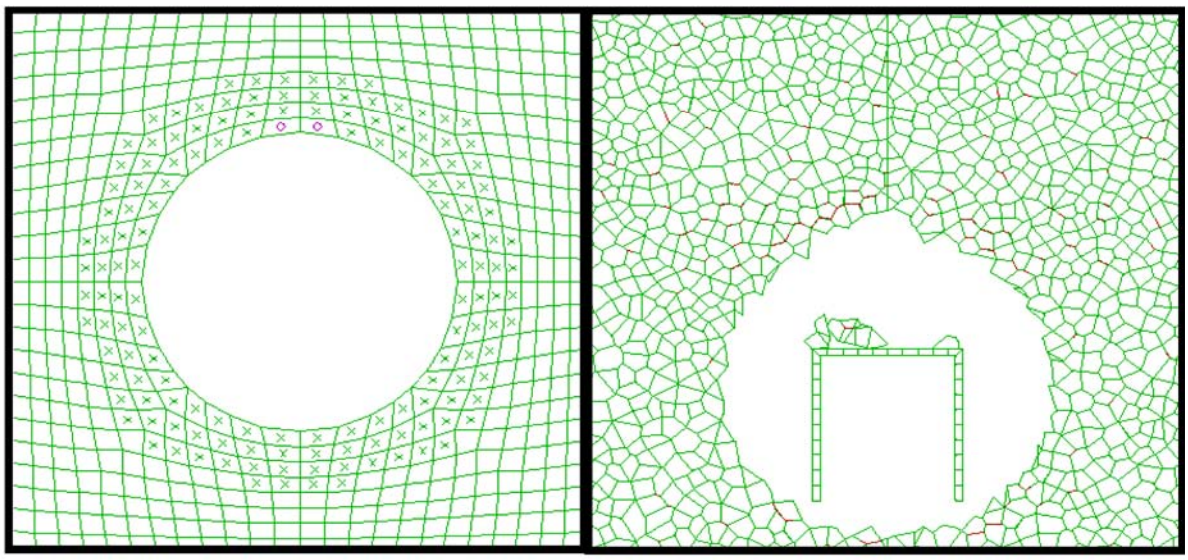

00387DC_027.ai

Source: BSC 2004a, Figure 7-7.

NOTE: The continuum approach models yield of the rock through use of a material model that enforces plasticity relations (note marked elements). Rock breakage and separation are not possible in this approach. The discontinuum approach also represents the rock mass using similar material models but provides the capability for the rock mass to fracture and break apart on potential fracture surfaces. The illustration on the right contains a simple rectangular representation of a drip shield.

Figure 4-6. Continuum (Left) and Discontinuum (Right) Approaches to Modeling Drift Stability

Continuum models use stress-strain relations to describe the mechanical behavior of a material. In rock, the mechanical effects of fractures and other features are typically assumed to be taken into account within a standard form of plasticity model without explicitly representing the features (e.g., see Hoek 2000). The specific characteristics of the rock mass, such as the rock type, the spacing and continuity of the fractures, and the roughness and alteration of the fracture surfaces, are taken into account by empirical adjustment of properties determined from testing of intact rock cores.

A linearly elastic–perfectly plastic material model with Mohr-Coulomb yield criteria is a constitutive model often used to represent mechanical behavior of a rock mass (e.g., Hoek 2000). Because the material strength of a perfectly plastic Mohr-Coulomb material under general conditions does not decrease as a function of plastic deformation, this model will show

indications of material yielding (i.e., plastic deformation) in different portions of the model, but will never actually predict instability that leads to rockfall. In order to predict rockfall, it is necessary to use a form of material model in which strength degrades as a function of deformation after the peak-strength of the material has been reached. Because representation of fracture and breakage in a continuum representation is speculative, a typical continuum modeling approach is not the primary method used to represent mechanical degradation and rockfall. Continuum models are, instead, used as a means of comparison to other approaches.

4.2.2.3 Development of a Discontinuum Approach to Representing the Mechanical Response of the Lithophysal Rock Mass

The estimation of rockfall requires that the modeling technique and mechanical material model be capable of representing fracture and separation of the intact rock mass into individual blocks of material. In particular, an estimate of the size distribution of particles is desired. Thus, the modeling technique must be based on use of a discontinuum numerical method (i.e., a method in which the rock is represented as blocks separated by fracture surfaces in which slip and separation of contacting rock blocks can be estimated).

The development of a mechanical material model and estimate of property ranges for the lithophysal material is based on use of the laboratory database described in Section 3 (primarily compression testing on cores with diameters of 290 mm) supplemented by numerical model extrapolation using the PFC and UDEC discontinuum programs. These extrapolation approaches are conducted in parallel as alternative numerical methodologies.

The database available for properties definition and model development includes: (1) uniaxial and triaxial compression and tensile testing of nonlithophysal rock; and (2) uniaxial compression testing of large-scale cores and in situ blocks of lithophysal tuff. As discussed in Section 3, the material properties of lithophysal rock are size-dependent due to the influence of the lithophysal pore space. Due to the difficulties in both obtaining and testing large samples of this rock, the laboratory testing data base is limited. However, it is possible to calibrate appropriate numerical models to reproduce the laboratory data. These models can then be used to extrapolate from the laboratory to the in situ scale for examination of the impact of the variability of lithophysal size, shape, and distribution on the range of rock mass strength and deformability. Thus, the model is used as a means of extending the laboratory data base.

This strategy, which combines laboratory testing, model calibration, and extrapolation for estimation of mechanical properties ranges is illustrated in Figure 4-7. In this section, an approach is described in which physics-based discontinuum numerical modeling programs—PFC2D (BSC 2004h), PFC3D (BSC 2004i), and UDEC (BSC 2002d)—are used as numerical "laboratories" to simulate and test the basic deformation and failure response mechanisms of lithophysal tuff. These programs were chosen due to their ability to simulate the physics of deformation and fracture of a bonded granular matrix that contains void space of varying shape, size, and porosity. Using two different approaches provides a check and greater confidence in the modeling. The UDEC program is additionally used as it allows constituent grains that are nonspherical in shape, and thus overcomes some simplifications used in the PFC approach. Specifically, it allows greater flexibility in modeling failure mechanisms under triaxial compression.

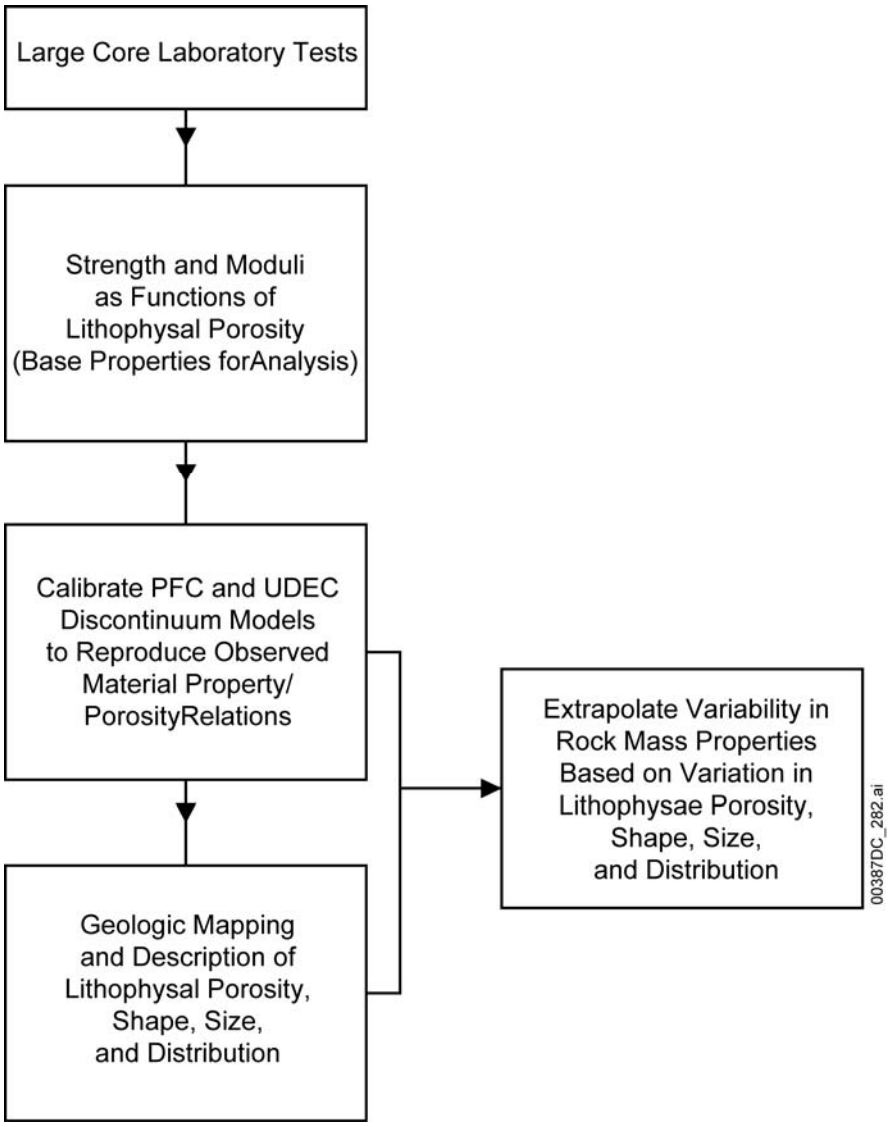

Figure 4-7. General Approach for Estimation of Lithophysal Rock Property Bounds

The approach has two steps. First, the programs are validated (Section 4.2.3) against the existing laboratory compression data, where it is demonstrated specifically that a detailed understanding of the basic physical mechanisms of the rock mass behavior can be obtained without resorting to empiricism or complex constitutive modeling. Next, the model is used to extend the laboratory data by conducting numerical experiments on simulated samples of lithophysal tuffs at various physical conditions of porosity, lithophysae shape and distribution, as well as various levels of confinement and applied stress. The outcomes of the modeling are estimates of the range of rock mass strength and stiffness for varying conditions of lithophysal porosity, size, shape, and distribution. Additionally, the results provide a means of understanding the size-scaling and variability issues introduced by lithophysae shape and distribution and their impact on rock mass properties and failure criteria.

The material model developed from the testing and PFC/UDEC extrapolation is embedded into a drift-scale UDEC model for conducting the parametric performance analyses of emplacement

drift stability. UDEC and PFC have a significant history of use in the mining and defense industries for analysis of tunnel stability and rock fracture simulation under in situ and seismic loading. The PFC2D, PFC3D, and UDEC programs have been qualified for use on the Yucca Mountain Project.

4.2.3 Validation of the Particle Flow Code–A Micromechanical Model Representation of the Mechanical Behavior of Lithophysal Rock

4.2.3.1 The Particle Flow Code Model

The PFC approach represents rock as a number of small, rigid, spherical grains that are bonded together at their contacts with shear and tensile strength, as well as a grain-to-grain friction angle after the "contact bond" has been broken. Details on the mechanics of the PFC program are provided in *Itasca Software—Cutting Edge Tools for Computational Mechanics* (Itasca Consulting Group 2002). The deformability of the contacts between particles is represented by normal and shear stiffness at the contact point. Porosity is developed naturally in the model by control of the shape and size of void space between chains of bonded grains. The contact properties and porosity distribution are referred to as "microstructural" properties. Thus, the input conditions necessary for the model are very simple, only contact strength and stiffness. However, extremely rich constitutive behavior may develop naturally based on void porosity and the few straightforward input properties and their variability throughout the rock.

When load is applied to the grain assembly, forces are transmitted across contacts. If the shear or tensile strength of the contact is reached, failure will occur, and the adjacent particles are free to slide past one another, or to separate. In either case, a fracture is formed and the forces must reorient in some fashion, thus redistributing loads. Realistic failure mechanisms may then develop which can be compared to those observed in the laboratory. Calibration of the model against laboratory testing is accomplished via sensitivity studies in which the contact strength and stiffness values are varied and the macroscopic stress-strain response is compared to that monitored.

The UDEC approach, although similar, is different specifically in that the grains may be of any arbitrary shape and size, and the contacts between grains are not point force contacts, but contact across a plane. Additionally, the UDEC grains may be deformable rather than rigid. The importance of this distinction is described later.

4.2.3.2 Particle Flow Code Model Calibration

The PFC model has been calibrated against the laboratory testing data discussed in Section 3. Sample numerical compression experiments were conducted for nonlithophysal and lithophysal tuffs using the same matrix properties (Figure 4-8). These matrix mechanical properties were derived by calibration of strength and modulus from the laboratory testing for a midrange lithophysal void porosity of approximately 15% (Table 4-2).

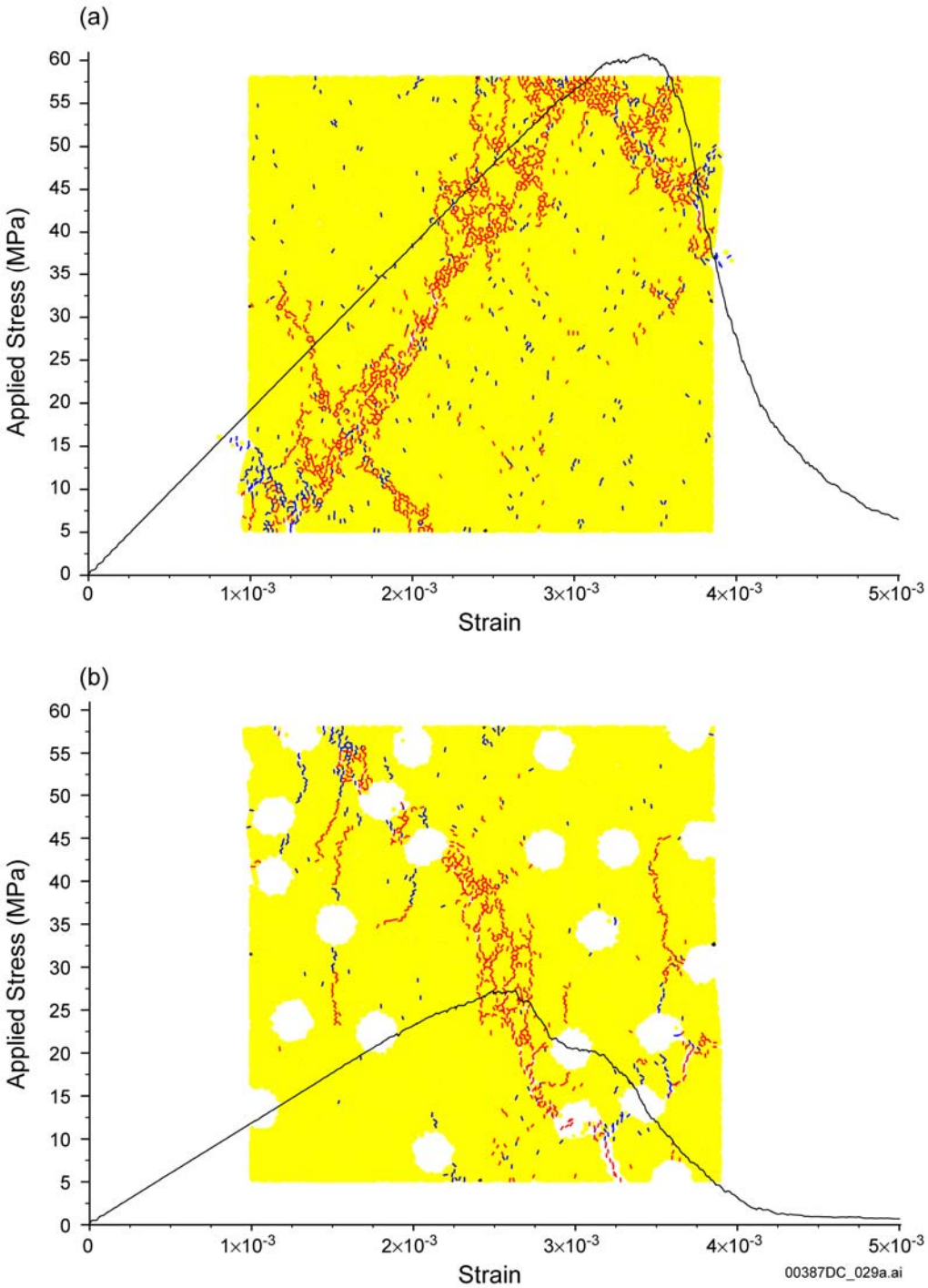

Source: BSC 2004j, Section 6.5.6, Figure 6.5-20.

NOTE: Stress strain curves have the same scale, so strength and modulus difference in lithophysal sample is evident. Red and black lines on samples are tensile and shear fracture, respectively, that have formed within the rock "samples" as they are loaded. Nonlithophysal sample shows typical macroscopic shear failure mechanism whereas lithophysal sample fails due to tensile splitting between voids. Calibration results are shown in Figure 4-9.

Figure 4-8. Particle Flow Code Calibration Compression Experiment "Samples" and Their Respective Uniaxial Stress-Strain Curves for (a) Nonlithophysal and (b) Lithophysal Rock

The nonlithophysal samples show a typical shear failure mechanism as evidenced by the coalescence of extension cracks to form major shear fractures. The model also shows highly linear (elastic) response just to the point of rock failure, followed by a brittle post–peak failure response due to the uniformity of bond strength set in the samples. This replicates the observed laboratory behavior of nonlithophysal samples.

Once the basic behavior of the nonlithophysal rock is represented, the samples can be populated with pores. Initially, simple circular holes were added to the nonlithophysal model to represent the lithophysal rock. The circular holes were added with a random spatial distribution to the model, and the correspondence between laboratory-derived strengths, modulus and porosity were examined. The model showed good comparison with general magnitude and trend of laboratory strength and modulus data (Figure 4-9).

A conclusion of this initial work with a simplistic void porosity model is that the primary strength-decreasing effect of the lithophysae is due to the formation of tensile splitting between neighboring lithophysae under compressive load. As porosity increases, the spacing between lithophysae decreases, and thus a greater propensity for tensile splitting at lower applied forces results due to the smaller solid bridges between voids.

The tensile splitting mechanism results in increasingly less-brittle post–peak response with increasing porosity. Additionally, the same matrix strength provides a reasonable fit to both nonlithophysal and lithophysal laboratory data (i.e., the void porosity is the primary driver in the mechanical properties reduction and not mineralogical differences in lithophysal and nonlithophysal rocks).

Further numerical testing was performed in which all of the actual lithophysal panel maps generated in the ECRB Cross-Drift (e.g., BSC 2004a, Appendix O) were discretized and used as compression test “specimens” for the calibrated model. As seen in Figure 4-10, the complex shape, size and distribution of lithophysal voids results in the same general failure mode (tensile splitting between voids) and same general trend of strength and modulus to void porosity (Figure 4-9); however, the variability tends to be greater primarily due to shape and distribution of voids. This is particularly true for samples whose lithophysal porosity is lower (e.g., around 10% to 15%). A few large voids with uneven distribution within a sample can result in lower strength, whereas widely spaced voids in a finite sample size can result in higher strength for the same sample with uniformly distributed voids.

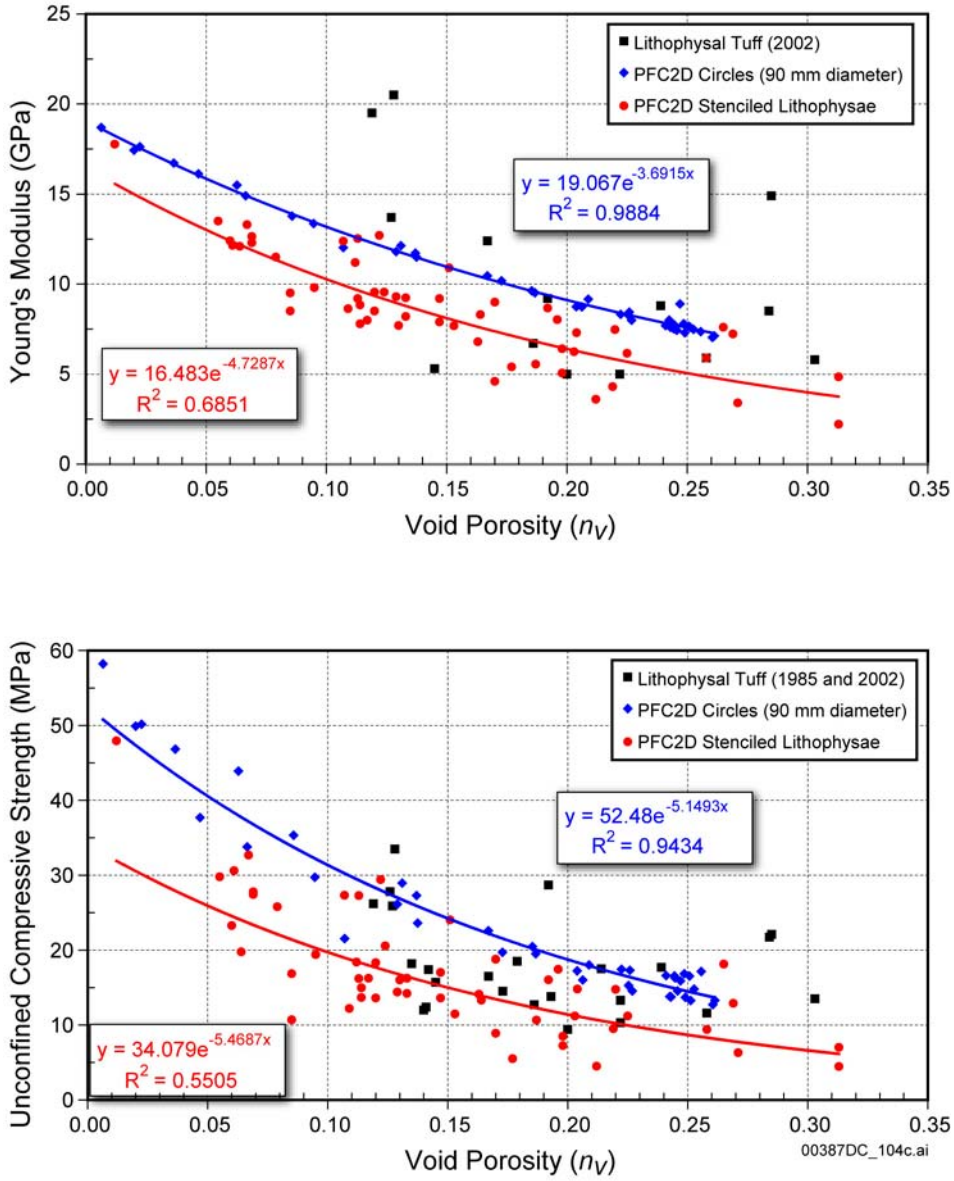

Source: BSC 2003a, Figures 9-22 and 9-23.

NOTE: Greater variability in the strength of the PFC samples for a given porosity is seen when true lithophysae shapes (stenciled) are introduced. This effect is particularly large at low porosities due to the greater variability of distribution and solid bridge lengths between lithophysae in a given sample volume. Test data is from large-core lithophysal tests and is the same as in Figure 3-12.

Figure 4-9. Plots Showing Data from Large Core Compression Testing of Tptpul and Tptpll Compared to Particle Flow Code Simulations Using Circular Shaped Lithophysae as well as Actual "Stenciled" Shapes from Enhanced Characterization of the Repository Block Panel Maps

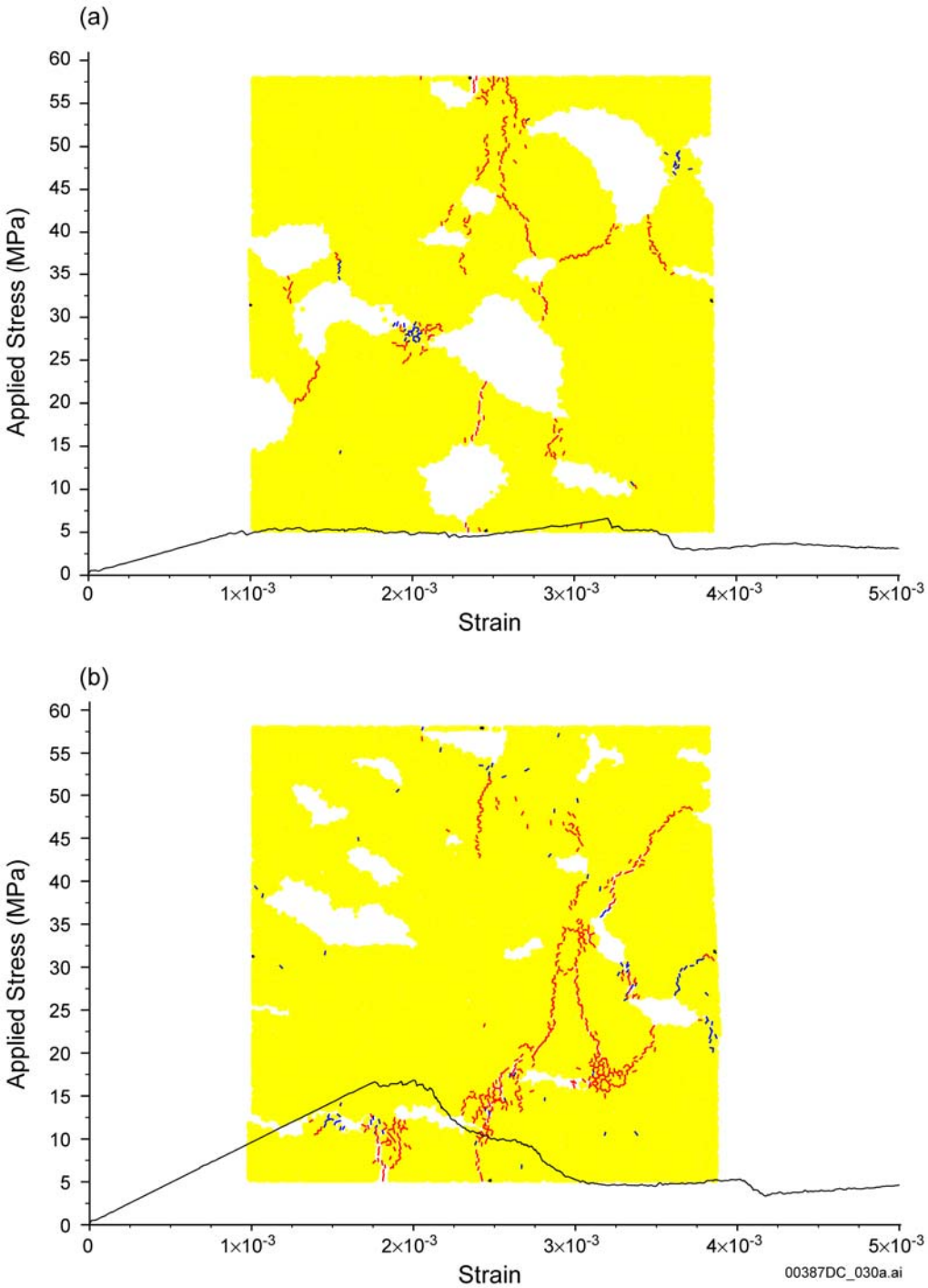

Source: BSC 2004j, Section 6.5.6, Figure 6.5-20.

Figure 4-10. Examples of Particle Flow Code Compression Tests Using Simulated Rock Specimens Developed by "Stenciling" Field Panel Maps in the Enhanced Characterization of the Repository Block

The result of all strength testing on both the simplest, circular void cases and the more complex, realistic shapes can be summarized as follows:

- The PFC model shows that the mechanism for strength reduction from nonlithophysal to intact rock results from tensile splitting of solid rock bridges between lithophysal voids. The smaller these rock bridges (i.e., the greater the porosity), the greater the strength reduction.

- The PFC model and laboratory data show a reasonable agreement with respect to strength and modulus change with lithophysal porosity. Strength and modulus show a generally logarithmic decrease with lithophysal porosity.

- Models with circular voids that are randomly distributed through the rock mass show less scatter and more uniform relation of mechanical properties to lithophysal porosity.

- Models with lithophysal voids with complex, irregular size and shape distribution show the same general trends as the circular void models, but with greater scatter of the strength or modulus. This scatter may partially account for the obvious size effect observed in the laboratory and in situ scale testing.

The conclusions from the PFC model calibration are that a viable tool has been developed for simulation of the mechanical response of lithophysal tuff to stressing and that this tool can be used, in addition to field and laboratory testing, to study variability in material response.

4.2.3.3 Extrapolation of Lithophysal Mechanical Response Using the Particle Flow Code Program

The calibrated PFC program is used as an extrapolation tool to examine the impact of lithophysae size, shape, porosity, and distribution on mechanical properties. Parametric studies have been conducted with simple (circular and triangular) lithophysae shapes, as well as with actual, complex shapes and distributions digitized directly from ECRB Cross-Drift panel maps. The results of these studies, shown in Figure 4-11, are used as a guide to understanding the variability of mechanical properties for a given porosity range. As seen in this plot, the results of the calibrated PFC shape studies from all ECRB Cross-Drift panels are overlaid on the large-core laboratory data for lithophysal rock showing the relationship of unconfined compressive strength to Young's modulus. Estimated upper and lower bounds of all the properties, including the results of the PFC extrapolations, are given on this plot. These upper and lower bounds are simply drawn to encompass all of the laboratory and extrapolated data, but the lines representing the bounding values are dashed outside the range of measured values. The range of data generated by the PFC extrapolations for size, shape, and distribution variability fall within the range of the laboratory testing with the exception of the highest levels of lithophysal porosity (e.g., less than 20%). It is seen that the saturated strength generally forms the lower bound of the data range, with a minimum strength value of approximately 10 MPa. The lower bound has been cut off at this 10-MPa strength level. This cutoff value is based on comparison of observations of current drift stability in the ECRB Cross-Drift and the ESF to drift-scale modeling studies performed assuming in situ stress conditions. Models indicate that extensive yield of the springlines of the ECRB Cross-Drift would be observed if the unconfined compressive strength

were below 10 MPa (BSC 2004a, Appendix E.4.1]). This is obviously not the case as the ECRB Cross-Drift shows stable conditions with generally unsupported sidewalls. Therefore, the PFC-extrapolated strength values below the laboratory data range appear to be related to local zones of high porosity. The impact of the spatial variability of lithophysal properties on drift-scale rock mass properties is discussed in Section 5.3.

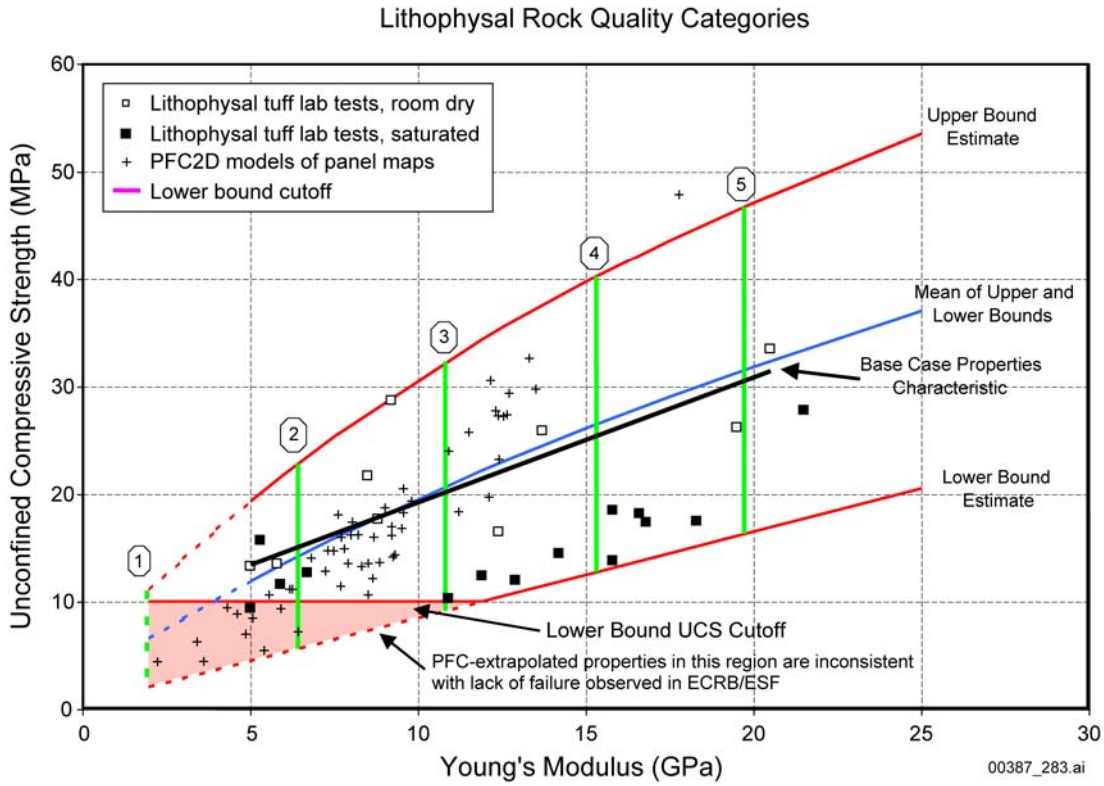

Source: BSC 2004a, Appendix E.4.1.

NOTE: The bounding curves are empirically derived to include all large core laboratory data, including 267-mm diameter saturated cores from Busted Butte. Base-case properties characteristic, derived from 305-mm diameter cores, are also shown. Extrapolated (PFC) strength values below 10 MPa are localized and inconsistent with observations of lack of yielding in ECRB Cross-Drift and ESF.

Figure 4-11. Estimated Upper and Lower Bounds of Unconfined Compressive Strength and Young's Modulus for Lithophysal Rock

4.2.4 Extrapolated Triaxial Behavior of Lithophysal Rock and Estimation of Rock Mass Constitutive Response

The previously described PFC calibration and analyses describe the basic comparison of the unconfined compression behavior and modulus of lithophysal rocks. As was discussed in Section 3, triaxial laboratory experiments have not been conducted on representative lithophysal samples due to the necessary size of the sample needed for lithophysal rock and the associated difficulties in obtaining pressure vessels and confining jacketing systems for samples with cavities.

An understanding of the confining pressure response is necessary for verification or for determination of a proper yield criteria for the lithophysal rocks to develop an understanding of how the basic rock mass failure parameters (rock mass cohesion, angle of internal friction, and dilatancy) are affected by lithophysal porosity. UDEC, a discontinuum program, similar in many respects to PFC, is used for this purpose due to its more general particle shape capability. The circular particle geometry employed by PFC simplifies the numerical algorithms, making it a good tool for conducting many parameter studies as shown in the previous calibration studies. However, the particle geometry also restricts the ability to examine post–peak failure mechanisms in detail due to dilational response of a circular particle model—this is not the case for the more general UDEC approach.

A series of uniaxial (extension and compression), triaxial compression experiments was conducted on the modeled samples, with circular lithophysal voids added randomly to create porosities of 10.3%, 17.8%, and 23.8%. These porosity values cover the approximate range of lithophysal porosity that spans the range of rock strength categories observed in the field panel maps. Figure 4-12 shows an example stress strain response for the case of 17.8% lithophysal porosity. The stress strain response for tensile testing and compression at a number of confining pressures are shown. Adjacent to each of the stress-strain curves is a figure of the sample in the failed state. Rock failure results from fracturing between the voids in a similar fashion as that demonstrated previously for the PFC modeling.

The general behavior is typical for brittle rock materials—increasing strength with confinement and conversion of the failure mode from axial splitting (in unconfined compression) to shear failure as the confining pressure increases. The material response is elastic-brittle at low confinement and elastic-plastic at higher confining levels.

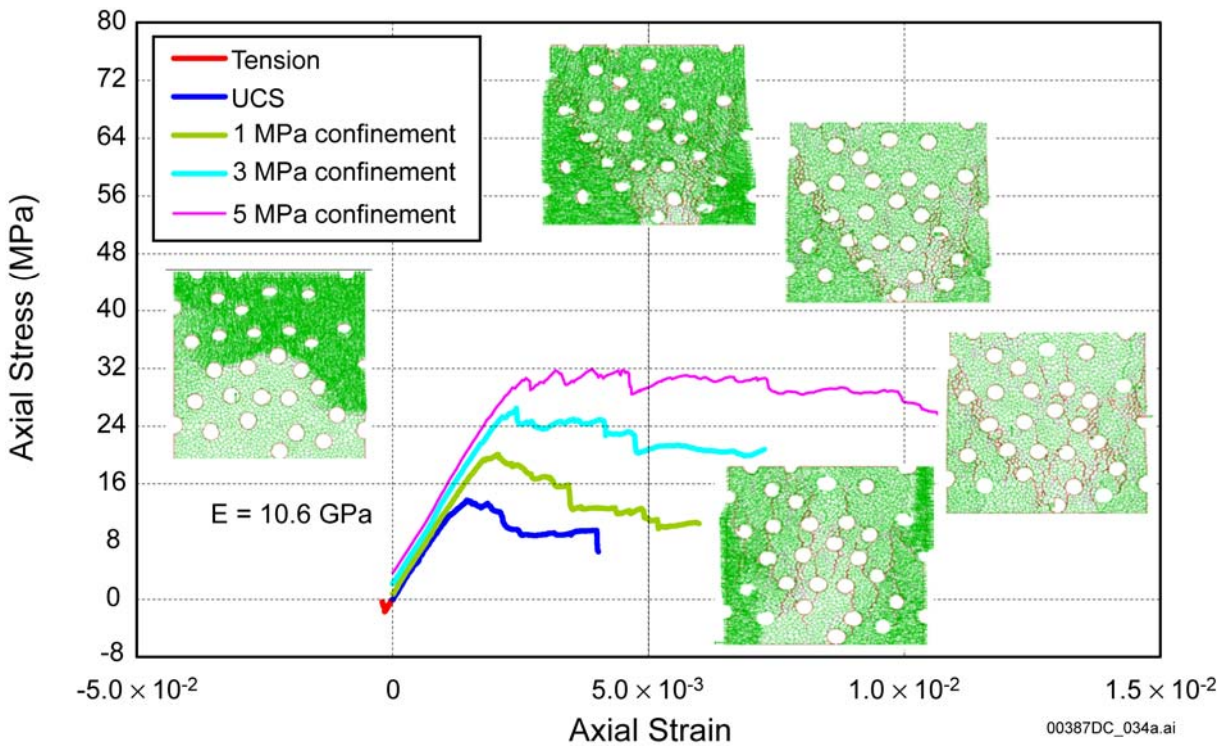

Source: BSC 2003a, Figure 9-34.

NOTE: Failure state of "samples" showed failed state for a particular confining pressure: counterclockwise from left are direct tension, unconfined, 1, 3 and 5 MPa confining stress, respectively. Circular voids distributed randomly throughout the sample.

Figure 4-12. Stress-Strain Response and Failure Mechanisms for Lithophysal Porosity of 17.8% as Predicted by the UDEC Model

4.2.5 Estimation of Linear and Nonlinear Failure Envelopes

The UDEC peak strength values for the numerical testing results can be used to construct traditional failure envelopes for the nonlithophysal as well as lithophysal samples. Figure 4-13 shows the peak strength values plotted in principal stress space with approximate Mohr-Coulomb (linear) and Hoek-Brown (nonlinear) failure envelopes fit to the results. Note that in each case, multiple UDEC simulations were made for each minimum principal (confining) stress level in which different random distributions of UDEC grain structure were used. The Mohr-Coulomb and Hoek-Brown strength parameters derived from the fits to these data are given in Table 4-3.

As seen, the primary effect of increasing lithophysal porosity is a reduction in the unconfined compressive and tensile strength components. There is little apparent impact of lithophysal porosity on the internal angle of friction of the material, which appears reasonable from a physical standpoint. These data can be used for definition of failure properties of the rock mass for performance analyses.

As seen in Figure 4-13, the best-fit Hoek-Brown envelopes (Hoek 2000, p. 179) for the UDEC simulations, yield nearly the same principal stress relations as the linear Mohr-Coulomb envelopes in the range of confining stresses given here.

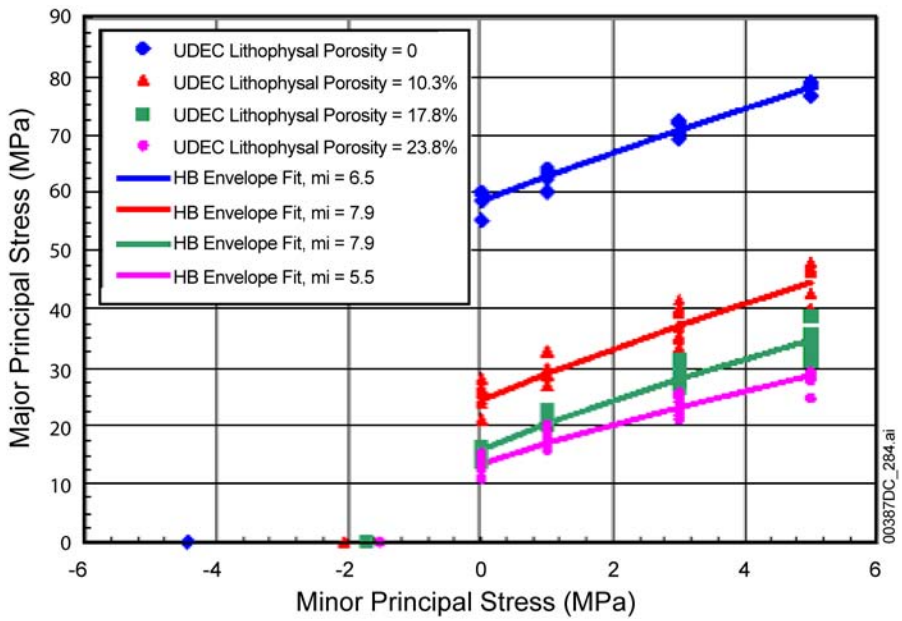

Source: BSC 2003a, Figure 9-40.

NOTE: HB = Hoek-Brown

Figure 4-13. Hoek-Brown Failure Envelopes Based on UDEC Simulations for Various Lithophysal Porosities

Table 4-3. Summary of Average Strength and Modulus for Variation In Lithophysal Porosity and Mohr-Coulomb (Linear) and Hoek-Brown (Nonlinear) Yield Criteria Parameters as Derived from UDEC Simulations

Lithophysal Porosity (%)	Estimated UCS (MPa)	Estimated Young's Modulus (GPa)	Estimated Friction Angle (°)	Estimated Cohesion (MPa)	Estimated Hoek-Brown UCS (MPa)	Estimated Hoek-Brown m_i
0	58.7	19.8	36	14.9	58.5	6.6
10	25.1	14.2	36	6.4	25.1	7.7
17	15.5	11.2	35	4.1	16.5	7.3
24	13.2	9.3	29	3.9	14.0	5.0

Source: BSC 2003a.

NOTE: Friction angle and cohesion are derived from best-fit linear envelope to data. Hoek-Brown "s" value is assumed to be 1 in deriving the Hoek-Brown estimated UCS values in this table, as the simulations are assumed to represent "intact" samples. Lithophysal porosities in this table can be related to in situ Tptpll rock mass properties categories via Figure 4-5. UCS = unconfined compressive strength.

4.2.6 Summary of Material Model Development

The following summarizes the material model and properties for analysis:

- A set of base-case rock mass strength and moduli were developed from large core laboratory testing. The properties were subdivided into a series of categories that span the range of in situ lithophysal porosities/rock qualities. These categories were related to approximate lithophysal porosities observed in existing tunnels at the Yucca Mountain site (Figure 4-5), providing a link between observation and rock quality. This data provides the basis for design and performance parameter analyses and for establishing an understanding of uncertainty in the analyses.

- The PFC and UDEC programs were calibrated to reproduce the basic strength and moduli as functions of lithophysal porosity as well as to provide a basic understanding of the mechanics of yield in this material. The models were used to extrapolate the mechanical properties for lithophysal rock masses over the range of in situ conditions determined from field mapping. These generated-data provide an estimate of the range of variability of the properties.

- Standard forms of yield conditions for rock masses (Mohr-Coulomb and Hoek-Brown) were fit to the laboratory and model extrapolation data, and their standard strength parameters were determined. This information, combined with the unconfined compressive strength and modulus ranges, provides the basis for development of drift-scale stability simulation models.

The material model can now be embedded into a general numerical method that is capable of simulating drift-scale problems and estimate rock mass degradation. This is described in the next section.

4.2.7 Development and Validation of a Drift-Scale Modeling Method for Lithophysal Rock Using the UDEC Program

Although the UDEC program has been shown to provide reasonable agreement to large-scale laboratory compression testing of lithophysal rock, it is not practical to attempt to model a full drift-scale problem with explicitly represented lithophysal cavities. The model would be excessively large with correspondingly large computational run times. However, it is not necessary to attempt to model individual lithophysae as long as the overall mechanical response of the rock mass behaves according to the material models and their strength and deformability parameters derived in the previous section.

Development of the drift-scale modeling approach for lithophysal rock requires calibration. The method used here is, first, to calibrate the rock mass material model and mechanical properties such that the UDEC discontinuum program (without explicit voids) is able to reproduce the observed large-scale laboratory moduli and strength behavior. Next, the model is validated against (1) observations of failure mechanism in the laboratory, (2) field observations of tunnel response in the ECRB Cross-Drift, and (3) thermally induced fracture development in the DST conducted in the ESF in the Tptpmn unit.

Figure 4-14 provides a flow chart illustrating the calibration and validation strategy for the drift-scale UDEC model. The following section describes the validation of the UDEC model and exploration of its limitations.

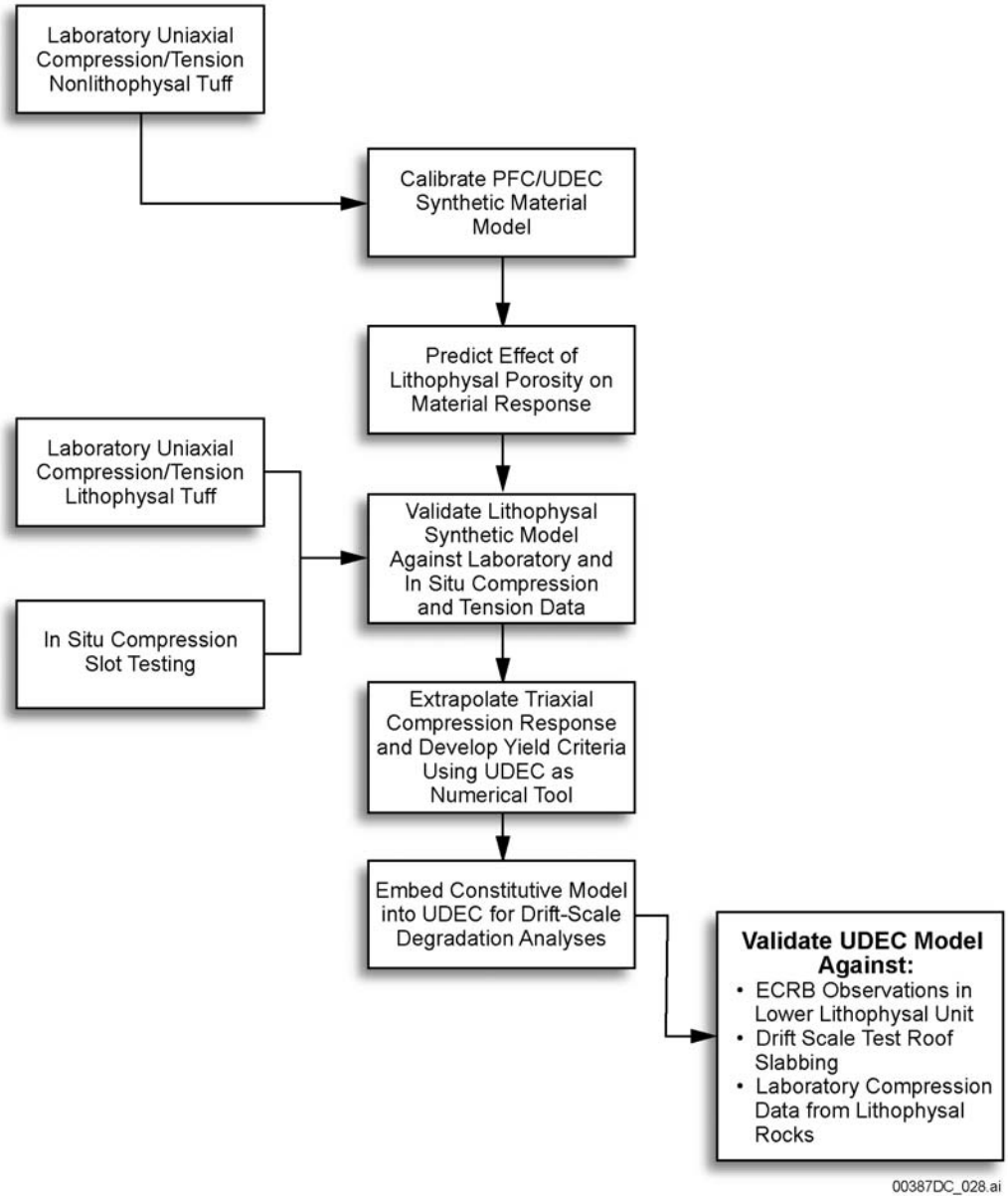

Figure 4-14. General Approach to Validation of Mechanical Material Model for Lithophysal Rocks

4.2.7.1 Drift-Scale Model Calibration

The drift-scale UDEC lithophysal model represents the rock mass as an assembly of polygonal, elastic blocks (Figure 4-15) bonded together across their boundaries to form a coherent solid. The goal is to provide a rock mass in which the overall mechanical behavior of the mass is consistent with the material model developed for the lithophysal rock, yet allow internal fracturing to form and blocks to loosen and detach as the evolving thermal and dynamic stress state dictate. In other words, the fractures are “invisible” to the model until yielding begins.

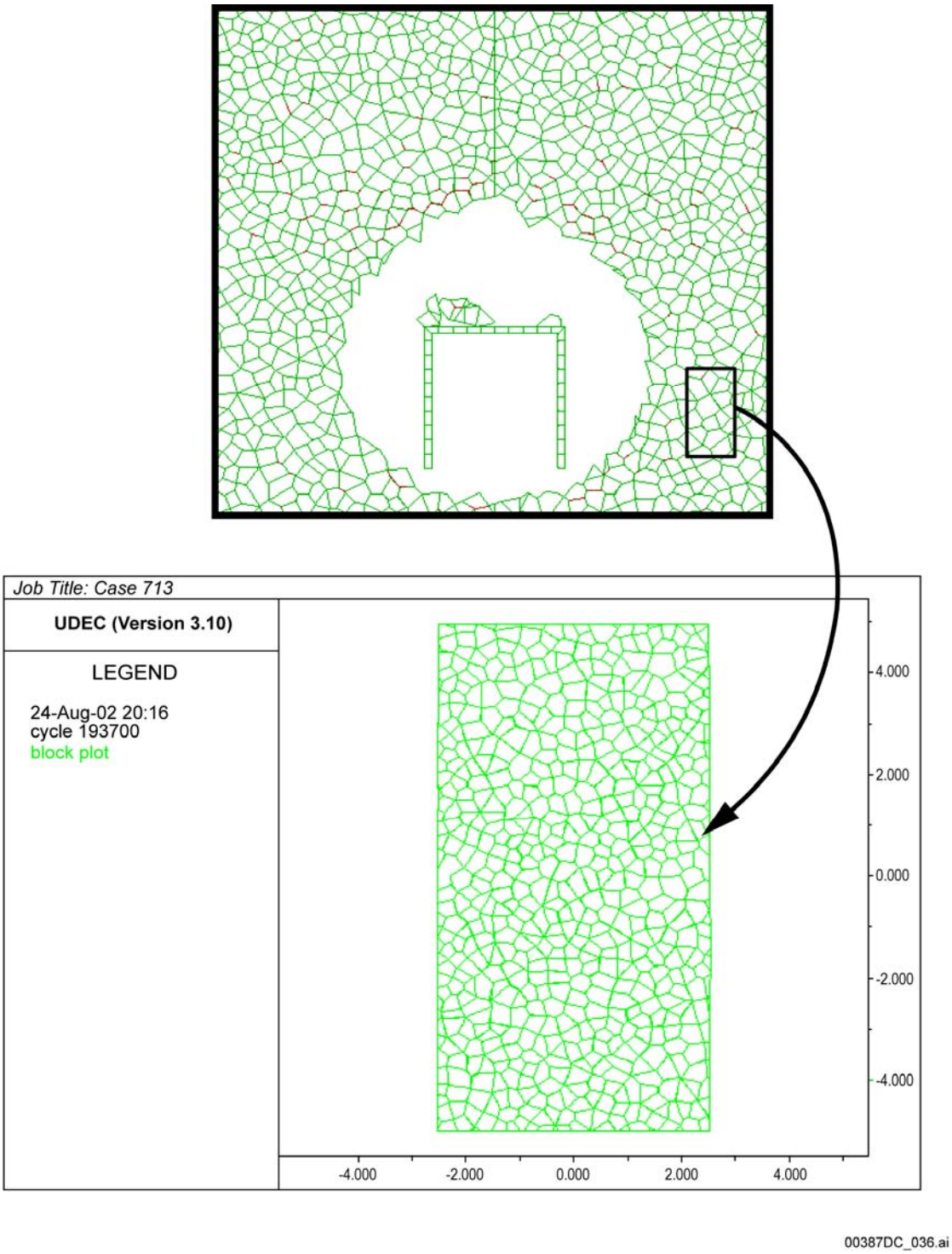

Source: BSC 2004a, Figure 7-20.

NOTE: Blocks are bonded at their contacts with a cohesion and tensile strength. When these break, the contacts become purely frictional. Specimen is "sampled" from equivalent rock mass representing the Tptpll.

Figure 4-15. UDEC Lithophysal Rock Specimen Composed of Many Irregular Blocks with Roughly Equal Side Lengths

Following calibration, the model can be used to conduct additional simulations under biaxial compression and tension to produce the yield criteria for the material, which can then be compared to that generated using the grain-scale models with explicitly modeled lithophysae in Section 4.2.4. Further details on the UDEC model calibration can be found in *Drift Degradation Analysis* (BSC 2004a).

4.2.7.2 Validation of the Numerical Model

Once calibrated, the UDEC model and its constituent properties require validation against field observations and testing. The model was validated against laboratory failure mechanisms and drift scale response through:

- Comparison of lithophysal test specimen failure mechanisms in the laboratory
- Comparison of the prediction of drift scale fracturing in the Tptpll at ECRB Cross-Drift depth to observations of tunnel sidewall fracturing in the ECRB Cross-Drift
- Comparison of roof spalling in the DST in the Tptpmn during thermal overdrive experiments to UDEC model predictions
- Comparison of several different numerical modeling techniques to UDEC for a field simulation of a liner-reinforced tunnel to dynamic loading from a blast.

The details of the validation comparisons are given in *Drift Degradation Analysis* (BSC 2004a). The validation tests showed that:

- The model is capable of reproducing the basic axial splitting fracturing and failure mode of lithophysal samples observed in uniaxial compression, while reproducing the proper strength and moduli.
- The model is capable of reproducing the springline shear fracturing observed occasionally in the Tptpll in the ESF and ECRB Cross-Drift. Figure 4-16 shows a photograph of the wall-parallel fractures occasionally observed in the large-diameter holes drilled for sampling at the springline. Although not common, this form of localized yielding has been observed in a few boreholes in the Tptpll. This form of fracturing behavior, typical of local in situ stress-related yield in hard rocks, is found only directly at the springline and extends to a depth of about 0.5 m into the sidewall. Due to the high vertical-low horizontal stress state, the greatest stress concentration occurs at this location directly at the springline. The UDEC model reproduces the local wall-parallel fractures and yield for strength Category 1, representative of localized, high porosity material. The model shows no fracturing for strength categories 2 or higher. This is consistent with the typical condition within the ESF and ECRB Cross-Drift, which shows no observation of sidewall yield. This observation is also consistent with the general lithophysal porosity mapped within the ECRB Cross-Drift (Figure 4-5), showing that the mean porosity is indicative of a strength category of 3, with about 97% being greater than a Category 1. In other words, the small number of observations of

sidewall spalling is consistent with the relatively infrequent occurrence of low strength categories.

- The model is capable of reproducing the roof crown spalling behavior observed during the thermal overdrive portion of the DST in the Tptpmn. In this test, the rock mass temperatures were driven to approximately 200°C at the conclusion of the test, at which time minor spalling in the form of plate-shaped fragments was observed in the crown of the tunnel. The UDEC model was calibrated against the large-sample strength (Figure 3-5) and in situ modulus (from plate bearing tests) of the Tptpmn in a similar manner to that described above for the Tptpll. The DST was modeled by imposing the in situ stress state and temperature history (as determined from field temperature measurements) onto the model. The roof crown-parallel fracturing extent and apparent mechanism were reproduced at the proper temperature levels without need for adjustment of properties (Figure 4-17). It was found that the fracturing was the result of the large horizontal, thermally induced stresses in the immediate roof. The crown is placed in a state of uniaxial compression, and when this stress reaches the strength of the material, extensional, wall-parallel fracturing occurs over a limited roof span. The system equilibrates when fracturing extends to a short depth.

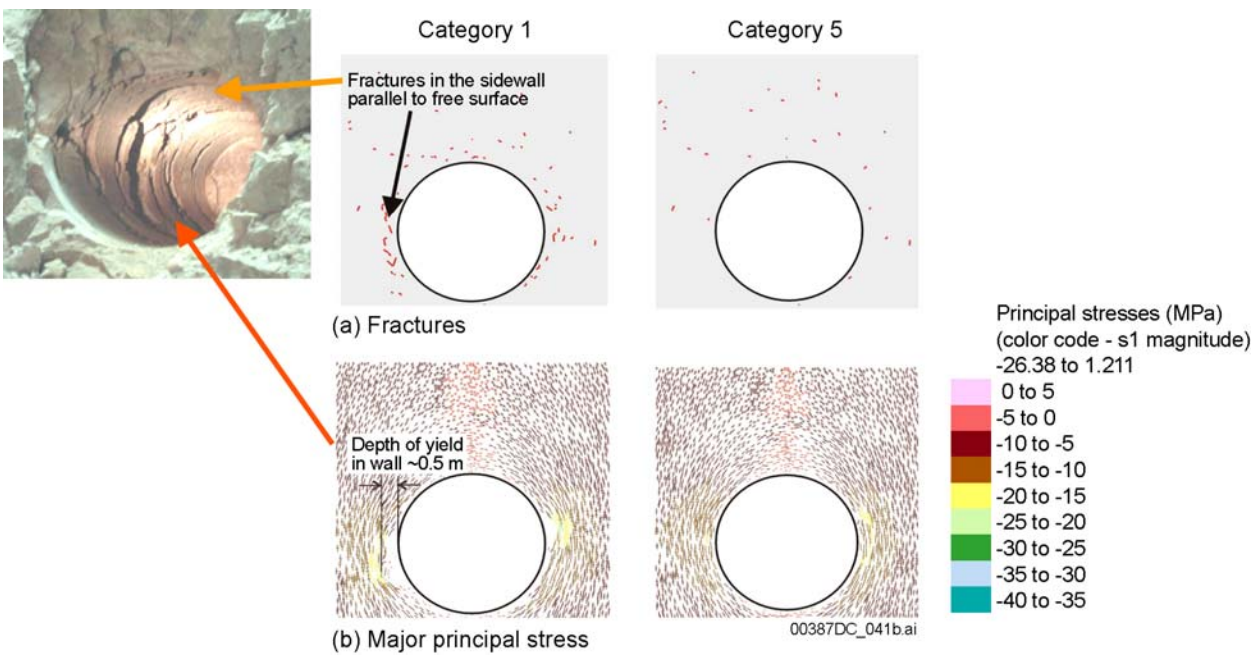

Source: BSC 2004a, Figure 7-28.

NOTE: The model shows that sidewall fracturing and yield does not occur for strength categories 2 or higher, which is consistent with the general observation of no sidewall fracturing. Localized fracturing is occasionally observed to a sidewall depth of about 0.5 m. The model reproduces wall-parallel springline fracturing to the proper sidewall depth for the lowest strength category only.

Figure 4-16. Validation of the UDEC Numerical Approach for Lithophysal Rock against Observation of Springline Wall-Parallel Fracturing in the Exploratory Studies Facility and Enhanced Characterization of the Repository Block

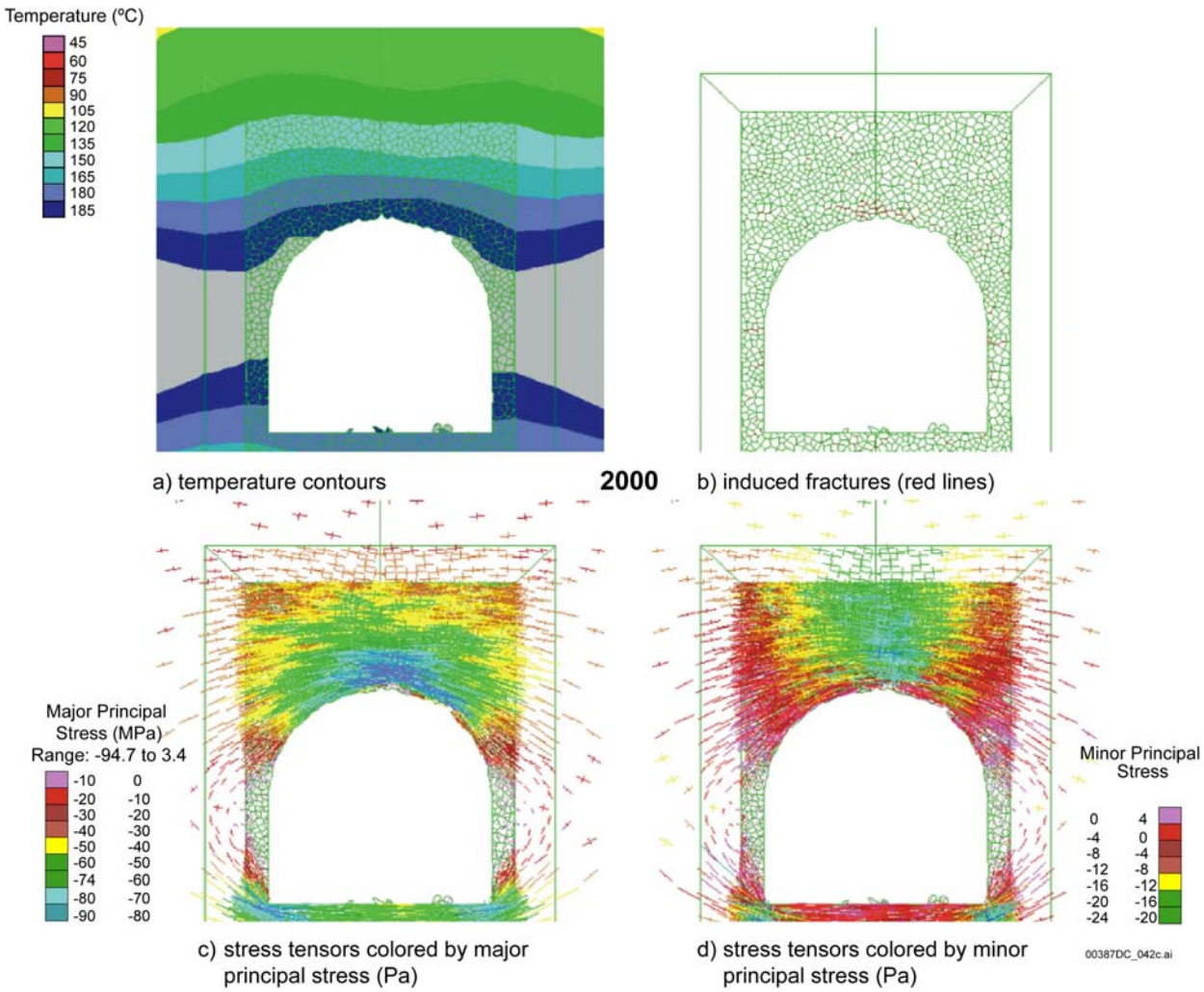

Source: DTNs: MO9807DSTSET01.000; MO9906DSTSET03.000; MO0001SEPDSTPC.000; MO0007SEPDSTPC.001; MO0107SEPDSTPC.003; MO0202SEPDSTTV.001; MO0002ABBLSLDS.000.

NOTE: Temperatures (a), fractures (b), minimum principal stress (c), and maximum principal stress (d). Temperatures were obtained from field thermal measurements; fracture and stress levels were predicted from the UDEC model. Conditions represent 3 years of heating in the heated drift. The temperature contours and induced fractures in (a) and (b) are outcomes of the model.

Figure 4-17. Results from Heated Drift Analysis with Temperature Conditions after 3 Years of Heating

4.3 ROCK MASS MODELING APPROACH FOR GROUND SUPPORT ASSESSMENT AND DESIGN

Postclosure modeling methods used for nonlithophysal and lithophysal rock masses, described in Sections 4.1 and 4.2, respectively, are based on the use of discontinuum numerical methods. These methods represent the rock mass as being composed of elastic rock blocks separated by fracture planes. Strength and modulus properties are assigned separately to the blocks and the fractures and the model accounts automatically for the interaction of blocks across the fractures and shearing or tension failure of the fractures during the simulation of applied stresses.

Another, more common approach to modeling fractured rock, is as a continuum material in which fractures are not modeled explicitly. Instead, the continuum model is assigned rock mass elastic and strength properties that include the overall effect of fractures and solid rock. Both approaches—continuum and discontinuum—produce the same approximate results (i.e., stress distributions and deformation, depth of yield, overall assessment of stability) as long as equivalent properties are used. The type of modeling approach used depends on the objectives of the modeling. Discontinuum methods, as used for postclosure analysis, are required in this application since the objective is to calculate estimates of size and amount of rockfall and the ultimate profile of the tunnels in response to in situ, thermal and seismic loading. Since continuum models do not explicitly represent fractures and their impact on rockfall, they are not capable of providing the information required for assessment of postclosure issues. However, for general assessment of excavation stability and ground support design, the continuum approach is reasonable, and has the advantage of simpler model setup and shorter analysis time.

A number of the RDTME Key Technical Issue agreements deal with preclosure issues and, specifically, with the assessment of rock mass properties and modeling methods for ground support design and analysis (e.g., Appendices B, D, F, G, and H). In these appendices, a summary of analyses performed with continuum-based numerical models for assessment of preclosure drift stability and ground support design is given. Rock mass properties for the lithophysal rock for these analyses are derived from the analyses presented in Section 4.2, and, specifically, the rock mass categories and strength and modulus ranges summarized in Figure 4-11.

Rock mass properties for the fractured nonlithophysal rock for these analyses were derived from the commonly used estimation method of Hoek and Brown (e.g., see Hoek, 2000). This method involves deriving estimates of rock mass mechanical properties from geotechnical rock mass classification, along with results from laboratory mechanical strength testing. The detailed derivation of the rock mass properties is described in detail in *Subsurface Geotechnical Parameters Report* (BSC 2003a, Section 8.5.2), and summarized here.

Using the Q rock quality designation system described by Hoek (2000), the U.S. Bureau of Reclamation and U.S. Geological Survey conducted geotechnical mapping of the Tptpmn in the ESF and ECRB Cross-Drift during the geological mapping immediately behind the advancing TBM. From the rock quality classification, the Hoek–Brown geologic strength index (GSI) was determined. Rock mass moduli, rock mass strength, and both Hoek–Brown and Mohr–Coulomb failure criteria parameters are derived from the GSI. Details of the relationships between the GSI, the rock mass modulus, compressive strength, and failure criteria parameters can be found

in *Subsurface Geotechnical Parameters Report* (BSC 2003a) or in the description of Hoek (2000). The results of these calculations show that the GSI for the Tptpmn follows a typical normal distribution with mean value of 59, a median rock mass modulus of 17 GPa and median rock mass compressive strength of 44 MPa. Table 4-4 provides a summary of the estimated in situ rock mass properties derived from the Hoek–Brown approach. For parametric evaluation, the variability of rock mass quality has been subdivided into five categories at 10th, 30th, 50th, 70th, and 90th percentile of the cumulative probability of occurrence within the Tptpmn.

Table 4-4. Rock Mass Mechanical Properties Estimates for the Tptpmn

Rock Mass Parameter	Rock Quality Category 1	Rock Quality Category 2	Rock Quality Category 3	Rock Quality Category 4	Rock Quality Category 5
Associated Cumulative Probability of Occurrence	10%	30%	50%	70%	90%
Rock Mass Cohesion, C (MPa)	7.6	8.7	9.5	10.4	11.8
Rock Mass Internal Angle of Friction, ϕ (degrees)	40	42	44	45	47
Rock Mass Compressive Strength, σ_{cm} (MPa)	33.5	39.7	44.4	49.5	57.7
Rock Mass Modulus, E_m (GPa)	10.3	13.7	16.7	20.2	26.2
Rock Mass Quality Parameter, Q_p	2.1	3.6	5.3	7.7	12.6
Hoek-Brown Geologic Strength Index, GSI	50	55	59	62	67

Source: BSC 2003a, Table 8-41.

5. ANALYSIS OF PRECLOSURE AND POSTCLOSURE DRIFT DEGRADATION UNDER GRAVITATIONAL, THERMAL, AND SEISMIC LOADING

5.1 INTRODUCTION

As discussed in Section 1, there are four primary mechanisms for drift degradation in the preclosure and postclosure time periods. These include rock mass yield and potential instability resulting from: (1) stresses induced by in situ gravitational loading, (2) stresses induced by waste package heat generation, (3) stresses and shaking induced by seismic ground motion, and (4) time-dependent strength loss from stress corrosion mechanisms. Drift degradation is defined here as the physical impact of the potential mechanical yield of the rock mass surrounding the emplacement drifts to application of these stresses or time-dependent strength change. A series of numerical calculations are discussed here that are aimed at predicting the drift degradation in physical terms that are easily understood:

- The extent and character of the fracturing around the emplacement drift tunnels as a function of time and stressing
- The character of rockfall that may occur as a result of this fracturing and the associated gravitational and seismic accelerations, including the size distribution of particles, the mass of the particles, and their velocities
- The evolution of the shape of the emplacement drifts and the dislodged rock as functions of loading and time.

To provide these results, it is necessary to use numerical modeling techniques that allow representation of preexisting rock structure and that represent fracturing explicitly, as described in Section 4. Thus, reliance is placed on the use of discontinuum numerical methods that allow displacement on preexisting rock mass structure and rock fracturing in a realistic fashion.

The following sections give a discussion of the modeling of emplacement drift stability and rockfall subject to postclosure loading. In addition, a description of the analysis of time-dependent drift stability is given. Due to the different modeling techniques required for nonlithophysal and lithophysal rock masses, the results are described separately.

5.2 PRECLOSURE GROUND SUPPORT ISSUES

Mechanical degradation analysis of the unsupported emplacement drift openings for an assumed 100 years of normal operation (Williams 2003) has shown that the drifts will remain intact and not collapse without engineered ground support (BSC 2003c). Those calculations consider static gravitational and thermal loads. The emplacement drift ground support, consisting of perforated stainless steel sheets (2 mm to 3 mm thick) and stainless steel friction rock bolts, is provided primarily for worker safety and to ensure the retrieval option.

The impact of in situ stress and preclosure rock temperatures on stability of unsupported tunnels was examined, as well as seismic events of 5×10^{-4} and 1×10^{-4} per year frequency of occurrence (or return periods of 2,000 and 10,000 years, respectively). Section 5.3 provides details of these calculations. Rockfall induced by preclosure seismic events was also estimated

to support the evaluation of the safety class of the ground support. These analyses were used to identify the largest potential rock size that could fall on a waste package (assuming no ground support). The results of these calculations were used to confirm that the waste package design was sufficient to preclude a breach of the waste package for the resulting rockfalls, and, thus, the ground support was classified as not important to safety (BSC 2004k).

Although this document primarily addresses postclosure performance issues, a number of the appendices discuss the ground support analyses in detail. Table 1-1 provides a list of NRC KTI agreements and the sections or appendices that discuss the associated issues. Most of these agreements deal with rock properties and modeling methods that apply to both the preclosure and postclosure drift degradation and seismic analyses.

5.3 ANALYSIS OF PRECLOSURE AND POSTCLOSURE DRIFT DEGRADATION

5.3.1 Emplacement Drift Degradation from In Situ and Thermal Stressing Effects

Thermal-mechanical modeling was performed to define drift stability under combined in situ and thermally induced stresses. Temperatures within the rock mass are determined from thermal analysis conducted using the NUFT program (LLNL 2002), which accounts for the details of heat transfer mechanisms within the drift, including heat removal due to ventilation in the preclosure period. The NUFT approach is two-dimensional, and thus assumes a cross section through a series of infinitely long emplacement drifts. Thus, this type of approach adequately represents the developing temperature distribution around emplacement drifts located centrally within the repository.

To examine three-dimensional geometric effects (which include both repository edge effects and topographic influences) on the temperature distribution, the FLAC3D (BSC 2002e) regional and local-scale models are used (Figure 5-1). Here, the heat flux into the rock mass at each tunnel, obtained from the NUFT program, is distributed over the plane of the repository as a function of time. The resulting temperature distributions are then used in drift-scale two- and three-dimensional models to determine the thermally induced stress state as a function of time. The details of the thermal-mechanical calculations are described in detail in *Drift Degradation Analysis* (BSC 2004a, Section 6.2 and Appendix C).

Three major cases of the drift-scale thermal calculation were carried out:

- **Case 1**–Base-case calculation with 1.45 kW/m initial heat load and 50-year preclosure ventilation (90% heat removal ratio, BSC 2004l, Section 5.1). Preclosure maximum may be 100 years, but base case is 50 years of ventilation.

- **Case 2**–Sensitivity calculation for thermal properties of repository rock material (Tptpll) with 1.45 kW/m initial heat load, 50-year preclosure ventilation, and 90% heat removal ratio. Values of thermal conductivity and specific heat one standard deviation less than the mean values were used:

- Thermal Conductivity (DTN: SN0208T0503102.007): 1.64 W/m·K (= 1.89 W/m·K – one standard deviation (0.25 W/m·K)) for wet conditions and 1.03 W/m·K (= 1.28 W/m·K – one standard deviation (0.25 W/m·K)) for dry conditions).

- Heat Capacity: 811 J/kg·K (= 954 J/kg·K – one standard deviation (143 J/kg·K)).

- **Case 3**–Sensitivity calculation for heat removal ratio. A heat removal ratio of 70% was used for the preclosure ventilation. This level is significantly below the estimated heat removal ratio during ventilation and examined only for the purpose of investigating preclosure ventilation rates. Figure 5-2 shows the linear heat load into the rock mass for each of these cases.

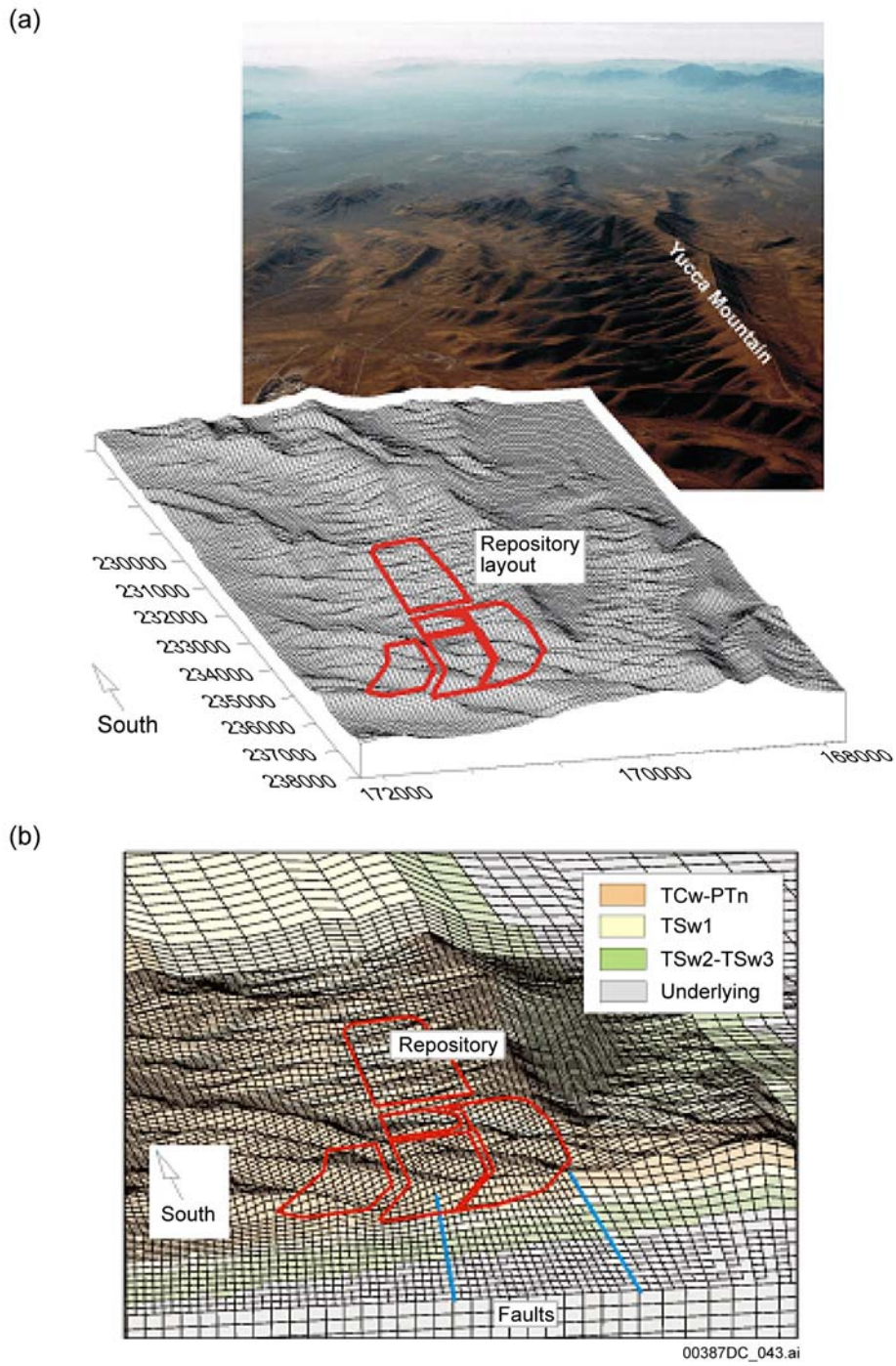

Source: BSC 2004a, Figure C-1.

NOTE: (a) View is toward south. (b) Repository panel outline is superimposed.

Figure 5-1. Aerial View of the Yucca Mountain Site and Digital Elevation Calculation Created from Topographic Information (a) and View of the Regional-Scale FLAC3D Thermal-Mechanical Model Constructed from the Digital Elevation Calculation and Available Geologic Information (b)

Temperature histories at the drift crown for all the cases of the thermal calculations are presented in Figure 5-3. The results exhibited the temperature increase from base case (Case 1) to sensitivity calculations (Cases 2 and 3). In particular, Case 3 showed a significant temperature increase at the preclosure period. The peak temperature for Case 1 was 138°C at around 75 years, while Cases 2 and 3 were 161°C and 153°C at around 75 years, respectively.

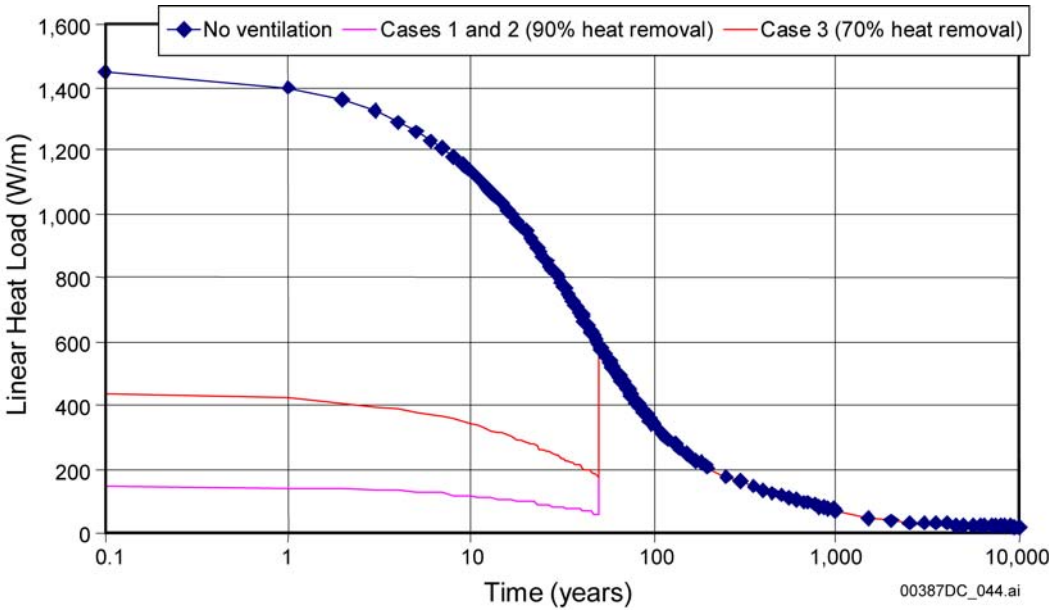

Source: BSC 2004a, Figure 6-31.

NOTE: The no ventilation curve is from BSC 2003g. Cases 1 and 2 use the 90% heat removal curve, while Case 3 uses the 70% heat removal curve.

Figure 5-2. Heat Decay Curves for Thermal Calculations

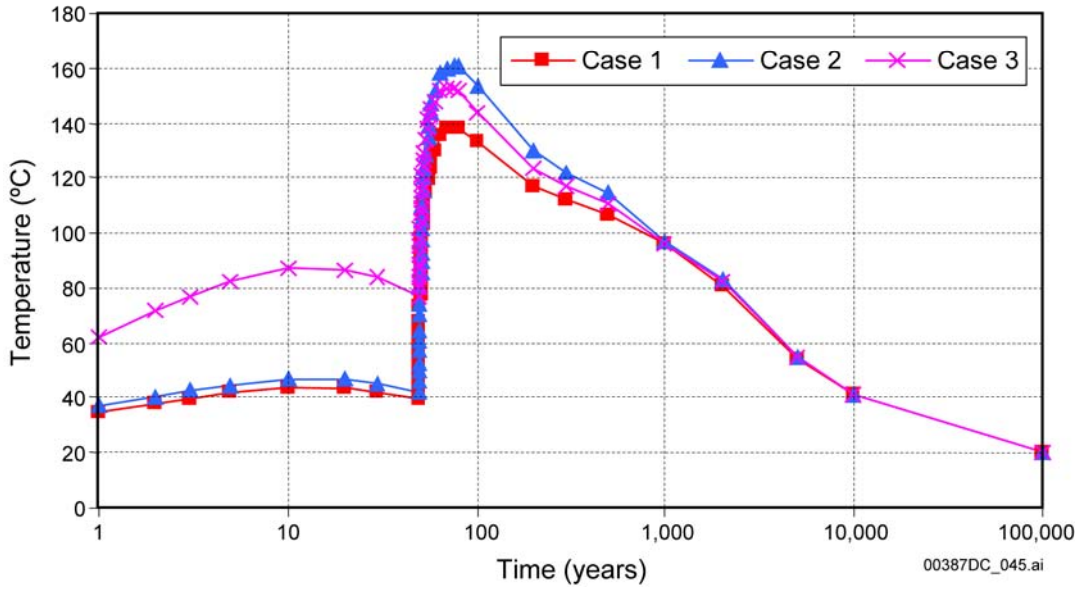

Source: BSC 2004a, Figure 6-32.

NOTE: This graphic assumes a 1.45 kW/m linear heat load and 50 years of preclosure ventilation.

Figure 5-3. Temperature History at the Drift Crown Due to the Linear Heat Load Presented in Figure 5-2

A comparison of temperature histories in the drift crown for Case 1, as determined in the drift-scale calculation (NUFT) and the coupled regional- and local-scale calculations (FLAC3D), is quite good, with the conditions in the middle of the repository representing the most conservative conditions. Details of these calculations are given in *Drift Degradation Analysis* (BSC 2004a).

A series of thermal-mechanical calculations are performed initially for the range of lithophysal and nonlithophysal mechanical rock properties (Table 4-2) to examine the potential for yield and degradation due to in situ stress and thermal loading alone.[14] The drift-scale UDEC model described in Section 4.2.7 is allowed to equilibrate under initial stress conditions, followed by application of the rock mass temperature history derived from the NUFT program. The nonlithophysal rock mass shows no thermally induced yield because the stresses are significantly below the yield condition of the rock mass (BSC 2004a). An example of the model output from the lithophysal rock, Case 1 thermal history is shown in Figure 5-4. Here, the temperature distribution and major and minor principal stress trajectories are plotted at 80 years (peak temperature and thermally induced stress for case of 50-year forced ventilation and closure) and 10,000 years near the completion of cool-down.

The in situ gravitational and thermally induced principal stress history paths for a series of radially oriented points, starting at the drift crown and springline and continuing into the rock mass, are given in Figures 5-5, 5-6, and 5-7 for the lithophysal rock mass. These figures represent the results of a number of thermal-mechanical simulations in which the rock mass temperatures given by Case 1 above are applied to an emplacement drift excavated and

[14] Impact of time-related strength degradation mechanisms are examined in Section 5.3.3.2.4.

equilibrated at the in situ stress condition. The path that the stress state then takes as a function of time as the rock mass is heated and cooled down over a 10,000-year time period are then given. The rock mass is assumed to have the moduli representative of the lowest quality lithophysal rock (Category 1, Figure 5-5), the highest quality lithophysal rock (Category 5, Figure 5-6) and the base case quality lithophysal rock (Category 3, Figure 5-7).

The calculations assume an elastic rock mass, but the associated failure envelope is superimposed on the principal stress history paths to allow estimation of the extent of failure into the rock mass as a function of time. As seen in these figures, the lowest quality (highest porosity-approximately 3% of the Tptpll) lithophysal rock indicates a small zone of yield of approximately 0.25 m directly at the springline of the tunnels from in situ stress. The depth of this yield zone changes only slightly from the thermal stresses and does not impact the overall stability of the tunnels. This small yield zone is the same as that discussed in Section 4.2.7.2 regarding calibration of the UDEC modeling approach.

Simulations for the lower porosity lithophysal rock (Category 5–approximately 30% of the Tptpll) indicate minor yielding of less than 0.25 m in the crown, whereas the base-case quality lithophysal rock (approximately 35% of the Tptpll) shows no failure. The conclusions from these analyses show that no significant yield or ground collapse mode is evident for emplacement drifts in either lithophysal or nonlithophysal rocks during the preclosure or postclosure time frames due to in situ or thermally induced stressing alone (i.e., in the absence of time-dependent strength change).

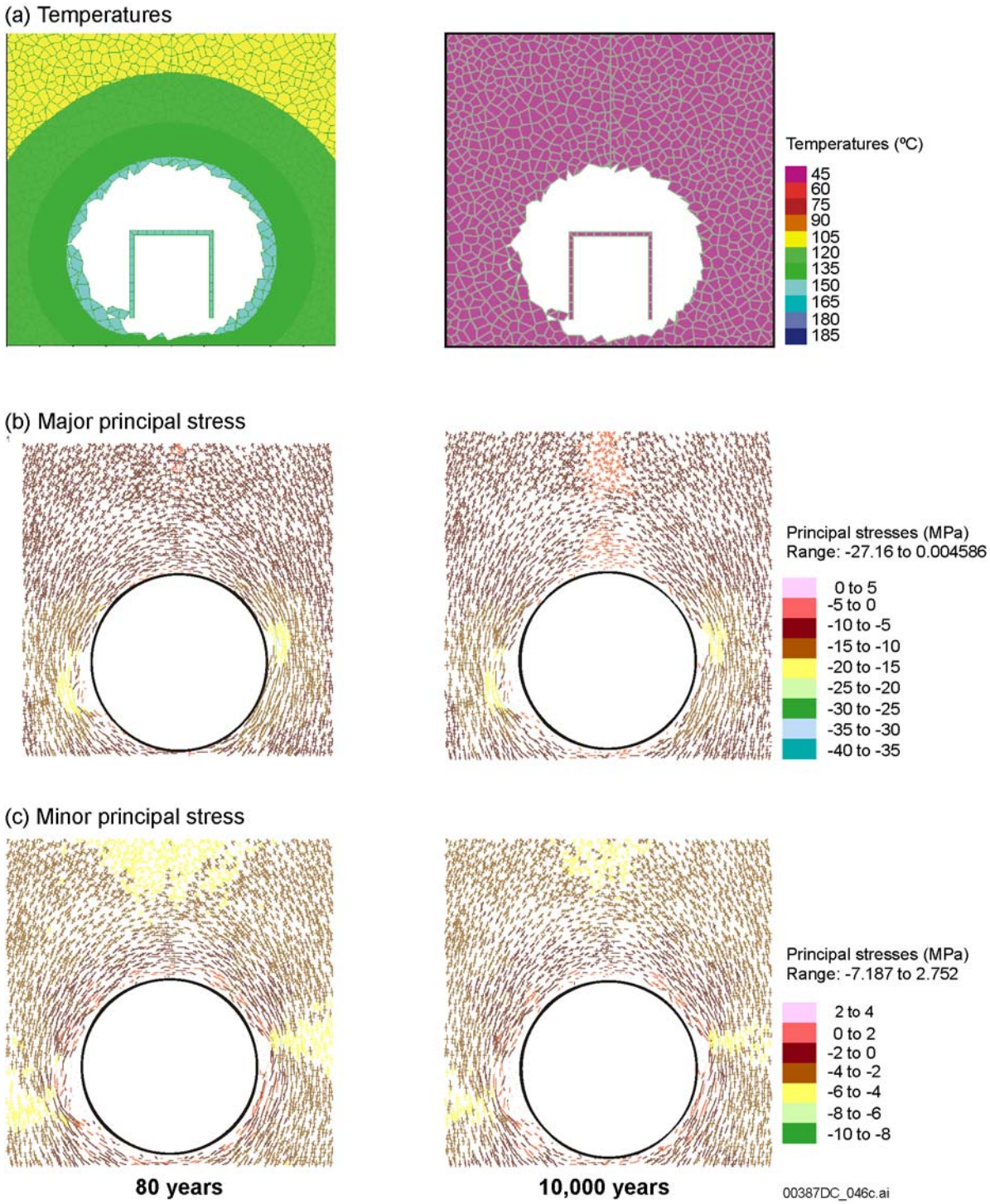

Source: BSC 2004a, Figure 6-142.

NOTE: Peak stress occurs at springline and small amount (0.25 m or less; seen as white zone with absence of stress vectors at wall) of yield is predicted from initial stress state. Depth of yield does not increase from heating alone.

Figure 5-4. Comparison of Temperatures, Major and Minor Principal Stress Trajectories at 80 (Peak Temperature) and 10,000 Years for Lithophysal Rock, Lowest Quality, Category 1

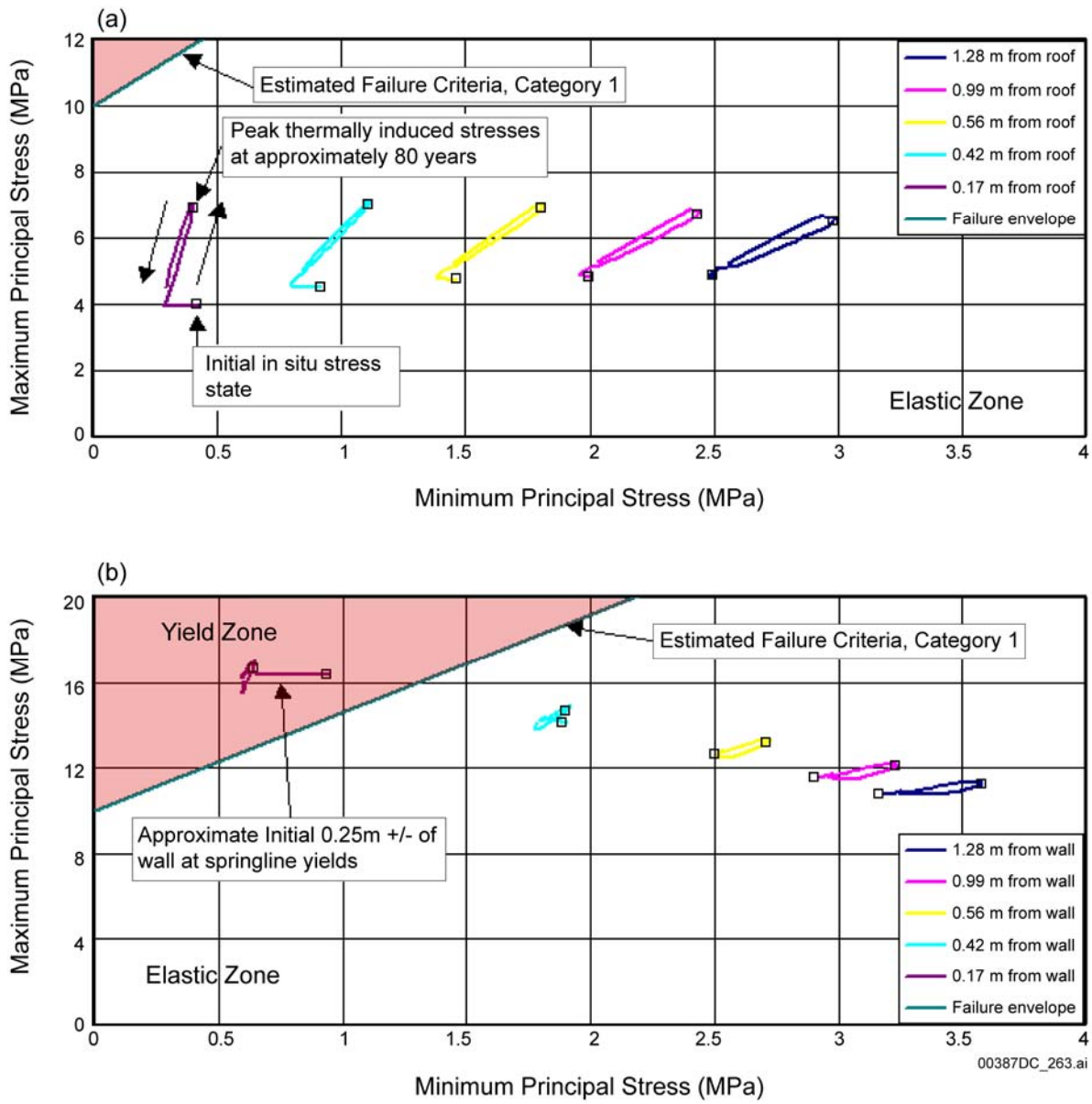

Source: BSC 2004a, Figures 6-144 and 6-143.

NOTE: Only minor yield (approximately 0.25 m depth) occurs in drift springline area for this lowest strength category. This yield is predicted to occur prior to initiation of heating. Estimated failure envelope is shown for comparison to the stress conditions. Initial point is at preheating stress state, followed by path through 10,000 years of heat-up and cool-down.

Figure 5-5. Elastic Principal Stress Path Histories for Points at Increasing Depth from Emplacement Drift Crown (a) and Springline (b) for Lithophysal Rock, Modulus from Lowest Quality Category 1

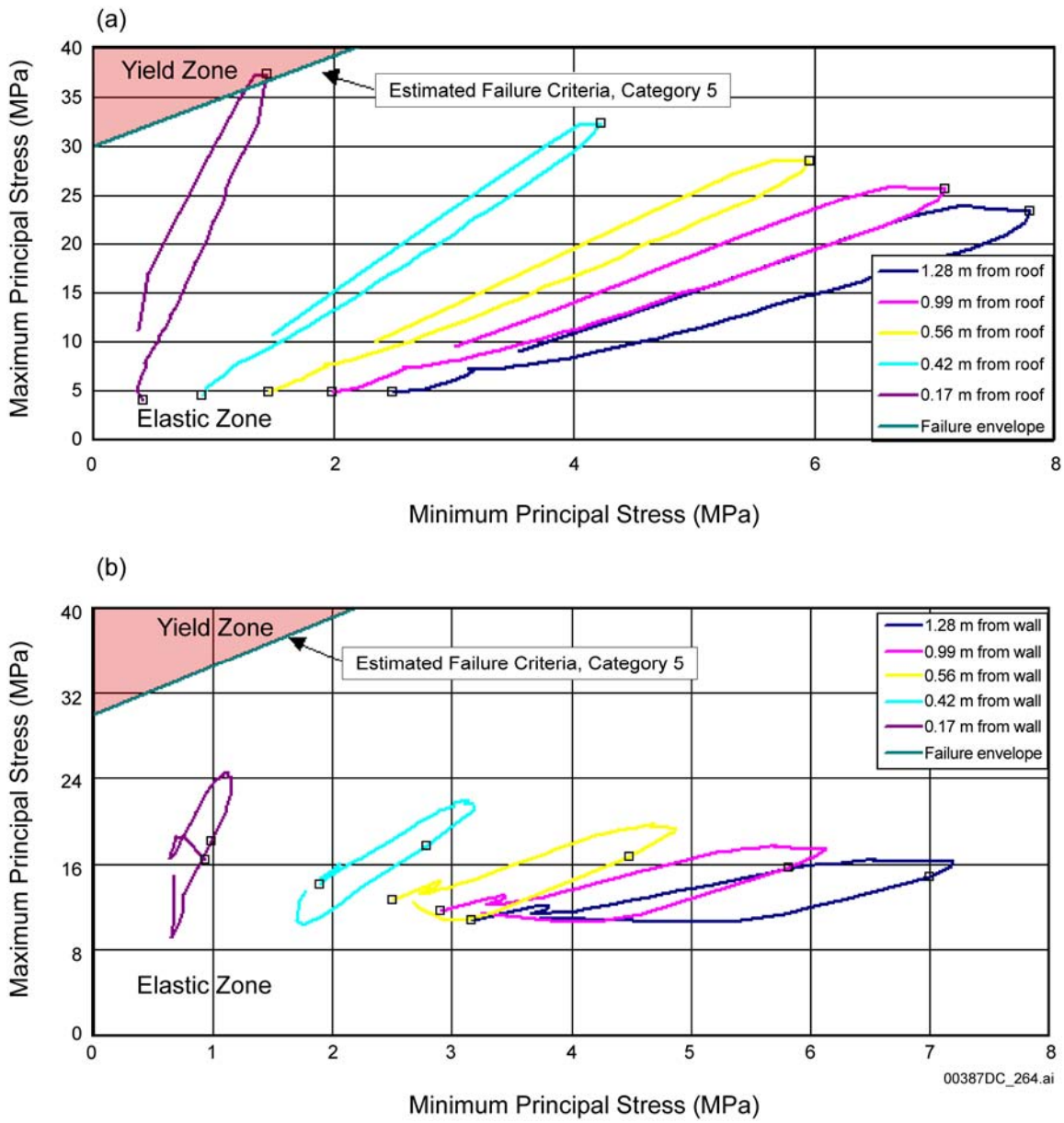

Source: BSC 2004a, Figures 6-146 and 6-145.

NOTE: Only minor yield (less than about 0.25 m depth) occurs in drift crown area for this highest lithophysal strength category. This yield is predicted to occur after 80 years of heating. Larger stress change occurs in crown for higher modulus category as compared to Figure 5-5. Estimated failure envelope is shown for comparison to the stress conditions. Initial point is at preheating stress state, followed by path through 10,000 years of heat-up and cool-down.

Figure 5-6. Elastic Principal Stress Path Histories for Points at Increasing Depth from Emplacement Drift Crown (a) and Springline (b) for Lithophysal Rock, Modulus from Highest Quality Category 5

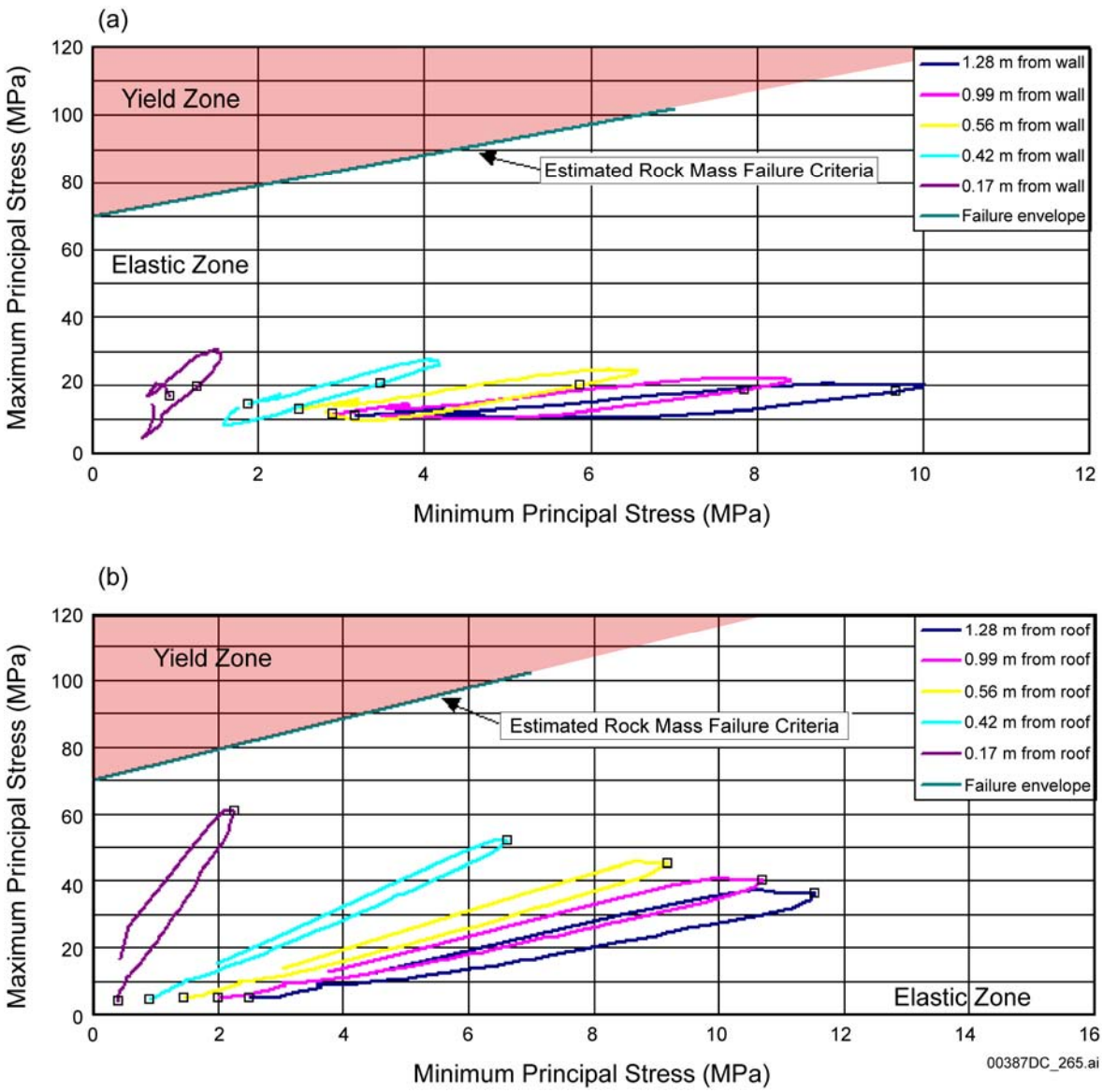

Source: BSC 2004a, Figures 6-84 and 6-85.

NOTE: No yield from in situ or thermally induced stresses occurs. Estimated failure envelope is shown for comparison to the stress conditions. Initial point is at preheating stress state, followed by path through 10,000 years of heat-up and cool-down.

Figure 5-7. Elastic Principal Stress Path Histories for Points at Increasing Depth from Emplacement Drift Crown (a) and Springline (b) for Nonlithophysal Rock, Strength Category 3

5.3.2 Analysis of Drift Degradation from Combined In Situ, Thermal, and Seismic Loading

5.3.2.1 Nonlithophysal Rocks

5.3.2.1.1 Introduction

The approach to modeling rock mass degradation and rockfall from combined in situ, thermal, and seismic loading in nonlithophysal rocks is illustrated in Figure 5-8. This approach involves modeling of emplacement drifts excavated within the stochastically defined, representative fractured rock mass volume, followed by application of in situ, thermal, and seismic load. A large number of parameter studies are conducted in which the tunnel location (and fracture geometry), rock fracture surface properties, and loading conditions are varied to derive a conservative range of performance response (in terms of rockfall mass, volume, and opening shape) that is indicative of the possible geologic conditions at depth. This data is then fed to analysis of the postclosure structural stability and determination of location and areal extent of localized yielding of the drip shield. This localized yielding is further abstracted into a damage model for of the titanium (e.g., tearing or stress corrosion cracking) with associated estimates of the drainage of seepage waters through the drip shield (BSC 2004e). The seismic consequence abstraction provides the final abstraction of damage consequences for drip shield and waste package to the total system performance assessment model.

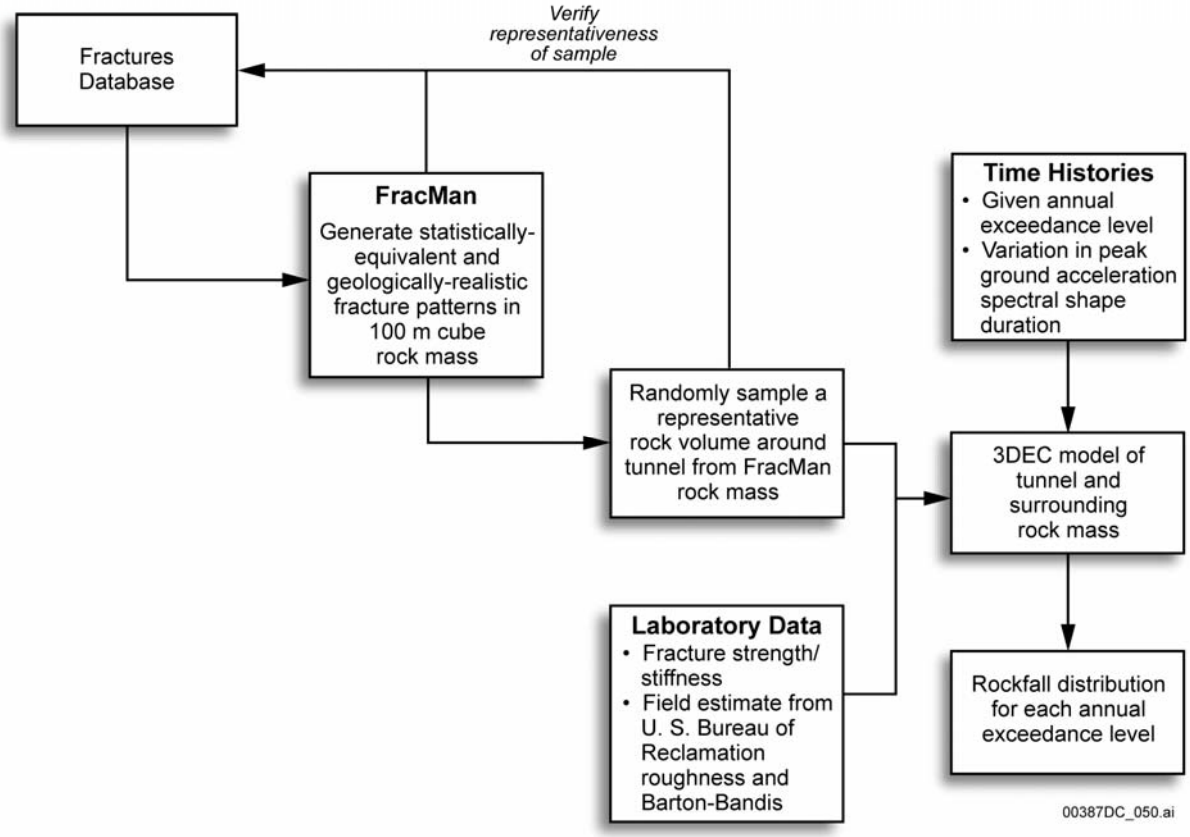

Figure 5-8. Approach to Analysis of Drift Degradation and Rockfall from Combined In Situ, Thermal, and Seismic Loading

5.3.2.1.2 3DEC Model Development

As described in Section 4.1, the FracMan program is used to develop the basic fracture input data for the 3DEC program. A 100-by-100-by-100-m representative fractured rock mass volume is generated and composed of the matrix blocks defined by approximately 90,000 fractures. A total of 50 emplacement drifts are randomly located and "excavated" within this rock mass such that the stochastic nature of the jointed medium and its impact on rockfall is adequately sampled. A random emplacement drift centroid coordinate is chosen within the cube, and a 25-by-25-by-25-m volume, oriented at the emplacement drift 72° azimuth, is extracted to contain the model emplacement drift (Figure 5-9). Within each emplacement drift, a rigid, rectangular block representing the drip shield is affixed to the invert of the tunnel. This drip shield block is placed only to facilitate the recording of block impacts (location and time of impact, block mass, velocity, and block shape) to the drip shield. For each rock that impacts the drip shield, and is not meant to represent its mechanical response, that modeling is accomplished in a separate calculation (BSC 2004m).

An algorithm was developed for applying the FracMan fracture geometry to the 3DEC model. Previous versions of the 3DEC program were set up to only efficiently handle through-going joint planes. The new algorithm allows incomplete fractures to be cut within a block, or to terminate against other fractures, thus creating realistic fracture patterns within the rock mass.[15] The resulting blocks within the 3DEC model are fully deformable as they are subdivided into tetrahedral finite difference zones, whose constitutive behavior may be elastic or conform to a desired constitutive law. Here, the blocks were assumed to be elastic due to the high intact strength of nonlithophysal rock, although later this assumption is reviewed in detail. The 3DEC model uses a fully dynamic solution algorithm to solve the laws of motions for the blocks, subject to contact restraints with surrounding blocks. The gridpoints that lie along the fracture surfaces act as contact points across which forces are transmitted, subject to shear and tensile yield conditions.

[15] The circular disc-shaped fractures prescribed by the FracMan output are initially cut to completely transect the blocks in which they occur. In a second step, the 3DEC model bonds those portions of the fracture that fall outside the fracture radius with the strength of the intact rock, thus simulating a partially-fractured block. During a simulation, the bonded portion of the fracture is free to fail in shear or tension if the stresses dictate, thus creating multiple blocks.

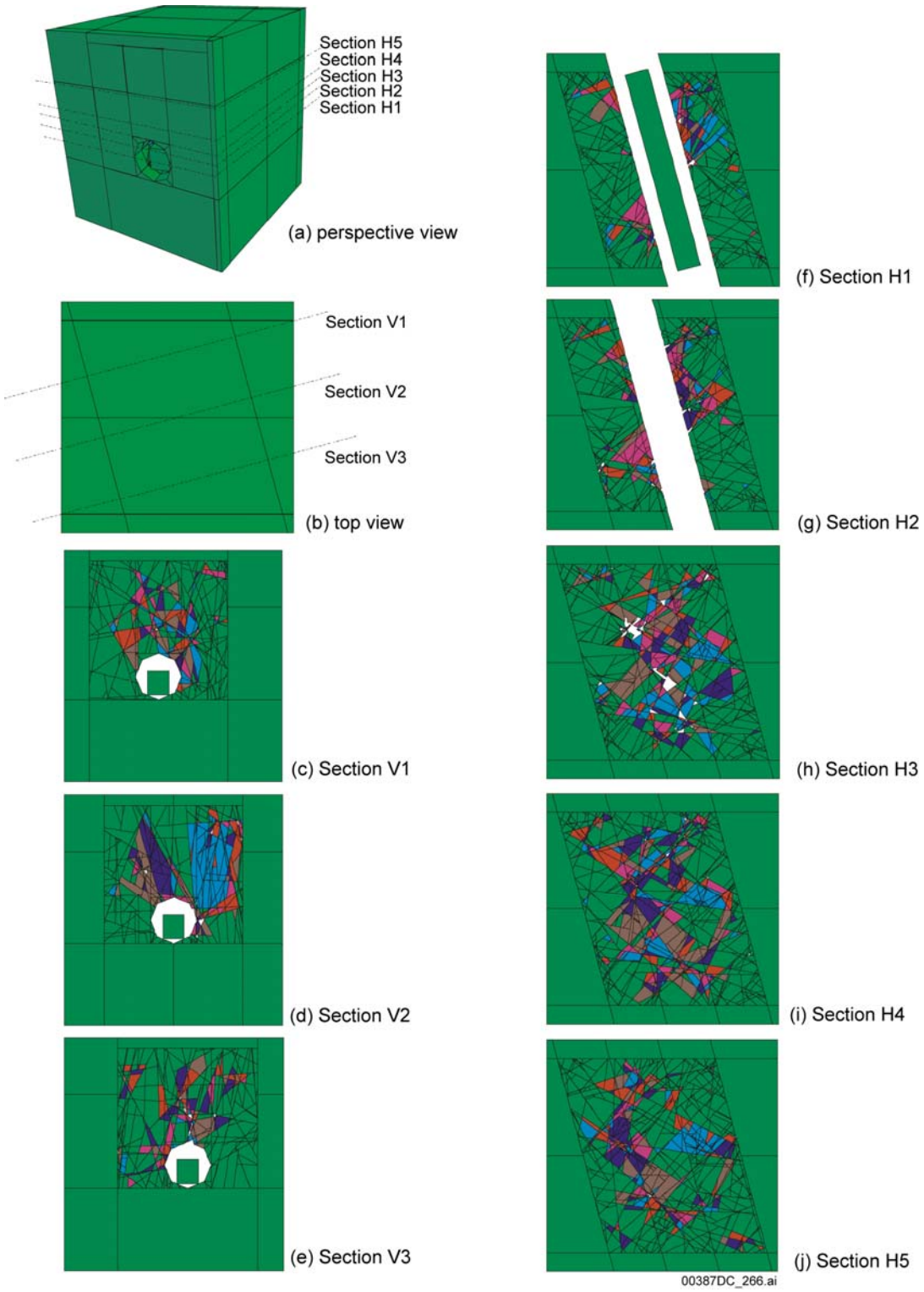

Source: BSC 2004a, Figure 6-41.

Figure 5-9. 3DEC Model Geometry and Cross Sections

5.3.2.1.3 Ground Motion

Site-specific ground motions were developed for the Yucca Mountain site through use of a formal process of expert elicitation resulting in development of a probabilistic seismic hazard assessment (PSHA). A summary of the PSHA can be found in *Characterize Framework for Seismicity and Structural Deformation at Yucca Mountain, Nevada* (BSC 2004n). Site-specific ground motion time histories for four levels of annual probability of exceedance, 10^{-4}, 10^{-5}, 10^{-6}, and 10^{-7}, were examined in *Drift Degradation Analysis* (BSC 2004a), with results described here. The development of the time histories are described in *Development of Earthquake Ground Motion Input for Preclosure Seismic Design and Postclosure Performance Assessment of a Geologic Repository at Yucca Mountain, NV* (BSC 2004c). The 10^{-4} ground motion level is for preclosure consideration, while the 10^{-5}, 10^{-6}, and 10^{-7} ground motion levels are for postclosure conditions. The 10^{-4} preclosure ground motion levels are also used in the analysis of access and emplacement drift seismic response for preclosure safety assessment and for analysis of ground support safety classification (BSC 2004k).

For higher frequency spectral accelerations (5 to 10 Hz) and an annual exceedance probability of 10^{-4}, results of the probabilistic seismic hazard analysis for Yucca Mountain indicate the ground motion hazard derives primarily from earthquakes in the magnitude range of 5.0 to 6.5 occurring at distances less than 15 km from the site. For lower-frequency spectral accelerations (1 to 2 Hz) at the same annual exceedance probability, the hazard shows, in addition to nearby sources, a significant contribution from earthquakes in the magnitude range of 7.0 to 8.0 occurring at an epicentral distance of about 50 km. For annual exceedance probabilities of 10^{-6} and 10^{-7}, nearby earthquakes in the magnitude range 5.5 to 7.0 are the dominant sources contributing to ground motion hazard at both higher and lower spectral accelerations. Discussion of the derivation of the site specific ground motion time histories can be found in *Technical Basis Document No. 14: Low Probability Seismic Events*.

A total of 15 sets of ground motion time histories were developed at the repository horizon for each annual postclosure hazard level. The multiple sets ensure a reasonable distribution of spectral shapes and time history duration. For each set of ground motion, two horizontal components (H1 and H2) and one vertical component (V) of acceleration, velocity, and displacement are supplied. Figure 5-10 shows the H1 velocity time history for four annual hazard levels. Only one ground motion time history set was provided for the preclosure hazard levels because of the deterministic-based approach for preclosure consideration.

The amplitude of the peak ground acceleration, velocity, and displacement, and the seismic-induced far-field stress for one of the ground motion sets from each hazard level are provided in Table 5-1. This table is used to demonstrate the typical ground motion parameters for the three hazard levels considered.

It is apparent that the preclosure ground motion levels have lower amplitude vibrations and hence lower induced rock mass stresses compared to the postclosure ground motion levels. The peak values for each postclosure hazard level vary depending on the hazard level. The complete data sets of the ground motion are contained in *Drift Degradation Analysis* (BSC 2004a).

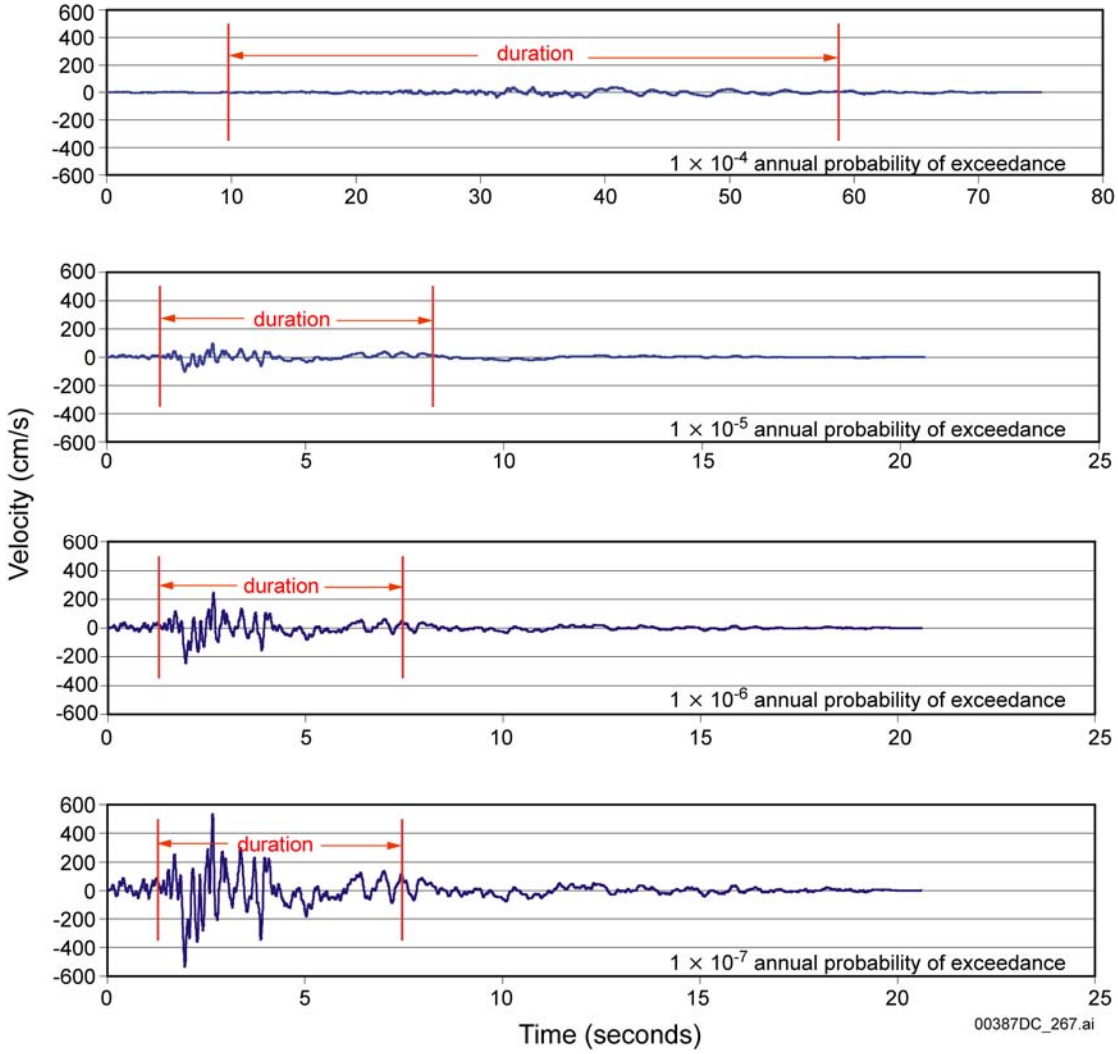

Source: DTNs: MO0211TMHIS104.002, MO0306SDSAVDTH.000, MO0301TMHIS106.001, MO0403AVTMH107.003; MO0402AVDTM105.001; BSC 2004a.

Figure 5-10. Examples of Ground Velocity Time Histories (H1) with Truncated Duration for Analysis

Table 5-1. Peak Ground-Motion Parameters

Annual Hazard Level	Ground Motion Component	Peak Acceleration (g)	Peak Velocity (cm/s)	Peak Displacement (cm)	Seismic Induced Stress Corresponding to Peak Velocity (Pa)*
10^{-4}	H1	0.39	38.38	44.44	2.20×10^6
	H2	0.37	43.78	45.3	2.51×10^6
	V	0.47	47.51	31.73	4.50×10^6
10^{-5} Ground Motion Set 1	H1	2.77	104.58	20.06	6.00×10^6
	H2	2.50	83.31	14.37	4.78×10^6
	V	2.63	70.88	13.00	6.71×10^6
10^{-6} Ground Motion Set 1	H1	7.42	244.14	26.76	1.40×10^7
	H2	6.74	195.41	26.78	1.12×10^7
	V	4.90	111.29	13.75	1.05×10^7
10^{-7} Ground Motion Set 1	H1	16.28	535.26	58.68	3.07×10^7
	H2	14.79	428.42	58.72	2.46×10^7
	V	13.15	298.44	36.86	2.83×10^7

Source: DTNs: MO0211TMHIS104.002, MO0306SDSAVDTH.000, MO0301TMHIS106.001, MO0403AVTMH107.003, MO0402AVDTM105.001.

NOTE: Seismic-induced stress is calculated based on elastic wave equations (Itasca Consulting Group 2002, Manuals/3DEC/Optional Features/Section 2: Dynamic Analysis, Section 2.5).

Ground motion at the location of the repository, in the form of three mutually perpendicular velocities (two horizontal and one vertical), are applied to the lower surface of the model, in terms of equivalent stress time histories. The motions, as supplied to the drift degradation modeling, include the effects of the free surface reflections, and, thus, the 3DEC model does not need to account for topography.

Nonreflecting vertical and upper model boundaries in 3DEC allow the wave to pass through the model, and free-field boundaries on the vertical sidewalls of the model prevent damping and distortion along the vertical sidewalls of the incoming wave. No material damping,[16] in addition to that supplied by sliding on fracture surfaces, is supplied to the model. Prior to use of the model for examination of drift degradation, seismic wave propagation of models without tunnels was run to ascertain that the wave passed through the model without significant distortion.

5.3.2.1.4 Combinations of Ground Motion and Fracture Modeling Region

A goal of these analyses is to provide an estimate of seismically induced rockfall that is derived from an adequate sampling of the variability of fracture geometries and ground motion time histories. As described previously, a 100-m cube was constructed from FracMan for providing the fracture network required in 3DEC analysis. A random selection of 105 emplacement drift centroid locations was conducted. These 105 centroid locations combined with the 15 sets of

[16] 0.3% of critical damping was used in a few analyses for numerical stability purposes.

ground motion data serve as the basis for sampling for numerical analysis. A simple Latin Hypercube sampling scheme was used for the pairing of ground motion and fracture modeling region (DTN: MO0301SPASIP27.004). A total of 50 sets of paired fracturing realizations (i.e., drift centroid locations) and ground motion data[17] were made for each postclosure annual exceedance frequency. For each of these analyses, a base case of block and fracture material properties were used so that the variability of the rockfall response was then a function of the fracture geometry and ground motion variability only. The base case rock and fracture properties are given in Table 5-2.

Table 5-2. Base-Case Material Properties for 3DEC Analysis

Joint strength properties	Joint cohesion (MPa)	0.1
	Joint friction (°)	41
	Joint dilation (°)	0
	Joint normal stiffness, K_n (MPa/m)	5×10^4
	Joint shear stiffness, K_s (MPa/m)	5×10^4
Intact rock deformation properties	Young's modulus (GPa)	33.03
	Poisson's ratio	0.21
	Bulk modulus (GPa)	19.2
	Shear modulus (GPa)	13.6
Intact bridge strength properties	Cohesion (MPa)	47.2
	Friction angle (°)	42
	Tensile strength (MPa)	11.56

NOTE: Values of cohesion and friction angle were derived from preliminary data with a slight deviation from the reported values in *Drift Degradation Analysis* (BSC 2004a, Section E3). An impact analysis was conducted with no difference in the results for rockfall prediction (BSC 2004a, Appendix Q). Joint dilation (BSC 2004a, Table E-3) is set to zero for the base-case analysis. With no dilation, joints are modeled as perfectly planar and smooth, resulting in a conservative (i.e., higher) estimation of rockfall.

5.3.2.1.5 Example of Seismic Analysis for Case of 10^{-6} Annual Exceedance Probability

The results for a complete set of 3DEC analyses, subjected to the postclosure hazard level of 10^{-6} annual probability of exceedance ground motion, are presented in this section. The analyses reviewed here are for nonthermal loading conditions; however, the impact of thermal load, in addition to gravitational and seismic stresses, is discussed later. A summary of the 10^{-4} simulations at other annual exceedance frequencies can be found in *Drift Degradation Analysis* (BSC 2004a).

[17] The adequacy of 50 analyses for representation of the variability of rockfall (at each exceedance level) was verified by calculation of the cumulative mean and standard deviation of rockfall parameters for successive analyses. As described in *Drift Degradation Analysis* (BSC 2003a), the mean and standard deviation of rockfall mass, for example, does not change after approximately 30 runs.

The block representing the drip shield is anchored at the invert, and is included in the model to record the information of the locations and relative velocities for the rockfall impact. Figure 5-11 shows a typical block impacting the drip shield in the 3DEC dynamic simulation.

Note that fallen blocks are automatically deleted after impacting the drip shield. The deletion is to facilitate a conservative approach of recording of all possible rockfall on the drip shield. If the blocks are not deleted for the heaviest of rockfall cases, the drip shield will be covered with fallen rocks so that some of the rockfall at the later stage of seismic shaking will not impact the drip shield. The simulation without deletion of the rock blocks after the impact was examined to define the conservatism in this present approach, indicating less rockfall impact without this deletion scheme.

The results of the 50 3DEC simulations are summarized in Table 5-3. All of the simulations predicted some level of rockfall associated with the 10^{-6} seismic shaking, resulting in an average of 398 m^3 of rockfall per kilometer of drift length. The associated impact parameters for these blocks from the analyses include the following:

- Rock block volume falling on the drip shields (unit in cubic meters)
- Relative impact velocity of rock block to the drip shields (unit in meters per second)
- Impact location.

Table 5-3. Summary of 3DEC Rockfall Prediction for 10^{-6} Annual Probability of Exceedance Hazard

Parameter	Value
Simulations Completed	50
Total Number of Rockfall	2,797
Total Volume of Rockfall (m^3)	497.7
Total Length of Drift Simulated (m)	1,250
Number of Blocks per km	2,238
Volume of Rockfall per km (m^3)	398.2

Source: BSC 2004a, Table 6-13.

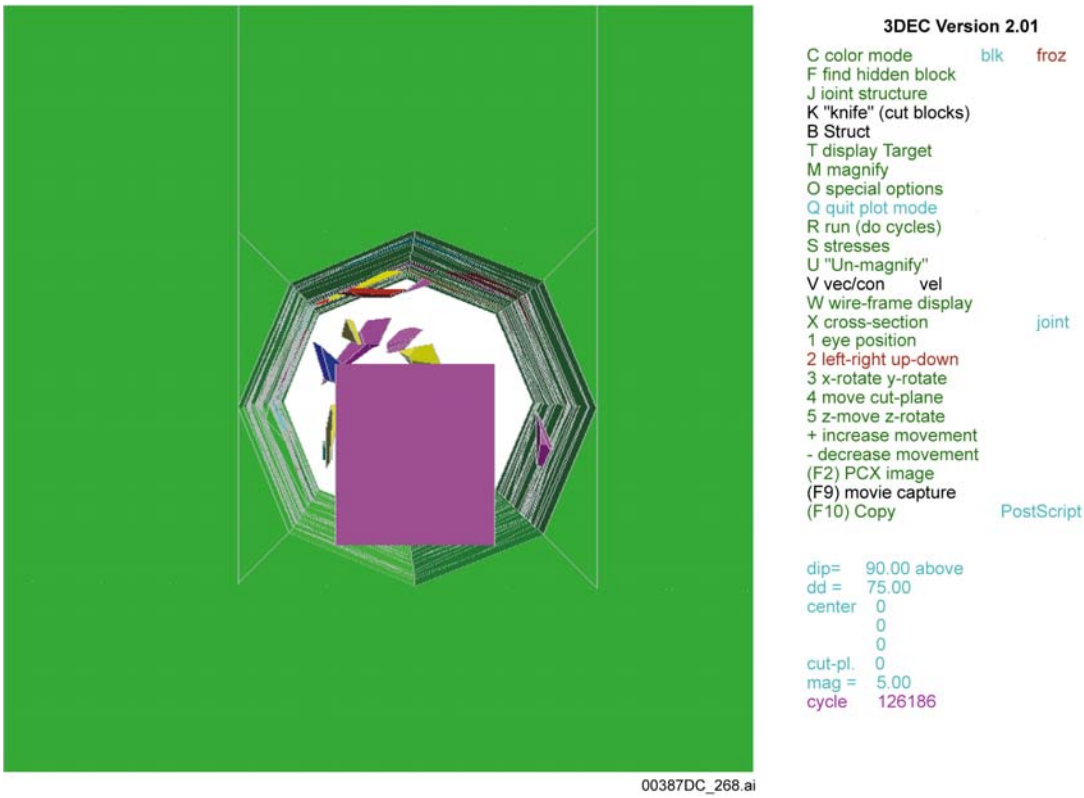

Source: BSC 2004a, Figure 6-56.

NOTE: 3DEC Simulation 22, 10^{-6} ground motion 5, at t = 5.24 s.

Figure 5-11. Simulation of Rockfall Impact to the Drip Shield

The distribution of the data for each parameter (i.e., block mass, relative impact velocity, impact angle, impact momentum, and impact energy) is presented using histograms (Figures 5-12 to 5-16). Also included in each histogram plot is the cumulative frequency of occurrence.

Due to the gravity effect, most of the rockfall will occur in the range of 48° to 132° (based on the drip shield coordinate system) as confirmed in Figure 5-14. The impact momentum and impact energy, both functions of block mass and impact velocity, were calculated as the required outputs for drip shield structural response calculation. Summary statistics for these parameters are provided in Table 5-4. The maximum rockfall block mass predicted is 28 MT with median block size of 0.13 MT. The predicted results (Table 5-4) show large variance and high skewness with the exception of impact velocity, as confirmed by the shape of the histograms. The block mass, impact angle, impact momentum and impact energy show the trend of exponential distribution with most of the data concentrated on the low end of the data range. The impact velocity shows a typical bell shape for the normal distribution. The distribution centers around 3 m/s with a standard deviation of approximately 1.7 m/s (BSC 2004a).

The relative low impact velocities indicate that block fallout is mainly due to gravitational free-fall. Differential acceleration or energy trapping to induce high ejection velocity is not observed.

Table 5-4. Statistical Summary of the Rockfall Impact Parameters, 10^{-6} Annual Probability of Exceedance Hazard, Variability in Fracture Geometry and Ground Motion

	Block Mass (MT)	Relative Impact Velocity (m/s)	Impact Angle (°)	Impact Momentum (kg·m/s)	Impact Energy (Joules)
Mean	0.43	3.23	136	1,217	2,350
Median	0.13	2.97	124	337	576
Standard Deviation	1.30	1.74	93	3,464	7,704
Skewness	11.61	1.06	0.87	11	12
Range	28.19	12.03	359	79,001	163,657
Minimum	0.02	0.07	0	2	0
Maximum	28.22	12.10	360	79,003	163,657
Sum	1200.43	N/A	N/A	3,403,555	6,573.633

Source: BSC 2004a, Table 6-14.

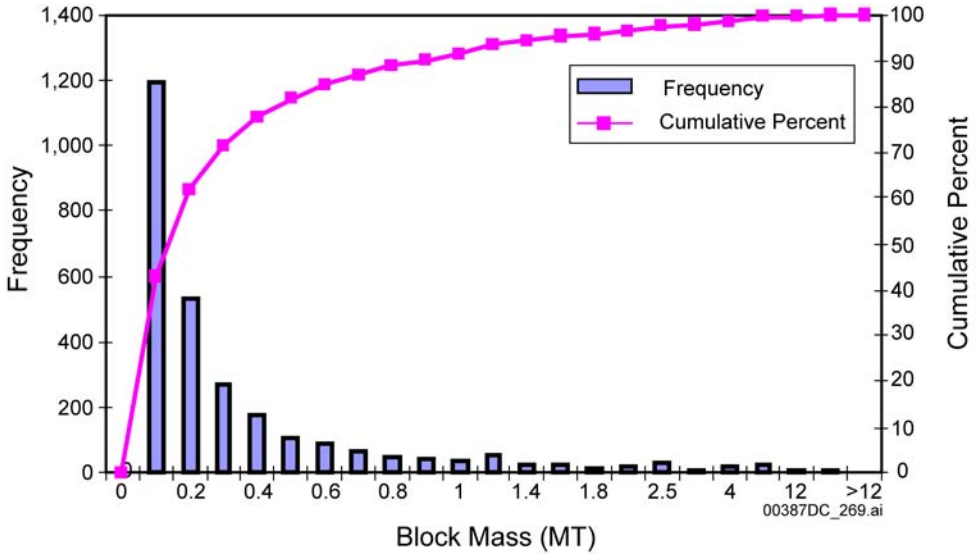

Source: BSC 2004a, Figure 6-59.

Figure 5-12. Histogram for Block Mass (10^{-6} Annual Probability of Exceedance Hazard)

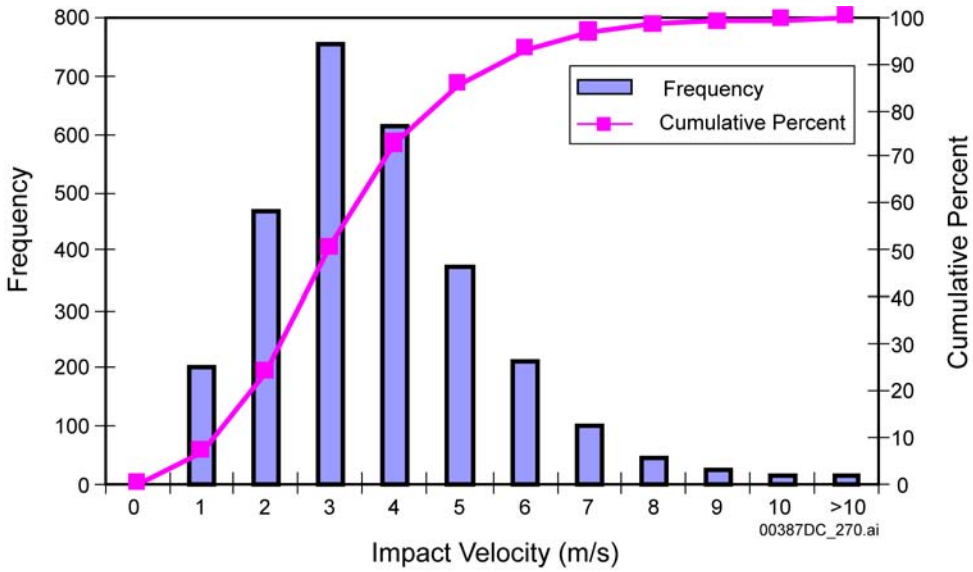

Source: BSC 2004a, Figure 6-60.

Figure 5-13. Histogram for Relative Impact Velocity (10^{-6} Annual Probability of Exceedance Hazard)

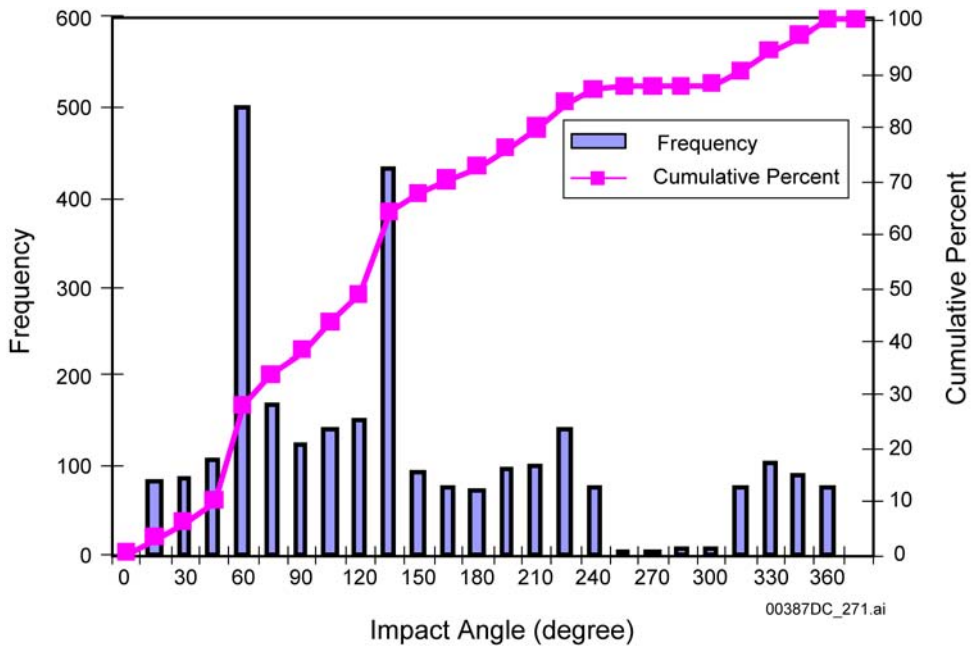

Source: BSC 2004a, Figure 6-61.

Figure 5-14. Histogram for Impact Angle (10^{-6} Annual Probability of Exceedance Hazard)

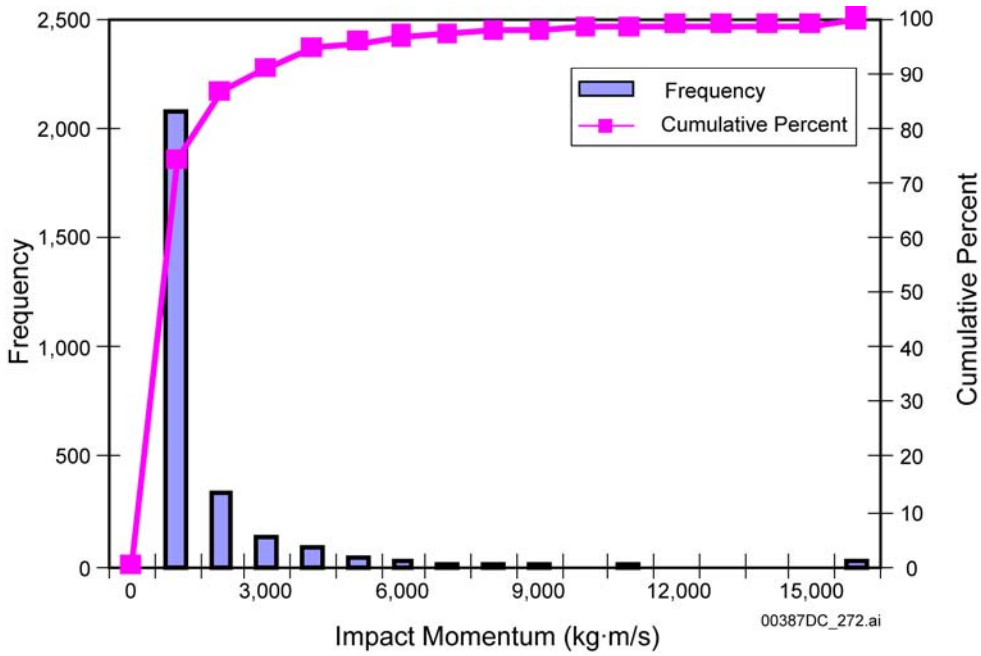

Source: BSC 2004a, Figure 6-62.

Figure 5-15. Histogram for Impact Momentum (10^{-6} Annual Probability of Exceedance Hazard)

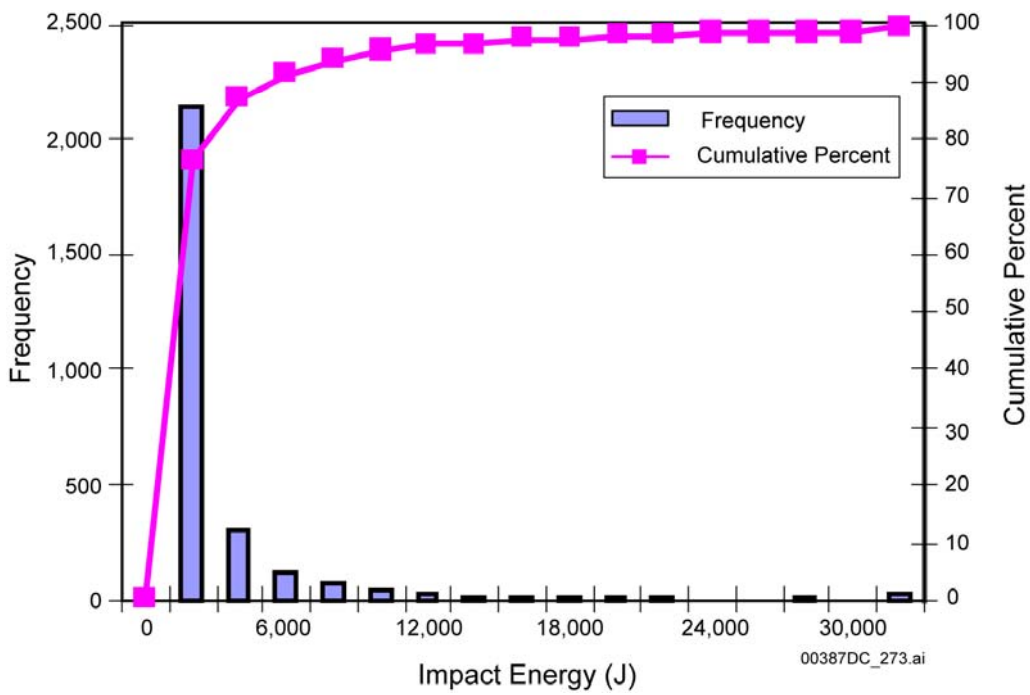

Source: BSC 2004a, Figure 6-63.

Figure 5-16. Histogram for Impact Energy (10^{-6} Annual Probability of Exceedance Hazard)

5.3.2.1.6 Summary of Nonlithophysal Rockfall from Preclosure and Postclosure Ground Motion

Analyses similar to that discussed in the previous section were also completed for 10^{-4}, 10^{-5}, and 10^{-7} motions. The exception is that only one ground motion set was provided for the preclosure cases, and 32, rather than 50, analyses were made.

Figure 5-17 shows a comparison of histograms of block mass for all three ground motion results. Essentially, the results show that all motions result in the same general distribution of block sizes with mean block masses of less than 0.2 MT, and an exponentially decaying distribution.

A comparison of the rockfall statistics for the preclosure and postclosure events is given in Table 5-5. The important comparison statistic here (due to the variable number of runs) is the number of blocks per km, which shows increase from 535 to 2,840 blocks in going from the 10^{-4} to 10^{-7} annual exceedance frequency.

Table 5-5. Comparison of Rockfall Statistics for Preclosure and Postclosure Events

Statistic	Ground Motion			
	10^{-4}	10^{-5}	10^{-6}	10^{-7}
Runs Completed	32	50	50	44
Total Number of Rockfall	428	1,764	2,797	3,219
Total Volume of Rockfall (m^3)	39.4	255.4	497.7	678.3
Total Length of Drift Simulated (m)	800	1,250	1,250	1,100
Number of Blocks per km	535	1,414	2,238	2,926
Volume of Rockfall per km (m^3/km)	49.3	204.3	398.2	616.6

Source: BSC 2004a, Table 6-22.

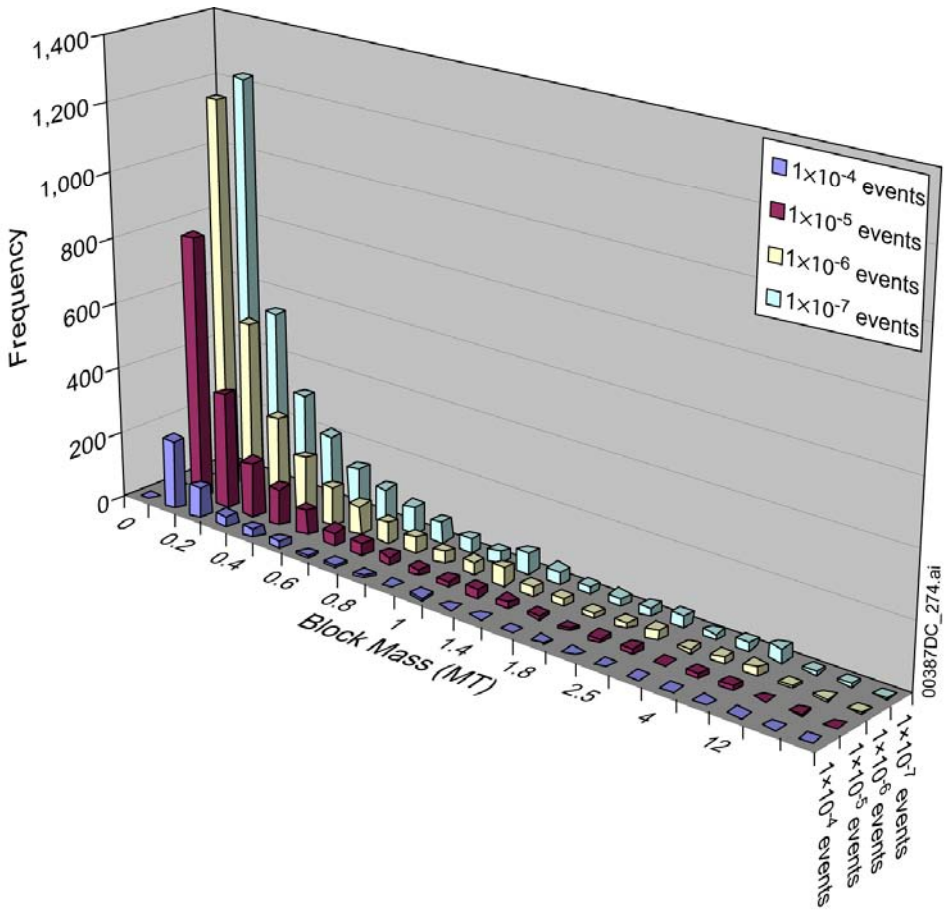

Source: BSC 2004a, Figure 6-87.1.

Figure 5-17. Comparison of Histograms of Block Mass from All Postclosure and Preclosure Ground Motion

5.3.2.1.7 Summary of Drift Profile

The three-dimensional depiction of an emplacement drift after 10^{-6} ground motion analyses provides a physical feel for the impact of seismically induced rockfall on drift profile. Figures 5-18 and 5-19 show the rockfall profile for the case showing the greatest amount of rockfall and for the case showing 50th percentile of quantity of rockfall.

Two particular cases of the 50 analyzed show larger amount of rockfall due to the fact that the two long, subvertical fracture sets strike at a low angle to the axis of the emplacement drift. This, coupled with the presence of closely spaced subhorizontal vapor phase partings or random sets, allows a number of roof and sidewall blocks to detach over a significant plan view area. As seen in the 50th percentile case, isolated wedges formed, again, by two subvertical and subhorizontal sets can occasionally occur.

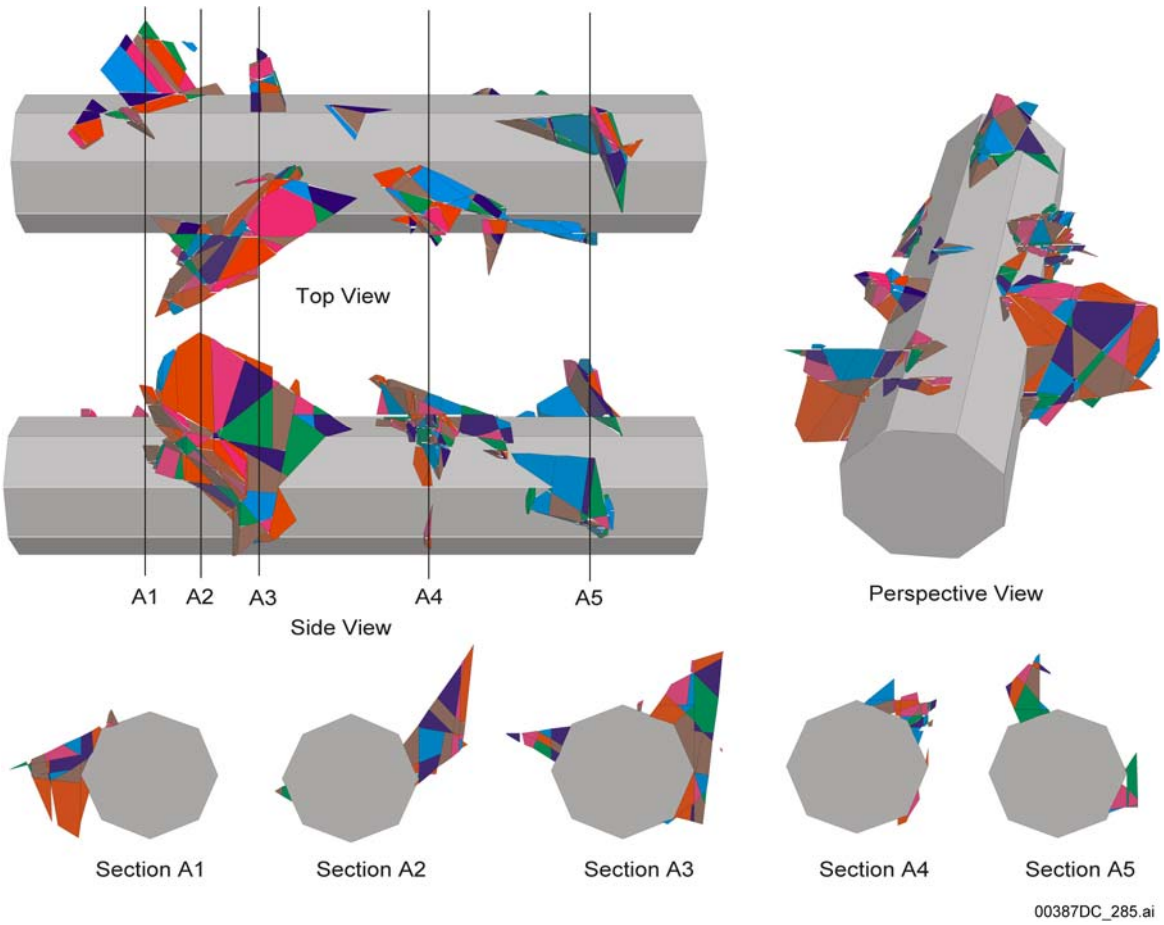

Source: BSC 2004a, Figure 6-114.

NOTE: Gray tube is emplacement drift as represented in the 3DEC model. This realization shows a case that has a 1 in 50 chance of occurrence.

Figure 5-18. Drift Profile Showing Blocks That Become Detached from Drift Wall during Simulation for 10^{-6} Hazard Level, Case with Greatest Amount of Rockfall of 50 Total Realizations

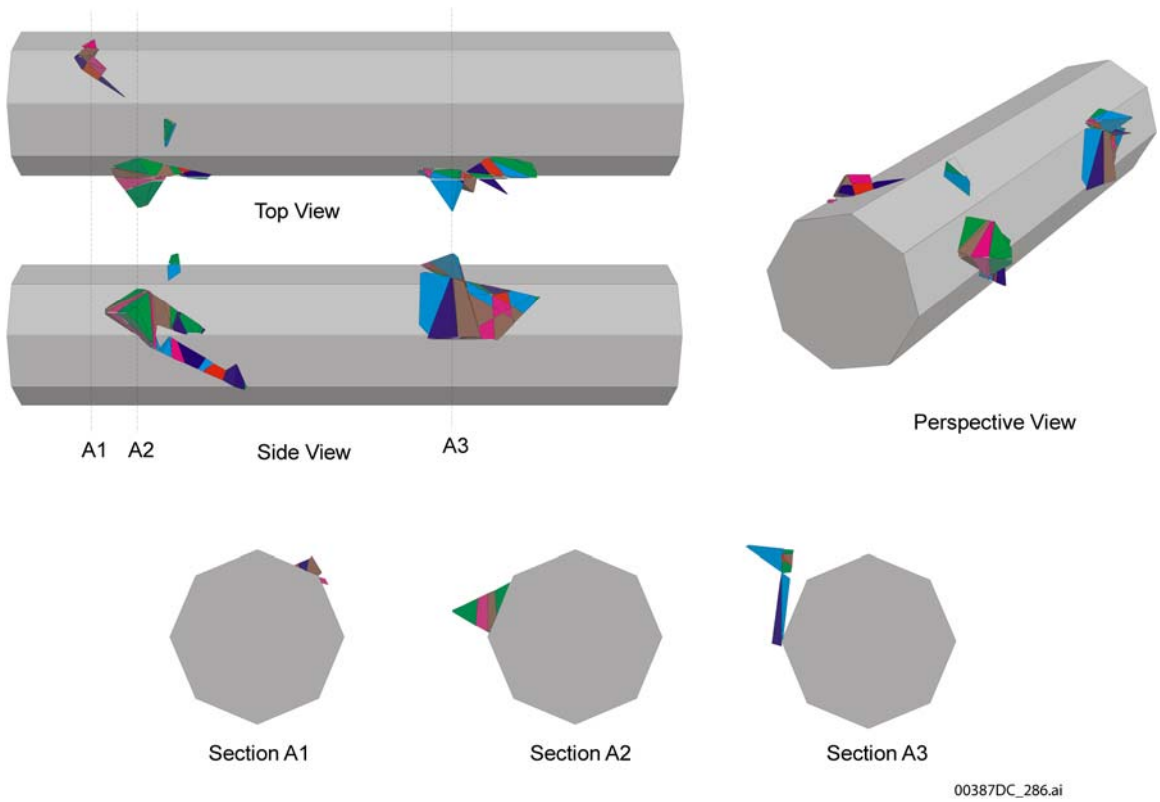

Source: BSC 2004a, Figure 6-115.

NOTE: This realization shows the mean case of 50 realizations.

Figure 5-19. Drift Profile Showing Blocks that Become Detached from Drift Wall During Simulation for 10^{-6} Hazard Level, 50th Percentile Case

5.3.2.1.8 Summary of Sensitivity Studies of the Input Parameters and Model Conditions

There are four major input data sets to the three-dimensional discontinuum analysis: ground motion, joint geometrical properties, joint and intact mechanical properties, and thermal stress history. Sensitivity studies of these input parameters were conducted to establish uncertainty in the predictions of rockfall and to identify the important controlling parameters. The following section provides a summary of the conclusions of these parameter studies. Details are presented in *Drift Degradation Analysis* (BSC 2004a).

Ground Motion Sensitivity–A total of 15 sets of ground motion data were used for each hazard level in the postclosure consideration to ensure a reasonable distribution of spectral shapes and time history durations. Sensitivity studies on the peak ground velocity, energy contents, duration, and orientation of horizontal motions in the 3DEC model to the rockfall prediction were examined and reviewed in the previous discussion. Correlation of the rockfall volume with the peak ground velocity and energy content in term of Arias Intensity shows that no strong relationship is observed for either of the parameters. The ground motion time histories were truncated at 5% and 95% energy content to shorten the time required to conduct the dynamic analyses. The analyses showed that the majority of the rockfall occurs coincident with the

arrival of the strong motion, which is typically within the first 15 seconds of shaking, and that truncating the ground motion had minimal impact on the amount of rockfall. However, the results were inspected at the end of the simulation, and, if it was determined that the simulation was terminated prematurely (i.e., there was indication of loose blocks), the simulation was continued until all loose blocks resulted in rockfall. Likewise, it was found that rotating the horizontal ground motion components by 90° had minimal impact on rockfall. This is understandable since the horizontal motions have, in general, similar peak amplitudes.

Joint Geometrical Properties–The variability of joint geometrical properties is incorporated in the application of FracMan to generate a 100-m cube fracture network. A total of 50 drift locations were selected from the 100-m cube fractured rock mass for the 3DEC analyses. Results from the analyses of 50 drift locations (or fracture modeling regions) reasonably explore the impact of the variability of joint geometrical properties (BSC 2004a, Appendix K).

Fracture Surface Property Variation and Fracture Strength Degradation–The base-case joint properties, listed in Table 5-2, were based on the rotary shear tests of the cored specimen as derived in *Drift Degradation Analysis* (BSC 2004a, Attachment V). Additional direct shear tests (Section 3.2.4.1) have been completed, and results from these tests are used to provide the range of variation tested in the sensitivity studies. With limited joint test results currently available and given the fact that the use of rotary shear devices in rock mechanics is not common, some of the parameters in the base case, such as cohesion and dilation angle, were scaled down from the testing results for conservatism, to allow for investigation of impact on increased rockfall.

A range of joint properties, as shown in Table 5-6, was selected for the sensitivity study. The values were established based on the residual friction angle of 30° and three tiers of dilation angles. The dilation angles were selected within the range of reported test results presented in *Drift Degradation Analysis* (BSC 2004a, Attachment V) and discussed in Section 3.2.4.2. Cohesion is conservatively set to be 0.1 MPa.

The results of these sensitivity studies show that the variation of joint mechanical properties is a secondary effect compared with the variation of fracture geometrical properties (i.e., fracture pattern). Results for the three categories are quite similar, irrespective of the variation of the mechanical properties used for each category.

Table 5-6. Three Categories of Joint Properties Used in the Sensitivity Study

Joint Category	Joint Cohesion (Pa)	Joint Dilation Angle	Peak Friction Angle	Joint Shear Stiffness (Pa/m)	Joint Normal Stiffness (Pa/m)
1	1.0×10^5	1.4	31.4	5.3×10^9	7.2×10^{10}
2	1.0×10^5	4.4	34.4	1.1×10^{10}	9.4×10^{10}
3	1.0×10^5	11	41	1.7×10^{10}	1.2×10^{11}

Source: BSC 2004a, Table 6-24.

Time Degradation of Joint Properties–The potential exists for time-dependent degradation of the rock mass surrounding the tunnels. In the nonlithophysal rock, the potential source of

time-dependency is the result of long-term shear failure along the preexisting fracture planes. A potential mechanism for time-dependent yield along rock fractures is the concentration of stress on joint asperities (i.e., roughness along the joint surfaces) with associated static fatigue failure when subjected to long-term constant shear stress. Static fatigue of hard rocks is typically associated with stress levels on the order of 60% to 80% of its unconfined compressive strength (see Section 5.3.2.2.4 for greater detail on time-dependent properties of welded tuff). Fatigue failure would presumably initiate along asperities on fracture surfaces, with the ultimate effect of reducing the fracture surface roughness. From a mechanical perspective, this failure would result in reducing or eliminating cohesion and dilation on the joint surface, as well as reducing the friction angle to its residual value.

The impact on drift stability due to the effect of rock joint degradation is assessed here based on a conservative estimate of the reduction of joint cohesion and friction angle. The reduced joint strength parameters are estimated to be in the range of the residual, postpeak shear displacement state with joint cohesion reduced to 0 and the joint friction angle reduced to 30°. The reduced friction angle is a typical value for a smooth joint reported by Goodman (1980, p. 158) and is consistent with the direct shear test results described in Section 3.2.4.1 (DTN: GS030283114222.001). Dilation angle is also conservatively presumed to be 0, considering that the asperities on fracture surfaces had been sheared off. The net result of these conservative assumptions is the potential for greater rockfall. The degraded joint strength and dilational properties were applied in the three 10^{-5} seismic motion cases that represent the case with greatest amount of rockfall, the median case, and the case producing no rockfall. The predicted number of detached rock blocks and the total rockfall volume show only a slight increase in rockfall is predicted for the degraded state. Thus, potential time-related joint strength degradation has a minor impact on drift stability in nonlithophysal rock.

Rock Bridge Strength– Solid rock bridges between fractures were automatically generated as the extension of finite trace length fractures to form the distinct blocks in the 3DEC model. A range of bridge strength parameters, in terms of cohesion, friction angle, and tensile strength, was selected for the sensitivity study. This range of intact rock properties was derived from the results of triaxial testing of rock cores from the Tptpmn (see Section 3.2.1). A total of 3 categories were included to cover the possible range of variation for bridge strength parameters and was subject to 10^{-5} motions. The base case joint strength parameters are used for Category 1 to represent the extreme case where all the bridges are sheared off to become fractures. The mean values of the intact Tptpmn strength parameters are used for Category 2. The mean plus one standard deviation values determined from triaxial testing are assigned as the strength parameters for Category 3. This category represents the upper bound for the rock bridge strength. The results show that within the range of variation for the intact strength parameters (Categories 2 and 3), rock bridge strength parameters have insignificant impact on rockfall prediction. However, if all rock bridges are sheared off, as represented by Category 1, a significant increase of rockfall volume occurs with smaller rock block size.

Intact Rock Block Strength–The base case parametric analyses assumed that all blocks are elastic and, therefore, do not yield. Thus, all rockfall is due to slip and separation along preexisting fracture surfaces. Further dynamic analyses were conducted to examine the impact of the postclosure ground motion on intact rock spalling mechanisms. In these analyses, the rock block strength, estimated to be approximately 70 MPa from back-analysis of the roof spalling in

the heated overdrive portion of the heated drift test (see Section 4.2.7.1; BSC 2004a), was used to limit the peak stress in the periphery of the excavations. The 10^{-7} motion and some of the 10^{-6} motions are capable of inducing significant spalling of intact rock, which could result in rockfall in the drift with small-scale spalled rock. This is very similar to the calculated postclosure response for the lithophysal rock, as given in the next section. The peak ground velocities associated with these low-probability events is very conservative (BSC 2004c).

Thermal Stress Effects on Seismically Induced Rockfall–The initial seismic loading studies were conducted assuming in situ stress and seismic loading only. An analysis of the 10^{-5} motion was conducted in which the base case thermal condition (see Figure 5-3, Case 1) stress state was added to the in situ stress conditions prior to ground motion application. Instead of conducting all 50 runs, three example cases were chosen: the case with the greatest amount of rockfall, a case showing the median amount of rockfall, and one case that showed no rockfall. The thermal state with the highest level of rock temperature and thermally induced rock stress (80 years after waste loading) was chosen. As illustrated in Figures 5-5, 5-6, and 5-7, the initial state (before heating began) and the state after 80 years of heating coincide with extreme points on thermally induced stress paths at a number of locations around the emplacement drift. The state after 80 years was felt to be of greatest interest because already-completed nonthermal analyses provide the other extreme thermal condition.[18]

As shown in Table 5-7, the impact of thermal loading in nonlithophysal rock is to stabilize the rock mass and reduce rockfall. The reason for this effect is that the rock mass expansion on heating induces tangential compression around the excavations. This compression tends to provide increased normal stresses to fractures, thus increasing their shearing resistance as well as minimizing joint opening during extensional loading during the seismic event. Thus, the most conservative thermal state, from a rockfall standpoint, is actually when the rock is at or near ambient temperature.

[18] It was demonstrated in *Drift Degradation Analysis* (BSC 2004a, Section 6.2.1.3) that little damage occurs in the rock mass from in situ stress and heating only; therefore, there is little yield and permanent deformation on cooldown.

Table 5-7. Impact of Thermal Loading on Rockfall for 10^{-5} Ground Motion, Nonlithophysal Rock

Case	Nonthermal Analysis			Thermal Stress Addition		
	Time of Event (years)	Number of Blocks Dislodged (Nonthermal)	Rockfall Volume (m^3)*	Time of Event (years)	Number of Blocks Dislodged (Thermal)	Rockfall Volume (m^3)
Greatest Rockfall Case	0 (Nonthermal)	173	42.03	80	56	13.59
Median Rockfall Case	0 (Nonthermal)	14	2.49	80	5	1.07
No Rockfall Case	0 (Nonthermal)	0	0.00	80	2	5.93

Source: BSC 2004a, Table 6-19.

NOTE: *Volume per 25-m modeled drift length.

5.3.2.1.9 Summary of Data Output Feeds from Nonlithophysal Analyses to Drip Shield Analysis and Design

The results of the nonlithophysal analyses provide primary input to the detailed structural analysis of the stability and damage assessment of the drip shield. In particular, the following rockfall block information for each analysis at each annual exceedance frequency is fed to the drip shield engineering design analysis: (1) mass and shape, (2) velocity components (relative to the drip shield), (3) impact location and energy, and (4) timing of impact. This information is used for assessment of stability (buckling) and damage (both breaching of the skin of the drip shield as well as yield) and forms the basis for the abstraction of damage as a function of peak ground velocity in *Seismic Consequence Abstraction* (BSC 2004e). Structural analysis of the effect of rockfall on the drip shield can be found in *Drip Shield Structural Response to Rock Fall* (BSC 2004m).

5.3.2.2 Lithophysal Rocks

5.3.2.2.1 Two-Dimensional Discontinuum Analysis of Lithophysal Rock Mass

The UDEC model, whose development was described in Section 4, was used to perform the rock mass degradation analyses discussed in this section. In the UDEC model, the rock mass is represented as an assembly of polygonal, elastic blocks. The entire domain is discretized into blocks using Voronoi tessellations (Itasca Consulting Group 2002). The joints between blocks are considered to be linearly elastic-brittle. The elastic behavior of joints is controlled by normal and shear stiffness (joint stiffness is constant). The joint stiffnesses produce a rock mass deformation modulus that is calibrated to reproduce the strength envelope of that given by lithophysal rock quality categories 1 to 5. Joints can sustain finite tensile stress as prescribed by the rock mass tensile strength. The Coulomb slip condition governs the onset of slip as a function of joint cohesion and friction angle, which have been calibrated to reproduce the

lithophysal rock mass in categories 1 to 5. If a joint fails either in tension or shear, tensile strength, friction and cohesion are reset to residual values.

This model allows for the formation of fractures between blocks, separation and instability (under action of gravity and seismic accelerations) of portions of the rock mass around a drift. No ground support was considered in the analyses. All cases of thermal and seismic loading considered in this section were also analyzed using a continuum, linearly elastic approximation by the finite difference code FLAC (Itasca Consulting Group 2002). The results of the continuum model were used as a reference for additional interpretation of the results from the more complex UDEC model.

The geometry of the UDEC model is shown in Figure 5-20. As indicated, only the region around the drift where inelastic deformation is expected is discretized into Voronoi blocks. The rest of the model is composed of a few large, elastic blocks that simply transmit far field stresses and ground motion from the boundary to the interior region.

Each of the individual UDEC models presented in this section considers the rock mass to be characterized by a single rock property category. For example, a UDEC Category 5 model will use Category 5 rock properties throughout the model region. In reality, the lithophysal rock mass can contain multiple rock property categories within a 5- to 10-m zone. The consideration of spatial variability of the rock mass porosity, is provided in *Drift Degradation Analysis* (BSC 2004a, Appendix S, Section S.4). The impact of spatial variability of porosity and the ultimate conservatism associated with the homogeneous properties approach used as a base condition is described later.

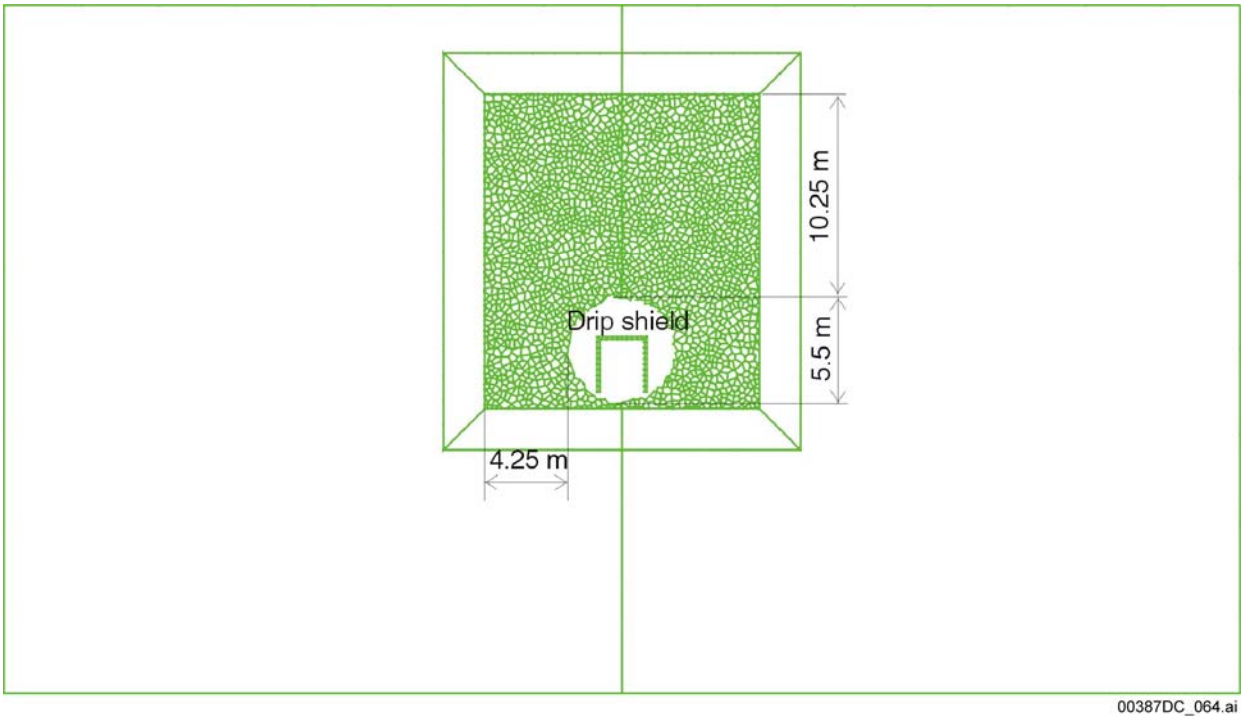

Source: BSC 2004a, Figure 6-118.

NOTE: Voronoi blocks represent near-field nonlinear behavior. Elastic blocks represent far-field behavior.

Figure 5-20. Geometry and Initial Conditions of the UDEC Model

5.3.2.2.2 Seismic Consideration in Lithophysal Units

Drift stability was analyzed for two preclosure and two postclosure ground motion data sets (5×10^{-4}, 10^{-4}, 10^{-5}, and 10^{-6} annual exceedance frequencies). One ground motion, (consisting of the three component motions) was supplied for each of the preclosure cases, whereas 15 sets of ground motion data were supplied for the postclosure case. For each of these ground motion data, the response for the range of rock mass properties categories was investigated.

An in situ (before excavation) stress state, defined by 7 MPa vertical and 3.5 MPa horizontal stresses, is used throughout the simulations, which is consistent with the 3DEC modeling discussed previously. The equilibrium state of the model after excavation of a drift represents the initial condition for the dynamic analysis. This equilibrium state is achieved by performing a quasi-static simulation whose geometry, static boundary, and initial conditions are illustrated in Figure 5-21.

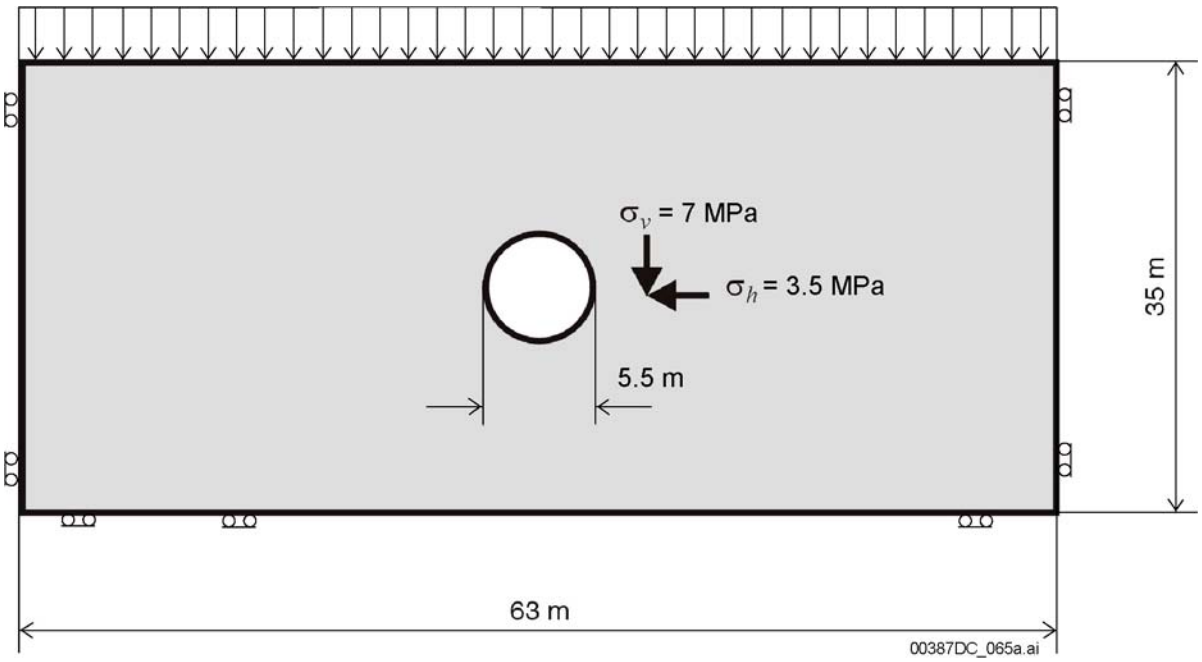

Source: BSC 2004a, Figure 6-119.

Figure 5-21. Dynamic Model, Initial and Boundary Conditions: Initial Static Simulation

The boundary conditions used in the dynamic analysis are illustrated in Figure 5-22. Quiet boundaries (indicated in Figure 5-22 as viscous boundaries) were used on all models outside boundaries. These boundaries prevent reflection of outgoing seismic waves back into the model. Quiet boundaries were combined with free-field boundaries on the vertical outside boundaries that prevent distortion of vertically propagating plane waves along the boundaries. Dynamic loading was applied at the bottom of the model, as propagating vertically upwards.

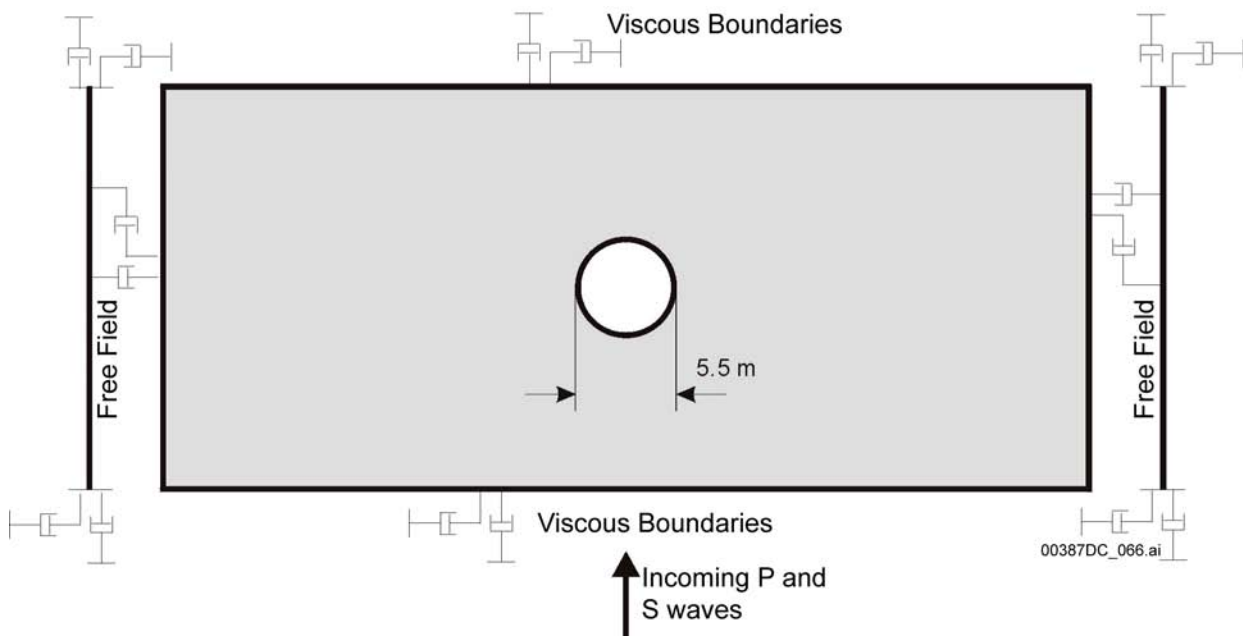

Source: BSC 2004a, Figure 6-120.

Figure 5-22. Dynamic Model Boundary Conditions for Dynamic Simulation

Preclosure Case–The preclosure ground motions, defined here as annual exceedance probabilities of 10^{-4} or greater, were conservatively examined for unsupported tunnels. The analyses indicate that ground motion with a probability of an annual occurrence of 5×10^{-4} and 10^{-4} will not induce any rockfall for rock mass categories 2 through 5. As discussed in Section 4.2.2.1, the estimated mean rock mass condition is Category 3, with about 90% of the Tptpll having Category 3 or greater properties. A relatively small amount of rockfall from the drift walls (shown in Figure 5-23) is expected, even for the lowest quality (less than 10% of all lithophysal rock) Category 1. In reality, no rockfall would occur in preclosure since the emplacement drifts are fully supported with rock bolts and surface steel sheeting (see Figure 1-4).

Stress monitoring locations within the rock mass surrounding the tunnel show that dynamic stress changes induced by this ground motion are small, and the rock mass remains well within the elastic range. The observed rockfall in the Category 1 case is simply the small springline zone of yielded rock from in situ stresses being shaken down. The conclusion is that only minor sidewall sloughing would be expected from this ground motion, and only in the poorest quality rock. Light bolting and surface support would easily contain this material.

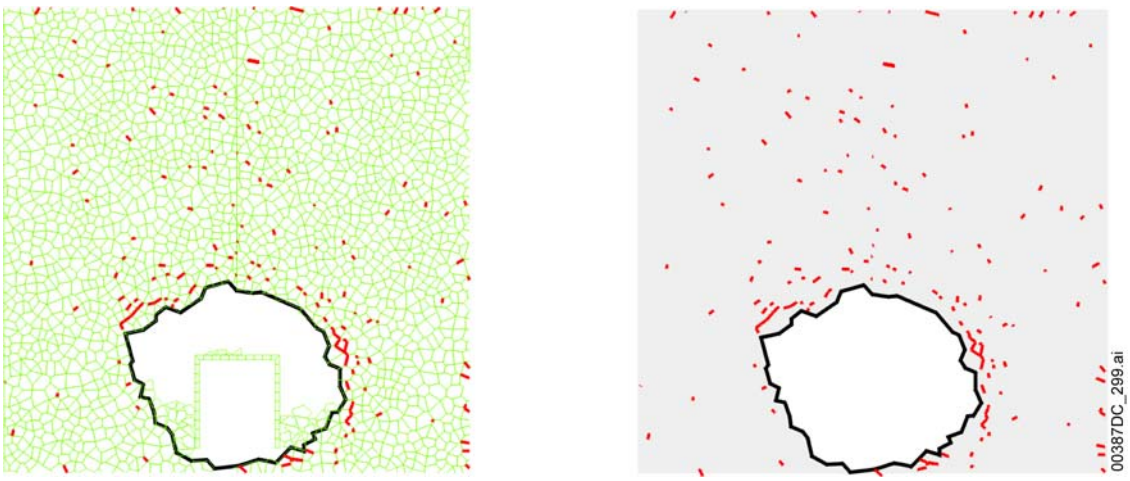

Source: BSC 2004a, Figure 6-127.

NOTE: Rock mass categories 2 to 5 show no damage from the 1×10^{-4} ground motion. Red lines indicate block bonds that have failed in shear or tension.

Figure 5-23. Geometry of the Model after Simulation for Preclosure Ground Motion (Probability 10^{-4}): Rock Mass Category 1

5.3.2.2.2.1 Postclosure Analyses

10^{-5} Ground Motion Parametric Analyses–All 15 sets of ground motion time histories were applied to unsupported base case rock mass strength Categories 1, 3, and 5 to provide a cross-section of response across the entire range of rock qualities. The level of damage induced by the ground motion is quantified here by the area (volume) of the rock that yields and is detached from the surrounding rock mass and falls into the tunnel. Since the model is two dimensional, it essentially represents a 1-m-thick slice of material parallel to the axis of the drift. The damage is this thus given in terms of volume per meter of emplacement drift, or cubic meters per meter. This could be converted to metric tons by multiplying by the density, which for the lithophysal rock is approximately 2 tons/m^3 (assuming a matrix density of approximately 2.5 tons/m^3).

10^{-5} Ground Motion Damage Assessment–Figures 5-24 to 5-26 show representative examples of the mechanism and level of damage induced for rock strength Categories 1, 3, and 5 for ground motion 12 (1.04 m/s peak ground velocity), 4 (1.52 m/s peak ground velocity), and 7 (3.33 m/s peak ground velocity). These ground motion data cover the approximate range of peak ground velocities for all 15 motions. The *Seismic Consequence Abstraction* (BSC 2004e) relates both rockfall and vibratory damage to the drip shield directly to the peak ground velocity of all three components of any particular ground motion. Since peak ground velocity and its variability are directly related to annual exceedance frequency, a correlation of damage to probability can be developed.

The drift damage levels are plotted for each rock mass strength category as a function of peak ground velocity in Figure 5-27. The analyses show that the damage is related to the magnitude of peak ground velocity, with significant variability at large peak ground velocity. Approximate linear upper and lower bounds are shown for each rock strength category, with a damage band shown that covers the range of variability. The variability in the response is a function of the

ground motion, not the rock properties, since constant modulus and strength are assumed for a given category. This variability at large peak ground velocity can be explained by examining the damage as a function of the total energy in the waveform. A Fast Fourier Transform (FFT) was used to perform an integration of each of the 15 10^{-5} velocity time histories (in terms of the velocity squared). The result of this integration is a spectral power density number that is proportional to the total kinetic energy (kinetic energy = $\frac{1}{2}(mv^2)$) of the time history.

The damage as a function of the velocity power spectral density for the ground motion component (either H1 or V, whichever has the maximum value of peak ground velocity) for each of the 45 analyses is plotted in Figure 5-28. This plot shows that the damage is linearly related to the kinetic energy associated with the velocity time history. Therefore, although the peak ground velocity is, in general, related to drift damage, the variability in that correlation is related to the total kinetic energy in the time history.

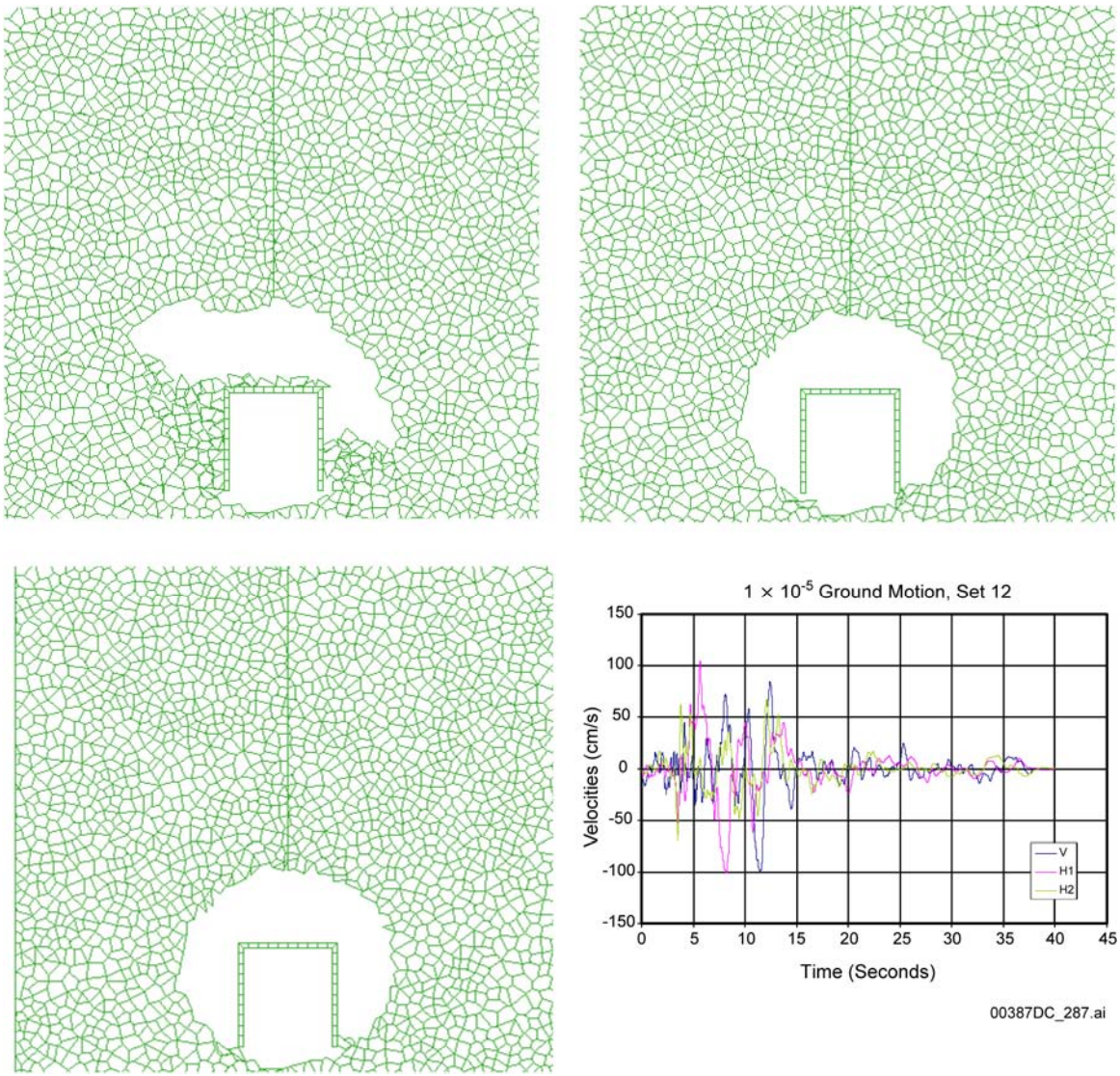

Source: BSC 2004a, Figure 6-128.

NOTE: (upper left) Rock Strength Category 1 (5.6 m^3/m drift length), (upper right) Category 3 (0.3 m^3/m), (lower left) Category 5 (0.2 m^3/m), and (lower right) Ground Motion History 12, peak ground velocity = 104 cm/s.

Figure 5-24. Example of Comparison of Damage Levels for Lower End of Peak Ground Velocity (104 cm/s) for 10^{-5} Annual Exceedance Level

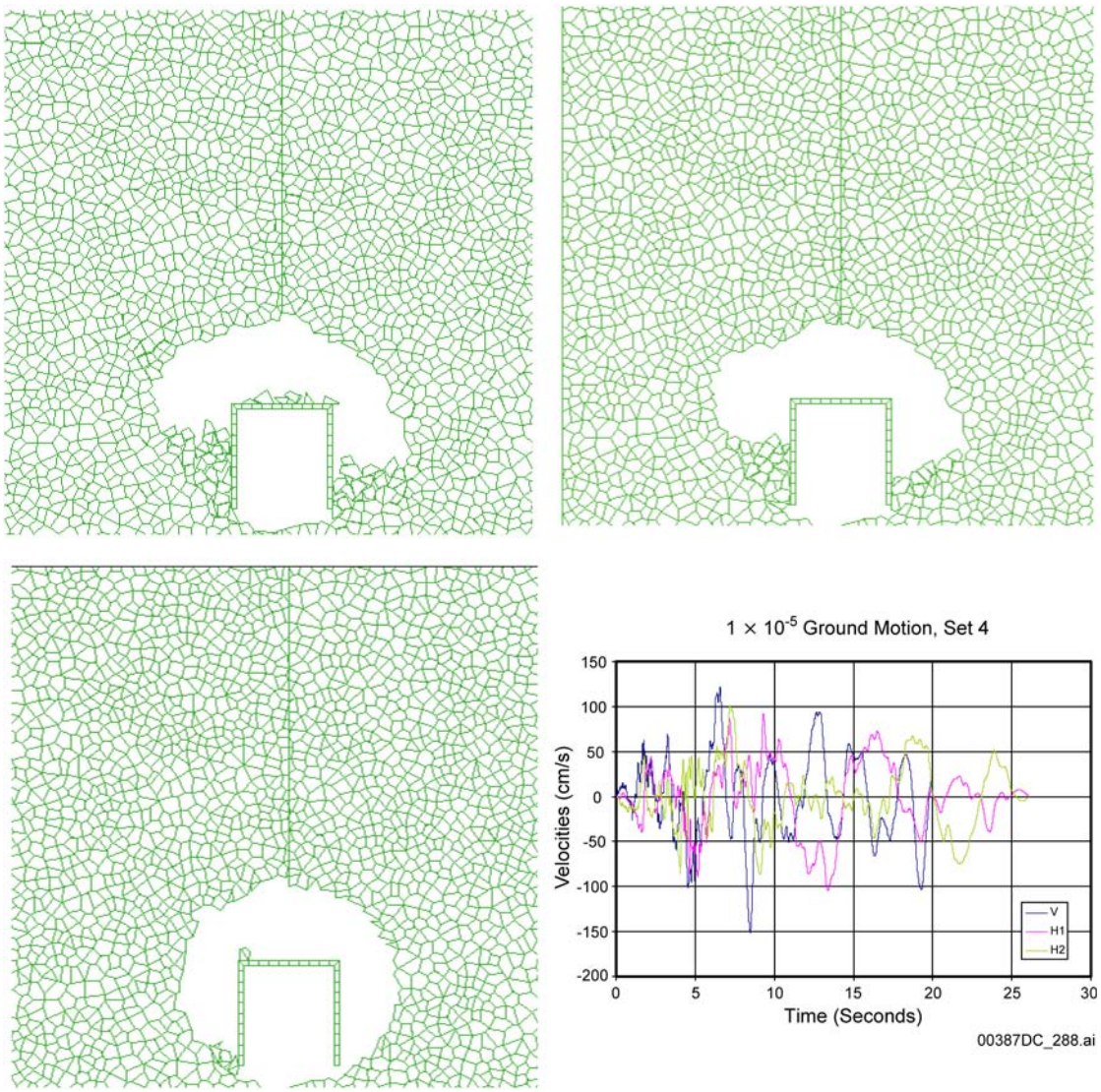

Source: BSC 2004a, Figure 6-129.

NOTE: (upper left) Rock Strength Category 1 (3.6 m^3/m drift length), (upper right) Category 3 (2.3 m^3/m), (lower left) Category 5 (0.3 m^3/m), and (lower right) Ground Motion History 4, peak ground velocity = 152 cm/s.

Figure 5-25. Example of Comparison of Damage Levels for Peak Ground Velocity of 152 cm/s for 10^{-5} Annual Exceedance Level

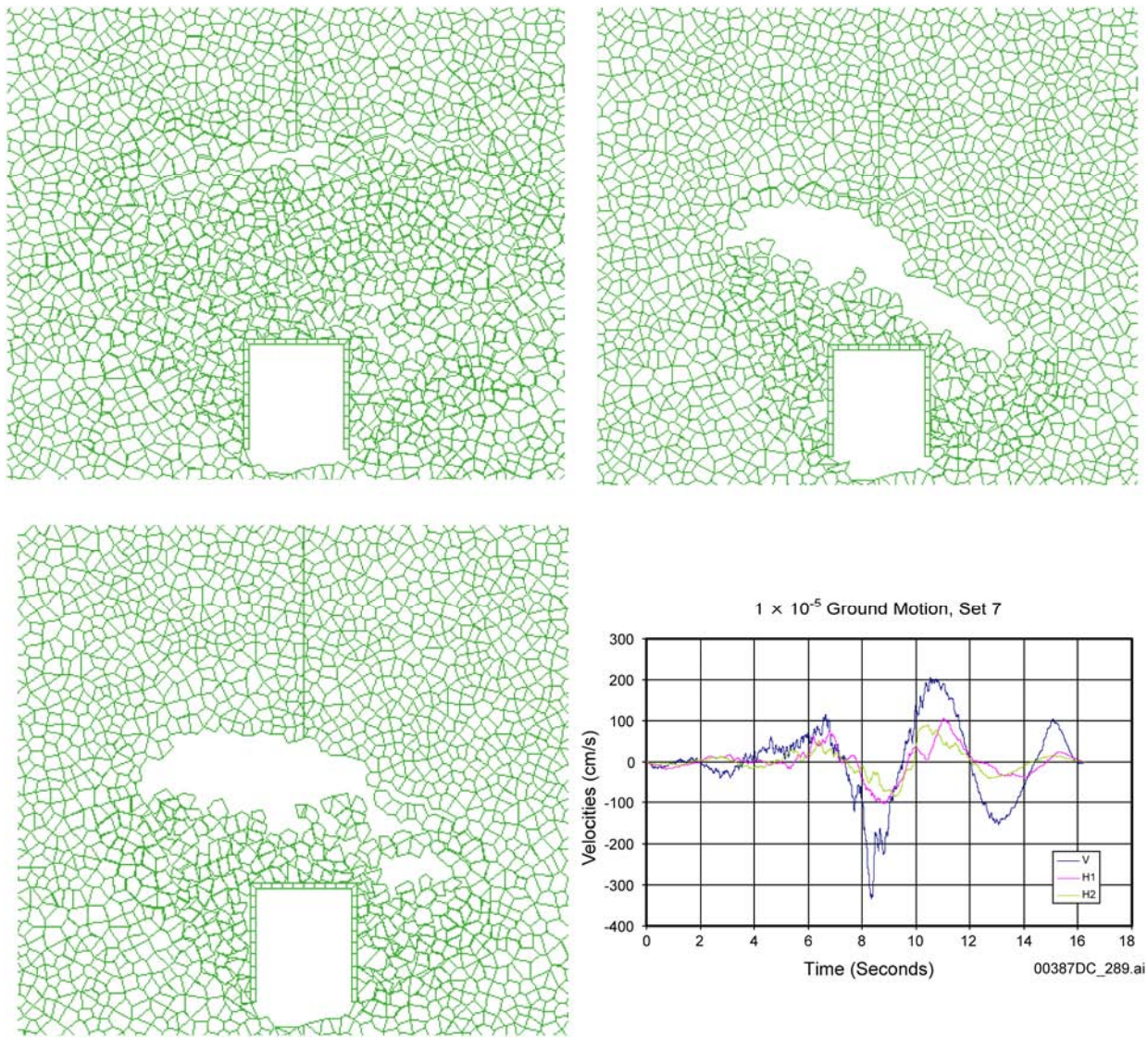

Source: BSC 2004a, Figure 6-130.

NOTE: (upper left) Rock Strength Category 1 (49.7 m^3/m drift length), (upper right) Category 3 (16.1 m^3/m), (lower left) Category 5 (21.1 m^3/m), and (lower right) Ground Motion History 7, peak ground velocity = 333 cm/s.

Figure 5-26. Example of Comparison of Damage Levels for Upper End of Peak Ground Velocity (333 cm/s) for 10^{-5} m/s

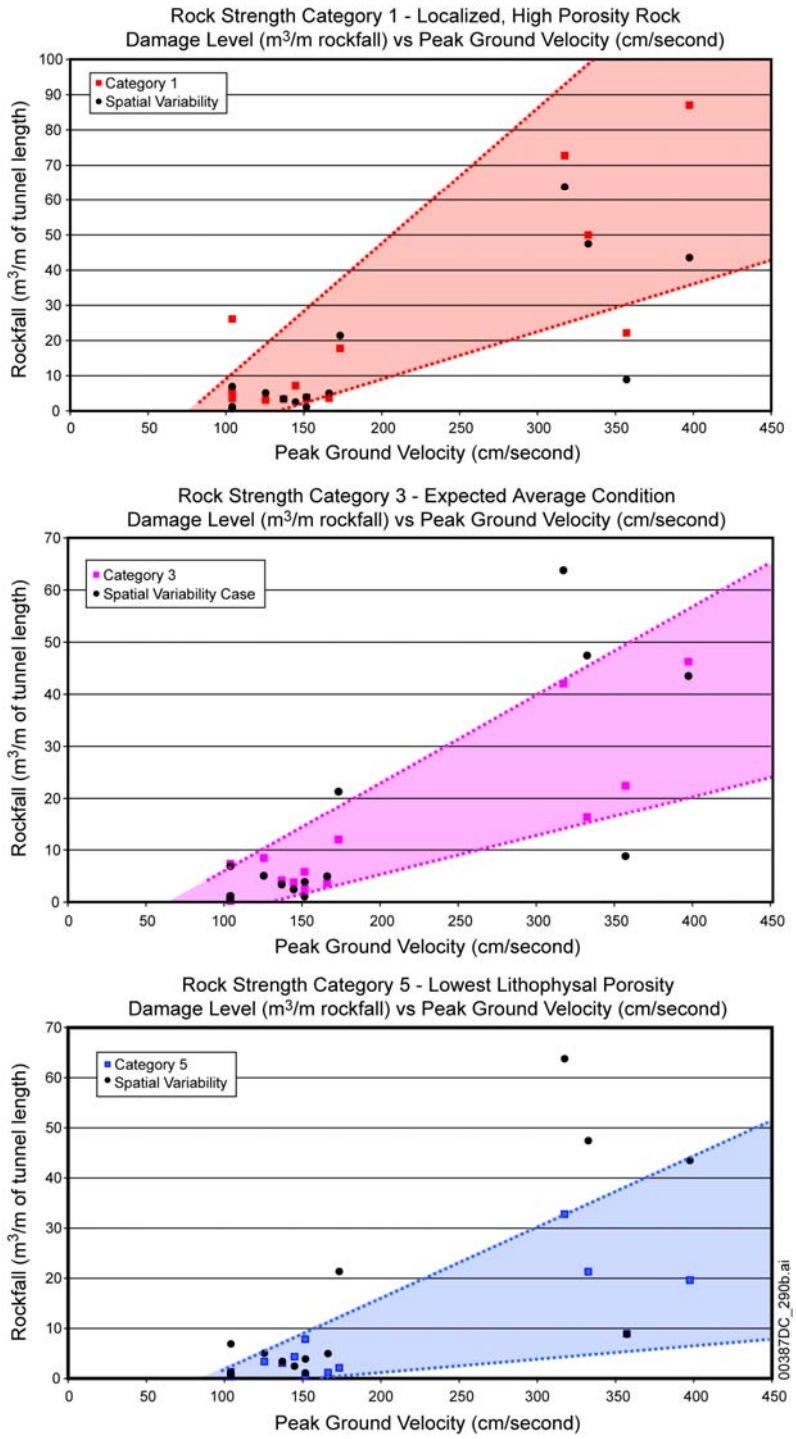

Source: BSC 2004a, Figure 6-131.

NOTE: Upper and lower linear bounds are drawn empirically to cover entire range of results for all 15°ground motion data and are given for visual reference only. Black data points are results for simulations in which rock mass has spatially-variable lithophysal porosity.

Figure 5-27. Estimate 10^{-5} Damage Level, Expressed as m^3/m of Emplacement Drift Length for Rock Strength Categories 1 (Top), 3 (Center), and 5 (Bottom) for All 15 Ground Motion Data.

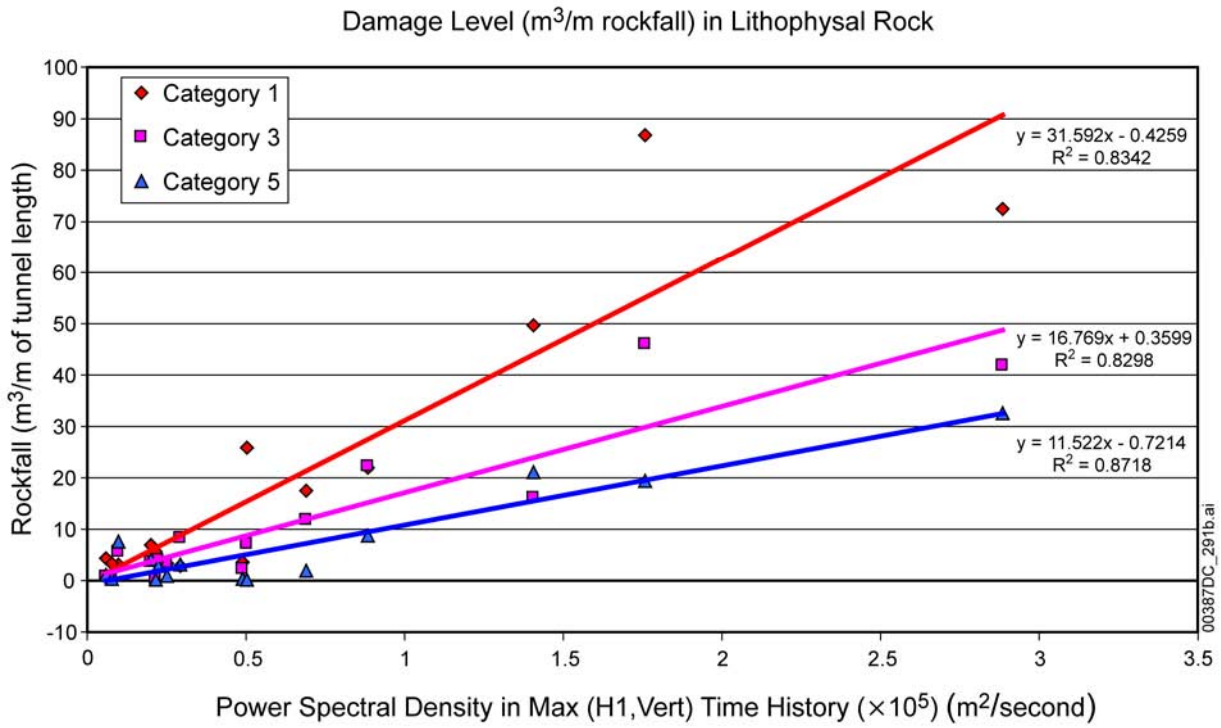

Source: BSC 2004a, Figure 6-132.

NOTE: The power spectral density is obtained by integrating the square of the velocity time history, producing a value proportional to the kinetic energy.

Figure 5-28. Rockfall Damage as a Function of the Energy Associated with the Vertical Velocity Time History

Damage Mechanism–The drift damage mechanism consists primarily of stress-induced failure of the rock mass resulting from the stress change associated with the velocity time history. The in situ stress field has major vertical and minor horizontal stress components. The vertical compression or horizontal shear wave essentially results in a free field dynamic stress increase equivalent to (Itasca Consulting Group 2002):

$$\sigma_{n,s} = \rho C_{p,s} V_{n,s}$$

where: $\sigma_{n,s}$ = dynamic induced normal (n) or shear (s) stress component
ρ = rock density
$C_{p,s}$ = speed of p-wave (p) or s-wave (s) propagation in rock medium
$V_{n,s}$ = peak normal (n) or shear (s) ground velocity

These dynamic components are superimposed on the existing in situ stress field to cause additional stressing or relaxation of the rock mass surrounding the drift. The end result of this superposition is that the stress tensor changes, both in magnitude and orientation of the principal stresses, as the ground velocities oscillate over the duration of the strong ground motion. Superposition of in situ and dynamic stresses can cause tensile or shear failure of rock mass, resulting in development of an elliptic shape of the opening as the rock mass yields and rockfall occurs and falls along the sides of the drip shield. Shear failure is most likely to start at the

springline, which is the location of the largest stresses under in situ stress conditions. The extent of shear failure and rockfall around the circumference of the tunnel, up and down from the springline, is due to both the general ratio of rock mass strength to stress, but also to the ratio of the vertical to horizontal peak ground velocity. The greater the horizontal component, the greater the rotation of the stress tensor, which results in greater inclination of the major principal stress. Generally, this shear failure mechanism occurs with the arrival of the peak ground velocities. Compressive stresses also appear responsible for some cases in which roof slabbing is observed where the rock mass strength and stiffness are larger (i.e., Category 5). A second failure mechanism observed includes tensile failure of the rock mass resulting from the reversal of the ground motion and inducement of dynamic tensile straining in the rock mass (i.e., when seismically-induced tensile stress exceeds in situ compressive stress and tensile strength, combined).

In general, it appears that the rock mass failure and thus rockfall occurs simultaneously with the arrival of velocity peaks in the time histories. In a similar fashion, the peak ground velocity has been recognized by many authors as the primary contributing factor to dynamic rock mass failure in mine tunnels, slopes and dams (e.g., Newmark 1965). In the present case, the shear or tensile failure mechanism results in a predicted creation of blocks resulting from fracture of the rock mass along the ubiquitous fracture network of the material. The blocks that contact the drip shield are relatively small in size and governed by the inherent fracture network and lithophysae spacing. The UDEC model studies have used primarily a 0.3 m average fracture spacing in developing the block structure, although simulations with 0.2 m spacing have also been conducted. In all cases, the transient dynamic stress changes, in addition to preexisting in situ stresses, results in breakage of the bonds between the blocks in the rockfall zone around the tunnel. In other words, the stressing does not create large blocks that impact the drip shield, but small component blocks defined by the inherent fracturing of the Tptpll.

Although the damage levels appear to correlate somewhat better to the energy content of the time history, correlation to peak ground velocity provides a simpler method for interpretation of the results. An approximate relationship of damage level to peak ground velocity in terms of both m^3/m of drift length and physical interpretation can be roughly approximated as follows:

- Damage level below 5 m^3/m results in minor damage to rock particles filling the invert along the sides of the drip shield – a peak ground velocity below about 1.5 m/s (see Figure 5-24).

- Damage level from 5 to 15 m^3/m results in rock particles covering the sides of the drip shield approximately to the height of the drip shield and may cover the top of the drip shield – this corresponds to peak ground velocity values of approximately 1.5 to 2 m/s (see Figure 5-25).

- Damage level above 15 m^3/m causes complete collapse of the tunnel, this corresponds to peak ground velocity values of approximately 2 to 3 m/s (see Figure 5-26).

Impact of Spatial Variability–In the previous analyses, the rock mass properties were considered homogeneous for a given drift cross section. Here, the impact of considering actual spatial variability of lithophysal porosity on damage from 10^{-5} ground motion is examined.

A representative section of the Tptpll was extracted from the upper portion of the lithophysal porosity model as described in Section 2.3.2. This model contains a range of lithophysal porosity from less than 10% to greater than 25%, averaging approximately 17.5%. The resulting UDEC model showing spatially variable porosity is given in Figure 5-29.

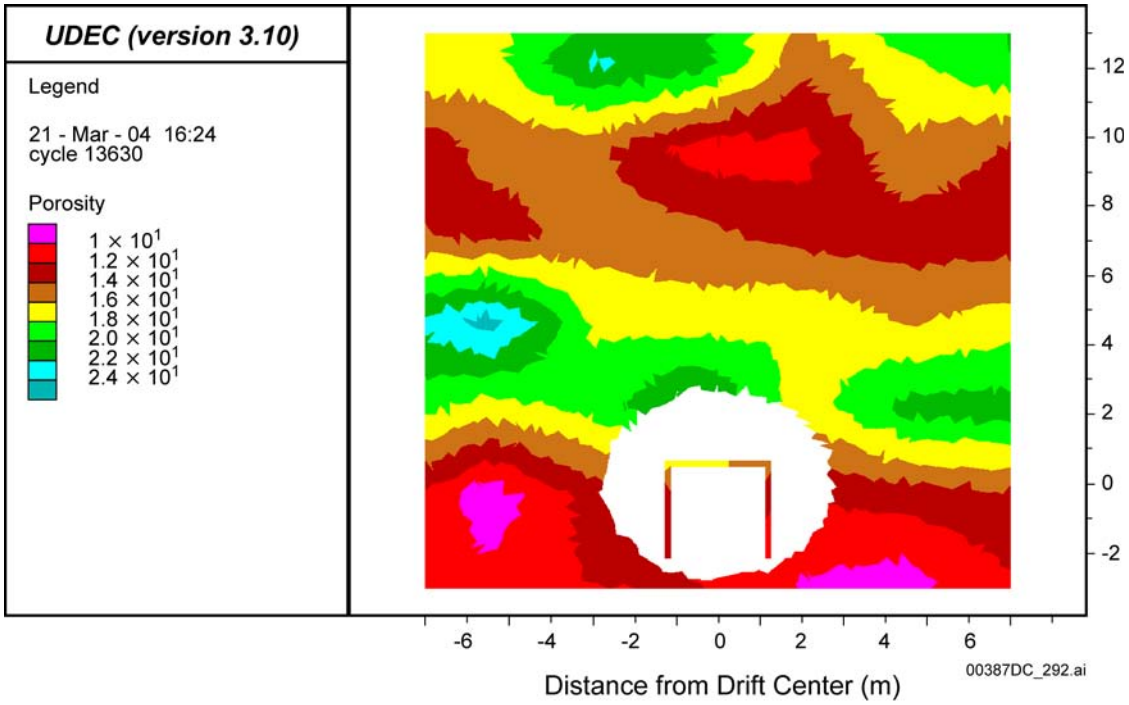

Source: BSC 2004a, Figure 6-133.

NOTE: Lithophysal porosity variability derived from Figure 2-11.

Figure 5-29. Contours of Lithophysal Porosity Contoured on the UDEC Spatial Variability Model (Top) and a Histogram Showing the Percentage of Lithophysal Porosity within the Model (Bottom)

Rock mass strength properties for Categories 1 to 5 were interpolated in the model based on the lithophysal porosity levels, achieving spatial variability in strength and moduli. This model was subjected by all 15 10^{-5} ground motion data, and damage levels determined. The results of the dynamic simulations, in terms of damage versus peak ground velocity, are shown in Figure 5-27. The damage levels are approximately in the range of the Category 3 rock mass as expected since the mean lithophysal porosity of the model falls within the range of the Category 3 levels. This analysis indicates that the use of homogenous rock properties that span the range of strength categories does, indeed, span the range of expected response, including conservative damage for the low strength categories.

Drip Shield Loading from Seismic Damage–The loading of the broken rock mass after drift collapse for the 10^{-5} case is examined for the assumption of rigid and deformable drip shields. Two cases of drip shield deformability are examined: (1) rigid, rectangular geometry, and (2) deformable, arched roof shape (Figure 5-30). The rigid assumption, used due to its simplicity, is the base case assumption. The deformable case provides a two-dimensional model

of the actual shape and deformability of the drip shield using the standard UDEC element structure. The drip shield is subdivided into 30 total segments of equal length. In the deformable case, the elements are assumed to be elastic. Since the UDEC model is two-dimensional and does not attempt to model the detailed structure of the drip shield, the stiffness of the elements must be adjusted to provide an equivalent overall deformability to the actual three-dimensional structure. The stiffness of the UDEC elements has been calibrated against the three-dimensional LS-DYNA model to reproduce the deformability of the actual drip shield design (BSC 2004a). The dynamic loading from detached rock particles during the seismic shaking (includes the effect of relative velocity between the drip shield and the falling rock) is examined here. The quasi-steady load on the drip shield once the seismic shaking stops and the system comes to force equilibrium, and, the dynamic loading of the drip shield when it is covered by broken rock and subjected to additional seismic events, are discussed in Section 5.3.2.3.

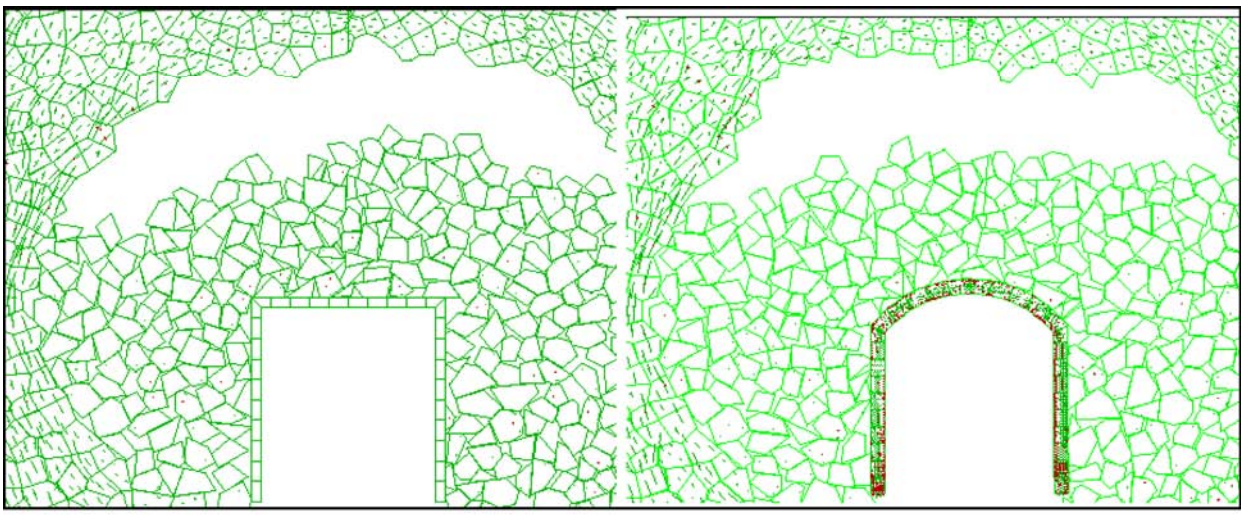

00387DC_293.ai

NOTE: Simple rigid, rectangular structure with footings rigidly fixed to the invert (left) and a deformable, actual geometry with footings pinned (i.e., translational motion slaved to the invert) (right). Drip shield footings can also slide on and separate from the invert.

Figure 5-30. Schematic Representation of Two Cases of Drip Shield Loading Showing (a) Rigid Rectangular Geometry and (b) Deformable Arched Geometry

5.3.2.2.2.2 Dynamic Impact Loading of the Drip Shield

An example of the dynamic impact loading from side and top impacts to the deformable drip shield resulting from the 10^{-5} ground motion (peak ground velocity = 3.33 m/s case) is given in Figure 5-31. In this figure, the average pressure across an element (in Pa) is given as a function of time (in seconds). In general, the transient pressure at any given element is approximately one order of magnitude greater than the eventual dead weight load of bulked rock for the case of a completely collapsed tunnel at equilibrium. However, due to the relatively small size of the rock particles developed in the lithophysal rock (in comparison to the much larger blocks in the nonlithophysal material), the nonlithophysal dynamic impact loading to the drip shield provides a more conservative, bounding case. Therefore, the nonlithophysal rockfall case is used to provide dynamic impact loading for the damage analysis and design of the drip shield.

Quasi-static loading of the dead weight of the rock on the drip shield is described in Section 5.3.2.3.

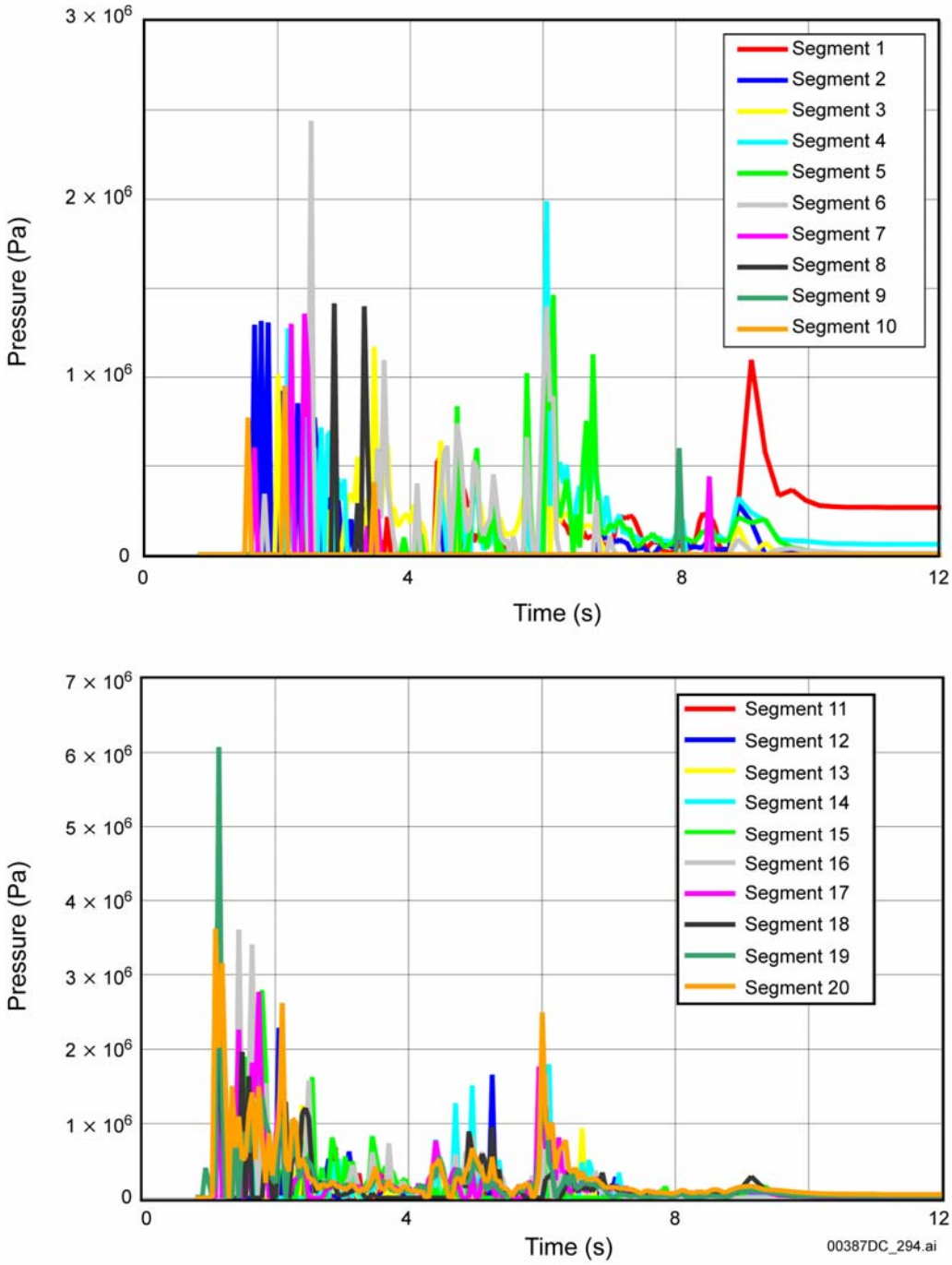

Source: BSC 2004a, Figure 6-135.

NOTE: Segments are numbered counterclockwise from the right side footing. Segments 1 to 10 are found along the right wall, 11 to 20 along the roof.

Figure 5-31. Example of Dynamic Impact Loading to the Right Wall (Top) and Roof (Bottom) of Deformable Drip Shield with Arched Roof

10^{-6} Ground Motion Parametric Analyses–Fifteen 10^{-6} ground motion time histories are characterized by the peak ground velocity of the H1 component of 2.44 m/s, resulting in a vertical component with mean of 1.11 m/s (Table 5-1 summarizes peak ground motion values). The analyses of the 10^{-5} ground motion showed extensive damage for peak ground velocity in excess of approximately 2 m/s, and therefore, similar damage is expected for all the 10^{-6} and 10^{-7} ground motion cases. A typical model geometry after simulation of the 10^{-6} motion is shown in Figure 5-32 showing complete collapse of tunnels in lithophysal rock. The extent of failure and detached rock mass forms a roughly elliptical shape that extends approximately one tunnel diameter into the roof of the drift. The rock mass failure mechanism, a combination of shear and tension failure, is similar to that described for the 10^{-5} case. As was discussed in the previous section, tunnel collapse occurs for peak ground velocity values in excess of approximately 2 to 3 m/s.

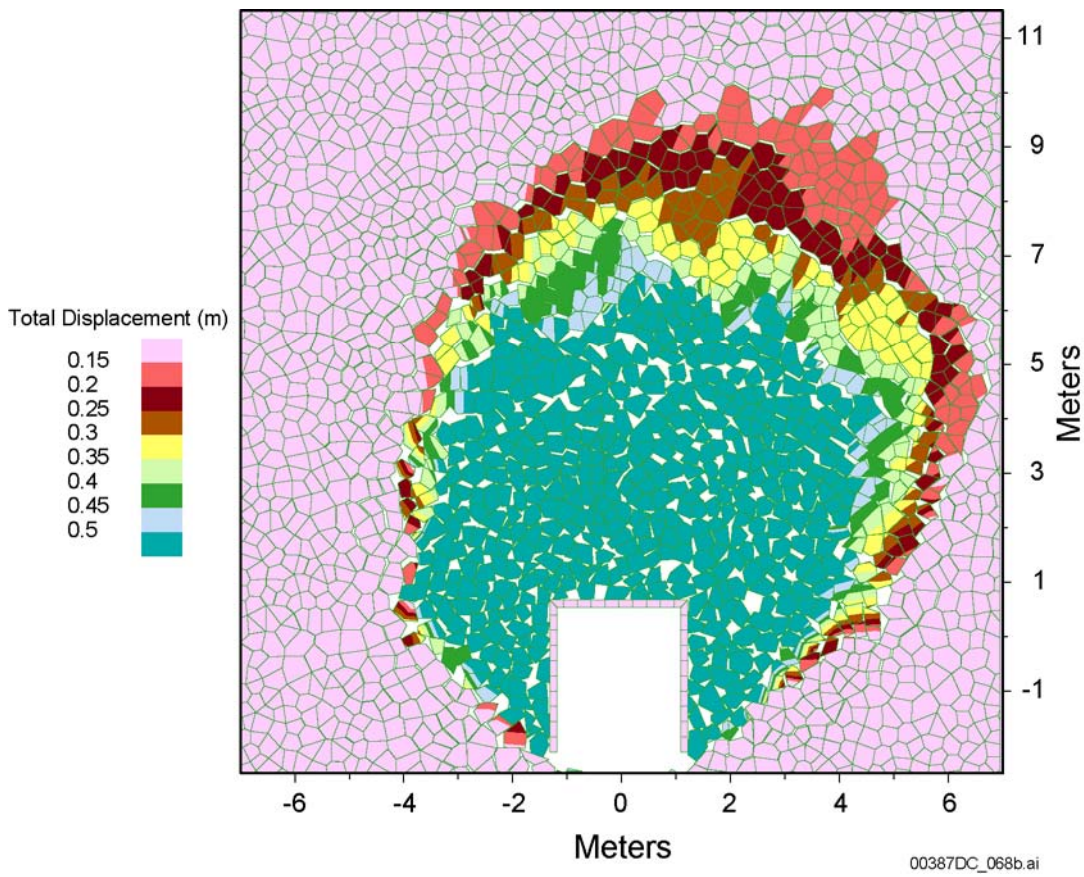

Source: BSC 2004a, Figure 6-133e.

NOTE: Blocks are colored by magnitude of displacement.

Figure 5-32 Typical Geometry of the Model after Simulations for Postclosure Ground Motion (Probability 10^{-6})

5.3.2.2.3 Combined Seismic, Thermal, and Time-Dependent Effect in Lithophysal Units

The initial condition for the seismic analysis discussed in the previous section was the in situ stress state perturbed only by excavation of the drifts. Throughout the postclosure phase, the rock mass temperature, and the associated thermally induced stress state will vary as discussed in Section 5.3.1. These stresses, particularly in the first one thousand years of postclosure time, are potentially significant as initial condition for to the transient seismic stressing. The impact of the thermal stresses is examined here.

Preclosure temperature and stress increase from heating is small and has no appreciable impact on drift degradation over and above preclosure seismic loading under in situ temperature conditions. Therefore, the maximum thermal condition (i.e., approximately 30 years after cessation of forced ventilation) is used as an initial condition for the seismic analysis (Figure 5-4).

Because the ground motion with 10^{-6} probability of annual occurrence results in complete drift collapse, it was not of particular interest to investigate the effect of that level of ground motion combined with thermally induced initial stresses. Instead, a ground motion of 5×10^{-4} probabilities of annual occurrence was considered. Rock mass categories 1 and 5 were considered in this analysis.

Seismic analysis using 1×10^{-4} ground motion after 80 years of heating for rock mass Category 1 (lowest strength) resulted in an increased rockfall compared to rockfall from the seismic shaking of the rock mass at the in situ stress state only (Figure 5-33, Category 1 (a)). Therefore, the heating induces additional damage (compared to damage caused by drift excavation), which does not necessarily result in a rockfall under static loading conditions but is shaken down by the 1×10^{-4} ground motion. No rockfall is induced in rock mass Category 5 in the case of 90% ventilation efficiency (Figure 5-33, Category 5 (b)).

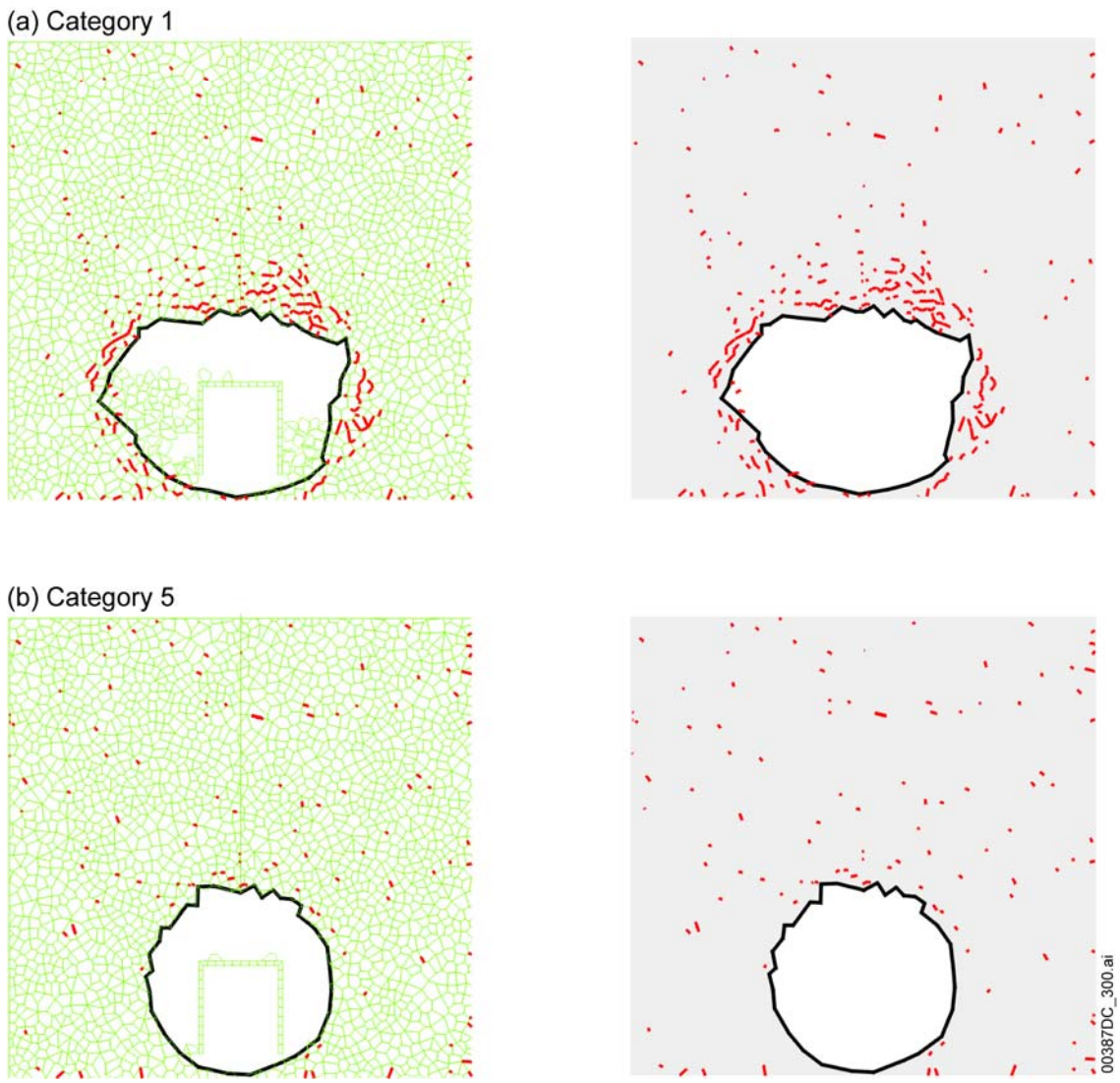

Source: BSC 2004a, Figures R-31 and R-32.

NOTE: Yield at the in situ stress condition for Strength Categories 1 and 5 can be found in Figure 4-17.

Figure 5-33. Rockfall and Fractures Induced around a Drift by 1×10^{-4} Preclosure Ground Motion after the Peak Thermal Condition Occurring at 80 Years of Heating (30 Years after Closure) in Rock Mass Categories 1 and 5

5.3.2.2.4 Time-Dependent Consideration in Lithophysal Units

Underground and surface excavations, which are designed to be stable after excavation, degrade with time, and some eventually collapse completely. The degradation of excavations in hard rocks has not been studied extensively because most underground excavations have service lives of 100 years or less and are maintained as required. However, there are many examples of stable, unsupported excavations associated with mining, and civil construction or naturally occurring caves in numerous rock types that are stable, or have suffered only minor instability for hundreds or even thousands of years (BSC 2002f, Section 3). Thus, there is no certainty that

collapse of unsupported excavations, particularly those subjected to low stress, relatively dry conditions, is inevitable.

The primary reason for eventual yield and collapse is that a hard rock mass, exposed to humidity and temperature of the open atmosphere, may undergo strength decay with time when it is loaded to stress levels higher than about 50% to 60% of its short-term strength. The rate of strength decay depends on, among other parameters, rock type (particularly the mineralogy and grain structure), stress state, relative humidity, and temperature. Stress corrosion is considered the primary mechanism causing strength degradation of hard rocks (Potyondy and Cundall 2001, Section 3).

The emplacement drifts at Yucca Mountain will be stable under currently existing conditions (in situ stresses and rock mass strength) with ground support as demonstrated by the calculations presented here. However, it is expected that the ground support will completely lose its integrity during the 10,000-year regulatory period, and drift degradation, to some extent, will occur due to strength decay of the rock mass. Drift degradation is an important issue for the repository design and performance as drifts have to remain open during the preclosure period; and eventually the caved rock resulting from degradation will load the drip shields possibly affecting their integrity and performance. Prediction of the rate of drift degradation for the duration of the 10,000-year regulatory period is a highly approximate task (it requires extrapolation of testing results, which have been done for a period of months, to a period of 10,000 years). Uncertainty in such predictions is quite large. The rate of drift degradation has been analyzed and is documented in detail in *Drift Degradation Analysis* (BSC 2004a, Appendix S).

Time-Dependent Drift Degradation Analysis Methodology–There is currently no accepted methodology for estimating the time-dependent degradation behavior of hard rocks. The empirical term “stand-up time” is often used in the mining industry to refer to an estimate of the amount of time that personnel can safely be sent beneath unsupported drill-and-blast tunnel headings without fear of loose material creating a working hazard (Bieniawski 1989). This “stand-up time” is typically on the order of hours or days, even for good quality rock masses, and is often confused with actual drift instability and collapse mechanisms.

Unsupported or lightly supported tunnels (although perhaps not safe from a personnel standpoint) can stand in stable condition for long time periods, particularly in good quality rock masses. For example, the ESF and ECRB Cross-Drift tunnels were constructed in 1995 to 1997 and in 1998, respectively. Although the ESF main loop is located largely in the Tptpmn, the ECRB Cross-Drift cuts through and exposes all of the repository host horizon units. The tunnels are, in general, lightly supported with friction rock bolts and light wire mesh in the tunnel roof, with occasional friction bolts in the tunnel walls. There is no evidence of significant deterioration or degradation of the rock mass in these tunnels since excavation, and no significant rockfall has occurred. Tunnel steel set load (CRWMS M&O 1998b) and deformation measurements (CRWMS M&O 1998c) have been regularly monitored since excavation, showing stable conditions as well. The rock mass is obviously in a stable and self-supporting mode with no obvious deterioration in 5 to 8 years.

A key mechanism of failure in low porosity, brittle, crystalline rocks is development in the propagation of cracks parallel to the greatest principal stress direction. Extensive studies over

the last 40 years have demonstrated that the critical parameters that control crack growth are stress, temperature, and the partial pressure of water at the crack tip. A crack grows due to the hydration and breaking of silicon–oxygen bonds at the tip of the crack. The rate at which the crack grows is controlled by the diffusion of water to the crack tip. This mechanism is commonly termed stress corrosion cracking. Experimental data on single crystals of quartz, as well as in rocks, have validated these mechanisms (e.g., Martin 1972; Kranz 1979).

In brittle rocks subjected to a constant stress, a crack will propagate in a time-dependent way. The diffusion of water to the crack tip controls the rate. Since the physical mechanism is hydration, there is a volume increase on the surface of the crack. Consequently, the propagation of water to the crack tip is controlled by diffusion along a crack surface where the aperture decreases and diffusivity decreases. This gives rise to a logarithmic time-dependent crack growth. The rate at which water diffuses to the crack tip decreases with time, the rate of crack growth slows down, and the observed deformation rate decreases. When the crack reaches a critical length, the rock fails. Furthermore, the lower the stress for a constant temperature, the longer the time to failure (Kranz 1980; Martin et al. 1997a).

With the understanding of the physical mechanisms of crack growth, it is reasonable to understand how the time dependence works. The rate dependence is a physical process that is scalable. The common experimental testing technique used to determine the time to failure for brittle rocks is the static fatigue compression test, which is essentially the same as a creep experiment. The rock sample is loaded in uniaxial or confined compression to a load that is a given percentage of its strength. This load is held constant until the sample fails, and the time to failure is recorded. Since the rate dependence is scalable, static fatigue experiments conducted for time frames from several minutes to several months can be extrapolated to much longer times with confidence. A limited amount of static fatigue compression test data on the Tptpmn is used as the basis for extrapolation of the "time-to-failure" as a function of applied stress conditions. This data is supplemented by the more extensive literature data on static fatigue of granite as a means of comparison of failure time-rock strength relationships.

The PFC stress corrosion model by Potyondy and Cundall (2001), developed for similar time-dependent predictions for the Canadian waste disposal research program, has been extensively documented and validated against time-dependent tunnel breakout in granite at the Underground Research Laboratory in Manitoba, Canada. The PFC stress corrosion model is first calibrated to reproduce the static fatigue response of LdB granite and interpolated for nonlithophysal tuff (i.e., the Tptpmn). The model is then used to investigate the impact of lithophysal porosity on the rate of time-dependence, resulting in the generation of a set of curves of time-to-failure versus applied stress level for various levels of lithophysal porosity.

A rock mass damage-time relationship, developed from the PFC simulations, is embedded in the same UDEC model used earlier to perform lithophysal stability calculations. This model is used to generate estimates of drift degradation as a function of time for a range of rock mass strength categories. The model is validated for short time periods against observations of the existing ESF and ECRB drifts, and for long time periods against observations of lack of observed yielding in the Tptpll. This work is reviewed here; details of the methodology and analysis methods are referred to *Drift Degradation Analysis* (BSC 2004a, Appendix S). Currently, a significant program in static fatigue measurement of Tptpmn cores is being conducted to

supplement the limited existing data base. This present work will be updated as this long-term testing data is developed.

Static-Fatigue Behavior of Granite and Tuff–Martin et al. (1997a) present static-fatigue results for a total of 16 specimens of welded (lithophysae poor) tuff from borehole NRG-7/7A at Yucca Mountain and from Busted Butte boulders taken from the same block of rock. The specimens were 2:1 aspect-ratio right circular cylinders with a diameter of 50.8 mm. Load application was rapid, with full load being reached in less than 10 seconds.

The seven borehole specimens were tested, drained, and vented to the atmosphere at a temperature of 225°C and a confining pressure of 10 MPa at differential stresses ranging from 40 to 130 MPa. None of these specimens had failed after loading for times ranging from 2.5×10^6 to 5.9×10^6 seconds. The nine Busted Butte specimens were tested at a pore water pressure of 4.5 MPa, a temperature of 150°C, and a confining pressure of 5 MPa at differential stresses ranging from 115 to 150 MPa. The high pore pressure (i.e., 4.5 MPa) ensured that pore water remained in the liquid state even though the temperature is above the boiling point. The test results are summarized in Table 5-8. The applied load in the axial direction and the effective confining pressure are denoted by σ_1 and P_c, respectively. The axial load at failure during a short-term test is denoted by σ_f. The stress difference maintained during a static-fatigue test conducted at a confining pressure of P_c is $\sigma = \sigma_1 - P_c$. The stress difference at failure during a short-term test is $\sigma_c = \sigma_f - P_c$.

To facilitate comparison between different data sets, static-fatigue curves were generated by plotting the logarithm of time-to-failure, t_f, versus the driving-stress ratio given by $\sigma / \sigma_c = (\sigma_1 - P_c) / (\sigma_f - P_c)$. Six of these specimens failed at times less than 2×10^6 seconds, while the remaining three specimens (BB-9392-H, -G, and -J) did not fail during the testing period. The times-to-failure for these six tests can be plotted versus applied load (Figure 5-34); however, the peak strength must be estimated in order to plot them versus driving-stress ratio for comparison with data from the Lac du Bonnet granite (Schmidtke and Lajtai 1985; Lau et al. 2000). For these purposes, the peak strength of the tuff samples at an effective confinement of 0.5 MPa is estimated to be 151 MPa, to give a failure time of one second for a driving-stress ratio of unity.[19]

Approximate linear relationships in semi log space have been fit to the unconfined and confined granite and tuff data. The granite data shows a flatter slope, or faster time-to-failure than the tuff for similar ratios of the applied stress to unconfined compressive strength in this plot. This would be expected as the tuff is a fine-grained volcanic that shows very little hysteresis on unloading until brittle failure occurs. The granite, on the other hand, is composed of coarser mineral grain structure of several different minerals and exhibits permanent deformation at lower strain levels.

[19] The unconfined compressive strength values by Martin et al. (1997a) for six saturated 50.8-mm-diameter Busted Butte specimens tested at a strain rate of 10^{-5}/s ranged from approximately 105 to 200 MPa, with a mean of approximately 128 MPa for the five weakest specimens.

Table 5-8. Static-Fatigue Data for Busted Butte Specimens

Specimen	P_c (MPa)	σ (MPa)	t_f (sec)	$\log(t_f)$ (sec)	σ_f (MPa)	σ/σ_c
BB-9392-K	0.5	149.0	1.2	0.08	151	0.99
BB-9392-N	0.5	141.0	4	0.60	151	0.94
BB-9392-E	0.5	134.6	250	2.40	151	0.89
BB-9392-C	0.5	134.2	636	2.80	151	0.89
BB-9392-F	0.5	132.8	5,848	3.77	151	0.85
BB-9392-B	0.5	127.8	1,960,000	6.29	151	0.85
BB-9392-H	0.5	131.4	1,180,000	6.07	151	0.87
BB-9392-G	0.5	131.3	732,000	5.86	151	0.87
BB-9392-J	0.5	115.0	2,000,000	6.30	151	0.76

Source: Martin et al. 1997a.

NOTE: Specimens were saturated and tested at a pore water pressure of 4.5 MPa and temperature of 150°C. Specimens were loaded directly to creep stress (σ_1) in less than 10 seconds. Specimen diameter is 50.8 mm. Specimens BB-9392-H, BB-9392-G, and BB-9392-J did not fail during the test.

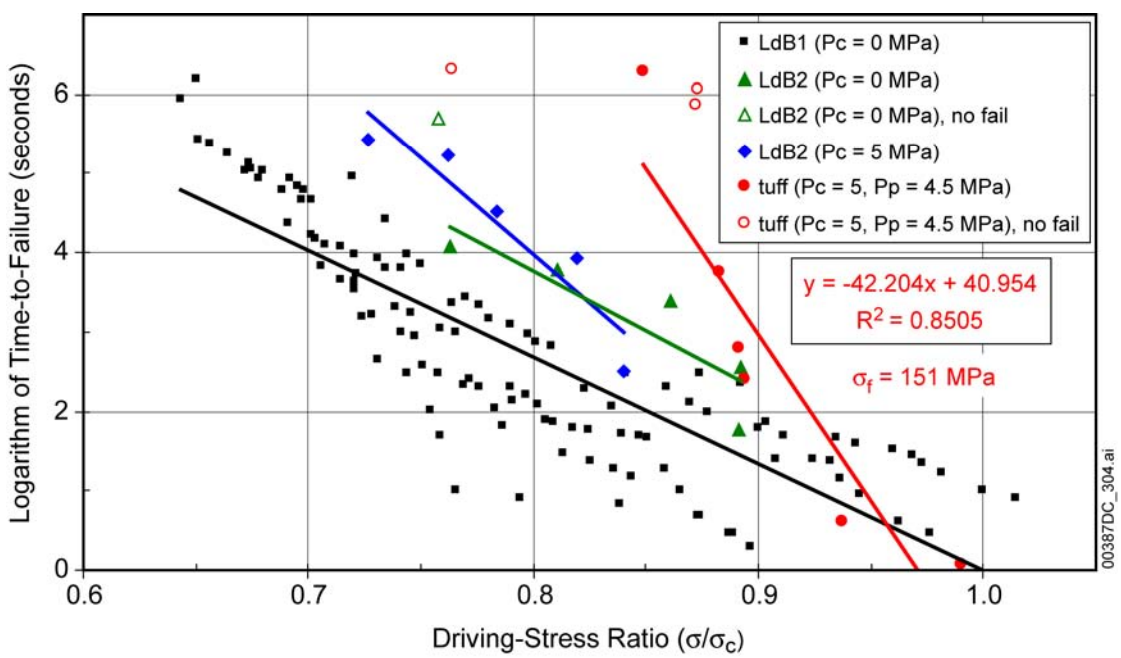

Source: BSC 2004a, Figure 6-148.

NOTE: Tests of Lac du Bonnet granite conducted at 25°C. Tuff tests conducted at 150°C. LdB = Lac du Bonnet.

Figure 5-34. Static-Fatigue Data for Welded Tuff and Lac du Bonnet Granite

PFC Corrosion Model Calibration and Examination of Impact of Lithophysal Voids–The static fatigue data for welded tuff shown in Figure 5-34 is for nonlithophysal samples. Since the majority of the repository lies within lithophysal rock, it is necessary to determine the impact of lithophysal voids on the static fatigue response (essentially, the slope of the best-fit lines in this figure).

Since the matrix material of the nonlithophysal and lithophysal tuff is mineralogically and mechanically similar, an approach to estimate the impact of lithophysae on the time-dependency can be developed based on the existing static fatigue data. The PFC program is first calibrated to reproduce the static fatigue response of the nonlithophysal rock. Using the same matrix properties, lithophysal porosity is added and time-dependency extrapolated. This is a reasonable approach because the primary effect of lithophysae is to adjust the internal stress condition of the sample, which, in turn, impacts the time-to-failure. PFC automatically determines the internal stress redistribution and concentration in the sample and thus accounts for this primary effect.

The PFC model for lithophysal tuff was described previously in Section 4. This PFC model (consisting of circular voids within a well-connected base material) has the same matrix material for which the stress-corrosion behavior is measured. The long-term behavior of the PFC material is characterized by performing a series of static-fatigue tests on the PFC lithophysal-tuff model. Recall that the PFC model consists of rigid, circular particles interconnected at their contact points. The macroscopic material behavior of the PFC model is governed by the strength and stiffness properties of the contact points. The PFC stress corrosion model uses the same construction and bonding characteristics as the model presented earlier, with the difference being that the bond strengths include time-related parameters consistent with a stress corrosion cracking mechanism. These time-dependent bond parameters (β_1, β_2, and $\bar{\sigma}_a$) are determined via calibration of the PFC model to static fatigue time-to-failure test data. These parameters do not affect the short-term behavior. The properties of the PFC2D material are obtained by numerically testing 1:1 aspect-ratio specimens (Figure 5-35) of one-meter diameter with void porosities of 0, 0.1, and 0.2 under static-fatigue conditions at confinements of 0.1 and 5 MPa.

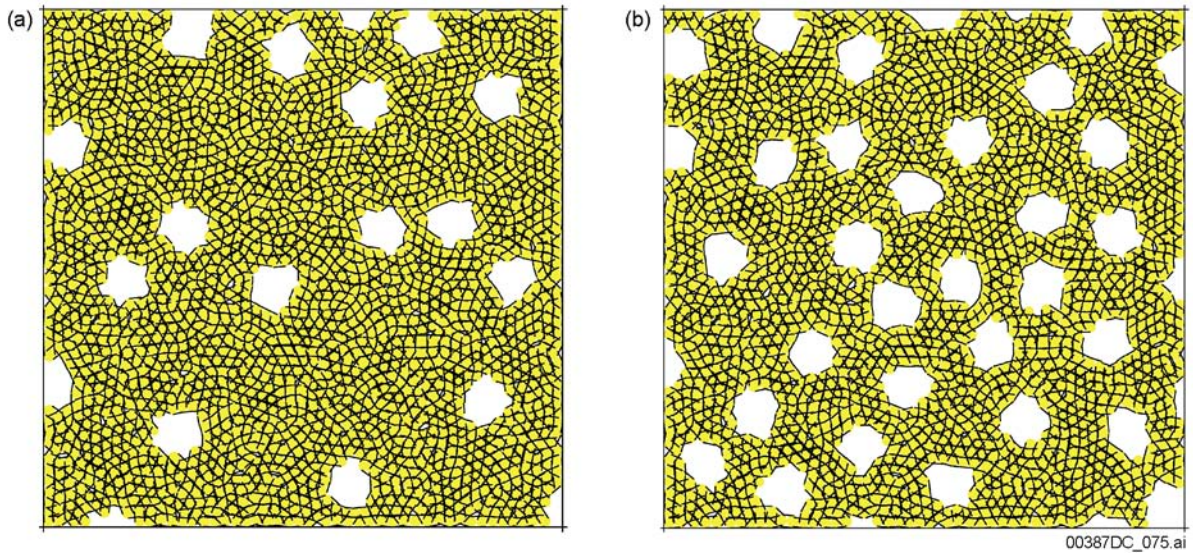

Source: BSC 2004a, Figure 5-5.

NOTE: Examples have void porosities of 0.107 (a) and 0.204 (b).

Figure 5-35. PFC2D Specimens of Tuff Material for Static Fatigue Testing

Figure 5-36 shows a typical "creep" curve and damage plot from a PFC nonlithophysal rock test in which the sample uniaxial load is held constant at 80% of the unconfined compressive strength. Damage occurs in the form of formation of cracks as a function of time. As seen, the sample undergoes time-dependent deformation until approximately 5,000 seconds, when creep rupture occurs and the sample fails. Numerical tests such as these are used first to calibrate the PFC model against the laboratory data for nonlithophysal tuff, but then to extrapolate the time-to-failure data to lithophysal rock with varying levels of lithophysal porosity.

Figure 5-37 shows a plot of the time-to-failure for different levels of sample porosity as a function of the ratio of applied stress to unconfined compression strength for lithophysal tuff samples. As one might expect, as the lithophysal porosity increases, the time-to-failure of the rock mass decreases, presumably due to the presence of increased level of tensile stresses in the material.

Inclusion of Time-Dependency Into an Engineering Approximation of Drift Degradation– To utilize the time-to-failure data for lithophysal tuff, it must be generalized into an engineering-based model that can predict the evolving stress state around excavations resulting from time-dependent strength degradation as well as from in situ, thermal, and seismic loading. The same UDEC approach that has been used for the previous calculations is used for this purpose. Because the UDEC model is used in a quasi-static mode in this regard, it is most convenient to frame the time-to-failure data in the form of a simple damage coefficient that represents the time-evolution of strength degradation.

Damage Coefficient Derivation–The axial load at failure (peak strength) during a short-term test performed at an elapsed time, t, since the start of a static-fatigue test is denoted by $\sigma^*_f = \sigma^*_f(t)$. The values of σ^*_f are bounded by:

$$\sigma^*_f(0) \leq \sigma_f$$

$$\sigma^*_f(t_f) \geq (\sigma/\sigma_c)\,(\sigma_f - P_c) + P_c \qquad \text{(Eq. 5-1)}$$

where (σ/σ_c) is the ratio of the driving stress to the unconfined compressive strength of the material, and P_c is the confining pressure of the test. The values of σ^*_f for times $0 < t < t_f$ are found by stopping the static-fatigue test at the desired time and measuring the peak strength.

The strength degradation is quantified by means of a damage coefficient:

$$D = 1 - \sigma^*_c / \sigma_c \qquad \text{(Eq. 5-2)}$$

where $\sigma^*_c = \sigma^*_f - P_c$ is the principal stress difference at failure. Substituting values from Equation 5-1 into this expression provides the following bounds for the damage coefficient:

$$D(0) = 0$$

$$D(t_f) = 1 - (\sigma/\sigma_c) \qquad \text{(Eq. 5-3)}$$

The time evolution of the damage coefficient for the nonlithophysal tuff material tested at a confinement of 0.1 MPa is shown in Figure 5-38. These results were produced by performing 10 numerical compression tests conducted on damaged "samples" derived from four static-fatigue tests at driving stress ratios of 0.8, 0.6, 0.4, and 0.2. In other words, the PFC stress corrosion model spontaneously produces stress corrosion fracturing as the simulated static fatigue test is run. To determine the impact of this damage on the strength of the sample, the static fatigue simulations are stopped at various elapsed times and the damaged "sample" compressed to determine its peak strength. The loss of cohesive and tensile strength, expressed as a ratio of the original strength, is termed the damage coefficient. Most damage occurs during the final stages of a static-fatigue test; tests performed at lower driving-stress ratios produce an earlier (in terms of normalized times-to-failure) onset of damage. Damage evolution for lithophysal tuff follows a similar form, with the time factor determined from the time-to-failure behavior illustrated in Figure 5-37.

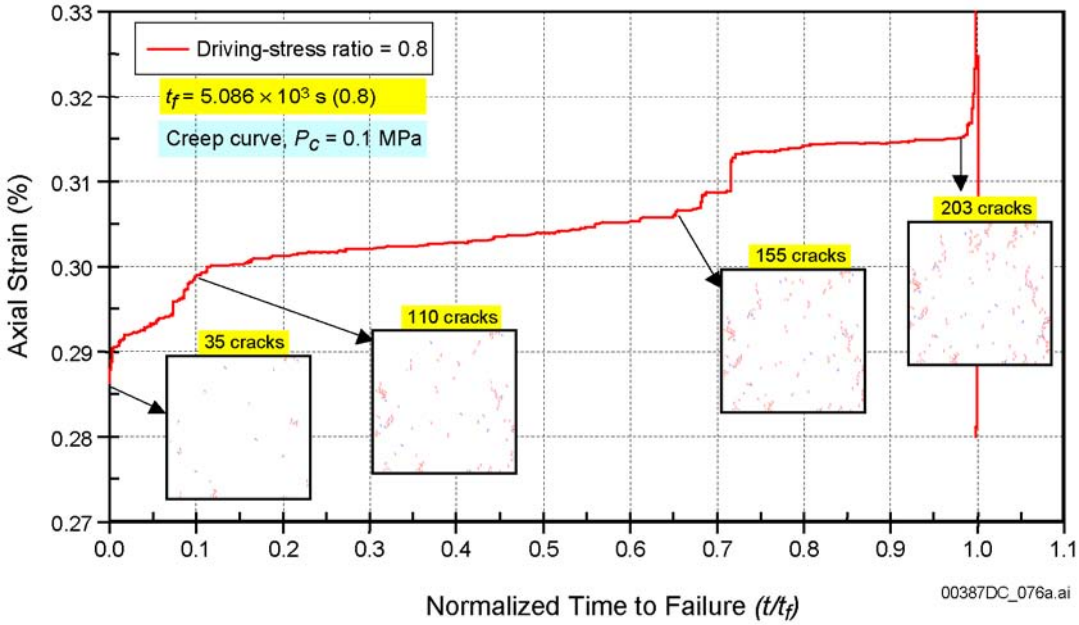

Source: BSC 2004a, Figure 5-12.

Figure 5-36. Creep Curve and Damage in mS50 Material for Static-Fatigue Test (0.1 MPa Confinement) at Driving-Stress Ratio of 0.8

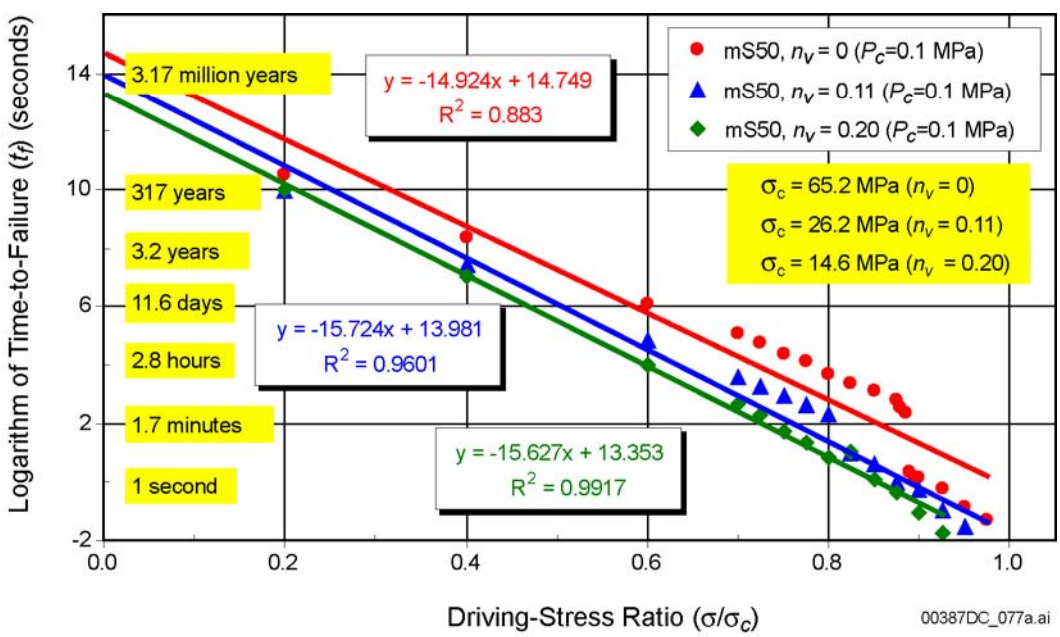

Source: BSC 2004a, Figure 5-16.

NOTE: The time-dependency has approximately the same slope for all void porosities. Straight-line fit.

Figure 5-37. Effect of Void Porosity on Static-Fatigue Curves (0.1 MPa Confinement) for Lithophysal Tuff Material (0% to 20% Void Porosity)

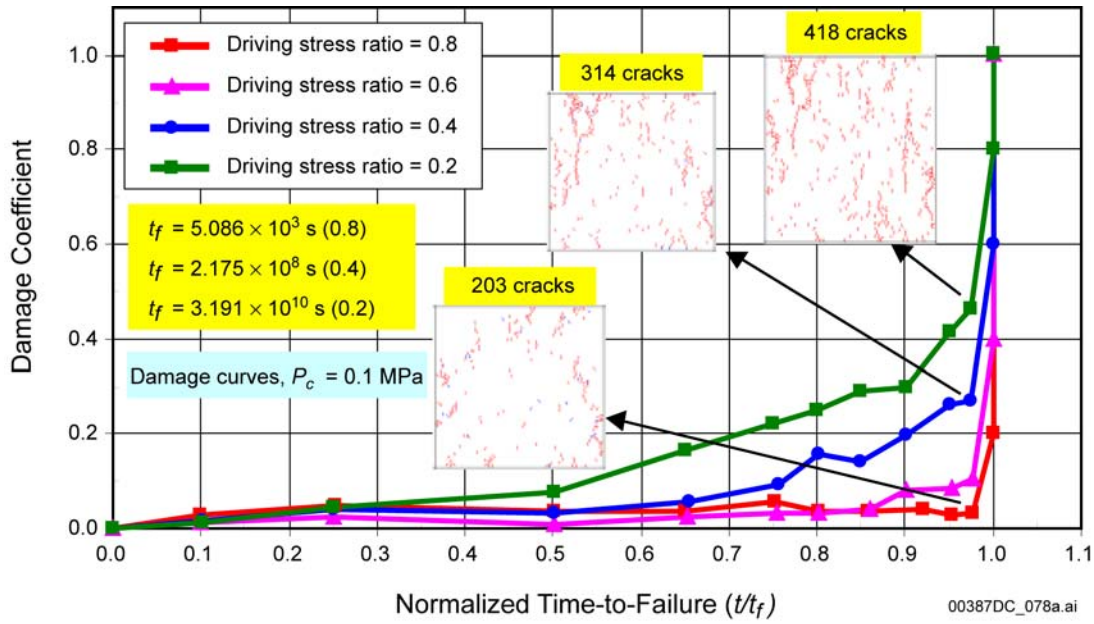

Source: BSC 2004a, Figure 5-21.

Figure 5-38. Time Evolution of Damage Due to Strength Degradation Coefficient for Nonlithophysal Tuff Material during Static-Fatigue Tests (0.1 MPa Confinement) at Driving-Stress Ratios Ranging from 0.2 to 0.8

Static-Fatigue Curves and the Evolution of Damage Due to Strength Degradation–The static-fatigue behavior of Lac du Bonnet granite and welded lithophysal tuff forms the basis of the UDEC model for stress corrosion around a drift. The static-fatigue curves provide the time-to-failure (t_f) of the material at a particular driving-stress ratio (σ/σ_c).

The static-fatigue data for Lac du Bonnet granite at 0 and 5 MPa confinement and tuff at 5 MPa confinement and 4.5 MPa pore pressure are shown in Figure 5-34. Each data set was fit with a straight line, and the line was extrapolated to encompass driving-stress ratios ranging from 0 to 1. This is a conservative assumption, because the curves most likely approach infinity at a driving-stress ratio less than about 0.5. Three lines for the tuff data are shown in Figure 5-39. The blue line in the figure is the least-square linear fit through the tuff data, while the purple line (best fit through origin curve) is the best-fit for the tuff data for unconfined compressive strength (i.e., failure at 1 s at the unit driving ratio of 1.0). Since the tuff data are very limited and are for confined conditions (effective confining stress of 0.5 MPa) only, the data input to UDEC uses a simplified best fit curve (red line) termed the "tuff best fit curve." The tuff best fit curve will be updated as the ongoing test data become available.

Using the time-to-failure versus stress-to-strength ratio (Figure 5-39) and the damage coefficient evolution plot, a simplified, general damage evolution curve in terms of time can be developed and used directly in the UDEC program for drift stability modeling. Figure 5-40 presents these relations for the tuff best-fit curve. This family of curves can be used to directly relate reduction in cohesive and tensile strength of the rock mass as a function of stress state and elapsed time since excavation.

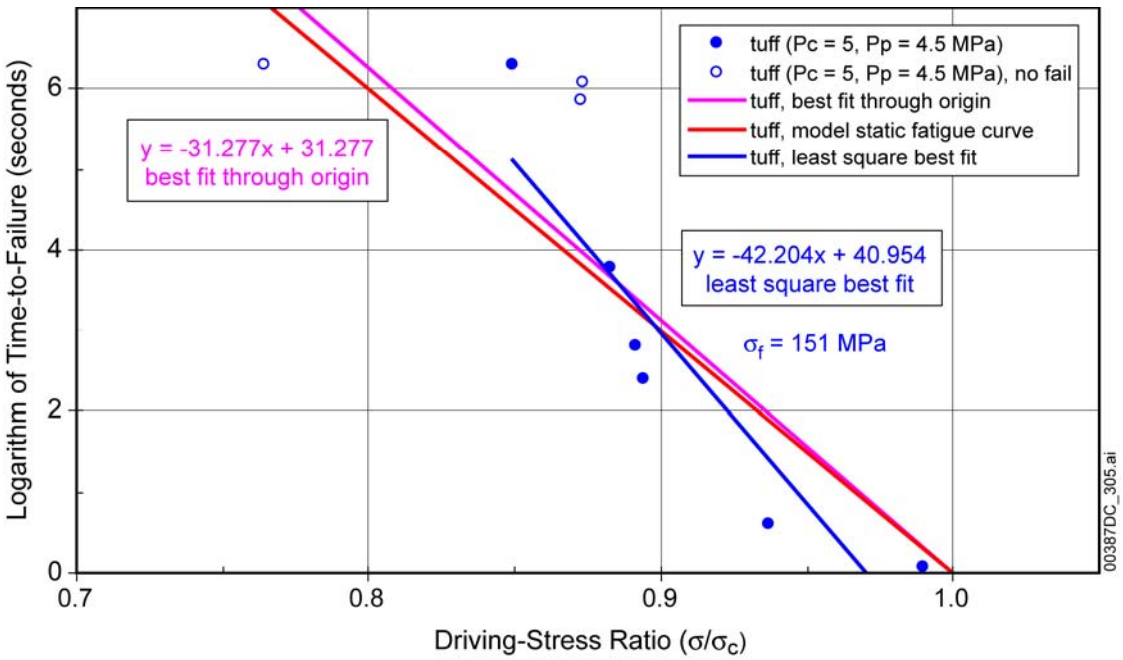

Source: BSC 2004a, Figure 5-25.

NOTE: LdB = Lac du Bonnet granite. Tuff tests were conducted at 150°C.

Figure 5-39. Static-Fatigue Curves Used as Input to the UDEC Analyses

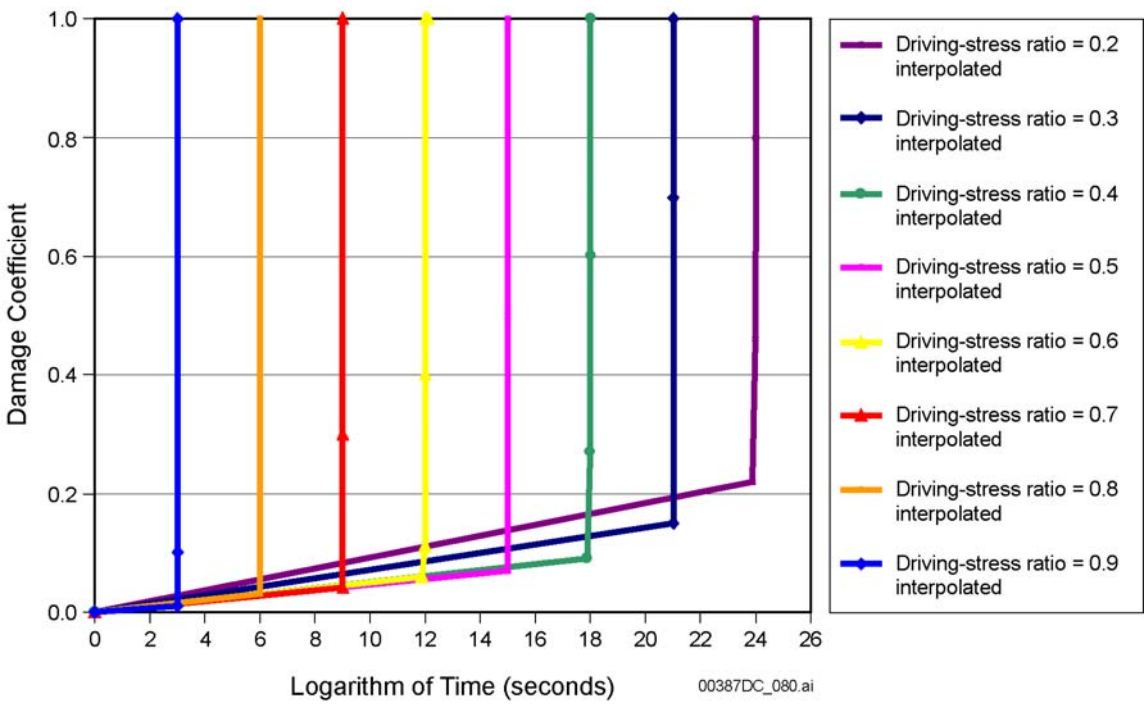

Source: BSC 2004a, Figure 5-28.

NOTE: Simplified curves are conservative in that complete damage (i.e., failure and loss of strength) is assumed to occur once time-to-failure is achieved.

Figure 5-40. Damage Curves Used as Input to the UDEC Tuff Best-Fit Analyses

Stress Corrosion Modeling with UDEC Drift Scale Model–The damage–time response illustrated in Figure 5-40 was embedded into the strength of the block contact surfaces of the UDEC lithophysal rock model used previously for drift scale stability calculations. Recall that the small, irregular-shaped blocks that compose the UDEC lithophysal mass are interconnected by shear (cohesive and frictional) and tensile strength components. The strength and stiffness parameters of these contacts are calibrated to the lithophysal strength categories. Here, it is assumed that the damage coefficients are related directly to the percentage loss of cohesion and tensile strength of these contacts; therefore, a damage coefficient of zero is no strength loss and a damage coefficient of 1 is 100% strength loss. The details of the generalization of the damage criteria within the contact strength logic in the UDEC program can be found in *Drift Degradation Analysis* (BSC 2004a, Appendix S).

UDEC drift stability analyses were initially conducted for in situ stress only. The time increments for solution of drift degradation were 1, 5, 10, 50, 100, 500, 1,000, 5,000, and 10,000 years. The damage states at 1, 5, and 10 years provide a means of back-analysis against existing observations in the ESF and ECRB Cross-Drift. Only the results for the best-fit tuff response are given here; additional analyses for the comparative granite time-to-failure data can be found in *Drift Degradation Analysis* (BSC 2004a).

Time-Dependent Effect from In Situ Stress Only in Lithophysal Units–Results for the predicted drift degradation for the selected time periods for the "best fit" tuff time-strength

relations for strength categories 1, 2, 3, and 5 are shown in Figures 5-41 to 5-44. Strength Category 1 (the poorest quality tuff) predicts immediate damage in the springline area of the drift characterized by extensive breakout which undergoes some, but not significant change over time. This means that the stress/strength ratio at the springline area is exceeded from in situ stress alone. This response is not observed in the existing ECRB Cross-Drift or ESF tunnels, and, as discussed in Chapter 5, the Category 1 strength level, corresponding to the poorest rock conditions, represents localized, poor rock conditions and is viewed as very conservative. It is noted that the springlines of the ECRB Cross-Drift are, in general, unsupported, and thus ground support is not preventing breakouts as predicted by this model. In a similar fashion, Category 2, representing about 7% of the Tptpll, shows springline damage levels immediately that are not observed in situ.

As discussed previously, back-analysis of current tunnel observations suggests that strength Category 3, which corresponds to approximate lithophysal porosity 15% to 20%, represents about 25% of the Tptpll, whereas Category 5 is indicative of the highest quality of lithophysal tuff and about 30% of the Tptpll. Little, if any, damage occurs for either of these rock strength categories due to in situ stress alone.

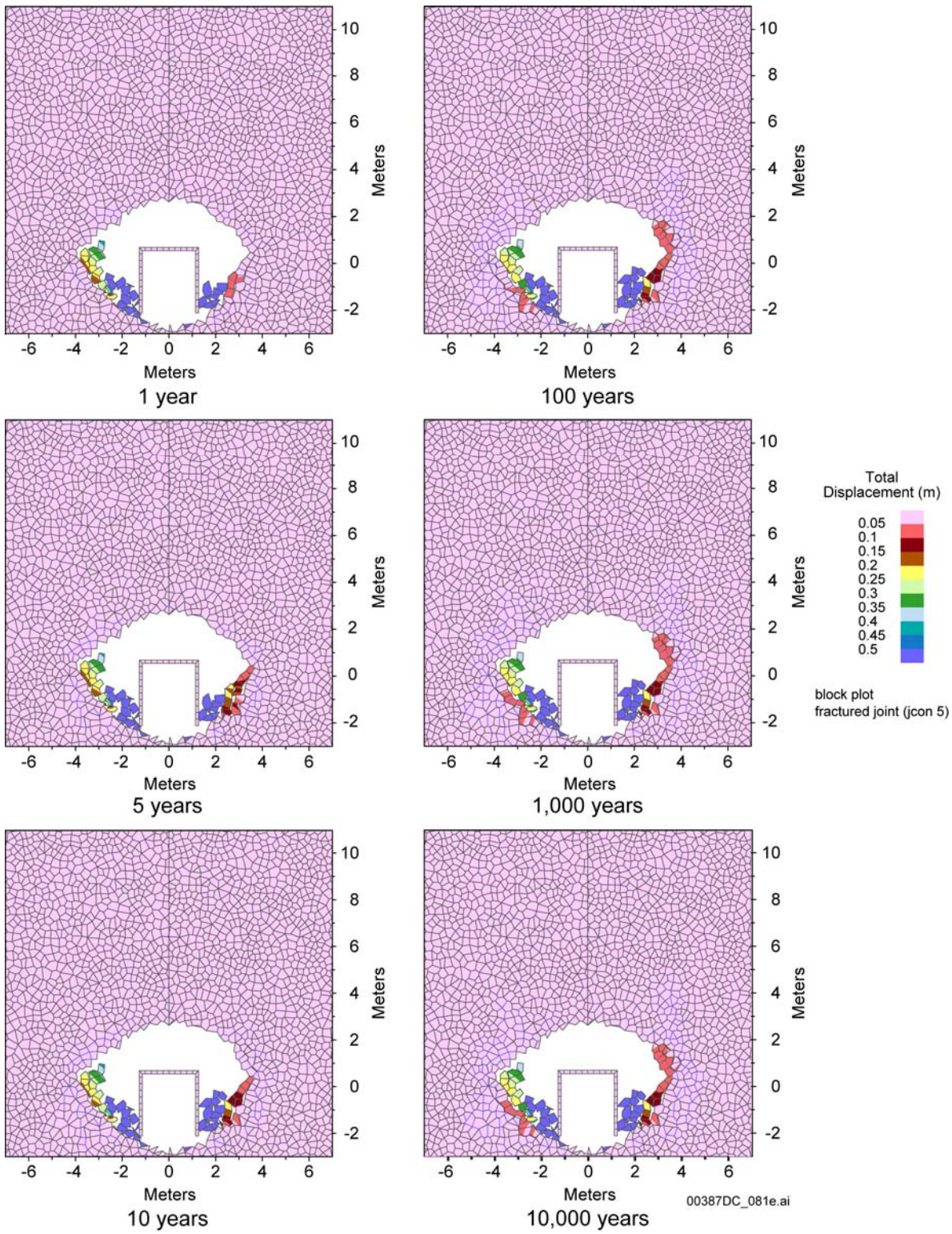

Source: BSC 2004a, Figure 5-36.

Figure 5-41. Predicted Evolution of Damage Due to Strength Degradation for Category 1–Tuff Best-Fit Static-Fatigue Curve, Applied In Situ Stress Only

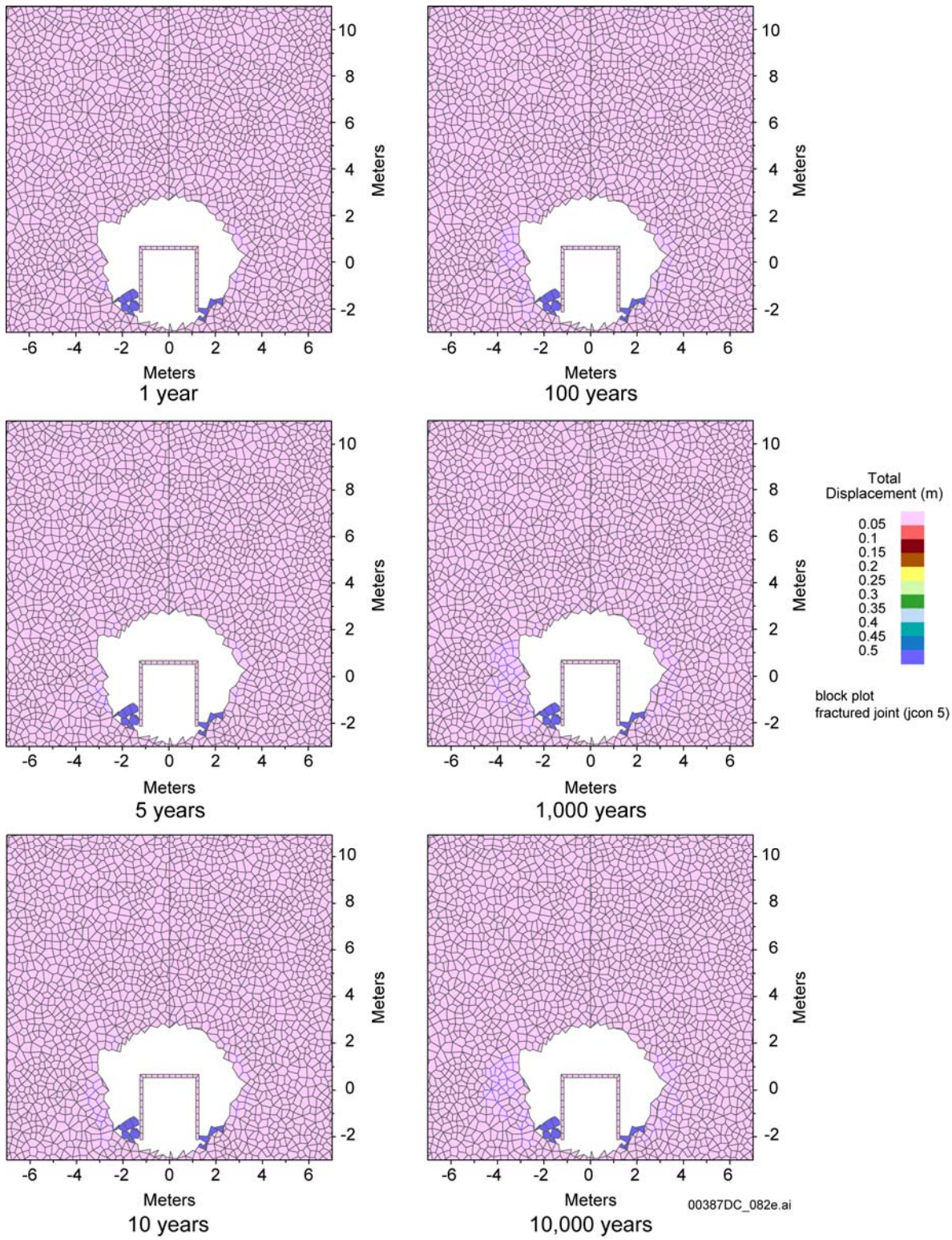

Source: BSC 2004a, Figure 5-37.

Figure 5-42. Predicted Evolution of Damage Due to Strength Degradation for Category 2–Tuff Best-Fit Static-Fatigue Curve, Applied In Situ Stress Only

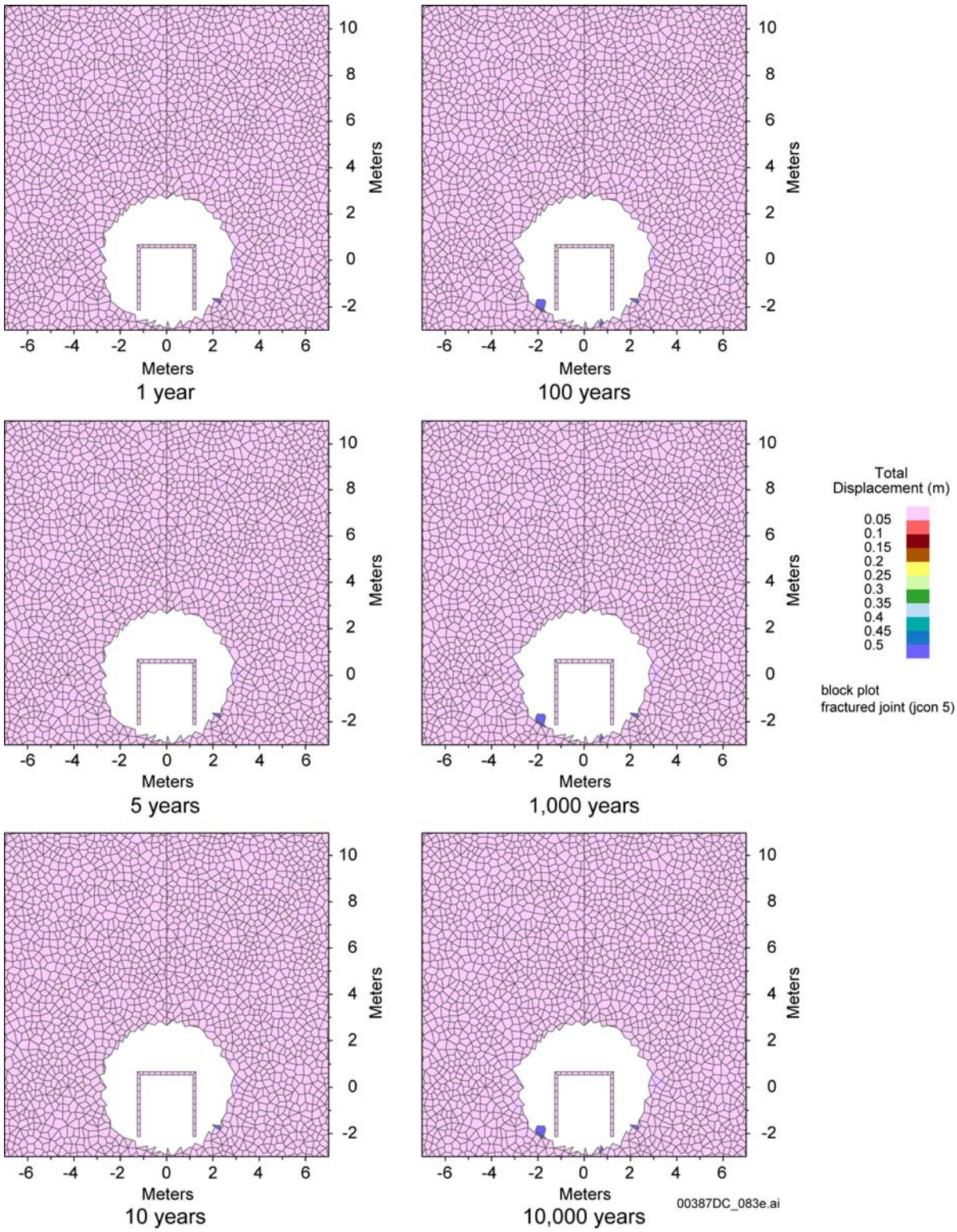

Source: BSC 2004a, Figure 5-38.

Figure 5-43. Predicted Evolution of Damage Due to Strength Degradation for Category 3–Tuff Best-Fit Static-Fatigue Curve, Applied In Situ Stress Only

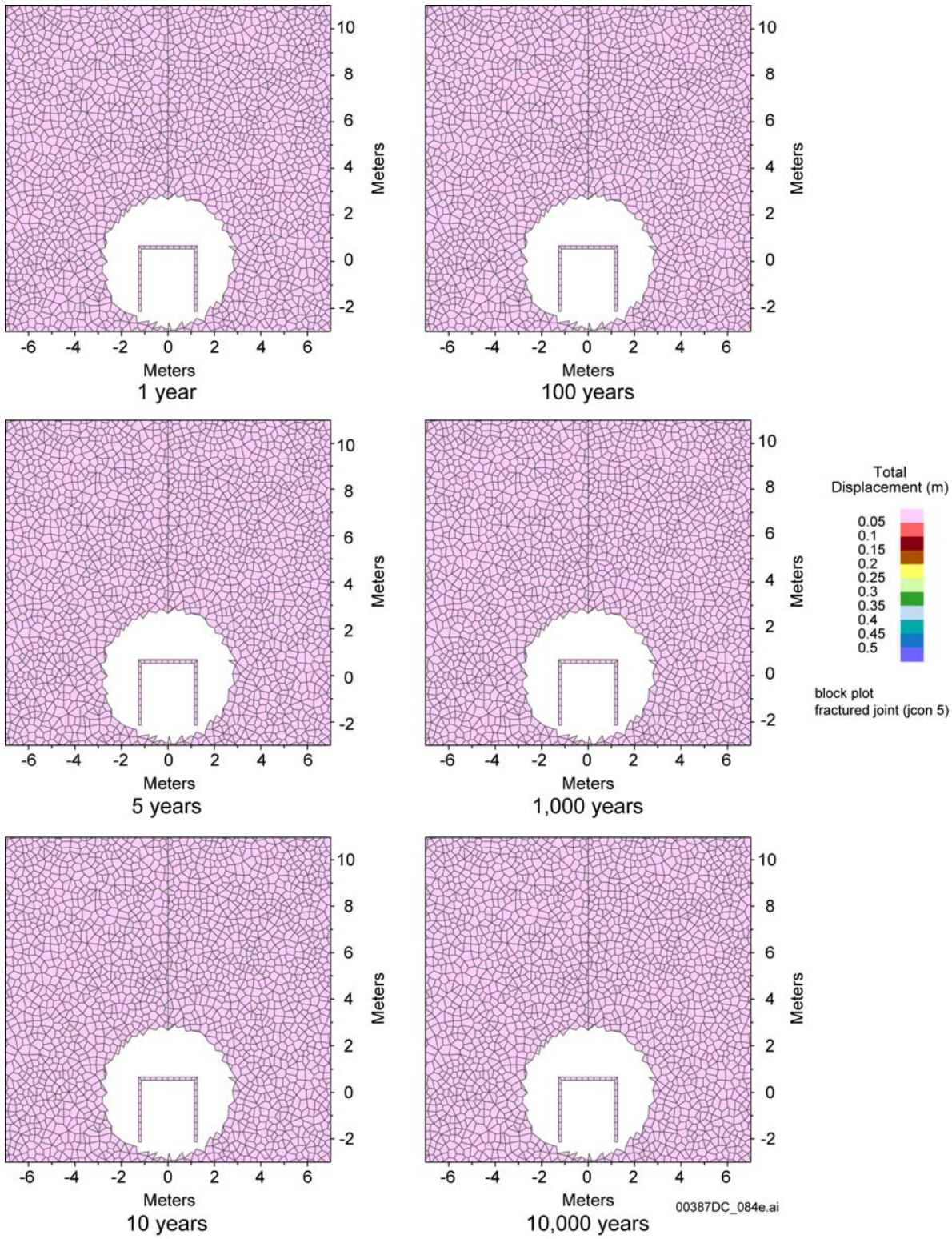

Source: BSC 2004a, Figure 5-39.

Figure 5-44. Predicted Evolution of Damage Due to Strength Degradation for Category 5–Tuff Best-Fit Static-Fatigue Curve, Applied In Situ Stress Only

Combined Thermal and Time-Dependent Effects in Lithophysal Units–Throughout the 10,000-year regulatory period, the emplacement drifts and surrounding rock mass will be subject to a cycle of heating and cooling. The time-dependent strength degradation will be a function of the in situ stress concentrations around the drifts as well as the transient, thermally induced stress changes. The addition of thermal stresses around the excavation will accelerate the process of strength degradation and potential drift instability. The results of numerical simulation of drift degradation as a result of these two stress states are shown in Figures 5-45 to 5-47 for Categories 2,[20] 3, and 5 rock strength conditions. Time-dependent strength degradation is assessed using the tuff best-fit static-fatigue testing data least-squares fit shown in Figure 5-39.

As expected, the greatest level of in situ, thermal, or time-dependent rockfall occurs for the Category 2 rock mass, as shown in Figure 5-45. Initially, most of rockfall comes from the walls, which are loaded to a near-yielding state for this rock mass category under in situ stress conditions alone. Strength degradation, combined with the increase in rock wall temperature, increases the tangential stress component in the walls, resulting in a small amount of rockfall from the walls within 5 to 10 years after emplacement of the waste. This localized spalling response would, in reality, be contained by ground support. The large increase in the temperature, and consequently in the immediate drift wall stresses, after the forced ventilation stops causes additional rockfall at the 80 years time frame when peak stress conditions are reached. Little additional rockfall occurs after that time as the rock mass slowly cools.

It might be expected that less rockfall would be predicted in Category 5 (Figure 5-47) than in Category 3 (Figure 5-46) due to the higher quality and lower porosity of the Category 5 rock mass. However, the greater modulus of the Category 5 lithophysal rock mass causes an increase in the tangential compressive stress and greater depth of yielding in the roof, in a fashion similar to that observed in the Tptpmn, Drift Scale Heater Test. This phenomenon is predicted to occur even for the case when time-dependency is not considered. In any case, Categories 3 and 5 show only small amounts of predicted rock degradation due to combined in situ and thermal stressing and time-dependent strength property change.

[20] Category 2 is used to represent the lower 10% of the rock mass quality. The response for Category 1 is similar.

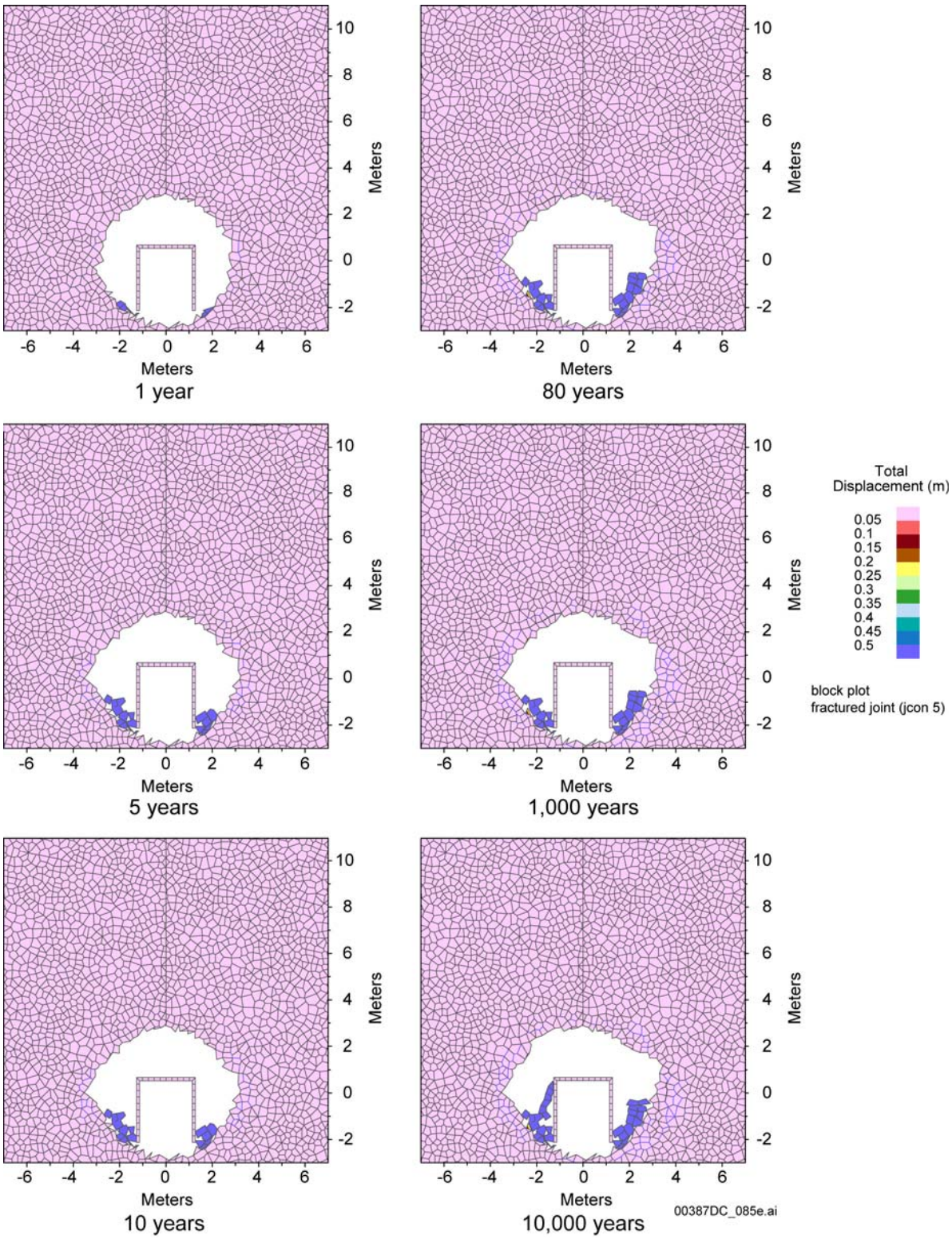

Source: BSC 2004a, Figure 5-41.

Figure 5-45. Predicted Evolution of Damage Due to Strength Degradation for Category 2–Tuff Best-Fit Static-Fatigue Fit, Combined In Situ and Thermal Stresses

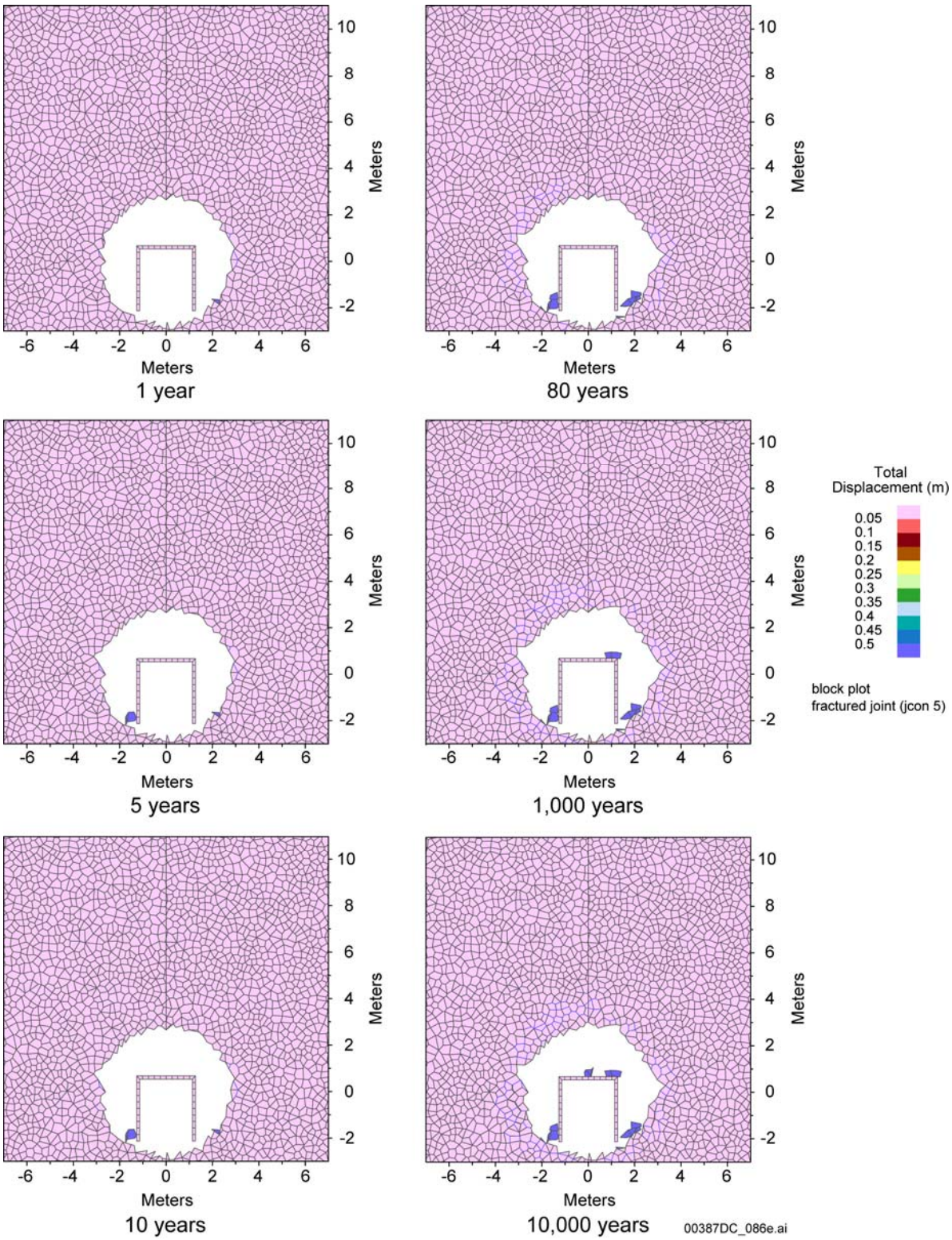

Source: BSC 2004a, Figure 5-42.

Figure 5-46. Predicted Evolution of Damage Due to Strength Degradation for Category 3–Tuff Best-Fit Static-Fatigue Curve, Combined In Situ and Thermal Stresses

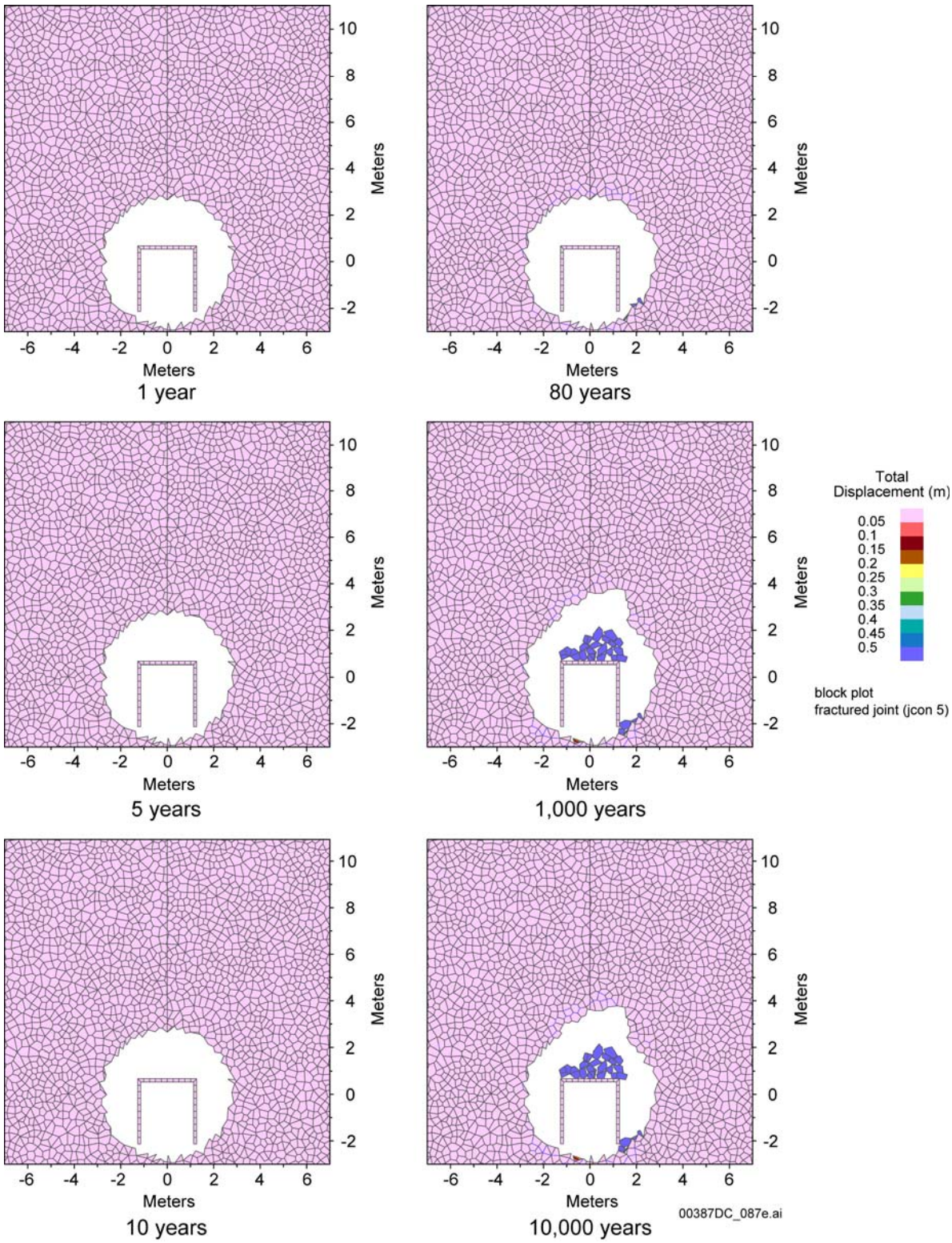

Source: BSC 2004a, Figure 5-43.

Figure 5-47. Predicted Evolution of Damage Due to Strength Degradation for Category 5–Tuff Best-Fit Static-Fatigue Curve, Combined In Situ and Thermal Stresses

Combined Seismic, Thermal, and Time-Dependent Effects in Lithophysal Units–The effect of a seismic event characterized by the 10^{-4} probability of annual recurrence, combined with in situ and thermal stressing, was investigated for time-dependent degradation modes for Categories 2 and 5 rock masses. The 10^{-4} seismic loading was chosen for this analysis as it may be considered that multiple events of this annual exceedance frequency could occur during the postclosure period. This work supplements previous seismic analyses in which thermal load was considered, but time-dependent strength loss was not.

The time frame when the combined in situ and thermally induced stress states reach their peak is at approximately 30 years after cessation of forced ventilation, or about 80 years after waste emplacement. However, when the time-dependent strength degradation is considered, the state when the maximum stresses are generated around the drift is not necessarily the critical state. The largest stresses occur relatively early during the regulatory period, and subsequently, the stresses decay gradually, returning to the state that existed prior to heating. At the same time the strength of the rock mass monotonically decreases as a function of time.

In order to investigate the extreme effects of the combination of in situ and thermal stress and seismic ground motion on drift stability, dynamic analyses were carried out for the model states at 80 and 10,000 years after waste emplacement.

The model geometry before and after the dynamic simulation is shown in Figures 5-48 and 5-49 for seismic ground motion 80 years after emplacement, and in Figures 5-50 and 5-51 for seismic ground motion 10,000 years after emplacement. In all the cases, additional rockfall is predicted due to the ground motion, which essentially shakes down the already-damaged rock mass resulting from the in situ and thermal stressing. This increase in the rockfall due to the 10^{-4} seismic loading is somewhat greater than that predicted for in situ and thermal stressing alone, particularly for the Category 2 case. There is also somewhat greater rockfall in the case of an earthquake 10,000 years, as opposed to 80 years, after waste emplacement.

Summary of Time-Dependent Degradation Results: Estimation of Drift Profile for Feeds to the Abstraction of Drift Seepage–The analyses presented here have provided an estimate of the extent of drift degradation due to in situ and thermally induced stresses as a function of time, combined with time-dependent rock mass strength change. Additionally, the effect of higher-probability preclosure ground motions on shaking down any damaged and loosened material from the degradation process was examined. The analyses show that a spectrum of drift damage is predicted ranging from wall breakouts with plan view diameter change of up to about 2 drift diameters (e.g., Figures 5-48 and 5-50) in the highest porosity rock (Categories 1 and 2: about 10% of the Tptpll) to minor breakouts along the walls and crown of the drifts in the average to lowest porosity conditions (e.g., Figures 5-49 and 5-51 for Categories 3 to 5: about 90% of the Tptpll). The modeling predicts that the majority of the damage is due to thermal stressing effects and occurs simultaneously with the peak thermal stressing about 30 years after ventilation shutdown. Time-dependency results in some small additional damage over time. However, the overall conclusion is that the drift profile change and drip shield loading (discussed in next section) from nonseismic degradation is minor in comparison to damage from seismic stressing.

The predicted drift profile change as a function of time is required as input for the estimates of time-related seepage flux into the emplacement drifts. Among other factors, the seepage flux depends on both the size and geometry of the drift and the capillary strength of the fractured rock surrounding the drift opening (BSC 2004o, Section 6.4.2.4). In partially or fully collapsed drifts, the larger size and potentially different crown shape after collapse will reduce the potential for flow diversion compared to the initial drift geometry; furthermore, the larger footprint of the collapsed drift leads to an increase in the total amount of percolation flux arriving at the drifts, which, in turn, can affect the total amount of seepage. In addition, the capillary-barrier behavior at the drift wall can be affected by the rubble rock particles filling the opening, as the capillary strength inside the opening will be different from the zero capillarity condition in the initially-open drift. Thus, the geometry of the degraded drift and the capillary strength of the rubble material inside the drift are of importance in this abstraction.

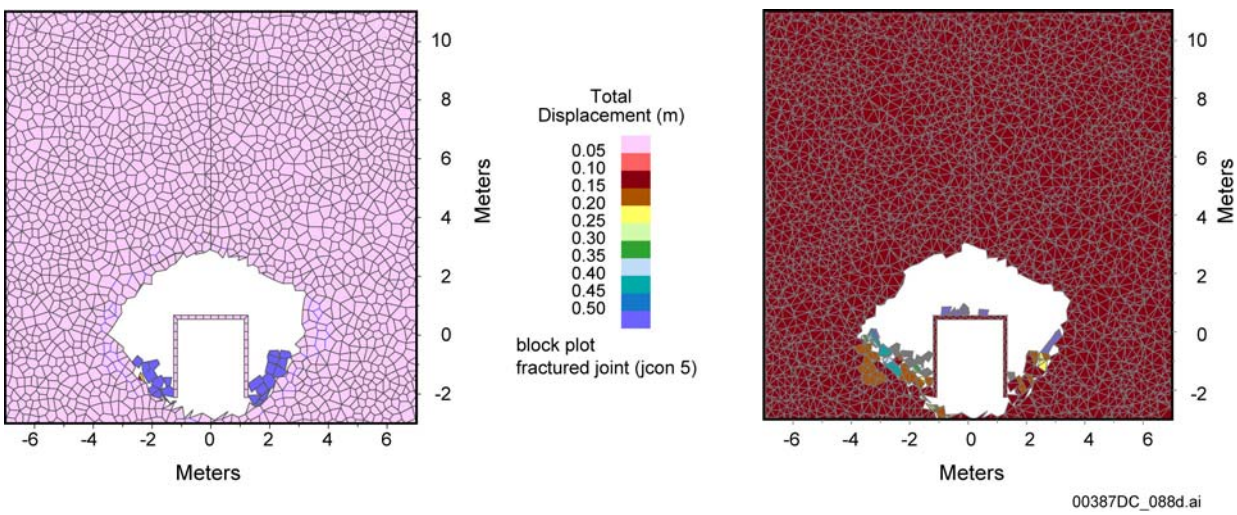

Source: BSC 2004a, Figure 5-44.

NOTE: Displacement magnitudes are in meters.

Figure 5-48. Effect of 10^{-4} Ground Motion after 80 Years of Heating in Category 2 before Seismic Shaking (Left) and after Seismic Shaking (Right): Blocks Colored by Contours of Displacement Magnitude

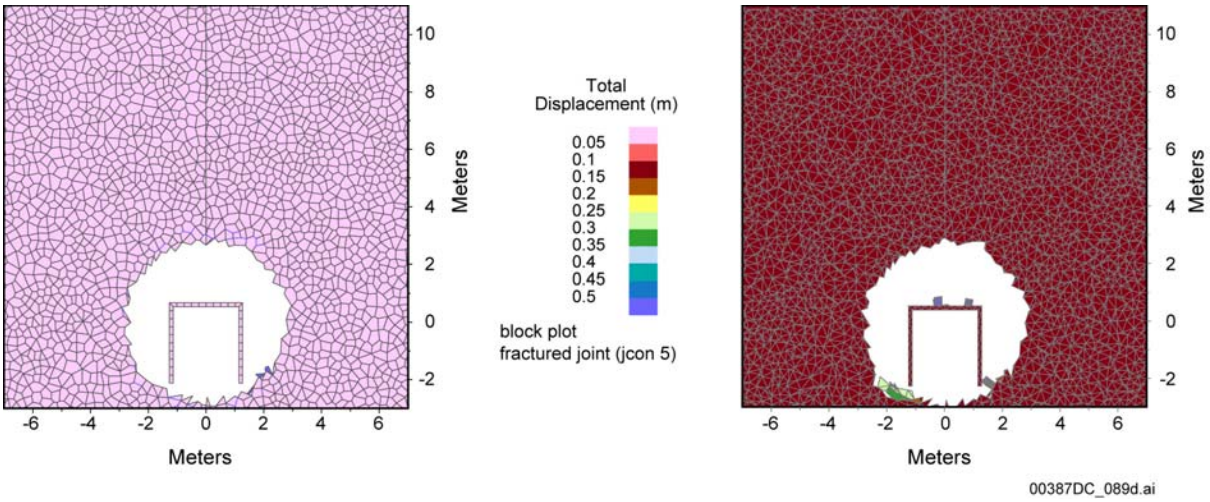

Source: BSC 2004a, Figure 5-45.

Figure 5-49. Effect of 10^{-4} Ground Motion after 80 Years of Heating in Category 5 before Seismic Shaking (Left) and after Seismic Shaking (Right): Blocks Colored by Contours of Displacement Magnitude

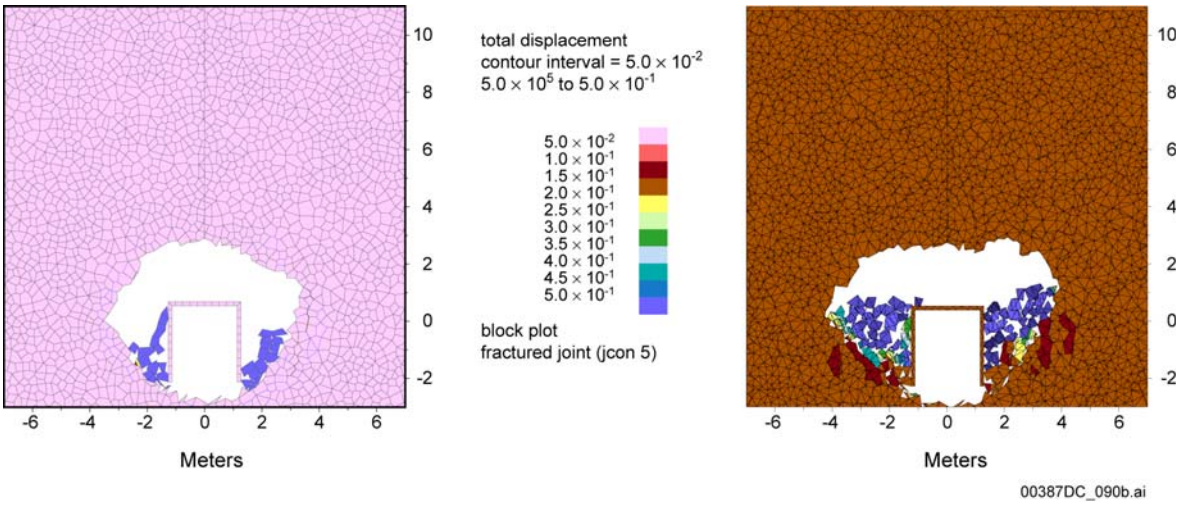

Source: BSC 2004a, Figure 5-46.

Figure 5-50. Effect of 10^{-4} Ground Motion after 10,000 Years of Heating in Category 2 before Seismic Shaking (Left) and after Seismic Shaking (Right) Contours of Displacement Magnitude

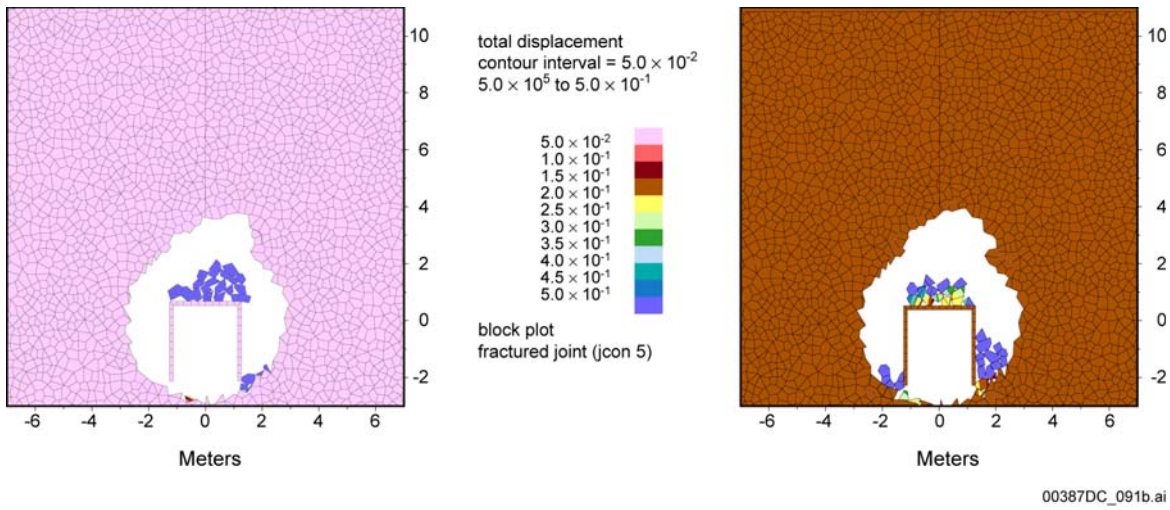

Source: BSC 2004a, Figure 5-47.

Figure 5-51. Effect of 10^{-4} Ground Motion after 10,000 Years of Heating in Category 5, before Seismic Shaking (Left) and after Seismic Shaking (Right): Blocks Colored by Contours of Displacement Magnitude

5.3.2.3 Quasi-Static Loading to the Drip Shield from Caved Lithophysal Rock

5.3.2.3.1 Introduction

The previous calculations of drift degradation from all sources of loading or strength (i.e., in situ stress, thermal stress, seismic stressing and shaking, and time-dependent strength degradation) have resulted in (1) dynamic loading of the drip shield from falling rock and (2) quasi-static load on the drip shield once the fallen rubble has come to rest. The primary concern for dynamic impact loading on the drip shield occurs in nonlithophysal rocks due to the larger size of rock wedges that can form in these units. Quasi-static loading is a potentially more important issue in the lithophysal rocks where potential collapse heights are greater and particle sizes are smaller. These factors can lead to larger quasi-static loads applied to the drip shield.

This section is concerned with prediction of the magnitude and distribution of the quasi-static loading. The time-dependency analyses presented in the previous section show that nonseismic drift degradation alone is not expected to result in complete tunnel collapse during the regulatory period. However, seismic loading and the accompanying rock mass failure can lead to collapse of the tunnels for postclosure ground motions of 10^{-5}, 10^{-6} or 10^{-7} annual exceedance frequency. In these cases, which are highly conservative due to the large and potentially physically unrealizable ground motions (BSC 2004c), the rock mass surrounding the drift fails and breaks into relatively small particles that fall under gravity to rest beside and on top of the drip shield. As shown in Figure 5-31(b), tunnel collapse during large (e.g., PGV greater than about 2 m/sec) seismic events is predicted to occur rapidly, within approximately 2 seconds. The analyses indicate that the drip shield is rapidly encased by the broken rubble, preventing further large translational motions.

The seismic calculations further provided an estimate of the maximum extent of caving that would occur in the sidewalls and roof accompanying these events. The drifts, which become

filled with rubble, attain an elliptical shape with maximum increase in dimension of about 1.5 times the original drift diameter. Similar estimates of the maximum collapse height can be determined by conducting discontinuum simulations in which the rock mass, under in situ loading is assumed to undergo a loss of cohesive (shear) and tensile strength such that it fails to its maximum caved height. This height is governed by the in situ stress conditions and the bulking of the broken and detached rock that fills the drift and provides a stabilizing back pressure to the excavation surfaces. Such an estimate represents a conservative upper bound of the load of the caved rock on the drip shield irrespective of the rate of strength decay and the residual strength of the rock mass. The quasi-static loads generated from these analyses are used as a design basis (along with the dynamic rockfall loads) for the drip shield stability calculations.

Predictions of ultimate drift collapse height and shape and the subsequent load of the broken rock on the drip shield were performed using three different approaches: analytically-based approximations, numerical continuum modeling approximations, and numerical discontinuum modeling. Three methods, with varying degrees of complexity, were used to provide load calculations from alternative conceptual models with the objective of providing an assessment of conservatism. Each of the methods uses certain assumptions regarding caving of the rock above the drifts and the transfer of the stresses within the broken rock mass. As discussed below, the level of conservatism is the greatest in the analytically-based approach and the smallest in the approach that represents the rock mass as a discontinuum. The analytical and numerical continuum models require assumption of the ultimate shape of the collapsed zone and the bulking factor of the rubble and do not take into account rock mass properties or in situ stresses. Load on the drip shield is estimated simply from the height of broken rock above it.

The discontinuum numerical modeling technique is judged to most closely represent the actual caving process. The only assumption made in this method is the size and shape of rock particles produced as the rock mass fails. The ultimate shape and size of the collapsed drift and the bulking factor of the caved rock are determined from the model. Load on the drip shield is determined directly from the interaction of the rubble and the drip shield. The drip shield is modeled using a two-dimensional representation in which the deformability and shape are correctly represented. The invert is modeled as a rigid boundary and the footings of the drip shield are free to slide or separate as forces dictate. The analyses here are aimed at determining the drip shield loading provided by the broken rock, and not to model the stability or perform design calculations of the drip shield. However, to provide an adequate determination of the load, the interaction of the broken rock and the structure needs to be modeled. These analyses provide a model of this interaction and the resulting stresses for the case of complete collapse. The resulting applied stresses are fed to the analysis of the drip shield in which the geometry and yield properties of the structure is modeled in detail.

5.3.2.3.2 Bulking of the Collapsed Rock Mass

When the rock mass above underground openings collapses it increases volume (i.e., it bulks). During the collapse, either sudden or gradual, the rock mass breaks into a number of pieces (blocks) that fall separately, and rotate as it falls and contacts the muck pile. When blocks equilibrate after caving, they do not fit together resulting in increased porosity and overall volume. The rock mass of volume V in the in situ conditions has volume V_B after caving, where:

$$V_B = (1 + B)V \qquad \text{(Eq. 5-4)}$$

where B is termed the "bulking factor."

The amount of bulking (i.e., the bulking factor, B) depends, among other things, on the lithology, preexisting internal structure (lithophysae, jointing, bedding), and the mechanism of collapse. For example, the density of crushed limestone is in the range between 1,360 kg/m^3 and 1,440 kg/m^3; while density of crushed dolomite is in the range between 1,280 kg/m^3 and 1,600 kg/m^3 (Fruchtbaum 1988). Considering that the specific gravity of limestone and dolomite is approximately 2.6 (Bauer et al. 1991), and using an in situ porosity of 20% (Goodman 1980), the in situ density of limestone and dolomite is approximately 2,200 kg/m^3. Consequently bulking of these rocks from in situ state to a crushed state is between 37.5% and 72%. Duncan et al. (1980) reported that porosity of rockfill for dams is between 23% and 36%. The rockfill used for dams is crushed to satisfy a certain size requirement and is compacted during construction, which leads to reduction of its porosity. It appears from this discussion that the bulking factor for caved rock can be conservatively selected to be in the range between 0.2 and 0.4, even for lithophysal rock, which has initial porosities ranging from about 20% to 35%.

Caving of the underground excavations is a self-limiting process in situations where the excavation diameter is much less than the depth below ground surface (i.e., where the depth is approximately 3 times or more of the tunnel radius, the depth is over 100 times the radius at Yucca Mountain). At a certain stage of caving, due to bulking, the volume of the caved rock completely fills the volume of the original excavation and the volume occupied by the collapsed rock before onset of collapse. When the cave is completely filled, the broken rock provides a backpressure, which prevents further collapse of the rock mass. This self-limiting concept of complete filling is a simplistic and conservative mechanism that provides the basis for the analytical approaches below.

In addition to the potential for complete filling as a cave-stabilizing mechanism, caving often results in formation of elliptical-shaped excavations, which, in turn, results in tangential stress concentrations at the cave crown where the radius of curvature is the greatest. These higher stresses can confine the rock, arresting cave development without complete filling of the tunnel. This is the case in many caves or other natural excavations that may form naturally arched, stable excavations. Analytical approaches do not examine the impact of in situ stress conditions, but this is accounted for when using the discontinuum modeling approaches that are used in the following analysis.

Analytical Models of Collapse Height and Shape–It is considered in this approach that the cave above the emplacement drift grows until it becomes filled with the broken rock, irrespective of the rock strength or rock mass stress state. The extent of the caved rock is calculated as a function of the bulking factor, *B*, considering that the cave stabilizes when it is completely filled with the broken rock. An additional unknown in this approach requiring assumption is the shape of the cave. In all cases, the entire dead weight of the material vertically overlying the drip shield is assumed to act on the drip shield. The frictional forces acting between the caved material and the stable sidewalls and within the caved particles themselves, is not taken into account, resulting in a lack of any portion of the vertical load being transferred to the surrounding rock mass. Two extreme conditions illustrated in Figures 5-52 and 5-53 and were considered.

The "piping" mode of roof collapse (Figure 5-52) may occur for conditions where the rock mass is horizontally bedded and there is a relatively large ratio of the span of the excavation to its depth. This type of roof collapse is sometimes induced to occur in coal mines (with a thinly-bedded overburden), using the longwall mining method, and often occurs suddenly. Roof piping collapse is not a likely mode of drift collapse at Yucca Mountain for the following reasons:

- None of the rock mass units are thinly stratified
- The ratio of depth to drift diameter is very large, and therefore the rock mass may be considered "infinite" in extent from a mechanical standpoint.
- Drift collapse due to time-dependent strength decay will evolve gradually over a long period of time.

The piping mechanism is considered here as a conservative extreme condition and is a mechanism that results in the largest vertical extent of the cave, *H*.

The other extreme conservative condition of the rock mass collapse around the underground opening (shown in Figure 5-53) corresponds to the limit equilibrium conditions around a shallow tunnel, which Terzaghi (1943) used to calculate the load on the tunnel support. Slip lines extend from the drift walls at an angle of $45° - \phi/2$ from the vertical direction, where ϕ is the friction angle.

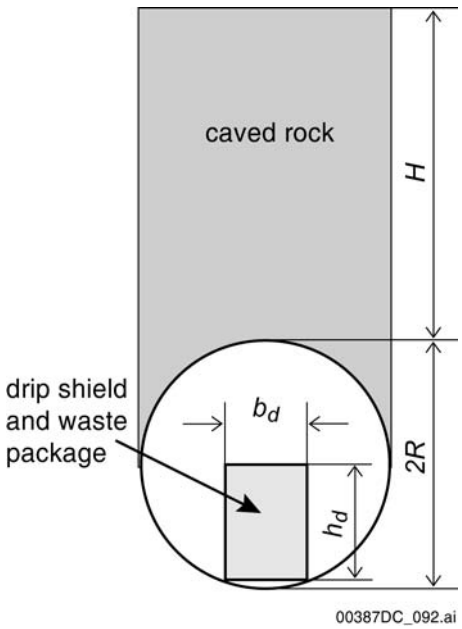

Source: BSC 2004a, Figure 6-156.

Figure 5-52. Piping Type of Caving Mechanism

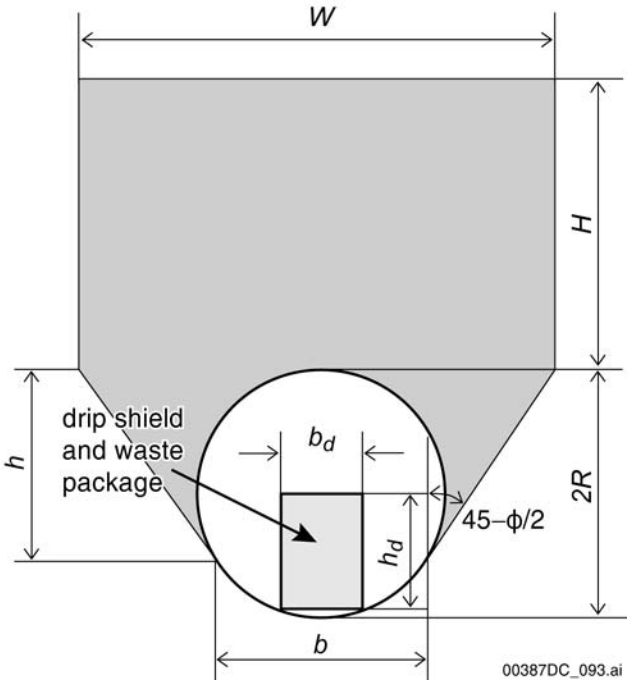

Source: BSC 2004a, Figure 6-157.

Figure 5-53. Terzaghi-Type Caving Mechanism

In both analytical representations, the cave height, and thus the dead weight of material that lies on the drip shield, is a function of the assumed bulking factor (BSC 2004a).

Numerical Continuum Approach to Simulate Piping and Terzaghi-Type Mechanisms–The next degree of greater detail in estimating cave formation and rubble loading is to use numerical modeling approaches. The simplest numerical model is one in which the rock mass and rubble are considered to be continuum materials. The analytical approaches do not take into account the effect of rock mass stress conditions and material properties. The use of numerical methods allows testing of the proposed piping and Terzaghi assumptions when the rock mass stresses and material properties are taken into account. The numerical models can also be used to examine the importance of potential stress arching within the broken rock that lies within the drift. However, continuum-based analyses also represent conservative, but more accurate, simulations of the collapse height than either the piping or Terzaghi-type mechanisms. A simplistic methodology was used in which the rock mass was represented as a Mohr-Coulomb material within FLAC, a continuum numerical code.

The estimated strength of the lowest quality lithophysal rock mass was used in the initial drift equilibrium state at excavation (Category 1). Subsequently, cohesion and tensile strength of the rock mass were reduced gradually, in steps to induce collapse. At each stage of strength reduction the model was run until either equilibrium was achieved, or there was clear indication that equilibrium could not be achieved (i.e., the rock mass around the drift was collapsing). Once the collapse was detected the model simulation was interrupted, and the cave height was calculated based on the bulking factor and the volume of the rock mass within the destabilized region. An example of the numerical prediction of collapse for the Terzaghi mechanism is shown in Figure 5-54.

It is noted that the bulking factor required for this analysis controls the ultimate cave propagation and is an uncertain parameter (as is the ultimate shape of the cave zone). Again, two limiting mechanisms were considered and generated using the numerical model: (1) the piping mechanism (where the caved rubble is assigned zero cohesive strength), in which the cave width was limited to the drift width and (2) the Terzaghi mechanism, in which cave width coincides with the width of the destabilized region of the rock mass under in situ stress conditions. Subsequently the drift and the caved region were filled with zones (caved rock selected to have no cohesive or tensile strength, and density accounting for the bulking factor), and the model was run to the equilibrium state to determine the load on the drip shield.

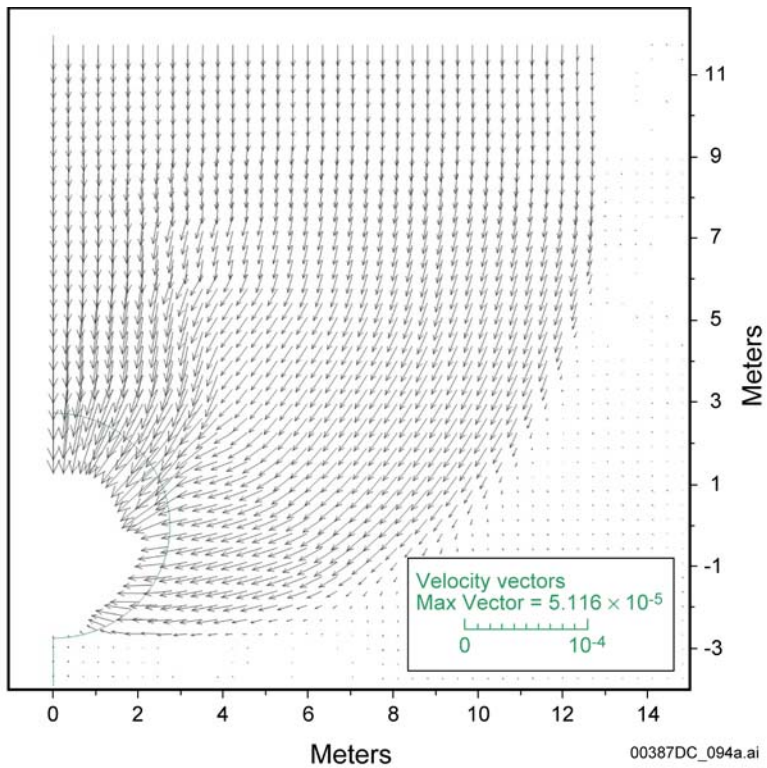

Source: BSC 2004a, Figure 6-160.

Figure 5-54. Failure Mechanism of a Deep Tunnel in Cohesionless Material

Discontinuum Numerical Approach to Estimating Drip Shield Load–The most detailed and representative approach to representing the actual caving behavior of a rock mass is the use of discontinuum numerical modeling. The collapse problem was simulated using the UDEC program to provide the most realistic prediction of caving by including actual site-specific material strength and in situ stress conditions. After initial stress equilibrium of the excavation was achieved for a circular 5.5 m diameter drift, the cohesion and tensile strength of the rock mass were subsequently reduced in a series of steps to provide the ultimate collapse height and shape of the excavation when the rubble eventually provides sufficient back pressure to the excavation to suppress further failure. The loading on the sides and top of the drip shield is then determined by the model.

The cohesive and tensile strengths are reduced in 5 increments from full strength properties (for a given rock strength category) to zero, allowing the rock to fail along its internal fracture boundaries, and to fall by gravity onto the invert and drip shield. In this model, the bulking of the caved rock is not an assumed model parameter but is the calculated result of the modeling. The bulking of the rubble depends on the size and shape of the falling blocks, which are predetermined by the size and the shape of the UDEC blocks in the model. The UDEC analyses use irregular-shaped blocks with a mean side length of 0.3 m. To ensure that the model estimates produce values of bulking factor that are considered to be low from common practice, additional analyses were performed with a 0.2 m block size so that the resulting bulking factor was equal or less than 0.2, the lower bound of the bulking factor expected in rocks gained from construction experience (described previously).

After the model has come to equilibrium under complete collapse, the broken rock blocks will rest on the drip shield and the invert of the drift (Figures 5-55 to 5-57). Figure 5-55 shows the geometry of the fully collapsed tunnel and rockfall in contact with the deformable drip shield. The contact of the footings with the drip shield is free to slide or separate on the invert. The exertion of the side-loading from rockfall results in lateral translation of the drip shield and more uniform loading distributions on the sides, with larger vertical loading to the crown. The ultimate collapsed height and shape of the cave is illustrated in Figure 5-56, which shows contours of displacement of the rock mass and rubble arising from the yield and collapse process. The ultimate collapse zone grows to approximately twice the original diameter of the tunnel. The rubble attains a bulking factor of approximately 19% in the case of 0.2 m block size. A total of 6 realizations of block shape (all assuming an average dimension of 0.2 m) were simulated, resulting in a range of potential loading conditions on the drip shield. The drip shield is subdivided into 30 segments, and average loads on each segment are defined. Figure 5-57 shows a histogram of the average pressure on each of the 30 elements for all six realizations. The mean of all the realizations is also plotted. As seen in this plot, the average loads from all realizations on the right and left hand sides are approximately the same, while the average pressure on the top of the drip shield is about 50% higher. Locally larger or lower point loads may exist, depending on the how the rubble falls and compacts around the drip shield.

5.3.2.4 Comparison of the Quasi-Static Drip Shield Loading from Various Methods

The predictions of average vertical pressure of the caved rock exerted on the top of the drip shield by all three approaches are summarized in Figure 5-58. This figure shows the pressure as a function of bulking factor. In the case of the analytical and continuum numerical model, the bulking factor is an assumed parameter. In the case of the discontinuum modeling, the bulking factor is determined directly from the results of the modeling and is the reason why the results are concentrated around a bulking factor of approximately 0.2. Results for the discontinuum modeling are given for assumptions of a deformable drip shield, as well as for a rectangular, rigid drip shield as a means of examining the impact of drip shield shape and deformability on stress arching in the rubble.

As expected, the analytical models yield the largest loads resulting from the overly conservative assumptions inherent in each approach. The continuum numerical model accounts more accurately for transfer of load by friction from the caved rock to the surrounding stable rock mass. Consequently predicted loads for small bulking factors and large cavity size are much smaller than analytical predictions. When the bulking factor is large, the height of the cave becomes small. Stress arching cannot be realized within the small column of the cave rock, and consequently the predictions from the analytical and continuum models are identical. The most realistic approach, using the discontinuum model, does not use an imposed (assumed) condition about the shape or extent of the caved region. It also accounts for load transfer through the caved rock in a reasonable fashion via frictional contact between rock blocks. A complete discussion of the various analyses leading to estimates of drip shield pressure distributions can be found in *Drift Degradation Analysis* (BSC 2004a). The predictions of the pressures on the drip shield using this approach are smaller than the predictions of the analytical and continuum models for all values of the bulking factor, but diverge significantly for bulking factors below approximately 0.2.

A number of analyses were also run to test the impact on quasi-static load due to seismic shaking on a previously collapsed drift. Figure 5-58 also shows the final loading on the drip shield when a previously collapsed drift (e.g., Figure 5-55) is subjected to shaking from subsequent ground motions with annual exceedance frequencies of 10^{-4}, 10^{-5}, and 10^{-6}. As seen, the effect of the additional seismic shaking on the loose rubble (approximately 20% initial bulking factor) is to cause additional compaction of the rubble, with a reduction in bulking factor. For example, the 10^{-4} motion has little effect on rubble compaction; however, the bulking factor decreases to approximately 14% and 10% for the 10^{-5} and 10^{-6} motions, respectively. However, the increased compaction does not lead to dramatically increased loads on the drip shield due to arching in the rubble.

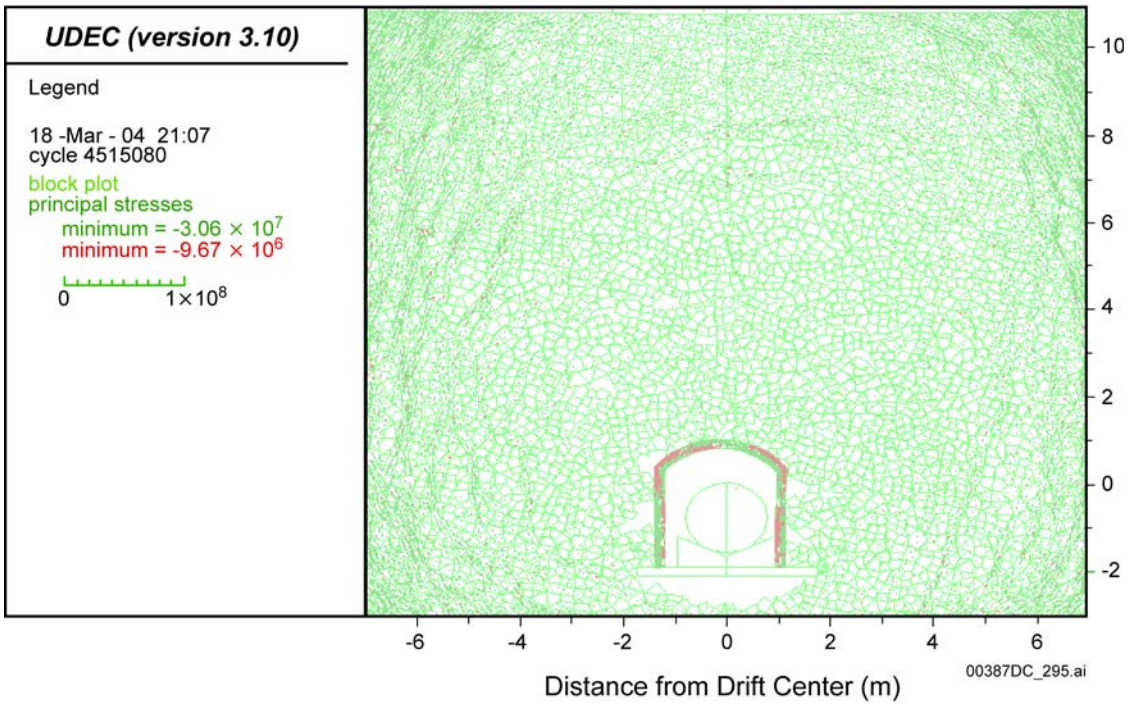

Source: BSC 2004a, Figure 6-164

NOTE: Stresses are given in Pascal.

Figure 5-55. Quasi-Static Drift Degradation, 0.2 m Block Size: Equilibrium State for Deformable Drip Shield with Arched Top, Footings Free to Slide or Detach from the Invert

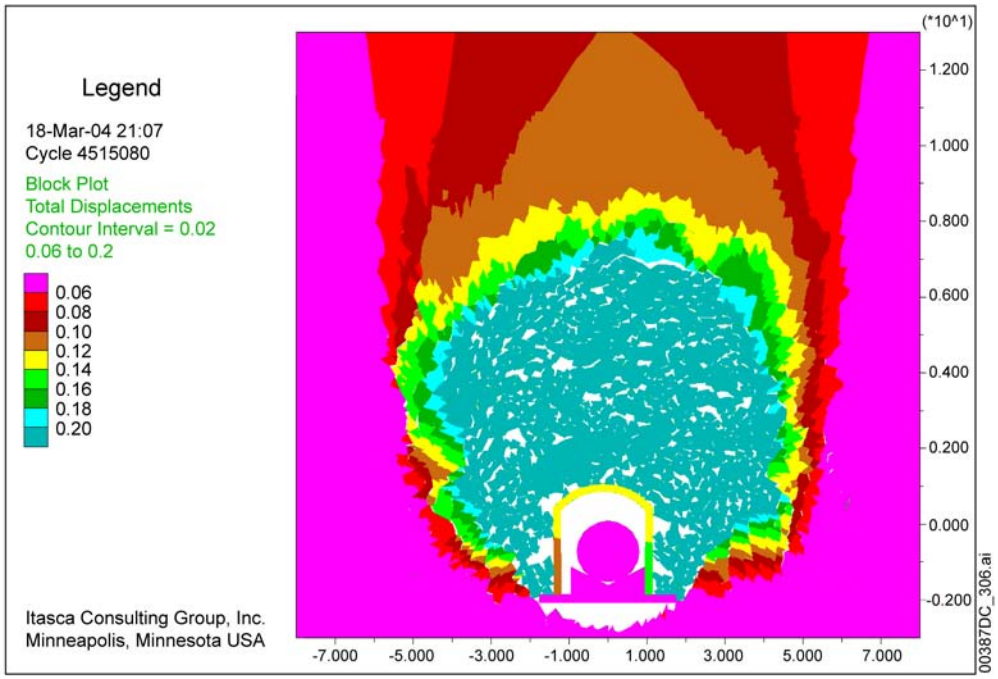

Source: BSC 2004a, Figure 6-165.

Figure 5-56. Quasi-Static Drift Degradation, 0.2 m Block Size: Contours of Displacement Magnitude for Deformable Drip Shield Showing Approximate Collapse Height of 7 m (about 6 m above Top of Drip Shield Crown)

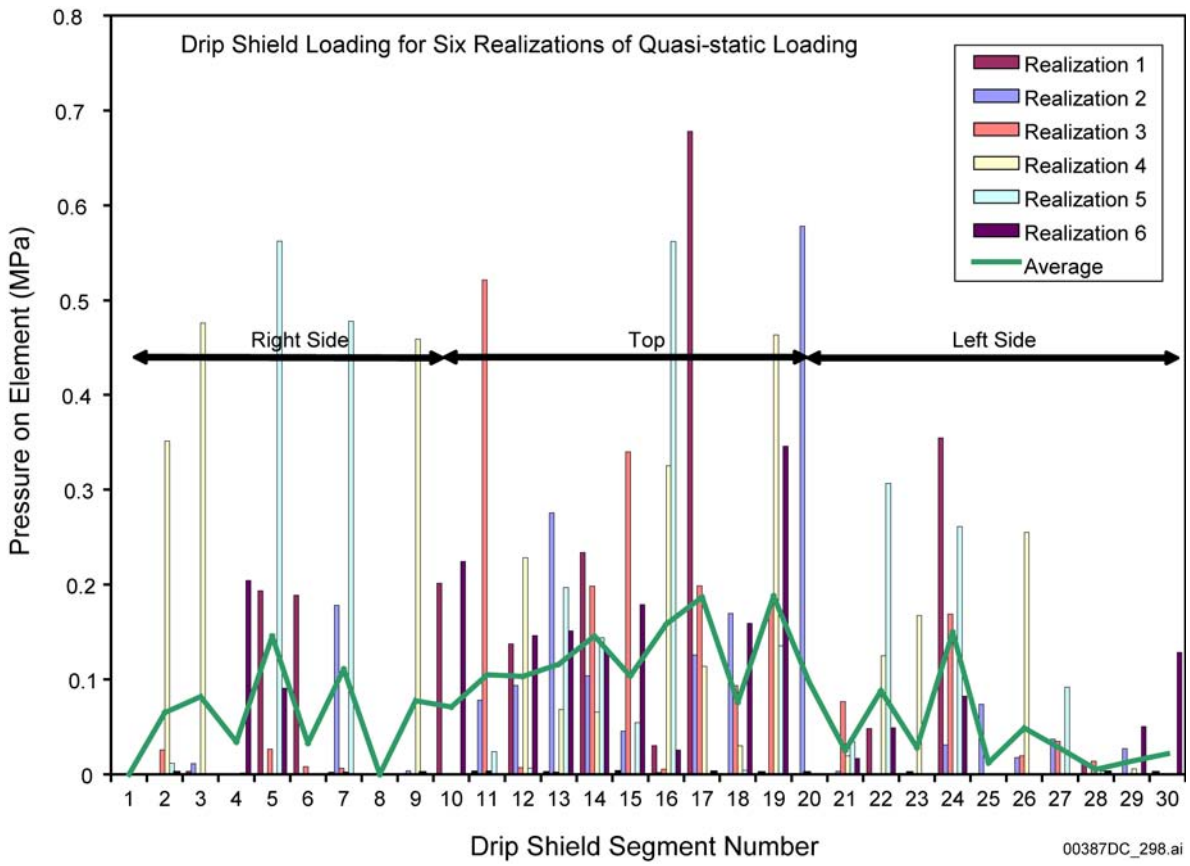

Source: BSC 2004a, Figure 6-166.

NOTE: Average pressure on each segment is shown for all six realizations. Segment numbering starts at 1 at right footing and continues counterclockwise to the left footing. Those elements on the right, top, and left sides of the drip shield are shown.

Figure 5-57. Quasi-Static Pressure on Drip Shield Segments for Six Realizations for Random, 0.2 m Block Geometries

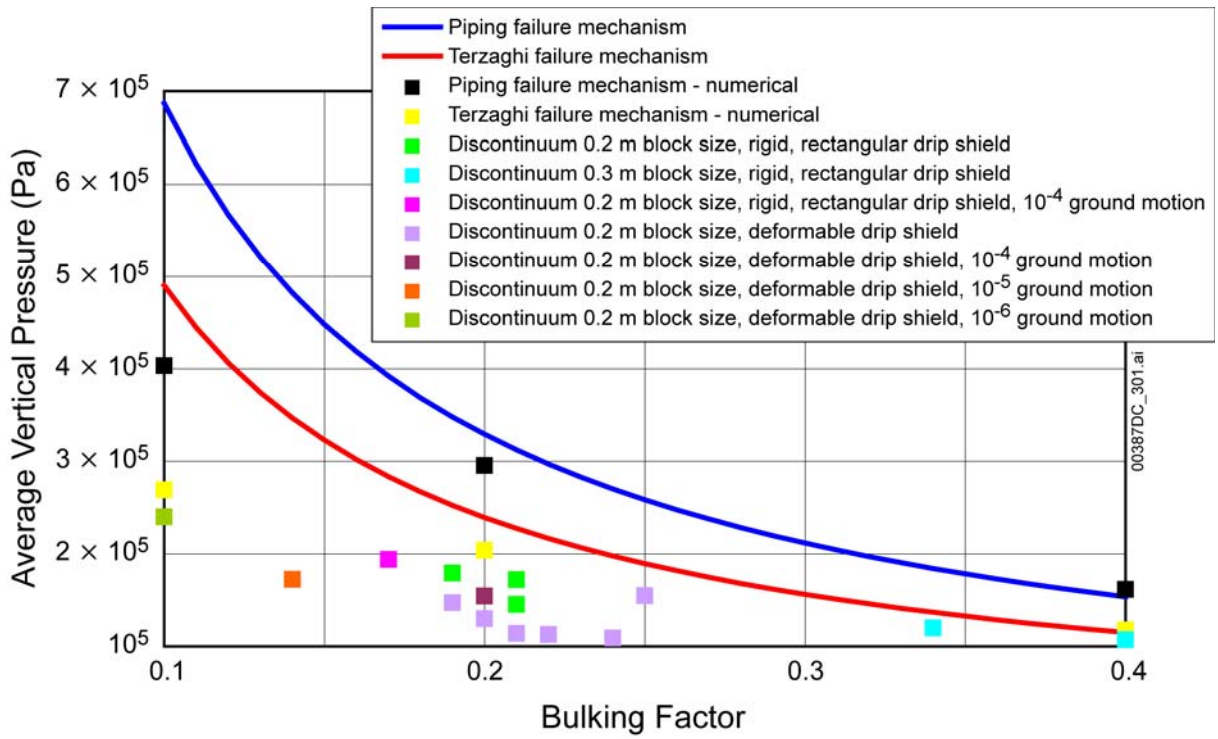

Source: BSC 2004a, Figure 6-170.

NOTE: Solid lines show the analytical methods. Symbols are numerical solutions.

Figure 5-58. Summary of Average Vertical Pressure on the Drip Shield as a Function of Bulking Factor for Analytical and Numerical Analysis

5.3.2.5 Rubble Load Feeds to Engineering Structural Analysis of the Drip Shield

The rubble loading estimates described above are ultimately used as input to the structural design analysis of the drip shield and are not part of this technical basis document. Three-dimensional finite element structural analyses are performed to examine stress and deflection of the drip shield and, in particular, buckling modes or excessive deformation that may result in contact with the waste package. The estimated rubble quasi-static loads derived from discontinuum modeling as depicted in Figure 5-57 are used as direct input to the structural analysis.

5.4 SUMMARY OF OUTPUT FROM THE DRIFT DEGRADATION ANALYSIS TO OTHER DISCIPLINES

The results of the drift degradation modeling provide feeds to several engineering calculations and abstraction models that eventually feed the TSPA model. This information is summarized here:

- **Preclosure Analysis of Rockfall and Waste Package Breach**–An analysis of potential rockfall due to preclosure in situ, thermal, and seismic loading was conducted for

unsupported[21] emplacement drifts and other repository excavations (BSC 2004k). This work provides an estimate of the maximum credible rock masses during the preclosure period and is used to show that damage of a waste package due to rockfall for unsupported openings is not a credible event.

- **Engineering Calculation of Drip Shield Stability and Damage from Rockfall**–This includes dynamic and quasi-static loading.

  – **Dynamic Loading**–Nonlithophysal rockfall masses, relative velocity components, impact location, and rockfall shapes are supplied to three-dimensional engineering structural analysis of the drip shield for each set of analyses at 10^{-5}, 10^{-6}, and 10^{-7} annual exceedance frequencies. In lithophysal rock, where particle sizes are relatively small, the dynamic stress time-history on each segment of the deformable drip shield is supplied to three-dimensional engineering structural analysis of the drip shield. Estimates of drip shield stability and yielded surface area are determined by the calculations in *Drip Shield Structural Response to Rock Fall* (BSC 2004m).

  – **Quasi-Static Loading**–A set of realizations of drift collapse were derived from discontinuum modeling. These realizations allowed complete collapse of the drift with filling of rubble until further collapse was arrested due to the back pressure to the excavation from the rubble. The stresses applied by the rubble to individual elements comprising the deformable drip shield at equilibrium were supplied to engineering for three-dimensional structural analysis of the drip shield. The engineering analysis examines buckling and deformation potential of the drip shield. The time-relation of the collapse does not enter into these analyses because the conservative condition of complete collapse of the excavations is being taken into account in the drip shield structural design.

- **Drift Seepage**–This includes the drift profile and drift periphery damage assessment.

  – **Drift Profile**–The cross-sectional profile of the emplacement drifts impacts the amount of seepage water that enters the tunnels. Drift collapse profiles for the range of rock strength categories for non-seismic and seismic loading conditions are fed to the drift seepage abstraction (BSC 2004o) for estimation of seepage inflow to the drifts. The drift is assumed to be filled with rubble, which is taken into account in the determination of the capillary barrier (as opposed to an empty drift).

  – **Drift Periphery Damage Assessment**–The rock mass strain and estimated change in fracture aperture around the periphery of the drift and the bulking factor and porosity of the collapsed rubble are provided for use in analysis of the drift capillary barrier for a collapsed drift.

[21] The excavations are assumed to be unsupported to support the case that ground support during preclosure is not important to safety.

- **Drift Environment**–This includes the drift collapse.
  - **Drift Collapse**–Drift collapse could have an impact on heat transfer from the waste package to the surrounding rock mass and, thus, affect waste package and drip shield temperature. This is particularly true if significant degradation were to occur during the time period in which temperatures are in excess of the boiling point (i.e., about 1,000 years). Time-dependent analyses show that, in the absence of seismic events with peak ground velocity greater than about 2 m/s, the drifts in either lithophysal or nonlithophysal rock remain largely intact during this time period.

6. SUMMARY AND INTERACTIONS WITH ENGINEERED AND NATURAL SYSTEMS

This document presented a description of the postclosure performance issues involving mechanical degradation of excavations.

6.1 SUMMARY

This report reviews the geologic, laboratory, field, and numerical analysis work that has been performed to document the degradation of the rock mass surrounding the emplacement drifts of a geologic repository at Yucca Mountain. The factors leading to drift degradation include the stresses from overburden (in situ) stresses, stresses induced by the heat released by the emplaced waste, the stresses due to seismically related ground motion, and the time-dependent strength degradation.

The strategy for resolution of these issues was described, and the studies performed to support this resolution were discussed in detail. The strategy was originally presented in March 2002 and documented by Board (2003) and reviewed in DOE-NRC Appendix 7 and Technical Exchange (April 2003 (Stablein and Gil 2003)) meetings. The studies included: (1) performance of detailed geologic and geotechnical mapping studies aimed at describing those geologic features relevant to geomechanical behavior, (2) development of data of mechanical and thermal rock properties for the primary repository host horizons, and (3) development and calibration of material and numerical models for prediction of rock mass response to loading.

These factors have been modeled and analyzed, resulting in the prediction of the general stability of the emplacement drifts, and, specifically, the amount and size distribution of rockfall in the repository drifts during both the preclosure and postclosure regulatory periods.

The following statements summarize the results from this drift degradation modeling and analysis activity and present the key conclusions:

- The rock mass at the repository host horizon has been geologically characterized to support the stability and rockfall modeling activities presented in this report. Drift degradation models have been developed for both nonlithophysal and lithophysal rock. A detailed description of the rock mass characteristics of the repository host horizon was performed. The available rock mass geotechnical data, including fracture geometry, lithophysal abundance and geometric characteristics, and geotechnical rock properties, are sufficient to support detailed drift degradation analyses using both continuum and discontinuum approaches.

- The drift-scale temperature history was calculated throughout the preclosure and postclosure periods of the repository. The temperature history was used to calculate the thermal stress state that develops within the rock mass due to the heat energy released from the stored nuclear waste, and appropriate thermal properties and boundary conditions for thermal loading have been applied. Three-dimensional, mountain-scale models of heat transfer in the rock have been conducted to determine topographical, repository shape, and drift location effects.

- A nonlithophysal rockfall model was developed using the three-dimensional discontinuum code, 3DEC, with the following features:

  - Appropriate boundary conditions are provided for thermal and seismic loading.

  - Critical fracture patterns are included from multiple sampling from a synthetic rock mass volume that contains a realistic fracture population based on field mapping data.

  - Appropriate thermal and mechanical properties of rock blocks and joints are used.

  - Long-term degradation of joint strength parameters is considered.

  - Site-specific ground motion time histories appropriate for both the preclosure (5×10^{-4}, 10^{-4} annual exceedance frequencies) and postclosure (10^{-5}, 10^{-6}, and 10^{-7} annual exceedance frequencies) time periods are included in the model.

- A lithophysal rockfall model was developed using the two-dimensional discontinuum code, UDEC, with the following features:

  - Appropriate thermal and mechanical properties of the lithophysal rock have been determined through a combination of large diameter laboratory testing, field-scale testing, and extrapolation using calibrated numerical models. The model extrapolation is used to examine the variability of mechanical properties with lithophysal porosity, shape, size, and distribution. The rock mechanical property range from testing has been subdivided into five quality "categories" that are functions of rock mass porosity. Categories 1 and 2 represent the lower end of the observed rock quality within the lithophysal rock, whereas Categories 3 and 4 represent an approximate average condition. Category 5 represents the higher quality, lower porosity portions of the Tptpll. These categories provide a basis for parametric calculations. A material model that accounts for the lithophysal rock mass behavior is developed. The majority of analyses were conducted for these bounding ranges of properties; however, a lithophysal porosity spatial variability model was developed to examine directly the impact of in situ variability on seismic and time-dependent drift stability.

  - Appropriate boundary conditions are provided for thermal and seismic loading.

  - The rock mass is represented as an assembly of polygonal, elastic blocks in which the bond strength of the blocks is calibrated such that the overall mechanical behavior of the mass is consistent with the material model developed for the lithophysal rock.

  - The discontinuum lithophysal rockfall model allows for the formation of stress-induced fractures between blocks (i.e., the formation of internal fracturing) separation and instability (under the action of gravity or seismic shaking) of the rock mass around the drift.

  - The effect of long-term degradation of rock mass strength is considered, assuming a stress corrosion mechanism that is dependent on time and applied stress level. An

timate of the degradation of emplacement drifts was developed by incorporating a time-related rock mass shear and tensile strength reduction factor into the drift degradation numerical model.

- Site-specific ground motion time histories appropriate for both the preclosure (5×10^{-4}, 10^{-4} annual exceedance frequencies) and postclosure (10^{-5} and 10^{-6} annual exceedance frequencies) time periods are included in the model.

- Model validation activities include: (1) validating the mechanical material models or representations for the two specific repository host rock types (i.e., lithophysal and nonlithophysal rocks), and (2) validating the implementation of these material models in general numerical modeling schemes.

- The results for the nonlithophysal units are summarized as follows:

  - Preclosure ground motion results in minor drift damage due to rockfall.

  - Postclosure ground motion results in a range of drift damage as a result of wedge-type rockfall (i.e., controlled by geologic structure). The mean block size is less than approximately 0.2 MT for all preclosure and postclosure motions. The large and highly conservative postclosure ground motions (particularly at the 10^{-7} level) can result, for some cases, in spalling of the intact rock blocks surrounding the excavations. The great conservatism in this result is questionable, as these large amplitude motions may not be physically realizable.

  - Thermal effects have a minor impact on rockfall.

  - Time-dependent strength degradation has a minor impact on rockfall.

- The results for the lithophysal units are summarized as follows:

  - Degradation is primarily controlled by stress conditions.

  - Rock block size produced by degradation is controlled by the intense fracturing due to natural cooling of the lithophysal rock matrix as well as the spacing of lithophysae, and is unrelated to the more widely spaced, longer cooling fractures. The spacing of fractures in the lithophysal rock averages approximately 0.05 m, with a resulting small block side length when the rock is overstressed.

  - Preclosure ground motion results in minor drift damage due to rock failure.

  - The 10^{-5} ground motion results in a range of response from no damage to collapse based on the highly variable amplitude of the individual time histories. A reasonable relationship between damage level and peak ground velocity or kinetic energy in the motion has been established. General collapse of the drifts occurs for peak ground velocity greater than about 2 m/s. The highly conservative 10^{-6} postclosure ground motion result in predicted collapse of the drift, with fragmented rock particle sizes on

the order of centimeters to decimeters. It is questionable whether these conservative motions are physically realizable.

- Thermal and time-dependent effects alone are expected to result in relatively small amounts of rockfall. Only in the poorest quality of rock are significant time-dependent breakouts expected. Time-dependent degradation is not expected to result in total collapse of the emplacement drifts. Nonetheless, a conservative approach to drip shield quasi-static loading has been assumed for drip shield structural design. The discontinuum model has been used to simulate complete collapse of the tunnels, and to estimate the subsequent vertical and lateral loads applied to the drip shield. These loads provide input loading conditions for drip shield structural analysis and design.

- Drift profiles based on complete collapse and rubble-filled drifts are used as input to the abstraction of drift seepage. These collapsed drift profiles are assumed at repository closure.

The drift degradation models and analyses documented in this report address the requirements of NRC/DOE agreements regarding rockfall and related issues to support the resolution of NRC KTI on Repository Design and Thermal-Mechanical Effects.

6.2 CLOSURE

The drift degradation models have adequately captured the physical phenomena associated with the various components of rock mass behavior anticipated within the repository horizon. Appropriate boundary and initial conditions have been applied to the models, and the technical bases for the development of these rockfall models have been adequately documented. Sufficient data have been collected to adequately model the drift degradation processes. The technical bases and ranges of data used in the rockfall models are documented.

Data uncertainty has been characterized through parameter sensitivity studies in the rockfall models. Model uncertainty has been characterized through an evaluation of alternative conceptual models, and the model results have been validated by comparison to field and laboratory data, alternative numerical approaches, and industry experience through external technical review.

The most significant uncertainties impacting the results of the rockfall models are those associated with the postclosure ground motion and time-dependent degradation. Some of the ground motion data provided are larger than the largest ground motion observed and may not be physically realizable. Therefore, predictions of complete drift collapse with postclosure ground motion may be unrealistic. Currently lacking a technical basis to limit such ground motion to smaller values, these inputs represent the best available information to support this work.

Prediction of the time-dependent degradation for the duration of the regulatory period of 10,000 years is a highly approximate task. Empirical data to provide evidence for tunnel collapse over hundreds to thousands of years are not available. A mechanics-based approach is used in which a stress corrosion crack model, based on static fatigue test data, is used for prediction of long-term stability of excavations. A small data base of time-dependent testing of

tuff is currently available to support this work. A significant program in static-fatigue measurement of Tptpmn cores is being conducted. This present work will be updated as the long-term testing data are developed.

The drift degradation and modeling activities summarized in this report are sufficient to support a license application. The data on rockfall size and amount are sufficient to provide input to drip shield design calculations, consequence models for the seismic scenario for the total system performance assessment for the license application, and seepage abstraction models for the nominal scenario for the total system performance assessment for the license application.

INTENTIONALLY LEFT BLANK

7. REFERENCES

7.1 DOCUMENTS CITED

Bauer, R.A.; Curry, B.B.; Graese, A.M.; Vaiden, R.C.; Su, W.J.; and Hasek, M.J. 1991. *Geotechnical Properties of Selected Pleistocene, Silurian, and Ordovician Deposits of Northeastern Illinois.* Environmental Geology 139. Champaign, Illinois: Illinois State Geological Survey. TIC: 253871.

Bieniawski, Z.T. 1989. *Engineering Rock Mass Classifications.* New York, New York: John Wiley & Sons. TIC: 226350.

Board, M. 2003. *Resolution Strategy for Geomechanically-Related Repository Design and Thermal-Mechanical Effects (RDTME).* REV 00. Las Vegas, Nevada: Bechtel SAIC Company. ACC: MOL.20030708.0153.

Brodsky, N.S.; Riggins, M.; Connolly, J.; and Ricci, P. 1997. *Thermal Expansion, Thermal Conductivity, and Heat Capacity Measurements for Boreholes UE25 NRG-4, UE25 NRG-5, USW NRG-6, and USW NRG-7/7A.* SAND95-1955. Albuquerque, New Mexico: Sandia National Laboratories. ACC: MOL.19980311.0316.

BSC (Bechtel SAIC Company) 2002a. *Thermal Testing Measurements Report.* ANL-NBS-HS-000041 REV 00. Las Vegas, Nevada: Bechtel SAIC Company. ACC: MOL.20021004.0314.

BSC 2002b. *Thermal Conductivity of the Potential Repository Horizon Model Report.* MDL-NBS-GS-000005 REV 00. Las Vegas, Nevada: Bechtel SAIC Company. ACC: MOL.20020923.0167.

BSC 2002c. *Software Code: 3DEC.* V2.01. PC/WINDOWS 2000/NT 4.0. 10025-2.01-00.

BSC 2002d. *Software Code: UDEC.* V3.1. PC/WINDOWS 2000/NT 4.0. 10173-3.1-00.

BSC 2002e. *Software Code: FLAC3D.* V2.1. PC/WINDOWS 2000/NT 4.0. 10502-2.1-00.

BSC 2002f. *Natural Analogue Synthesis Report.* TDR-NBS-GS-000027 REV 00 ICN 02. Las Vegas, Nevada: Bechtel SAIC Company. ACC: MOL.20020520.0288.

BSC 2003a. *Subsurface Geotechnical Parameters Report.* 800-K0C-WIS0-00400-000-00A. Las Vegas, Nevada: Bechtel SAIC Company. ACC: ENG.20040108.0001.

BSC 2003b. *Longevity of Emplacement Drift Ground Support Materials for LA.* 800-K0C-TEG0-01200-000-00A. Las Vegas, Nevada: Bechtel SAIC Company. ACC: ENG.20030922.0004.

BSC 2003c. *Ground Control for Emplacement Drifts for LA.* 800-K0C-TEG0-00100-000-00A. Las Vegas, Nevada: Bechtel SAIC Company. ACC: ENG.20031016.0001.

BSC 2003d. *Scoping Analysis on Sensitivity and Uncertainty of Emplacement Drift Stability.* 800-K0C-TEG0-00600-000-000. Las Vegas, Nevada: Bechtel SAIC Company. ACC: ENG.20031125.0002.

BSC 2003e. *Underground Layout Configuration.* 800-P0C-MGR0-00100-000-00E. Las Vegas, Nevada: Bechtel SAIC Company. ACC: ENG.20031002.0007.

BSC 2003f. *Heat Capacity and Thermal Expansion Coefficients Analysis Report.* ANL-NBS-GS-000013 REV 00. Las Vegas, Nevada: Bechtel SAIC Company. ACC: DOC.20030820.0002.

BSC 2003g. *Repository Design, Repository/PA IED Subsurface Facilities.* 800-IED-EBS0-00403-000-00B. Las Vegas, Nevada: Bechtel SAIC Company. ACC: MOL.20030109.0147.

BSC 2004a. *Drift Degradation Analysis.* ANL-EBS-MD-000027 REV 03A. Las Vegas, NV: Bechtel SAIC Company. ACC: MOL.20040513.0081.

BSC 2004b. *Ground Control for Non-Emplacement Drifts for LA.* 800-KMC-SSD0-00700-000-00A. Las Vegas, Nevada: Bechtel SAIC Company. ACC: ENG.20040302.0022.

BSC 2004c. *Development of Earthquake Ground Motion Input for Preclosure Seismic Design and Postclosure Performance Assessment of a Geologic Repository at Yucca Mountain, NV.* MDL-MGR-GS-000003 REV 00, with errata. Las Vegas, Nevada: Bechtel SAIC Company. ACC: DOC.20031201.0001; DOC.20040401.0004.

BSC 2004d. *D&E / PA/C IED Emplacement Drift Configuration and Environment.* 800-IED-MGR0-00201-000-00B. Las Vegas, Nevada: Bechtel SAIC Company. ACC: ENG.20040326.0001.

BSC 2004e. *Seismic Consequence Abstraction.* MDL-WIS-PA-000003 REV 0, with errata. Las Vegas, Nevada: Bechtel SAIC Company. ACC: DOC.20030818.0006; DOC.20040218.0002.

BSC 2004f. *Yucca Mountain Site Description.* TDR-CRW-GS-000001 REV 02 ICN 01. Two volumes. Las Vegas, Nevada: Bechtel SAIC Company. ACC: DOC.20040419.0003.

BSC 2004g. *D&E / PA/C IED Subsurface Facilities.* 800-IED-WIS0-00103-000-00A. Las Vegas, Nevada: Bechtel SAIC Company. ACC: ENG.20040309.0028.

BSC 2004h. *Software Code: PFC2D.* V2.0. PC/WINDOWS 2000. 10828-2.0-01.

BSC 2004i. *Software Code: PFC3D.* V.2.0. PC/WINDOWS 2000. 10830-2.0-01.

BSC 2004j. *Lithophysal Rock Mass Mechanical Properties of the Repository Host Horizon.* 800-K0C-SS00-00200-000-00Aa. Las Vegas, Nevada: Bechtel SAIC Company. ACC: MOL.20040510.0200.

BSC 2004k. *Bounding Characteristics of Credible Rockfalls of Preclosure Period.* 800-00C-MGR0-00200-000-00A. Las Vegas, Nevada: Bechtel SAIC Company. ACC: ENG.20040315.0009.

BSC 2004l. *Ventilation Model and Analysis Report.* ANL-EBS-MD-000030 REV 03 ICN 03, Errata 2. Las Vegas, Nevada: Bechtel SAIC Company. ACC: DOC.20031216.0002; DOC.20040202.0004; DOC.20040325.0003.

BSC 2004m. *Drip Shield Structural Response to Rock Fall.* 000-00C-SSE0-00300-000-00A. Las Vegas, Nevada: Bechtel SAIC Company. ACC: ENG.20040405.0019.

BSC 2004n. *Characterize Framework for Seismicity and Structural Deformation at Yucca Mountain, Nevada.* ANL-CRW-GS-000003 REV 00, with errata. Las Vegas, Nevada. Bechtel SAIC Company. ACC: DOC.20040223.0007

BSC 2004o. *Abstraction of Drift Seepage.* MDL-NBS-HS-000019 REV 00 ICN 01. Las Vegas, Nevada: Bechtel SAIC Company. ACC: DOC.20031112.0002; DOC.20040223.0001.

Buesch, D.C.; Spengler, R.W.; Moyer, T.C.; and Geslin, J.K. 1996. *Proposed Stratigraphic Nomenclature and Macroscopic Identification of Lithostratigraphic Units of the Paintbrush Group Exposed at Yucca Mountain, Nevada.* Open-File Report 94-469. Denver, Colorado: U.S. Geological Survey. ACC: MOL.19970205.0061.

CRWMS M&O (Civilian Radioactive Waste Management System Management and Operating Contractor) 1997a. Data Transmittal Package (DTP) for "Hydraulic Fracturing Stress Measurements in Test Hole: ESF-AOD-HDFR#1, Thermal Test Facility, Exploratory Studies Facility at Yucca Mountain. DTN: SNF37100195002.001, TDIF 305878. Las Vegas, Nevada: CRWMS M&O. ACC: MOL.19970717.0005; MOL.19970717.0006; MOL.19970717.0007; MOL.19970717.0008.

CRWMS M&O 1997b. *Yucca Mountain Site Geotechnical Report.* B00000000-01717-5705-00043 REV 01. Two volumes. Las Vegas, Nevada: CRWMS M&O. ACC: MOL.19971017.0736; MOL.19971017.0737.

CRWMS M&O 1998a. *Preliminary Block Size Calculation.* BCAA00000-01717-0210-00001 REV 00. Las Vegas, Nevada: CRWMS M&O. ACC: MOL.19981106.0282.

CRWMS M&O 1998b. *ESF Design Confirmation Steel Set Loads Analysis.* BABEE0000-01717-5705-00006 REV 00. Las Vegas, Nevada: CRWMS M&O. ACC: MOL.19981014.0001.

CRWMS M&O 1998c. *Deformation Monitoring Analysis.* BABEE0000-01717-5705-00005 REV 00. Las Vegas, Nevada: CRWMS M&O. ACC: MOL.19981014.0002.

CRWMS M&O 2000. *Fracture Geometry Analysis for the Stratigraphic Units of the Repository Host Horizon.* ANL-EBS-GE-000006 REV 00. Las Vegas, Nevada: CRWMS M&O. ACC: MOL.20000918.0286.

Duan, F. 2003. "A White Paper by Nick Barton." E-mail from F. Duan to D. Kicker, May 28, 2003, with attachment. ACC: MOL.20030603.0132; MOL.20030219.0058.

Duncan, J.M.; Byrne, P.; Wong, K.S.; and Mabry, P. 1980. *Strength, Stress-Strain and Bulk Modulus Parameters for Finite Element Analyses of Stresses and Movements in Soil Masses.* UCB/GT/80-01. Berkeley, California: University of California, College of Engineering, Office of Research Services. TIC: 253873.

Fruchtbaum, J. 1988. "Handling Special Materials." *Bulk Materials Handling Handbook.* Pages 327-375. New York, New York: Van Nostrand Reinhold. TIC: 253872.

George, J.T.; Finley, R.E.; and Riggins, M. 1999. "Conduct of Plate Loading Tests at Yucca Mountain, Nevada." *Rock Mechanics for Industry, Proceedings of the 37th U.S. Symposium, Vail, Colorado, USA, 6-9 June, 1999.* Amadei, B.; Kranz, R.L.; Scott, G.A.; and Smeallie, P.H.; eds. 2721-2727. Brookfield, Vermont: A.A. Balkema. TIC: 245246.

Goodman, R.E. 1980. *Introduction to Rock Mechanics.* New York, New York: John Wiley & Sons. TIC: 218828.

Hoek, E. 2000. *Practical Rock Engineering.* 2000 Edition. Toronto, Ontario, Canada: RocScience. TIC: 253544.

Itasca Consulting Group 2002. *Itasca Software—Cutting Edge Tools for Computational Mechanics.* Minneapolis, Minnesota: Itasca Consulting Group. TIC: 252592.

Kranz, R.L. 1979. "Crack Growth and Development during Creep in Westerly Granite." *International Journal of Rock Mechanics and Mining Sciences, 16,* 23–36. New York, New York: Elsevier. TIC 255955.

Kranz, R.L. 1980. "The Effects of Confining Pressure and Stress Difference on Static Fatigue of Granite." *Journal of Geophysical Research, 85,* 1854–1866. Washington, D.C.: American Geophysical Union. TIC 255950.

Lau, J.S.O.; Gorski, B.; Conlon, B.; and Anderson, T. 2000. *Long-Term Loading Tests on Saturated Granite and Granodiorite.* Report No. 06819-REP-01300-10061-R00. Toronto, Ontario, Canada: Ontario Power Generation, Nuclear Waste Management Division. TIC: 254970.

LLNL (Lawrence Livermore National Laboratory) 2002. *Software Code: NUFT.* V3.0s. SUN/SunOS 5.6 and 5.7. 10088-3.0s-01.

Martin, R.J. 1972. "Time-Dependent Crack Growth in Quartz and Its Application to the Creep of Rocks." *Journal of Geophysical Research, 77,* 1406–1419. Washington, D.C.: American Geophysical Union. TIC 224770.

Martin, R.J.; Noel, J.S.; Boyd, P.J.; and Price, R.H. 1997a. "Creep and Static Fatigue of Welded Tuff from Yucca Mountain, Nevada." *International Journal of Rock Mechanics and Mining Sciences, 34,* (3/4), 382. New York, New York: Elsevier. TIC: 250241.

Martin, R.J.; Noel, J.S.; Boyd, P.J.; and Price, R.H. 1997b. *Creep Properties of the Paintbrush Tuff Recovered from Borehole USW NRG-7/7A: Data Report.* SAND95-1759. Albuquerque, New Mexico: Sandia National Laboratories. ACC: MOL.19971017.0661.

Martin, R.J., III; Price, R.H.; Boyd, P.J.; and Noel, J.S. 1993a. *The Influence of Strain Rate and Sample Inhomogeneity on the Moduli and Strength of Welded Tuff.* SAND92-2152C. Albuquerque, New Mexico: Sandia National Laboratories. TIC: 254873.

Martin, R.J., III.; Price, R.H.; Boyd, P.J.; and Noel, J.S. 1993b. *Unconfined Compression Experiments on Topopah Spring Member Tuff at 22º C and a Strain Rate of 10-9 s-1: Data Report.* SAND92-1810. Albuquerque, New Mexico: Sandia National Laboratories. ACC: NNA.19930728.0088.

Martin, R.J., III; Price, R.H.; Boyd, P.J.; and Noel, J.S. 1995. *Creep in Topopah Spring Member Welded Tuff.* SAND94-2585. Albuquerque, New Mexico: Sandia National Laboratories. ACC: MOL.19950502.0006.

Mongano, G.S.; Singleton, W.L.; Moyer, T.C.; Beason, S.C.; Eatman, G.L.W.; Albin, A.L.; and Lung, R.C. 1999. *Geology of the ECRB Cross Drift - Exploratory Studies Facility, Yucca Mountain Project, Yucca Mountain, Nevada.* [Deliverable SPG42GM3]. Denver, Colorado: U.S. Geological Survey. ACC: MOL.20000324.0614.

Newmark N.M. 1965. "Effects of Earthquakes on Dams and Embankments." *Geotechnique, 15,* (2), 139–160. London, England: Thomas Telford. TIC: 255743.

Nimick, F.B. and Connolly, J.R. 1991. *Calculation of Heat Capacities for Tuffaceous Units from the Unsaturated Zone at Yucca Mountain, Nevada.* SAND88-3050. Albuquerque, New Mexico: Sandia National Laboratories. ACC: NNA.19910308.0017.

Nimick, F.B.; Price, R.H.; Van Buskirk, R.G.; and Goodell, J.R. 1985. *Uniaxial and Triaxial Compression Test Series on Topopah Spring Tuff from USW G-4, Yucca Mountain, Nevada.* SAND84-1101. Albuquerque, New Mexico: Sandia National Laboratories. ACC: MOL.19980602.0332.

Olsson, W.A. and Jones, A.K. 1980. *Rock Mechanics Properties of Volcanic Tuffs from the Nevada Test Site.* SAND80-1453. Albuquerque, New Mexico: Sandia National Laboratories. ACC: NNA.19870406.0497.

Potyondy, D. and Cundall, P. 2001. *The PFC Model for Rock: Predicting Rock-Mass Damage at the Underground Research Laboratory.* Report No. 06819-REP-01200-10061-R00. Toronto, Ontario, Canada: Ontario Power Generation, Nuclear Waste Management Division. TIC: 253569.

Price, R.H. 1983. *Analysis of the Rock Mechanics Properties of Volcanic Tuff Units from Yucca Mountain, Nevada Test Site.* SAND82-1315. Albuquerque, New Mexico: Sandia National Laboratories. ACC: NNA.19870406.0181.

Price, R.H. 1986. *Effects of Sample Size on the Mechanical Behavior of Topopah Spring Tuff.* SAND85-0709. Albuquerque, New Mexico: Sandia National Laboratories. ACC: NNA.19891106.0125.

Price, R.H. and Bauer, S.J. 1985. "Analysis of the Elastic and Strength Properties of Yucca Mountain Tuff, Nevada." *Research & Engineering Applications in Rock Masses, Proceedings of the 26th U.S. Symposium on Rock Mechanics, Rapid City, South Dakota, June 26-28, 1985.* Ashworth, E., ed. Pages 89-96. Boston, Massachusetts: A.A. Balkema. TIC: 218790.

Price, R.H. and Jones, A.K. 1982. *Uniaxial and Triaxial Compression Tests Series on Calico Hills Tuff.* SAND82-1314. Albuquerque, New Mexico: Sandia National Laboratories. ACC: NNA.19900810.0480.

Price, R.H.; Jones, A.K.; and Nimick, K.G. 1982. *Uniaxial Compression Test Series on Bullfrog Tuff.* SAND82-0481. Albuquerque, New Mexico: Sandia National Laboratories. ACC: HQS.19880517.1700.

Price, R.H.; Martin, R.J., III; and Boyd, P.J. 1993. "Characterization of Porosity in Support of Mechanical Property Analysis." *High Level Radioactive Waste Management, Proceedings of the Fourth Annual International Conference, Las Vegas, Nevada, April 26-30, 1993.* 2, 1847–1853. La Grange Park, Illinois: American Nuclear Society. TIC: 208542.

Price, R.H.; Nimick, F.B.; Connolly, J.R.; Keil, K.; Schwartz, B.M.; and Spence, S.J. 1985. *Preliminary Characterization of the Petrologic, Bulk, and Mechanical Properties of a Lithophysal Zone Within the Topopah Spring Member of the Paintbrush Tuff.* SAND84-0860. Albuquerque, New Mexico: Sandia National Laboratories. ACC: NNA.19870406.0156.

Price, R.H. and Nimick, K.G. 1982. *Uniaxial Compression Test Series on Tram Tuff.* SAND82-1055. Albuquerque, New Mexico: Sandia National Laboratories. ACC: HQS.19880517.1699.

Price, R.H.; Nimick, K.G.; and Zirzow, J.A. 1982. *Uniaxial and Triaxial Compression Test Series on Topopah Spring Tuff.* SAND82-1723. Albuquerque, New Mexico: Sandia National Laboratories. ACC: NNA.19870406.0063.

Price, R.H.; Spence, S.J.; and Jones, A.K. 1984. *Uniaxial Compression Test Series on Topopah Spring Tuff from USW GU-3, Yucca Mountain, Southern Nevada.* SAND83-1646. Albuquerque, New Mexico: Sandia National Laboratories. ACC: NNA.19870406.0252.

Schmidtke, R.H. and Lajtai, E.Z. 1985. "The Long-Term Strength of Lac du Bonnet Granite." *International Journal of Rock Mechanics and Mining Science & Geomechanics Abstracts, 22,* (6), 461-465. New York, New York: Pergamon. TIC: 254874.

Schuhen, M. and Sobolik, S. 2003. *Rock Modulus Slot Test #3, Location 21+25 in ECRB.* Scientific Notebook SN-SNL-SCI-027-V1, Attachment Volume 8. ACC: MOL.20030319.0019.

Sobolik, S.R. 2002a. *Rock Mass Mechanical Properties TDIF, Pressurized Slot Test #1, ESF Station 57+77, 5/8/2002, Description of Analysis.* Albuquerque, New Mexico: Sandia National Laboratories. ACC: MOL.20021022.0151.

Sobolik, S.R. 2002b. *Rock Mass Mechanical Properties, Slot Test #2, Location 63+83 in ESF*. Scientific Notebook SN-SNL-SCI-027-V1, Attachment Volume 6. ACC: MOL.20030319.0040.

Stablein, N.K. and Gil, A.V. 2003. Summary Highlights of NRC/DOE Technical Exchange Meeting on Repository Design and Thermal-Mechanical Effects Key Technical Issue. Meeting held May 6 to 8, 2003, Las Vegas, Nevada. Washington, D.C.: U.S. Nuclear Regulatory Commission. ACC: MOL.20030708.0032.

Stock, J.M.; Healy, J.H.; Hickman, S.H.; and Zoback, M.D. 1985. "Hydraulic Fracturing Stress Measurements at Yucca Mountain, Nevada, and Relationship to the Regional Stress Field." *Journal of Geophysical Research, 90,* (B10), 8691-8706. Washington, D.C.: American Geophysical Union. TIC: 219009.

Terzaghi, K. 1943. *Theoretical Soil Mechanics*. New York, New York: John Wiley & Sons. TIC: 223837.

USGS (U.S. Geological Survey) 1999. *Software Code: FracMAN*. V.2.511. PC/Windows NT. 10114-2.511-00.

Williams, N.H. 2003. "Contract No. DE-AC28-01RW12101 – Licensing Position-034, Preclosure Period Duration." Letter from N.H. Williams (BSC) to J.D. Ziegler (DOE/ORD), December 15, 2003, 1209039726, with enclosure. ACC: MOL.20040107.0059.

7.2 CODES, STANDARDS, AND REGULATIONS

10 CFR 63. Energy: Disposal of High-Level Radioactive Wastes in a Geologic Repository at Yucca Mountain, Nevada. Readily available.

7.3 DATA, LISTED BY DATA TRACKING NUMBER

GS000608314224.004. Provisional Results: Geotechnical Data for Station 35+00 to Station 40+00, Main Drift of the ESF. Submittal date: 06/20/2000.

GS000608314224.006. Provisional Results: Geotechnical Data for Station 26+00 to 30+00, North Ramp and Main Drift of the ESF, Full-Periphery Geotechnical Maps (Drawings OA-46-222 through OA-46-226) and Rock Mass Quality Ratings Report. Submittal date: 06/28/2000.

GS030283114222.001. Direct Shear Data from Selected Samples of the Topopah Spring Tuff. Submittal date: 02/20/2003.

GS960708314224.008. Provisional Results: Geotechnical Data for Station 30 + 00 to Station 35 + 00, Main Drift of the ESF. Submittal date: 08/05/1996.

GS960708314224.010. Provisional Results: Geotechnical Data for Station 40+00 to Station 45+00, Main Drift of the ESF. Submittal date: 08/05/1996.

GS960908314224.015. Provisional Results: Geotechnical Data for Stations 30+00 to 40+00, Main Drift of the ESF, Full-Periphery Geotechnical Maps and Rock Mass Quality Ratings Report. Submittal date: 09/09/1996.

GS960908314224.016. Provisional Results: Geotechnical Data for Station 40+00 to 50+00, Main Drift of the ESF, Full-Periphery Geotechnical Maps and Rock Mass Quality Ratings Report. Submittal date: 09/09/1996.

GS960908314224.020. Analysis Report: Geology of the North Ramp - Stations 4+00 to 28+00 and Data: Detailed Line Survey and Full-Periphery Geotechnical Map - Alcoves 3 (UPCA) and 4 (LPCA), and Comparative Geologic Cross Section - Stations 0+60 to 28+00. Submittal date: 09/09/1996.

GS971108314224.025. Revision 1 of Detailed Line Survey Data, Station 26+00 to Station 30+00, North Ramp and Main Drift, Exploratory Studies Facility. Submittal date: 12/03/1997.

GS990408314224.004. Full-Periphery Geologic Maps for Station 10+00 to 15+00, ECRB Cross Drift. Submittal date: 09/09/1999.

LL980411104244.061. DST Baseline REKA Probe Measurements for Thermal Conductivity and Diffusivity. Submittal date: 04/24/1998.

LL980902104244.070. DST Baseline REKA Probe Measurements for Thermal Conductivity and Diffusivity. Submittal date: 09/03/1998.

MO0001SEPDSTPC.000. Drift Scale Test (DST) Temperature, Power, Current, and Voltage Data for June 1, 1999 through October 31, 1999. Submittal date: 01/12/2000.

MO0002ABBLSLDS.000. As-Built Borehole Locations and Sensor Locations for the Drift Scale Test Given in Local (DST) Coordinates. Submittal date: 02/01/2000.

MO0007SEPDSTPC.001. Drift Scale Test (DST) Temperature, Power, Current, and Voltage Data for November 1, 1999 through May 31, 2000. Submittal date: 07/13/2000.

MO0107SEPDSTPC.003. Drift Scale Test (DST) Temperature, Power, Current, and Voltage Data for December 1, 2000 through May 31, 2001. Submittal date: 07/06/2001.

MO0202SEPDSTTV.001. Drift Scale Test (DST) Temperature, Power, Current, and Voltage Data for June 1, 2001 through January 14, 2002. Submittal date: 02/28/2002.

MO0211TMHIS104.002. Acceleration, Velocity, and Displacement Time Histories for the Repository Level at 5X10-4 Annual Exceedance Frequency. Submittal date: 11/14/2002.

MO0301SPASIP27.004. Sampling of Stochastic Input Parameters for Rockfall Calculations and for Structural Response Calculations Under Vibratory Ground Motions. Submittal date: 01/15/2003.

MO0301TMHIS106.001. Acceleration, Velocity, and Displacement Time Histories for the Repository Level at 10-6 Annual Exceedance Frequency. Submittal date: 01/28/2003.

MO0306SDSAVDTH.000. Seismic Design Spectra and Acceleration, Velocity, and Displacement Time Histories for the Emplacement Level at 10-4 Annual Exceedance Frequency. Submittal date: 06/26/2003.

MO0402AVDTM105.001. Acceleration, Velocity, and Displacement Time Histories for the Repository Level at 10-5 Annual Exceedance Frequency. Submittal date: 02/09/2004.

MO0403AVTMH107.003. Acceleration, Velocity, and Displacement Time Histories for the Repository Level at 10-7 Annual Exceedance Frequency. Submittal date: 03/22/2004.

MO9807DSTSET01.000. Drift Scale Test (DST) Temperature, Power, Current, Voltage Data for November 7, 1997 through May 31, 1998. Submittal date: 07/09/1998.

MO9906DSTSET03.000. Drift Scale Test (DST) Temperature, Power, Current, and Voltage Data for September 1, 1998 through May 31, 1999. Submittal date: 06/08/1999.

SN0206F3504502.012. Revised Thermal Conductivity, Volumetric Heat Capacity and Thermal Diffusivity Data for ECRB Thermal K Test 1 (Two-Hole Test). Submittal date: 06/07/2002.

SN0206F3504502.013. Revised Thermal Conductivity, Volumetric Heat Capacity and Thermal Diffusivity Data for ECRB Thermal K Test 3 (Three-Hole Test, with Results from 1/22/2002 through 4/9/2002). Submittal date: 06/07/2002.

SN0208F3504502.019. Thermal Conductivity, Volumetric Heat Capacity and Thermal Diffusivity Data for ECRB Thermal K Test 2 (Six-Hole Test). Submittal date: 08/30/2002.

SN0208L01B8102.001. Thermal Expansion Properties of Lithophysal Tuff, Batch #1 (Test Dates: August 3, 2002 through August 16, 2002). Submittal date: 08/28/2002.

SN0208L0207502.001. Mechanical Properties of Lithophysal Tuff, Batch #1 (Test Dates: July 31, 2002 through August 16, 2002). Submittal date: 08/20/2002.

SN0208T0503102.007. Thermal Conductivity of the Potential Repository Horizon Rev 3. Submittal date: 08/26/2002.

SN0211L01B8102.002. Thermal Expansion Properties of Lithophysal Tuff, Batch #2 (Test Dates: October 20, 2002 through October 25, 2002). Submittal date: 11/13/2002.

SN0211L0207502.002. Mechanical Properties of Lithophysal Tuff, Batch #2 (Test Dates: October 22, 2002 through October 25, 2002). Submittal date: 11/13/2002.

SN0305L0207502.006. Porosity of Laboratory Mechanical Properties Test Specimens for Batch #1 and Batch #2. Submittal date: 05/20/2003.

SN0306L0207502.008. Revised Mechanical Properties Of Welded Tuff From The Lower Lithophysal Zone Of The Topopah Spring Tuff, Batch #3 (Test Dates: March 6, 2003 Through April 18, 2003). Submittal date: 06/20/2003.

SN0307T0510902.003. Updated Heat Capacity of Yucca Mountain Stratigraphic Units. Submittal date: 07/15/2003.

SNF37100195002.001. Hydraulic Fracturing Stress Measurements in Test Hole: ESF-AOD-HDFR1, Thermal Test Facility, Exploratory Studies Facility at Yucca Mountain. Submittal date: 12/18/1996.

SNL01A05059301.005. Laboratory Thermal Conductivity Data for Boreholes UE25 NRG-4, NRG-5; USW NRG-6 and NRG-7/7A. Submittal date: 02/07/1996.

SNL01B05059301.006. Laboratory Thermal Expansion Data for Boreholes UE25 NRG-4, NRG-5; USW NRG-6 and NRG-7/7A. Submittal date: 02/07/1996.

SNL02112293001.001. Results from Shear Stress Experiments on Natural Fractures on Samples from NRG-4 and NRG-6 Drillholes. Submittal date: 08/18/1994.

SNL02112293001.003. Results from Shear Stress Experiments on Natural Fractures from NRG-4 & NRG-6. Submittal date: 03/13/1995.

SNL02112293001.005. Mechanical Properties of Fractures in Specimens from Drillhole USW SD-9. Submittal date: 07/15/1996.

SNL02112293001.006. Mechanical Properties of Fractures in Specimens from Drillhole USW SD-7 and ESF-TMA-MPBX-3 at Elevated Temperature. Submittal date: 07/30/1996.

SNL02112293001.007. Mechanical Properties of Fractures in Specimens from Drillholes USW NRG-7/7A and USW SD-12. Submittal date: 08/08/1996.

UN0106SPA013GD.004. Drift Scale Thermal Test (DST) REKA Probe Developed Data for Thermal Conductivity and Diffusivity for the Period 05/01/1998 to 04/30/2001 (Heated Measurements for Boreholes 151, 152, and 153). Submittal date: 06/28/2001.

UN0201SPA013GD.007. DST REKA Probe Developed Data for Thermal Conductivity and Diffusivity for the Period 05/01/2001 to 12/31/2001 (Heated Measurements for Boreholes 151 and 152). Submittal date: 01/07/2002.

APPENDIX A

ROCK-MASS CLASSIFICATION FOR LITHOPHYSAL ROCK (RESPONSE TO RDTME 3.05)

Note Regarding the Status of Supporting Technical Information

This document was prepared using the most current information available at the time of its development. This Technical Basis Document and its appendices providing Key Technical Issue Agreement responses that were prepared using preliminary or draft information reflect the status of the Yucca Mountain Project's scientific and design bases at the time of submittal. In some cases this involved the use of draft Analysis and Model Reports (AMRs) and other draft references whose contents may change with time. Information that evolves through subsequent revisions of the AMRs and other references will be reflected in the License Application (LA) as the approved analyses of record at the time of LA submittal. Consequently, the Project will not routinely update either this Technical Basis Document or its Key Technical Issue Agreement appendices to reflect changes in the supporting references prior to submittal of the LA.

APPENDIX A

ROCK-MASS CLASSIFICATION FOR LITHOPHYSAL ROCK (RESPONSE TO RDTME 3.05)

This appendix provides a response to Key Technical Issue (KTI) agreement Repository Design and Thermal-Mechanical Effects (RDTME) 3.05. The agreement relates to concerns regarding the effects of lithophysal cavities on mechanical properties of the rock mass.

A.1 KEY TECHNICAL ISSUE AGREEMENT

A.1.1 RDTME 3.05

Agreement RDTME 3.05 was reached during the U.S. Nuclear Regulatory Commission (NRC)/U.S. Department of Energy (DOE) Technical Exchange and Management Meeting on Repository and Design Thermal-Mechanical Effects held February 6 to 8, 2001, in Las Vegas, Nevada (Reamer and Williams 2001). There has been no submittal related to this KTI agreement to the NRC.

The wording of the agreement is as follows:

RDTME 3.05

> Provide the Rock Mass Classification Analysis (or some other document) including the technical basis for accounting for the effects of lithophysae. The DOE will provide a rock mass classification analysis (or other document), including the technical basis for accounting for the effects of lithophysae, expected to be available to NRC in FY 2002.

The agreement focuses on a concern regarding the effects of lithophysal cavities (lithophysae) on rock-mass mechanical properties and on whether conventional rock-mass classification systems that are widely used in mining and rock engineering for jointed rock masses are suitable for estimating rock-mass mechanical properties of lithophysal rocks. The concern is further elaborated in *Integrated Issue Resolution Status Report* (NRC 2002, Section 2.1.7.3.3.2, pp. 2.1.7-14 and 2.1.7-15). The NRC concerns are as follows:

- Use of empirical correlations between rock-mass mechanical properties and rock-mass quality indices, such as the Barton's Q index or the Bieniawski's rock-mass rating, to account for the effects of lithophysae is unprecedented and not supported by any data on or model investigation of the effects of lithophysae on the mechanical characteristics of rock.

- Barton's Q index or Bieniawski's rock-mass rating index may be appropriate for accounting for the effects of fractures. Some modification of these index values would be necessary if the DOE uses the indexes to account for the effects of lithophysae. The

technical basis for such modification is all the more important because about 75%[1] of the emplacement area may lie within the lithophysal rock units.

A.1.2 Related Key Technical Issue Agreements

RDTME 3.02–This KTI agreement requires that drift degradation and ground support analyses be conducted for critical combinations of in situ, thermal, and seismic stresses. These load combinations are addressed in Section 5.

RDTME 3.04–This KTI agreement involves providing a geotechnical parameters report that includes rock-mass property estimates of the lithophysal rocks of the Topopah Spring formation. RDTME 3.05 deals specifically with providing estimates of the lithophysal rock-mass properties. Thus, the work performed to resolve RDTME 3.05 also forms a portion of the geotechnical parameters report that is used to resolve RDTME 3.04. Sections 3 and 4 examine the rock-mass properties estimates.

RDTME 3.10–This KTI agreement requires verification of the adequacy of the use of two-dimensional models for analysis of drift degradation. Sections 4.2.2.2 and 5.3.3.1.2 discuss the use of two- and three-dimensional models for drift degradation analysis.

RDTME 3.11–This KTI agreement requires examination of the long-term degradation of the rock mass in lithophysal and nonlithophysal rocks. This appendix discusses the methodology for accounting for lithophysae in the mechanical rock-mass properties and material models. Section 5.3.3.2.4 summarizes the specific approach to accounting for long-term strength degradation of material properties via use of static fatigue testing of tuffs.

RDTME 3.12–This KTI agreement requires a dynamic analysis of ground support systems during the preclosure phase using site-specific ground motions and discontinuum numerical modeling. The technical basis document centers on the postclosure dynamic analysis of lithophysal and nonlithophysal rocks using discontinuum methods. The preclosure dynamic analysis of ground support is provided in *Scoping Analysis on Sensitivity and Uncertainty of Emplacement Drift Stability* (BSC 2003a).

RDTME 3.13–This KTI agreement requires technical justification for boundary conditions for models used in drift degradation and ground support analyses. Section 5 discusses static and dynamic mechanical and thermal boundary and initial conditions.

TSPAI 2.02, Items 58 and 62–TSPAI 2.02, Items 58 and 62 related to the inclusion of rockfall and its potential mechanical impacts on engineered barriers and on the thermal-mechanical impacts of long-term rock-mass degradation on engineered barriers and potential hydrologic changes in the rock mass. RDTME 3.05 deals specifically with the estimation of rock-mass properties of the lithophysal rocks of the Topopah Spring formation and the development of rock-mass material and numerical models for representing fracture, rockfall, and long-term degradation under in situ, thermal, and seismic loading. The estimates made for rockfall and

[1] Although 75% is used in *Integrated Issue Resolution Status Report* (NRC 2002), the actual percentage is approximately 85%.

long-term degradation and change of opening shape feed performance assessment studies of the engineered barriers. Section 1 describes this integration in more detail.

A.2 RELEVANCE TO REPOSITORY PERFORMANCE

Agreement RDTME 3.05 deals with demonstrating an understanding of the material properties of the lithophysal rock mass. The material properties of importance to repository design and performance are the thermal, deformability, and strength properties and their potential changes with time, as well as variability within the repository host horizon. A description of geotechnical properties is given in Section 3, and a detailed characterization of all properties is given in *Subsurface Geotechnical Parameters Report* (BSC 2003b). These properties are used as direct input to numerical models that predict the drift degradation behavior of the emplacement drifts when subjected to in situ, thermal, and seismic loading, as well as time-dependent changes in mechanical properties. The results of these calculations are estimates of the volume and size of potential rockfall and the change in the shape of the tunnels as functions of time. This information directly feeds calculations of the structural stability of waste packages and drip shields due to rockfall in the preclosure and postclosure time frames. The rockfall also potentially causes an insulating effect around the drip shields, which could impact in-drift temperatures as a function of time. The change in the shape of the tunnels as a function of time feeds the analysis of seepage to emplacement drifts.

A.3 RESPONSE

The strategy for developing estimates of rock-mass properties and material models for lithophysal rocks was presented by Board (2003). The strategy does not rely on rock-mass classification methods for empirically deriving the rock-mass mechanical properties for the lithophysal rock. Instead, the approach for determining the effects of lithophysae involves:

1. Conducting a detailed site-specific geologic description of the lithophysal rock mass in the Exploratory Studies Facility (ESF) and Enhanced Characterization of the Repository Block (ECRB) Cross-Drift.

2. Testing of large-diameter core in the laboratory and in situ slot testing to establish properties of rock material as functions of specimen size and lithophysal porosity for a limited data set.

3. Calibrating the PFC (i.e., collectively, the PFC2D (BSC 2002a) and PFC3D (BSC 2002b) and UDEC (BSC 2002c) discontinuum numerical models of unfractured lithophysal rock to provide a mechanics-based predictive tool of lithophysal behavior. This is described in Section 4.2.3.

4. Utilizing the models to extrapolate rock-mass mechanical behavior to a wide range of rock-mass lithophysal conditions, including the size, shape, porosity, and distribution of lithophysae to establish their impact on variability of the rock-mass properties.

5. Developing bounding rock-mass mechanical properties ranges based on the laboratory testing, numerical extrapolation, and examination of the spatial variability of lithophysal porosity.

The development and technical basis for the above strategy is documented in *Lithophysal Rock Mass Mechanical Properties of the Repository Host Horizon* (BSC 2004a) and the *Subsurface Geotechnical Parameters Report* (BSC 2003b). The results from these assessments are implemented in design calculations and sensitivity analyses presented in detail in *Drift Degradation Analysis* (BSC 2004b) and *Evaluation of Emplacement Drift Stability for KTI Resolutions* (BSC 2004c) and summarized in Sections 4 and 5.

The strategy is summarized below.

Geologic Description of the Physical and Mineralogical Characteristics of Lithophysae within the Lower Lithophysal Unit (Tptpll)–A mapping program was undertaken in the ECRB Cross-Drift to describe the statistical variability of the size, shape, porosity, and distribution of lithophysae, as well as interlithophysal fracturing across the entire Tptpll. This work provides the basis for understanding the physical variability of the lithophysal rock mass and is discussed in Section 2.3.2.

Laboratory and Field Testing of Lithophysal Rock–Large-scale testing is necessary to determine the mechanical properties of lithophysal rock due to the presence of the lithophysal voids. A laboratory (approximately 0.3 m diameter samples) and in situ (approximately 1.1 m samples) testing program was used to obtain and mechanically test large specimens of the upper lithophysal unit (Tptpul) and the lower lithophysal unit (Tptpll). These laboratory data provide a base (in addition to the small core testing database) for relating strength and modulus to lithophysal porosity as well as determining the relationship between modulus and strength. Additionally, the field-scale testing provides information on the effects of scale involving a greater specimen size and variability of shape, size, and distribution of lithophysal porosity. Section 3.2.1 discusses the mechanical properties of intact rock, including correlation of these properties with rock porosity. Section 3.2.3 discusses the in situ mechanical testing of lithophysal rock.

Development of the Numerical Modeling Approach for the Representation of Lithophysal Rock–The rock sample size-dependency and variability in lithophysal rock-mass properties introduced by the lithophysae make a conventional, statistically based laboratory testing program impractical. An essential part of the resolution strategy is the development of a numerical modeling approach that is capable of simulating the mechanics of deformability and yield of the lithophysal rock. Different discontinuum numerical modeling approaches, the PFC and UDEC models, are used to examine the basic mechanisms of how lithophysae affect the failure characteristics and moduli of the Tptpul and Tptpll. These models were chosen because of their ability to represent physical voids in a material and for their capability to model complex failure mechanisms, such as fracture initiation and propagation between voids. PFC3D was used to explore the suitability of the two-dimensional modeling.

The model matrix (containing no voids or fractures) strength and elastic moduli were first calibrated through comparison of the model response to the results from laboratory testing of nonlithophysal rocks. The models were then validated for lithophysal rocks by assuming the same matrix as the nonlithophysal case, and then adding voids of varying size to replicate the lithophysal porosity of the rock mass. Simulated uniaxial compression tests were then compared to laboratory and field testing results to verify the general predictability of the approach. An

outcome of this process was an explanation for the mechanisms of strength and modulus reduction that accompanies additional porosity. Triaxial compression experiments were used to develop estimated yield criteria and dilation angles for lithophysal rocks as a function of porosity. Sections 4.2.1 and 4.2.3 and this appendix discuss the numerical modeling approach, material model requirements, and validation of the adopted models for predicting lithophysal rock behavior.

Extrapolation of the Variability of Lithophysal Rock-Mass Properties Using Numerical Models–The calibrated PFC model is used for extrapolation purposes to supplement the laboratory and field testing database. The variability of rock mechanical properties due to lithophysae shape and spatial distribution is studied by randomly creating voids of simple shape (e.g., circle, triangle, or star) in the matrix material and by modeling realistic void shapes and distributions corresponding to lithophysal cavities identified in ECRB Cross-Drift panel maps (1 × 3 m). Variability in the rock response and size effect appears to be a function primarily of the distribution of the lithophysae (i.e., percentage porosity and how evenly distributed it is through the rock mass), and, to a lesser extent, the deviation of the shape of true voids from circular voids. The property scatter apparent at given values of lithophysal porosity reduces significantly when the data are plotted in terms of strength versus Young's modulus, suggesting that this correlation is independent of void geometry. Section 4.2.2 and this appendix discuss how the numerical models for lithophysal rock were calibrated and used to model lithophysal rock behavior.

Establishing the Range of Material Properties of Lithophysal Rocks for Design and Performance Assessment–The laboratory and field data are integrated with the computational property variability estimates to establish the range of strengths and moduli that represent the rock-mass properties in the ECRB Cross-Drift and, especially, the Tptpll. A bounding approach based on parametric modeling over the entire range of estimated rock-mass properties is used for conducting drift degradation analyses. These rock parameters ranges are then used as a basis for excavation stability calculations. Sections 4.2.3 and 4.2.4 and this appendix describe how lithophysal rock mass properties estimates were developed and bounded.

Development of a Drift-Scale Emplacement Drift Degradation Modeling Tool–The impact of modeled spatial variability of lithophysal porosity in the Tptpll and establishment of the conservatism of use of a bounding range approach is examined through numerical analysis of nonhomogeneous rock-mass strength and deformability. A discontinuum model based on the UDEC program was developed and calibrated to represent the range of strength and moduli (discussed above). The range of rock mass properties that were used to calibrate the UDEC model are presented in Sections 4.2.3 and 4.2.4. Validation of the UDEC model was performed against laboratory and field observations, as described in Section 4.2.7. The UDEC model was then used to estimate the stability and rockfall for in situ, thermal, and seismic loading, as well as time-dependent strength degradation. A parametric study was conducted using the range of strength and moduli to provide lower-bound, mean, and upper-bound estimates of rock-mass yield and rockfall for the Tptpll. Section 4.2 and this appendix provide further explanation of how lithophysal rock mass properties were calibrated, developed, and bounded.

The information in this appendix is responsive to KTI agreement RDTME 3.05 made between the DOE and NRC for the following reasons:

- The impact of lithophysae on mechanical properties is accounted for based on laboratory and field testing at various physical scales.
- Numerical analyses of rock containing lithophysae have been used to enhance understanding and provide evidence of the mechanisms impacting mechanical properties of rock.
- The spatial variability of lithophysae and bulk porosity in the Tptpll is accounted for based on geologic field mapping and numerical extrapolation.
- This variability is also accounted for in design analyses through parametric studies that cover a bounding range of rock parameters.

The approach of applying numerical modeling to the rock containing lithophysae is corroborated with laboratory and field test data and observation of excavation effects in the ECRB Cross-Drift in the Tptpll unit.

The information in this report is responsive to agreement RDTME 3.05 made between the DOE and NRC. The report contains the information that DOE considers necessary for NRC review for closure of this agreement.

A.4 BASIS FOR THE RESPONSE

The Yucca Mountain exploratory excavations for the repository are located within a portion of the Topopah Spring formation, a volcanic welded tuff subdivided into four subunits characterized by their geologic features and structure. These four subunits are the upper lithophysal unit (Tptpul), the middle nonlithophysal unit (Tptpmn), the lower lithophysal unit (Tptpll), and the lower nonlithophysal unit (Tptpln). The nonlithophysal units (Tptpmn and Tptpln) are fine-grained, low porosity (i.e., approximately 11%), strong volcanic rocks that contain abundant but relatively nonpersistent cooling fractures. The lithophysal units (Tptpul and Tptpll) are composed of the same fine-grained matrix material but have additional porosity contributed by lithophysae (i.e., open voids that are a result of gas localization during the cooling process) and by rims and spots formed from the crystallization of vitric rock in the presence of vapor. These lithophysae, which vary in size from the millimeter to meter scale, make up about 10% to 30% of the volume of the Tptpll subunit, averaging approximately 15%. Rim and spot material has a porosity averaging 30% and makes up about 4% of the volume of the Tptpll, ranging from about 1% to 12%.

Agreement RDTME 3.05 addresses the means by which the presence of lithophysae will be accounted for in thermal and mechanical analysis models. At the time of the writing of that agreement (Reamer and Williams 2001), the use of modified empirical classification and design methods typically used in rock mechanics (e.g., Barton's Q index and Bieniawski's rock-mass rating classification schemes) to account for lithophysae was being considered. In response to

NRC concerns, it was determined that an alternative approach based on development of site-specific rock-mass properties data for the lithophysal rocks was warranted.

The present approach being used in estimating lithophysal rock-mass properties relies on a program incorporating site-specific laboratory and field testing supplemented by numerical modeling of lithophysal rock. As a result, the DOE has conducted and analyzed tests on lithophysal rock in the Tptpul and Tptpll units, consisting of large-diameter core (up to 0.3 m diameter) and in situ compression tests (slot tests up to 1.1 m across). Additionally, the Tptpll portion of the ECRB Cross-Drift has been systematically mapped to identify lithophysal rock characteristics (abundance, shape, and size variability), and work is underway to similarly map portions of the Tptpul unit in the ECRB Cross-Drift as well. Lastly, two- and three-dimensional numerical modeling of larger-scale samples (1 m scale) with realistic lithophysal voids have been carried out using the PFC and UDEC discontinuum programs. These numerical simulations have been utilized to further develop the stress-strain response of lithophysal rocks and to establish rock parameter ranges necessary to extrapolate the possible behavior and material properties of lithophysal bulk rock. This appendix deals specifically with the geotechnical characterization of the lithophysal rock mass and the impact of lithophysal porosity on mechanical properties. The impact of lithophysal porosity on thermal properties is derived from laboratory and field thermal testing and is discussed in Section 3.2.5.

A.4.1 Geologic Mapping of Physical and Mineralogical Characteristics of Lithophysae

Documentation of the variability of physical and mineralogical characteristics of lithophysae forms the basis for further analytical modeling. These field characteristics are documented via the use of several techniques using tape and survey measurements of lithophysae sizes taken at specified intervals across the unit thickness of the Tptpll exposed within the ECRB Cross-Drift. Detailed mapping and photography of 1 × 3 m panels maps along the walls of the ECRB Cross-Drift serves as a core of site-specific documentation (Figure A-1).

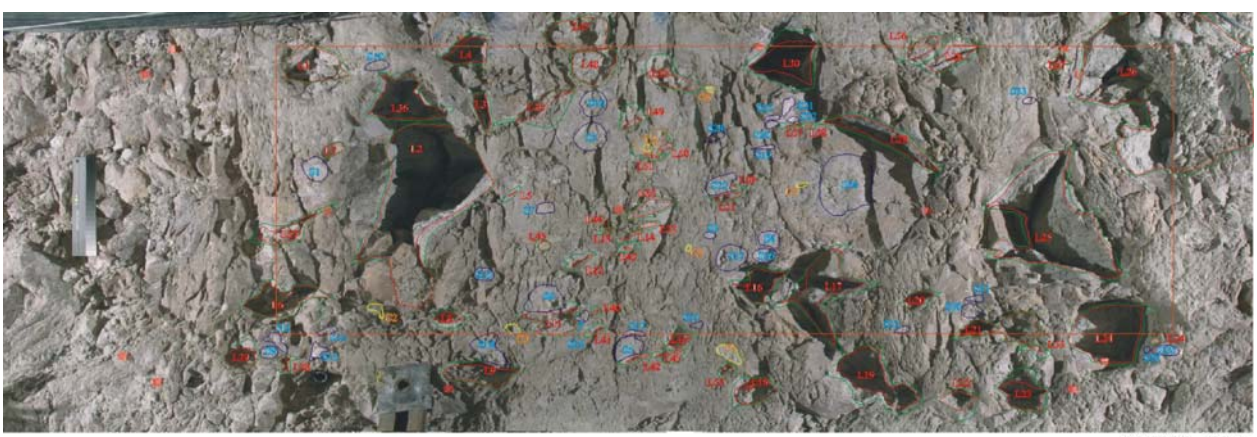

00387DC_100.ai

Figure A-1. Example Tptpll Panel Map and Showing Lithophysae, Rims, Spots, and Lithic Clasts

The results of this work are summarized in this appendix and described in *Subsurface Geotechnical Parameters Report* (BSC 2003b, Section 8.8.4). Each of these techniques has resulted in an estimate of the lithophysal porosity along the tunnel, as well as estimates of the abundance of the lithophysae rims and spots and the shape and size distribution of the

lithophysal porosity. The distribution of lithophysal porosity and other features obtained from the 15 m averaged tape traverse data corrected to panel map and angular traverse data is presented in Figure A-2. This figure shows that average lithophysal porosities greater than 20% makes up only a small (about 10%) of the Tptpll. The greatest abundance of porosity levels is found in the range of approximately 10% to 20%. Since lithophysal porosity is the greatest controlling factor in the mechanical properties of the rock mass, the abundance of lithophysal porosity can be directly related to the abundance of mechanical properties, as discussed Section A.4.5.

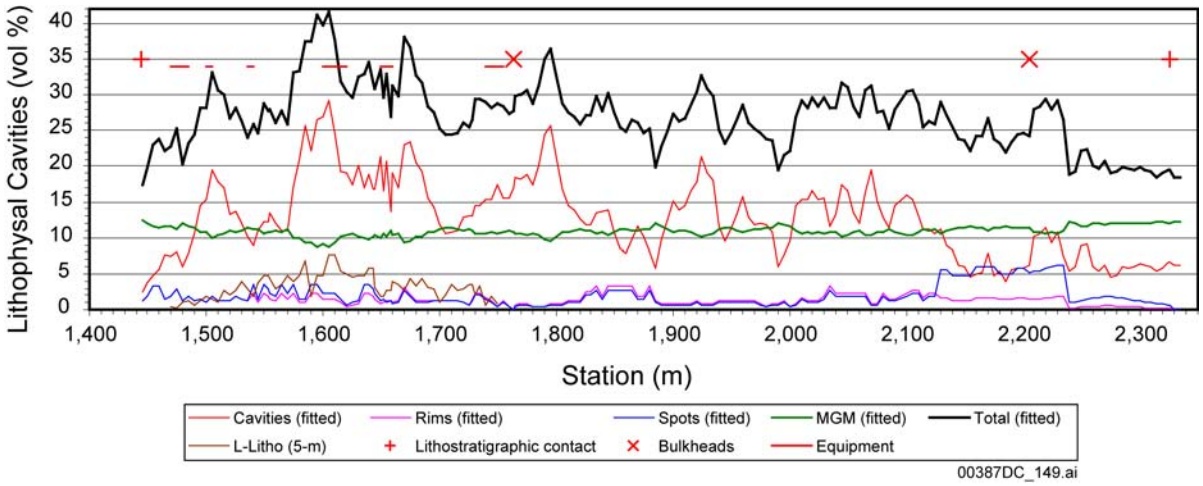

Source: BSC 2003b, Attachment VII, Figure VII-15.

NOTE: Relatively thin bands of highest lithophysal porosity (greater than 20%) occur near the top of the Tptpll, with decreasing values near the bottom of the subunit. Higher and lower localized volumes of lithophysal porosity may be present. The 5 m averaged large-lithophysae inventory (brown) is not included as part of the lithophysal or total porosity curves.

Figure A-2. Example of Calculated Porosity of Lithophysal Cavities (red), Rims (violet), Spots (blue), Matrix-Groundmass (green), and the Total Porosity (black) in the Tptpll Exposed along the ECRB Cross-Drift

Field mapping (an example of the fitted lithophysal cavity porosity is shown in Figure A-2) has been used to develop a model for simulating the spatial variability of lithophysal porosity within the Tptpll (see Section 2.3.2). The observed variations in lithophysal porosity within the Tptpll are assumed to be laterally continuous across the volume of rock sampled and to vertically show a statistically distinguishable sequence of stratiform subzones. The ECRB Cross-Drift transects the entire Tptpll unit allowing determination of the stratiform nature of laterally continuous subzones of lithophysal porosity within the Tptpll. The lateral continuity of lithostratigraphic features and the projection of these features along the apparent dip of the ECRB Cross-Drift are used to develop a vertical cross section of the distribution of lithophysal porosity within the Tptpll.

Figure A-3 presents two simulated (overlapping) vertical projections of lithophysal porosity for 50-m-tall vertical cross sections extending from the top and bottom of the Tptpll. Each of the cells of these cross sections represent a volume of the Tptpll and have a lithophysal porosity associated with it. As seen in these cross sections, the lithophysal porosity occurs as stratiform subzones, with the highest values (i.e., 20% or higher) occurring in thin bands near the top of the

subzone. The lowest lithophysal porosities occur in the lower portions of the subzone near the contact with the Tptpln. These simulated cross sections are used as a basis for examining the impact of spatial variability on rock-mass mechanical response and comparing assumptions of homogenous rock-mass properties.

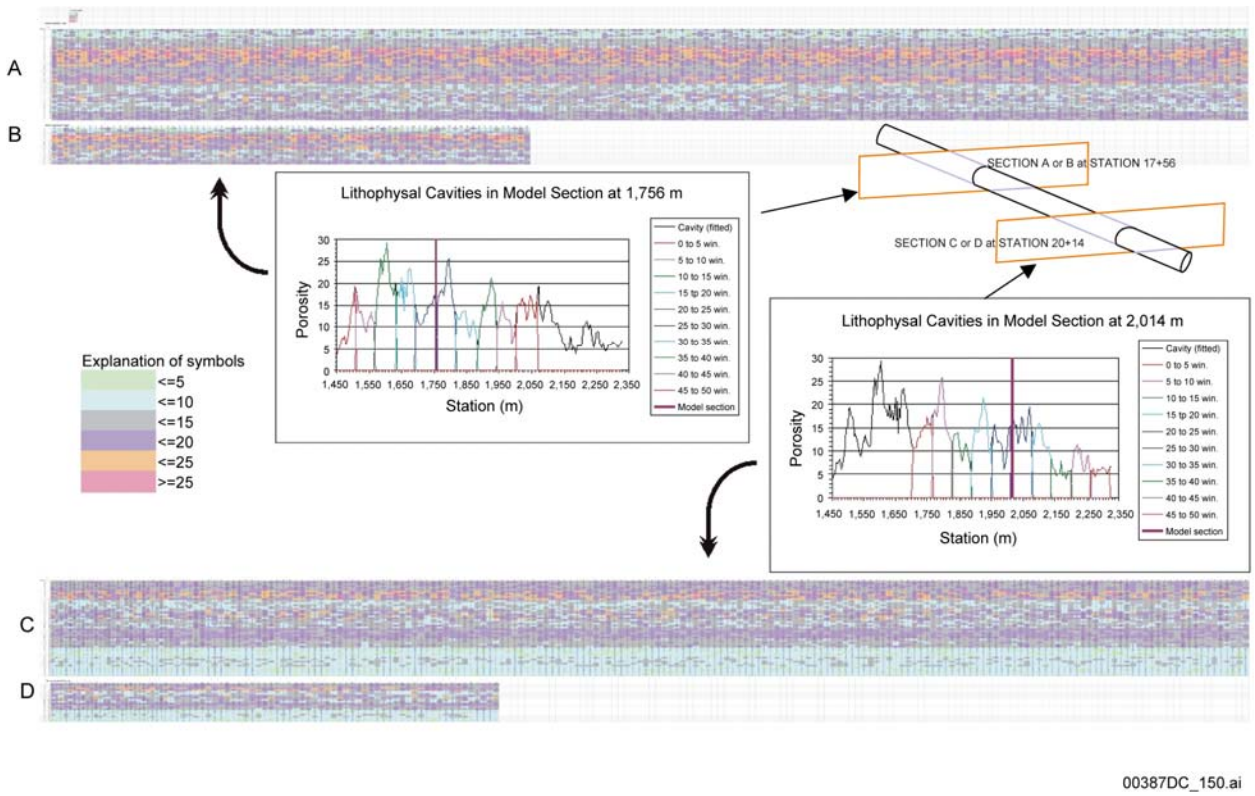

Source: BSC 2003b, Section 9.4, Figure 9-46.

NOTE: Cross section A is a 50 × 200 cell table representing a 1 × 1 m grid and cross section B is a 20 × 80 cell table representing a 2.5 × 2.5 m grid for the simulated section at 17 + 56 in the ECRB. Cross sections C and D represent simulated section at 20 + 14 in the ECRB.

Figure A-3. Illustration of the Process of Sampling and Modeling Spatial Variability Using Lithophysal Porosity—Two 50 × 200 m Simulated Cross Sections at Overlapping Upper (A/B) and Lower (C/D) Sections of the Tptpll

Results of Geological Mapping–Geological mapping studies in the Tptpll have provided the baseline information required for inclusion in the thermal and mechanical analyses. This information includes a determination of the following:

- Abundance of lithophysal cavities, rims, and spots in the Tptpll
- The size distribution of lithophysae
- An inventory of lithophysae shapes

- Panel map sampling of the two-dimensional spatial variability of lithophysal porosity within the Tptpll (i.e., the distribution of lithophysal cavity space versus solid rock bridge length).

A.4.2 Laboratory and In Situ Thermal and Mechanical Testing of Lithophysal Rocks

A series of laboratory and field tests of mechanical and thermal properties of Tptpul and Tptpll rock have been completed and reviewed in Section 3.2.1 and have been documented in detail in *Subsurface Geotechnical Parameters Report* (BSC 2003b), which reviews the available geotechnical database. A review of the results presented in Section 4.2 follows. *Lithophysal Rock Mass Mechanical Properties of the Repository Host Horizon* (BSC 2004a) provides a detailed assessment of the relationship between porosity and mechanical rock properties.

Laboratory Testing–Due to the variable size of lithophysae, only large-diameter core samples (e.g., ideally about several lithophysae diameters in diameter) can be used for estimating rock strength values. In 1985, compression tests were conducted on cores with a diameter of 0.27 m (10.5 in.) taken from the Tptpul at Busted Butte. An extensive drilling program was undertaken in the ESF and ECRB in 2002 to provide representative large diameter (0.29 m, 11.5 in.) core samples of lithophysal rock from the Tptpul and Tptpll zones within the repository host horizon. Fourteen suitable specimens were recovered and tested in uniaxial compression at dry, saturated, and room–moisture conditions. The lithophysal porosity of these core samples, estimated from the surface line counting of features, ranges from approximately 10% to 30%. The results of these tests, in terms of unconfined compressive strength versus Young's modulus, are shown in Figure A-4.

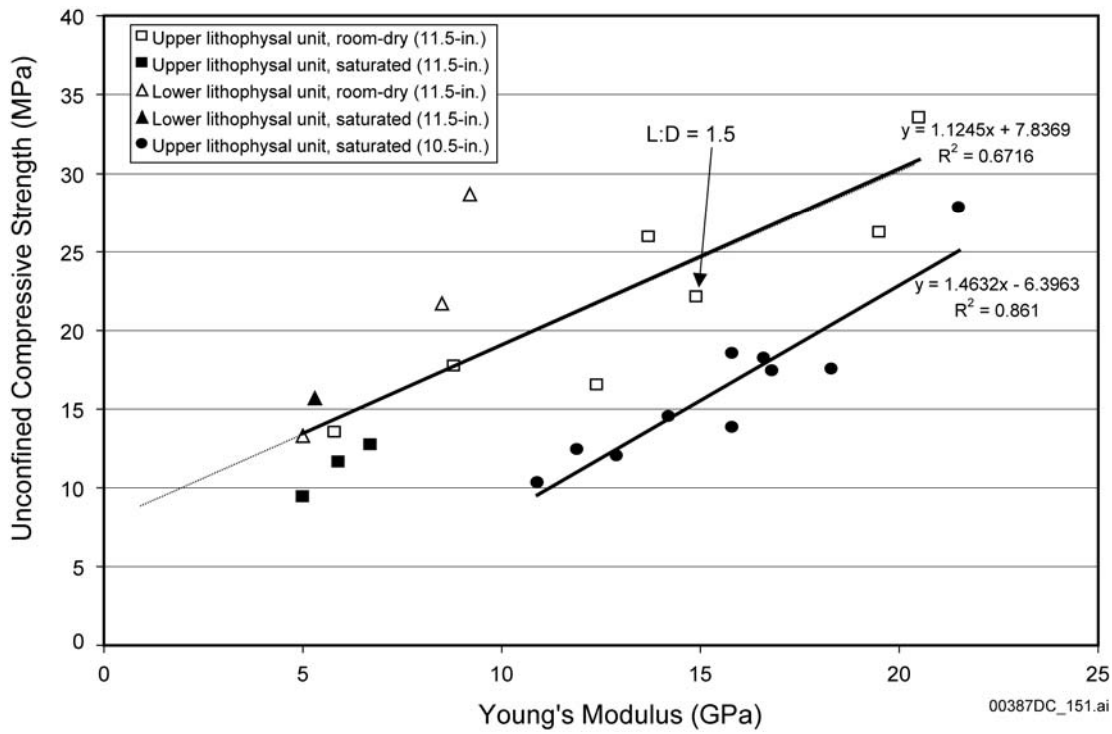

NOTE: Variation in range of strength and modulus is primarily a function of lithophysal porosity and level of saturation. Linear fits to data presented for 0.29 and 0.27 m cores separately.

Figure A-4. Unconfined Compressive Strength versus Young's Modulus for 0.29 m (11.5 in.) and 0.27 m (10.5 in.) Diameter Cores of Tptpul and Tptpll

In Situ Mechanical Testing–Three in situ flatjack slot tests were conducted on 1.1 m span samples in the Tptpll and Tptpul (see Section 3.2.3). The tests involve cutting two thin, parallel slots, separated by approximately 1.1 m, in the sidewall or floor of the tunnel. The lithophysal content from the face and slots of the blocks were mapped to define the size, shape, and percentage of lithophysae and spots. Steel flatjack bladders were inserted into the slots and pressurized to load the sample in a state of near-uniaxial compression (the ends of the sample are not freed, thus there is some confinement from the sample ends). Deformations of the block were determined in a central, internal borehole to allow calculation of the stress-strain response of the rock mass.

These tests have shown that the in situ deformation modulus is approximately 1.0 to 3.0 GPa (one test was located in the poorest quality failed rock in the tunnel springline area, yielding a modulus of 0.5 GPa). In general, it has been concluded that these tests illustrate the impact of mining and stress-related damage in the immediate sidewall of the tunnels and are not necessarily indicative of rock-mass strength and moduli. However, the tests illustrate some component of the size effect present in sample size increased from 0.3 m to approximately 1 m.

A.4.3 Development of Basic Mechanical Constitutive Models for Lithophysal Rock through Calibration of Numerical and Analytical Models

Conducting a statistically significant number of large core mechanical tests and in situ scale tests on lithophysal rocks as a means of determining the variability of rock-mass properties is not practical, due to sampling difficulties and laboratory testing limitations. Instead, the strategy described by Board (2003) suggested that calibration and validation of a suitable mechanical numerical modeling approach could be used to supplement available laboratory and field testing and to clarify understanding of the mechanical response of lithophysal rock. This approach allows investigation of the effects of lithophysae size, shape, and porosity distribution on mechanical constitutive behavior of lithophysae-containing rock. The PFC program employs a micromechanical modeling approach, which represents the rock matrix as a large number of rigid circular or spherical particles that are bonded together at their contact points with simple shear and tensile bonds and normal and shear stiffness. The UDEC program, also based on a discontinuum approach, is used as an alternative computational model to simulate compressive load testing on lithophysal rock specimens.

As a simulated PFC rock specimen is stressed, the inter-particle bonds can fail, leading to frictional sliding between particles. This conceptually simple model can exhibit complex constitutive behavior including realistic growth of stress-induced fracturing. Of importance to the present problem is that holes of arbitrary shape, size, and distribution can be represented in the model as physical entities. Thus, stress concentrations and fracturing between holes can be represented in a realistic way, allowing detailed examination of deformation and failure mechanisms.

The PFC model has been calibrated against the laboratory testing data discussed in Section 4.2.3.2. Numerical compressive strength experiments were conducted first for nonlithophysal welded tuff to derive strength properties of the matrix (Figure A-5). In subsequent analyses, simple uniformly distributed circular (and later triangular) holes were added to the model, and the relationship between laboratory-derived strengths, moduli, and porosities was examined. The modeling results showed good agreement with laboratory data (Figure A-6). Results indicated that the primary strength-decreasing effect of the lithophysae is due to initiation and propagation of tensile splitting between lithophysae under compressive load. As porosity increases, the spacing between lithophysae decreases, and rock acquires a greater propensity for tensile splitting at the lower applied stresses.

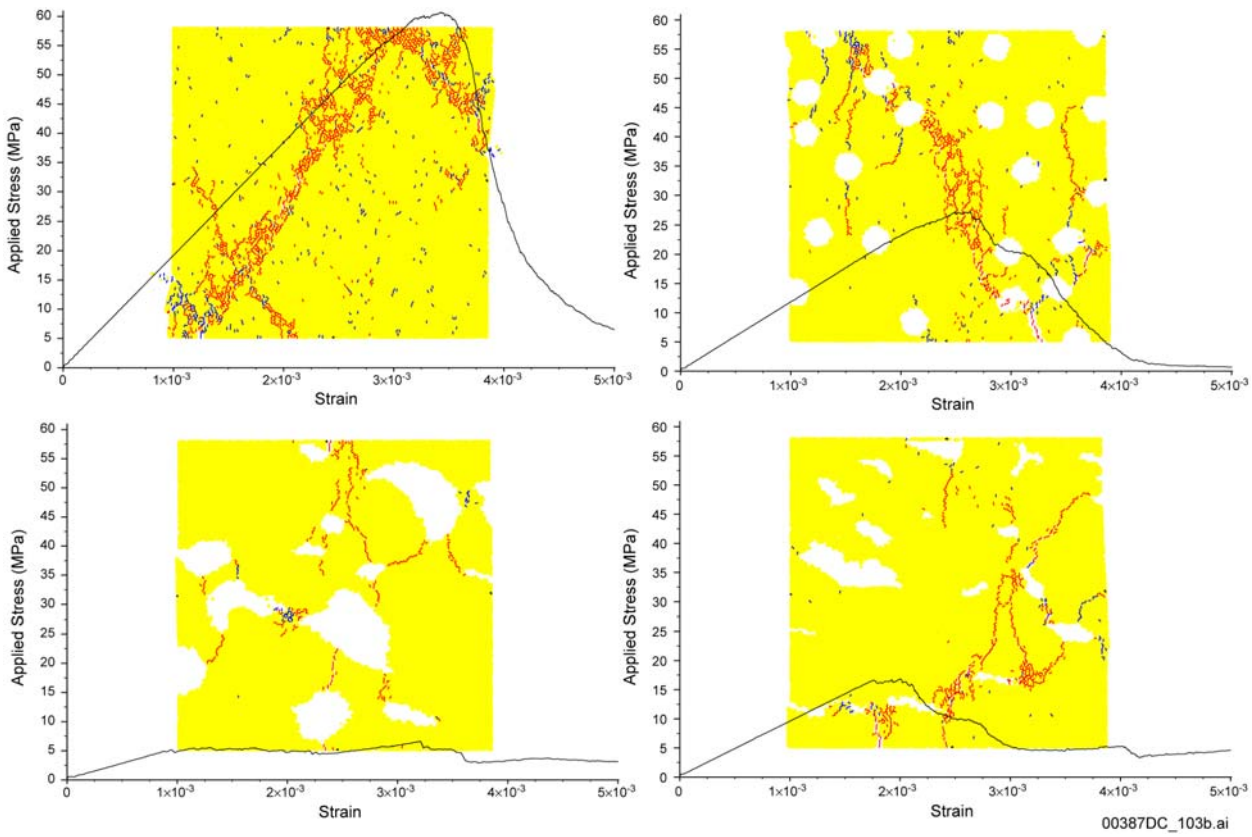

Source: BSC 2004a, Section 6.5.6, Figure 6.5-20.

NOTE: Nonlithophysal welded tuff (upper left) is calibrated to provide matrix properties. Circular holes (upper right) provide a simple model of lithophysae, whereas lower models provide more realistic (hand-stenciled and digitized) shapes from Tptpll panel maps. Nonlithophysal rock fails in a brittle fashion through propagation of a major shear fracture (composed of small tensile fractures) through the sample. Lithophysal samples fail due to tensile splitting (each red line is a bond breakage between small particles) between holes. Variability in lithophysal strength arises due to abundance, shape, and distribution of the holes throughout the sample.

Figure A-5. PFC Calibration Experiment Samples and Their Respective Unconfined Stress–Strain Curves for Cases of Circular and Stenciled Lithophysae Shapes

Further PFC numerical testing was performed during which lithophysal panel maps (see Figure A-1) were discretized and used as 1.0 × 1.0 m compressive test specimens (Figure A-5) for the model. As shown in Figure A-6, the simple models containing circular holes display less variability in results than similar analyses that utilize actual lithophysae shapes. Actual shapes result in greater variability in test results (particularly at low porosities) and a lower estimate of mean strength and modulus.

The conclusion drawn from the PFC model calibration is that this approach provides a reasonable methodology for simulating the mechanical response of lithophysal welded tuff to stressing and that this tool can be used to study variability in material response in addition to laboratory and field testing.

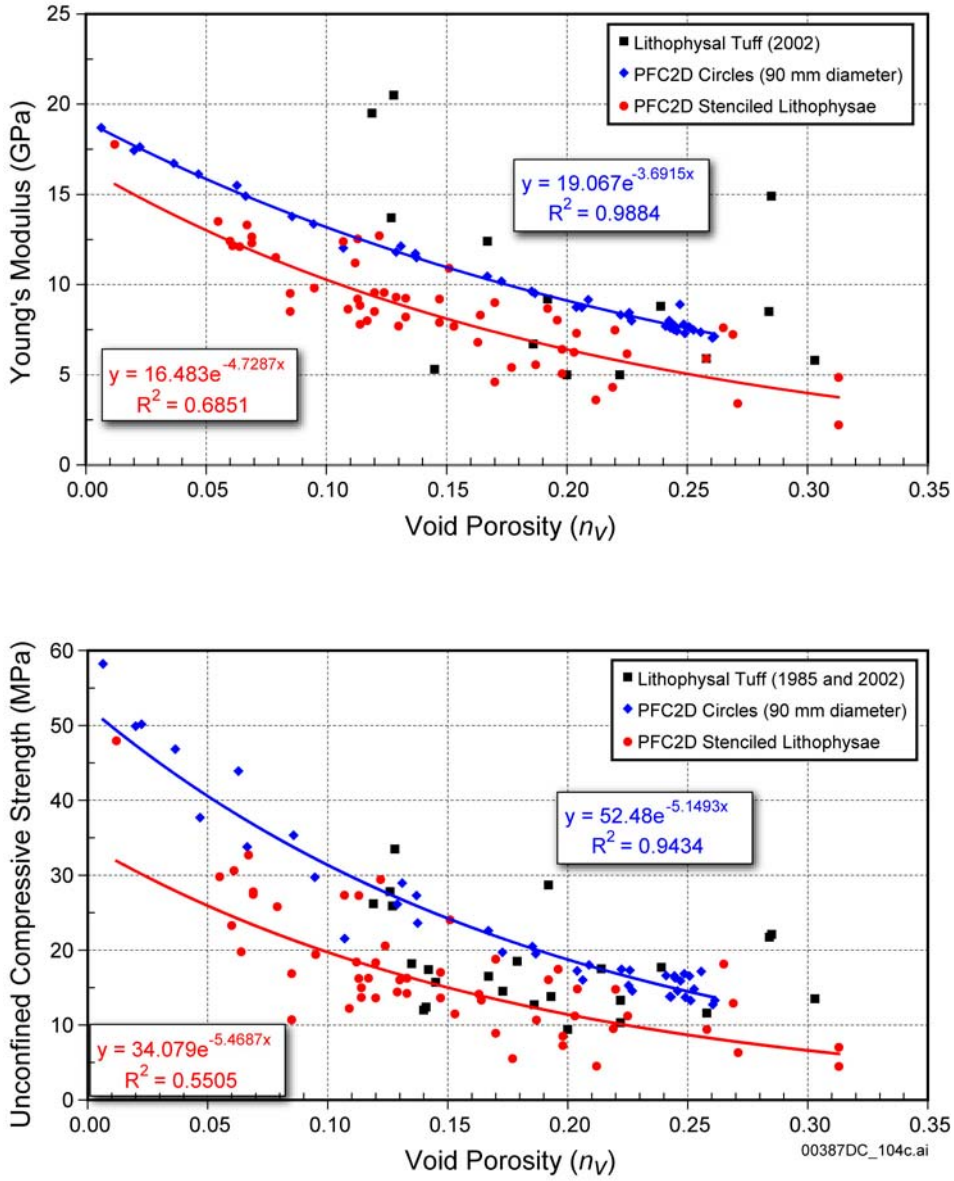

Source: BSC 2004a, Section 6.5.2, Figures 6.5-13 and 6.5-14.

NOTE: For a given porosity, there is a greater variability in the strength of the PFC samples when true lithophysae shapes are introduced. This effect is particularly significant at low porosities due to the greater variability of distribution and solid bridge lengths between lithophysae in a given sample volume.

Figure A-6. Plots Showing Data from Large Core (0.29 diameter) Compression Testing of Tptpul and Tptpll Compared to PFC Simulations Using Circular and Triangular Shaped Lithophysae as well as Actual Stenciled Shapes from Enhanced Characterization of the Repository Block Panel Maps

A.4.4 Extrapolation of Mechanical Response Using the PFC Program—Establishing Bounding Ranges for Rock-Mass Properties

The calibrated PFC and UDEC computational models are used as an extrapolation tool to examine the impact of lithophysae size, shape, porosity, and distribution on rock-mass

mechanical properties. Parametric studies have been conducted with simple (e.g., circular and triangular) shapes of lithophysae as well as actual, complex shapes and distributions digitized from ECRB Cross-Drift panel maps. The results of these studies (shown in Figure A-6) are used as a guide to understand the variability of mechanical properties for a given level of lithophysal porosity. Figure A-7 shows the large-core laboratory mechanical test data given in Figure A-4 plotted with the results of the PFC modeling studies assuming realistic lithophysae shapes and distributions from panel maps. As seen in this plot, approximate bounding estimates of the unconfined compressive strength and Young's Modulus have been drawn for the range of saturated and unsaturated laboratory data as well as the PFC panel map extrapolations of lithophysal shape and porosity variability. The linear fit to the 0.29 m core data, which is used as a base-case measure of the mechanical properties for room dry conditions, is shown as is the mean of the two bounding curves. The plots are dashed for those points that fall outside the range of the data. The laboratory data shows that the saturated environmental conditions form a lower bound to the property ranges and that the PFC extrapolations of shape variability fall within the bounding curves.

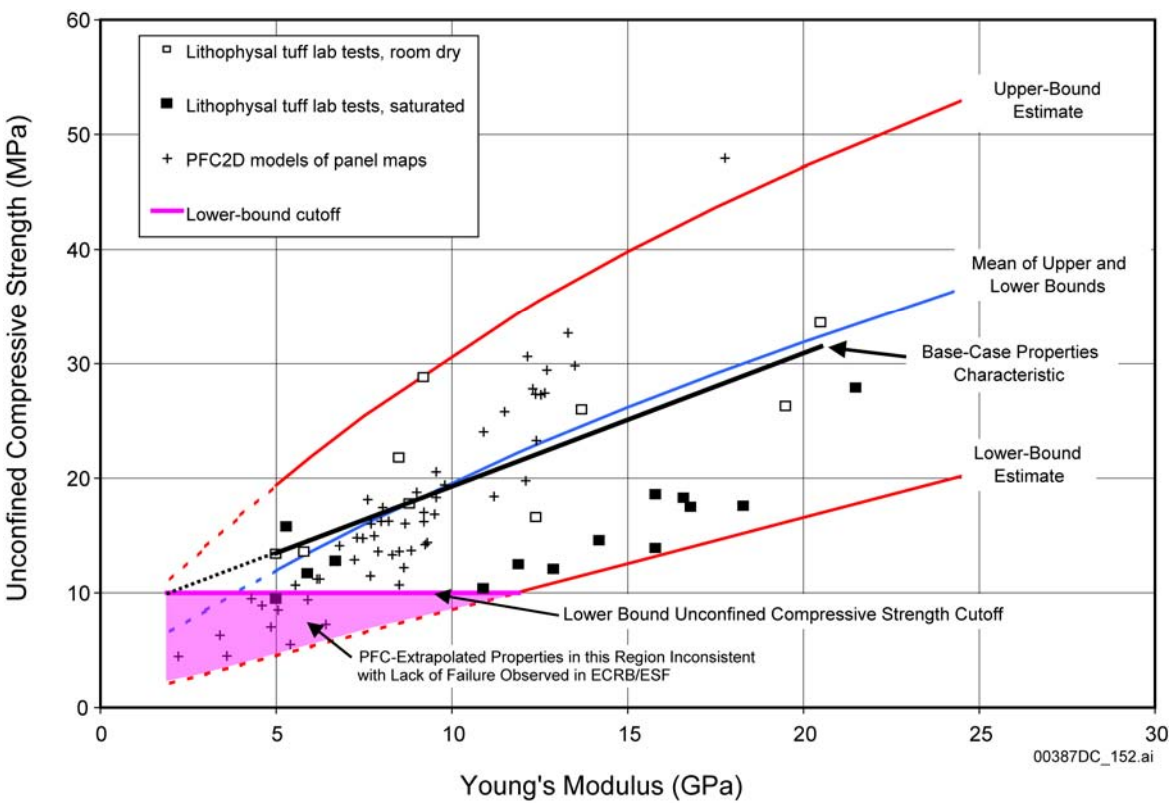

Source: BSC 2004a, Section 6.6.3, Figures 6.6-5 and 6.6-7.

NOTE: The bounding curves are empirically derived to include all large core laboratory data, including 0.267 m diameter saturated cores from Busted Butte. Characteristic base-case properties, derived from 0.29 m diameter cores, are also shown. Extrapolated (PFC) strength values below 10 MPa represent small samples with large lithophysae and inconsistent with observations of lack of yielding in ECRB and ESF.

Figure A-7. Estimated Upper and Lower Bounds of Unconfined Compressive Strength and Young's Modulus for Lithophysal Rock.

The PFC models estimate the impact of lithophysae shape and distribution on the strength of small (meter scale) samples of rock. When the lithophysae size is roughly proportional to the sample size (the case in some of the PFC panel map models), it is possible to produce strengths that are unrealistically low. This sample size effect can be seen in Figure A-7 in the shaded region in which no laboratory data are available, and only PFC-extrapolated values are seen. To test whether these lower strengths can actually occur in the field or are due to the extrapolation procedure, they were used as input to a number of drift-scale stability models of the ECRB subjected to in situ stress conditions. The results of these simulations, in terms of expected stability of the tunnel, were compared to field observations to assess if such low strength values are possible. The UDEC discontinuum program was run for the range of strengths shown in Figure A-7. It was found that unconfined compression strengths with values below about 10 MPa predict that significant sidewall spalling of the ECRB Cross-Drift and the ESF would be observed in the lithophysal rock. Significant sidewall spalling, as predicted by the model, would involve obvious shear failure of the tunnel springlines and breakout of the sidewall. On the contrary, these drifts are stable and in good structural condition despite the fact that only light bolting (none in the sidewalls of most of the drift) is used. Therefore, a lower-bound strength cutoff of 10 MPa, which coincides with the lowest strength properties measured from large core compression, is assumed.

A.4.5 Abstraction of the Thermal and Mechanical Constitutive Response into Numerical Predictive Models

Estimate of Rock Strength Categories for Bounding Property Range Analysis–The basic constitutive behavior defined by testing and PFC extrapolations must be abstracted into a design assessment tool capable of representing the lithophysal rock-mass response as well as allowing for modeling of the drift degradation process. To accomplish these objectives, a similar two-dimensional discontinuum approach is used and implemented in the UDEC program, which is similar to PFC but more efficiently examines large-scale mechanical problems. The process of implementation, calibration, and validation of this approach for representation of lithophysal rock is reviewed here and described in detail in *Drift Degradation Analysis* (BSC 2004b, Section 7).

A UDEC model is developed with a finely discretized block structure in which the block sizes are approximately equal to the spacing of the ubiquitous fracture fabric of the lithophysal rock mass (Figure A-8). The fracture fabric within the Tptpll was mapped in a series of small-scale fracture panel maps as discussed in *Drift Degradation Analysis* (BSC 2004b, Section 6.1.4.1). The 18 m of traverse shows multiple fracture sets with an average spacing of 0.05 m and an average trace length of 0.29 m. The blocks themselves are elastic but bonded at their contacts with a Mohr-Coulomb material capable of simulating shear and tensile failure. Thus, the overall response of the rock mass is that of an equivalent Mohr-Coulomb material but with the ability to fracture between blocks in shear or tension as the stresses dictate. This fracturing, along with gravitational or seismic accelerations, may cause detachment of rock fragments and rockfall.

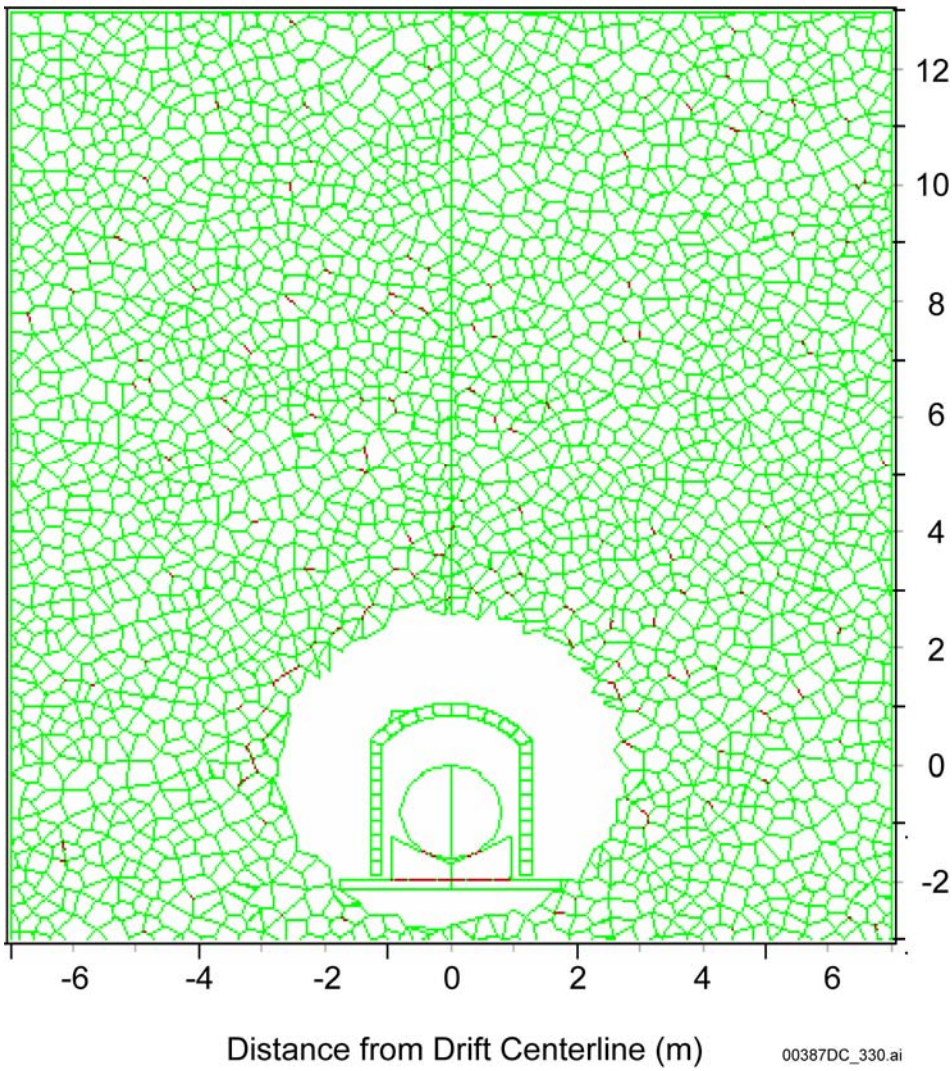

NOTE: Overall, the model behaves as an equivalent Mohr-Coulomb rock mass until fracture occurs between blocks, allowing detachment of rock fragments and rockfall.

Figure A-8. Discretization of the UDEC Discontinuum Model into Small and Irregular Blocks to Represent the Lithophysal Rock Mass

For the model to represent the lithophysal rock mass, it must be calibrated to reproduce the modulus and compressive strength ranges that have been determined from the laboratory testing and PFC extrapolations (see Figure A-7). The approach to modeling used here is to assume the rock-mass properties are constant and homogeneous for any given tunnel cross section. This assumption is justified for two reasons:

- The lithophysae are, in general, much smaller than the diameter of the tunnel and, thus, do not need to be modeled explicitly. Instead, the effect of the porosity is accounted for in the overall strength and modulus of the rock mass

- Although the rock mass porosity is variable for any given cross section, use of a bounding range approach assuming constant properties is conservative. This assumption was examined by representing spatial variability of lithophysal porosity (and the associated strength and modulus spatial variability) and is presented in Section 5.4.2.2.2.1 and discussed below. The results show that accounting for spatial variability produces rock mass strength and moduli that tend toward the mean of the lithophysal porosities within a given cross section. Thus, use of parametric analysis utilizing constant properties that encompass the range of material properties values will produce conservative estimates of degradation.

The impact of variability of the mechanical properties of the Tptpll on drift stability is accounted for by conducting parametric stability analyses that cover the entire range of probable rock-mass properties (i.e., from the highest porosity and lowest strength and modulus to the lowest porosity and highest strength and modulus). To accomplish this task, the strength and modulus range of the large-scale laboratory testing results is divided into five equally spaced categories (Figure A-9). By conducting numerical analyses over this range of data, the levels of rock quality and rock-mass response (from lowest to highest porosity ranges and size effects) can be covered.

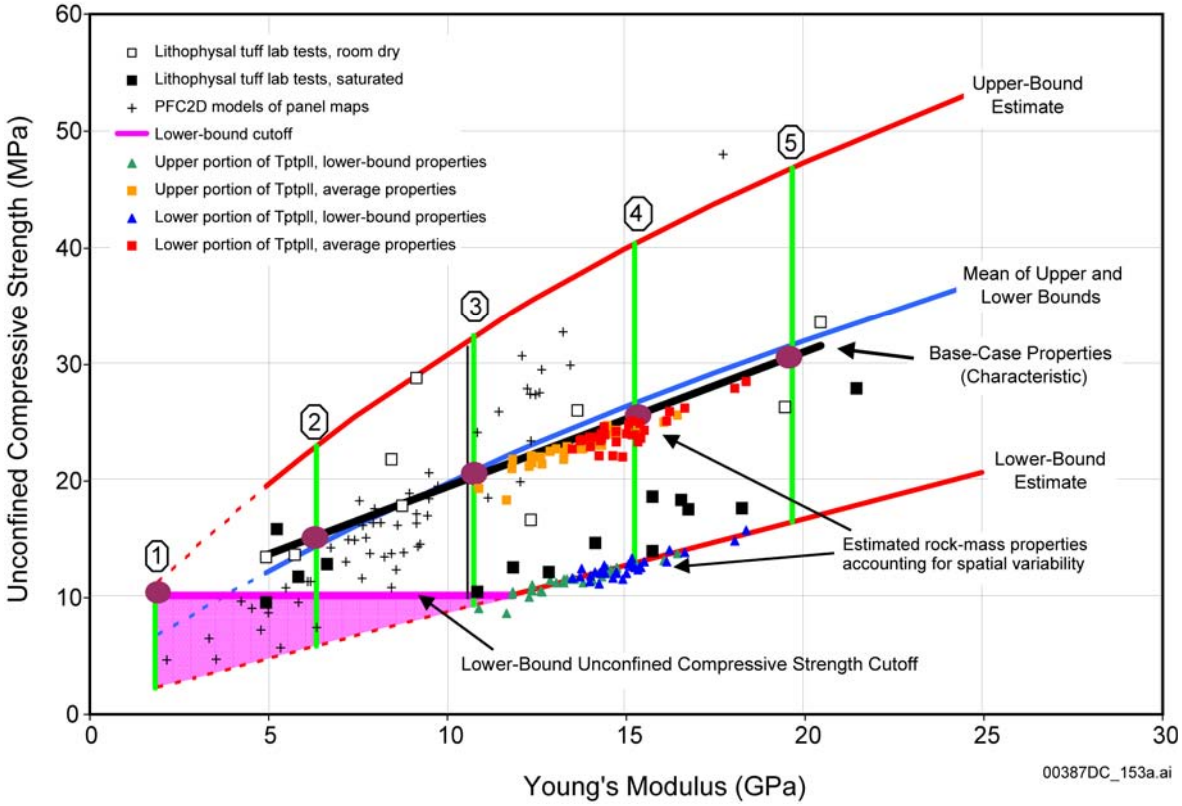

Source: BSC 2004a, Section 6.6.3, Figure 6.6-7.

NOTE: Base-case average properties defined for each category are the mean and the upper and lower bounds of each range. Category 1 is highest porosity, lowest quality rock and category 5 is lowest porosity, highest quality rock. Results of rock-mass strength estimates from spatial variability studies are shown assuming mean and lower bound properties.

Figure A-9. Lithophysal Rock Strength and Modulus Range Divided into Five Rock Strength Categories Covering the Large Core Laboratory Testing and PFC Extrapolation Lithophysal Shape Extrapolation Studies

The abundance of occurrence of these rock-mass categories in the Tptpll, and thus their importance from a stability standpoint, is demonstrated by the mapped lithophysal cavities shown in Figure A-2. The data in Figure A-9 are divided into five lithophysal porosity categories that roughly correspond to the five rock-mass strength categories shown in the same figure. Table A-1 presents an approximate relationship between lithophysal porosity abundance and strength categories.

Table A-1. Approximate Relationship of Rock Strength Category to Lithophysal Porosity Abundance in the Tptpll

Rock Strength Category	Approximate Lithophysal Porosity Range (%)	Abundance in Tptpll (%)
1	>25	3
2	20 to 25	7
3	15 to 20	26
4	10 to 15	34
5	<10	30

Source: BSC 2004a, Sections 6.6.1 and 6.6.2, Table 6.6-1.

Impact of Spatial Variability of Lithophysal Rock Properties–The approach described above assumes that the rock properties are constant for a given tunnel cross section. Field mapping shows that lithophysal porosity is not uniform and homogeneous but varies over a distance scale of perhaps a few meters (see Figure A-2). Therefore, in reality, the rock mass at the drift scale has spatially variable lithophysal porosity, and thus spatially variable mechanical properties. The question arises as to whether the use of ranges of constant properties in drift stability modeling is a conservative approach or whether there needs to be an explicit accounting for spatial variability in properties.

To investigate the impact of lithophysal spatial variability on mechanical properties ranges, the simple model of Tptpll lithophysal variability (see Figure A-3) was used as a basis for a numerical examination of its impact on rock-mass mechanical properties. Numerical compression experiments, similar to the PFC modeling studies, were conducted on 5×10 m rock-mass samples selected randomly from the Tptpll spatial variability model. The selected samples were of a drift scale to sample the range of lithophysal variability seen from the top to bottom of the Tptpll. Each sample was subdivided into meter-scale elements which were assigned (from the spatial variability model) a lithophysal porosity and, in turn, unconfined compression strength and Young's modulus obtained from the mean or lower bound values in Figure A-6.

Typical samples may have zones of lithophysal porosity ranging from less than 10% to greater than 20%. These spatially variable samples were then subjected to compression testing to define their mechanical properties. Two sets of tests were run using mean and lower bound properties assumptions (given in Figure A-7). The results of these experiments (see Figure A-9) show that the rock-mass compressive strength and moduli of spatially variable samples tends toward the mid-point of the properties ranges roughly corresponding to the mean porosity of the samples. The average rock strength condition tends toward an equivalent strength category of 3 to 4, which is also the most prevalent lithophysal porosity condition mapped underground. This illustrates, on a drift scale, the use of constant rock properties in models to represent that strength categories 1 and 2 are conservative and represent only localized regions of poor quality rock.

Calibration of the Drift Scale UDEC Discontinuum Model to Rock Strength Categories– The model calibration to the rock properties categories is accomplished by subjecting samples of the UDEC discontinuum model rock mass to uniaxial and triaxial compressive strength tests. During these tests, fitting of the Mohr-Coulomb strength parameters (cohesion and tensile

strength) and the fracture stiffness values is performed to achieve the measured modulus and compressive strength average and lower bound for each rock strength category (Figure A-10). As seen in Figure A-10, the calibration involved generation of stress-strain curves for the equivalent material. The calibrated UDEC discontinuum model was then validated by comparisons to the stability condition of the existing excavations. Field observations show good ground conditions (e.g., stable conditions and lack of tunnel deterioration over time even though minimal ground support is used) in the Tptpll or Tptpul. There are a small number of locations where minor springline surface fracturing can be observed in large diameter boreholes in the Tptpll in the ECRB Cross-Drift. Additionally, minor roof spalling was observed under thermal overdrive conditions in the Tptpmn heated drift test. Both of these observations, as well as comparisons to laboratory failure modes, were used as validation examples in *Drift Degradation Analysis* (BSC 2004b) and are reviewed in Section 4.2.7.2.

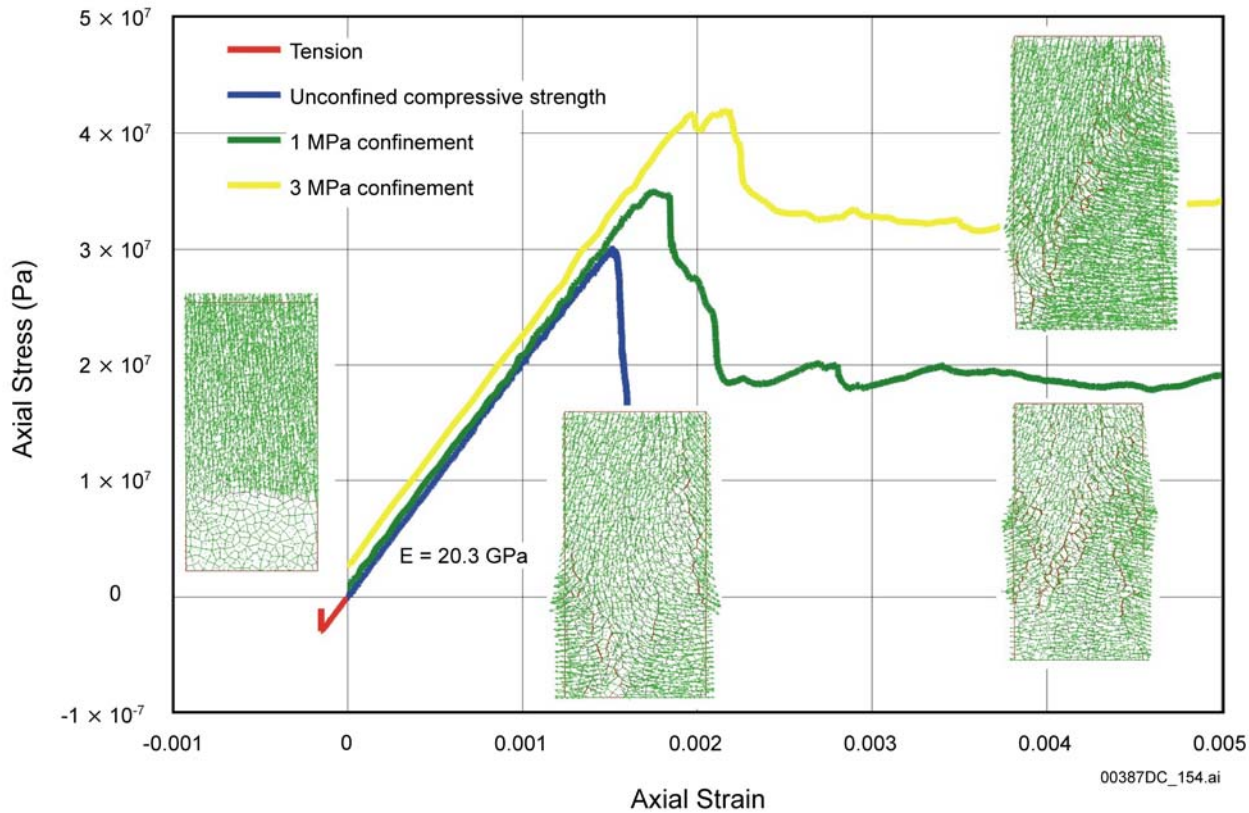

Source: DTN: MO0306MWDDDMIO.001.

NOTE: Model fracture stiffness, shear, and tensile strength calibrated to reproduce laboratory values of Young's Modulus and unconfined compressive strength. Samples show fracturing and failure modes in tension and unconfined and confined compression.

Figure A-10 Example of the Calibration of the UDEC Discontinuum Block Model to Laboratory Testing Results in Unconfined and Confined Compression and Tension, Strength Category 5

Consideration of Long Trace Length Fracturing in the Tptpll–The discussion heretofore has centered on the role of lithophysal porosity and the ubiquitous short-length fractures as the primary controllers of lithophysal rock-mass behavior. There are also longer trace length

fractures (length greater than 1 m) that are fairly widely spaced. *Drift Degradation Analysis* (BSC 2004b, Section 6.4) provides an analysis of potential failure modes involving these longer fractures. A simulated network of these fractures was developed using the FracMan program (USGS 1999) based on detail line survey mapping as described in this technical basis document. A series of 76 three-dimensional 3DEC models of these longer fractures in the Tptpll were analyzed to determine if any kinematically admissible wedges were possible. Even with the unrealistic use of zero cohesion and friction, there were no moveable wedges formed by these structures in the Tptpll. Therefore, the assumption that rock-mass strength controlled by lithophysal porosity and the ubiquitous, small scale fracturing is valid.

A.4.6 Conclusions

RDTME 3.05 deals with the strategy for developing a methodology to determine rock-mass mechanical properties and their variability for lithophysal rocks. It was determined that reliance on empirical rock-mass classification methods for estimating lithophysal rock properties was not appropriate at this time as insufficient excavation experience in this rock is available upon which to develop property correlations. The approach taken to establish lithophysal rock-mass properties and constitutive models was based on site-specific geological mapping, laboratory and field testing, and numerical model calibration. The testing and material property extrapolations accomplished utilizing numerical modeling as a tool were used to provide an estimate of the mean and range of rock-mass parameter values as a function of the lithophysal porosity. The porosity has been determined to be the primary factor in controlling the rock-mass mechanical properties, with significant impact on rock-mass strength and deformation modulus.

For parametric evaluation of rock-mass behavior, it is appropriate to subdivide the range of rock-mass porosities into a number of categories that allow direct relation of in situ geologic mapping to the associated rock-mass properties. Estimation of rock-mass properties at the drift scale and the impact of spatial variability of lithophysal porosity was performed based on geologic mapping and laboratory testing. Inclusion of spatial variability has shown that rock-mass properties tend toward the center of the range used in parametric stability calculations. This result is expected as the rock-mass properties tend toward that defined by the average lithophysal porosity. Thus, the use of parametric stability analysis based on constant rock-mass properties allows conservatism in the analyses to be assured. Numerical analysis of drift degradation under the influence of in situ, thermal, and seismic loading is accomplished by using a parametric approach for all rock-mass quality categories. This strategy and the results obtained are considered responsive to this KTI agreement.

A.5 REFERENCES

A.5.1 Documents Cited

Board, M. 2003. *Resolution Strategy for Geomechanically Related Repository Design and Thermal-Mechanical Effects (RDTME)*. REV 00. Las Vegas, Nevada: Bechtel SAIC Company. ACC: MOL.20030708.0153.

BSC (Bechtel SAIC Company) 2002a. *Software Code: PFC2D*. V2.0. PC WINDOWS 2000/NT 4.0. 10828-2.0-00.

BSC 2002b. *Software Code: PFC3D*. V.2.0. PC. 10830 2.0-00.

BSC 2002c. *Software Code: UDEC*. V3.1. PC WINDOWS 2000/NT 4.0. 10173-3.1-00.

BSC 2003a. *Scoping Analysis on Sensitivity and Uncertainty of Emplacement Drift Stability*. 800-KOC-TEG0-00600-000-000. Las Vegas, Nevada: Bechtel SAIC Company. ACC: ENG.20031125.0002.

BSC 2003b. *Subsurface Geotechnical Parameters Report*. 800-K0C-WIS0-00400-000-00A. Las Vegas, Nevada: Bechtel SAIC Company. ACC: ENG.20040108.0001.

BSC 2004a. *Lithophysal Rock Mass Mechanical Properties of the Repository Host Horizon*. 800-K0C-SS00-00200-000-00A. Las Vegas, Nevada: Bechtel SAIC Company. ACC: MOL.20040510.0200.

BSC 2004b. *Drift Degradation Analysis*. ANL-EBS-MD-000027 REV 03A. Las Vegas, NV: Bechtel SAIC Company. ACC: MOL.20040513.0081.

BSC 2004c. *Evaluation of Emplacement Drift Stability for KTI Resolutions*. 800-KMC-SSE0-00200-000-00A. Las Vegas, Nevada: Bechtel SAIC Company. ACC: MOL.20040510.0199.

NRC (U.S. Nuclear Regulatory Commission) 2002. *Integrated Issue Resolution Status Report*. NUREG-1762. Washington, D.C.: U.S. Nuclear Regulatory Commission, Office of Nuclear Material Safety and Safeguards. TIC: 253064.

Reamer, C.W. and Williams, D.R. 2001. Summary Highlights of NRC/DOE Technical Exchange and Management Meeting on Repository Design and Thermal-Mechanical Effects. Meeting held February 6-8, 2001, Las Vegas, Nevada. Washington, D.C.: U.S. Nuclear Regulatory Commission. ACC: MOL.20010307.0511 through MOL.20010307.0521.

USGS (U.S. Geological Survey) 1999. *Software Code: FracMAN*. V.2.511. PC Windows NT. 10114-2.511-00.

A.5.2 Data, Listed by Data Tracking Number

MO0306MWDDDMIO.001. Drift Degradation Model Inputs and Outputs. Submittal date: 06/19/2003.

INTENTIONALLY LEFT BLANK

APPENDIX B

SCOPING ANALYSIS OF INPUT DATA AND SENSITIVITY AND UNCERTAINTY ANALYSIS OF EMPLACEMENT DRIFT STABILITY (RESPONSE TO RDTME 3.06)

Note Regarding the Status of Supporting Technical Information

This document was prepared using the most current information available at the time of its development. This Technical Basis Document and its appendices providing Key Technical Issue Agreement responses that were prepared using preliminary or draft information reflect the status of the Yucca Mountain Project's scientific and design bases at the time of submittal. In some cases this involved the use of draft Analysis and Model Reports (AMRs) and other draft references whose contents may change with time. Information that evolves through subsequent revisions of the AMRs and other references will be reflected in the License Application (LA) as the approved analyses of record at the time of LA submittal. Consequently, the Project will not routinely update either this Technical Basis Document or its Key Technical Issue Agreement appendices to reflect changes in the supporting references prior to submittal of the LA.

APPENDIX B

SCOPING ANALYSIS OF INPUT DATA AND SENSITIVITY AND UNCERTAINTY ANALYSIS OF EMPLACEMENT DRIFT STABILITY (RESPONSE TO RDTME 3.06)

This appendix provides a response for Key Technical Issue (KTI) agreement Repository Design and Thermal-Mechanical Effects (RDTME) 3.06. This agreement relates to concerns regarding the design sensitivity and uncertainty of input parameters to preclosure drift stability.

B.1 KEY TECHNICAL ISSUE AGREEMENT

B.1.1 RDTME 3.06

Agreement RDTME 3.06 was reached during the U.S. Nuclear Regulatory Commission (NRC)/U.S. Department of Energy (DOE) Technical Exchange and Management Meeting on Repository and Design Thermal-Mechanical Effects held February 6–8, 2001, in Las Vegas, Nevada (Reamer and Williams 2001). There has been no submittal related to this KTI agreement to the NRC.

The wording of this agreement is as follows:

RDTME 3.06

> Provide the design sensitivity and uncertainty analyses of the rock support system. The DOE will prepare a scoping analysis to determine the significance of the input parameters for review by NRC staff by August 2002. Once an agreed set of significant parameters has been determined by the DOE and NRC staff, the DOE will prepare an analysis of the sensitivity and uncertainty of the preclosure rock support system to design parameters in a revision to Ground Control for Emplacement Drifts for SR, ANL-EBS-GE-000002 (or other document) supporting any potential license application. This is expected to be available to NRC in FY 2003.

The agreement focuses on a concern regarding the design sensitivity and uncertainty of input parameters to the stability of the drifts and the ground support system. The concern is further elaborated in the *Integrated Issue Resolution Status Report* (NRC 2002, Section 2.1.7). The NRC concerns are paraphrased as follows:

- Mechanical-property uncertainties were not discussed in the DOE analyses of ground-support performance for site recommendation (CRWMS M&O 2000). There are considerable uncertainties in all the mechanical properties needed for design analyses. The influence of such uncertainties on the assessment of the performance of the subsurface structures, systems, and components should be clearly identified, and the identification should be supported with adequate technical basis (NRC 2002, p. 2.1.7-21).

- Effect of lithophysae and fractures are not adequately accounted for in rock-mass properties estimates used in numerical models (NRC 2002, pp. 2.1.7-14 to 2.1.7-16).

- Other concerns on specific rock-mass properties including rock-mass Young's modulus (NRC 2002, p. 2.1.7-16), rock-mass strength (NRC 2002, p. 2.1.7-17), rock-mass thermal expansivity (NRC 2002, p. 2.1.7-18), rock-mass thermal properties (NRC 2002, p. 2.1.7-18), and spatial and temporal variation of mechanical properties (NRC 2002, p. 2.1.7-19).

B.1.2 Related Key Technical Issue Agreements

Agreement RDTME 3.05 (Appendix A) is related to RDTME 3.06. RDTME 3.05 addresses rock-mass mechanical properties of lithophysal rock. The rock-mass properties estimate, based on the approach described in resolution of RDTME 3.05 (Appendix A), is used for resolution of RDTME 3.06.

B.2 RELEVANCE TO REPOSITORY PERFORMANCE

The preclosure safety analysis demonstrates the safety of the proposed design and operations in the geologic repository operations area with regard to the overall preclosure performance objectives. The safety strategy for the preclosure operating period is to demonstrate that the ground control system is not required to prevent or mitigate credible rockfall. This demonstration relies upon analyses that show that the waste package does not breach when impacted by credible rock blocks. The safety analysis comprises a systematic examination of the site, design, potential hazards, initiating events and their resulting event sequences, and the potential radiological exposures to workers and the public (10 CFR 63.112).

The emplacement drifts are an array of horizontal tunnels trending at 72° azimuth. Each drift has a diameter of 5.5 m and will be separated from the adjacent drifts by a center-to-center distance of 81 m (BSC 2003a; Williams 2002). The emplacement drifts provide the subsurface access and openings for the structures, systems, and components used for emplacement and retrieval operations. The emplacement area host rock provides shielding for the rest of the underground facilities from radiation emanating from the waste packages.

The rock-mass surrounding the emplacement drifts will be subjected to loadings from in situ stress, thermal loading, and seismic ground motion. Both the design of the emplacement drifts and the surrounding rock mass are relevant for determining emplacement drift stability and repository performance.

B.3 RESPONSE

The response to RDTME 3.06 is based upon a series of parametric analyses prepared to assess the sensitivity and uncertainty of input parameters that govern drift stability and the performance of the ground support system. Although this document deals largely with postclosure drift degradation issues, the rock mass properties and numerical modeling approaches summarized here are also used to investigate preclosure drift stability and ground support performance issues. A description of the derivation of the basic tools used for resolution of RDTME 3.06 is given in

Sections 3.2 and 4.3. The use of continuum- and discontinuum-based numerical modeling approaches for analysis of lithophysal and nonlithophysal units is described in Section 4.2.2.2 and in Appendix D. The analyses summarized below are described in detail in *Scoping Analysis on Sensitivity and Uncertainty of Emplacement Drift Stability* (BSC 2003b).

The items summarized in this appendix for resolution of RDTME 3.06 include:

- Identification of input parameters
- Assessment of drift stability, considering the sensitivity and uncertainty of the following rock-mass mechanical properties and related parameters
  - The effect of lithophysae on the lithophysal rock-mass properties and the associated uncertainties
  - The effect of fractures on the nonlithophysal rock-mass properties and the associated uncertainties
  - Spatial variation of rock-mass mechanical properties
  - Consideration of the excavation-disturbed zone
  - Consideration of the range of rock strength within each rock category
- Conduct analysis to address the sensitivity and uncertainty of thermal modeling-related parameters to drift stability
  - Uncertainties associated with thermal properties
  - Off-normal thermal scenarios
  - Waste emplacement sequence and repository edge effect.

A summary of the scoping analysis in response to these items is provided below:

- Unsupported emplacement drifts are expected to be stable, with relatively small rock displacements and minor yield zones induced by excavation for drifts located in both lithophysal units and nonlithophysal units. Thermal and seismic loads during the preclosure period are small in comparison to the rock mass strength (see Section 5.3.2). With the exception of minor yielding in the immediate periphery of emplacement drifts for the poorest lithophysal rock mass strength category, elastic rock mass response is predicted for the in situ, thermal, and seismic loading stresses. The resulting safety factor against yield for unsupported emplacement drifts in the preclosure period is at least 2 (BSC 2003c, Section 6.1.3; BSC 2003b, Sections 6.1.1 and 6.1.2). An example of contours of a factor of safety is given in Figure B-1. The ground support system is, therefore, not required for overall drift stability; the main function of the ground support is to provide retainment of loose and detached rock particles around the periphery of the excavation.

- As discussed in Section 4.2, lithophysal rock mass models assume a range of homogeneous (constant) rock mass properties. In reality, the rock mass properties are variable, based on the variability of the lithophysal porosity. The suitability of the homogeneous property versus spatially variable property approach to drift stability assessment is examined. Assessment of the spatial variation of the rock mass properties in lithophysal rock is based on the simulated in situ lithophysal porosity variability, as discussed in Section 2.3.2. The overall rock mass response, assuming in situ variability of strength and modulus around the drifts, is predicted to be approximately equivalent to the response predicted assuming a constant, homogeneous rock mass characterized by the median rock mass quality for lithophysal rock (e.g., rock strength Category 3). This same conclusion was reached in regard to postclosure seismic damage assessment (Section 5.3.2.2.2.1). The conclusions from these analyses is that the results of homogeneous property parametric analyses for bounding rock properties ranges are reasonable and provide conservative results (BSC 2003b, Section 6.3.1).

- The analysis considers the effect of an excavation-disturbed zone. This disturbed zone is a thin zone of more heavily fractured rock around the excavation periphery due to mining or stress-induced yield. Rock mass mechanical properties to describe the disturbed zone are derived from in situ slot testing that was conducted in the Tptpll and Tptpul disturbed zone in the ESF (see Section B.4.1.4 of Appendix B and Section 3.2.2 of the technical basis document). The inclusion of this more fractured rock mass produces lower stress concentration at the wall and higher deformation around the opening, but the unsupported drift remains stable (BSC 2003b, Section 6.3.3.1). This conclusion is confirmed by observations in the ESF tunnel of stable 7.62-m-diameter tunnels in which walls are only occasionally supported with rock bolts.

- The effect of strength variation within a fixed strength category in the lithophysal rock is analyzed considering the bounding range of rock strength presented in Section A.4.5 in Appendix A. The results indicate that, even with the lower-bound strength, the emplacement drifts are predicted to be stable (BSC 2004a, Section 6.2).

- Sensitivity of rock mass strength parameters (cohesion and friction angle) for the nonlithophysal rock was assessed for estimated rock mass properties and the Hoek-Brown failure criterion (Section 4.3) (Hoek et al. 2002). The results show that the strength properties have little impact on the outcome of the analysis results (BSC 2003b, Section 6.3.4).

- Values of thermal conductivity and specific heat with one standard deviation more and less than the mean values are used as an upper bound and a lower bound while evaluating thermal property uncertainties. The peak temperature values at the drift crown are about ±5°C different from that of the base case due to the variation of thermal conductivity. An additional ±1.5°C is added to this peak temperature due to the heat capacity changes (BSC 2003b, Section 6.4.2).

- Off-normal thermal scenarios considered various ventilation shutdown durations at different preclosure times. The results demonstrated a rapid temperature increase of

14°C in the 1-week shutdown cases and less than 2°C increase in the 1-day shutdown case. The temperature jump diminished rapidly, with temperature returning to the temperature history unaffected by the shutdown, after the ventilation was restored. An extreme case with 1-month shutdown was also performed. This case shows a rapid temperature increase of 28°C and a relatively slow decrease of temperature after the ventilation was restored. Analysis of drift stability for a preclosure seismic event (10^{-4} annual exceedance frequency), combined with the off-normal thermal scenario, show negligible impact on stability (BSC 2003b, Section 6.4.3).

- Effects of the waste emplacement sequence were investigated using a two-drift NUFT preclosure calculation. The results of the emplacement sequence calculations exhibited minor temperature changes in the first and the second drifts from the base case NUFT calculation (BSC 2003b, Section 6.4.4).

The information in this report is responsive to agreement RDTME 3.06 made between the DOE and NRC. This report contains the information that DOE considers necessary for NRC review for closure of this agreement.

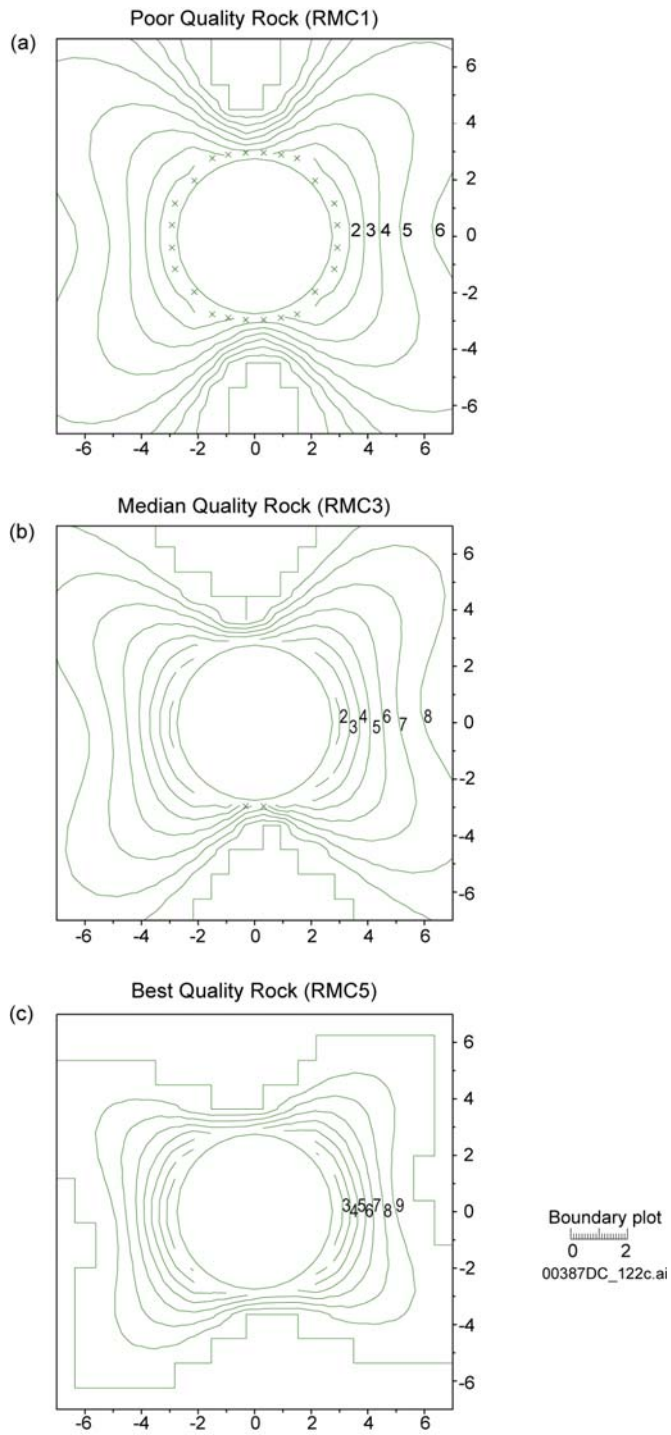

Source: BSC 2003b, Figure 6-11.

NOTE: Areas marked with an x in the figure exhibited yielding during the simulation process but equilibrated to an elastic state at the end of the simulation. RMC = rock mass category.

Figure B-1. Yield Zone and Safety Factor Contours after Seismic Shaking, Lithophysal Rock

B.4 BASIS FOR THE RESPONSE

A two-dimensional plane-strain thermal-mechanical parameter analysis is used to assess the stability of unsupported emplacement drifts. The two-dimensional finite-difference code FLAC (Itasca Consulting Group 2002) is used for the analysis. A combination of in situ, thermal, and seismic loadings is included in the analysis. The continuum-based analyses assume the rock mass conforms to a Mohr-Coulomb failure criteria, with property variations for lithophysal and nonlithophysal rock described in Sections 4.2 and 4.3, respectively (BSC 2003b, Section 6.1).

B.4.1 Analysis to Address the Sensitivity and Uncertainty of Rock-Mass Mechanical Property-Related Parameters to Drift Stability

A number of parametric studies are summarized in the following sections to highlight the sensitivity and uncertainty aspects. Detailed results of the analyses are presented in *Scoping Analysis on Sensitivity and Uncertainty of Emplacement Drift Stability* (BSC 2003b).

B.4.1.1 Effect of Lithophysae on Lithophysal Rock-Mass Properties and the Associated Uncertainties

The effect of lithophysae on lithophysal rock-mass mechanical properties (i.e., strength and modulus) has been addressed in the RDTME 3.05 resolution (Appendix A). A range of rock-mass mechanical properties has been estimated that represents the range of rock mass lithophysal porosity variability present in the Tptpll and Tptpul (e.g., Appendix A, Figure A-9). The sensitivity of the parameter ranges was investigated in the scoping analysis with consideration of in situ stress, preclosure thermal loading, and seismic ground motion (BSC 2003b, Section 6.1.1). Figure B-1 showed the yield zone and contours of safety factor against yield after seismic shaking with 5×10^{-4} ground motion for the best quality lithophysal rock (Category 5), the median quality lithophysal rock (Category 3), and the poorest quality lithophysal rock (Category 1). Minor yielding at the drift perimeter is observed for the poorest quality rock only. Stress paths[1] for locations around the opening surrounded by the median quality rock, as predicted during thermal loading and seismic shaking, are presented in Figures B-2 and B-3. It is evident that the stress states are well below the yield surface, and the stress-strain response is in the elastic (nonfailed) regime.

B.4.1.2 Effect of Fractures on Nonlithophysal Rock-Mass Properties and the Associated Uncertainties

The effect of fractures on nonlithophysal rock-mass properties has been included in this analysis based on the conventional approach for jointed rock medium by Hoek et al. (2002). A range of rock-mass mechanical properties has been estimated based on this conventional approach, which correlates the rock-mass mechanical properties to rock quality indices derived from field geotechnical characterization and laboratory testing. The sensitivity of the parameter range was investigated in the scoping analysis with consideration of in situ stress, preclosure thermal

[1] Stress path refers to a history of the principal stress at a point in the rock mass as it undergoes the transient loading and unloading associated with heating and cooling or seismic stressing. Plotting of the transient stress path on a standard plot of principal stresses with superimposed Mohr-Coulomb yield criteria (e.g., Figure B-2) allows easy identification of the location, timing, and extent of yield of the rock mass.

loading, and seismic ground motion (BSC 2003b, Sections 6.1.2 and 6.3.4). Stress paths for locations around the opening surrounded by median quality rock predicted during thermal loading and seismic shaking are presented in Figures B-4 and B-5. The yield criteria shown in these plots are based on a conservative estimate of Mohr-Coulomb strength parameters derived from a tangent to a nonlinear Hoek-Brown envelope at low (5 MPa) minor principal stress. This results in a very conservative estimate of the equivalent rock mass unconfined compressive strength (i.e., 21 MPa in Figures B-4 and B-5). The typical but less conservative approach to derivation of strength properties is to use a best-fit linear Mohr-Coulomb criteria to the near-linear portion of the Hoek-Brown envelope (see Hoek et al. 2002). In that case, the rock mass compressive strength for the median quality case is approximately 44 MPa (Section 4.3) (BSC 2003b), and the factor of safety against yield would be significantly larger than that implied by the stress paths in Figures B-4 and B-5. Even using the conservative estimate of rock mass strength properties, the stress states are well below the yield surface for all loading conditions, and the predicted stress-strain response is in the elastic (nonfailed) regime.

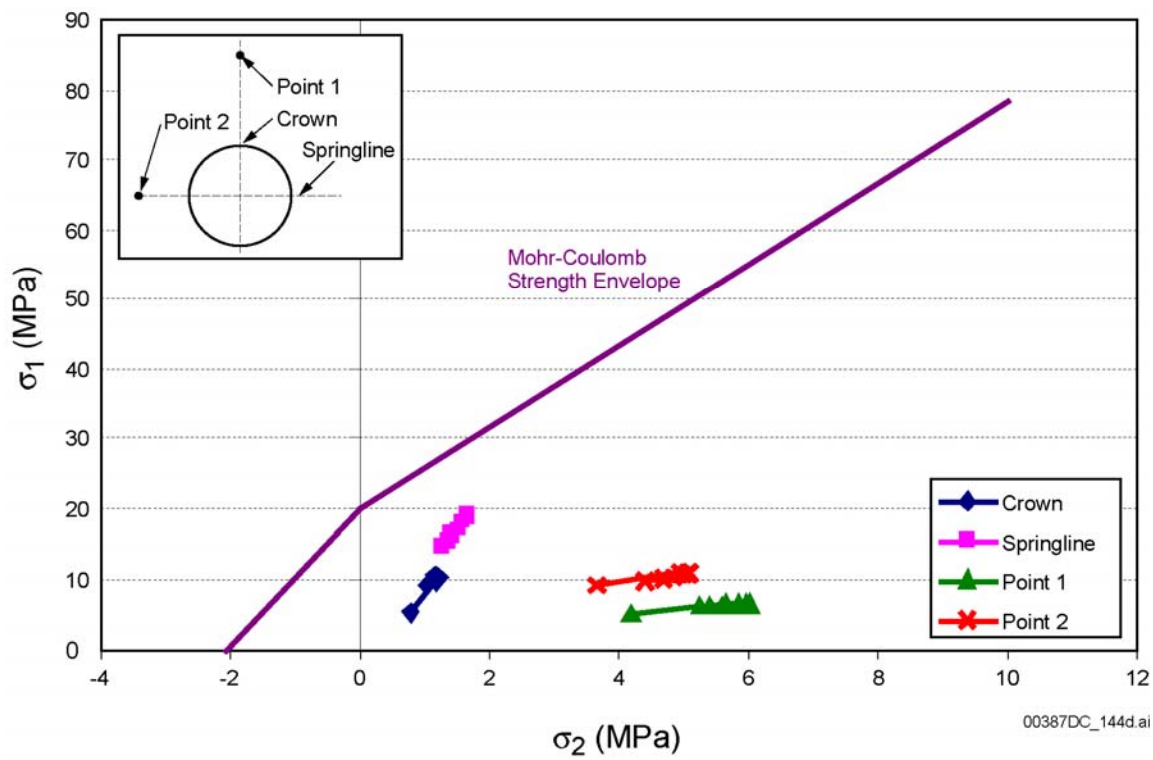

Source: BSC 2003b, Figure 6-5.

NOTE: Regions of plot beneath the strength envelope represent elastic (nonfailed) stress conditions.

Figure B-2. Stress Path for Selected Locations during Thermal Loading, Lithophysal Rock, Median Quality Rock (Compression as Positive)

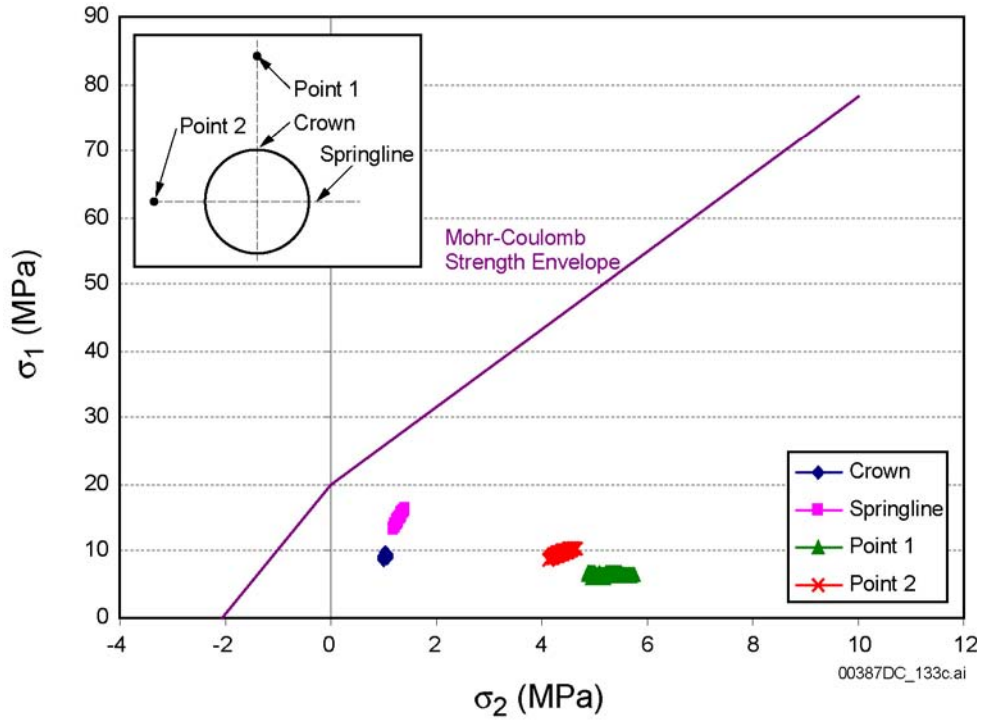

Source: BSC 2003b, Figure 6-12.

NOTE: Regions of plot beneath the strength envelope represent elastic (nonfailed) stress conditions.

Figure B-3. Stress Path for Selected Locations during Seismic Loading, Lithophysal Rock, Median Quality Rock (Compression as Positive)

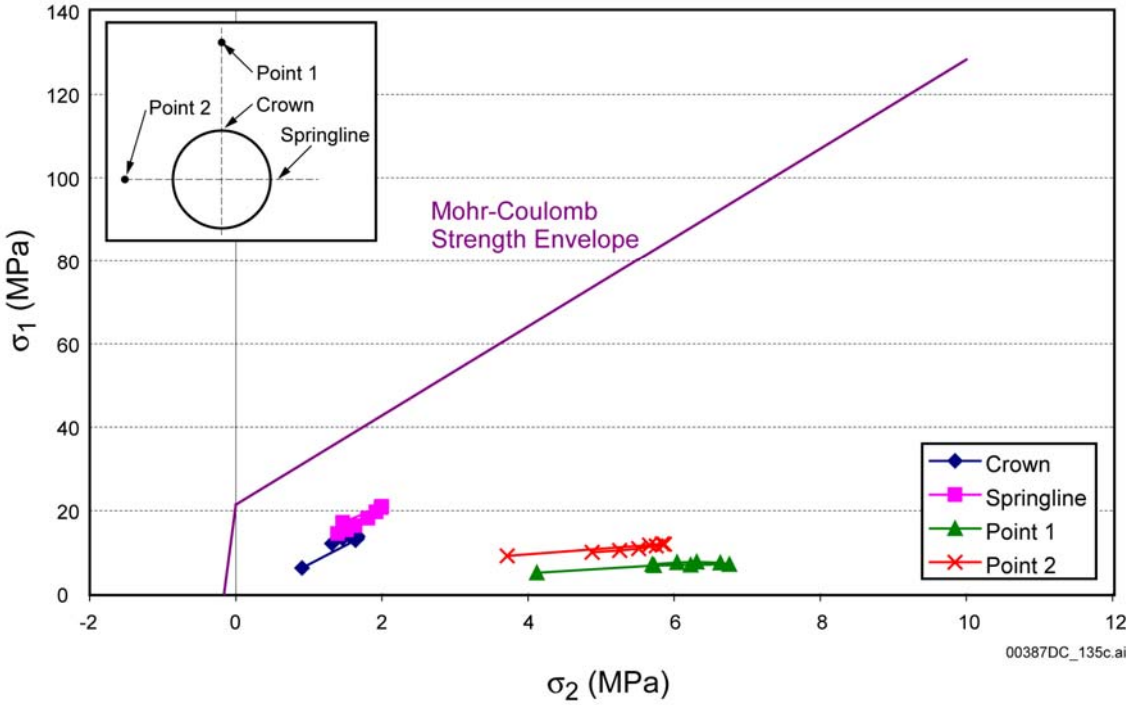

Source: BSC 2003b, Figure 6-18.

NOTE: Regions of plot beneath the strength envelope represent elastic (nonfailed) stress conditions.

Figure B-4. Stress Path for Selected Locations during Thermal Loading, Nonlithophysal Rock, Median Rock Quality (Compression as Positive)

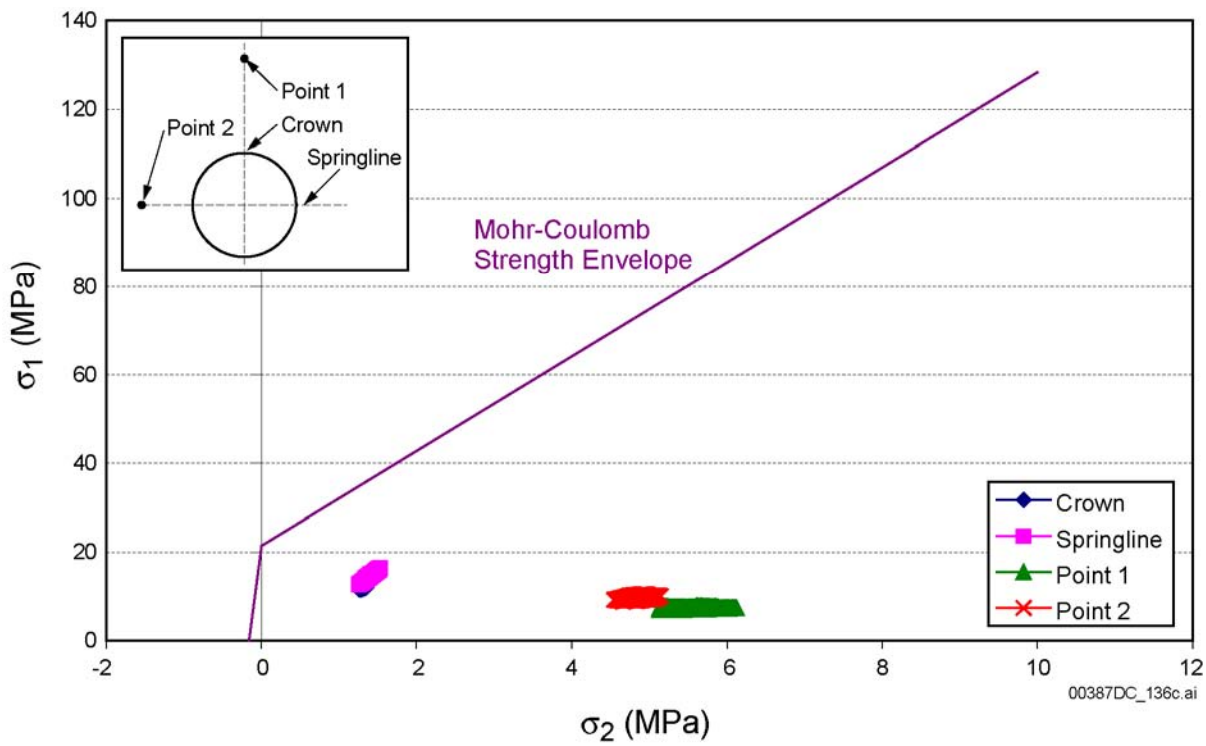

Source: BSC 2003b, Figure 6-21.

NOTE: Regions of plot beneath the strength envelope represent elastic (nonfailed) stress conditions.

Figure B-5. Stress Path for Selected Locations during Seismic Loading, Nonlithophysal Rock, Median Rock Quality (Compression as Positive)

B.4.1.3 Spatial Variation of Rock-Mass Mechanical Properties

Spatial variation of rock-mass mechanical properties is discussed in Sections 2.3.2 and 5.3.2.2.2.1 and is considered in the scoping analysis report (BSC 2003b, Section 6.3.1). The variation of lithophysal porosities within a model cross-sectional area is simulated based on mapped lithophysal porosity data and the assumption that the lithophysal porosity variation occurs in a stratiform layering that is conformal to the dip of units. A detailed description of the lithophysal porosity simulation is provided in the scoping analysis (BSC 2003b, Attachment I). The correlation between lithophysal porosity and the strength and modulus developed from large-scale laboratory testing and the PFC model extrapolations (e.g., Table A-1 and Figure A-9 of Appendix A) are used for estimating the corresponding variation of the strength and modulus in the analysis region. Figure B-6 shows the contours of rock mass cohesion (i.e., rock mass strength), illustrating the spatial variation of lithophysal porosity estimated from field panel mapping in the ECRB Cross-Drift. The magnitude of deformation and stresses predicted for the case with spatial parameter variation are approximately equivalent to similar predictions in which homogeneous, median rock quality category rock (Category 3) is assumed. Figure B-7 shows the comparison of the principal stress contours between the case with spatial variation and the case with Category 3 rock. The Category 3 rock is, therefore, considered to be a reasonable mechanical representation of the in situ rock considering spatial variation.

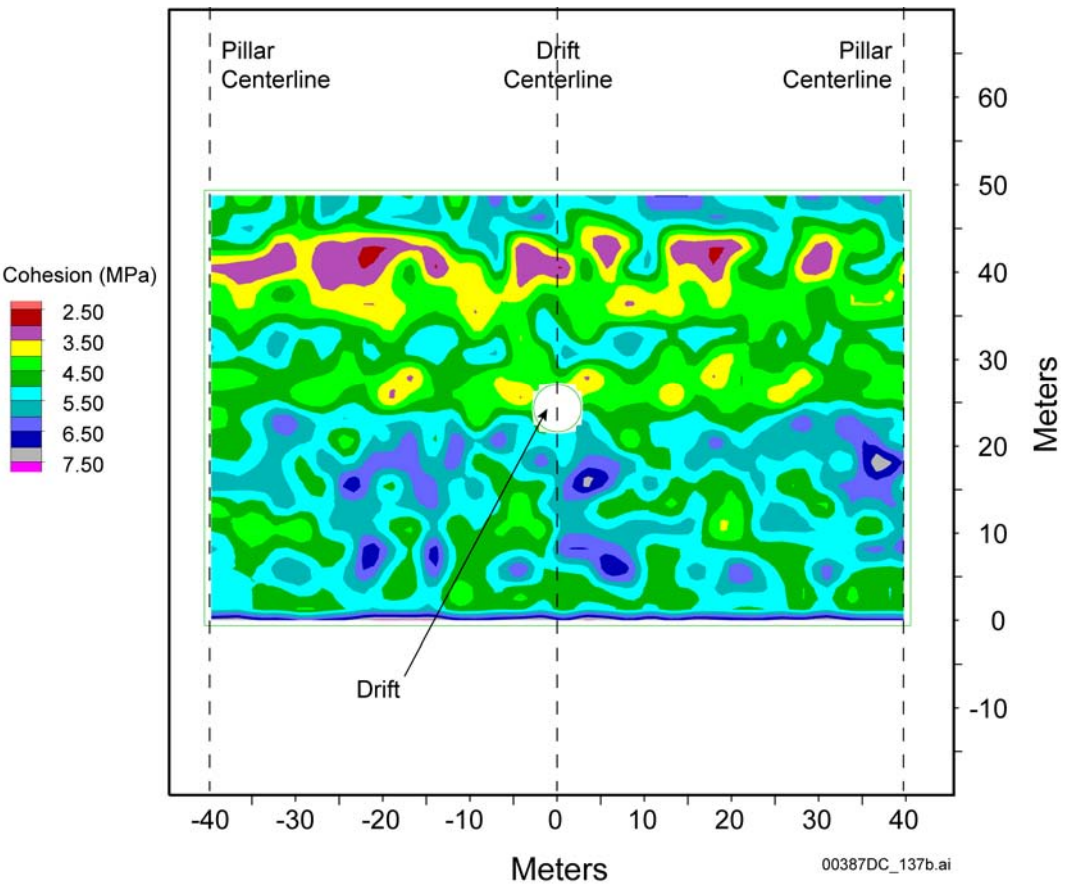

Source: BSC 2003b, Figure 6-46.

NOTE: Cohesion is proportional to rock mass shear strength, which is, in turn, a function of lithophysal porosity. Regions of high cohesion are indicative of low porosity.

Figure B-6. Contours of Rock Mass Cohesion (Shear Strength) in the Tptpll Surrounding an Emplacement Drift for a Representation of Spatial Variability of Lithophysal Porosity

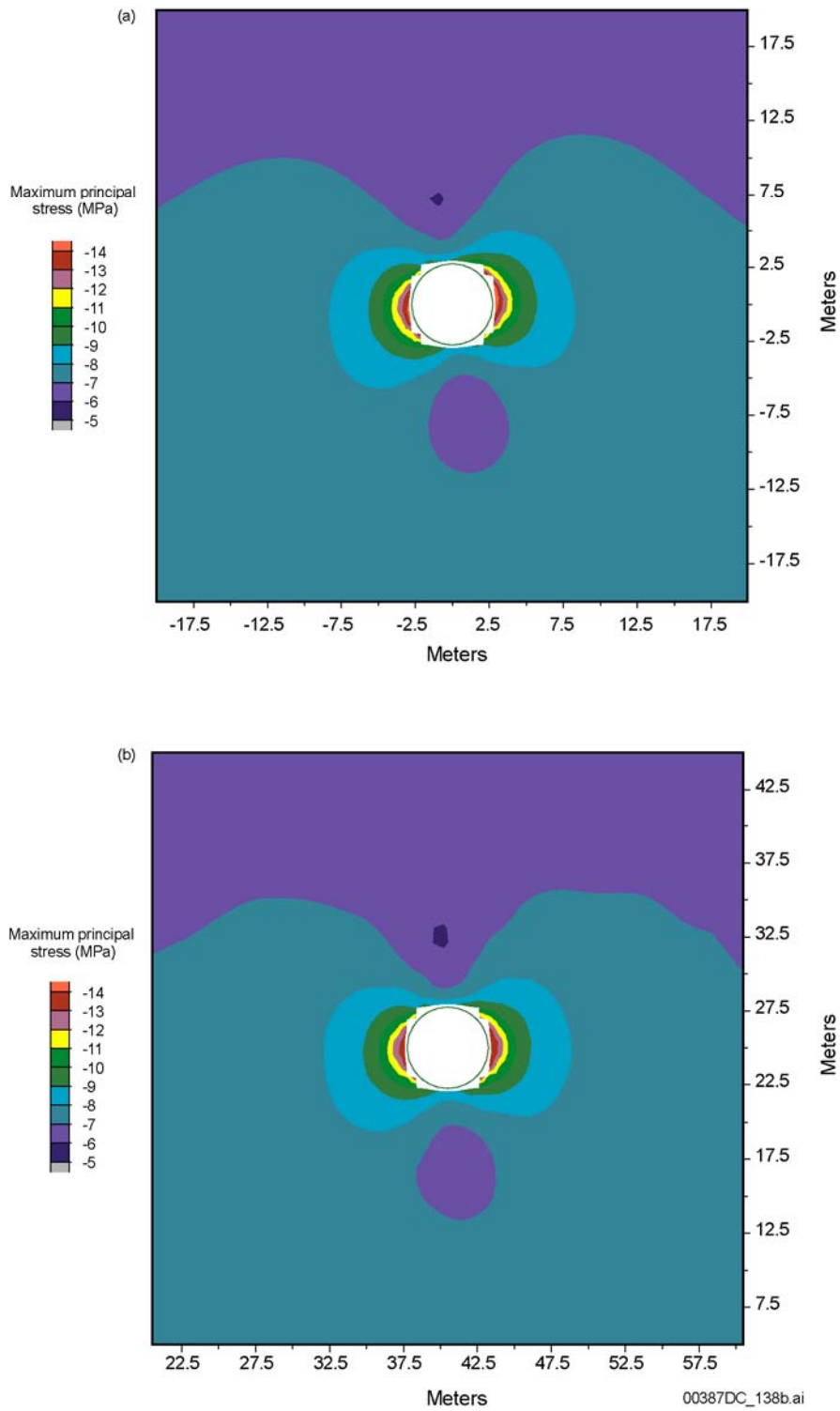

Source: BSC 2003b, Figure 6-51.

Figure B-7. Maximum Principal Stress Contours Comparison (a) with Assumption of Homogeneous Rock Mass, Category 3 Rock, and (b) with Representation of Rock Mass with Spatially-Variable Rock Properties

B.4.1.4 Consideration of Excavation-Disturbed Zone in Lithophysal Rock

An additional lithophysal rock strength category was created to account for the test results from the in situ slot tests, which were conducted in the disturbed zone at the ESF tunnel springline. It is believed that the low moduli and strength values measured near the tunnel wall are characteristic of the excavation-disturbed zone (BSC 2003b, Section 6.3.3.1). The low values, although conservative, are considered to be unrepresentative of the rock mass in the confined state away from the immediate tunnel periphery. A sensitivity analysis, including the effect of the excavation-disturbed zone represented by a 2-m ring of disturbed rock mass, was conducted. The modulus and strength results from the in situ slot tests (see Table 3-3 of the technical basis document) were used to represent the disturbed rock zone, while strength Category 1 rock was used to represent the surrounding rock mass in the model. The soft inclusion produces lower stress concentration and higher deformation. The maximum closure reaches 90 mm with consideration of excavation-disturbed zone compared to 55 mm of maximum closure for the case without the excavation-disturbed zone during thermal loading. Although the inclusion of the excavation-disturbed zone results in a larger yielding area and lower safety factor (BSC 2003b, Section 6.3.3.1), the unsupported opening remains stable.

B.4.1.5 Consideration of the Range of Rock Strength within a Fixed Category

The effect of strength variation within a fixed category in the lithophysal rock was analyzed considering the bounding range presented in Section A.4.5 and Figure A-9 in Appendix A (BSC 2004a, Section 6.2). The relationship of unconfined compressive strength to elastic modulus for lithophysal rock is reproduced in Figure B-8. Both the upper and lower bounds of rock mass categories 1, 3, and 5 have been considered. Load combinations include in situ stress, thermal loading, and seismic loading. Results indicate that the drift closures and stresses in rock adjacent to emplacement drifts are sensitive to the variation in rock mass strength. Coupled ground support analyses were also conducted. Increase of drift closures and axial forces in bolts is observed for the lower-bound cases, while increase of stresses was found for upper-bound cases. The emplacement drifts are predicted to be stable even with the lower-bound strength considered (BSC 2004a, Section 6.2).

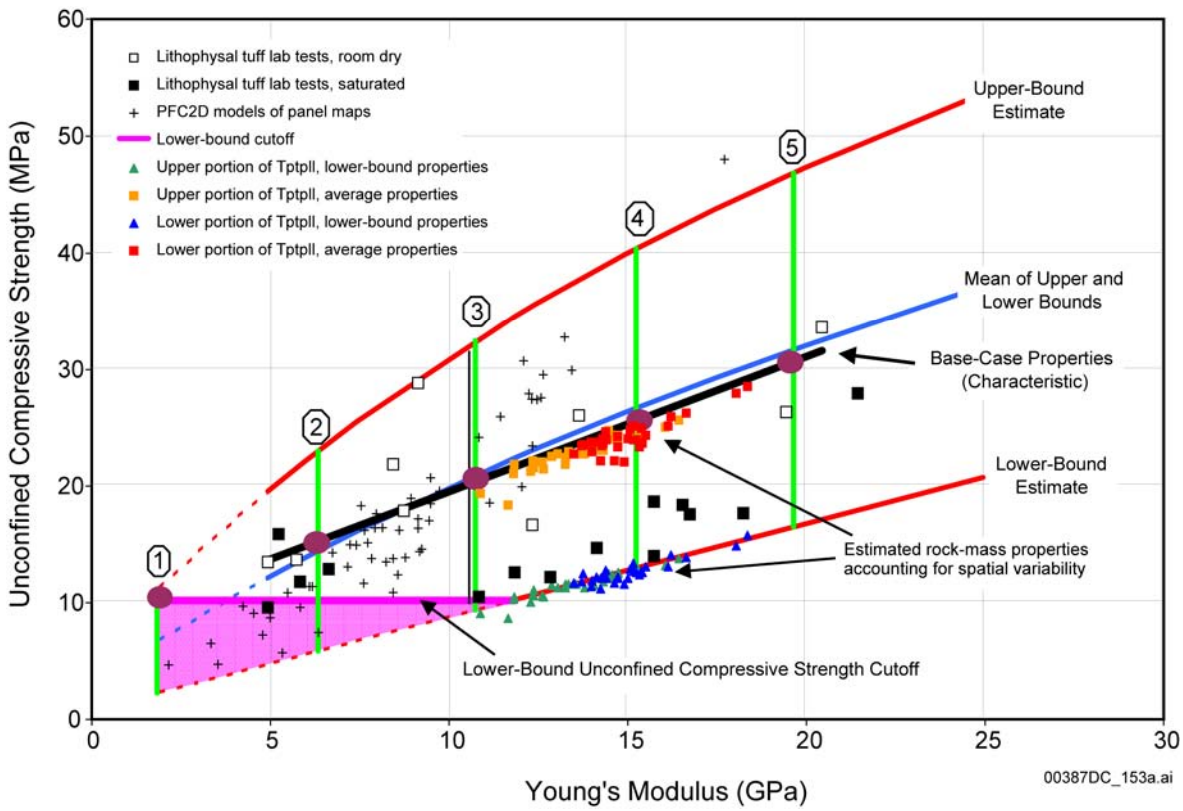

Source: BSC 2004b, Section 6.6.3, Figures 6.6-5 and 6.6-7.

NOTE: Base-case average properties defined for each category are the mean and the upper and lower bounds of each range. Category 1 is highest porosity, lowest quality rock and category 5 is lowest porosity, highest quality rock. Results of rock-mass strength estimates from spatial variability studies are also shown for mean and lower bound properties.

Figure B-8. Lithophysal Rock Strength and Modulus Range Divided into Five Rock Strength Categories Covering the Large Core Laboratory Testing and PFC Extrapolation Lithophysal Shape Studies

B.4.2 Analysis to Address the Sensitivity and Uncertainty of Thermal Modeling–Related Parameters to Drift Stability

B.4.2.1 Uncertainties Associated with Thermal Properties

Uncertainties in thermal properties, such as thermal conductivity, heat capacity, and the thermal expansion coefficient are evaluated by examining their effects on the performance of emplacement drifts (BSC 2003b, Sections 6.4.2 and 6.6.2). Values of thermal conductivity and specific heat with one standard deviation greater and less than the mean values are used as an upper bound and a lower bound for the thermal property uncertainties. Results of the thermal sensitivity calculations are presented in Figure B-9. The peak temperature values at the drift crown are about ±5°C different from that of the base case due to the variation of thermal conductivity. An additional ±1.5°C is added to the peak temperature due to the heat capacity changes.

In thermal-mechanical analyses with consideration of lower thermal conductivity and specific heat, the deformation and stress around the opening are shown to be very close to the normal thermal case. Similar results are also observed for cases with higher thermal expansion coefficient (BSC 2003b, Section 6.6.2).

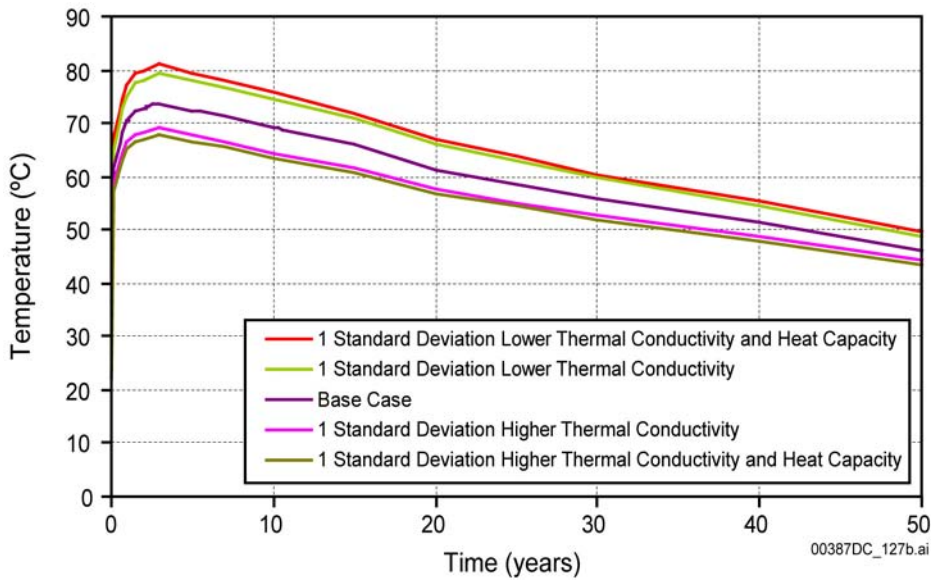

Source: BSC 2003b, Figure 6-88.

NOTE: Waste package loading = 1.45 kW/m (linear heat source), ventilation flow rate = 15 m^3/s.

Figure B-9. Temperature at the Drift Crown as a Function of Time after Emplacement, NUFT Preclosure Thermal Sensitivity Calculations

B.4.2.2 Uncertainties Associated with Off-Normal Thermal Scenarios

Off-normal thermal scenarios with various ventilation shutdown durations (i.e., 1 day, 1 week, and 1 month) occurring at various preclosure times (e.g., 2 years, 5 years, 10 years) are considered in the analysis (BSC 2003b, Sections 6.4.3 and 6.6.1). The NUFT preclosure calculations are conducted for the off-normal thermal scenarios. The results demonstrate a rapid temperature increase of 14°C in the 1-week shutdown case and less than 2°C increase in the one-day shutdown case (Figure B-10). The initially-rapid increase of temperature declined rapidly after the normal ventilation was resumed. A case with a 1-month shutdown was also performed. The result shows a rapid temperature increase of 28°C and a relatively slow decrease of temperature after the ventilation is resumed. The ventilation was assumed to be completely lost for 30 days in this case, which is judged to be conservative since backup fan capability and maintenance measures should ensure limited shutdown times. Additionally, natural air circulation due to the chimney effect induced by the heated air buoyancy effect and associated pressure gradient would occur naturally should the ventilation system be interrupted. In addition, loss of forced ventilation for as long as 30 days would also be very unlikely (BSC 2004c). Therefore, this case is not considered a typical scenario in the design.

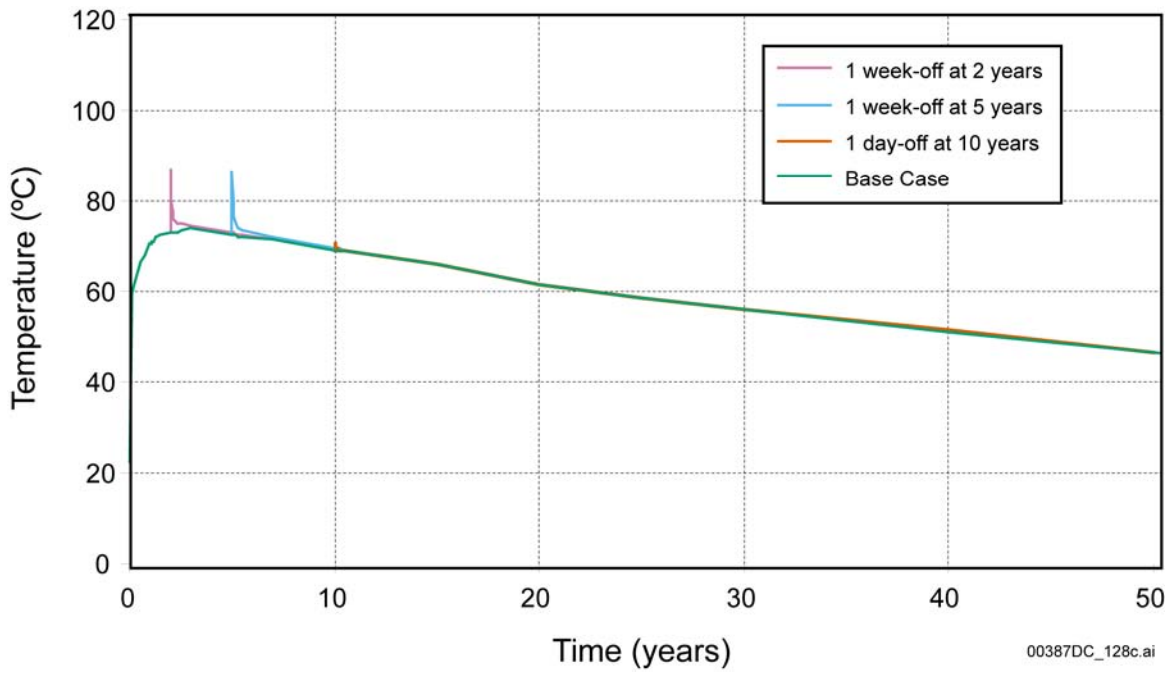

Source: BSC 2003b, Figure 6-89.

Figure B-10. Temperature at the Drift Crown for Base Case and Three Possible Off-Normal Scenarios

The off-normal thermal scenarios are used for thermal-mechanical analyses. Predicted drift closures and major principal stresses in rock near the springline and the crown are shown in Figure B-11, under the off-normal thermal scenario 1 and 2. Compared with those predicted under the normal thermal condition, differences in rock displacements and stresses are not significant, even though the drift wall temperatures are 16°C to 28°C higher under the off-normal situations than the normal condition. Predicted yield zones and contours of strength-to-stress ratios also show a minor difference from the normal thermal case.

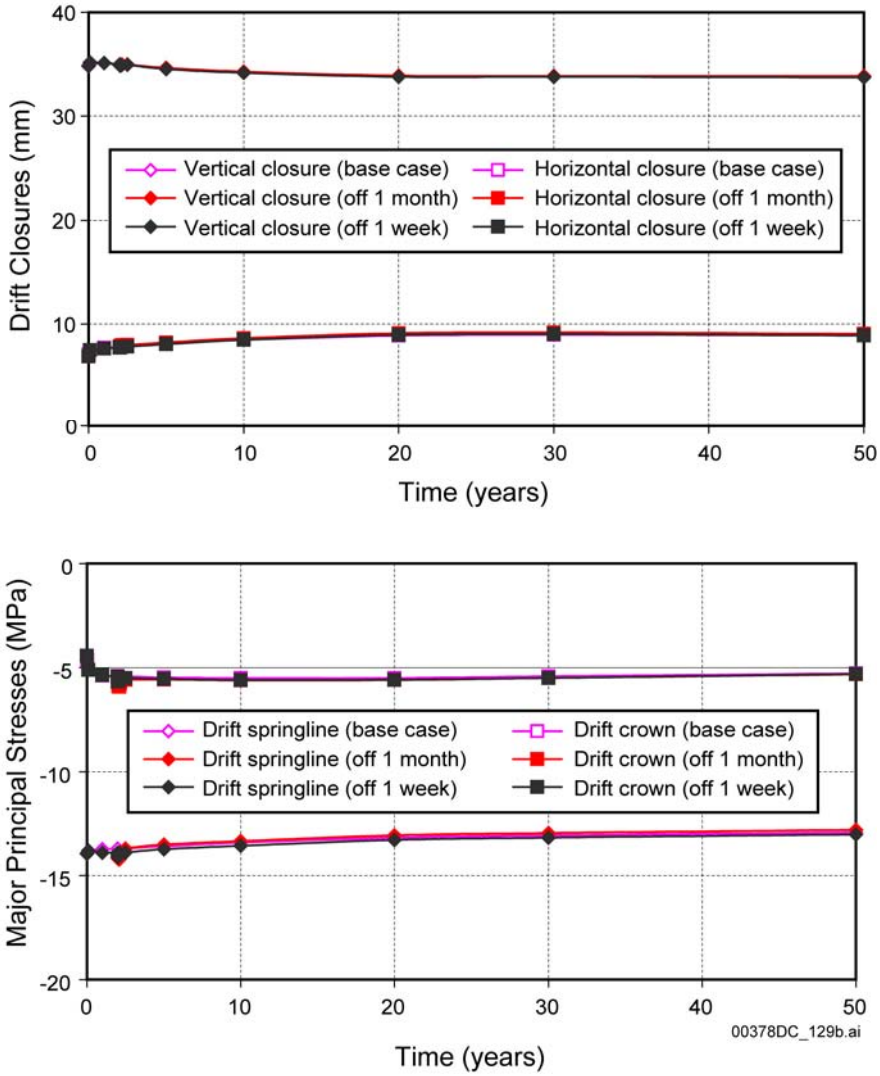

Source: BSC 2003b, Figure 6-143.

Figure B-11. Time Histories of Drift Closures and Major Principal Stresses in Rock under In Situ and Thermal Loads for Various Off-Normal Thermal Conditions

B.4.2.3 Uncertainties Associated with Waste Emplacement Sequence and Repository Edge Effect

Effects of the waste emplacement sequence, in terms of time intervals of emplacement, are investigated using a two-drift NUFT preclosure calculation (BSC 2003b, Sections 6.4.4 and 6.6.3). Several different emplacement time intervals were selected (e.g., 1 year, 5 years, and 10 years) to simulate the temperature distribution and gradient compared to the simultaneous emplacement calculation. In addition to the waste emplacement sequence calculation, repository edge effect is also investigated by placing no heat source in the second drift during the entire preclosure period. Temperatures at the drift crown for the effects for waste emplacement sequence and repository edge are presented in Figures B-12 and B-13. The results of the emplacement sequence calculations exhibited minor temperature changes in the first and the

second drifts from the normal thermal case with the temperature curves of the second drift shifted with delayed emplacement.

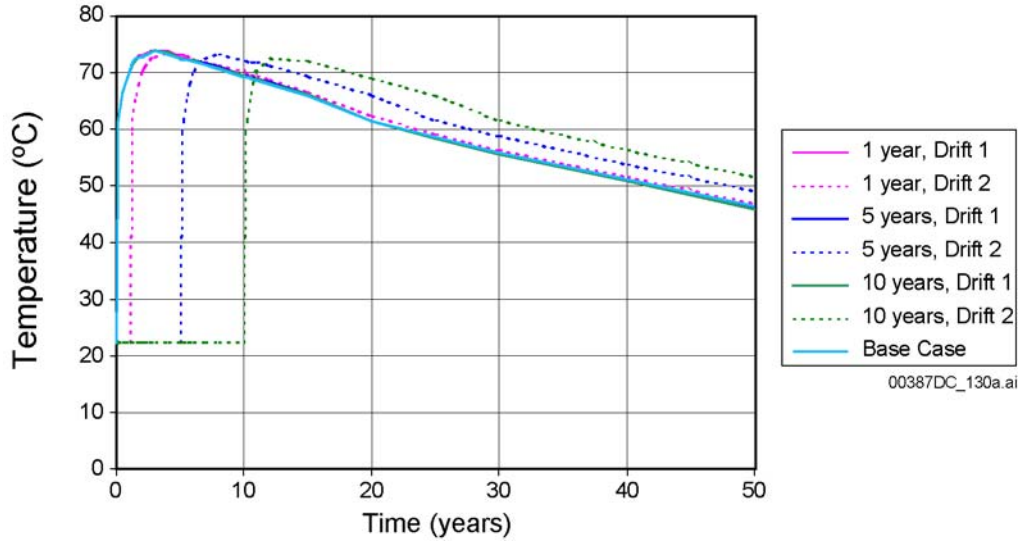

Source: BSC 2003b, Figure 6-93.

NOTE: Drift 1 curves are close to identical to base case.

Figure B-12. Temperatures at the Drift Crown Resulting from Effects of the Waste Emplacement Sequence

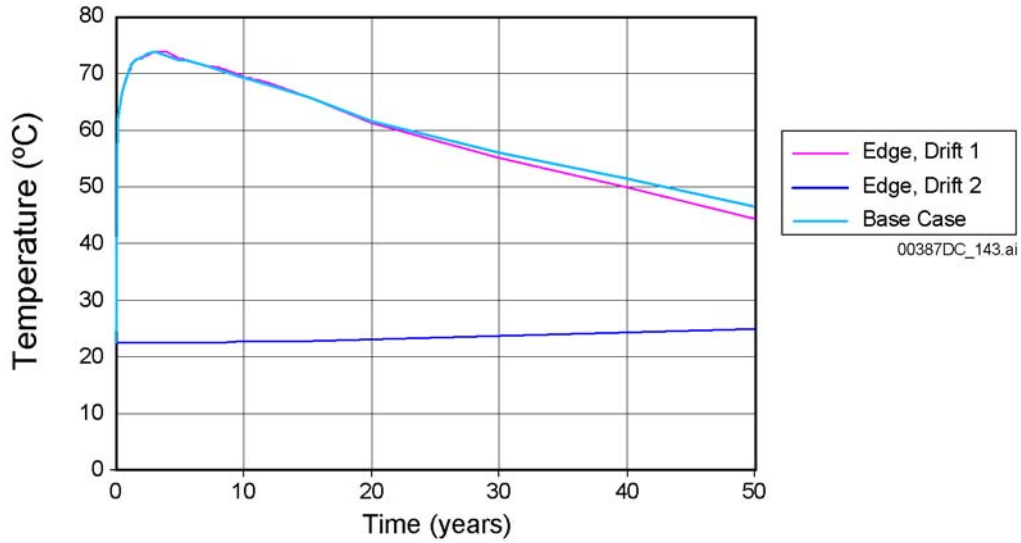

Source: BSC 2003b, Figure 6-94.

Figure B-13. Temperatures at the Drift Crown Resulting from the Effects of the Waste Repository Edge

A thermal-mechanical analysis, consisting of two drifts with 10 years delayed emplacement for the second drift, is used to investigate the impact of emplacement sequence and edge effect on drift stability. Time histories of predicted drift closures and major principal stresses in the rock near the springline and the crown of the second drift during heating for lithophysal rock strength

Category 5 rock are presented in Figure B-14. A sharp increase in stress and displacement at around 10 years is shown both at the crown and at the springline. The magnitude of the maximum stress or closure is slightly less than the magnitude of the maximum stress predicted for the drifts located in the center of a panel. The results for the springline left and right are similar, indicating that the edge effect is insignificant. There are no noticeable differences in the predicted yield zone and safety factor contours compared to the normal thermal case. These results indicate that the emplacement sequence and edge effect has an insignificant impact on drift stability.

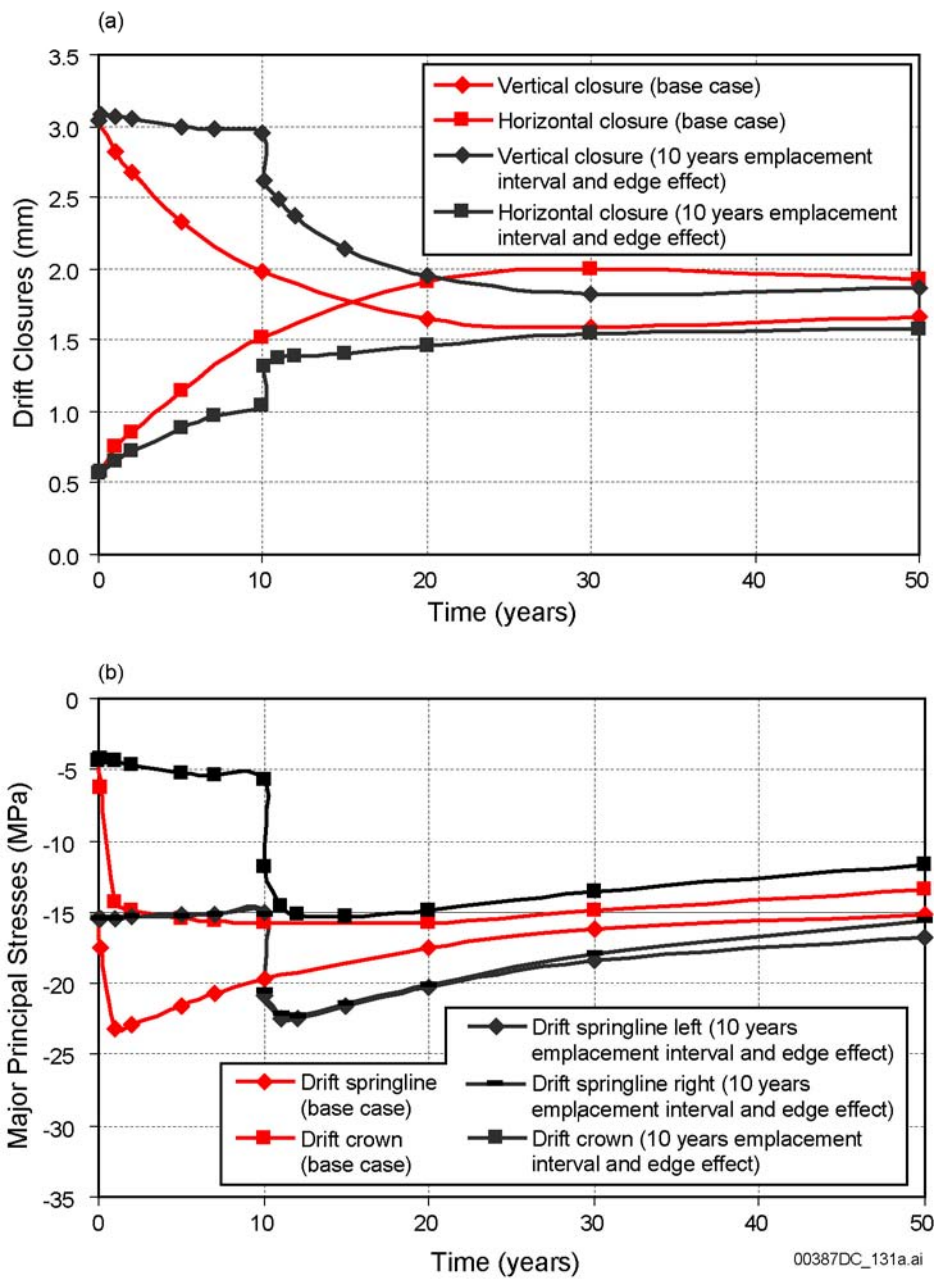

Source: BSC 2003b, Figure 6-152.

NOTE: Drift closure is the net inward displacement of the drift across a given diameter.

Figure B-14. Time Histories of Drift Closure and Major Principal Stresses in Rock under In Situ and Thermal Loads for the Second Drift with Consideration of Emplacement Sequence and Edge Effect, Rock Quality 5

B.4.2.4 Conclusions

In response to RDTME 3.06, a large parametric analysis of the impact of input rock mass properties and parameter assumptions on the prediction of unsupported emplacement drift stability in lithophysal and nonlithophysal rock units was performed. The sensitivity and

uncertainty of unsupported drift stability was examined using a continuum-based numerical modeling method for the bounding ranges of mechanical and thermal rock mass properties for critical preclosure loading conditions, including in situ, thermal, and seismic stresses. The results are summarized here and described in detail in *Scoping Analysis on Sensitivity and Uncertainty of Emplacement Drift Stability* (BSC 2003b). A summary of the conclusions from this study are given in Section B.4.3. The analyses indicate that emplacement drifts within both lithophysal and nonlithophysal units are stable in an unsupported mode for all parameter variations and loading conditions. It is concluded that the ground support is not required to maintain drift stability, but that its primary purpose is retention of potentially loosened material along the excavation periphery. These analyses are considered to be sufficient for resolution of RDTME 3.06.

B.5 REFERENCES

B.5.1 Documents Cited

BSC (Bechtel SAIC Company) 2003a. *Underground Layout Configuration*. 800-P0C-MGR0-00100-000-00E. Las Vegas, Nevada: Bechtel SAIC Company. ACC: ENG.20031002.0007.

BSC 2003b. *Scoping Analysis on Sensitivity and Uncertainty of Emplacement Drift Stability*. 800-K0C-TEG0-00600-000-000. Las Vegas, Nevada: Bechtel SAIC Company. ACC: ENG.20031125.0002.

BSC 2003c. *Ground Control for Emplacement Drifts for LA.* 800-K0C-TEG0-00100-000-00A. Las Vegas, Nevada: Bechtel SAIC Company. ACC: ENG.20031016.0001

BSC 2004a. *Evaluation of Emplacement Drift Stability for KTI Resolutions.* 800-KMC-SSE0-00200-000-00A. Las Vegas, Nevada: Bechtel SAIC Company. ACC: MOL.20040510.0199.

BSC 2004b. *Lithophysal Rock Mass Mechanical Properties of the Repository Host Horizon.* 800-K0C-SS00-00200-000-00Aa. Las Vegas, Nevada: Bechtel SAIC Company. ACC: MOL.20040510.0200.

BSC 2004c. *Subsurface Construction and Emplacement Ventilation*. 800-P0C-MGR0-00200-000-00B. Las Vegas, Nevada: Bechtel SAIC Company. ACC: ENG.20040304.0002.

CRWMS M&O (Civilian Radioactive Waste Management System Management & Operating Contractor) 2000. *Ground Control for Emplacement Drifts for SR.* ANL-EBS-GE-000002 REV 00. Las Vegas, Nevada: CRWMS M&O. ACC: MOL.20000414.0875.

Hoek, E.; Carranza-Torres, C.; and Corkum, B. 2002. "Hoek-Brown Failure Criterion – 2002 Edition." *5th North American Rock Mechanics Symposium and 17th Tunnelling Association of Canada Conference: NARMS-TAC 2002, July 7-10, University of Toronto.* Toronto, Ontario, Canada: Rocscience. Accessed March 17, 2003. TIC: 253954.

Itasca Consulting Group 2002. *Itasca Software–Cutting Edge Tools for Computational Mechanics*. Minneapolis, Minnesota: Itasca Consulting Group. TIC: 252592.

NRC (U.S. Nuclear Regulatory Commission) 2002. *Integrated Issue Resolution Status Report.* NUREG-1762. Washington, D.C.: U.S. Nuclear Regulatory Commission, Office of Nuclear Material Safety and Safeguards. TIC: 253064.

Reamer, C.W. and Williams, D.R. 2001. Summary Highlights of NRC/DOE Technical Exchange and Management Meeting on Repository Design and Thermal-Mechanical Effects. Meeting held February 6-8, 2001, Las Vegas, Nevada. Washington, D.C.: U.S. Nuclear Regulatory Commission. ACC: MOL.20010307.0511 through MOL.20010307.0521.

Williams, N.H. 2002. "Thermal Inputs for Evaluations Supporting TSPA-LA." Interoffice memorandum from N.H. Williams (BSC) to Distribution, September 16, 2002, 0911024159, with enclosures. ACC: MOL.20021008.0141.

B.5.2 Codes, Standards, and Regulations

10 CFR Part 63. Energy: Disposal of High-Level Radioactive Wastes in a Geologic Repository at Yucca Mountain, Nevada. Readily available.

INTENTIONALLY LEFT BLANK

APPENDIX C

ROCKFALL IN EMPLACEMENT DRIFTS
(RESPONSE TO RDTME 3.15, RDTME 3.16, RDTME 3.17, RDTME 3.19, AND GEN 1.01 (COMMENT 3))

Note Regarding the Status of Supporting Technical Information

This document was prepared using the most current information available at the time of its development. This Technical Basis Document and its appendices providing Key Technical Issue Agreement responses that were prepared using preliminary or draft information reflect the status of the Yucca Mountain Project's scientific and design bases at the time of submittal. In some cases this involved the use of draft Analysis and Model Reports (AMRs) and other draft references whose contents may change with time. Information that evolves through subsequent revisions of the AMRs and other references will be reflected in the License Application (LA) as the approved analyses of record at the time of LA submittal. Consequently, the Project will not routinely update either this Technical Basis Document or its Key Technical Issue Agreement appendices to reflect changes in the supporting references prior to submittal of the LA.

APPENDIX C

ROCKFALL IN EMPLACEMENT DRIFTS (RESPONSE TO RDTME 3.15, RDTME 3.16, RDTME 3.17, RDTME 3.19, AND GEN 1.01 (COMMENT 3))

This appendix provides a response for Key Technical Issue (KTI) agreements Repository Design and Thermal-Mechanical Effects (RDTME) 3.15, RDTME 3.16, RDTME 3.17, RDTME 3.19, and General Agreement (GEN) 1.01 (comment 3). The RDTME KTI agreements relate to providing the technical basis for the design, construction, and operation of the geologic repository operations area with respect to preclosure and postclosure performance objectives, taking into consideration long-term thermal-mechanical processes.

C.1 KEY TECHNICAL ISSUE AGREEMENTS

C.1.1 RDTME 3.15, RDTME 3.16, RDTME 3.17, RDTME 3.19, and GEN 1.01 (Comment 3)

Agreements RDTME 3.15, RDTME 3.16, RDTME 3.17, and RDTME 3.19 were reached during the U.S. Nuclear Regulatory Commission (NRC)/U.S. Department of Energy (DOE) Technical Exchange and Management Meeting on Repository and Design Thermal-Mechanical Effects held February 6 to 8, 2001, in Las Vegas, Nevada (Reamer and Williams 2001). There have been no submittals related to these KTI agreements to the NRC.

During the NRC/DOE Technical Exchange and Management Meeting on Thermal Operating Temperatures, held September 18 to 19, 2001, the NRC provided an additional comment related to RDTME 3.15, RDTME 3.16, RDTME 3.17, and RDTME 3.19 (Reamer and Gil 2001). This comment (GEN 1.01, comment 3) relates to the analysis of potential consequences of drift collapse. DOE provided an initial response to this comment at that meeting (Reamer and Gil 2001).

The wording of these agreements and of DOE's initial response to the general agreement comment is as follows:

RDTME 3.15

> Provide field data and analysis of rock bridges between rock joints that are treated as cohesion in DRKBA modeling together with a technical basis for how a reduction in cohesion adequately accounts for thermal effects. The DOE will provide clarification of the approach and technical basis for how reduction in cohesion adequately accounts for thermal effects, including any additional applicable supporting data and analyses. Additionally, the adequacy of the cohesion reduction approach will be verified according to the approach described in Subissue 3, Agreement 19, of the Repository Design and Thermal-Mechanical Effects Technical Exchange. This will be documented in a revision to the Drift Degradation Analysis, ANL-EBS-MD-000027, expected to be available to NRC in FY 2003.

RDTME 3.16

Provide a technical basis for the DOE position that the method used to model joint planes as circular discs does not under-represent the smaller trace-length fractures. The DOE will analyze the available small trace-length fracture data from the Exploratory Studies Facility and Enhanced Characterization of the Repository Block, including their effect on block development. This will be documented in a revision to the Drift Degradation Analysis, ANL-EBS-MD-000027, expected to be available to NRC in FY 2003.

RDTME 3.17

Provide the technical basis for effective maximum rock size including consideration of the effect of variation of the joint dip angle. The DOE will provide the technical basis for effective maximum rock size including consideration of the effect of variation of the joint dip angle. This will be documented in revisions to the Drift Degradation Analysis, ANL-EBS-MD-000027, and the Rockfall on Drip Shield, CAL-EBS-ME-000001, expected to be available to NRC in FY 2003.

RDTME 3.19

The acceptability of the process models that determine whether rockfall can be screened out from performance assessment abstractions needs to be substantiated by the DOE by doing the following: (1) provide revised DRKBA analyses using appropriate range of strength properties for rock joints from the Design Analysis Parameters Report, accounting for their long-term degradation; (2) provide an analysis of block sizes based on the full distribution of joint trace length data from the Fracture Geometry Analysis Report for the Stratigraphic Units of the Repository Host Horizon, including small joints trace lengths; (3) verify the results of the revised DRKBA analyses using: (a) appropriate boundary conditions for thermal and seismic loading; (b) critical fracture patterns from the DRKBA Monte Carlo simulations (at least two patterns for each rock unit); (c) thermal and mechanical properties for rock blocks and joints from the Design Analysis Parameters Report; (d) long-term degradation of rock block and joint strength parameters; and (e) site-specific ground motion time histories appropriate for postclosure period; provide a detailed documentation of the analyses results; and (4) in view of the uncertainties related to the rockfall analyses and the importance of the outcome of the analyses to the performance of the repository, evaluate the impacts of rockfall in performance assessment calculations. DOE believes that the Drift Degradation Analysis is consistent with current understanding of the Yucca Mountain site and the level of detail of the design to date. As understanding of the site and the design evolve, DOE will: (1) provide revised DRKBA analyses using appropriate range of strength properties for rock joints from a design parameters analysis report (or other document), accounting for their long-term degradation; (2) provide an analysis of block sizes based on the full distribution of joint trace length data from the Fracture Geometry Analysis

for the Stratigraphic Units of the Repository Host Horizon, ANL-EBS-GE-000006, supplemented by available small joint trace length data; (3) verify the results of the revised DRKBA analyses using: (a) appropriate boundary conditions for thermal and seismic loading; (b) critical fracture patterns from the DRKBA Monte Carlo simulations (at least two patterns for each rock unit); (c) thermal and mechanical properties for rock blocks and joints from a design parameters analysis report (or other document); (d) long-term degradation of joint strength parameters; and (e) site-specific ground motion time histories appropriate for postclosure period. This will be documented in a revision to the Drift Degradation Analysis, ANL-EBS-MD-000027, expected to be available to NRC in FY 2003. Based on the results of the analyses above and subsequent drip shield calculation revisions, DOE will reconsider the screening decision for inclusion or exclusion of rockfall in performance assessment analysis. Any changes to screening decisions will be documented in analyses prior to any potential license application.

GEN 1.01 (Comment 3)

None of the uncertainty and/or sensitivity analyses performed in the SSPA include the effects of drift collapse. Analyzing the potential consequences of drift collapse should be done to satisfy the basic TSPAI alternative conceptual model requirement.

DOE Initial Response to GEN 1.01 (Comment 3)

The SSPA rockfall sensitivity analyses (Sect. 6.3.4) were limited to examining the potential importance of three key uncertainties on rockfall. These uncertainties included 1) multiplier of fracture trace lengths, 2) Terzaghi correction factor, and 3) number of Monte Carlo simulations. These subsystem analyses did not substantially change the results of the rockfall model from that presented in the SR wherein we concluded rockfall did not significantly impact performance. As efforts were focused on other aspects of EBS performance, DOE did not perform system level SSPA Volume 2 calculations that included rockfall. DOE is continuing to do uncertainty analyses and examining an alternative model to improve the basis for screening rockfall from performance assessment abstractions per KTI agreements RDTME 3.15, RDTME 3.16, RDTME 3.17, and RDTME 3.19. If it is determined from these additional analyses that rockfall may significantly impact repository performance then, rockfall will be evaluated for abstraction into the TSPA calculations for any potential LA.

The foregoing statements focus on concerns regarding seismic, thermal, and time-dependent effects on rockfall and drift degradation. The effect on rockfall is further elaborated in *Integrated Issue Resolution Status Report* (NRC 2002, Section 3.3.2.4.4.1), where the NRC comments:

- The rationale for the DOE approach is that the additional shear stress induced on fracture surfaces from a temperature distribution (thermal loading) or earthquake

(seismic loading) and the weakening of fracture surfaces by time-dependent degradation can all be represented by the specified reduction of the cohesion and friction-angle parameters. DOE did not present a satisfactory mathematical basis to relate the cohesion reduction to the temperature distribution or the friction-angle reduction to the seismic loading to support an argument that the applied fracture-strength reductions appropriately represent the thermal and seismic loadings for the repository (NRC 2002, p. 3.3.2-29).

- The seismic data used for the drift degradation analysis were the design basis seismic ground motions for both Category 1 and 2 events. These seismic ground motion parameters are appropriate for preclosure-related design and analysis but are not proper for any postclosure considerations (NRC 2002, pp. 3.3.2-30 to 3.3.2-31).

C.1.2 Related Key Technical Issues

These RDTME agreements are related to:

CLST 2.02–This agreement requires rockfall loading estimates for the drip shield (postclosure) and waste package (preclosure) performance. RDTME KTI agreements 3.15, 3.16, 3.17, and 3.19 address the estimation of rockfall (mass, shape, and momentum) induced by in situ, thermal, and seismic loading as well as time-dependent strength changes. Section 5 summarizes the seismic rockfall analyses for lithophysal and nonlithophysal rocks.

CLST 2.08–This agreement requires estimation of rockfall for examination of drip shield and waste package performance. RDTME KTI agreements 3.15, 3.16, 3.17, and 3.19 address the estimation of rockfall (mass, shape, and momentum) induced by in situ, thermal, and seismic loading as well as time-dependent strength changes. Section 5 summarizes the seismic rockfall analyses for lithophysal and nonlithophysal rocks.

CLST 2.09–This agreement requires examination of the drip shield and waste package mechanical response under seismic excitation. RDTME KTI agreements 3.15, 3.16, 3.17, and 3.19 deal with the estimation of rockfall (mass, shape, and momentum) induced by in situ, thermal, and seismic loading as well as time-dependent strength changes. Section 5 summarizes the seismic rockfall analyses for lithophysal and nonlithophysal rocks.

RDTME 3.08–This agreement requires sensitivity analysis to establish design uncertainty for ground support design and drift degradation estimates with respect to the variability of the fracture system in the nonlithophysal and lithophysal rocks. RDTME KTI agreements 3.15, 3.16, 3.17, and 3.19 are linked to 3.08 primarily through determination of rockfall from in situ, thermal, and seismic loading as well as through long-term strength changes in the rock mass. This document addresses the methodology for analyzing the fracture patterns in Sections 4.1 and 4.2, and the postclosure drift degradation analyses in Section 5. Analysis of the variability of fracturing and its impact on ground support design is discussed in *Ground Control for Emplacement Drifts for LA* (BSC 2003).

SDS 2.04–This agreement requires a seismic risk assessment be conducted to provide the impact of site-specific ground motion on engineered barrier performance. This agreement is linked to the RDTME agreements in this appendix via the conduct of rockfall analyses. Section 5 summarizes the seismic rockfall analyses for lithophysal and nonlithophysal rocks.

TSPAI 2.02–RDTME 3.17 is linked to TSPAI 2.02, Items 62, 78, and 79. RDTME 3.19 is related to TSPAI 2.02, items 62, 78, and 79. TSPAI 2.02 Items 58 and 62 related to the inclusion of rockfall and its potential mechanical impacts on engineered barriers (Item 58) and on the thermal-mechanical impacts of long term rock mass degradation on engineered barriers and potential hydrological changes in the rock mass. RDTME 3.05 deals specifically with the estimation of rock mass properties of the lithophysal rocks of the Topopah Spring formation and the development of rock mass material and numerical models for representing fracture, rockfall, and long-term degradation under in situ, thermal, and seismic loading. The estimates made for rockfall and long-term degradation and change of opening shape feed performance assessment studies of the engineered barriers. (Refer to Section 1 for further details on this integration.)

C.2 RELEVANCE TO REPOSITORY PERFORMANCE

Over time, changes will occur to both the stress condition and the strength of the rock mass as a result of thermal stress, seismic ground motion, and time-dependent strength degradation of the rock mass. These effects may cause rock blocks to become detached or loosen from the rock mass surrounding the emplacement drifts and eventually fall into the drift as ground support functionality diminishes during postclosure. Potential rockfall is a concern that could affect waste package and drip shield performance. In the preclosure period, although the amount of rockfall could impact ventilation and waste package surface conditions, there are no credible rock blocks, with or without ground support, that can cause breach of an emplaced waste package. During preclosure, as rockfall occurs, the size and shape of the emplacement drift will change. Changes in local drift geometry could affect percolation of groundwater around the drifts and create the potential for water seepage into drifts. Substantial postclosure rockfall could also impact waste package temperature due to the insulating effect of coarse granular material surrounding the drip shield. The analyses of drift degradation and rockfall are relevant for determining emplacement drift stability and repository performance.

C.3 RESPONSE

Because RDTME 3.15, RDTME 3.16, RDTME 3.17, and RDTME 3.19 are related to rockfall in emplacement drifts, the response to each agreement is combined in this appendix. The approach to the analysis of seismic, thermal, and time-dependent effects on rockfall and drift degradation are summarized in this appendix. This information is further described in *Drift Degradation Analysis* (BSC 2004a) and summarized in Section 5. The drift degradation analysis includes the development and validation of rockfall models that approximate phenomena associated with various components of rock mass behavior anticipated within the repository horizon.

The subject KTI agreements request greater detail in the use of the DRKBA rockfall model keyblock approach to estimating rockfall. Since the time of writing of these agreements, the approach to estimating drift degradation has changed, as presented in March 2002 and documented by Board (2003) and reviewed in DOE/NRC Appendix 7 and Technical Exchange

(Stablein and Gil 2003) meetings. The current approach to rockfall analyses no longer relies on the DRKBA numerical code. The limitations associated with DRKBA have been addressed through the use of the distinct element codes UDEC (BSC 2002a), a two-dimensional discontinuum code, and 3DEC (BSC 2002b), a three-dimensional discontinuum code. These codes can explicitly apply both seismic and thermal loads (as discussed in Section 5.3.2), which satisfies the requirements of RDTME 3.15, RDTME 3.16, RDTME 3.17, and RDTME 3.19 for the following reasons:

First, the rock mass at the repository host horizon has been geologically characterized to support the rockfall modeling activities (see Section 2) and input requirements for UDEC and 3DEC. Drift degradation models have been developed for both nonlithophysal and lithophysal rock. A detailed description of the rock mass characteristics of the repository host horizon is provided in *Drift Degradation Analysis* (BSC 2004a, Section 6.1). The available rock mass geotechnical data, including fracture geometry (BSC 2004a, Sections 6.1.4.1, 6.1.6, and Appendix B), lithophysal abundance and geometric characteristics (BSC 2004a, Section 6.1.4.2 and Appendix O), and geotechnical rock properties (BSC 2004a, Section 6.1.3 and Appendix E) are sufficient to support drift degradation analyses using both continuum and discontinuum approaches.

Second, the drift-scale temperature history is calculated throughout the preclosure and postclosure periods of the repository (see Section 5.3.2) (BSC 2004a, Section 6.2). The temperature history is used to calculate the thermal stress state that develops within the rock mass due to the heat energy released from the stored high-level radioactive waste and appropriate boundary conditions for thermal loading have been applied (BSC 2004a, Sections 6.2, 6.3.1.3, 6.4.1.2, and Appendix W). Appropriate thermal properties have been used in the thermal-mechanical calculation (Section 3.2.5; BSC 2004a, Sections 4.1 and E5).

Third, small trace-length fracture data have been analyzed, including their effect on block development (BSC 2004a, Section 6.3.3). The DRKBA probabilistic key-block code was used to analyze stability of blocks under static conditions generated from the fracture database including fractures of trace length greater than 1 m and including the small trace-length fracture database for fractures less than 1 m. About 10% more blocks with significantly smaller maximum volume blocks are formed when small trace length fractures are included in the analysis (BSC 2004a, Table 6-31). It was concluded that ignoring the small length fractures results in conservative analyses as larger mass blocks with higher waste package and drip shield impact energy are formed.

Fourth, a nonlithophysal rockfall model was developed using 3DEC with the following features (see Sections 4.1 and 5.3.3):

- Appropriate boundary conditions are provided for in situ, thermal and seismic loading (BSC 2004a, Sections 6.3.1.2 and 6.3.1.3).

- Critical fracture patterns are included from multiple sampling from a synthetic rock mass volume that contains a realistic fracture population based on field mapping data (BSC 2004a, Section 6.1.6).

- Appropriate thermal and mechanical properties of rock blocks and joints are used (BSC 2004a, Appendix E).

- Long-term degradation of joint strength parameters is considered (BSC 2004a, Section 6.3.1.5).

- Site-specific ground motion time histories appropriate for both the preclosure (10^{-4} annual hazard level) and the postclosure (10^{-5}, 10^{-6}, and 10^{-7} annual hazard levels) time period are included in the model (BSC 2004a, Section 4.1.5). Since the drifts collapse for all cases under the 10^{-7} motions, explicit modeling of the 10^{-8} annual hazard level was unnecessary.

- The maximum rock size and shape is taken directly from the 3DEC output, which includes the variation in joint strike, dip, spacing, and persistence. The variation of joint geometry parameters is based on field mapping data from the ESF and ECRB, which have been input into the rockfall models.

Finally, a lithophysal rockfall model was developed using UDEC with the following features (Sections 4.2 and 5.3.3):

- Appropriate boundary conditions are provided for thermal and seismic loading (BSC 2004a, Sections 6.4.2.2 and 6.4.2.3).

- The rock mass is represented as an assembly of polygonal, elastic blocks in which the bond strength of the blocks is calibrated such that the overall mechanical behavior of the mass is consistent with the material model developed for the lithophysal rock (BSC 2004a, Section 7.7.4).

- The lithophysal rockfall model allows for the formation of stress-induced fractures between blocks (i.e., the formation of internal fracturing) and separation and instability (under the action of gravity or seismic shaking) of the rock mass around the drift (BSC 2004a, Section 6.4).

- Appropriate thermal and mechanical properties of rock blocks and joints are used (BSC 2004a, Appendix E).

- Long-term degradation of rock mass strength is considered (BSC 2004a, Section 6.4.2.4).

- Site-specific ground motion time histories appropriate for both the preclosure (10^{-4} annual hazard level) and the postclosure (10^{-6} annual hazard levels) time period are included in the model (BSC 2004a, Section 4.1.5). Since the 10^{-6} annual hazard level results in complete collapse of emplacement drifts in lithophysal rock, it was not necessary to analyze the 10^{-7} or 10^{-8} annual hazard levels.

The information in this report is responsive to agreements RDTME 3.15, RDTME 3.16, RDTME 3.17, RDTME 3.19, and GEN 1.01 (Comment 3) made between the DOE and NRC.

The report contains the information that DOE considers necessary for NRC review for closure of these agreements.

C.4 BASIS FOR THE RESPONSE

This section describes the strategy, technical basis, and approach for resolving the RDTME 3.15, 3.16, 3.17, and 3.19.

C.4.1 Overview of Resolution Strategy

As a general approach for resolving the geomechanical issues related to the RDTME KTIs and addressing the associated NRC and DOE agreements, a resolution strategy was outlined in *Resolution Strategy for Geomechanically-Related Repository Design and Thermal-Mechanical Effects (RDTME)* (Board 2003), as discussed in Section 6.1. This strategy, as it relates to rockfall analyses associated with RDTME 3.15, 3.16, 3.17, and 3.19, is illustrated in Figures C-1 and C-2 for nonlithophysal and lithophysal rocks, respectively.

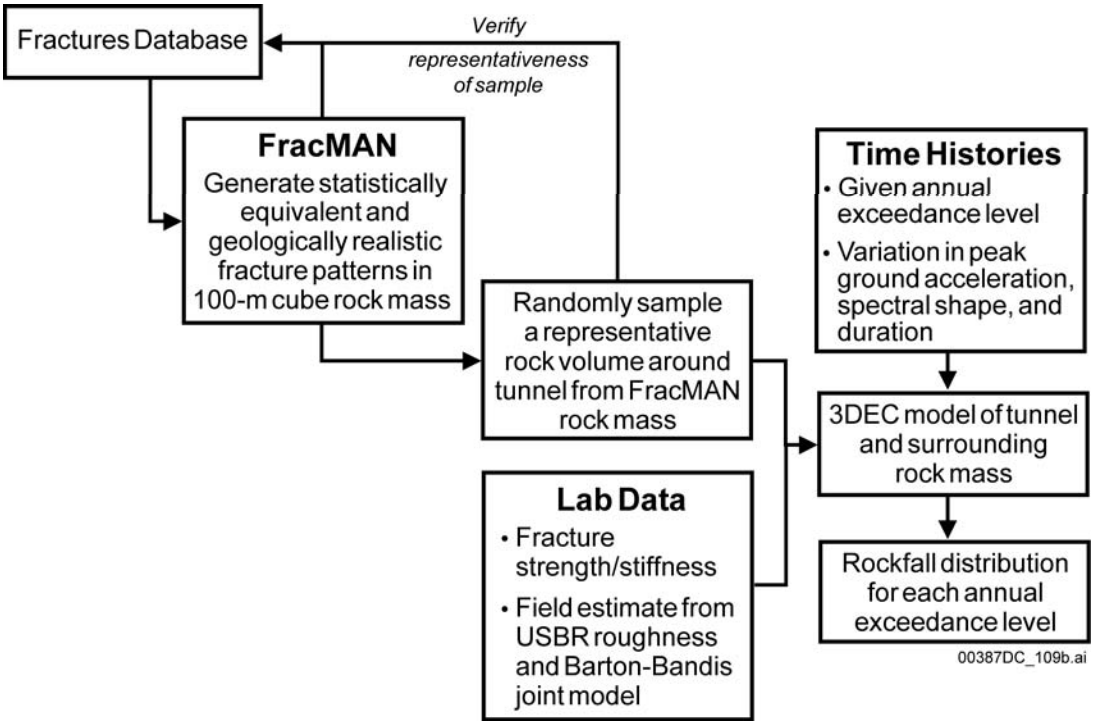

Source: Board 2003, Figure 32.

NOTE: USBR = U.S. Bureau of Reclamation.

Figure C-1. General Methodology for Rockfall Analyses in the Nonlithophysal Rocks

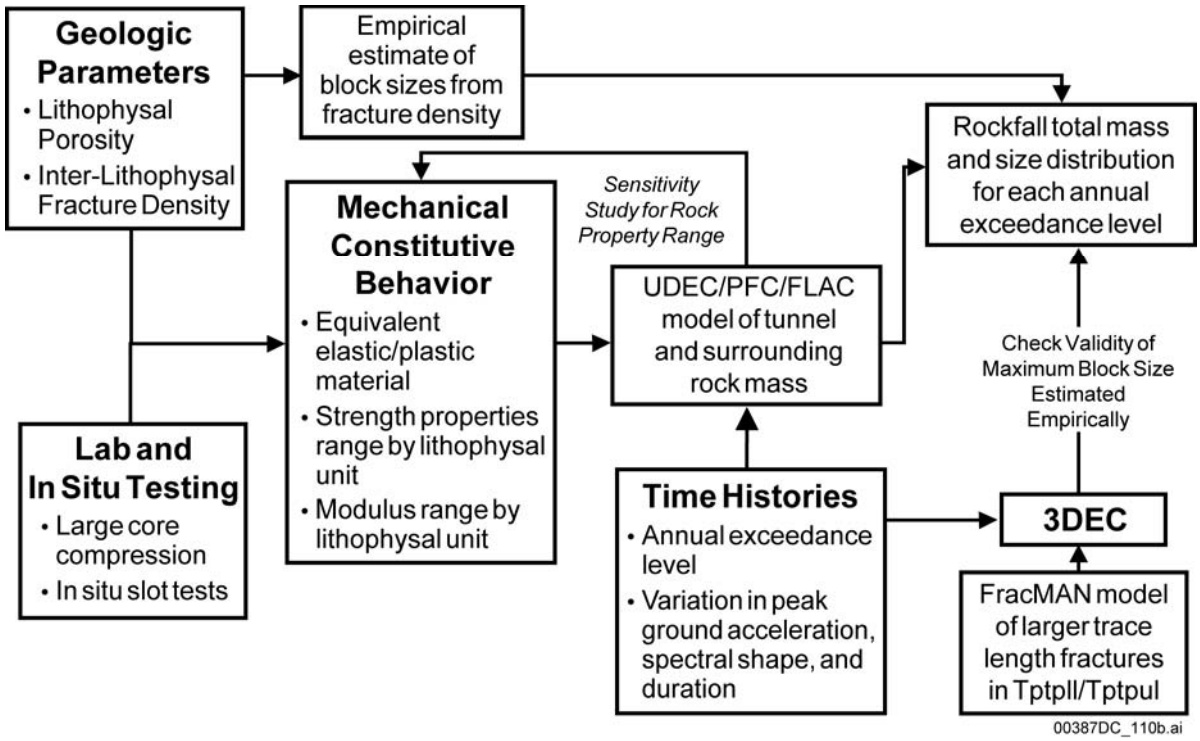

Source: Board 2003, Figure 33.

Figure C-2. General Methodology for Rockfall Analyses in the Lithophysal Rocks

In *Drift Degradation Analysis* (BSC 2004a) the analysis of seismic, thermal, and time-dependent effects on rockfall and drift degradation is included. It is the analysis that supports the resolution of these KTI agreements.

A summary of the basis for the resolution of RDTME 3.15, RDTME 3.16, RDTME 3.17, and RDTME 3.19 is provided in the following section.

C.4.2 Basis for Resolution of RDTME 3.15

The emphasis of this agreement is to determine the adequacy of the DOE approach for accounting for thermal effects in the analyses of drift degradation. In a previous approach, thermal effects were indirectly accounted for through a reduction in joint cohesion using the DRKBA rockfall model. The joint cohesion reduction approach was used, since the DRKBA rockfall model did not have a mechanism to apply thermal stresses in the rock mass. This joint cohesion reduction approach is no longer used to account for thermal effects. Instead, the drift degradation analyses use UDEC and 3DEC to model thermal loads explicitly (BSC 2004a, Sections 6.2, 6.3, and 6.4), thus providing an improved thermal-mechanical model. A detailed, mountain-scale three-dimensional thermal analysis was performed to verify proper thermal boundary conditions and the impact of emplacement drift location on emplacement drift thermal history (BSC 2004a, Appendix C). The DRKBA approach now provides only a confirmatory role in the assessment of drift degradation.

Thermal-mechanical modeling was performed to define drift stability under combined in situ and thermally induced stresses. The stability of the drift due to thermal loading was analyzed using both 3DEC and UDEC discontinuum models, as described in *Drift Degradation Analysis* (BSC 2004a, Sections 6.3 and 6.4). For consistency with other thermal calculations performed for performance assessment at Yucca Mountain, the 3DEC and UDEC programs were not used to determine the rock mass temperatures. Instead, the evolution of the temperature field after waste emplacement was obtained using the hydro-thermal code NUFT, which is one of the component submodels of the line-averaged heat source, drift-scale, thermal-hydrologic (LDTH) model, described in *Multiscale Thermohydrologic Model* (BSC 2004b). The temperature or thermally induced stress fields were imported sequentially into 3DEC and UDEC for 45 time-steps after waste emplacement, making sure that the temperature change between two stages was relatively small (i.e., it did not result in a large stress change). The thermal stresses due to temperature changes were calculated, and the models were solved for equilibrium for the selected thermal times.

The NUFT approach is two-dimensional and, thus, assumes a cross section through a series of infinitely long emplacement drifts. Therefore, this approach adequately represents the developing temperature distribution around emplacement drifts located centrally within the repository.

Additional clarification and technical basis for this thermal approach are provided in Section 5.3.1 and in *Drift Degradation Analysis* (BSC 2004a, Section 6.2, Appendix C, and Appendix U).

The adequacy of the current methods to account for thermal effects on drift degradation (i.e., using UDEC and 3DEC) has been validated in *Drift Degradation Analysis* (BSC 2004a, Sections 7.7 and 7.8).

C.4.3 Basis for Resolution of RDTME 3.16

The available small trace-length fracture data have been analyzed and included in *Drift Degradation Analysis* (BSC 2004a, Section 6.3.3), which documents their effect on block development. The probabilistic key-block code DRKBA, with its efficient key-block simulation algorithm, is used to assess the impact of small trace-length fractures on possible rockfalls. The DRKBA approach models small trace-length fractures as circular discs, which is consistent with the 3DEC approach for fractures greater than 1 m (see Section 4.1.1). The DKRBA rockfall assessment is based on static conditions by comparing the results of two cases. Case 1 provides the standard fracture representation, which includes multiple joint sets, with joint trace lengths greater than 1 m. Case 2 is identical to Case 1, except it includes an additional random joint set for small trace-length fracture data (i.e., less than 1 m).

Figure C-3 presents the key-block analysis results in the format of cumulative frequency of occurrence for both cases. The block sizes predicted from Case 2 are, in general, similar to Case 1. As shown in Figure C-3, the inclusion of small trace-length fractures results in a higher frequency of smaller blocks (i.e., block volumes less than 0.05 m^3). The maximum block predicted is 7.36 m^3 for Case 1, without small trace-length fractures, compared to 3.25 m^3 for Case 2, including the small trace-length fractures. The results also show that by considering the

small trace-length fractures, more blocks would form. A total of 347 blocks were generated in Case 2 with inclusion of the small trace-length fractures, compared to 325 blocks predicted in Case 1 without the small trace-length fractures (BSC 2004a, Table 6-31). Approximately 10% more blocks are predicted when considering the small trace-length fractures. Since the inclusion of small trace-length fractures decreases the maximum block size with a relatively small increase in the number of blocks, it is concluded that small trace-length fractures have a minor impact on key-block development in the nonlithophysal units.

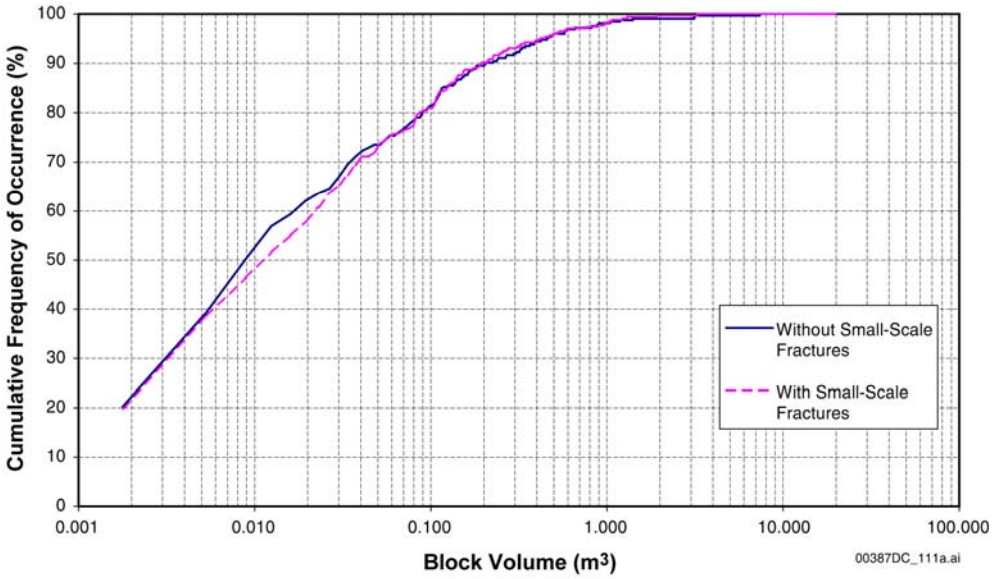

Source: BSC 2004a, Figure 6-111.

Figure C-3. Impact of Small Trace-Length Fractures on Block Size Distribution

C.4.4 Basis for Resolution of RDTME 3.17

The emphasis of this agreement is to verify the adequacy of the DOE approach in determining the geometry of various block sizes. In a previous approach, the geometry of blocks predicted was not available as direct output from the DRKBA rockfall model due to the limitation of the postprocessing capability of the DRKBA code. Therefore, the previous approach used UNWEDGE to calculate block geometry based on a systematic variation of the orientation of the three dominant joint sets. The approach for determining the effective maximum rock size has been revised in *Drift Degradation Analysis* (BSC 2004a, Appendix I). Varying the joint geometry input to UNWEDGE is no longer applied. The maximum rock size and shape is taken directly from the 3DEC output, which is based on stochastic variation in joint strike, dip, spacing, and persistence (see Section 4.1.2). The variation of joint geometry parameters is based on field mapping data from the ESF and the ECRB, which have been input into the rockfall model (BSC 2004a, Sections 6.1.6 and 6.3).

The predicted rock blocks impacting the waste package and drip shield have many different sizes and shapes. Since the block geometry information is mainly used for drip shield impact calculations, the geometry of the largest blocks is provided in *Drift Degradation Analysis* (BSC 2004a, Appendix I), showing six different views of each block with a listing of corner point

coordinates. Rock block masses, including relative velocity components, impact location, and rockfall shapes, are supplied to three-dimensional engineering structural analysis of the drip shield for each set of analyses at 10^{-5}, 10^{-6}, and 10^{-7} annual exceedance frequencies.

C.4.5 Basis for Resolution of RDTME 3.19

Part 1–This agreement addresses the inclusion of an appropriate range of geotechnical data from a design parameters analysis report (or other report). *Drift Degradation Analysis* is the approved report documenting the appropriate range of geotechnical data (BSC 2004a, Appendix E). In the current revision of *Drift Degradation Analysis* (BSC 2004a), the DRKBA analyses provide a confirmatory role only in the assessment of drift degradation. The primary analyses for degradation of nonlithophysal rock are provided using 3DEC (BSC 2004a, Section 6.3), while lithophysal rock is analyzed using UDEC (BSC 2004a, Section 6.4). An appropriate range of joint strength properties for nonlithophysal rock and estimated rock mass strength and moduli for lithophysal rocks has been applied in the drift degradation analyses, with the variability accounted for through parametric studies that cover a bounding range of parameters (see Section 4.2.2.1, Table 4-2; Section 5.3.2.1.8, Table 5-6).

Underground and surface excavations, which are designed to be stable after excavation, degrade with time, and some may eventually show partial or complete collapse. The main reason for these observations is that the strength of a rock mass exposed to humidity and temperature of the open atmosphere decays with time when it is loaded to a stress level higher than 50% to 60% of its short-term strength. The rate of strength decay depends on, among other parameters, rock type, stress state, relative humidity, and temperature. Stress corrosion is considered the main mechanism causing strength degradation of the rocks (Potyondy and Cundall 2001, Section 3).

A small number of existing as well as ongoing uniaxial static fatigue tests on nonlithophysal rock samples from the Tptpmn form the basis for estimating the time-dependency of the intact rock. PFC[1] (BSC 2002c), with an appropriate time-dependent strength model based on a stress corrosion crack growth model, was calibrated against the existing static fatigue data for nonlithophysal rocks and then used to extrapolate the impact of lithophysal porosity on the time dependency. The resulting estimate of the time-dependent change in the strength of the rock mass (in terms of loss of cohesive strength) is encapsulated in the drift scale UDEC model used for drift degradation analysis in lithophysal rocks. This work is reviewed in Section 5.3.3.2.4 and in *Drift Degradation Analysis* (BSC 2004a, Appendix S).

The drift stability impact due to the effect of rock joint degradation in nonlithophysal units is assessed based on a conservative estimate of the reduction of joint cohesion and friction angle (BSC 2004a, Section 6.3.1.5). The reduced joint strength parameters are estimated to be in the range of the residual state with joint cohesion reduced to zero and the joint friction angle reduced to 30°. The reduced friction angle is a typical value for a smooth joint reported by Goodman (1980, p. 158) and is consistent with the direct shear test results (DTN: GS030283114222.001). Dilation angle is also conservatively presumed to be zero considering the asperities on fracture

[1] The PFC code used for time-dependent analysis was developed initially for analysis of time-dependent yield in tunnels at the Underground Research Laboratory, Atomic Energy Commission of Canada (Potyondy and Cundall 2001). This same model, calibrated for the Topopah Spring Tuff data, is used in *Drift Degradation Analysis* (BSC 2004a) for time-dependency analysis.

surfaces had been sheared off, resulting in greater rockfall. The degraded joint strength and dilatational properties were applied in 10^{-6} seismic motion cases (BSC 2004a, Table 6-21). While a slight increase in rockfall is predicted for the degraded state, joint strength degradation has a minor impact on drift stability in nonlithophysal rock.

Predictions of the time-dependent drift degradation in lithophysal rock were examined using the UDEC model described in Section C.3. The time-related change in drift shape and rockfall associated with strength reduction in the rock mass work is reviewed in Section 5.3.3.2.4 and in *Drift Degradation Analysis* (BSC 2004a, Appendix S). The subsequent load of the broken rock on the drip shield is estimated using three different approaches: analytical, continuum numerical modeling, and discontinuum numerical modeling (BSC 2004a, Section 6.4.2.5). Cohesion and tensile strength of the rock mass are considered to degrade to zero in the degradation model. Each of the methods uses certain conditions regarding caving of the rock above the drifts and transfer of the stresses within the broken rock mass. Those conditions make the model results (i.e., cave size and pressures on the drip shield) conservative in each of three approaches (i.e., the conditions result in higher pressures). The level of conservatism is the largest in the analytical results and the smallest in the approach that represents rock mass as a discontinuum.

The predictions of pressure of the caved rock on the drip shield by the three modeling approaches are summarized in Figure C-4 (BSC 2004a, Section 6.4.2.5). The analytical model yields the largest loads due to overly conservative conditions. The continuum numerical model accounts more accurately for transfer of load by friction from the caved rock to the surrounding stable rock mass. Consequently, predicted loads for small bulking factors and large cavity size are much smaller than analytical predictions. When the bulking factor is large, the height of the cave becomes small. Stress arching cannot be realized within the small column of the caved rock and, consequently, predictions between analytical and continuum models are identical. The most accurate approach, using the discontinuum model, does not use an imposed condition about the shape of the caved region. It also correctly accounts for load transfer through the caved rock. The predictions of the pressures on the drip shield using this approach are smaller than the predictions of the analytical and continuum models for all values of the bulking factor.

Part 2–An analysis of block sizes based on the full distribution of joint trace length data has been included in the *Drift Degradation Analysis* (BSC 2004a, Sections 6.1.4 and 6.1.6). The joint trace length data used are consistent with the data from *Fracture Geometry Analysis for the Stratigraphic Units of the Repository Host Horizon* (CRWMS M&O 2000), and are discussed in Section 4.1.

To improve the method for estimating rockfall in the repository host horizon, a fracture network texture representation has been developed for the four subunits comprising the repository host horizon (BSC 2004a, Section 6.1.6 and Appendix B). The fracture network texture representation provides the basis for geologically representative drift degradation scenarios. The synthetic fracture network in three dimensions has been constructed using the FracMan methodology. The actual data from the ESF main loop and ECRB Cross-Drift are used to condition the fracture network texture representation. These data are detailed line survey and full periphery geologic map data collected from the tunnel walls during and after construction. The fracture data include strike and dip, trace length, truncation style, and intensity/density of fracturing.

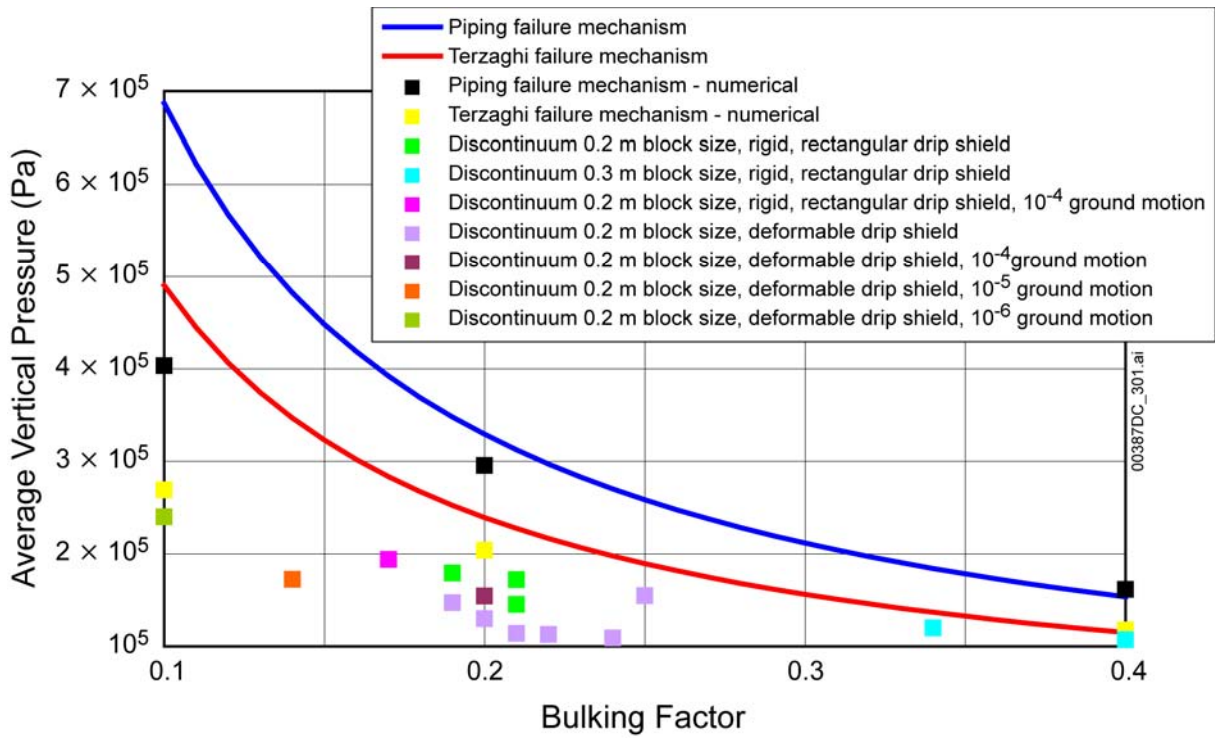

Source: BSC 2004a, Figure 6-170.

NOTE: Analytical methods are shown by solid lines. Continuum numerical modeling methods include "Piping failure mechanism – numerical" and "Terzaghi failure mechanism – numerical." All other points are determined using a discontinuum numerical modeling approach.

Figure C-4. Predictions of Pressure of the Degraded Lithophysal Rock on the Drip Shield as a Function of Bulking Factor

The confidence building for the development of synthetic fracture geometries is both qualitative and quantitative. A visual comparison to mapped field data is used qualitatively to evaluate synthetic fracture networks. Although qualitative, the visual comparison of a synthetic full periphery geologic map with the observed full periphery geologic map allows a synthetic fracture network to be abstracted from the observed data. Qualitative comparisons are provided in Part 3b of this section.

Quantitative comparison was done through comparison of orientation distributions (synthetic stereonets and observed stereonets), as well as comparison of trace length distribution and inter-fracture distance distribution, both synthetic and observed (BSC 2004a, Section 6.1.6).

The analysis of block sizes also includes the available small joint trace length data (see Section C.4.3).

Part 3–As indicated in Section C.4.2, the DRKBA results now provide a confirmatory role in the assessment of drift degradation. 3DEC has replaced DRKBA as the primary code for analyzing structural block development in the nonlithophysal rock units. The 3DEC and DRKBA results

are in good agreement, since the DRKBA block sizes are generally bounded by the 3DEC results (BSC 2004a, Section 7.8.4).

Part 3a–Appropriate boundary conditions for thermal and seismic loading have been included in the rockfall models (BSC 2004a, Sections 6.3.1.1, 6.4.2.2, and 6.4.2.3). At the initial consolidation stage and the later thermal loading period for the analysis of nonlithophysal rock using 3DEC, fixed velocity boundaries were used to ensure the boundary effect does not impact the stress distribution around the opening. For the 3DEC seismic analysis, a nonreflecting boundary is used for both the top and bottom of the model, whereas a free field boundary is imposed at the perimeter of the model (BSC 2004a, Figure 6-42). The free field boundaries ensure that plane waves propagating upward suffer no distortion at the boundary. A description of the free-field boundary is provided in *Drift Degradation Analysis* (BSC 2004a, Appendix H). Dynamic loading was applied at the bottom of the model as a prescribed stress boundary, and propagated vertically upward.

For the seismic analysis of lithophysal rock using UDEC, quiet (nonreflecting) boundaries are used on the outside boundaries of each model (BSC 2004a, Section 6.4.2.2). These boundaries prevent reflection of outgoing seismic waves back into the model, which is an essential modeling consideration since the reflection has been accounted for in the ground motion time histories. Quiet boundaries are combined with free field boundaries on the vertical outside boundaries. The free field boundaries perform one-dimensional simulation of vertically propagating plane waves representing motion of truncated, semi-infinite medium. They prevent distortion of vertically propagating plane waves along the quiet boundaries. Dynamic loading was applied at the bottom of the model, as propagating vertically upward. Although the dynamic loading was specified as velocity histories, it was applied at the bottom model boundary as a stress boundary condition. The conversion of the ground motion velocity to input seismic stress is discussed in *Drift Degradation Analysis* (BSC 2004a, Section 6.4.2.2).

For the thermal analysis of lithophysal rock using UDEC, boundary conditions are discussed in *Drift Degradation Analysis* (BSC 2004a, Section 6.4.2.3). The UDEC model does not perform complete thermal-mechanical simulation. Instead, temperature fields calculated with the code NUFT for 1.45 kW/m and 50 years of forced ventilation are imported into UDEC. Two cases of ventilation efficiency are considered, as discussed in Section 5.3.1: 90% and 70% heat removal. Stresses are calculated for each new temperature state based on the temperature increment (from the previous temperature state) and the coefficient of thermal expansion.

Part 3b–The previous DRKBA approach used a built-in joint generator for simulating joints in three-dimensional space. The DRKBA joint generator was limited in its ability to fully populate the model space, and typically created a joint density that was highest in the center of the model region. For the 3DEC analyses, the software FracMan (USGS 1999) provides fracture geometry input, which is used to provide an improved method of generating joints.

A representative FracMan simulation of the actual fracture network has been constructed based on standard detailed line survey and full periphery geologic map data (BSC 2004a, Section 6.1.6). These data consist of fractures with trace lengths of 1 m or greater. The premise to this simulation is that a cube 100 m on a side results in a representative fracture network within which emplacement drifts can be excavated. The fractures are simulated, and their

location, orientation, and size are inputs for the rockfall analyses. Individual 100 m cubes are constructed for each lithostratigraphic unit. For structural rockfall analyses, the Tptpll and Tptpmn units are representative of lithophysal and nonlithophysal rock, respectively, within the repository.

For nonlithophysal rock, 50 FracMan fracture patterns have been sampled from the 100 m Tptpmn FracMan cube and analyzed using 3DEC. The number of fracture patterns sampled was determined based on a sufficiency assessment to ensure that rockfall data (including block size, relative impact velocity, and impact energy of the rock to the drip shield) are converging to a stable value (BSC 2004a, Appendix K). These FracMan fractures are drawn from the same fracture population used in the DRKBA analyses (BSC 2004a, Sections 6.3.1.1 and 6.4.3), which includes joint geometry data collected from geologic mapping in both the ESF and the ECRB Cross-Drift. Comparisons of full periphery geologic maps from the ECRB Cross-Drift to simulated full periphery geologic maps from the FracMan cube are shown in Figures C-5 and C-6 for the lithophysal and nonlithophysal rocks, respectively. Fracture intensity, trace length, and orientation are similar for both the field data and the synthetic FracMan data (see Section 4.1.2).

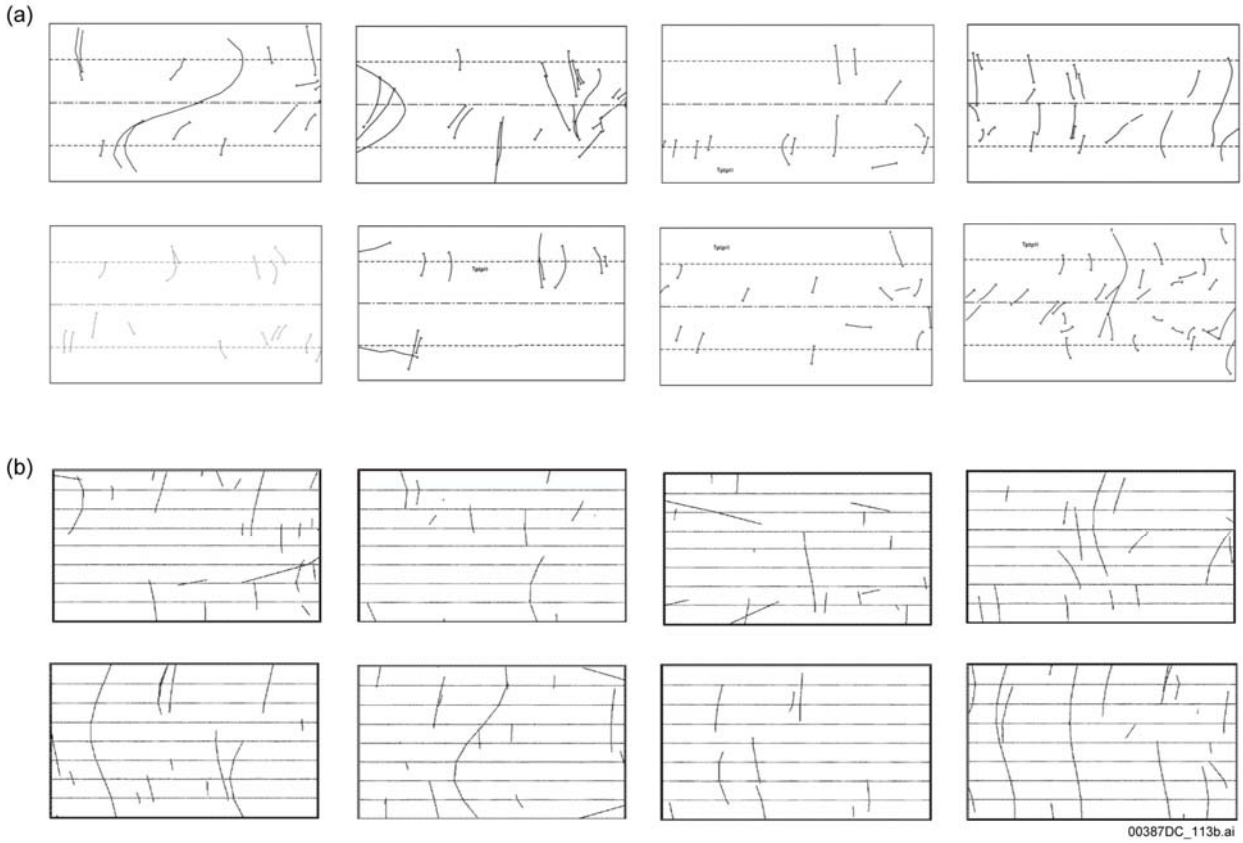

Source: BSC 2004a, Figure 6-20.

Figure C-5. Comparison of Full Periphery Geologic Maps from the Tptpll in the ECRB Cross-Drift (a) with Simulated Full Periphery Geologic Maps from the FracMan Cube (b)

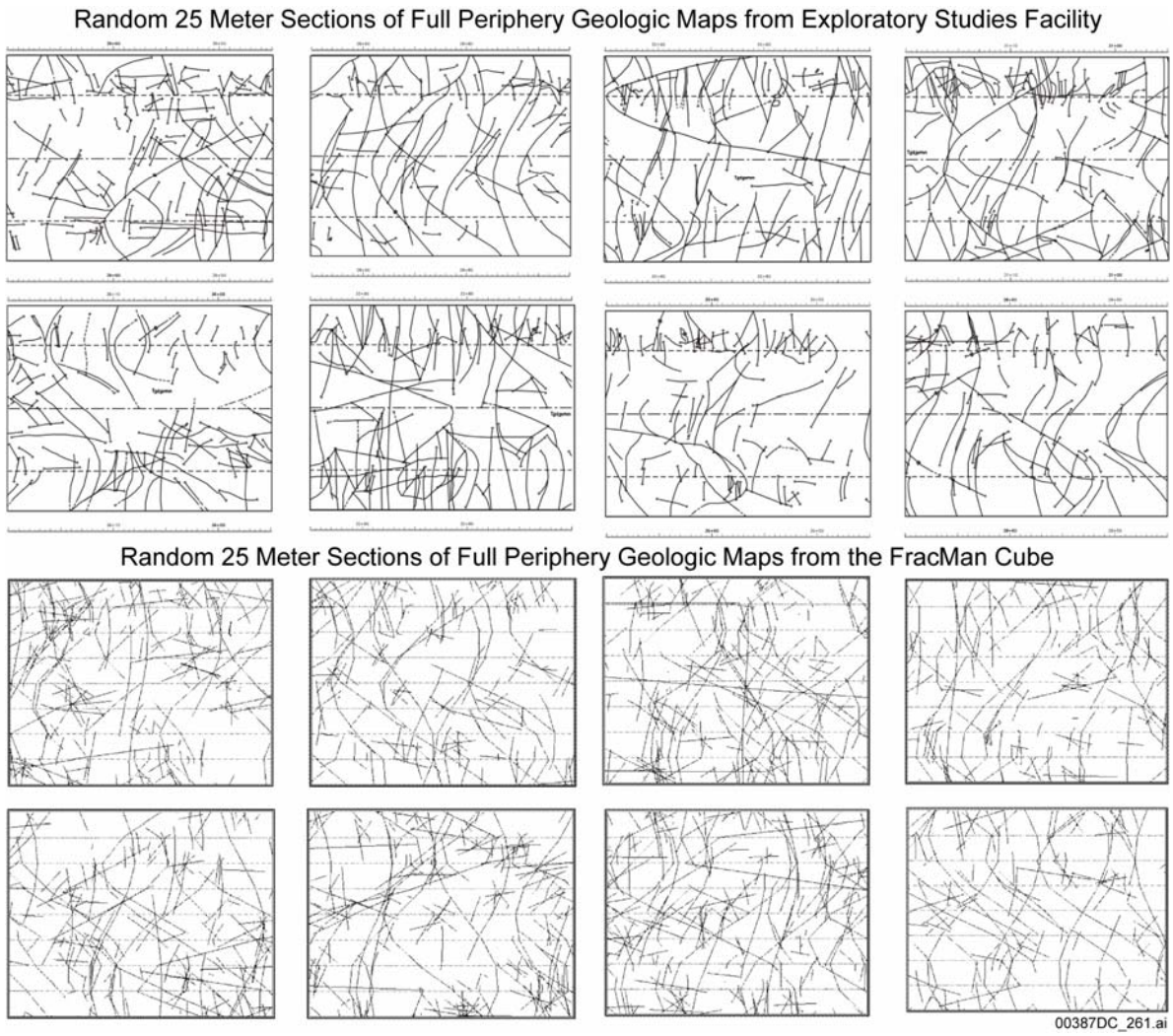

Source: BSC 2004a, Figure 6-28.

Figure C-6. Comparison of Full Periphery Geologic Maps from the Tptpmn in the ECRB ESF to Simulated Full Periphery Geologic Maps from the FracMan Cube

Part 3c–Thermal and mechanical properties for rock blocks and joints are available in the Technical Data Management System, as documented in *Drift Degradation Analysis* (BSC 2004a, Section 4.1 and Appendix E).

Sensitivity calculations for thermal properties were conducted for a range including the mean value down to one standard deviation less than the mean for thermal conductivity and specific heat (BSC 2004a, Sections 6.2, 6.3.1.3, and 6.4.1.2). The sensitivity case results in an approximately 23°C higher peak temperature compared with the base case with minor impact to the rockfall prediction.

Based on the discussion provided in Section 3.2, a sufficient amount of intact rock physical and mechanical properties data have been collected for the nonlithophysal rock units. Conversely, the amount of intact rock physical and mechanical properties data for the lithophysal units is

limited. To account for the uncertainty of intact data for the lithophysal units in the UDEC lithophysal rockfall model, five categories of rock properties were included in the model to assess the impact of the bounding ranges in intact properties data. The difference of rockfall prediction for the range of properties considered is provided in *Drift Degradation Analysis* (BSC 2004a, Section 6.4), and in Appendix A, which address RDTME 3.05.

Part 3d–Long-term joint strength degradation in nonlithophysal rock and long-term rock mass strength degradation in lithophysal rock has been documented in *Drift Degradation Analysis* (BSC 2004a, Sections 6.3.1.5 and 6.4.2.4). The drift stability impact due to the effect of rock joint degradation in nonlithophysal units is assessed based on a conservative estimate of the reduction of joint cohesion and friction angle (BSC 2004a, Section 6.3.1.5). While a slight increase in rockfall is predicted for the degraded state, joint strength degradation has a minor impact on drift stability in nonlithophysal rock.

The time-related change in drift shape and rockfall associated with strength reduction in the rock mass work in lithophysal rock is reviewed in Section 5.3.3.2.4 and in *Drift Degradation Analysis* (BSC 2004a, Appendix S). Cohesion and tensile strength of the lithophysal rock mass are considered to degrade to 0 in the degradation model, resulting in collapse of the drift. The subsequent load of the broken rock on the drip shield was then estimated. Additional discussion of long-term strength degradation is provided in Part 1 of this section.

Part 3e–Site-specific ground motion time histories were developed based on a site response model. The modeling approach implements a random-vibration theory, equivalent-linear formulation to calculate site response effects on ground motions. A detailed description for the development of the site specific ground motion time histories is provided in *Development of Earthquake Ground Motion Input for Preclosure Seismic Design and Postclosure Performance Assessment of a Geologic Repository at Yucca Mountain, NV* (BSC 2004c).

Site-specific ground motions for three postclosure levels of annual probability of exceedance, 10^{-5}, 10^{-6}, and 10^{-7}, are included in *Drift Degradation Analysis* (BSC 2004a, Section 6.3.1.2.1). A total of 15 sets of Point B ground motion (i.e., ground motion developed at the repository horizon) were selected for each annual postclosure hazard level. The multiple sets ensure a reasonable distribution of spectral shapes and time history durations. For each set of ground motion, two horizontal components (H1 and H2) and one vertical component (V) of acceleration, velocity, and displacement are supplied. Figure C-7 shows example H1 velocity time histories for four annual hazard levels. A preclosure ground motion level (10^{-4} annual probability of exceedance) is included in this figure for comparison to the postclosure levels.

These site-specific ground motions are included in both the 3DEC nonlithophysal rockfall model and the UDEC lithophysal rockfall model, as documented in *Drift Degradation Analysis* (BSC 2004a, Sections 6.3.1.2 and 6.4.2.2).

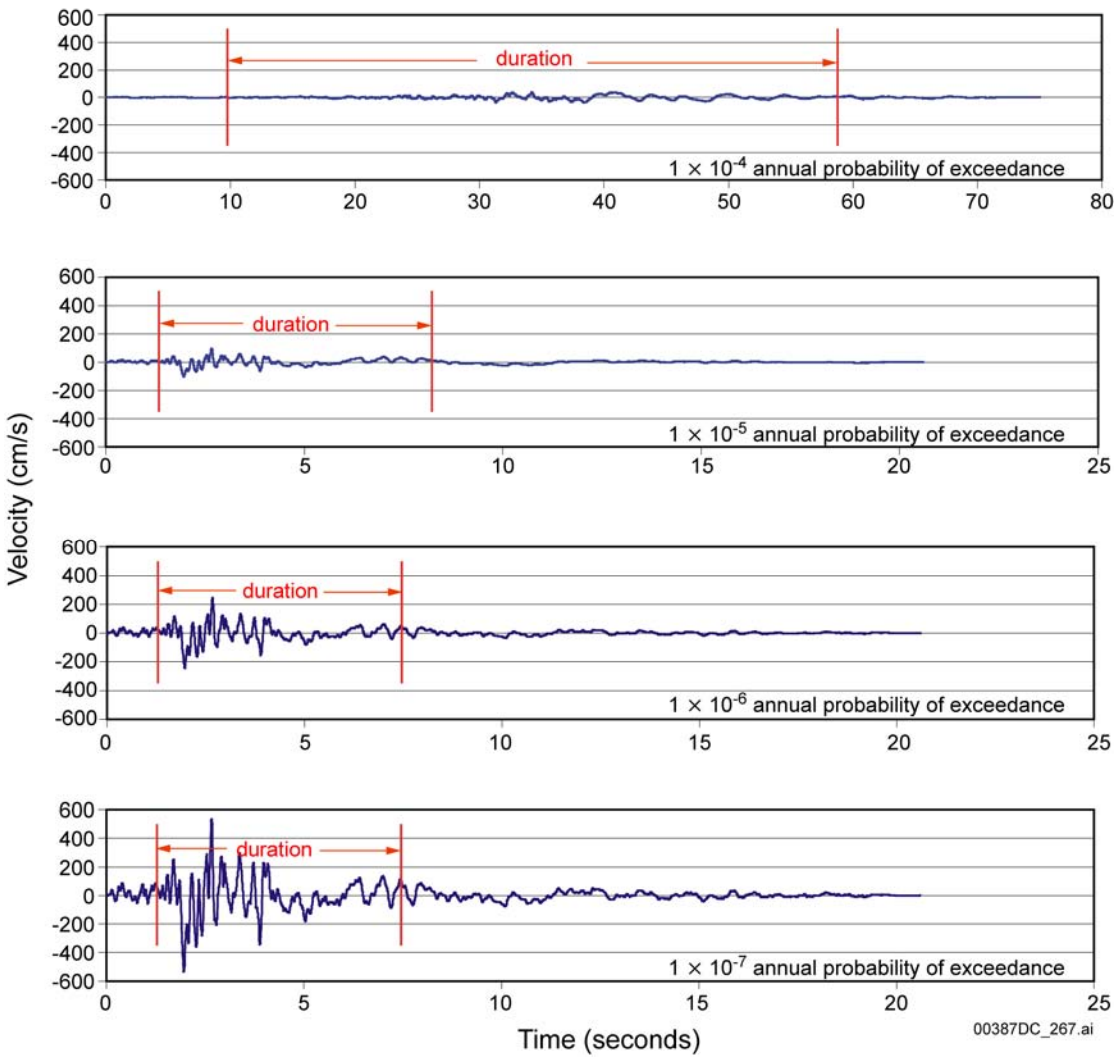

Source: BSC 2004a, Figure 6-43.

Figure C-7. Examples of Ground Velocity Time Histories with Truncated Duration for Analysis

Part 4–The impacts of rockfall on performance are discussed in Section 1.2.2.2. The rockfall results described in this appendix provide input to performance assessment calculations that evaluate rockfall impacts. The impact of seismic-induced rockfall on engineered barrier system components, including the drip shield, the waste package, and the fuel cladding, has been evaluated in *Seismic Consequence Abstraction* (BSC 2004d). The impact of drift shape changes caused by rockfall has been evaluated in seepage models for performance assessment (BSC 2004e). These performance calculations provide probability distributions of relevant parameters affected by rockfall for use in the TSPA-LA.

C.4.6 Conclusions

The current approach to rockfall analyses no longer relies on the DRKBA numerical code. The limitations associated with DRKBA have been addressed through the use of the distinct element codes UDEC, a two-dimensional discontinuum code, and 3DEC, a three-dimensional

discontinuum code. These codes can explicitly apply both seismic and thermal loads, which satisfies the requirements of RDTME 3.15, RDTME 3.16, RDTME 3.17, and RDTME 3.19.

Drift degradation has the potential to affect drip shield integrity directly, waste package integrity indirectly, and thermal-hydrologic environments within drifts. The results of this modeling and analysis activity provide rockfall data to support structural analyses of the ground support system, the drip shield, and waste package. The drift degradation analysis also provides the changes in drift profile due to rockfall, which supports analyses of seepage into the emplacement drift during the period of compliance for postclosure performance.

C.5 REFERENCES

C.5.1 Documents Cited

Board, M. 2003. *Resolution Strategy for Geomechanically-Related Repository Design and Thermal-Mechanical Effects (RDTME)*. REV 00. Las Vegas, Nevada: Bechtel SAIC Company. ACC: MOL.20030708.0153.

BSC (Bechtel SAIC Company) 2002a. Software Code: UDEC. V3.1. PC/WINDOWS 2000/NT 4.0. 10173-3.1-00.

BSC 2002b. *Software Code: 3DEC*. V2.01. PC/WINDOWS 2000/NT 4.0. 10025-2.01-00.

BSC 2002c. *Software Code: PFC2D*. V2.0. PC/WINDOWS 2000/NT 4.0. 10828-2.0-00.

BSC 2003. *Ground Control for Emplacement Drifts for LA*. 800-K0C-TEG0-00100-000-00A. Las Vegas, Nevada: Bechtel SAIC Company. ACC: ENG.20031016.0001.

BSC 2004a. *Drift Degradation Analysis*. ANL-EBS-MD-000027 REV 03A. Las Vegas, NV: Bechtel SAIC Company. ACC: MOL.20040513.0081.

BSC 2004b. *Multiscale Thermohydrologic Model*. ANL-EBS-MD-000049 REV 01. Las Vegas, Nevada: Bechtel SAIC Company. ACC: DOC.20040301.0004.

BSC 2004c. *Development of Earthquake Ground Motion Input for Preclosure Seismic Design and Postclosure Performance Assessment of a Geologic Repository at Yucca Mountain, NV with Errata*. MDL-MGR-GS-000003 REV 00. Las Vegas, Nevada: Bechtel SAIC Company. ACC: DOC.20031201.0001; DOC.20040401.0004.

BSC 2004d. *Seismic Consequence Abstraction*. MDL-WIS-PA-000003 REV 0, with errata. Las Vegas, Nevada: Bechtel SAIC Company. ACC: DOC.20030818.0006; DOC.20040218.0002.

BSC 2004e. *Abstraction of Drift Seepage*. MDL-NBS-HS-000019 REV 00 ICN 01. Las Vegas, Nevada: Bechtel SAIC Company. ACC: DOC.20031112.0002; DOC.20040223.0001.

CRWMS M&O (Civilian Radioactive Waste Management System Management and Operating Contractor) 2000. *Fracture Geometry Analysis for the Stratigraphic Units of the Repository Host Horizon*. ANL-EBS-GE-000006 REV 00. Las Vegas, Nevada: CRWMS M&O. ACC: MOL.20000918.0286.

Goodman, R.E. 1980. *Introduction to Rock Mechanics*. New York, New York: John Wiley & Sons. TIC: 218828.

NRC (U.S. Nuclear Regulatory Commission) 2002. *Integrated Issue Resolution Status Report.* NUREG-1762. Washington, D.C.: U.S. Nuclear Regulatory Commission, Office of Nuclear Material Safety and Safeguards. TIC: 253064.

Potyondy, D. and Cundall, P. 2001. *The PFC Model for Rock: Predicting Rock-Mass Damage at the Underground Research Laboratory*. Report No. 06819-REP-01200-10061-R00. Toronto, Ontario, Canada: Ontario Power Generation, Nuclear Waste Management Division. TIC: 253569.

Reamer, C.W. and Gil, A.V. 2001. Summary Highlights of NRC/DOE Technical Exchange and Management Meeting of Range on Thermal Operating Temperatures, September 18-19, 2001. Washington, D.C.: U.S. Nuclear Regulatory Commission. ACC: MOL.20020107.0162.

Reamer, C.W. and Williams, D.R. 2001. Summary Highlights of NRC/DOE Technical Exchange and Management Meeting on Repository Design and Thermal-Mechanical Effects. Meeting held February 6-8, 2001, Las Vegas, Nevada. Washington, D.C.: U.S. Nuclear Regulatory Commission. ACC: MOL.20010307.0511 through MOL.20010307.0521.

Stablein, N.K. and Gil, A.V. 2003. Summary Highlights of NRC/DOE Technical Exchange Meeting on Repository Design and Thermal-Mechanical Effects Key Technical Issue. Meeting held May 6 to 8, 2003, Las Vegas, Nevada. Washington, D.C.: U.S. Nuclear Regulatory Commission. ACC: MOL.20030708.0032.

USGS (U.S. Geological Survey) 1999. *Software Code: FracMAN*. V.2.511. PC/Windows NT. 10114-2.511-00.

C.5.2 Data, Listed by Data Tracking Number

GS030283114222.001. Direct Shear Data from Selected Samples of the Topopah Spring Tuff. Submittal date: 02/20/2003.

INTENTIONALLY LEFT BLANK

APPENDIX D

ANALYSIS OF LOAD COMBINATION AND MODELING APPROACH RELATED TO EVALUATION OF EMPLACEMENT DRIFT STABILITY (RESPONSE TO RDTME 3.02, RDTME 3.10, AND RDTME 3.13)

Note Regarding the Status of Supporting Technical Information

This document was prepared using the most current information available at the time of its development. This Technical Basis Document and its appendices providing Key Technical Issue Agreement responses that were prepared using preliminary or draft information reflect the status of the Yucca Mountain Project's scientific and design bases at the time of submittal. In some cases this involved the use of draft Analysis and Model Reports (AMRs) and other draft references whose contents may change with time. Information that evolves through subsequent revisions of the AMRs and other references will be reflected in the License Application (LA) as the approved analyses of record at the time of LA submittal. Consequently, the Project will not routinely update either this Technical Basis Document or its Key Technical Issue Agreement appendices to reflect changes in the supporting references prior to submittal of the LA.

APPENDIX D

ANALYSIS OF LOAD COMBINATION AND MODELING APPROACH RELATED TO EVALUATION OF EMPLACEMENT DRIFT STABILITY (RESPONSE TO RDTME 3.02, RDTME 3.10, AND RDTME 3.13)

This appendix provides a response for Key Technical Issue (KTI) agreements Repository Design and Thermal-Mechanical Effects (RDTME) 3.02, 3.10, and 3.13. These agreements relate to issues regarding the critical load combinations and modeling approaches related to the evaluation of emplacement drift stability and ground support performance during the preclosure period. These issues are addressed together in this appendix due to their related content.

D.1 KEY TECHNICAL ISSUE AGREEMENTS

D.1.1 RDTME 3.02, RDTME 3.10, and RDTME 3.13

Agreements RDTME 3.02, RDTME 3.10, and RDTME 3.13 were reached during the U.S. Nuclear Regulatory Commission (NRC)/U.S. Department of Energy (DOE) Technical Exchange and Management Meeting on Repository Design and Thermal-Mechanical Effects held February 6 to 8, 2001, in Las Vegas, Nevada (Reamer and Williams 2001). There have been no submittals related to these KTI agreements to the NRC.

The wording of these agreements is as follows:

RDTME 3.02

> Provide the critical combinations of in-situ, thermal, and seismic stresses, together with their technical bases, and their impacts on ground support performance. The DOE will examine the critical combinations of in-situ, thermal, and seismic stresses, together with their technical bases and their impacts on preclosure ground support performance. These results will be documented in a revision to the Ground Control for Emplacement Drifts for SR, ANL-EBS-GE-000002 (or other document) supporting any potential license application. This is expected to be available to NRC in FY 2003.

RDTME 3.10

> Provide technical basis for the assessment that two-dimensional modeling for emplacement drifts is considered to be adequate, considering the fact that neither the in-situ stress field nor the principle fracture orientation are parallel or perpendicular to emplacement drift orientation. The DOE will provide the technical bases for the modeling methods used in ground control analysis in a revision to the Ground Control for Emplacement Drifts for SR, ANL-EBS-GE-000002 (or other document) supporting any potential license application. This is expected to be available to NRC in FY 2003.

RDTME 3.13

> Provide technical justification for boundary conditions used for continuum and discontinuum modeling used for underground facility design. The DOE will provide the technical justification for boundary conditions used in modeling for preclosure ground control analyses in a revision to the Ground Control for Emplacement Drifts for SR, ANL-EBS-GE-000002 (or other document) supporting any potential license application. This is expected to be available to NRC in FY 2003.

These agreements focus on issues regarding the effects of critical load combinations and numerical modeling-related parameters on emplacement drift stability and ground support performance. The concerns are further elaborated in the *Integrated Issue Resolution Status Report* (NRC 2002, Section 2.1.7). The NRC concerns are paraphrased as follows:

- DOE has set performance criteria for several structures, systems, and components that call for a design against the worst-case load combinations. In the stability analyses of emplacement drifts for site recommendation (BSC 2001), the worst-case load combination was assumed to be achieved by superimposing seismic loading on thermal loading at the time when the drift-wall temperature was close to its peak value. Since the effect of critical load combinations depend to a large extent on the potential failure modes of structures, systems, and components, several different loading combinations need to be considered to determine the appropriate load combinations for design (NRC 2002, pp. 2.1.7-8 to 2.1.7-9).

- Concern about the appropriateness of two-dimensional thermal-mechanical modeling of emplacement drifts arises because the in situ horizontal principal stresses and several of the fracture sets are oblique to the proposed drift alignment (252° azimuth, that is S72°W) (BSC 2003a, Section 5.1.4). The ambient minimum principal stress is horizontal and oriented N60°W-N65° W, which is 40 to 45 degrees from the drift-normal plane, which is the assumed orientation of the minimum principal stress for the two-dimensional modeling. Also, the dip direction of the subhorizontal fractures lies in the 40 to 60 degree range (i.e., 10 to 30 degrees from the drift orientation). Therefore, the two-dimensional models are not favorably oriented to detect slip on the subhorizontal fractures. Three-dimensional modeling may be necessary to determine the effects of these structural features that are oblique to the drift alignment. Other areas for which three-dimensional modeling may also be necessary include (1) stability of the turnout area, which may be subjected to a combination of vertical tension and high-horizontal compression; (2) effects of greater heat conduction rates through the drift floor because steel members in the floor (invert and pallet) that are in direct or indirect contact with the waste package provide a faster heat-flow path into the rock; (3) stability of the structural components of the invert and the interaction of the transverse beams with the drift wall under heated conditions; and (4) effects of ground-surface topography drift-parallel thermal gradients on thermal stress and, consequently, drift stability (NRC 2002, pp. 2.1.7-12 to 2.1.7-13).

- Thermal-mechanical analyses of the emplacement drifts were conducted using a drift-scale model truncated at a distance of 50 m above and below the emplacement drift axis. The base of the model was held at zero vertical displacement, whereas the model top was held at constant normal traction equivalent to the preemplacement in situ stress. Such a model is inappropriate because it allows excessive free upward thermal expansion, thereby interfering with the development of thermally induced stress that is consistent with the geometry of the emplacement area (NRC 2002, p. 2.1.7-10).

D.1.2 Related Key Technical Issue Agreements

Agreements RDTME 3.05 (addressed in Appendix A) and RDTME 3.06 (addressed in Appendix B) are related to RDTME 3.02, RDTME 3.10, and RDTME 3.13. RDTME 3.05 addresses rock-mass mechanical properties of lithophysal rock. The rock-mass properties estimate, based on the approach described in resolution of RDTME 3.05, is used for resolution of RDTME 3.02, RDTME 3.10, and RDTME 3.13. RDTME 3.06 addresses sensitivity and uncertainty related to evaluation of emplacement drift stability. The results from the parameter study conducted for resolution of RDTME 3.06 assist the resolution of RDTME 3.02 and RDTME 3.13.

D.2 RELEVANCE TO REPOSITORY PERFORMANCE

The preclosure safety analysis is used to demonstrate the safety of the proposed design and operations in the geologic repository operations area with regard to the overall preclosure performance objectives through a systematic examination of the site, design, potential hazards, initiating events and their resulting event sequences, and the potential radiological exposures to workers and the public (10 CFR 63.112). This safety analysis demonstrates that the ground control system is not required to prevent or mitigate credible rockfall. This demonstration relies upon analyses that show that the waste package does not breach when impacted by credible rock blocks. The emplacement drifts are an array of horizontal tunnels trending at 72° azimuth. Each drift will have a nominal diameter of 5.5 m and will be separated from the adjacent drifts by a nominal center-to-center distance of 81 m (BSC 2003a, Section 5.3.1; Williams 2002). The emplacement drifts provide the subsurface access and openings for the structures, systems, and components used for emplacement and retrieval operations.

The rock-mass surrounding the emplacement drifts will be subjected to loadings from in situ, thermal, and seismic stresses. The performance of emplacement drifts and ground support is analyzed based on the technically justified numerical modeling approach with appropriate boundary conditions and load combinations. The emplacement drift stability analysis demonstrates (1) the stability of the emplacement drifts with or without the installation of ground support, and (2) satisfaction of ground support performance, under the critical combinations of in situ, thermal, and seismic stresses during the preclosure period.

D.3 RESPONSE

The analyses that address resolution of RDTME 3.02, RDTME 3.10, and RDTME 3.13 are summarized in this appendix. Detailed information is provided in *Evaluation of Emplacement Drift Stability for KTI Resolutions* (BSC 2004a). Additional detail on rock mass properties

derivation and numerical model development and validation are given in the technical basis document. The items covered in this appendix include:

- Analysis for resolution of RDTME 3.02
  - Describe each type of load, including the bounds of each and how these loads are estimated
  - Identify potential critical load combinations for emplacement drift stability and ground support performance
  - Conduct analyses based on critical load combinations
- Analysis for resolution of RDTME 3.10
  - Discuss the ground support functions and their implementation in a numerical model
  - Conduct two- and three-dimensional analyses using assumed and true in situ stress conditions and compare their results
  - Provide the basis for the acceptability of the analyses
- Analysis for resolution of RDTME 3.13
  - Describe and justify model dimension and boundary conditions used in numerical modeling
  - Conduct two-dimensional analysis for sensitivity of variations in model dimension.

The summary and conclusions from various analyses responding to these RDTME issues are provided below:

D.3.1 Response to RDTME 3.02

- The critical load combinations include in situ plus preclosure seismic stress and in situ plus preclosure thermal plus seismic stress. In the latter load combination, two potentially critical thermal conditions are: (1) when the drift wall temperature reaches its peak value, and (2) when the preclosure period (or the considered repository service life) ends, which gives the longest duration of heating or thermal expansion (BSC 2004a, Section 6.1).
- Under the load combinations considered, the emplacement drifts are predicted to be stable during the preclosure period, with a minimum factor of safety of 2 for the weakest estimate lithophysal rock strength category (BSC 2004a, Section 6.1).
- For the estimated weak rock strength (Category 1; see Section 4.2.2, Table 4-2 of the technical basis document for definition) with low deformation modulus, the load combination of in situ plus preclosure seismic stress governs the stability of

emplacement drifts. Changes in stresses during the seismic ground motions overshadow those induced by heating over the entire preclosure period. This is because the increase in temperature is relatively moderate and the rock mass modulus is relatively low, resulting in a low thermally induced stress (BSC 2004a, Section 6.1).

- Stresses in the rock adjacent to emplacement drifts are sensitive to the elevated temperatures, especially for the higher strength category rock (e.g., Category 5, which has a high modulus value). The ratio of modulus to strength controls stability sensitivity to the thermal load. If the ratio is large, the effect of heating on the drift stability is greater. For lithophysal rock, the ratio increases with rock strength category number. The worst conditions of thermal loading are for the best quality rock mass (Category 5; see Section 4.2.2 of the technical basis document for definition). The maximum stresses are generally anticipated to be associated with the peak temperature following waste emplacement. For emplacement drifts excavated in good quality rock, a load combination that includes thermal effect may be the most important from a stability standpoint (BSC 2004a, Section 6.1).

- The duration of heating has an effect on the performance of emplacement drifts and ground support. This is because an increasing amount of heat will be transferred into the rock mass over time, even though the temperature on the drift wall is decreasing. The more heat accumulated within the rock, the more thermal expansion the rock will have, resulting in additional rock deformations and stresses (BSC 2004a, Section 6.1).

- For rock bolt performance, the in situ and preclosure seismic load combination is the governing loading state. The peak axial forces in rock bolts installed near the springline and the crown are induced under combined in situ and preclosure seismic loading conditions. During the early stage of heating, the axial forces in bolts actually decrease due to the difference in coefficient of thermal expansion between rock bolt steel and rock mass and may become compressive if the axial loads are relatively low prior to heating. Depending on the length of heating, however, the axial forces in rock bolts are predicted to increase with time. This suggests that a thermal condition at the end of the preclosure period should also be combined with the preclosure seismic loading condition as a potentially governing load combination (BSC 2004a, Section 6.1).

D.3.2 Response to RDTME 3.10

Use of two-dimensional analyses for evaluation of emplacement drift stability and ground support performance is a generally-accepted practice. In these two-dimensional analyses, the bounding scenarios are considered in terms of rock properties and load conditions. Results based on the bounding scenarios are usually more conservative than those from three-dimensional analyses using more realistic input data of in situ stress field and fractures (BSC 2004a, Section 6.5).

To assess the effect of fractures in rock mass on instability due to wedge-type failures, a three-dimensional discontinuum model is required (BSC 2004b). The predicted rockfall information can then be used to evaluate the performance of ground support based on uncoupled calculations (see Appendix F of this document). The size, mass, and location of blocks can be

used to perform simple static structural calculations to ensure that the ground support is capable of maintaining stability.

Results from two-dimensional stability analyses from FLAC models are compared with those from the three-dimensional FLAC3D models. It appears that the two-dimensional models yield more conservative results and, therefore, are justified for use in the ground support design (BSC 2004a, Section 6.5).

D.3.3 Response to RDTME 3.13

The thermal-mechanical impacts of three models with vertical dimensions of 50, 100, and 200 m and corresponding thermal-mechanical boundary conditions are considered. The analyses are based on the rock mass properties for the lithophysal unit and base thermal loading and forced ventilation conditions (BSC 2004a, Section 6.7).

Use of a model with a vertical dimension of 100 m is adequate from the standpoint of ground support design. Additional increase in the model dimension has little effect on the predicted drift stability and ground support performance and is not necessary (BSC 2004a, Section 6.7).

Reduction of the model dimension to 25 m measured from the drift center to the top boundary may result in an overestimate of drift closures and stresses near the drift opening (BSC 2004a, Section 6.7).

The information in this report is responsive to agreements RDTME 3.02, RDTME 3.10, and RDTME 3.13 made between the DOE and NRC. This report contains the information that the DOE considers necessary for NRC review for closure of these agreements.

D.4 BASIS FOR THE RESPONSE

This section describes the technical basis and approach for resolving RDTME 3.02 (Section D.4.2), RDTME 3.10 (Section D.4.3), and RDTME 3.13 (Section D.4.4).

D.4.1 Overview of Resolution Strategy

A general strategy for resolving the geomechanical issues related to the RDTME KTIs is outlined in *Resolution Strategy for Geomechanically-Related Repository Design and Thermal-Mechanical Effects (RDTME)* (Board 2003). This technical basis document provides a summary of the testing and analyses that have been conducted based on this strategy. Although this technical basis document is primarily concerned with postclosure performance issues, the rock mass properties derived from these studies and the modeling tools developed are also applied to preclosure issues such as emplacement drift stability and ground support design. A number of documents describing preclosure applications have been developed, including: *Scoping Analysis on Sensitivity and Uncertainty of Emplacement Drift Stability* (BSC 2003b) and *Evaluation of Emplacement Drift Stability for KTI Resolutions* (BSC 2004a). These documents were developed specifically to resolve RDTME KTI agreements related to preclosure issues. These documents present detailed information regarding the analyses of emplacement drift stability and ground support performance, and support the resolution of these KTI agreements.

D.4.2 Basis for Resolution of RDTME 3.02

The focus of this agreement is the technical basis for selecting the critical[1] load combinations of in situ, thermal, and seismic stresses to support an evaluation of emplacement drift stability and ground support performance during the repository preclosure period.

D.4.2.1 Consideration of Sources of Loads

In a design analysis of emplacement drift stability and ground support performance, stresses resulting from three sources are considered: in situ (including excavation effects), thermal (radioactive waste heat decay), and seismic stresses. In situ stresses are present before drift excavation and will be altered in the vicinity of openings due to drift excavation. Thermal stresses occur following the initiation of waste emplacement and are transient in nature. The magnitude of thermally induced stresses at a particular location in the vicinity of the emplacement drifts is dependent upon the position relative to the emplaced waste packages and the airflow rate used in ventilation during the preclosure period. Seismic stresses are dynamic and transitory in nature. The magnitude of seismically induced stresses and the duration of the earthquake event are a function of the intensity of the earthquake, the distance from the event to the repository, and the direction and size of the seismic wave relative to the drift openings. The applicability and magnitude of some of the design loads will vary depending on the type of ground support system. Some of the loads, such as thermal loads, will only apply to the final ground support system.

Detailed discussion on how each of these three loads is estimated and applied in the design analysis of emplacement drift stability and ground support performance during the preclosure period is presented in *Evaluation of Emplacement Drift Stability for KTI Resolutions* (BSC 2004a, Section 6.1). The in situ, thermal, and seismic loads considered in the analysis of drift degradation are discussed in Section 5.

D.4.2.2 Selection of Load Combinations

The following load combinations have been considered to support a design analysis of emplacement drift stability and ground support performance during the repository preclosure period (BSC 2003c):

- In situ
- In situ plus seismic
- In situ plus thermal (as a function of time)
- In situ plus thermal plus seismic.

Of these combinations, the last three are considered more important in terms of governing the design.

[1] The term, critical means that these load combinations have the greatest potential impact on drift stability. Critical is not meant to imply that the load combinations result in impending instability.

For the rock mass adjacent to the emplacement drift and ground support components that are in compression due to excavation-induced rock displacements, the critical load combinations will be (1) in situ plus thermal and (2) in situ plus thermal plus seismic.

In Situ and Thermal Loading Combination–There are two significant times during the preclosure period that are critical from the ground-support design perspective. The first time is the point at which the drift wall reaches its peak temperature (Figure D-1). Including this point in the analysis of emplacement drift stability is appropriate because the increase in compressive stresses in the rock mass immediately adjacent to the drift is proportional to the increase in the rock temperature.

The second time is the end of the preclosure period. The emplacement drifts will be loaded with waste packages sequentially, together with ventilation provided. Once the loading is completed, the drift wall temperature will go down, as long as a ventilation airflow rate is maintained. As indicated in Figure D-1, the drift wall temperature peaks at about 2 years after emplacement for a forced ventilation airflow rate of 15 m^3/s. The drift wall temperature then gradually decreases with time due to the effect of continuous ventilation. However, the rock mass temperature away from the drift will continue to rise after the drift wall temperature peaks because the ventilation cannot remove 100% of the heat generated by the waste package (see rock temperatures at about 19 m from the skin of drift opening, shown in Figure D-1). As the temperature of the rock mass continues to rise, it causes additional expansion of the rock mass, which results in thermal stress increase that must be accounted for in estimation of drift stability and ground support performance. As more rock mass is heated, the cumulative effect of continuous rock thermal expansion plays a key role in governing the applied preclosure applied stresses.

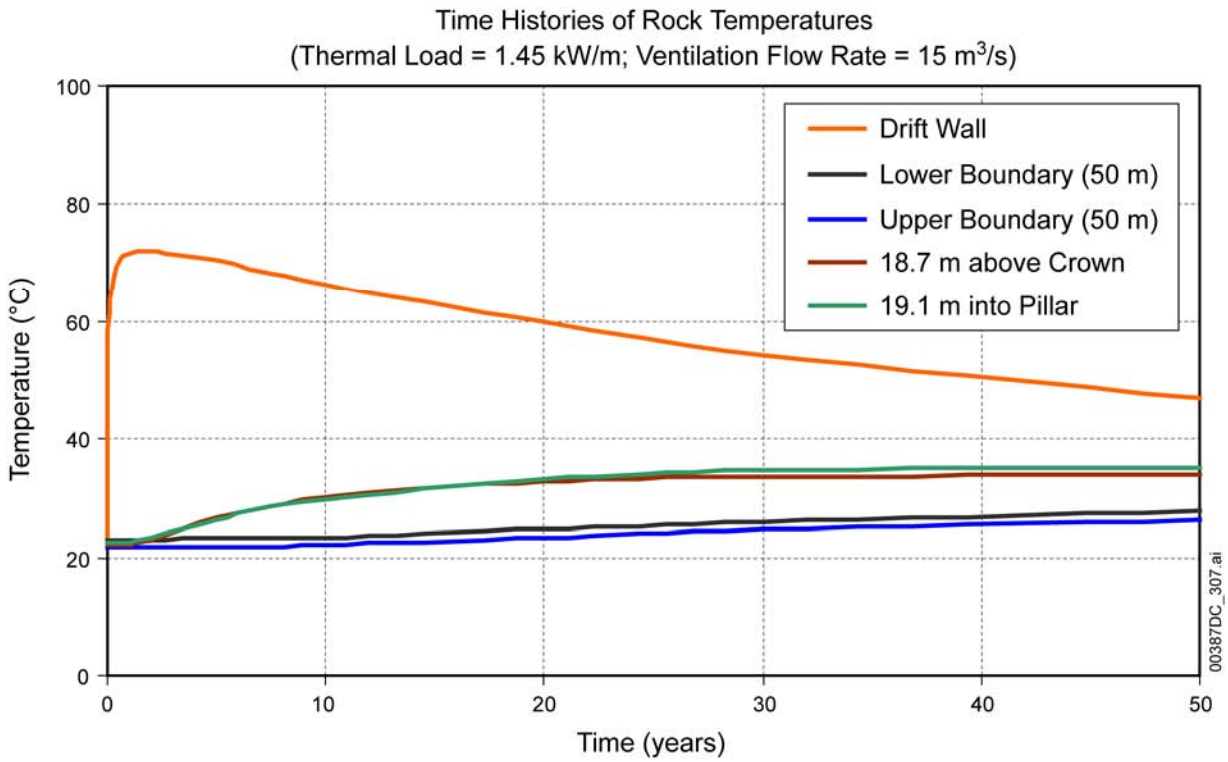

Source: DTN: MO0306MWDALAFV.000, ANSYS-LA-Fine.xls and la600c24.rth.

NOTE: These are temperatures predicted at 600 m from the drift air inlet.

Figure D-1. Rock Temperatures as a Function of Time at the Drift Wall and Various Positions within the Rock Mass

Thus, there are two time frames (i.e., from the beginning of emplacement to the time when the drift wall temperature peaks, and then the end of the preclosure period) to be considered in evaluating the effects of thermal load and its combination with other loads.

The in situ plus thermal load combination may be considered less critical, or less conservative, when a potential failure mode of rock mass or ground support components is due to tension. For example, rock bolts are generally in tension under excavation-induced rock deformation. The coefficient of thermal expansion for steel of rock bolts is usually similar to or higher than that of the rock mass. The elevated rock temperatures will result in induced compression in the bolts, which, as a result, will offset their preexisting tensile forces. Thus, thermal load is less important to rock bolt performance.

In Situ, Thermal and Seismic Loading Combination–Because the seismically-induced ground motions will induce both tensile and compressive stresses in the rock mass and in rock bolts, their effects should be combined with those of all other loads. The seismic load is dynamic in nature, while the in situ and thermal loads are essentially static in comparison. The required safety margin for the former (dynamic load) is usually lower than that for the latter (static load). For this reason, a load combination without the seismic load, such as in situ plus thermal, is also considered as critical due to a higher factor of safety required.

D.4.2.3 Effect and Sensitivity of Various Load Combinations

Two-Dimensional Continuum Modeling Approach–From a ground support design perspective, stability of emplacement drifts is judged by overall rock mass displacements and stresses. A two-dimensional plane-strain thermal-mechanical parameter analysis is used to assess the stability of emplacement drifts. The two-dimensional finite-difference code FLAC (Itasca Consulting Group 2002) is used for the analysis. A combination of in situ, thermal, and seismic loadings is included in the analysis. The continuum-based analyses assume the rock mass conforms to a Mohr-Coulomb failure criteria, with property variations for lithophysal rock described in Section 4.2 of this technical basis document.

Range in Variation of Rock Mass Properties for Lithophysal Rock–In the FLAC models, rock mass properties for the lithophysal rock properties reflect the effects of lithophysae and fractures on rock mass properties; their values are presented in *Evaluation of Emplacement Drift Stability for KTI Resolutions* (BSC 2004a, Table 4-5a, as well as Section 4.2, Table 4-2, and Appendix A of this technical basis document). For the bounding case scenarios, the rock mass mechanical properties corresponding to strength Category 1 (the weakest rock), and strength Category 5 (the strongest rock), are specifically considered. Under the in situ or seismic loading conditions, the stability of emplacement drifts is governed by the mechanical properties associated with the weakest rock, so use of the Category 1 rock mass properties represents the worst case scenario. However, under the thermal loading condition, the drift stability may depend on the modulus of the rock mass, since a relatively stiff rock (i.e., a good quality rock) may result in higher thermal stresses under elevated temperatures (because the thermal stress is proportional to modulus). Use of the Category 5 rock mass properties that give a relatively high modulus value are considered as a bounding case scenario in the analysis.

In Situ Stress State Variation and Rock Mass Yield Criterion–The measured vertical stress component at the Yucca Mountain site is maximum and equal to the gravitational component. The ratio of the minimum and maximum horizontal stress to vertical is estimated at 0.36 and 0.62 (see Table 2-2 of the technical basis document). Since a two-dimensional analysis is conducted here, bounding horizontal-to-vertical stress ratios (K_0), 0.3 and 1.0, are used in the analyses to encompass the potential range of in situ horizontal components in the plane normal to the emplacement drift axis (BSC 2004a, Table 6.1-1). Only results for a K_0 value of 0.3 are reviewed here as it provides the most critical combination of in situ stresses. The mechanical failure response of rock mass is assumed to conform to Mohr-Coulomb yield criterion. The use of the Mohr-Coulomb yield criteria is a typical assumption for rock (Hoek 2000) and was verified for lithophysal tuff in Section 4.2.5 of the technical basis document.

Model Configuration and Boundary Conditions–Figure D-2 illustrates the configuration of a typical FLAC model. The vertical dimension of the model is 100 m, and the horizontal is 81 m, equal to the drift spacing. The boundary conditions associated with the analyses for in situ, thermal, and seismic loading conditions are shown in Figure D-3. *Evaluation of Emplacement Drift Stability for KTI Resolutions* (BSC 2004a, Section 6.1.3) contains details on how each type of load is applied in the analyses.

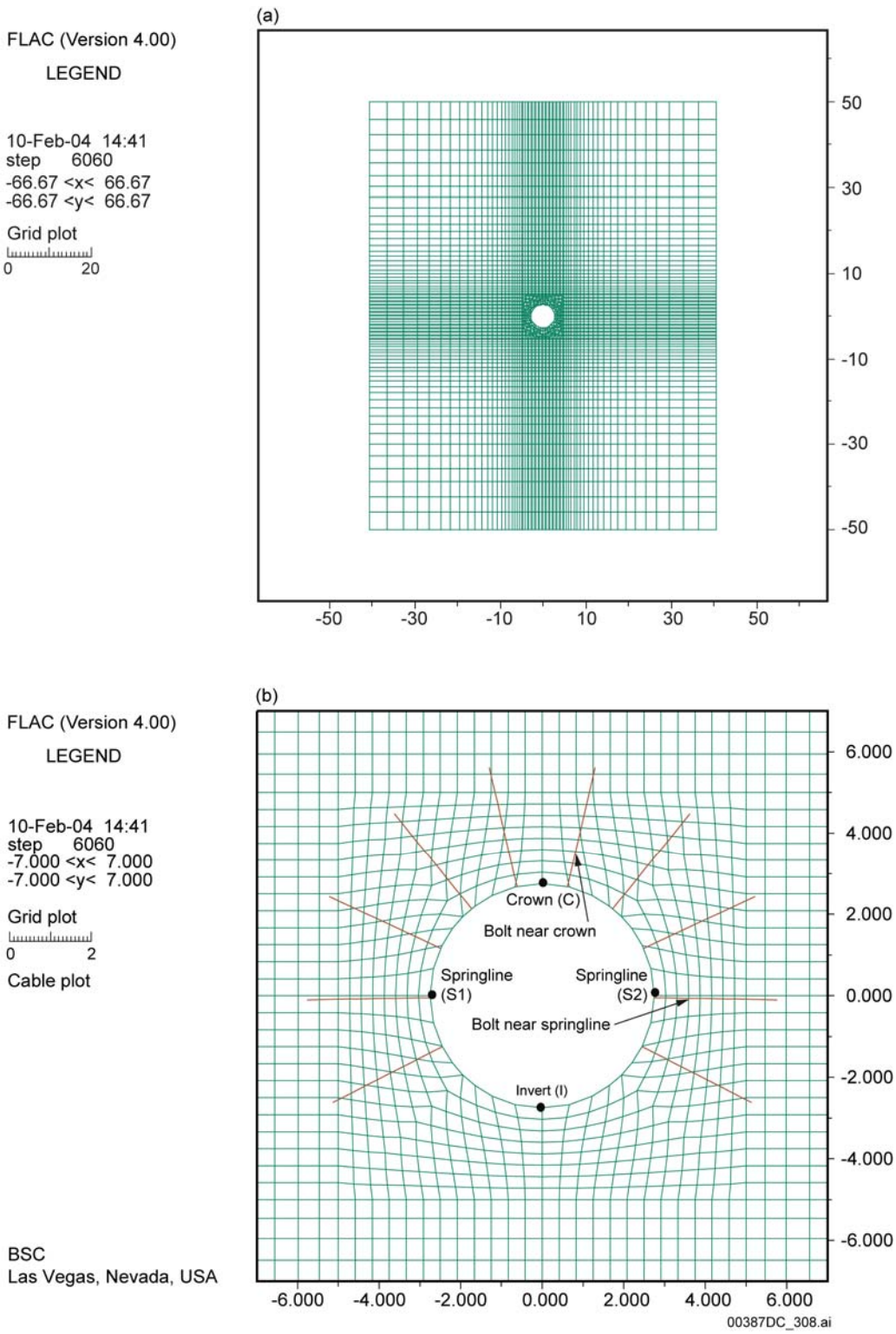

Source: BSC 2004a, Figure 6.1-5.

Figure D-2. Configuration of a Typical FLAC Model: (a) Mesh; (b) Rock Bolts (in Meters)

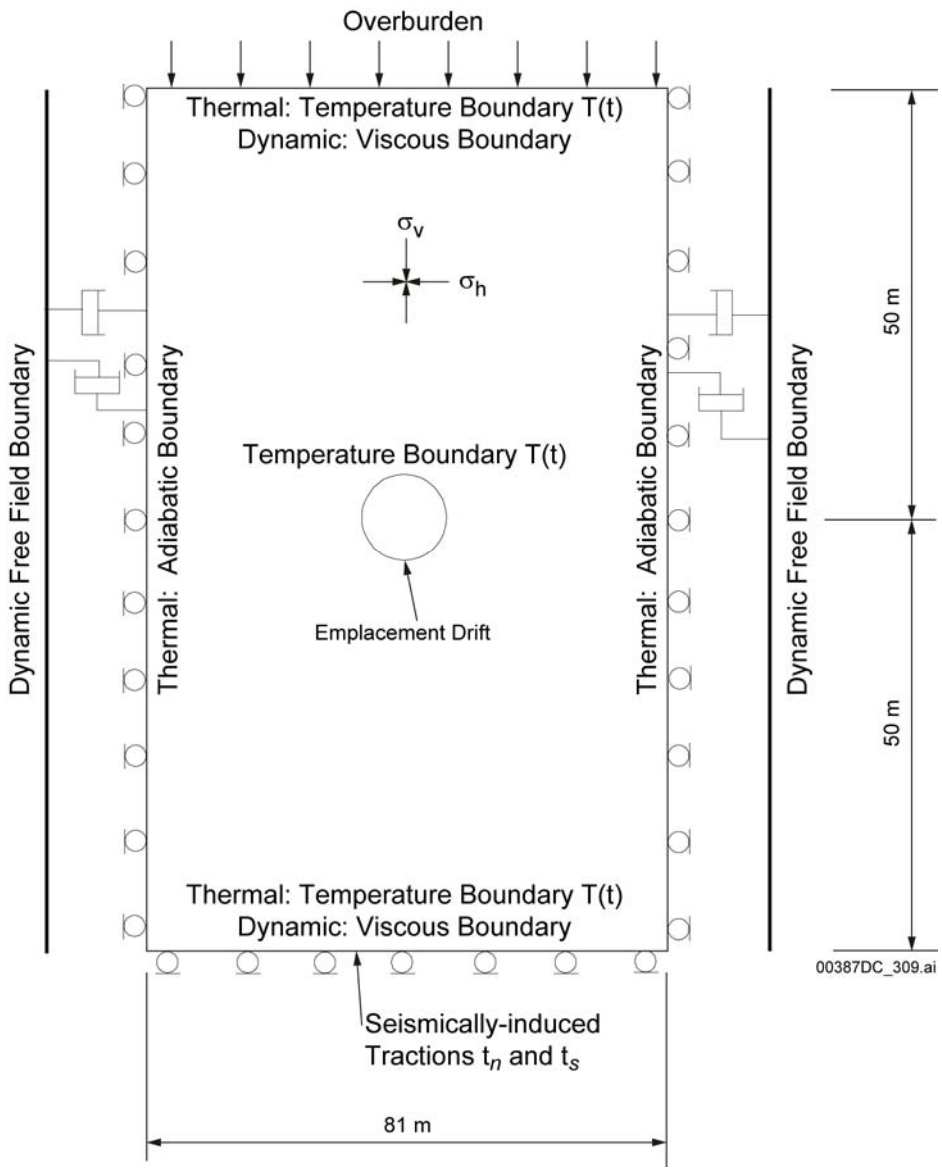

Figure D-3. Geometry and Boundary Conditions for a Typical Two-Dimensional Model

Additionally, to evaluate the sensitivity of rock bolt performance under various load combinations, rock bolts (such as the Swellex bolts proposed for the emplacement drifts (BSC 2003c, Section 6.3.2) are also included in the FLAC models. These bolts are simulated by rock bolt elements available as a standard feature within the FLAC program. As shown in Figure D-2, there are a total of ten 3-m-long bolts in each modeled cross section. The drift axial spacing of each row of rock bolts is 1.25 m. Two-dimensional modeling of the bolts with regular spacing in the drift axial direction involves averaging the three-dimensional effect over the distance between the adjacent rows of bolts. Linear scaling of rock bolt material properties is required in the FLAC models, as described by Itasca Consulting Group (2002), to account for the impact of spacing in the axial direction. This scaling is achieved by dividing the actual property by the bolt spacing along the drift. The material properties that need to be scaled include the modulus of elasticity, the tensile strength, and the normal and shear bonding stiffness, K_{bond} and S_{bond} of the bolt-borehole contact. Rock bolt properties are derived from laboratory or field pull

testing. Data used in these analyses are summarized in *Evaluation of Emplacement Drift Stability for KTI Resolutions* (BSC 2004a, Section 6.1.4). Axial force outputs from the models are then multiplied by the bolt spacing to obtain the actual loads.

In considering the combination of in situ, thermal, and seismic loading conditions, two subcases are analyzed. One subcase imposes the seismic motions at 2 years after waste emplacement, which corresponds to a state that the temperature reaches its peak value on the drift wall; and the other subcase applies the seismic load at 50 years, which is the end of the preclosure ventilation period.

Results of Analyses–Results of the analyses for the three different load combinations and two bounding rock mass categories (i.e., Categories 1 and 5 only) are shown in Figures D-4 to D-23. The observations based on a comparison of these results can be summarized as follows:

- The analyses define the most important loading combinations in regard to tunnel stability and rock bolt loading. In all cases analyzed, tunnels are stable with approximate strength-to-stress ratios of 2 to 4 for the lowest and highest lithophysal strength categories, respectively. Even though modeling of rock bolts was inherent in these analyses as shown in Appendix B, the tunnels are stable in an unsupported fashion. Therefore, the role of ground support is not to ensure opening stability under preclosure in situ, thermal and seismic loadings, but to retain any small, loosened rock particles.

- Drift closure, defined as the relative displacement between the invert and the crown for the vertical closure and between the walls at the springline for the horizontal closure (see Figure D-2b), are not significantly affected by either preclosure heating or preclosure seismic ground motions, as indicated in Figures D-4 and D-5. Heating after waste emplacement induces additional drift closure, especially in the horizontal direction, but the increases are on the order of millimeters. Changes in the drift closures during the seismic ground motion are generally independent of whether the drift is heated or not. Compared to heating from waste packages, seismic ground motions have greater impact on the drift closures, but the impact is inconsequential in comparison to initial closure of the drift from excavation alone and do not affect drift stability (see Figures D-4a and D-4b).

- Under the load combinations and bounding lithophysal rock mass properties considered, the emplacement drifts are predicted to be stable. The stress paths[2] near the springline and the crown, as shown in Figure D-6, remain within the Mohr-Coulomb yield criteria, meaning that the rock mass adjacent to the emplacement drifts behaves elastically under all load combinations. A stress path located below the yield criteria indicates that the transient stress variation is such that the rock mass remains within the elastic range.

- For the weakest lithophysal rock case (Category 1), the load combination of in situ plus seismic is considered to be critical for the stability of emplacement drifts. Changes in

[2] The term, stress path refers to a history of the principal stress at a point in the rock mass as it undergoes the transient loading and unloading associated with heating and cooling or seismic stressing. Plotting of the transient stress path on a standard plot of principal stresses with superimposed Mohr-Coulomb yield criteria (e.g., Figure B-2) allows easy identification of the location, timing, and extent of yield of the rock mass.

stresses during the seismic ground motions are greater than those induced by heating over the entire preclosure period (see Figure D-7). This is because the increase in rock mass temperature is relatively moderate and the rock mass modulus value is also low, resulting in a low thermally induced stress.

- Stresses in the rock adjacent to emplacement drifts increase with elevated temperatures, especially for the stiffer rock (see Figure D-8). The maximum stresses are generally anticipated to be associated with the peak temperature occurring at 2 years following waste emplacement. For emplacement drifts excavated in good quality rock, a load combination that includes thermal effect may potentially be critical.

- Overall factors of safety or strength-to-stress ratio for emplacement drifts are not significantly affected by variations in loading conditions, as shown in Figures D-9 and D-10. They are controlled by the quality or strength of the rock mass considered. For the weakest lithophysal rock (Category 1), the average factor of safety in a region of 3-m-thick annulus around the drift is about 2 for the governing load combination, while for the strong rock (Category 5), it is greater than 4.

- For rock bolt performance, the in situ and seismic load combination is governing. As shown in Figures D-11 and D-12, the peak axial forces in rock bolts installed near the springline and the crown are induced under combined in situ and seismic loading conditions. Under thermal loading conditions, however, the axial forces in bolts initially decrease, and then gradually increase with time. The axial forces may become compressive if they are relatively low prior to heating (see Figure D-12). By comparing Figure D-11 with Figure D-12, it can also be seen that the axial forces in bolts are very sensitive to the stiffness of rock: the lower the stiffness is, the higher the tensile axial forces. It should be noted that the in situ drift scale heating test, which was located in nonlithophysal rock (rock mass modulus at least as high as Category 5 lithophysal rock) was heated to temperatures of nearly 200°C, followed by a cool-down phase. The rock bolts utilized for ground support in this drift have showed no signs of loss of function. As discussed in Section 4.2.7 of this technical basis document, the thermally-induced roof tangential compressive stresses were actually high enough to equal the rock mass compressive strength at the maximum temperature to induce minor spalling. Even under this extreme condition, the rock bolts continued functioning and maintained suspension of wire mesh in the roof.

- The duration of heating has some impact on the performance of emplacement drifts and ground support. This is because an increasing amount of heat will be transferred into the rock mass over time, even though the temperature on the drift wall is decreasing. The more heat accumulated within the rock, the more thermal expansion of the rock, resulting in additional rock deformation and stressing. Axial forces in rock bolts are also predicted to increase with time due to continuous heating. This indicates that a thermal condition at the end of the preclosure period should be combined with seismic loading condition as a potentially critical load combination.

- Inclusion of the seismic condition is considered critical, and the load combination of in situ and thermal alone does not control the emplacement drift stability and ground support performance.

The observations made above are based on the analyses using rock mass properties for the lithophysal units. Similar observations can be made if rock mass properties for the nonlithophysal units are used (BSC 2003c, Sections 6.1.2 and 6.1.3).

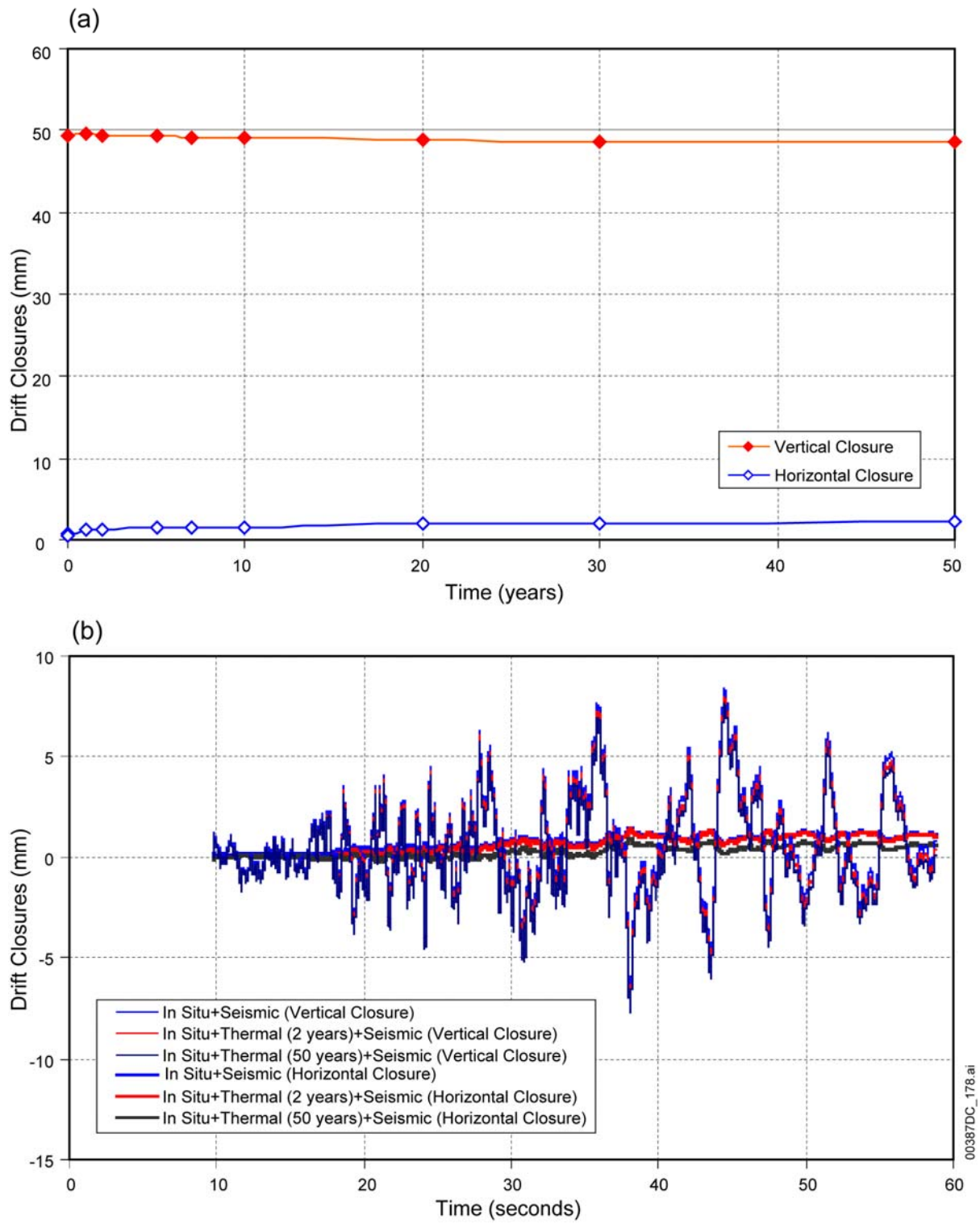

Source: BSC 2004a, Figure 6.1-6.

NOTE: The displacement values shown in (b) are initialized prior to seismic shaking.

Figure D-4. Drift Closure for Various Load Combinations (Category 1 and K_0 = 0.3): (a) In Situ plus Thermal; (b) In Situ plus Seismic and In Situ plus Thermal plus Seismic

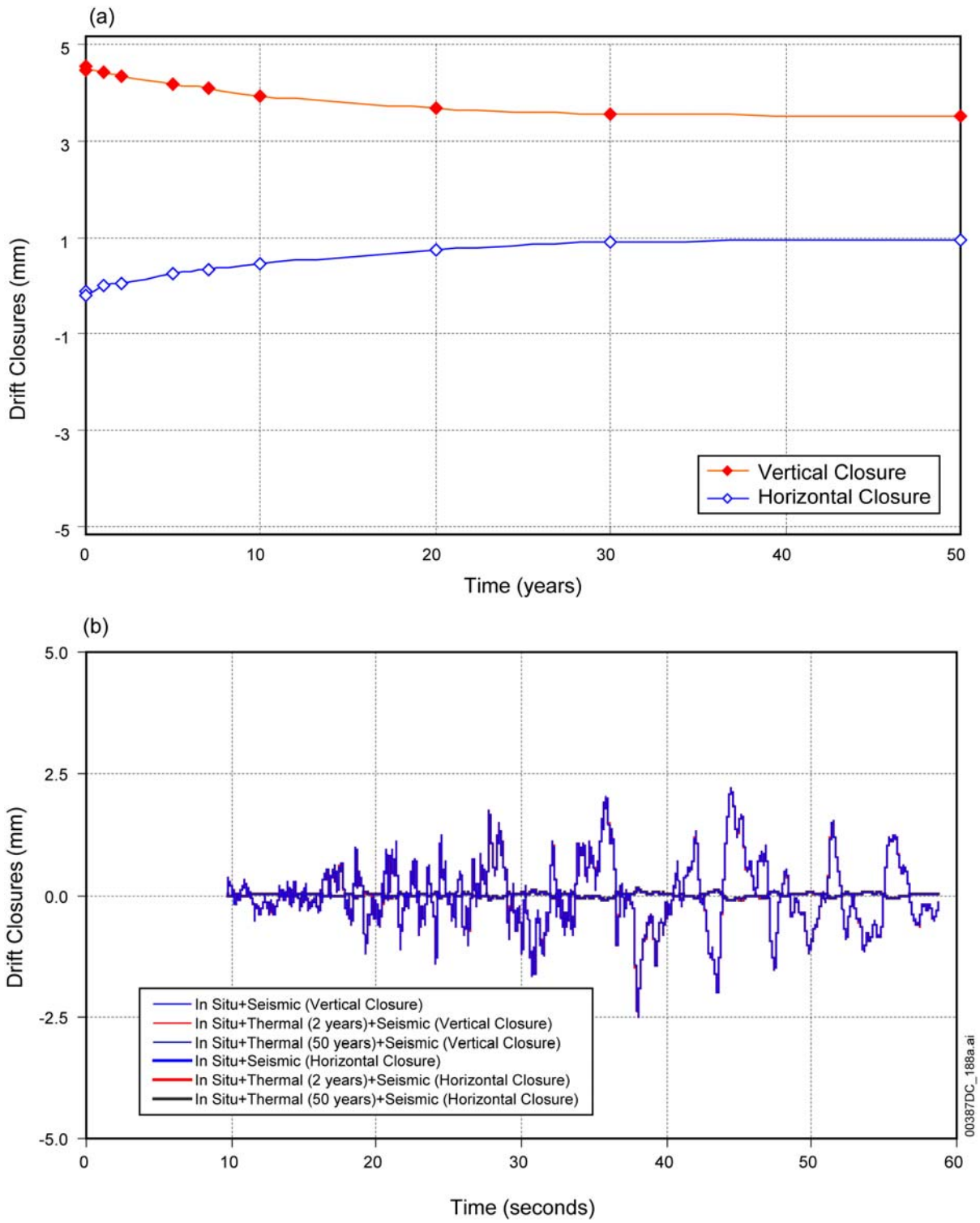

Source: BSC 2004a, Figure 6.1-16.

NOTE: The displacement values shown in (b) are initialized prior to seismic shaking.

Figure D-5. Drift Closures for Various Load Combinations (Category 5 and K_0 = 0.3): (a) In Situ plus Thermal; (b) In Situ plus Seismic and In Situ plus Thermal plus Seismic

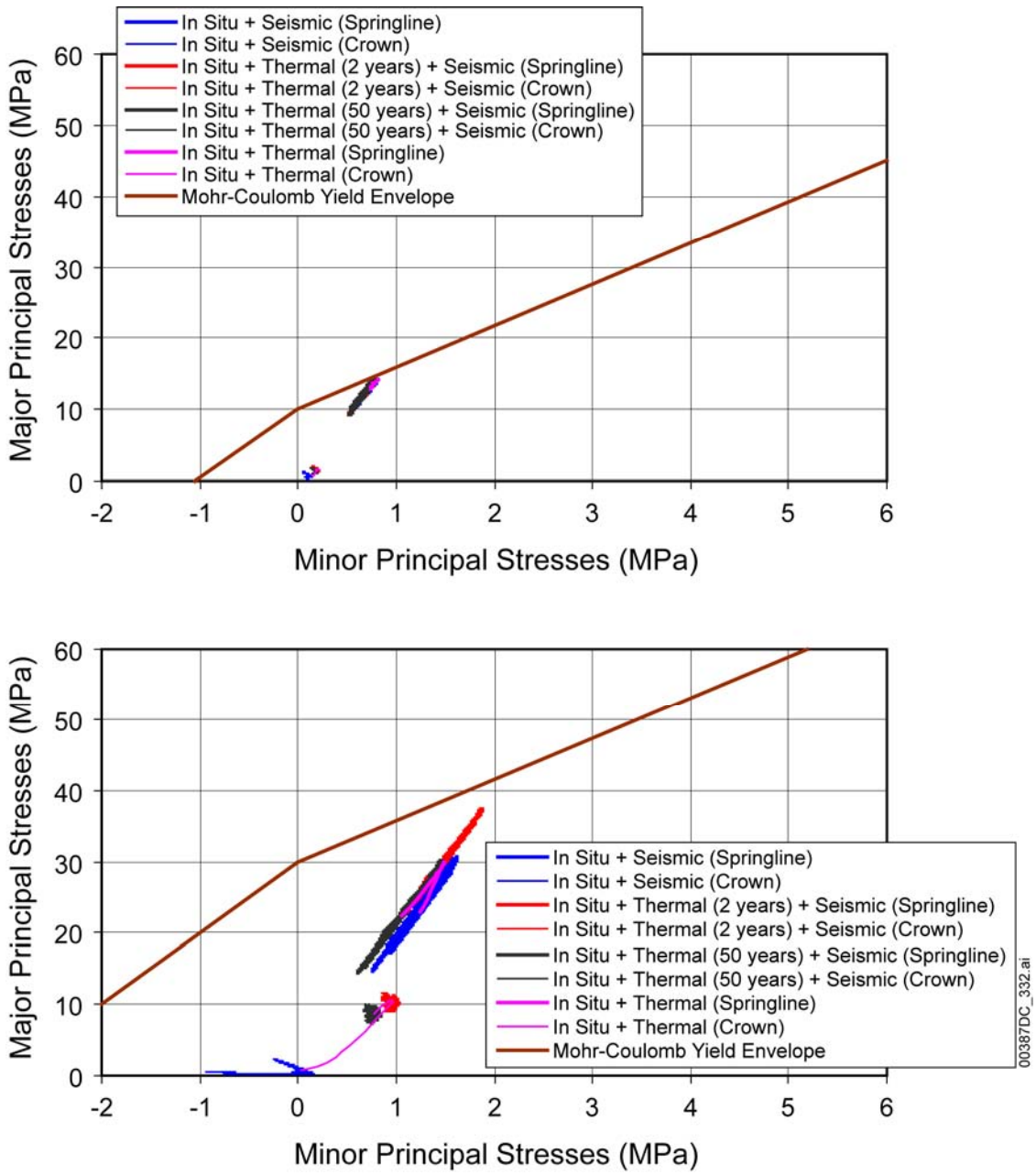

Source: BSC 2004a, Figures 6.1-7 and 6.1-17.

Figure D-6. Stress Paths near Springline and Crown for Various Load Combinations (a) Lithophysal Rock Strength Category 1 (Lowest Strength and Modulus) and (b) Lithophysal Rock Strength Category 5 (Highest Strength and Modulus)

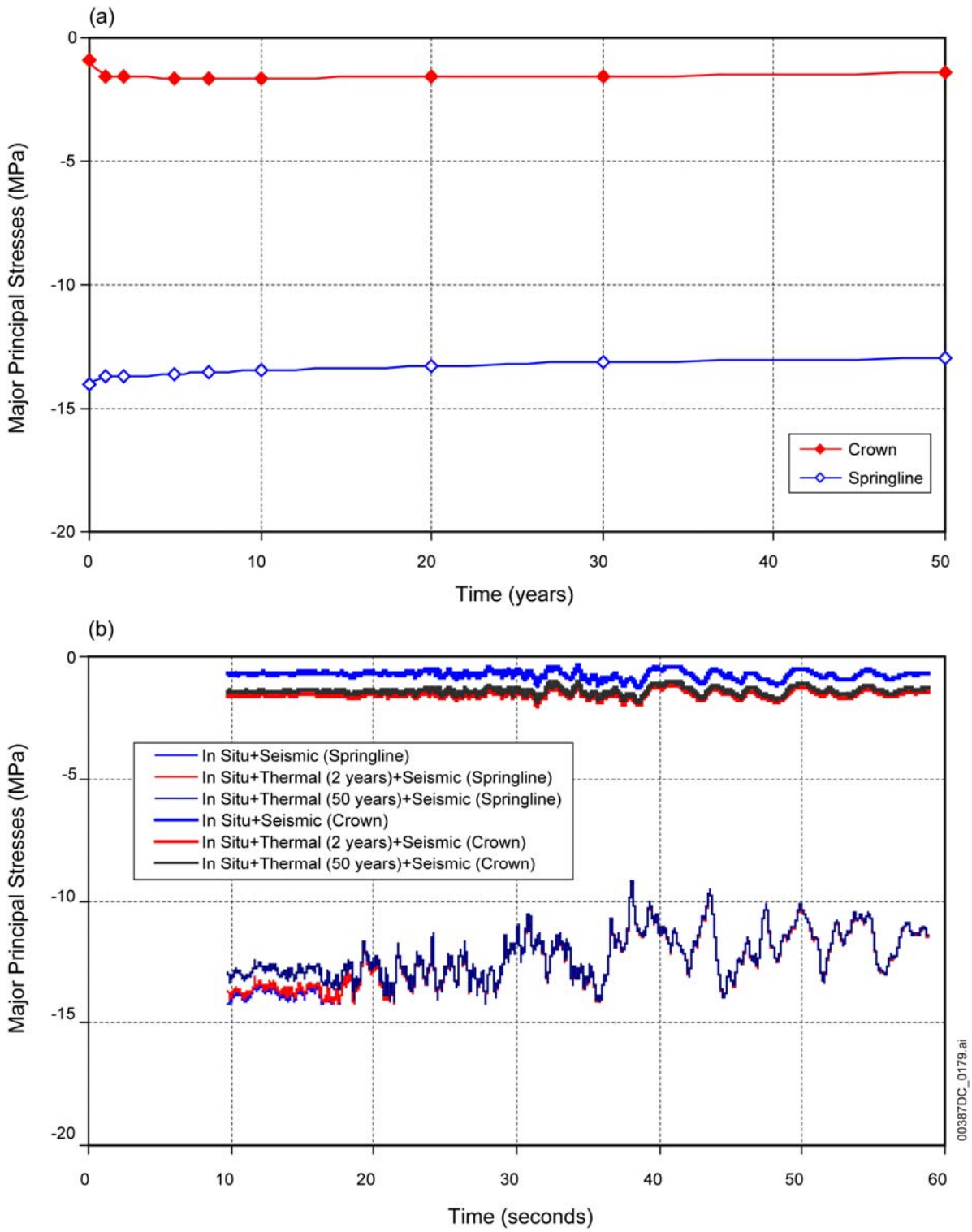

Source: BSC 2004a, Figure 6.1-8.

Figure D-7. Major Principal Stresses near Drift Opening for Various Load Combinations (Category 1 and K_0 = 0.3): (a) In Situ plus Thermal; (b) In Situ plus Seismic and In Situ plus Thermal plus Seismic

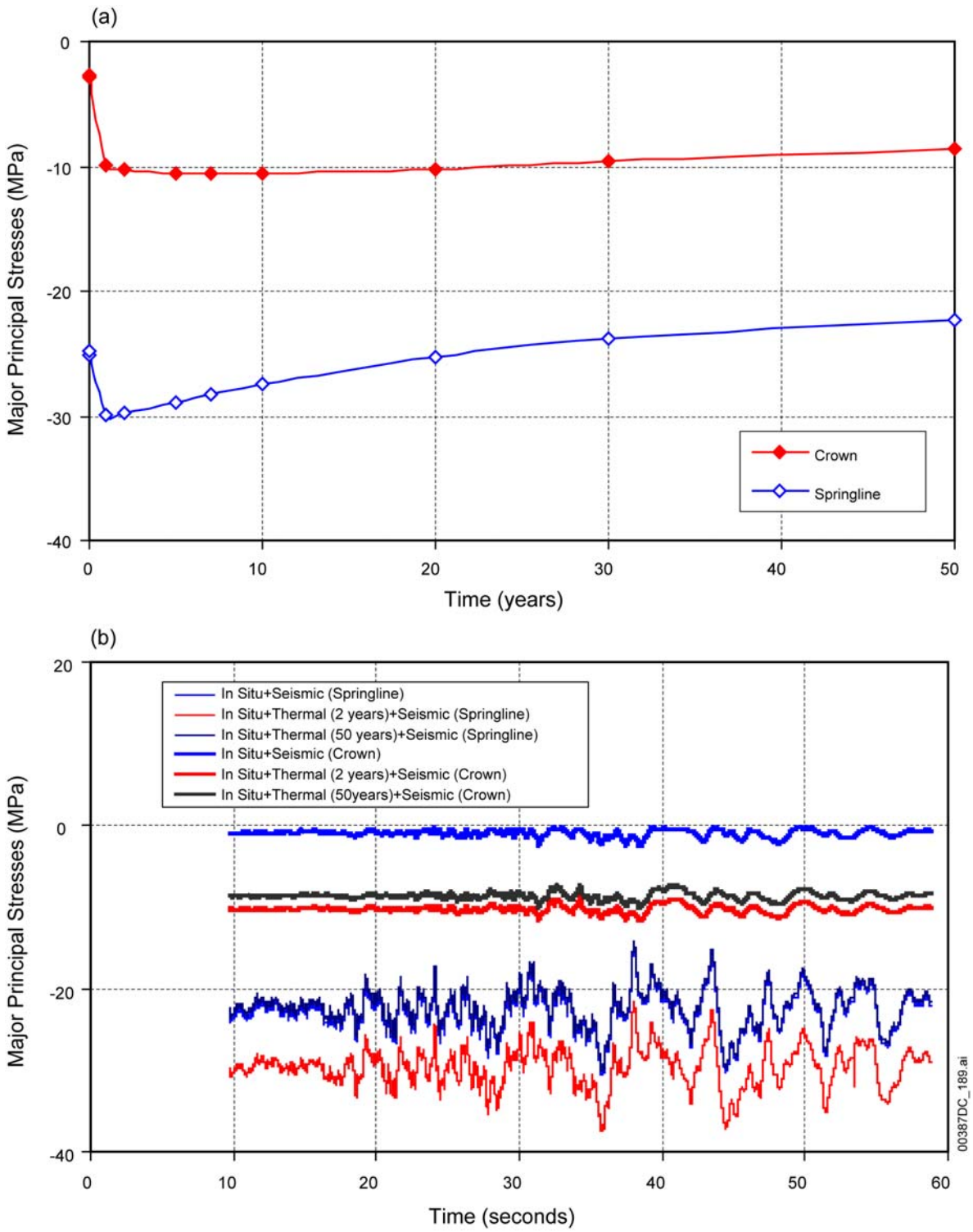

Source: BSC 2004a, Figure 6.1-18.

Figure D-8. Major Principal Stresses near Drift Opening for Various Load Combinations (Category 5 and K_0 = 0.3): (a) In Situ plus Thermal; (b) In Situ plus Seismic and In Situ plus Thermal plus Seismic

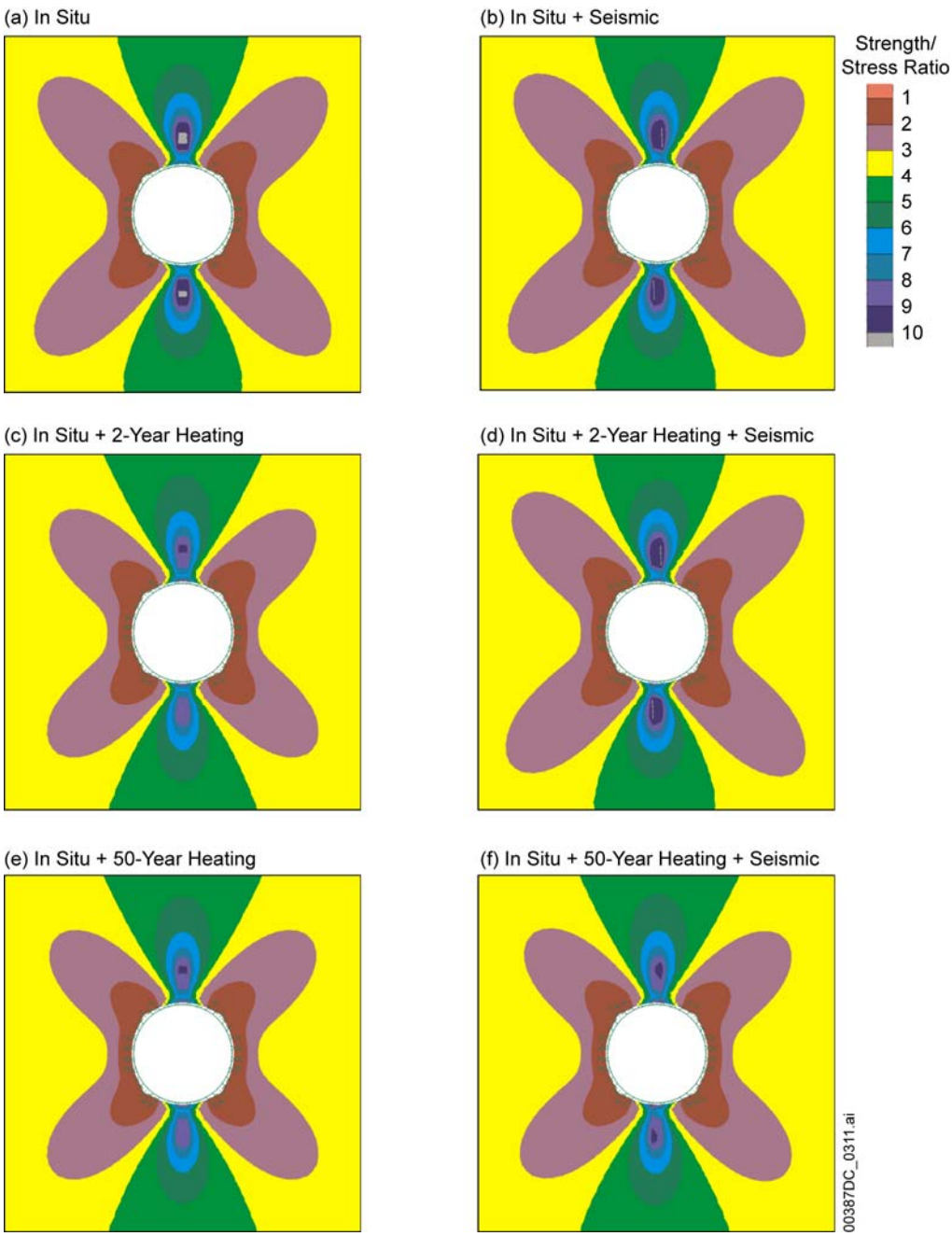

Source: BSC 2004a, Figure 6.1-9.

Figure D-9. Contours of Strength-to-Stress Ratios around Emplacement Drifts under Various Load Combinations (Category 1 and $K_0 = 0.3$)

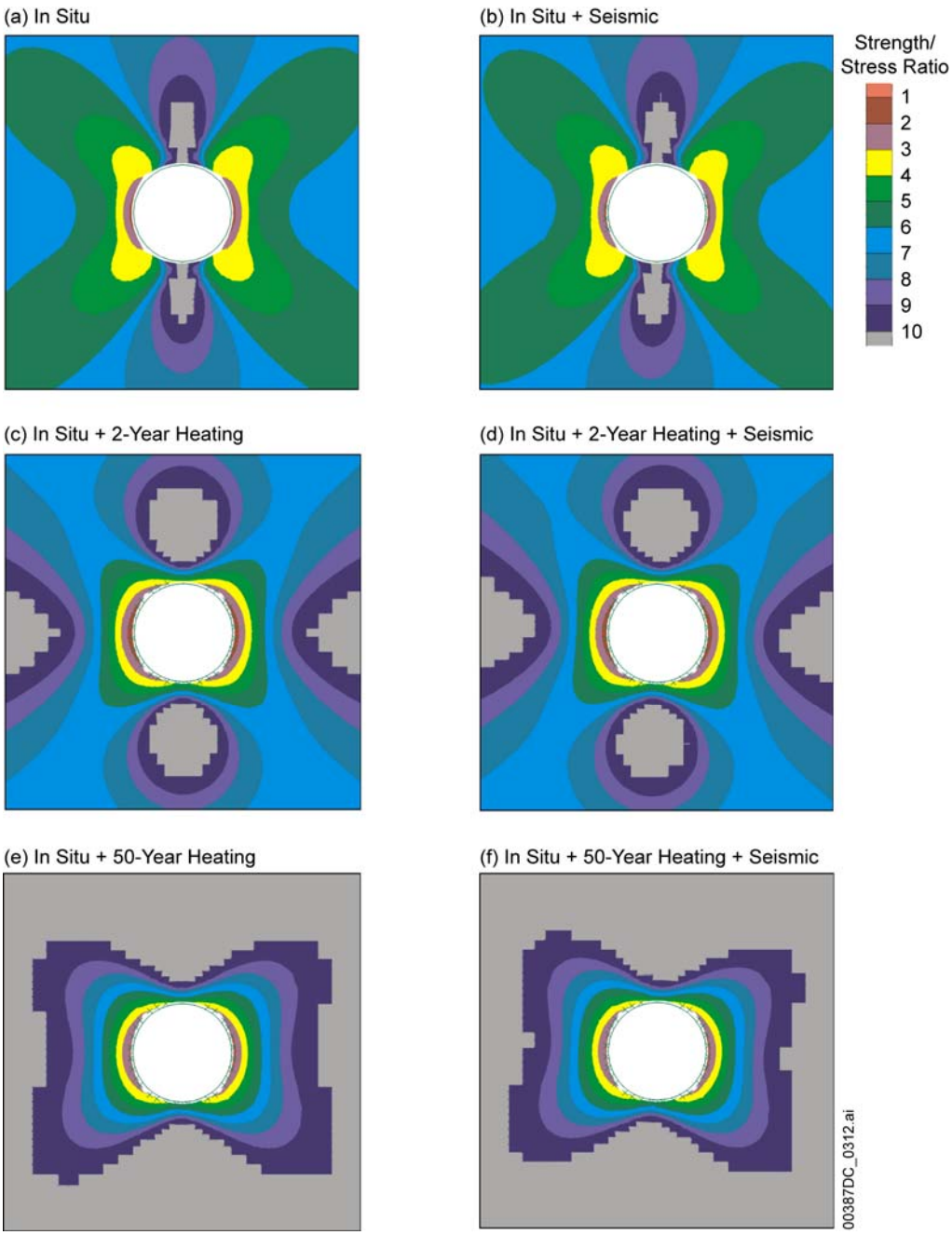

Source: BSC 2004a, Figure 6.1-19.

Figure D-10. Contours of Strength-to-Stress Ratios around Emplacement Drifts under Various Load Combinations (Category 5 and $K_0 = 0.3$)

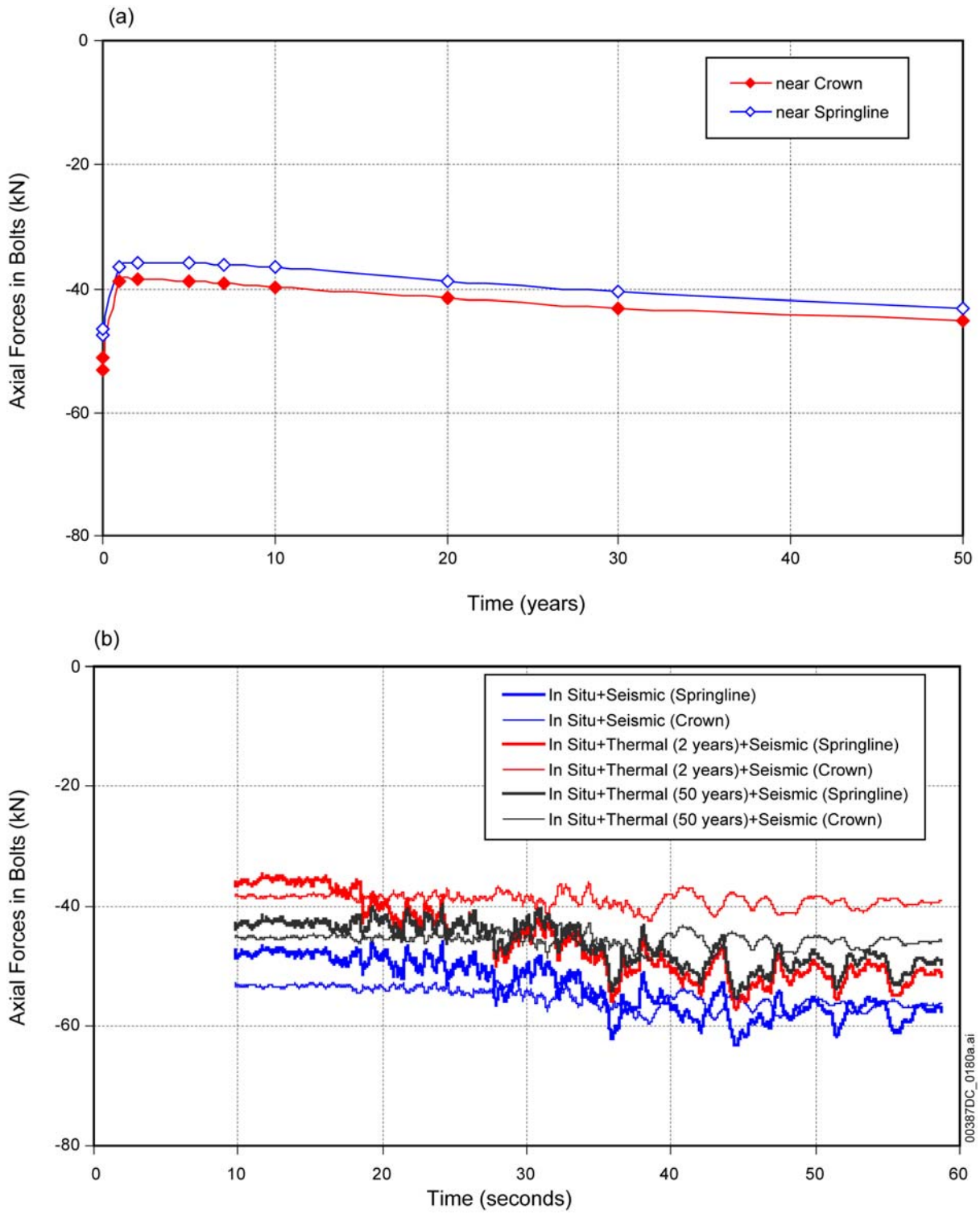

Source: BSC 2004a, Figure 6.1-10.

Figure D-11. Axial Forces in Rock Bolts Installed near Springline and Crown for Various Load Combinations (Category 1 and K_0 = 0.3): (a) In Situ plus Thermal; (b) In Situ plus Seismic and In Situ plus Thermal plus Seismic

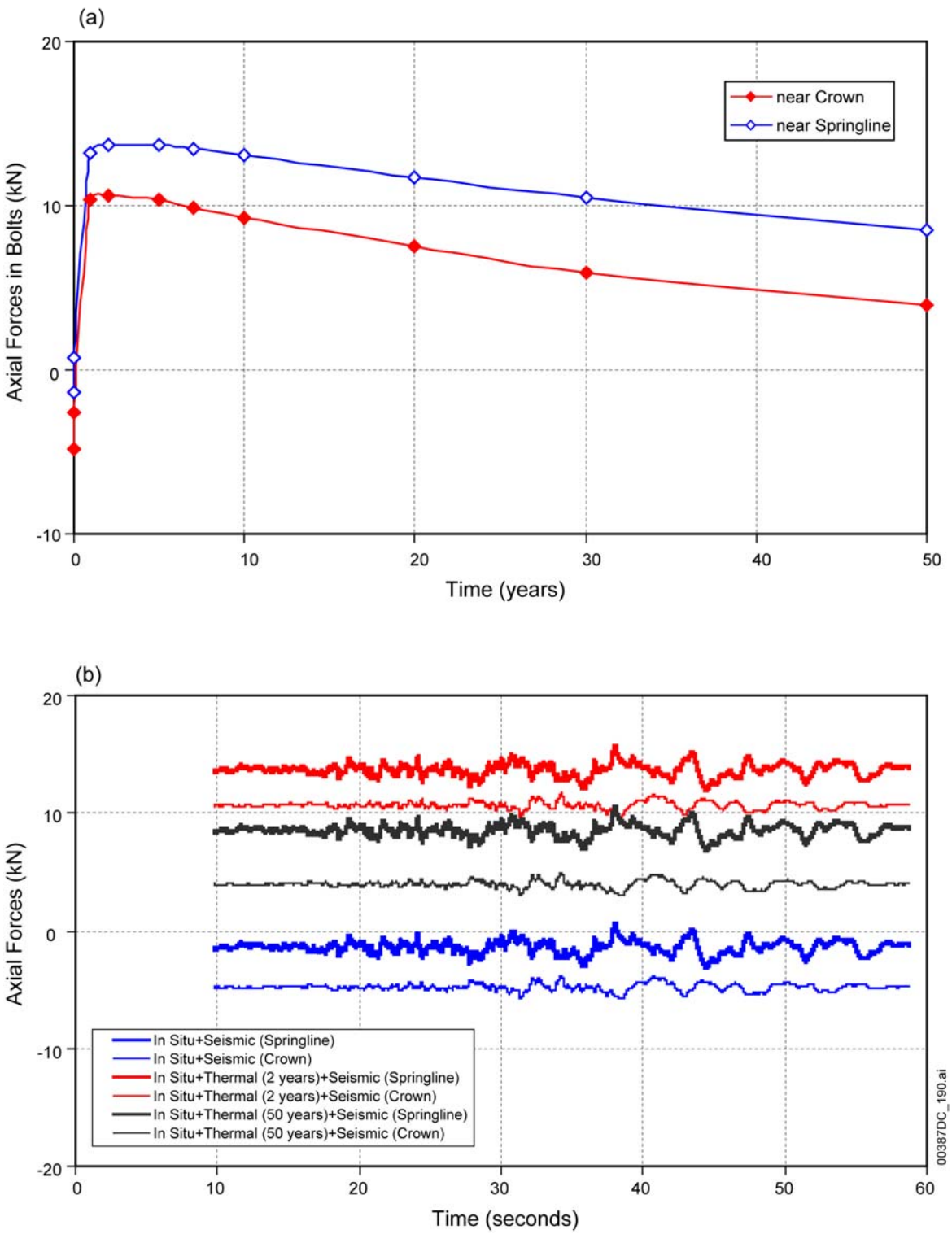

Source: BSC 2004a, Figure 6.1-20.

Figure D-12. Axial Forces in Rock Bolts Installed near Springline and Crown for Various Load Combinations (Category 5 and K_0 = 0.3): (a) In Situ plus Thermal; (b) In Situ plus Seismic and In Situ plus Thermal plus Seismic

D.4.2.4 Uncertainty Associated with Analyses of Load Combination Effect

The following factors may contribute to uncertainties associated with the analyses of load combination effects on the emplacement drift stability and ground support performance:

- Variation of modeling approaches. The analyses presented in this appendix for the RDTME 3.02 agreement are based on a two-dimensional continuum approach. This approach is considered appropriate from the standpoint of ground support design. In the study of drift degradation, a three-dimensional analysis based on a discontinuum approach is used to assess the effect of fractures on rockfall (Sections 5.3.1 and 5.3.2 of this technical basis document) (BSC 2004b). The predictions of potential rockfalls under various load combinations during the preclosure period are provided in Appendix F of this document. The conclusion from these studies is that unsupported drifts in fractured rock subjected to preclosure thermal and seismic loading are stable.

- Variation in thermal properties and ventilation shutdown. Appendix B (Section B.4.2) presents results from BSC 2003b, Sections 6.4.2 and 6.6.2, in which the impact of variability of thermal conductivity, coefficient of thermal expansion, and specific heat on drift stability were examined. The impact of variation of these parameters as well as credible periods of ventilation shutdown on stability of unsupported drifts in the preclosure was found to be negligible.

D.4.2.5 Summary of Analyses for Resolution of RDTME 3.02

The critical preclosure load combinations include in situ plus seismic and in situ plus thermal plus seismic. In the latter load combination, two potentially "critical" thermal conditions are: (1) when the drift wall temperature reaches its peak value, and (2) when the preclosure period ends. These load combinations, as well as bounding ranges in rock mass properties and in situ stress conditions, were considered in the evaluation of emplacement drift stability and ground support performance. The conclusion from these analyses, coupled with similar analyses for unsupported drifts presented in Appendix B, show that the emplacement drifts are stable with a minimum strength to stress ratio of approximately 2 for the lowest strength lithophysal rock.

D.4.3 Basis for Resolution of RDTME 3.10

The emphasis of this agreement concerns the technical basis for using two-dimensional continuum models for evaluation of emplacement drift stability and ground support performance during the repository preclosure period.

D.4.3.1 Methods of Analyses for Ground Support Design

Both empirical and numerical methods are widely used in mining and tunneling industries for design of ground support. The empirical methods are primarily tools for assessing the needs for initial ground support. They may also be used to develop preliminary estimates of the final ground support system(s) to be used. Design issues such as personnel safety, constructibility, and geologic mapping requirements may be factored into the design of the ground support system at this stage. Then, with the aid of computer modeling, the stability of underground openings may be further assessed and the recommended ground support system analyzed.

In the case of a waste repository, evaluation of the stability of emplacement drifts and the performance of ground support relies on numerical methods, due primarily to the complex nature of the combined in situ, thermal, and seismic loads.

Emplacement drifts will be excavated primarily in two different types of densely welded tuff: lithophysal and nonlithophysal (BSC 2003a, Table II-2). The drift response to anticipated loads will depend on the characteristics of rock where the drifts are located. The approaches used in design analyses reflect this difference.

D.4.3.1.1 Consideration of Geologic Features in Choice of Modeling Approach

D.4.3.1.1.1 Analysis for Drifts in Lithophysal Rocks

The application of numerical methods to assessing the stability of repository drifts in the lithophysal rock depends on the rock mass structure, material properties, and failure mechanisms. As discussed in the Section 2.3 of this technical basis document, the characteristics of this type of rock is primarily controlled by the presence of lithophysae and the short fractures interconnecting lithophysae, particularly in the lower lithophysal unit (Board 2003) (Section 3.4 of this technical basis document). Joint sets with a spacing of greater than 2 m also exist, but are not judged to be a key factor that governs the deformation and failure mechanism (BSC 2004b). Since the lithophysae roughly uniformly distributed through the lithophysal units, it is reasonable to assume that a mechanical constitutive model, dependent on porosity and matrix strength properties, can capture the general failure mechanisms. In addition, the lithophysal cavity radius is much smaller than the radius of emplacement drifts. Individual lithophysal cavities will, in general, have negligible impact on the predicted overall stability of the drifts, as long as the effect of lithophysae is accounted for in the properties used in the analysis (see Section 4.2 of this technical basis document for a discussion about the modeling approach for lithophysal rocks). Therefore, it is appropriate to use a two-dimensional continuum approach based on equivalent rock mass properties derived from a constitutive model (Mohr-Coulomb) representing the lithophysal rocks for analysis of stress distribution, deformation and yield estimation. Quantitative analysis of rockfall in emplacement drifts needed for postclosure performance assessment purposes, requires a discontinuum approach to modeling since the continuum approach is not capable of explicit modeling of fracture or detachment of blocks from the rock mass.

In the equivalent continuum approach, the rock structural features such as lithophysae and short-length fractures are not modeled explicitly. Rather, the effects of these features are reflected in the material properties and failure mechanisms defined. The general stress distribution, deformation, and yield predicted by this approach is approximately equivalent to models that explicitly represent the fractures as the overall response of the rock mass is assumed to conform to a Mohr-Coulomb yield condition. Section 4.2 of this technical basis document describes the process of development of rock mass properties and verification of the mechanical constitutive model for lithophysal rock in detail.

D.4.3.1.1.2 Analysis for Drifts in Nonlithophysal Rocks

The strength and modulus of intact blocks of the nonlithophysal rock mass is large in comparison to the applied preclosure stress levels. Primary structural features of the nonlithophysal rocks are four fracture sets with a mean spacing on the order of 1 m or more (see Section 2.3 of this technical basis document). The mechanical response of emplacement drifts in the non-lithophysal rocks is generally assumed to be anisotropic and three-dimensional in nature as the fracture set orientations are not perpendicular and parallel the drift axis. With the discontinuum approach, interaction between joints and rock blocks that are bounded by joints can be simulated explicitly and in detail. The characteristics of joints, such as joint geometry and frequency, are the direct inputs to numerical models. Such detail is necessary when the model is used to explicitly calculate rockfall, as is the case in postclosure performance analysis.

However, when the goal of the analysis is to estimate overall stability of the excavations, and, in particular, to examine stress distributions, deformations and yield potential for ground support estimation, a discontinuum modeling approach is not required. A sophisticated three-dimensional discontinuum model is rarely used in the mining or tunneling industry for ground support design purposes. Typical industrial applications of three-dimensional discontinuum modeling include problems such as examination of the impacts of faults or block detachment in large excavations in blocky ground. Common practice (Hoek 2002) in excavation stability assessment and ground support design is the use of empirical methods based on geotechnical classification for initial support specification. The empirical methods are often supplemented by the use of continuum-based numerical modeling using estimated equivalent rock mass properties for detailed analysis of excavation stability. A two-dimensional model based on the equivalent continuum approach is conventionally accepted for simulating the response of jointed rock mass. The success of the two-dimensional continuum approach is due primarily to the conservatism built in the two-dimensional analysis and the high factor of safety used in most of the conventional tunnel and mining design.

D.4.3.1.2 Consideration of Loading Conditions

In situ stress conditions at the repository host horizon are not isotropic in the horizontal plane. The vertical stress, resulting from overburden gravitational weight, is the major principal stress component. The major horizontal principal stress is estimated to be 62% of the vertical stress acting in the N15°E, whereas the minor horizontal principal stress is estimated to be 36% of the vertical stress acting in the N75°W. This was observed from field in situ stress measurements (DTN: MO0007RIB00077.000). In a two-dimensional analysis, this anisotropic stress condition cannot be simulated. In addition, the emplacement drifts are oriented at an azimuth of 72° (N72°E) (BSC 2003a, Section 5.1.4). This indicates that the drifts are neither perpendicular to nor parallel with the horizontal principal stress components. In a two dimensional, cross-sectional tunnel design analysis, vertical and horizontal stresses are applied to the model horizontal and vertical boundaries. Thus, the drift longitudinal axis is assumed to orient perpendicular to, or parallel with, the principal stresses. The effect of this model simplification on the ground support design depends on how the in situ stress condition is considered in the two-dimensional analysis.

In *Ground Control for Emplacement Drifts for LA* (BSC 2003c), the bounding scenarios of in situ stress conditions were considered for the design calculation of ground support. The horizontal stress was assumed to be isotropic, but horizontal-to-vertical stress ratio (K_0) of 0.3 and 1.0 were used. These were considered the lower and upper bounds of anticipated stress conditions (Sun 2002, Table 3-2). Results from these bounding conditions capture the worst case scenario and, therefore, are considered more conservative than those based on the anisotropic condition.

D.4.3.1.3 Consideration of Drift Behavior

The purpose of the analyses discussed in *Evaluation of Emplacement Drift Stability for KTI Resolutions* (BSC 2004a, Section 6.3), is to examine drift stability to preclosure loading conditions and rock mass property variability. As discussed above, a two-dimensional continuum modeling approach is considered adequate for this purpose. Rockfall induced by preclosure seismic ground motions is examined using three-dimensional discontinuum models (Appendix F). However, for the purposes of emplacement drift ground support design, two-dimensional models are used to predict the drift deformation, stability, and approximate drift strength to stress ratios for bounding ranges of conditions for unsupported drifts. The ground support function and requirements are determined from the deformations and depth of yield from these models in a conventional fashion without explicitly modeling the ground support. As described below, additional modeling is performed in which the rock bolts are represented explicitly within the model to verify their functionality.

In some repository nonemplacement areas, such as intersections, three-dimensional modeling is used to examine stability since the geometry of these areas dictates a three-dimensional stress condition. For this reason, the design analyses for the intersections and other openings where three-dimensional behavior dominates are based on three-dimensional models (BSC 2004c, Section 6.5.1.2).

D.4.3.2 Effect of Ground Support Components in Numerical Model

In general, the rock mass elastic deformation as a result of tunnel excavation is largely complete before rock support is installed because the support is typically installed some distance behind the advancing tunnel face. Thus, the rock support will actually experience only small strains from deformations related to tunnel excavation if the rock mass is not actively yielding. Since elastic conditions are predicted for emplacement drift excavation, the primary loading of tunnel support is the result of preclosure thermal and seismic loading.

Ground support components installed in emplacement drifts, such as proposed rock bolts and perforated steel sheets, also have a very limited effect on the strains and stresses in rock mass predicted in numerical models. The effect is limited because, as a reinforcement member, rock bolts have much lower stiffness compared to that of the rock mass. Therefore, from a practical standpoint, since the emplacement drifts do not undergo yield and significant closure strain, ground support components have negligible impact on the modeled results. Results from the analyses of unsupported emplacement drifts can be used for estimation of drift stability and deformation, and thus provide an indication of the stability state and, therefore, the ground support requirements.

D.4.3.3 Adequacy of Two-Dimensional Modeling

To further demonstrate the adequacy of two-dimensional modeling for evaluation of emplacement drift stability and ground support performance, several comparisons between two-dimensional and three-dimensional analyses are presented below.

D.4.3.3.1 Comparison of Drift and Regional Scale Thermal-Mechanical Analyses

In *Drift Degradation Analysis* (BSC 2004b, Section 6.2 and Appendix C), coupled thermal-mechanical processes in the rock mass surrounding the repository drifts are examined using a drift-scale calculation as well as a coupled regional- and drift-scale calculation.

The drift-scale calculation (both thermal and mechanical) considers an infinite extent (perpendicular and in the direction of the drifts) of the repository. Consequently, the problem is two-dimensional in nature and only a single drift need be included in the calculation with a symmetry boundary condition on a plane midway between the emplacement drifts (BSC 2004b, Section 6.2). The thermal part of the drift-scale calculation was performed by the NUFT thermal-hydrology software (LLNL 2002) simulating two-dimensional drift-scale thermal-hydrologic behavior. The temperature history results from the NUFT software calculation were imported to the FLAC code model that calculates the thermal strain and stress around an emplacement drift. Algorithms for importing temperatures from NUFT to other models is described in *Drift Degradation Analysis* (BSC 2004b, Appendix U)

The coupled regional- and drift-scale thermal-mechanical calculation was conducted to support this drift-scale calculation by assessing repository-scale effects, including edge effects and the effects of finite repository size and depth on predicted temperatures and stresses (BSC 2004b, Appendix C) (Section 5.3.1 of this technical basis document). These calculations are three-dimensional, and the analysis was carried out in two steps. First, the regional-scale thermal-mechanical calculation was used to determine temperature and stress changes on the scale of the entire mountain. Second, the drift-scale thermal-mechanical analysis was performed such that boundary conditions for temperature and stress fields (functions of time) were determined from the regional-scale calculation. Thus, this calculation did not use any simplifying assumptions (e.g., infinite extent of the repository) for the boundary conditions. Both components of the regional- and drift-scale thermal-mechanical calculations were performed using FLAC3D (BSC 2002).

Stresses in the drift wall and crown for conditions in the middle of the repository for 10 years after waste emplacement, as predicted by the drift-scale calculations (FLAC) and coupled regional- and drift-scale calculations (FLAC3D), are shown in Figure D-13.

Agreement of the tangential stresses in the crown is good, as seen in Figure D-13. The vertical stress in the wall predicted from the FLAC drift-scale model is slightly higher than that from the FLAC3D coupled regional- and drift-scale calculation, but the difference is not significant.

These results suggest that use of a two-dimensional drift-scale model, as adopted in the ground support design analysis, is justified and is more conservative if loading conditions with bounding loads are considered.

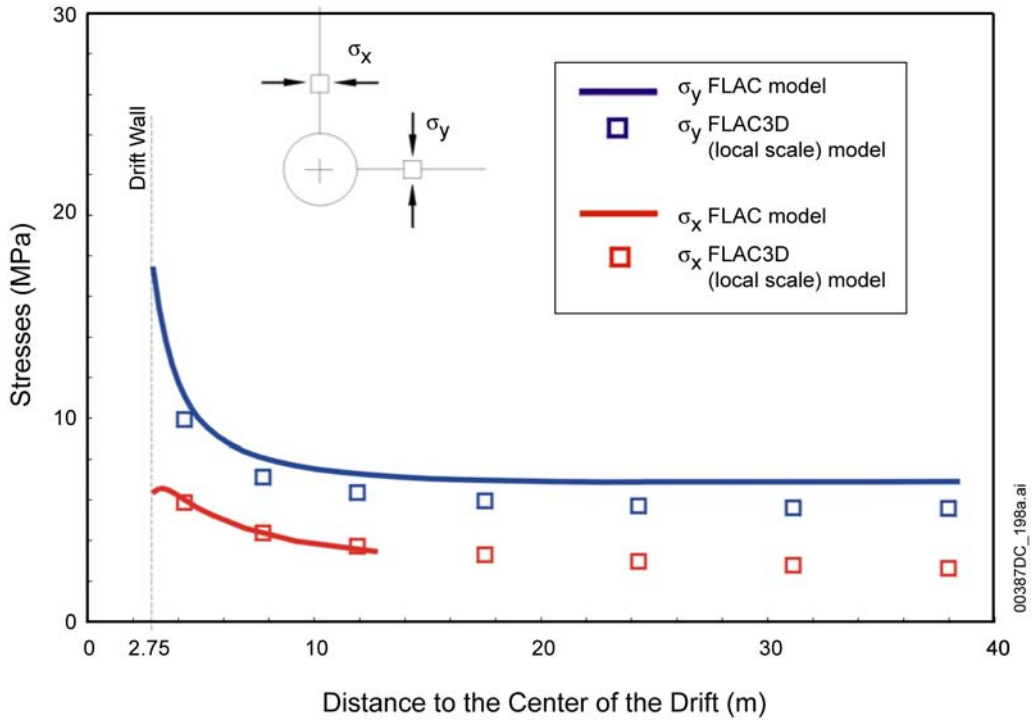

Source: BSC 2004b, Figure 6-34.

NOTE: Stresses shown are positive in compression.

Figure D-13. Comparison between the FLAC Code and FLAC3D Code Predictions of Stresses around the Drift after 10 Years of Heating

D.4.3.3.2 Comparison of Two-Dimensional (FLAC) and Three-Dimensional (FLAC3D) Drift-Scale Mechanical Analyses

FLAC3D Model with Anisotropic Stress Condition–A three-dimensional FLAC3D model based on an anisotropic in situ stress condition was developed (BSC 2004a, Section 6.5.3.2). The major horizontal principal stress is 62% of the vertical stress acting in the N15°E, whereas the minor horizontal principal stress is 36% of the vertical stress acting in the N75°W. In addition, the emplacement drift is oriented at an azimuth of 72° (N72°E). The model is constructed so that the y-axis is parallel to the drift axis (pointing to N72°E), x-axis pointing N162°E, and z-axis upward. The horizontal components of principal stresses are not along x- or y-axes. In addition to the normal stress components, an initial shear component is also defined. To achieve the anisotropic stress condition, the model boundaries are fixed in three orthogonal (x, y, z) directions. Figure D-14 shows a perspective view of model mesh and a horizontal section (plan) view of the initial principal stress field. The orientation of the short bars depicted in Figure D-16b indicates the direction of the horizontal principal stresses. It is evident that an anisotropic stress field is developed, and this stress field is neither perpendicular nor parallel to the drift axis.

The FLAC3D model is run for the in situ stress condition using the lithophysal rock mass properties for rock strength Categories 1, 3, and 5. The predicted drift vertical and horizontal

closures are compared in Figure D-15 with those from FLAC analyses with K_0 values of 0.3, 0.5, and 1.0. Drift closures predicted from the FLAC3D analysis are generally consistent with those from the FLAC analyses using a K_0 value of 0.5. This suggests that the effect of an isotropic stress field with a K_0 value of 0.5 is similar to the actual stress condition (see Section 2.3.3 of this technical basis document). The results also indicate that the scenarios represented by the K_0 values of 0.3 and 1.0 can bound the anticipated stress condition. Using the K_0 values of 0.3 and 1.0 overestimates the vertical and horizontal closures by about 5 mm and 25 mm, respectively, for the weakest rock case (Category 1). Therefore, use of the two-dimensional modeling with the bounding stress conditions is appropriate and justified.

D.4.3.4 Summary of Analyses for Resolution of RDTME 3.10

From the overall preclosure drift stability and ground support design perspective, use of two-dimensional modeling is conventional and justified as long as the bounding scenarios in terms of loading and rock conditions are considered. However, if the problem of interest is the effect of fractures on rockfalls, three-dimensional analysis based on discontinuum approach is required.

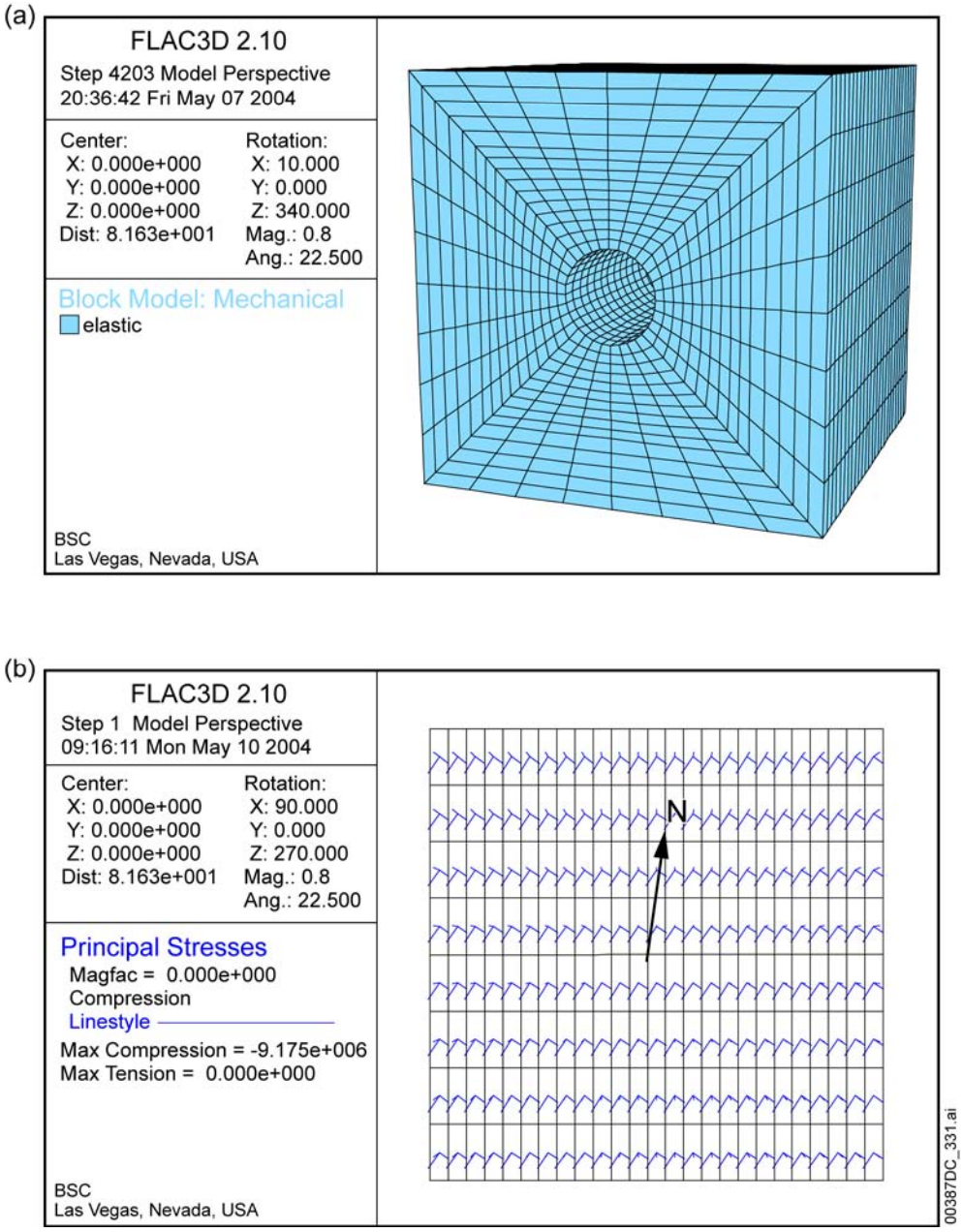

Source: BSC 2004a, Figure 6.5-4.

Figure D-14. FLAC3D Model Mesh and Initial Principal Stress Field

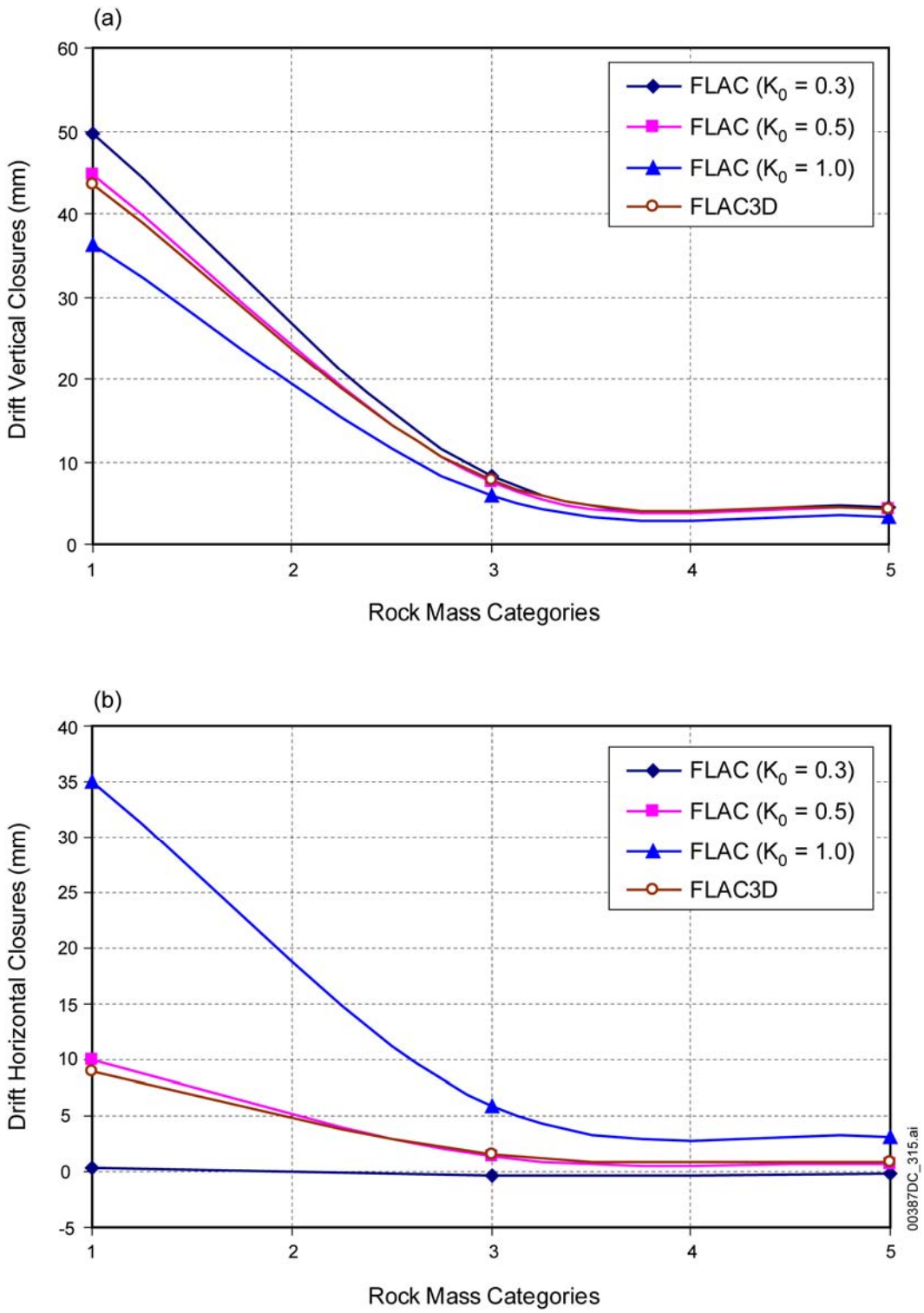

Source: BSC 2004a, Figure 6.5-5.

Figure D-15. Comparisons of Drift Closures from FLAC and FLAC3D Predictions for Various Rock Mass Categories

D.4.4 Basis for Resolution of RDTME 3.13

As discussed in Section D.4.2, thermal-mechanical analyses of the emplacement drifts were conducted using a drift-scale model truncated at a distance of 50 m above and below the centerline of emplacement drifts (100 m total model vertical dimension). The base of the model was fixed in the vertical direction, whereas the top of the model was prescribed a constant normal traction equivalent to the in situ stress and given no constraint in displacements (see Figure D-3). NRC questioned the appropriateness of such a model in simulating the development of thermally induced stress and believed that the model might allow excessive free upward thermal expansion during heating (NRC 2002, p. 2.1.7-10). To investigate the sensitivity of predicted drift and ground support performance to variations in the model (vertical) dimension and boundary conditions, additional thermal-mechanical analyses have been conducted. Sections D.4.4.1 to D.4.4.3 describe the results obtained from this endeavor.

D.4.4.1 Selection of Model Dimensions and Boundary Conditions

For mechanical analyses of a deep excavation in hard rock (i.e., the diameter of the tunnel is much less than the depth to ground surface), a model dimension equal to about 5 to 10 times the diameter is generally sufficient to preclude boundary effects on mechanical predictions (Itasca Consulting Group 2002, Sections 3.2.1 and 3.3.4.2). This is particularly true when the rock mass behaves in an elastic fashion. It is not necessary to fully extend the top boundary of the model to the ground surface, as long as a normal traction is applied to the top boundary that is equal to the load applied by the remaining overburden. In this case the top boundary is allowed to move in the vertical direction as the stress conditions dictate.

For thermal analyses of the effect of heating that continues more than thousands of years, a large model dimension is required or the boundary is set at the location where the boundary condition is known or can be easily defined. For example, the lateral boundaries for thermal analyses of emplacement drifts are located at the middle of the pillar between two adjacent drifts because these boundaries can be conservatively assumed to be adiabatic due to thermal symmetry. The top and bottom boundaries cannot be located too close to the emplacement drifts because the region of influence by heating in emplacement drifts may eventually extend to the ground surface within thousands of years. A ground surface that is about 400 m from the emplacement drifts as the top boundary is used in the thermal analyses of the ventilation model for predicting the temperatures during the preclosure period (BSC 2004d). To ensure consistency of the thermal-mechanical analyses described here with the thermal analyses of the ventilation model, transient temperature distributions from the ventilation model are imported to the mechanical models used for thermal-mechanical analyses of emplacement drift stability and ground support performance for the license application design (BSC 2003c). The procedure for importing temperatures from the thermal model to the mechanical model are described in (BSC 2004b, Appendix U).

The model output parameters of interest in thermal-mechanical analyses are the principal stresses (and stress path) and displacement in the rock mass adjacent to an emplacement drift during heating. Heating in rock mass is expected to result in thermal strain and stress in the regions at a distance of several times the drift diameter from the drift opening, such as near the middle of pillar or the ground surface. The thermal strain and stress in these regions may not have adverse

effect on emplacement drift stability and ground support performance. So selection of the model dimension should be based on the criterion that the selected dimension is judged adequate if any additional increase in the model dimension with associated boundary conditions has no, or negligible, impact on the calculated principal stresses and excavation wall displacement.

To further examine whether the model dimension used in the thermal-mechanical analyses of ground support design is appropriate, ,sensitivity study was conducted (BSC 2003b, Section 6.2.1). In this sensitivity study, three different total model vertical dimensions, equal to 50, 100, and 200 m, were used.

A total vertical dimension of 50 m (upper and lower boundaries of 25 m from the drift centerline) is considered as a lower bound in terms of the opening size because the top and the bottom boundaries are located at a distance of about five times the drift diameter (5.5 m). Further reduction in the vertical dimension may result in some degree of boundary effect on the results of interest (Itasca Consulting Group 2002). On the other hand, a vertical dimension of 200 m is considered as a reasonable upper bound for the thermal-mechanical analyses.

As shown in Figure D-16, noticeable increases of temperature occur at a distance of 25 m above and below the drift center, while those at a distance of 50 m or 100 m from the drift are less than 1°C over the entire preclosure period. Therefore, results from the model using the upper bound vertical dimension can be used to examine boundary impacts for the base case of a total model dimension of 100 m (50 m up and down from drift centerline) as was assumed for analyses presented in *Evaluation of Emplacement Drift Stability for KTI Resolutions* (BSC 2004a, Section 6.7).

Figure D-17 shows the configurations and meshes of three different models for these additional analyses. To allow comparison, the figure also presents a close-up view of the mesh refinement. It is noted that the mesh sizes within a region of 10 × 10 m around the drift opening are actually identical in these three models.

Boundary conditions for the models with different vertical dimensions are identical, as shown in Figure D-3, except the magnitude of normal traction applied on the top of a model and the prescribed (imported from the ventilation thermal model) transient temperatures on both the top and the bottom boundaries. The normal traction is equivalent to the vertical component of in situ stress at the elevation of the top boundary of a model, and therefore dependent on the overburden thickness above that boundary. For an emplacement drift excavated at a depth of 400 m, the overburden thickness is 375, 350, and 300 m for the model vertical dimensions of 50, 100, and 200 m, respectively. As a result, in situ stresses are the same at any comparable location within the models with different vertical dimensions.

D.4.4.2 Description of Analyses for Examination of the Impact of Model Dimension

Continuum thermal-mechanical analyses based on the models with different vertical dimensions are performed for combined in situ, preclosure thermal, and preclosure seismic loading conditions. The seismic ground motions are applied at 50 years after waste emplacement. The analyses are conducted using lithophysal rock mass properties for bounding strength Categories 1 and 5 and bounding K_0 values of 0.3, 0.5, and 1.0. For comparison purposes, only

the results associated with a K_0 value of 0.5 are presented because the conclusions drawn are applicable to those for K_0 values of 0.3 and 1.0.

D.4.4.2.1 Effects of Model Dimension on Predicted Temperature Distributions

In Figure D-18, temperature contours at 10 and 50 years following waste emplacement are compared for total model vertical dimensions of 50, 100, and 200 m. The transient temperatures from the ventilation model, with 400 m dimension, are imported into all internal elements of these truncated models. However, at the upper and lower boundaries, a constant temperature (at any given time step) is assumed. Therefore, it is possible that slight temperature effects could occur near the boundaries. It can be seen that temperature distributions within comparable regions of the models with vertical dimensions of 100 and 200 m are nearly identical, and only a small degree of discrepancy occurs near the corners of the smallest model (50-m vertical dimension) compared to those in the other two models. This small discrepancy is a result of the boundary effect described previously. Overall, temperatures within an annulus of about 3 to 4 times the drift diameter are not distinguishable among the three models.

D.4.4.2.2 Effects of Model Dimension on Predicted Rock Displacements

Comparisons of the drift closures induced under combined in situ and thermal loads are shown in Figure D-19. There are almost no noticeable differences in both vertical and horizontal drift closures for the Category 1 rock mass. Only a small discrepancy exists for Category 5 rock mass between the predicted closures from the smallest model (50-m vertical dimension) and those from the other two modeled vertical dimensions. It appears that thermally induced rock displacements in the model with a small vertical dimension are slightly more sensitive to elevated temperatures. Results clearly indicate that use of a vertical dimension of 100 m is adequate, and there is no evidence that use of a vertical dimension of 100 m will underestimate the effect of thermal loading conditions.

Drift closures due to preclosure seismic ground motions ($1x10^{-4}$ annual exceedance) that occur at 50 years after heating are shown in Figure D-20. As shown, the effect of model size variations is negligible.

D.4.4.2.3 Effects of Model Dimension on Predicted Stress Changes

Time histories of the major principal stresses at locations for models of various dimension are shown in Figure D-21. Similar to what is observed for the drift closures, changes in the model dimension only have an impact on the smallest model when used in conjunction with Category 5 rock mass properties. Increase in the model size beyond 100 m has no, or minimal effect on stress. These can also be observed from the stress paths, shown in Figure D-22.

Also included in Figure D-22, are the stress paths at locations about 6 m from the wall measured horizontally and 4 m from the crown measured vertically. The differences among these three models are negligible.

The effect of preclosure seismic ground motions ($1x10^{-4}$ annual exceedance) on stresses is shown in Figure D-23. Results indicate that the predicted changes of stresses due to ground motions are nearly independent of the model dimension.

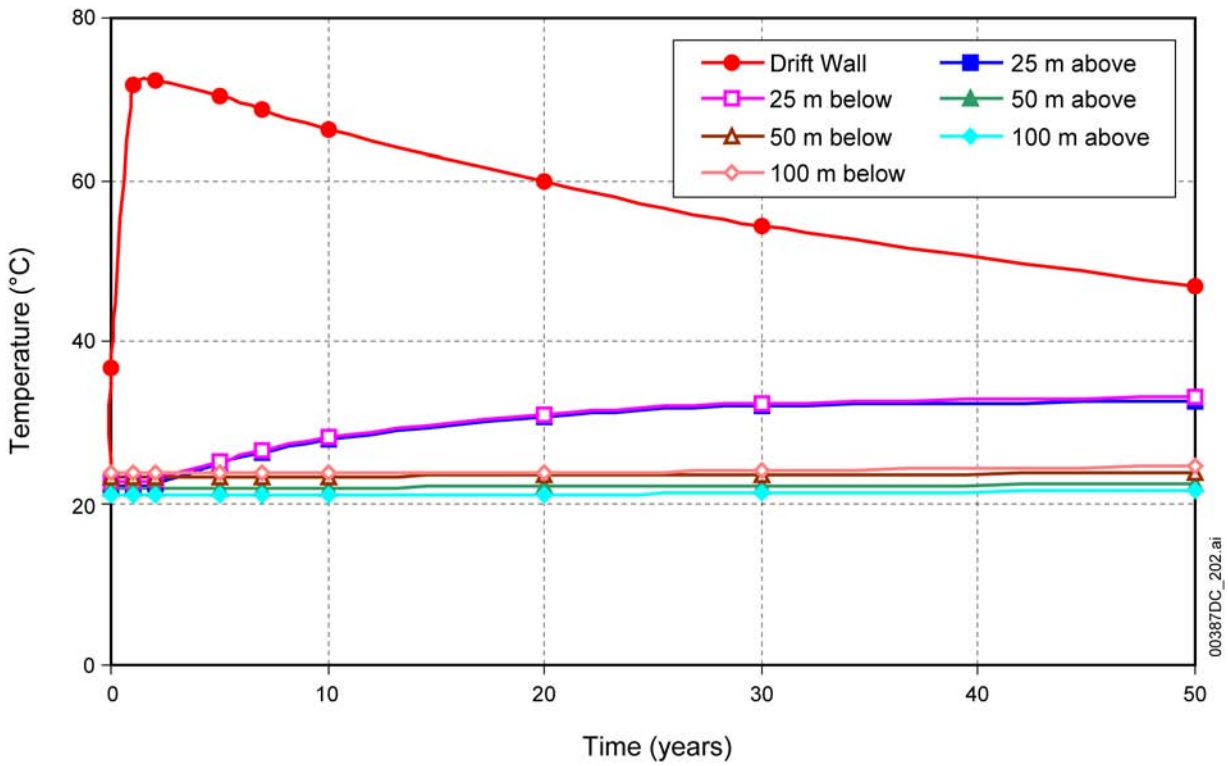

Source: BSC 2004a, Figure 6.7-1.

Figure D-16. Time Histories of Rock Temperatures on Model Boundaries

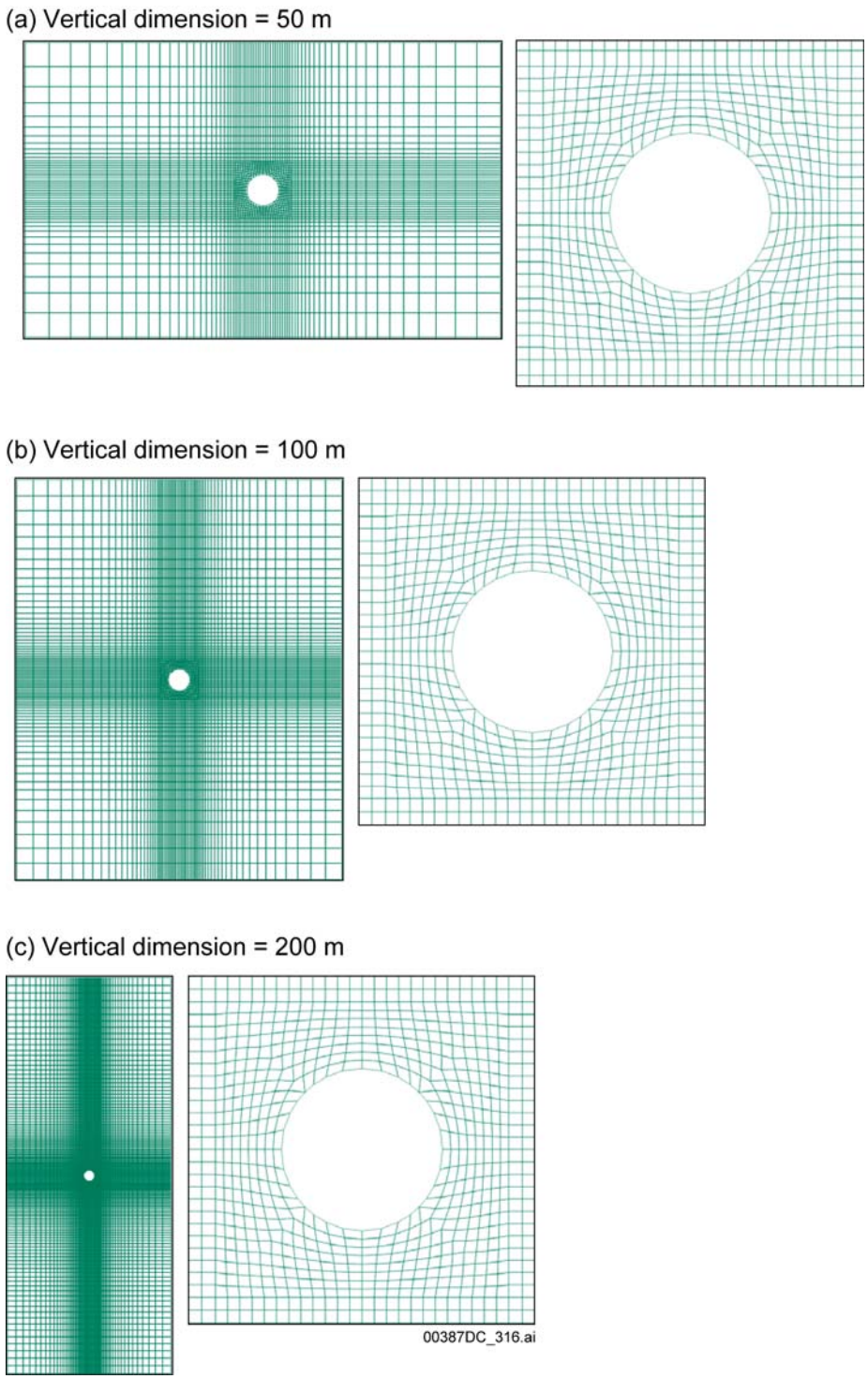

Source: BSC 2004a, Figure 6.7-2.

Figure D-17. Comparisons of Configurations and Meshes for Models with Different Vertical Dimensions

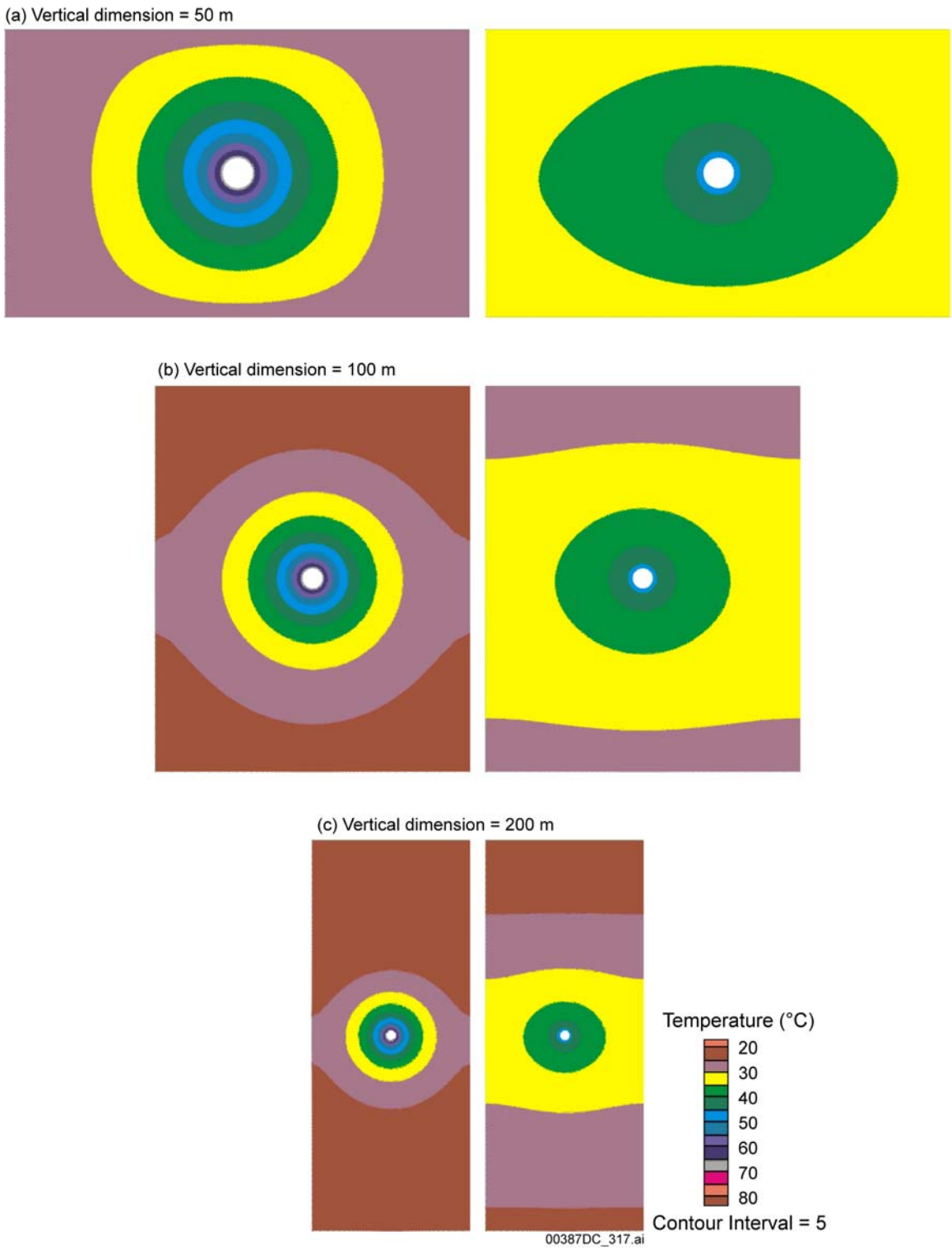

Source: BSC 2004a, Figure 6.7-4.

Figure D-18. Comparisons of Temperature Distributions in Models with Different Vertical Dimensions at 10 and 50 Years after Waste Emplacement

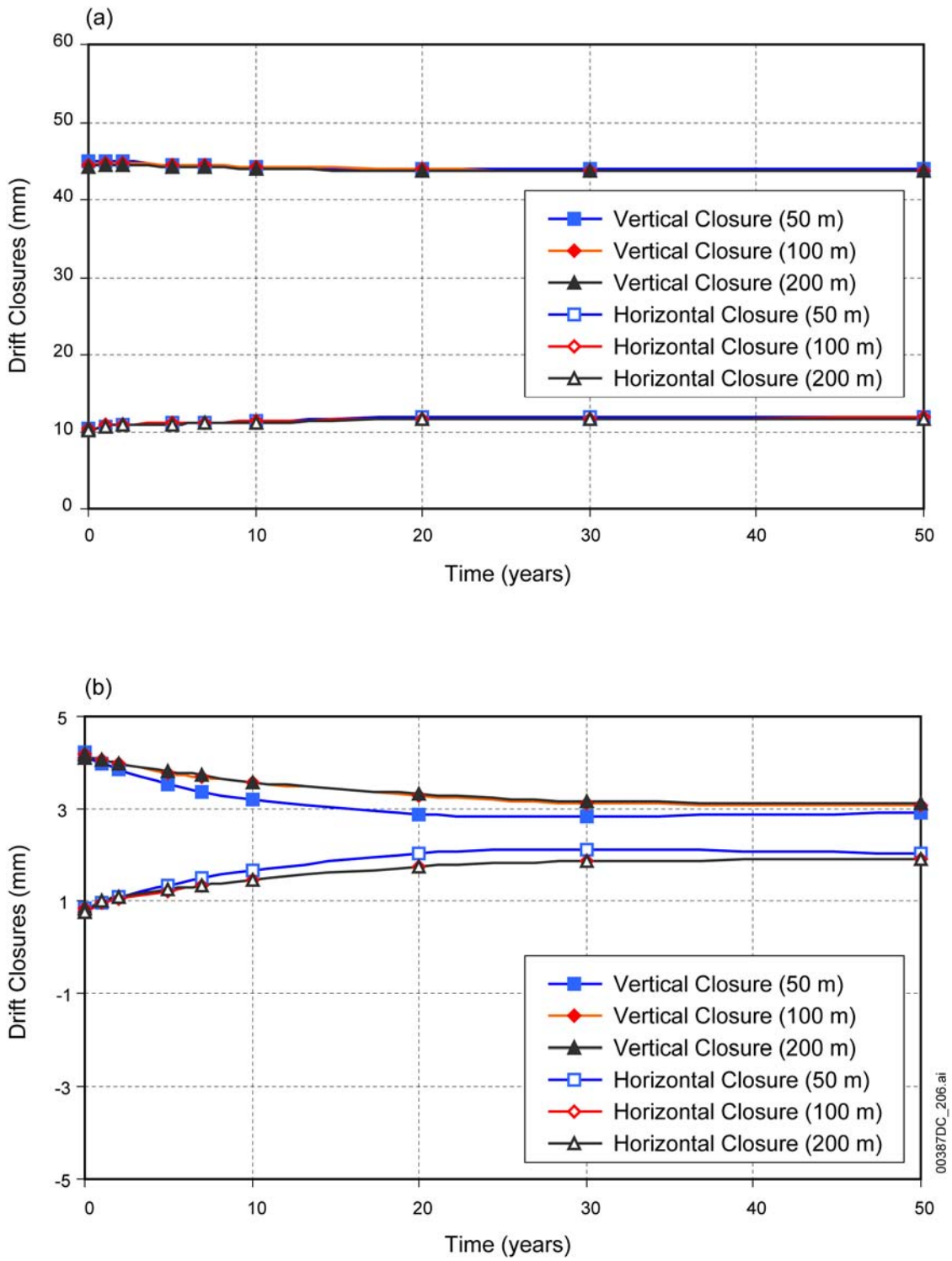

Source: BSC 2004a, Figure 6.7-5.

Figure D-19. Comparisons of Drift Closures for Models with Different Vertical Dimensions

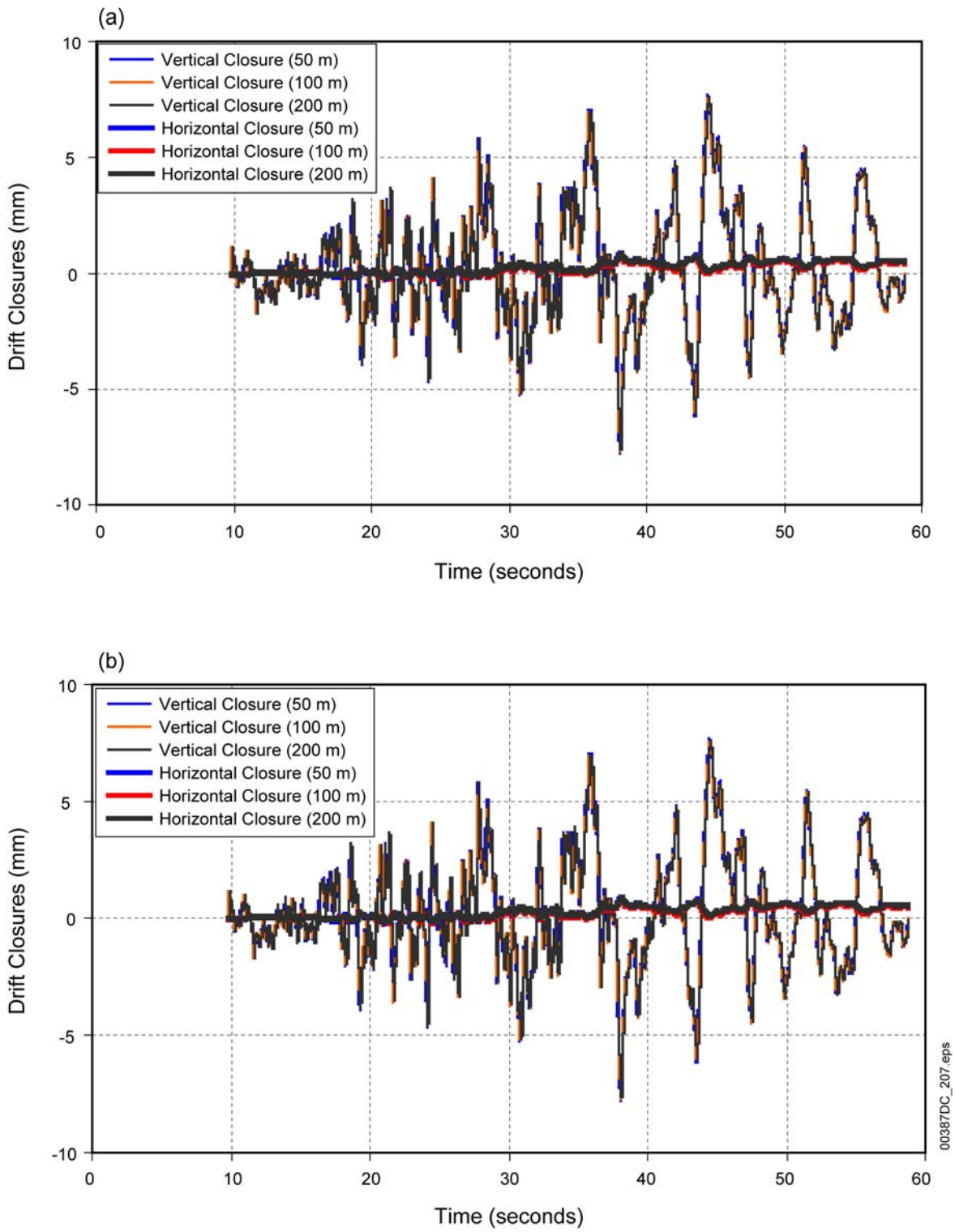

Source: BSC 2004a, Figure 6.7-6.

Figure D-20. Comparisons of Drift Closures under Seismic Ground Motions for Models with Different Vertical Dimensions

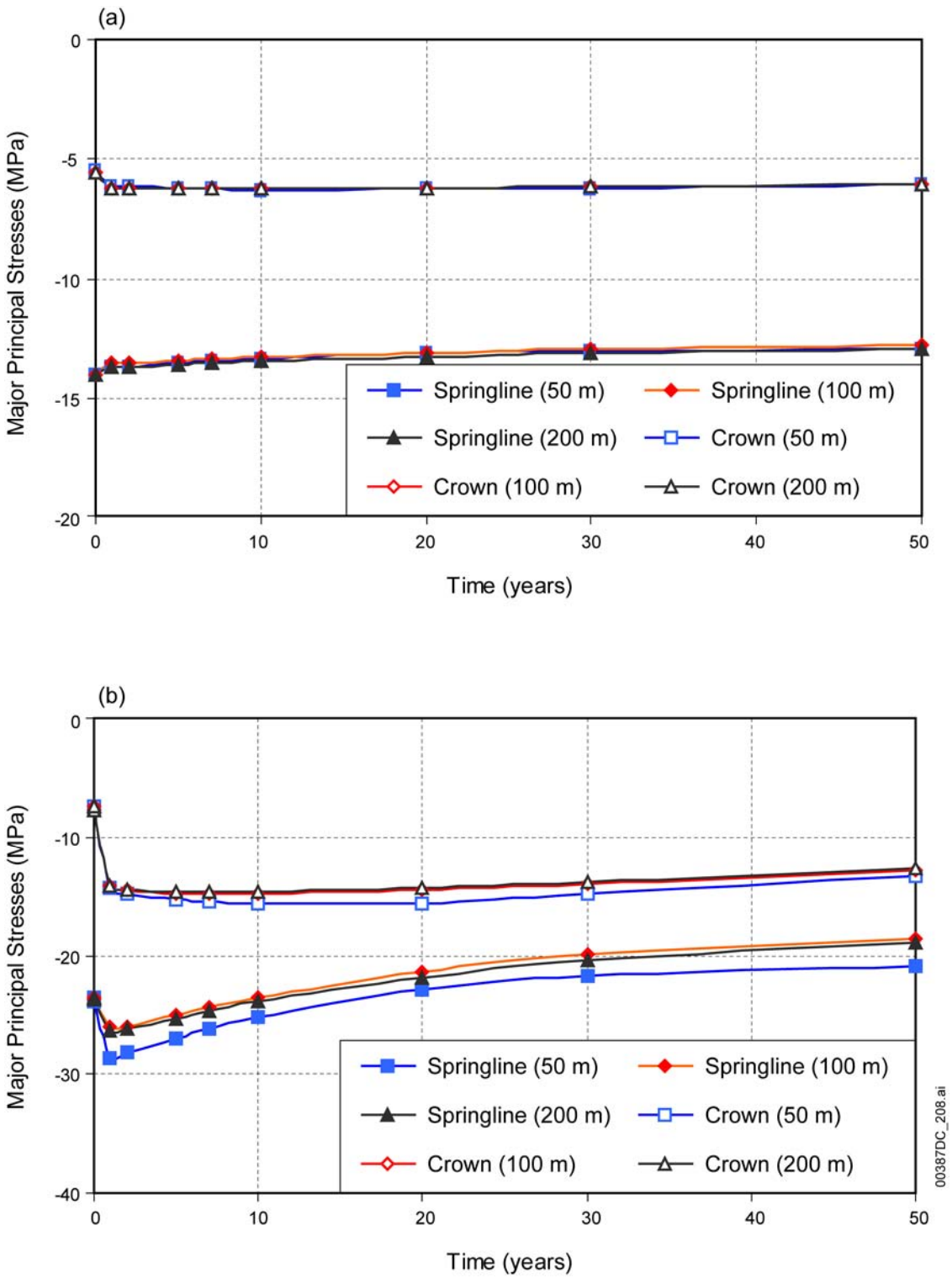

Source: BSC 2004a, Figure 6.7-13.

Figure D-21. Comparisons of Major Principal Stresses for Models with Different Vertical Dimensions

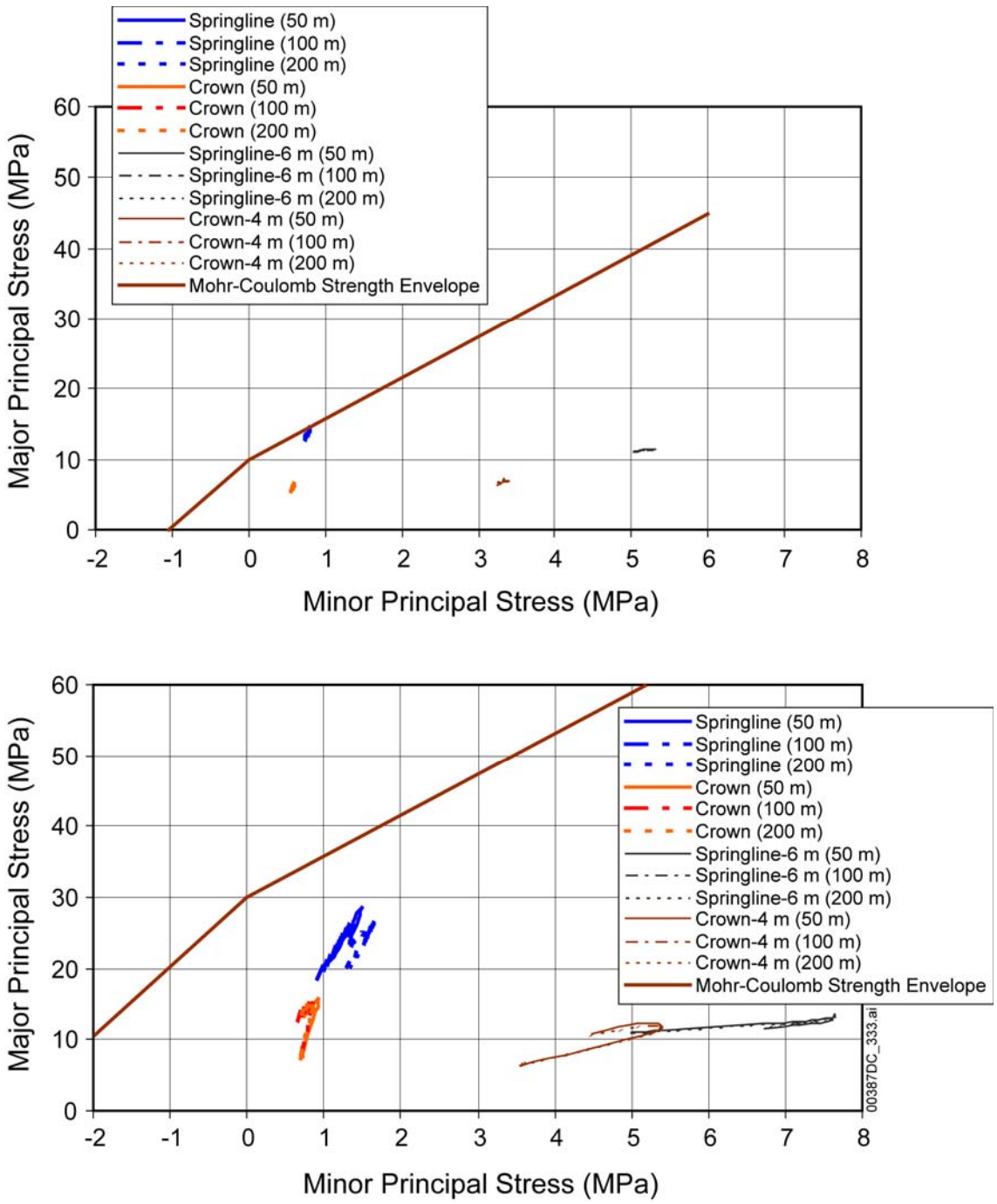

Source: BSC 2004a, Figure 6.7-14.

Figure D-22. Comparisons of Stress Paths for Models with Different Vertical Dimensions

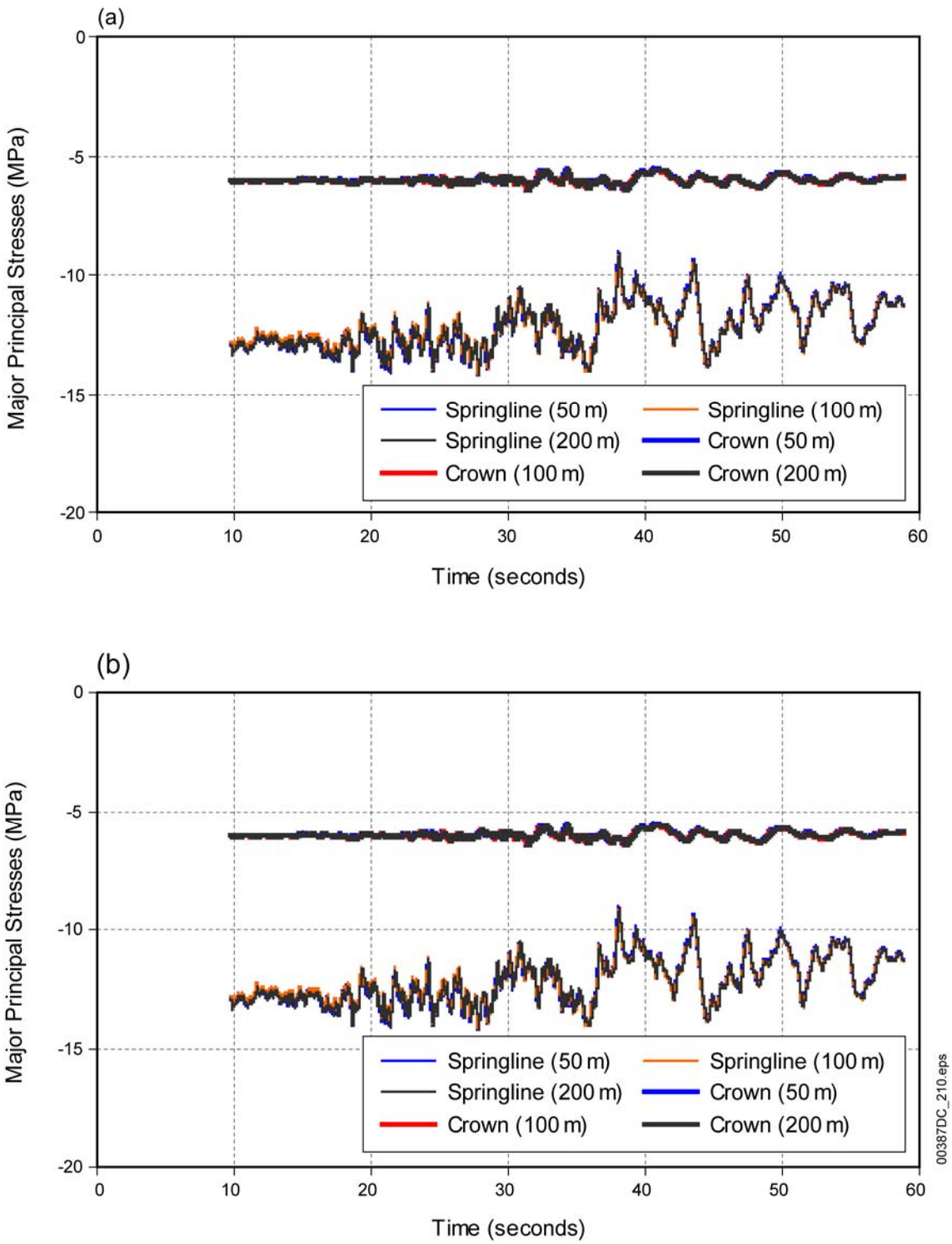

Source: BSC 2004a, Figure 6.7-15.

Figure D-23. Comparisons of Major Principal Stresses under Seismic Ground Motions for Models with Different Vertical Dimensions

D.4.4.2.4 Effects of Model Dimension on Predicted Strength to Stress Ratios for the Rock Mass Surrounding Emplacement Drifts

Contours of strength-to-stress ratios for emplacement drifts from different model dimensions are compared in Figures D-24 and D-25 at 50 years after waste emplacement. The minimum strength to stress ratio ranges from about 2 for drifts in the weakest lithophysal rock (Category 1) to greater than 4 in the strongest lithophysal rock (Category 5). In the pillar, the factor of strength to stress ratio is well above 5 for the cases analyzed. The results are consistent among all models and are not sensitive to the model sizes.

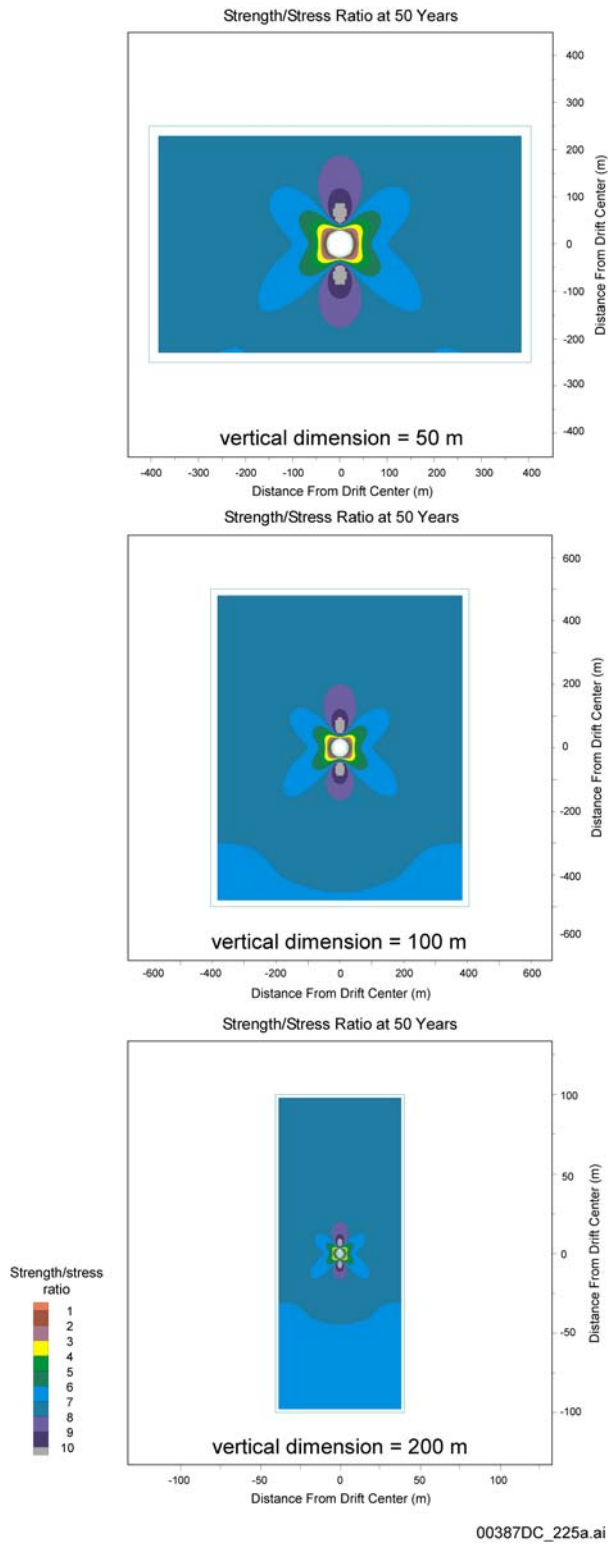

Source: BSC 2004a, Figure 6.7-18.

Figure D-24. Comparisons of Strength-to-Stress Ratios at 50 Years after Waste Emplacement in Models with Different Vertical Dimensions (Category 1, $K_0 = 0.5$)

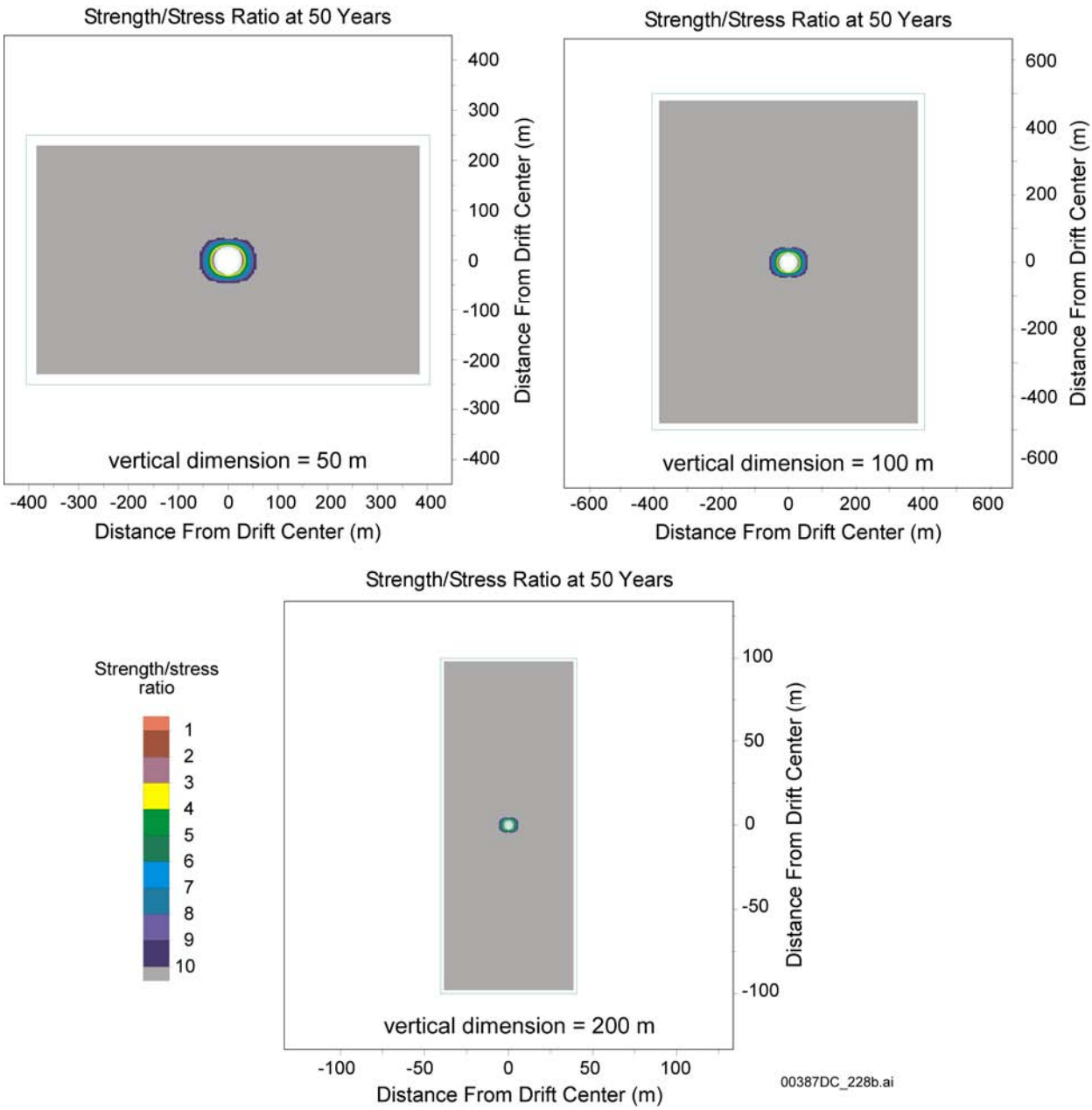

Source: BSC 2004a, Figure 6.7-27.

Figure D-25. Comparisons of Strength-to-Stress Ratios at 50 Years after Waste Emplacement in Models with Different Vertical Dimensions (Category 5, $K_0 = 0.5$)

D.4.4.2.5 Effects of Model Dimension on Predicted Axial Force in Bolts

Axial forces in various bolts at different stages of the repository preclosure period are illustrated in Figures D-26 and D-27. By comparing the plots from different models, it can be seen that the predicted axial forces from these models are generally consistent, and the difference is negligible.

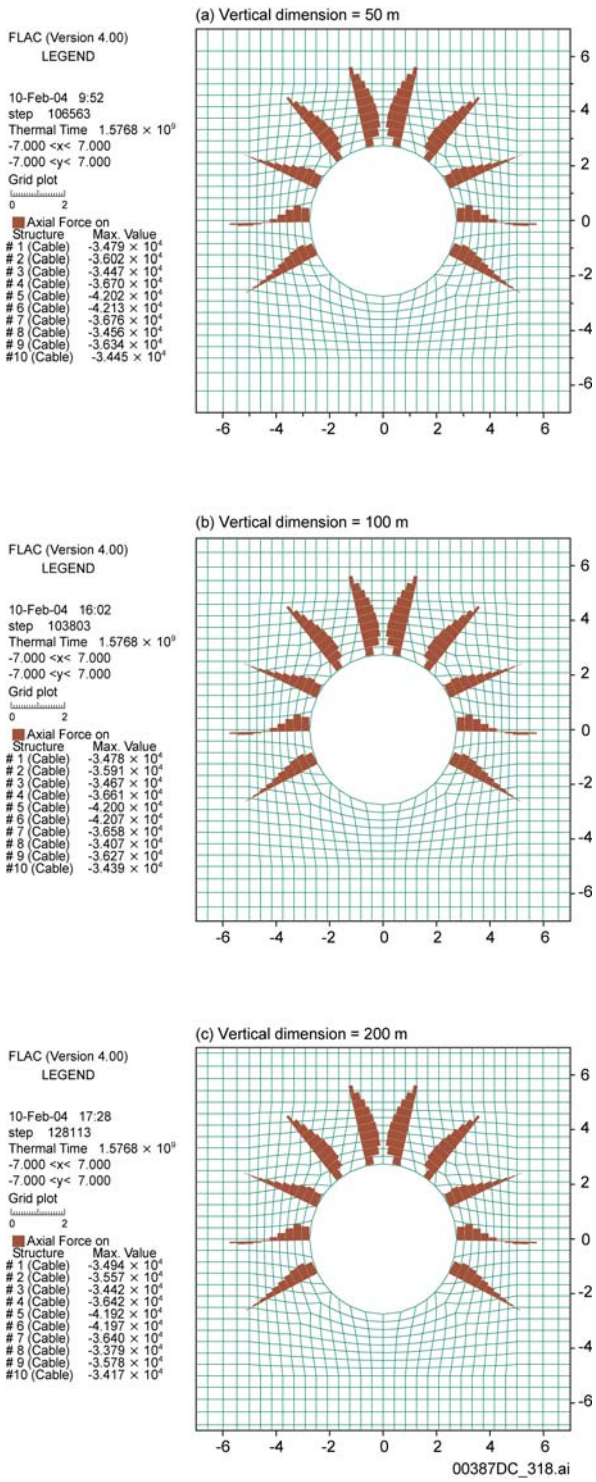

Source: BSC 2004a, Figure 6.7-30.

Figure D-26. Comparisons of Axial Forces (N) in Bolts at 50 Years after Waste Emplacement in Models with Different Vertical Dimensions (Category 1, $K_0 = 0.5$)

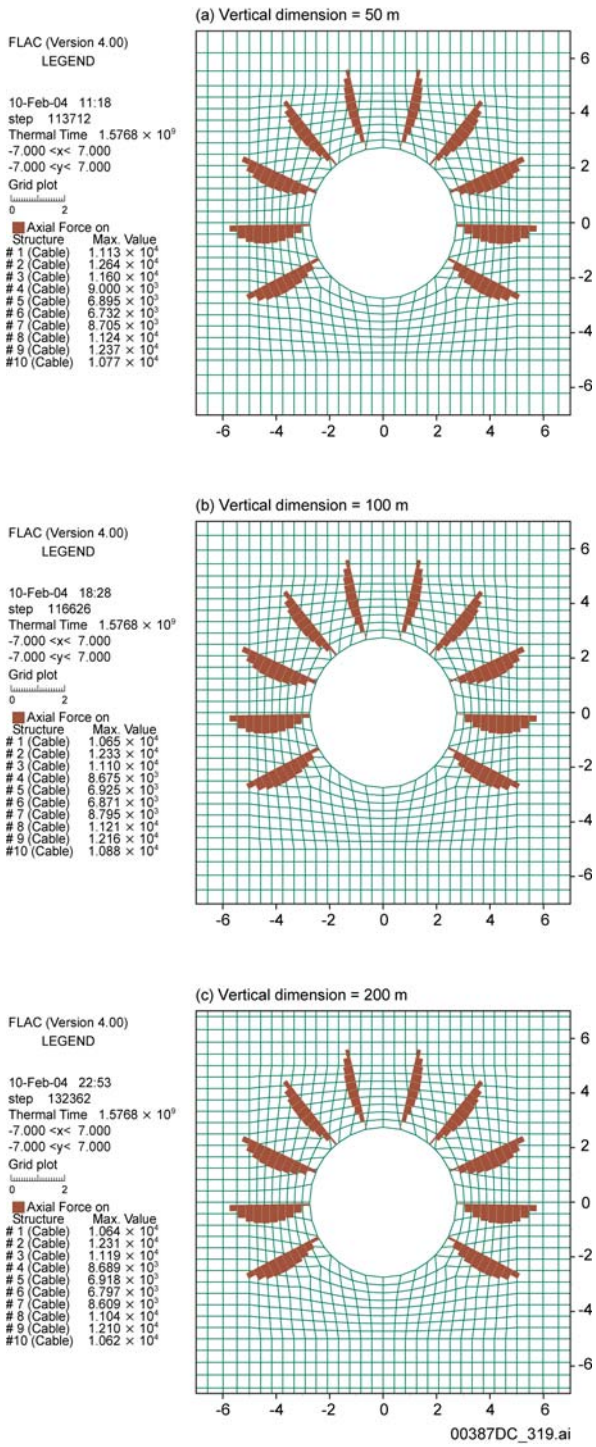

Source: BSC 2004a, Figure 6.7-33.

Figure D-27. Comparisons of Axial Forces in Bolts at 50 Years after Waste Emplacement in Models with Different Vertical Dimensions (Category 5, $K_0 = 0.5$)

D.4.4.3 Effect of Model Dimension on Rockfall Predictions Discontinuum Modeling

The dimension of the three-dimensional discontinuum models becomes an important issue due to the large run times required for conducting the dynamic rockfall analyses. The postclosure rockfall study utilized a base-case 3DEC discontinuum model with a size of $25 \times 27.5 \times 25$ m (BSC 2004b) (Section 5.3.2.1.2 of this technical basis document). The region with detailed fractures imported from the FracMan model is one diameter at the side of the drift and two diameters on top of the drift. Analyses with three model dimensions were conducted to investigate the sensitivity of rockfall prediction to model.

The study indicates that the distinct blocks increase as the model dimension increases. The model, with a dimension smaller than that of the base-case model, underestimates the amount of rockfall, whereas the base-case and the larger models predict roughly the same amount of rockfall. Generally speaking, the base case appears to be adequate to provide a reasonable answer for rockfall (BSC 2004b, Section 6.3.1.6.4).

D.4.4.4 Summary of Analyses for Resolution of RDTME 3.13

The comparisons presented above indicate that use of a model with a vertical dimension of 100 m, in conjunction with the thermal-mechanical boundary conditions described here is adequate to minimize boundary influence. Additional increase in the model dimension beyond this level does not significantly improve the accuracy of prediction of emplacement drift performance. Reduction in the total model vertical dimension from 100 m to 50 m results in an overestimate of the drift closures and stresses near the drift opening. A total model dimension of 100 m was used as the base case condition in ground support analysis studies presented in *Evaluation of Emplacement Drift Stability for KTI Resolutions* (BSC 2004a, Section 6.7.

In conclusion, assuming a free-moving boundary located at 50 m above the drift centerline, coupled with importing temperatures from a large scale ventilation model, are sufficient to minimize both mechanical and thermal boundary effects. Use of the 100 m total model dimension will not result in an underestimate of potential failure mechanisms of emplacement drifts, and therefore, is justified.

D.5 REFERENCES

D.5.1 Documents Cited

Board, M. 2003. *Resolution Strategy for Geomechanically-Related Repository Design and Thermal-Mechanical Effects (RDTME).* REV 00. Las Vegas, Nevada: Bechtel SAIC Company. ACC: MOL.20030708.0153.

BSC (Bechtel SAIC Company) 2001. *Ground Control for Emplacement Drifts for SR.* ANL-EBS-GE-000002 REV 00 ICN 01. Las Vegas, Nevada: Bechtel SAIC Company. ACC: MOL.20010627.0028.

BSC 2002. *Software Code: FLAC3D.* V2.1. PC/WINDOWS 2000/NT 4.0. 10502-2.1-00.

BSC 2003a. *Underground Layout Configuration*. 800-P0C-MGR0-00100-000-00E. Las Vegas, Nevada: Bechtel SAIC Company. ACC: ENG.20031002.0007.

BSC 2003b. *Scoping Analysis on Sensitivity and Uncertainty of Emplacement Drift Stability*. 800-K0C-TEG0-00600-000-000. Las Vegas, Nevada: Bechtel SAIC Company. ACC: ENG.20031125.0002.

BSC 2003c. *Ground Control for Emplacement Drifts for LA*. 800-K0C-TEG0-00100-000-00A. Las Vegas, Nevada: Bechtel SAIC Company. ACC: ENG.20031016.0001.

BSC 2004a. *Evaluation of Emplacement Drift Stability for KTI Resolutions.* 800-KMC-SSE0-00200-000-00A. Las Vegas, Nevada: Bechtel SAIC Company. ACC: MOL.20040510.0199.

BSC 2004b. *Drift Degradation Analysis*. ANL-EBS-MD-000027 REV 03A. Las Vegas, Nevada: Bechtel SAIC Company. ACC: MOL.20040513.0081.

BSC 2004c. *Ground Control for Non-Emplacement Drifts for LA*. 800-KMC-SSD0-00700-000-00A. Las Vegas, Nevada: Bechtel SAIC Company. ACC: ENG.20040302.0022.

BSC 2004d. *Ventilation Model and Analysis Report.* ANL-EBS-MD-000030 REV 03 ICN 03, Errata 2. Las Vegas, Nevada: Bechtel SAIC Company. ACC: DOC.20031216.0002; DOC.20040202.0004; DOC.20040325.0003.

Hoek, E. 2000. *Practical Rock Engineering, 2000 Edition.* Toronto, Ontario, Canada: RocScience. TIC: 253544.

Itasca Consulting Group 2002. *Itasca Software–Cutting Edge Tools for Computational Mechanics*. Minneapolis, Minnesota: Itasca Consulting Group. TIC: 252592.

LLNL (Lawrence Livermore National Laboratory) 2002. Software Code: NUFT. V3.0s. Sun/SunO.S. 5.6 & 5.7. 10088-3.0s-01.

NRC (U.S. Nuclear Regulatory Commission) 2002. *Integrated Issue Resolution Status Report.* NUREG-1762. Washington, D.C.: U.S. Nuclear Regulatory Commission, Office of Nuclear Material Safety and Safeguards. TIC: 253064.

Reamer, C.W. and Williams, D.R. 2001. Summary Highlights of NRC/DOE Technical Exchange and Management Meeting on Repository Design and Thermal-Mechanical Effects. Meeting held February 6-8, 2001, Las Vegas, Nevada. Washington, D.C.: U.S. Nuclear Regulatory Commission. ACC: MOL.20010307.0511 through MOL.20010307.0521.

Sun, Y. 2002. *Ground Control Methodology for Emplacement Drifts*. TDR-GCS-GE-000002 REV 00. Las Vegas, Nevada: Bechtel SAIC Company. ACC: MOL.20021118.0097.

Williams, N.H. 2002. "Thermal Inputs for Evaluations Supporting TSPA-LA." Interoffice memorandum from N.H. Williams (BSC) to Distribution, September 16, 2002, 0911024159, with enclosures. ACC: MOL.20021008.0141.

D.5.2 Codes, Standards, and Regulations

10 CFR Part 63. Energy: Disposal of High-Level Radioactive Wastes in a Geologic Repository at Yucca Mountain, Nevada. Readily available.

D.5.3 Data, Listed by Data Tracking Number

MO0007RIB00077.000. In Situ Rock Conditions. Submittal date: 07/18/2000.

MO0306MWDALAFV.000. ANSYS-La-Fine Ventilation. Submittal date: 06/23/2003.

APPENDIX E

SITE-SPECIFIC PROPERTIES OF THE HOST ROCK (RESPONSE TO RDTME 3.04)

Note Regarding the Status of Supporting Technical Information

This document was prepared using the most current information available at the time of its development. This Technical Basis Document and its appendices provide Key Technical Issue Agreement responses that were prepared using preliminary or draft information reflect the status of the Yucca Mountain Project's scientific and design bases at the time of submittal. In some cases this involved the use of draft Analysis and Model Reports (AMRs) and other draft references whose contents may change with time. Information that evolves through subsequent revisions of the AMRs and other references will be reflected in the License Application (LA) as the approved analyses of record at the time of LA submittal. Consequently, the Project will not routinely update either this Technical Basis Document or its Key Technical Issue Agreement appendices to reflect changes in the supporting references prior to submittal of the LA.

APPENDIX E

SITE-SPECIFIC PROPERTIES OF THE HOST ROCK (RESPONSE TO RDTME 3.04)

This appendix provides a response for Key Technical Issue (KTI) agreement Repository Design and Thermal-Mechanical Effects (RDTME) 3.04. This agreement relates to the physical, thermal, and mechanical properties of the host rock used as part of license application activities.

E.1 KEY TECHNICAL ISSUE AGREEMENT

E.1.1 RDTME 3.04

Agreement RDTME 3.04 was reached during the U.S. Nuclear Regulatory Commission (NRC)/U.S. Department of Energy (DOE) Technical Exchange and Management Meeting on Repository and Design Thermal-Mechanical Effects held February 6 to 8, 2001, in Las Vegas, Nevada (Reamer and Williams 2001). There has been no submittal related to this KTI agreement to the NRC.

The wording of the agreement is as follows:

RDTME 3.04

> Provide in the Design Parameter Analysis Report (or some other document) site-specific properties of the host rock, as a minimum those included in the NRC handout, together with the spatial and temporal variations and uncertainties in such properties, as an update to the information contained in the March 1997 Yucca Mountain Site Geotechnical Report. The DOE will: (1) evaluate the adequacy of the currently available measured and derived data to support the potential repository licensing case and identify areas where available data may warrant additional field measurements or testing to reduce uncertainty. DOE will provide a design parameters analysis report (or other document) that will include the results of these evaluations, expected to be available to NRC in FY 2002; and (2) acquire data and/or perform additional analyses as necessary to respond to the needs identified in (1) above. The DOE will provide these results prior to any potential license application.

RDTME Agreement 3.04 appears in the NRC's *Integrated Issue Resolution Status Report* (NRC 2002, Appendix A). This agreement focuses on providing an update to the project rock properties geotechnical database in the form of a geotechnical parameters report. Specific NRC concerns include addressing the uncertainty, spatial variability, and temporal variability of these rock properties at the repository site and identifying where additional data gathering activities or analyses or both may be warranted to reduce the existing uncertainties. The NRC also requested an evaluation of the adequacy of the project geotechnical database for supporting the repository licensing case.

E.1.2 Related Key Technical Issue Agreements

RDTME 3.05 (Appendix A)–This KTI agreement requires the characterization of the rock mass mechanical properties of lithophysal rock, which includes a description of the uncertainty and variability of these properties. Section 3.2.1 of this technical basis document summarizes the site-specific properties of lithophysal rock and Section 4.2 discusses the development of rock mass properties for lithophysal rock. The spatial variability of lithophysal rock properties based on their correlation with rock porosity is addressed in Sections 2.3.2 and 5.3.2.2.

RDTME 3.07–This KTI agreement requires a description of how mechanical intact rock strength is expected to vary over time as a result of sustained loading. The response to the agreement provides a summary of laboratory testing, field investigations, scientific and engineering analyses, and modeling efforts used in estimating and confirming the time-dependent performance of rock mass and rock fracture strength. Section 5.3.2.2.4 discusses many of these issues, and the agreement will be fully addressed separate from this technical basis document.

RDTME 3.08 (Appendix F)–This KTI agreement requires a description of the uncertainty and variability of the fracture geometry in nonlithophysal and lithophysal rocks and a corresponding sensitivity analysis with respect to fracture geometry to establish design uncertainty for ground support design and drift degradation estimates. Sections 3.2, 4.1, and 5.3 discuss these issues.

RDTME 3.15, 3.16, 3.17, and 3.19 (Appendix C)–These KTI agreements require a summary of in situ fracture geometry measurements, including small trace-length fracture data, and a description of the representative modeling of fractures for the repository horizon. They also require a discussion of the uncertainties in the thermal and mechanical properties of rock blocks and fractures, including their long-term degradation. Sections 3.2, 4.1, and 5.3 discuss these issues.

E.2 RELEVANCE TO REPOSITORY PERFORMANCE

The license application will include an adequate summary of thermal-mechanical properties needed for subsurface design, preclosure repository safety analysis, and repository performance after permanent closure. It is necessary to demonstrate that data inputs for license application are a traceable to an appropriate source, are transparent to users of the data, and are sufficient for their intended use. In particular, the NRC regulations employ a risk analysis approach for license application requires that rock property inputs have defined uncertainties, as well as established spatial and temporal variations that can be propagated through the products that support the repository performance licensing case.

To facilitate meeting these objectives, a preliminary collection of site-specific subsurface geotechnical properties and parameters was made and evaluated for its adequacy to support license application. As a result of this evaluation, additional laboratory, field, computational, and geostatistical work was initiated to improve the geotechnical database for lithophysal rock, to better characterize the spatial representations of fractures and rock properties for the repository, and to describe the temporal variation of rock parameters. While this work was being accomplished, a comprehensive effort was made to improve the defensibility of the historical

data and to summarize the important contextual information associated with particular rock parameters in order to ensure appropriate use of the parameters by users of the data. Finally, a current summary of site-specific subsurface geotechnical parameters was prepared by the DOE, including a summary of parameter uncertainties and variability, which updates data in *Yucca Mountain Site Geotechnical Report* (CRWMS M&O 1997). The updated summary of acquired and developed geotechnical properties was issued as *Subsurface Geotechnical Parameters Report* (BSC 2003a) and is supplemented by information found in *Drift Degradation Analysis* (BSC 2004a). Sections 3 and 4 of this technical basis document summarize the characterization of these rock properties.

E.3 RESPONSE

DOE has evaluated the adequacy of the previously available data, acquired additional data to reduce data uncertainty, and published an update of geotechnical data and parameters in *Subsurface Geotechnical Parameters Report* (BSC 2003a). This section describes actions leading to its development.

In 1997, the DOE issued *Yucca Mountain Site Geotechnical Report* (CRWMS M&O 1997). Included in the report were the site-specific data resulting from field and laboratory testing available through June 1996 (CRWMS M&O 1997, p.1-1). This report evaluated the sufficiency of the existing geotechnical data available in the geotechnical database for a viability assessment of constructing a repository at Yucca Mountain, and for license application.

In the ensuing years, substantial effort was made to acquire the additional data considered necessary to support the design and analyses for the license application. These investigative activities encompassed a range of data obtained from a number of sources including field measurements, laboratory testing, in situ testing, numerical modeling, and analytical assessment. Results of historical as well as recent activities were summarized in *Subsurface Geotechnical Parameters Report* (BSC 2003a). The report incorporates the additional data available to the project as of the summer of 2003. The primary source data are based on qualified data obtained within a framework of the DOE quality assurance procedures. Where available, additional (corroborative) data are also presented in *Subsurface Geotechnical Parameters Report* (BSC 2003a).

The general properties focused on in *Subsurface Geotechnical Parameters Report* (BSC 2003a) included fracture geometry parameters; rock density and porosity data; intact rock thermal and mechanical parameters; rock mass quality estimates; and estimated rock mass physical, thermal, and mechanical parameters. Site geology, stratigraphy, stratigraphic nomenclature, and lithostratigraphic structural features are also included to provide a framework for presentation of the rock and rock mass property data.

Subsurface Geotechnical Parameters Report (BSC 2003a) presents simple statistical summaries of parameters where sufficient data are available. Where an incomplete or inadequate understanding of rock behavior and parameters existed, other approaches were used to gain a deeper understanding of rock behavior and to estimate the uncertainty of rock unit parameters. For example, to better understand the mechanical behavior of lithophysal rock, a conceptual model of lithophysal rock was devised, implemented within suitable computational codes, and

used in addition to the large-core test results. In particular, the large core mechanical tests (including room dry and saturated conditions) and computational results were used to relate strength and modulus to lithophysal porosity, which is the primary factor controlling the variability of the mechanical behavior in lithophysal rocks. The spatial variation of mechanical rock properties was then developed using a surrogate porosity process in which field measurements of lithophysal voids were used to build a simple geostatistical model that was then coupled with the property–porosity correlations. Preliminary modeling of time degradation of mechanical rock parameters is presented in Section 5.3.2.2.4 and is fully addressed by response to RDTME 3.07, to be provided separately.

A general discussion of the adequacy of geotechnical parameters for underground design and modeling purposes is given in *Subsurface Geotechnical Parameters Report* (BSC 2003a). The updated summary of laboratory tests, field tests, field mapping, construction records, numerical modeling, and geostatistical modeling provides sufficient supporting rock data for design and analysis needs. Several key geotechnical analysis and modeling reports support the license application. The adequacy of the geotechnical database for these analyses is discussed in Sections 5 and 6 and, individually, in the following reports:

- *Drift Degradation Analysis* (BSC 2004a)
- *Ground Control for Emplacement Drifts for LA* (BSC 2003b)
- *Ground Control for Non-Emplacement Drifts for LA* (BSC 2004b)
- *Scoping Analysis on Sensitivity and Uncertainty of Emplacement Drift Stability* (BSC 2003c).

The information in this report is responsive to agreement RDTME 3.04 made between the DOE and NRC. The report contains the information that DOE considers necessary for NRC review for closure of this agreement.

E.4 BASIS FOR THE RESPONSE

The scope and methodology for achieving an adequate set of site-specific data for characterizing the complex subsurface conditions was progressively developed from a series of geotechnical review panel meetings held in 2001 and 2002, and from work proposals prepared and reviewed by its participants. The review panel consisted of BSC personnel and geomechanics experts from Sandia National Laboratories, U.S. Bureau of Reclamation, U.S. Geological Survey, University of Nevada, Las Vegas, University of Nevada, Reno, New England Research, Itasca Consulting Group, and Nick Barton and Associates. The DOE approach for addressing the identified geomechanical needs is summarized in Section 1.2.3 of this technical basis document and in *Resolution Strategy for Geomechanically-Related Repository Design and Thermal-Mechanical Effects (RDTME)* (Board 2003).

The overall approach adopted to resolve these geomechanical issues consisted of obtaining new laboratory and field data, supplemented by utilizing a combination of analyses, studies, and

calculations to maximize the utility of the available site-specific data. The following steps were identified and taken:

1. Collection and geotechnical analysis of the existing (2001) geological and geotechnical characterization data for suitability to support the analyses listed in E.3. The analysis identified additional laboratory and in situ thermal-mechanical testing needs.

2. Development and execution of a laboratory and field-testing plan. This consisted of extensive mapping of features within Yucca Mountain's excavated tunnels, the mechanical testing of lithophysal rock given the limited data set existing in 2001, augmenting the thermal-mechanical test database, and planning for time-dependent testing needed to better characterize the temporal variation of rock properties.

3. Development, calibration, and validation of numerical models capable of representing the thermal-mechanical behavior of lithophysal and nonlithophysal rocks and geostatistical models to characterize the geologic spatial variability (lithophysal porosity and fracture geometry).

4. Utilization of these computational models to supplement the material properties database and to explore the impact of spatial variability of properties on the geomechanical response in rock, primarily lithophysal rocks.

5. Exploration by means of numerical sensitivity studies to further investigate the impact of parameter uncertainty on preclosure ground support and postclosure drift degradation and seismic stability.

A preliminary 2001 summary of site-specific geotechnical properties of the host rock appears in *Subsurface Geotechnical Parameters Report* (BSC 2003a, Attachment IV). A qualitative analysis of this summary resulted in an assessment of data needs required for license application. These needs and a description of new measurement data and analyses are described below.

Field Collection of Fracture Geometry and Rock Mass Quality Data–For nonlithophysal rock, field characterization was carried out using a large database of meter-scale fracture geometry data produced from mapping the ESF and ECRB tunnels. Evaluation of this database of the tunnel full-periphery structure maps produced a statistical database, by fracture set, of fracture geometry data, such as fracture orientation, spacing, and trace length (BSC 2003a, Section 8.8.2; BSC 2004a, Sections 4.11 and 6.14, Appendix B). A secondary aspect of the program involved collecting rock quality data for rock classification purposes for lithostratigraphic units (BSC 2003a, Section 8.8.3) and mapping smaller scale fractures (less than 1 m) in the ESF and ECRB tunnels. Section 2.3.1 of this technical basis document discusses the characterization of fractures.

Field Characterization of Lithophysal Rock Features–For lithophysal rock within the repository host horizon, the primary aspect of field characterization involved mapping the shape, size, and abundance of lithophysae, spots, and rims (BSC 2003a, Section 8.8.4). This augmented the existing field characterization from geophysical borehole logging to indirectly determine

vertical variation of bulk density and porosity data. Section 2.3.2 discusses the characteristics and distribution of lithophysae.

Laboratory Characterization of Nonlithophysal Rock Properties–Laboratory tests were performed on intact core samples of nonlithophysal rock. This laboratory database has been analyzed to identify the key factors impacting the thermal and mechanical properties of intact rock (BSC 2003a, Sections 8.2, 8.3, and 8.4). The general mechanical and thermal behavior of nonlithophysal rock is adequately understood and sufficient parameter summaries have been prepared. Direct shear testing of five fractures was performed to help characterize the mechanical behavior of fractures by fracture set in nonlithophysal rock (BSC 2003a, Section 8.6). Section 3.2.1 discusses the mechanical properties of intact rock, and Section 3.2.4 discusses the mechanical properties of fractures.

Laboratory Characterization of Lithophysal Rock Properties–Several important thermal and mechanical rock properties are strongly dependent on rock porosity and lithophysal rock sample size. The mechanical elastic and rock strength parameters and thermal conductivity represent typical examples. Additional laboratory testing has been conducted to better characterize the thermal intact rock properties of thermal conductivity, heat capacity, and coefficient of thermal expansion (BSC 2003a, Section 8.3). Additional mechanical testing of large core specimens of lithophysal rock was undertaken to better characterize rock parameter dependencies on porosity and size. Results and analysis are presented in *Subsurface Geotechnical Parameters Report* (BSC 2003a, Section 8.4) and in *Lithophysal Rock Mass Mechanical Properties of the Repository Host Horizon* (BSC 2004c). However, sampling difficulties and laboratory testing limitations made it impractical to adequately characterize of lithophysal rock parameters, so computational methods were developed to augment the limited data. Section 3.2.1 discusses the mechanical properties of intact rock, including correlation of these properties with rock porosity.

In Situ Field Testing–Additional thermal and mechanical field testing was planned and carried out along the ESF and ECRB Cross-Drift to improve characterization of rock properties and validation of property estimates (BSC 2002a). A summary of in situ thermal and mechanical rock tests is reported in *Subsurface Geotechnical Parameters Report* (BSC 2003a, Sections 8.3 and 8.7). The in situ testing program extends from small-scale borehole testing of thermal and mechanical behaviors to meter-scale mechanical and thermal testing of rock blocks (e.g., the Single Heater Test, plate loading tests, slot tests) to drift-scale tests in both repository host horizon nonlithophysal (Drift Scale Test) and lithophysal rock (planned for the future for purposes of confirmation). In particular, in situ lithophysal rock testing (slot tests) was necessary to help confirm models and ranges of rock behavior. Section 3.2.3 discusses the in situ mechanical testing of nonlithophysal and lithophysal rocks.

Analysis and Modeling of Thermal Rock Mass Properties–New analyses of thermal laboratory and field measurements have been carried out to better characterize and model thermal properties. The most important of these recent efforts include *Thermal Testing Measurements Report* (BSC 2002a), *Heat Capacity and Thermal Expansion Coefficients Analysis Report* (BSC 2003d), *Thermal Conductivity of the Potential Repository Horizon Model Report* (BSC 2002b), and *Thermal Conductivity of Non-Repository Lithostratigraphic Layers* (BSC 2004d). The conceptual, analytical, and numerical modeling of thermal behavior of both a nonlithophysal and lithophysal rock mass is relatively well developed and is summarized in the

Subsurface Geotechnical Parameters Report (BSC 2003a, Section 8.3) for the rock mass thermal properties of thermal conductivity, heat capacity, and coefficient of thermal expansion. Section 3.2.5 discusses the thermal properties of the repository host rocks.

Derived Estimate of Nonlithophysal Rock Mass Properties–The mechanical rock mass behavior of nonlithophysal rock is controlled largely by the geometry of fractures that separates the relatively strong and stiff pieces of intact rock. The rock mass parameters of the repository host horizon nonlithophysal rock from tunnel data have been developed from an established empirical approach and are summarized in *Subsurface Geotechnical Parameters Report* (BSC 2003a, Section 8.5). A statistically representative fracture model of the repository site was required for addressing the spatial variability of properties and for meeting design and analysis needs. Fracture model results have been developed using the FracMan program and are reported in *Subsurface Geotechnical Parameters Report* (BSC 2003a, Section 9.3) and *Drift Degradation Analysis* (BSC 2004a, Section 6.1.6 and Appendix B).

Derived Estimate of Lithophysal Rock Mass Properties–The mechanical rock mass behavior of lithophysal rock is controlled largely by stress conditions and voids within the rock that can lead to failure of the bulk lithophysal rock. *Lithophysal Rock Mass Mechanical Properties of the Repository Host Horizon* (BSC 2004c) provides a detailed analysis of the relationship between porosity and mechanical rock properties and develops estimates of the rock mass mechanical properties of the lithophysal units of the Topopah Spring Tuff. The strength and modulus base-case estimates and ranges are developed based on laboratory testing of lithophysal rock and supplemented by numerical modeling. Numerical modeling of lithophysal rock was used to study the dependence of rock behavior on sample size, and lithophysal geometry (e.g., shape, size, and spatial distribution of voids). The development, calibration, and validation of these numerical models of lithophysal rock are summarized in the above report and *Subsurface Geotechnical Parameters Report* (BSC 2003a, Sections 9.1 and 9.2). These numerical approaches are shown to be successful in reproducing observed complex rock behavior, such as allowing for the development of interlithophysae fracturing. Section 4.2 and the response to RDTME 3.05 (Appendix A) provides further explanation of how lithophysal rock mass properties were developed.

Spatial Variation of the Mechanical Properties of Lithophysal Rock–The spatial variability of lithophysal rock mechanical parameters could not be directly developed from laboratory and field data. Instead, an indirect approach was adopted that combines the modeled spatial variation of lithophysal porosity in the field with the previously developed correlations between rock porosity and its mechanical properties. A preliminary simulation of the spatial variation of lithophysal porosity has been completed and is described in *Subsurface Geotechnical Parameters Report* (BSC 2003a, Section 9.4). Further discussion of this surrogate property approach for estimating the spatial variability of mechanical and thermal properties is described in *Subsurface Geotechnical Parameters Report* (BSC 2003a, Section 10.2). The application of this approach for lithophysal rock is developed in *Lithophysal Rock Mass Mechanical Properties of the Repository Host Horizon* (BSC 2004c). The spatial variability of lithophysal rock properties based on their correlation with rock porosity is addressed in Sections 2.3.2 and 5.3.2.2.

Temporal Variation of the Mechanical Properties of Lithophysal Rock–Estimates of the temporal variation in rock properties will be addressed separately in conjunction with

RDTME 3.07. A discussion of static fatigue testing and estimates of long-term strength is provided in *Drift Degradation Analysis* (BSC 2004a, Appendix S). This is based on laboratory static-fatigue testing of lithophysal rock as well as reliance on numerical modeling. The numerical modeling program is required due both to the limited number of rock samples tested under sustained loading and the relatively short time available in laboratories relative to the 10,000-year prediction of behavior. Conceptual models have been developed and implemented within computational codes to better understand and predict the time-related mechanical behavior of lithophysal rock. For nonlithophysal rock, the temporal variation in mechanical rock mass behavior is assumed to substantially relate to the degradation of the fracture strength parameters. A summary of laboratory static fatigue testing, as well as time-dependent numerical modeling and residual fracture strength data will be provided in the next revision of *Subsurface Geotechnical Parameters Report* (BSC 2003a) and will be specifically addressed in the response to RDTME 3.07. A summary of the long-term loading effect on rock strength is discussed in Section 5.3.2.2.4.

Conclusions–The uncertainty related to several key thermal and mechanical geotechnical properties has been substantially reduced as a result of additional data that have been collected and analyzed since 1997. This new work is summarized in *Subsurface Geotechnical Parameters Report* (BSC 2003a), *Lithophysal Rock Mass Mechanical Properties of the Repository Host Horizon* (BSC 2004c), and *Drift Degradation Analysis* (BSC 2004a) and specifically includes:

- Updated analysis of geophysical bulk density and porosity from Yucca Mountain boreholes
- Updated analysis of rock mass quality ratings and classifications of the underground openings
- Field mapping and analysis of lithophysae and other features in lithophysal rock
- Field mapping and analysis of small-scale fractures within the repository horizon
- Updated analysis and modeling of field fracture geometry within the repository horizon
- Creation of a new database of thermal and mechanical properties of intact rock of the Yucca Mountain stratigraphy, with an updated analyses of these intact rock properties
- Direct shear testing of repository horizon rock fractures and an updated analysis of mechanical fracture properties of the Yucca Mountain stratigraphy
- New estimates of rock mass thermal properties of the Yucca Mountain stratigraphy
- New estimates of nonlithophysal rock mass mechanical properties of the Yucca Mountain stratigraphy
- Laboratory testing of large cores of lithophysal rock
- Numerical testing to better characterize the properties of lithophysal rock

- New estimates of lithophysal rock mass mechanical properties in the repository horizon
- In situ thermal-mechanical field testing of rock within the repository horizon
- Static fatigue testing of repository horizon rock
- Estimates of the spatial variation of rock mass mechanical properties based on the spatial variation of lithophysae
- Estimates of the temporal variation of rock properties based on laboratory results and numerical analysis.

Completion of the above work, together with the anticipated completion of in-progress activities, is considered sufficient to reduce thermal and mechanical rock property uncertainties to acceptable risk levels for license application.

E.5 REFERENCES

Board, M. 2003. *Resolution Strategy for Geomechanically-Related Repository Design and Thermal-Mechanical Effects (RDTME)*. REV 00. Las Vegas, Nevada: Bechtel SAIC Company. ACC: MOL.20030708.0153.

BSC (Bechtel SAIC Company) 2002a. *Thermal Testing Measurements Report.* ANL-NBS-HS-000041 REV 00. Las Vegas, Nevada: Bechtel SAIC Company. ACC: MOL.20021004.0314.

BSC 2002b. *Thermal Conductivity of the Potential Repository Horizon Model Report.* MDL-NBS-GS-000005 REV 00. Las Vegas, Nevada: Bechtel SAIC Company. ACC: MOL.20020923.0167.

BSC 2003a. *Subsurface Geotechnical Parameters Report*. 800-K0C-WIS0-00400-000-00A. Las Vegas, Nevada: Bechtel SAIC Company. ACC: ENG.20040108.0001.

BSC 2003b. *Ground Control for Emplacement Drifts for LA.* 800-K0C-TEG0-00100-000-00A. Las Vegas, Nevada: Bechtel SAIC Company. ACC: ENG.20031016.0001.

BSC 2003c. *Scoping Analysis on Sensitivity and Uncertainty of Emplacement Drift Stability*. 800-KOC-TEG0-00600-000-000. Las Vegas, Nevada: Bechtel SAIC Company. ACC: ENG.20031125.0002.

BSC 2003d. *Heat Capacity and Thermal Expansion Coefficients Analysis Report.* ANL-NBS-GS-000013 REV 00. Las Vegas, Nevada: Bechtel SAIC Company. ACC: DOC.20030820.0002.

BSC 2004a. *Drift Degradation Analysis*. ANL-EBS-MD-000027 REV 03A. Las Vegas, NV: Bechtel SAIC Company. ACC: MOL.20040513.0081.

BSC 2004b. *Ground Control for Non-Emplacement Drifts for LA.* 800-KMC-SSD0-00700-000-00A. Las Vegas, Nevada: Bechtel SAIC Company. ACC: ENG.20040302.0022.

BSC 2004c. *Lithophysal Rock Mass Mechanical Properties of the Repository Host Horizon.* 800-K0C-SS00-00200-000-00Aa. Las Vegas, Nevada: Bechtel SAIC Company. ACC: MOL.20040510.0200.

BSC 2004d. *Thermal Conductivity of Non-Repository Lithostratigraphic Layers.* MDL-NBS-GS-000006 REV 00, with errata. Las Vegas, Nevada: Bechtel SAIC Company. ACC: DOC.20030815.0001; DOC.20040115.0001.

CRWMS M&O (Civilian Radioactive Waste Management System Management and Operating Contractor) 1997. *Yucca Mountain Site Geotechnical Report*. B00000000-01717-5705-00043 REV 01. Two volumes. Las Vegas, Nevada: CRWMS M&O. ACC: MOL.19971017.0736; MOL.19971017.0737.

NRC (U.S. Nuclear Regulatory Commission) 2002. *Integrated Issue Resolution Status Report*. NUREG-1762. Washington, D.C.: U.S. Nuclear Regulatory Commission, Office of Nuclear Material Safety and Safeguards. TIC: 253064.

Reamer, C.W. and Williams, D.R. 2001. Summary Highlights of NRC/DOE Technical Exchange and Management Meeting on Repository Design and Thermal-Mechanical Effects. Meeting held February 6-8, 2001, Las Vegas, Nevada. Washington, D.C.: U.S. Nuclear Regulatory Commission. ACC: MOL.20010307.0511 through MOL.20010307.0521.

APPENDIX F

DESIGN SENSITIVITY AND UNCERTAINTY ANALYSES OF THE FRACTURE PATTERNS WITH DISCONTINUUM APPROACH (RESPONSE TO RDTME 3.08 AND RDTME 3.12)

Note Regarding the Status of Supporting Technical Information

This document was prepared using the most current information available at the time of its development. This Technical Basis Document and its appendices providing Key Technical Issue Agreement responses that were prepared using preliminary or draft information reflect the status of the Yucca Mountain Project's scientific and design bases at the time of submittal. In some cases this involved the use of draft Analysis and Model Reports (AMRs) and other draft references whose contents may change with time. Information that evolves through subsequent revisions of the AMRs and other references will be reflected in the License Application (LA) as the approved analyses of record at the time of LA submittal. Consequently, the Project will not routinely update either this Technical Basis Document or its Key Technical Issue Agreement appendices to reflect changes in the supporting references prior to submittal of the LA.

APPENDIX F

DESIGN SENSITIVITY AND UNCERTAINTY ANALYSES OF THE FRACTURE PATTERNS WITH DISCONTINUUM APPROACH (RESPONSE TO RDTME 3.08 AND RDTME 3.12)

This appendix provides a response for Key Technical Issue (KTI) agreements Repository Design and Thermal-Mechanical Effects (RDTME) 3.08 and 3.12. These agreements focus on U.S. Nuclear Regulatory Commission (NRC) concerns regarding the design sensitivity, uncertainty of fracture patterns, and applying site-specific ground motion to the stability of the drifts and the ground support system. These agreements are addressed together in this appendix due to the similar nature of the issues.

F.1 KEY TECHNICAL ISSUE AGREEMENTS

F.1.1 RDTME 3.08 and RDTME 3.12

Agreements RDTME 3.08 and 3.12 were reached during the NRC/U.S. Department of Energy (DOE) Technical Exchange and Management Meeting on Repository and Design Thermal-Mechanical Effects held February 6 to 8, 2001, in Las Vegas, Nevada (Reamer and Williams 2001). There has been no submittal related to these KTI agreements to the NRC.

The wording of these agreements are as follows:

RDTME 3.08

> Provide the design sensitivity and uncertainty analyses of the fracture pattern (with respect to Subissue 3, Component 1). The DOE will provide sensitivity and uncertainty analysis of fracture patterns (based on observed orientation, spacing, trace length, etc) on the preclosure ground control system design in a revision to the Ground Control for Emplacement Drifts for SR, ANL-EBS-GE-000002 (or other document) supporting any potential license application. This is expected to be available to NRC in FY 2003.

RDTME 3.12

> Provide dynamic analyses (discontinuum approach) of ground support system performance using site specific ground motion time history as input. The DOE will provide appropriate analyses to include dynamic analyses (discontinuum approach) of preclosure ground support systems, using site specific ground motion time histories as input, in a revision to the Ground Control for Emplacement Drifts for SR, ANL-EBS-GE-000002 (or other document) supporting any potential license application. This is expected to be available to NRC in FY 2003.

NRC concerns are further elaborated in the *Integrated Issue Resolution Status Report* (NRC 2002, Section 2.1.7) and are paraphrased as follows:

- Discontinuum models used in the thermal-mechanical analyses for site recommendation (CRWMS M&O 2000) were based on a regular fracture pattern composed from the mean fracture-set attitudes (dip and dip direction) and spacing, but the uncertainties in the fracture-set properties and their effects on the calculated results were not discussed (NRC 2002, p. 2.1.7-13).

- Seismic loading was represented in the models as a sinusoidal velocity history with a frequency of 10 Hz, an amplitude equal to the estimated peak ground velocity for the site, and a duration of 3 seconds for site recommendation (CRWMS M&O 2000). The site-specific ground-motion time history would differ from the model velocity history in terms of frequency content, amplitude variation, and duration of loading, so a comparison of the two might examine the total energy delivered to the rock in either case and the amount of that energy available to cause rock failure (e.g., by fracture slip) (NRC 2002, pp. 2.1.7-13 to 2.1.7-14).

F.1.2 Related Key Technical Issue Agreements

Agreements RDTME 3.02 and RDTME 3.13 (Appendix D) are related to RDTME 3.08 and RDTME 3.12. RDTME 3.02 addresses the critical combination of in situ, thermal, and seismic stresses. RDTME 3.13 addresses the technical justification for boundary conditions for the numerical models.

F.2 RELEVANCE TO REPOSITORY PERFORMANCE

The preclosure safety analysis is used to demonstrate the safety of the geologic repository operations area with regard to the overall preclosure performance design and operations objectives. The safety strategy for the preclosure operating period is to demonstrate that the ground control system is not required to prevent or mitigate credible rockfall. This demonstration relies upon analyses that show that the waste package does not breach when impacted by credible rock blocks.

The jointed rock mass surrounding the emplacement drifts for nonlithophysal rock will be subjected to loadings from in situ stress, thermal loading, and seismic ground motion. The results of the sensitivity and uncertainty analyses for fracture patterns provide the design basis rock blocks for evaluation of the waste package.

F.3 RESPONSE

A summary of analyses for resolving agreements RDTME 3.08 and RDTME 3.12 follow. These analyses are discussed in Sections 4.1 and 5.3 and covered in detail in *Evaluation of Emplacement Drift Stability for KTI Resolution* (BSC 2004a). The approach for addressing the KTIs include:

- Development of a three-dimensional stochastically-defined synthetic fracture network using the FracMan program, and based on the mapped fracture orientation, spacing, and

trace length from repository rock units exposed in the ESF and ECRB Cross-Drift excavations.

- Development of site-specific ground-motion time histories with representative frequency content and variability, amplitude variation, and duration of loading for seismic shaking.

- Development of a three-dimensional dynamic discontinuum (3DEC) model that incorporates the synthetic fracture model developed from the FracMan program to address the issues of design sensitivity and uncertainty of fracture patterns. A total of 32 fracture patterns are selected to represent the variability of fracture patterns.

- Conducting the dynamic discontinuum analyses using site-specific ground-motion time histories for unsupported drifts.

The summary and conclusions from the discontinuum analyses are provided below:

- A three-dimensional synthetic fracture network was generated for the uncertainty and sensitivity analysis of fracture patterns. The generation was based on the observed orientation, spacing, and trace length (Section 4.1 of this technical basis document).

- The 3DEC model, incorporating the stochastically-defined synthetic fracture network that addresses the design sensitivity and uncertainty of fracture patterns for preclosure analysis, was used to conduct analysis for identification of potential unstable blocks (Section 5.3.3 of this technical basis document). Dynamic discontinuum analyses using site-specific ground-motion time histories were conducted to provide correct input of frequency content, amplitude variation, and duration of loading for seismic shaking (BSC 2004a, Section 6.3).

- Limited areas of unstable blocks were observed in the discontinuum analyses for the unsupported openings when subjected to seismic shaking. A total of 32 simulations with stochastically-defined fracture patterns were conducted for preclosure ground motions. Calculation of the ground support response based on an uncoupled method (i.e., the ground support was not modeled directly in the 3DEC analysis) demonstrated that the factor of safety of the rock bolt tension capacity versus the median weight of unstable wedges is more than 10. The combination of rock bolts and steel sheets provides ample support for the extreme scenario with unfavorable block orientation (BSC 2004a, Section 6.3).

The information in this appendix is responsive to agreements RDTME 3.08 and RDTME 3.12 made between the DOE and NRC. This report contains the information that the DOE considers necessary for NRC review for closure of these agreements.

F.4 BASIS FOR THE RESPONSE

F.4.1 Development of Three-Dimensional Synthetic Fracture Network Using FracMan

The description of the fracture characteristics at the repository host horizon is provided in Section 2.3.1 of this technical basis document. Relatively short trace length and partially

nonpersistent joints are observed at the ESF and ECRB Cross-Drift (BSC 2004b, Section 6.1). Analysis of seismic response in emplacement drifts in fractured rock is a three-dimensional problem requiring the rock mass to be represented as an explicitly fractured assemblage. The FracMan program (Section 4.1 of this technical basis document) was used to provide a statistically-similar fracture network geometry as compared to that observed in the exploratory tunnels. This fracture network was used to develop a representative volume of jointed rock mass within which example emplacement drifts could be excavated. The existing fracture mapping database provides the basic input to the FracMan program, which develops sets of planar, circular fractures that conform to the statistical variability of the geometric characteristics of the input data. A detailed description of the synthetic fracture network generation process is provided in *Drift Degradation Analysis* (BSC 2004b, Section 6.1).

F.4.2 Development of Site-Specific Ground-Motion Time History

A description regarding the development of the site-specific ground motion time history is provided in *Development of Earthquake Ground Motion Input for Preclosure Seismic Design and Postclosure Performance Assessment of a Geologic Repository at Yucca Mountain, NV* (BSC 2004c). The site-specific ground-motion time history was developed based on a site response model. The modeling approach implements a random-vibration theory and equivalent-linear modeling formulation to calculate site response effects on ground motion. Resulting seismic velocity time histories for the mean annual exceedance probability of 10^{-4} are shown in Figure F-1. Two horizontal components (H1 and H2) and one vertical component (V) of acceleration, velocity, and displacement are supplied, as discussed in Section 5.3.2.1.3 of this technical basis document.

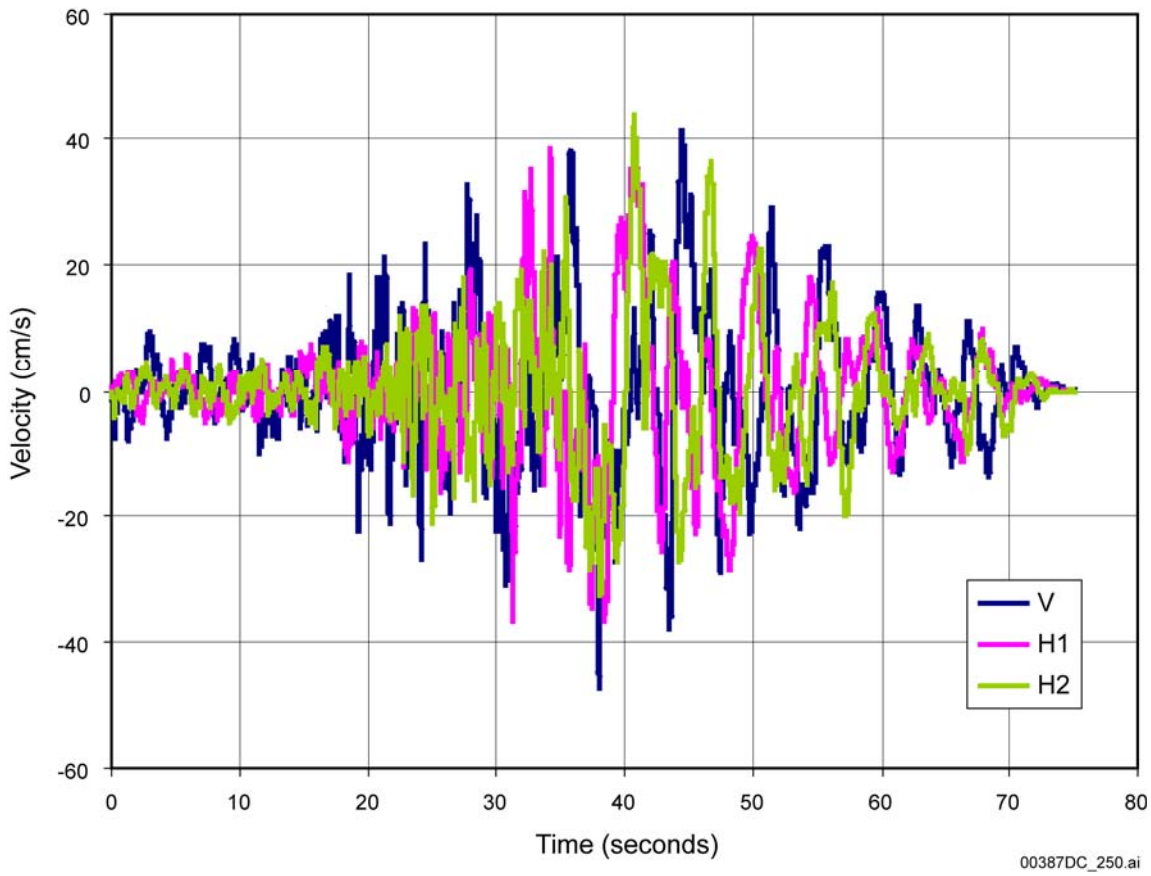

Source: DTN: MO0306SDSAVDTH.000.

Figure F-1. Time Histories of Velocity Components of Seismic Motion at Repository Horizon, Mean Annual Exceedance Probability of 10^{-4}

F.4.3 Three-Dimensional Discontinuum Analysis of Jointed Rock Mass

The three-dimensional discontinuum analysis is used for simulating the mechanical behavior of the jointed rock mass in the nonlithophysal units for loading conditions in which the stability response will be controlled by the fractures. The possibility that wedge-type failure occurs in the lithophysal units has been investigated and found to be very small (approximately 1 block per kilometer) with consideration of the variation of fracture patterns (BSC 2004b, Section 6.4.3). A minor sidewall shear failure mechanism is considered more appropriate for the lithophysal units, as discussed in Sections 4.2 and 5.3.3.2 of this technical basis document.

The 3DEC program was selected for its capability of simulating a jointed rock mass under both thermal and seismic loadings (see Section 4.1.1 of this technical basis document). The jointed rock mass is represented as a number of intact rock blocks separated by interface planes whose mechanical behavior is represented by a standard Coulomb slip criterion. The intact blocks are subdivided into tetrahedral finite difference zones and can be assigned a suitable mechanical constitutive law (Itasca Consulting Group 2002). Because of the high intact rock strength in the nonlithophysal units (Section 3.2.1 of this technical basis document), rock blocks are considered to behave elastically. Ground support is not included in the model so that a general stability of

the unsupported openings is assessed. Unstable blocks identified in the 3DEC analyses are then used in a separate, uncoupled ground support calculation presented in Section F.4.4.

To account for the heterogeneous nature of the jointed medium, 32 fracture patterns were selected from a 100–m cube of stochastically-defined FracMan rock mass for preclosure consideration (see Section 4.1 of this technical basis document). Justification of conducting 32 fracture patterns to cover the range of variability of the fracture patterns is provided in *Drift Degradation Analysis* (BSC 2004b, Appendix K). A representative tunnel volume, approximately two tunnel diameters around the emplacement drift centroid and 25 m long, is created at each of these locations to contain fractures generated in FracMan. This volume is considered sufficient to generate an appropriate representation of damaged rock and of sufficient length (approximately five times the tunnel diameter and approximately 10 times the median joint trace length) to provide a representative volume of unstable blocks for estimation of the rockfall hazard.

One of the 3DEC models including the region with detailed fractures imported from FracMan is shown in Figure F-2. Three vertical and five horizontal cross-sectional views are included in Figure F-2 to illustrate the fractures and blocks around the excavation. The dominant north–west trending subvertical fracture set is clearly shown in the cross-sectional views. That portion of the rock mass in which fractures do not form blocks is shown in green, while distinct blocks are identified by other colors. Some of the fractures shown in the cross-sectional views were artificially generated during the block-cutting process or to facilitate mesh generation and are bonded and not allowed to slip (BSC 2004b, Section 6.3.1). The drip shield is represented as a stiff block fixed to the invert of the drift. Although the drip shield does not exist during the preclosure period, the drip shield block is placed to collect information on the locations and relative velocities of the rockfall impact. Modeling parameters, such as the mechanical properties of intact rock and joints, in situ stress, and boundary conditions used in the 3DEC model, are provided in *Drift Degradation Analysis* (BSC 2004b, Section 6.3).

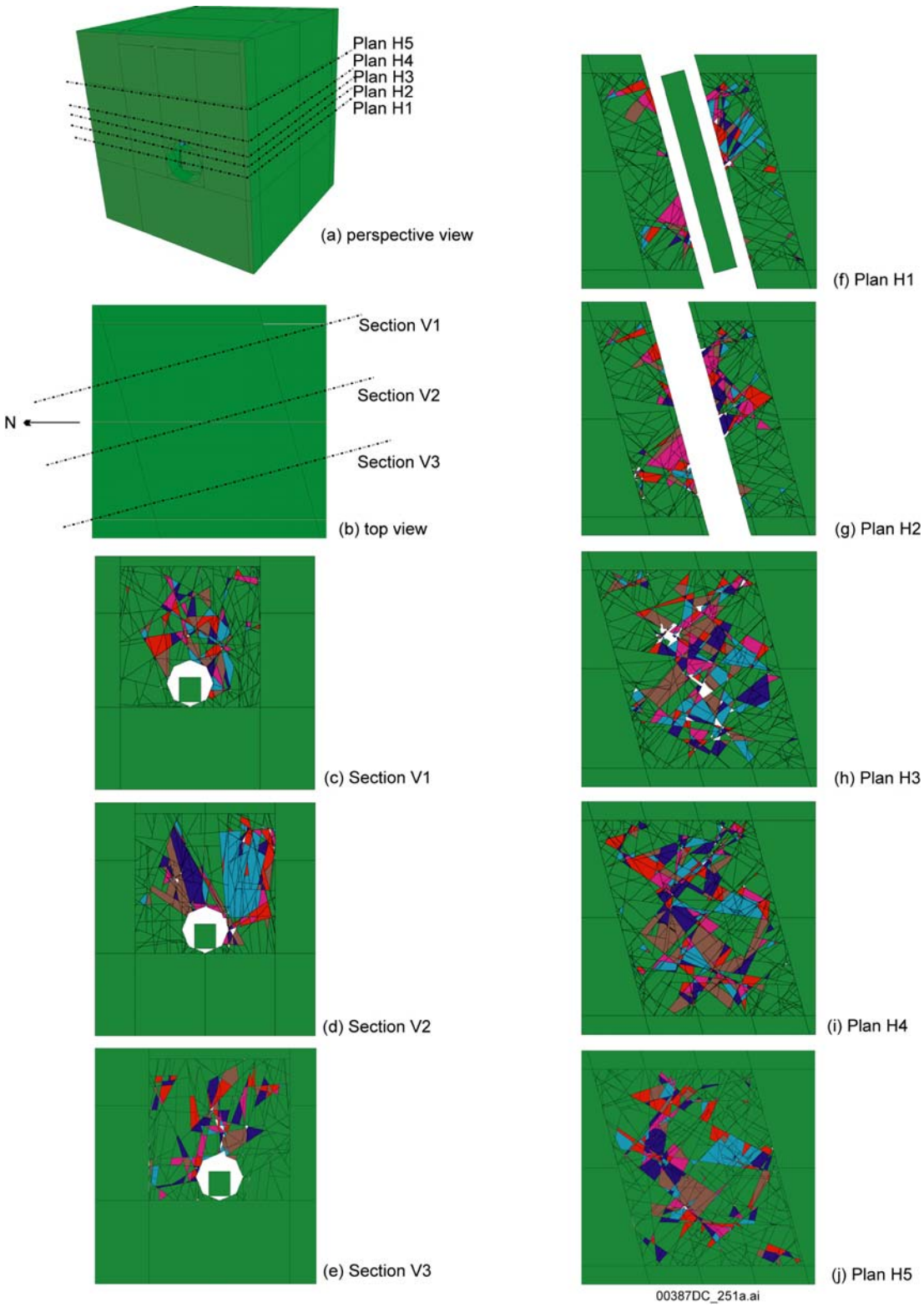

Source: BSC 2004a, Figure 6.3-11.

Figure F-2. 3DEC Model Geometry and Cross Sections

Figure F-3 compares the input ground motion (H1) with the recorded velocities at the center of the model. The results confirm the correct wave inputs and proper wave propagation in the 3DEC model. Time histories of normal and shear stresses for joints close to the opening were recorded during seismic shaking in the 3DEC model. The stress paths of selected fracture subcontacts are plotted against the Coulomb slip criterion, as shown in Figure F-4. The fracture properties assigned to the model are reviewed in Section 3.2.4 of this technical basis document. The coordinates of the subcontacts and their relative location to the drift are presented in Figure F-5. The in situ stress state before seismic shaking is also included as the orange square for each subcontact location in Figure F-4. The in situ stress state at subcontact *a* is very close to the Coulomb slip criterion. The fracture containing this subcontact has undergone yielding during seismic motions. Seismic shaking-induced normal and shear stress are in the range of 6 MPa. The stress paths for fractures containing subcontacts *b* and *c* are well under the yield criterion and representative of most of the rock mass.

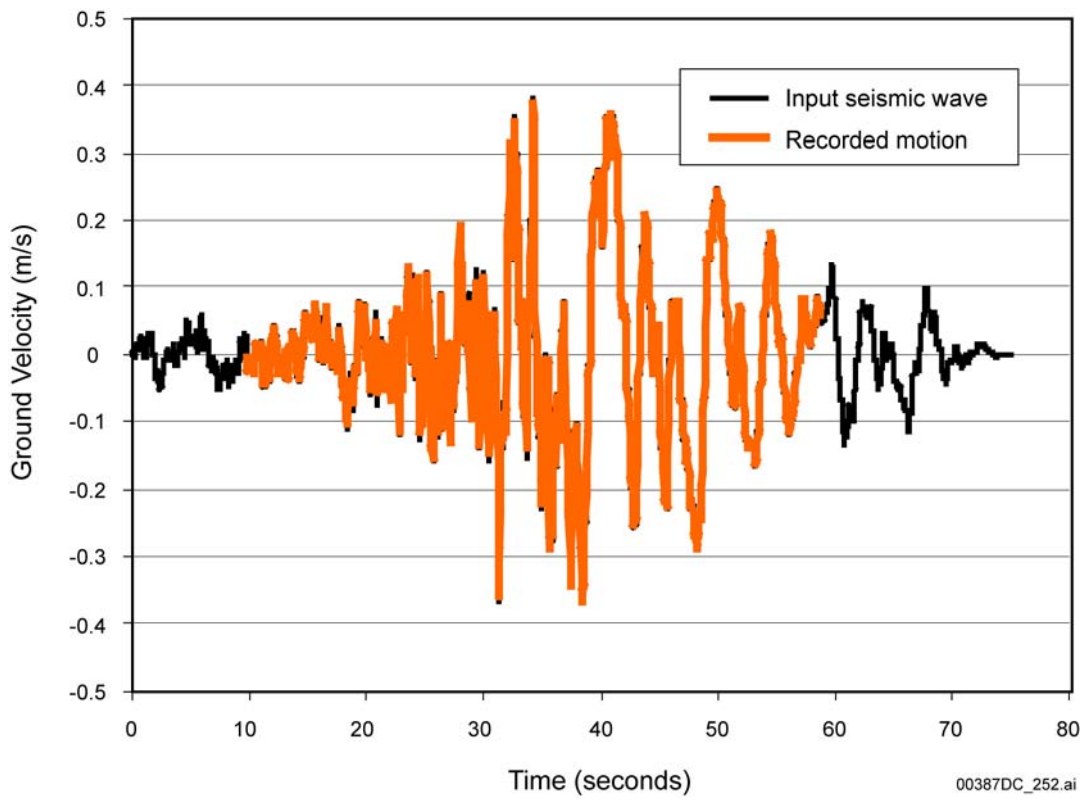

Source: BSC 2004a, Figure 6.3-13.

Figure F-3. Comparison of Input Seismic Wave and Recorded Velocities (H1) in the 3DEC Model

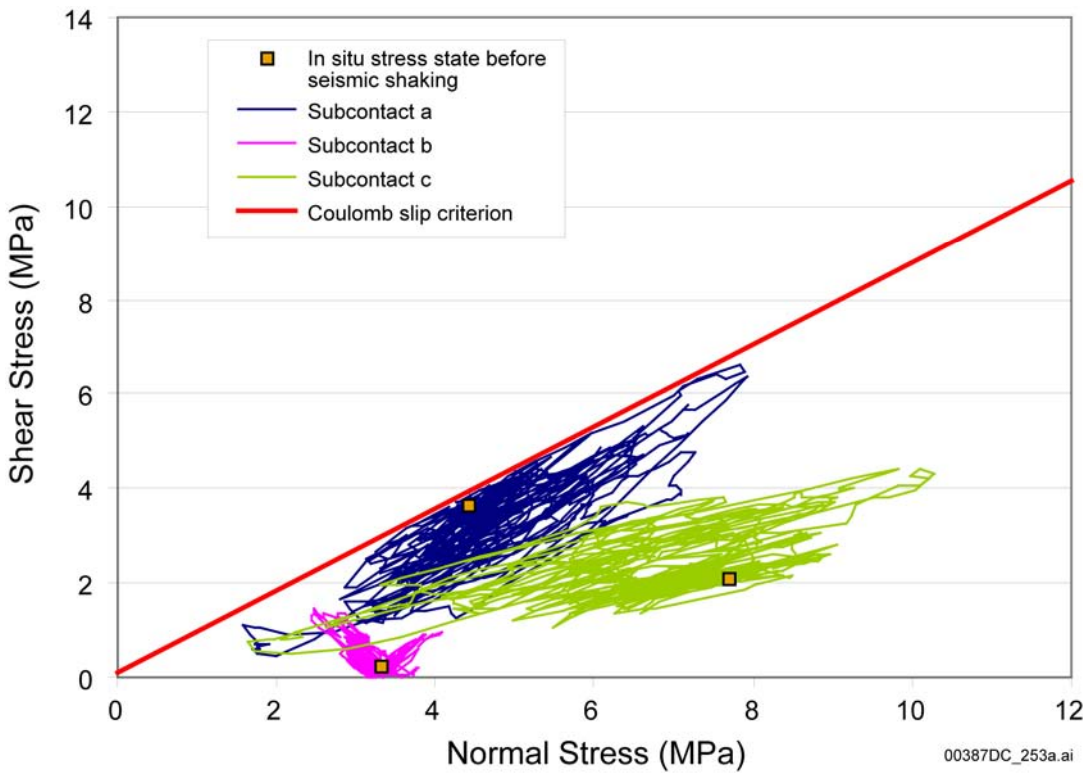

Source: BSC 2004a, Figure 6.3-14.

Figure F-4. Stress Path at Selected Fracture Subcontacts (3DEC Simulation 16)

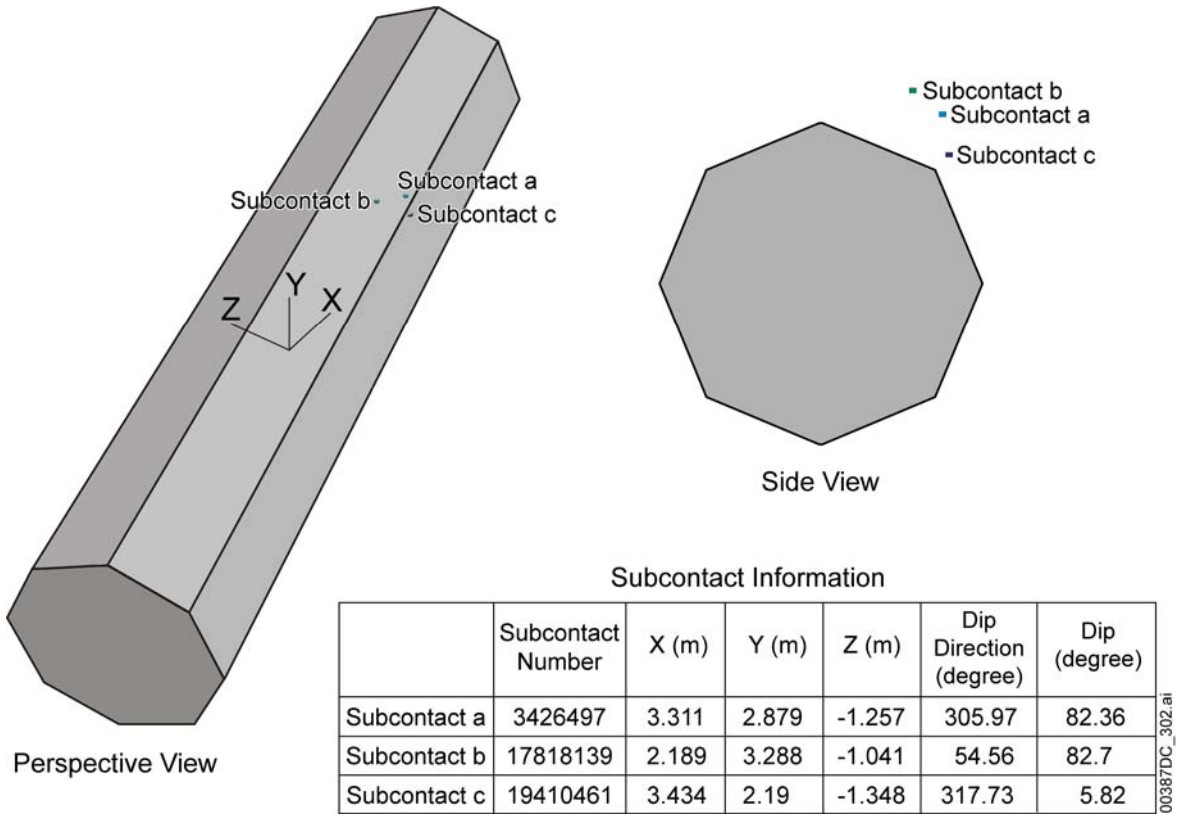

Subcontact Information

	Subcontact Number	X (m)	Y (m)	Z (m)	Dip Direction (degree)	Dip (degree)
Subcontact a	3426497	3.311	2.879	-1.257	305.97	82.36
Subcontact b	17818139	2.189	3.288	-1.041	54.56	82.7
Subcontact c	19410461	3.434	2.19	-1.348	317.73	5.82

Source: BSC 2004a, Figure 6.3-15.

Figure F-5. Information for the Subcontacts for Stress Path Presentation (3DEC Simulation 16)

The unstable blocks resulting from preclosure seismic shaking were identified in the 3DEC simulations, with results summarized in Table F-1. The total number and volume of unstable blocks for each simulation are summed and ranked in order in Table F-1. Figure F-6 presents the histogram and the cumulative frequency of occurrence for the size of the unstable blocks. The blocks are generally small. The maximum rockfall block mass predicted is 2.72 MT, with a median block size of 0.12 MT. The histogram shows it is highly skewed toward small-size blocks, which is the same trend depicted for rockfall for postclosure ground motions shown in Section 5.3.2.1.6 of this technical basis document.

Table F-1. Total Number and Volume of Unstable Blocks for Each 3DEC Simulation

Rank Order	3DEC Simulation Case Number	Synthetic Fracture Pattern Number	Number of Unstable Blocks	Total Volume of Unstable Blocks (m^3)	Percentile
1	38	29	62	7.169	100
2	39	37	29	3.487	97
3	56	98	28	3.433	94
4	23	5	22	3.129	91
5	16	30	35	2.684	88
6	28	25	16	2.481	84
7	25	17	16	2.375	81
8	41	42	13	1.979	78
9	22	23	15	1.686	75
10	40	99	17	1.286	72
11	19	10	13	1.232	69
12	44	65	22	1.186	66
13	34	75	23	0.990	63
14	45	39	5	0.858	59
15	33	102	9	0.709	56
16	24	6	10	0.576	53
17	55	16	10	0.570	50
18	35	33	5	0.565	47
19	43	59	15	0.544	44
20	18	26	17	0.544	41
21	53	4	9	0.405	38
22	20	19	4	0.238	34
23	15	21	5	0.197	31
24	32	7	1	0.181	28
25	29	3	4	0.152	25
26	14	22	3	0.146	22
27	31	79	2	0.140	19
28	36	78	6	0.129	16
29	21	9	5	0.108	13
30	42	24	3	0.098	9
31	27	14	3	0.094	6
32	17	27	1	0.045	3

Source: BSC 2004a, Table 6.3-5.

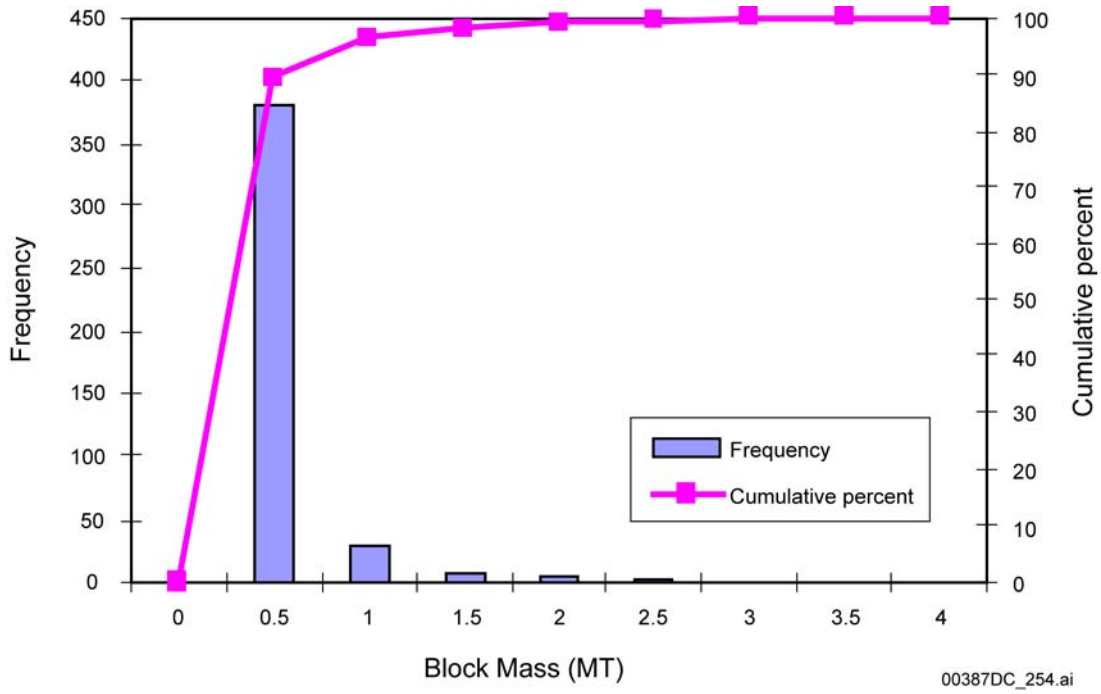

Source: BSC 2004a, Figure 6.3-16.

Figure F-6. Histogram for Block Mass

The unstable blocks are identified in each simulation. Limited areas of unstable blocks are observed for most of the simulations. A typical case is shown in Figure F-7 with 10 unstable blocks and a total volume of 0.57 m^3. The side view, perspective view, and cross-sectional view in through which most of the rockfall occurred are provided. The blocks are small, and most of them are clustered in the one location. Figure F-8 presents the results for the worst case in terms of the unstable block volume. A total of 62 unstable blocks and a volume of 7.17 m^3 are predicted for this case. Most of the blocks are clustered at four locations. A cluster of blocks with a pyramid shape is formed at the roof crown. The cross section shown in Figure F-8 intersects this pyramid cluster. A catalog of unstable blocks identified in each simulation is provided in *Evaluation of Emplacement Drift Stability for KTI Resolutions* (BSC 2004a, Attachment I).

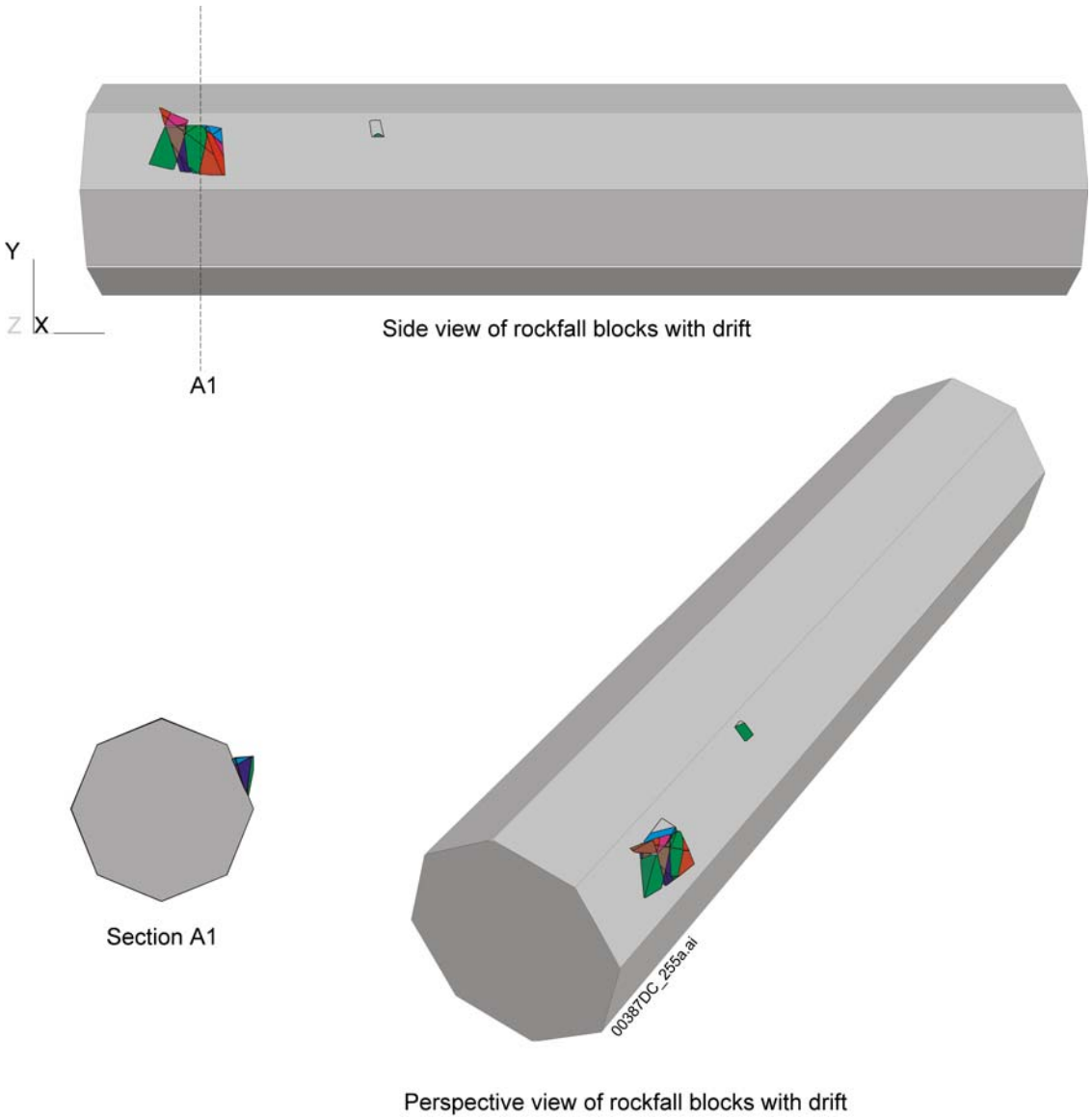

Source: BSC 2004a, Figure 6.3-17.

Figure F-7. Unstable Blocks for Typical Case (Simulation 55, 50 Percentile)

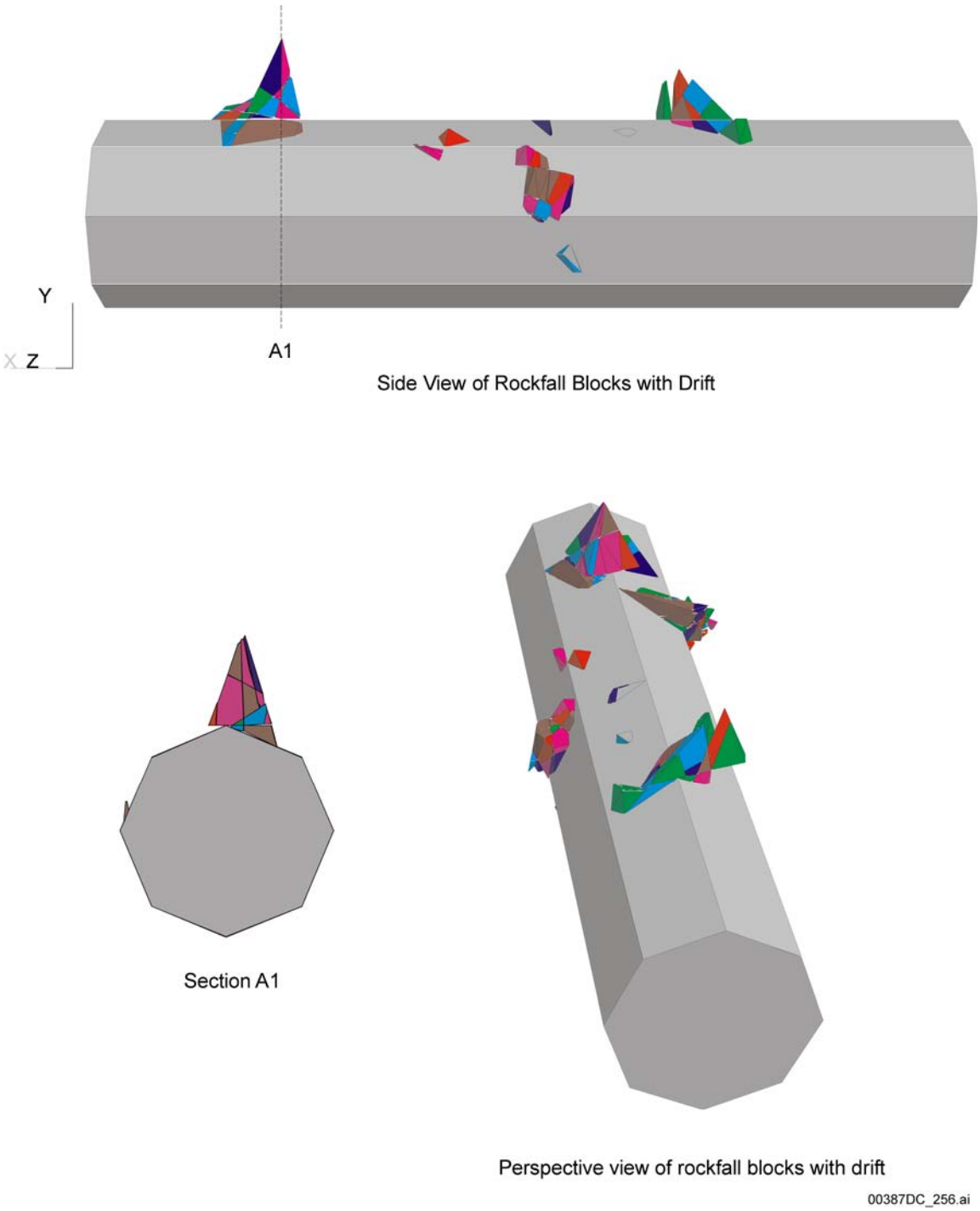

Source: BSC 2004a, Figure 6.3-18.

Figure F-8. Unstable Blocks for the Case with Greatest Amount of Rockfall (Simulation 38; 100 Percentile)

F.4.4 Uncoupled Ground Support Calculation

Frictional rock bolts and thin perforated steel sheets (held to the rock surface with the rock bolts) are selected as the ground support methods for the emplacement drifts (BSC 2003, Section 6.3). The design for the ground support system utilizes 3-m-long bolts and perforated steel sheets with approximately 240° coverage around the tunnel periphery above the invert. Radially oriented rock bolts with faceplates provide the required holding capacity and are placed in an approximately 240° coverage pattern around the drift periphery (Figure F-9). Bolts are spaced 1.25 m apart radially. The longitudinal spacing of the rows of rock bolts is also 1.25 m. Both the frictional rock bolts and the perforated steel sheets are made of Stainless Steel Type 316 with thickness of 3 mm (equivalent to Stainless Steel Type 316).

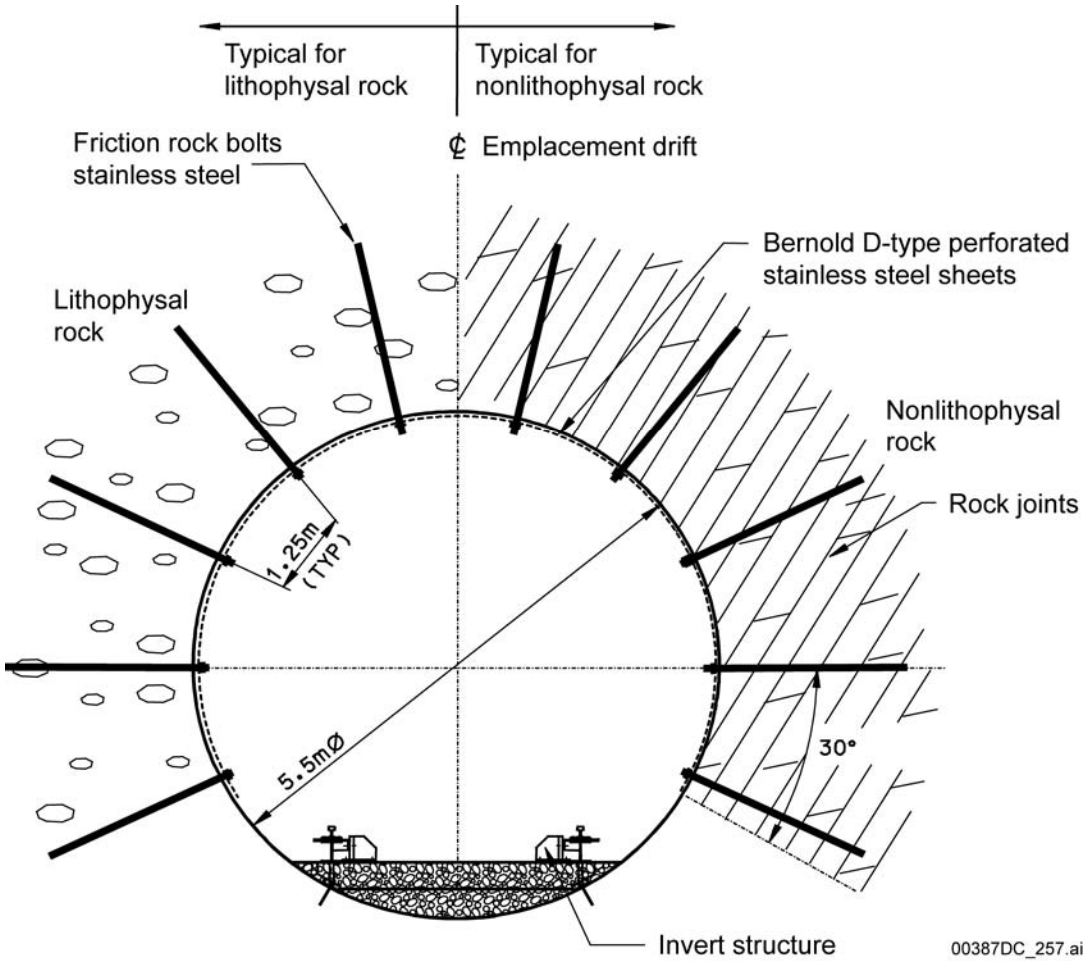

NOTE: The diameter of the rock bolt is 54 mm, and the thickness of the perforated plate is 3 mm.

Figure F-9. Ground Support Methods Recommended for Emplacement Drifts

For the uncoupled ground support calculation, six cases were selected to cover the range of predicted rockfall caused by preclosure seismic shaking. These six cases have rank order numbers 1, 2, 3, 7, 9, and 17 (listed in Table F-1) corresponding to three cases of greatest volume of rockfall, two above-average volume cases, and the median volume case. This selection

provides a conservative catalog of unstable blocks for ground support calculation. Figure F-10 shows the cross section of unstable blocks with superimposed ground supports for each selected simulation.

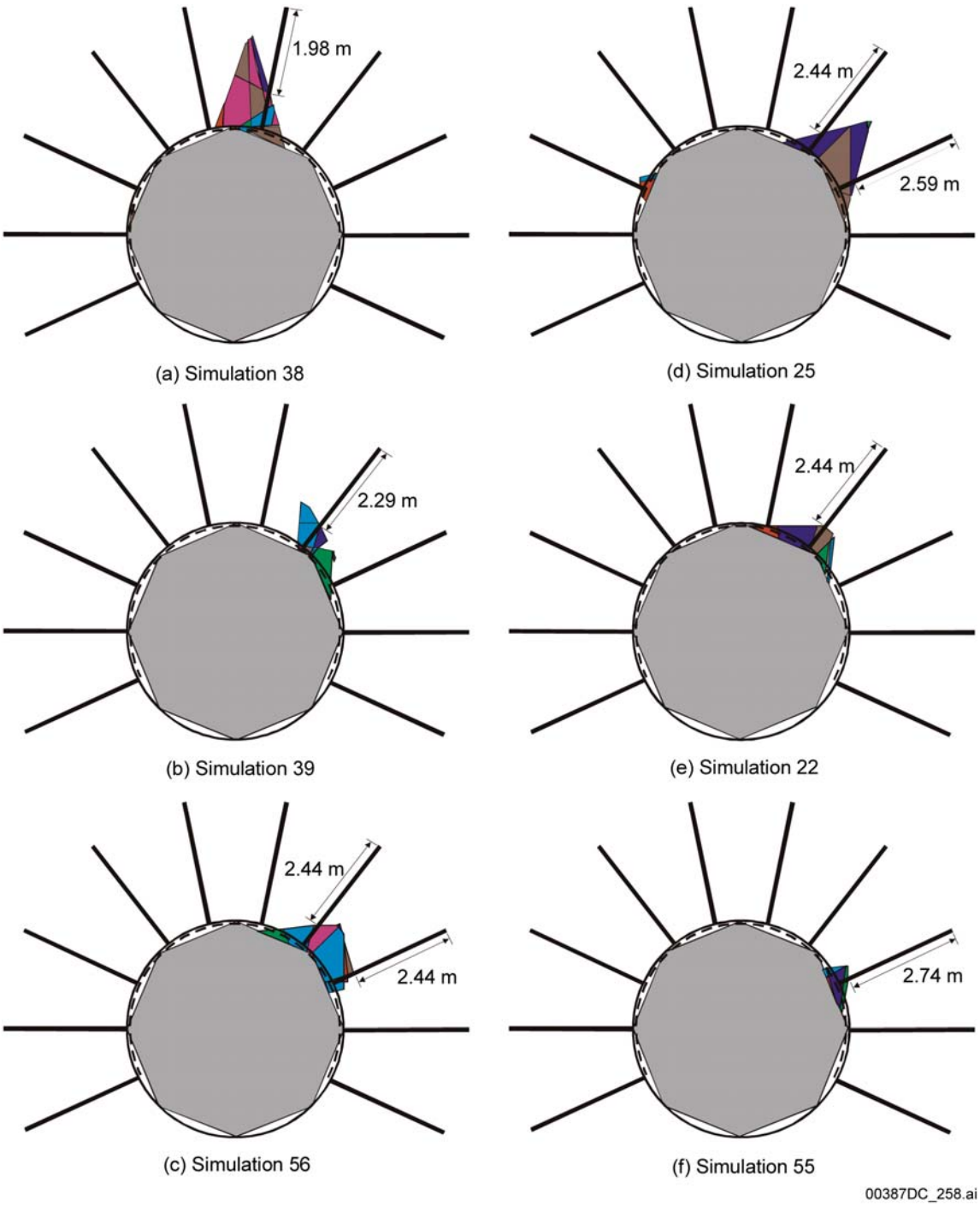

Source: BSC 2004a, Figure 6.3-20.

Figure F-10. Identified Unstable Blocks with Ground Support

The uncoupled ground support calculation concerning the bolt capacity assumes free fall of unstable blocks due to seismic shaking (i.e., there is no credit taken for the frictional resistance along the sliding surface of the block and surrounding rock mass). Thus, the entire weight of the block is assumed to be carried by the bolt. The footprint of the blocks on the opening are ignored in the calculation (i.e., the blocks may be supported by more than one bolt for some of the cases with a larger footprint).

The weight of the unstable blocks, the calculated bolt resistance capacity, and the calculated factor of safety are listed in Table F-2. The design capacity for the rock bolt is specified to be 20 tons (BSC 2003, Section 6.4). Bolt capacity was adjusted based on the anchored length (shown in Figure F-10) and a discount of the capacity due to excavation-induced deformation. A discount of 2.25 tons is used based on the coupled numerical analysis reported in *Ground Control for Emplacement Drifts for LA* (BSC 2003, Figure 6-47). The weight of the unstable blocks listed in Table F-2 is conservatively estimated based on the 3DEC simulations. For most of the cases, the total weight of the unstable blocks predicted in the 25-m drift is used as the weight of the blocks in the localized area. The calculations show that the factor of safety for most of the cases is in the range of 3 to 5, with the lowest value of 1.6 for the worst case (Simulation 38). However, for Simulation 55 (which represents the median stability case among all 32 runs completed) the factor of safety is higher than 10. The results clearly indicate that the rock bolts alone will provide sufficient support for unstable blocks.

Table F-2. Uncoupled Load-Capacity Calculation for Rock Bolts

Simulation	Anchored Bolt Length (m)		Adjusted Bolt Capacity (tons)		Weight of Unstable Blocks (tons)	Factor of Safety
	Bolt 1	Bolt2	Bolt 1	Bolt2		
38	1.98	NA	11.73	NA	7.2	1.6
39	2.29	NA	13.53	NA	4.2	3.2
56	2.44	2.44	14.43	14.43	8.3	3.5
25	2.44	2.59	14.43	15.33	5.7	5.2
22	2.44	NA	14.43	NA	4.1	3.5
55	2.74	NA	16.23	NA	1.4	11.6
38, blocks rotated	0.78	NA	4.61	NA	7.2	0.6
25, blocks rotated	1.56	NA	9.21	NA	5.7	1.6

Source: BSC 2004a, Table 6.3-6.

Consideration was also given to the possibility of the blocks slightly rotating to the most unfavorable orientation and the rock bolts penetrating through the peak of the unstable blocks, resulting in shorter anchored length (see Figure F-11). Simulations 25 and 38 were selected for this assessment because of the depth of the blocks. The calculation is included in Table F-2 with a relatively low safety factor outcome for these two rotated cases. Clearly, the adjusted single bolt capacity is not sufficient for Simulation 38. The capacity of the perforated steel sheets will be required to support the unstable blocks for this scenario. The remaining load required for the perforated sheet to support is approximately 2.7 tons.

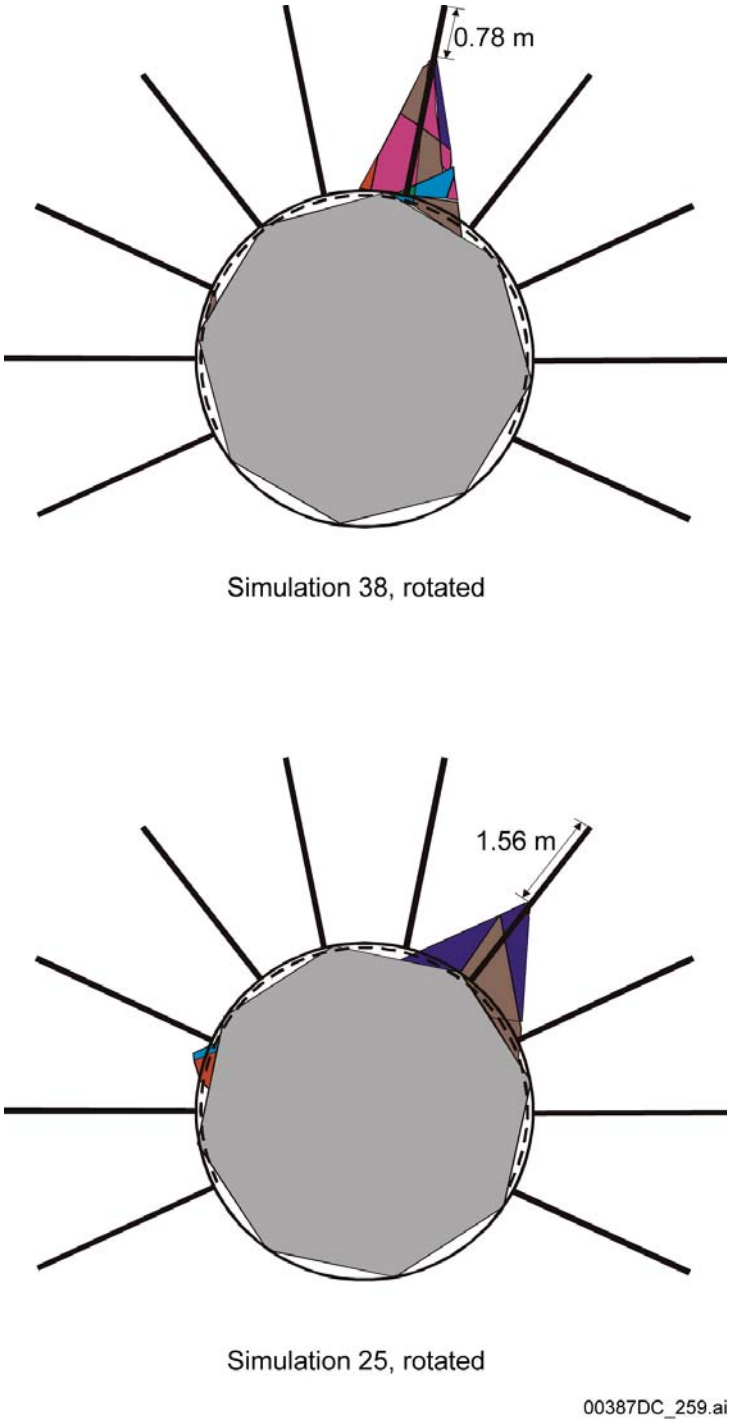

Source: BSC 2004a, Figure 6.3-21.

Figure F-11. Unstable Blocks Aligned along the Most Unfavorable Orientation

To evaluate the performance of the perforated steel sheets against the unstable blocks for Simulation 38, the calculation procedure in *Ground Control for Emplacement Drifts for LA* (BSC 2003, Section 6.4.3) was used. To simplify the calculation, the pyramid shape was assumed for

the assembly of the unstable blocks. The base dimension *l* can be calculated with known volume and height of the pyramid:

$$l = \sqrt{\frac{3 \times V}{h}} \qquad \text{(Eq. F-1)}$$

where *V* and *h* is the volume and height of the pyramid, respectively.

The volume of the block assemblage at the pyramid location is estimated to be 3 m^3 based on the 3DEC simulation results. With a volume of 3 m^3 and a height of 2.22 m from Simulation 38 rotated (Figure F-10), the base dimension *l* is calculated as 2 m. Figure F-12 shows that the actual footprint of the unstable block is larger than the base of the pyramid; hence, the calculation result is on the conservative side.

If the remaining dead load (2.7 MT) is spread uniformly over the entire area of the perforated sheet, the unit load is

$$w = \frac{W}{A} = \frac{2.7 * 0.008896}{2^2} = 0.006 \quad MN / m^2 \qquad \text{(Eq. F-2)}$$

where 0.008896 is a constant for conversion from metric ton to meganewton (MN).

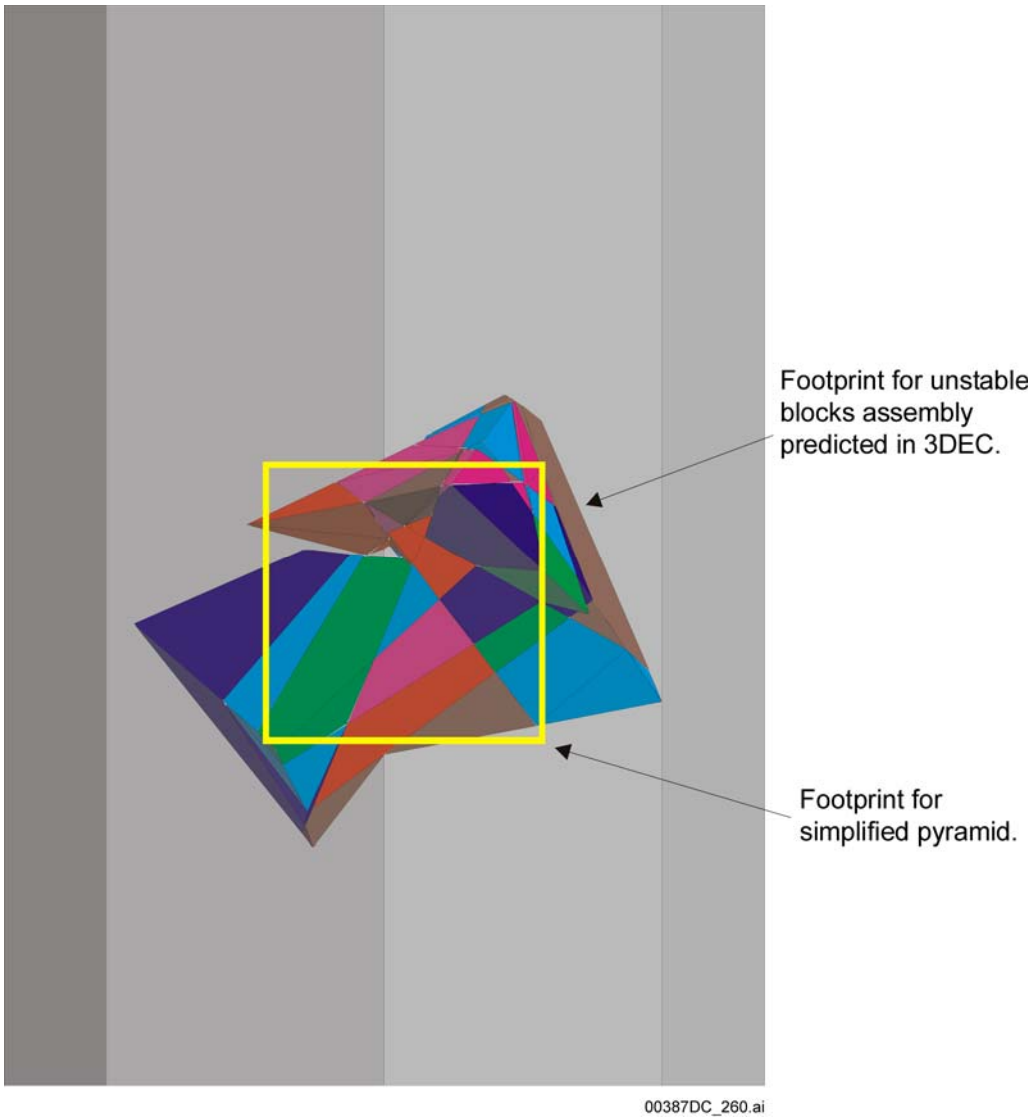

Source: BSC 2004a, Figure 6.3-22.

Figure F-12. Top View for the Footprints of the Unstable Blocks Assembly Predicted in 3DEC Simulation 38 and the Simplified Pyramid

The thin-walled, corrugated stainless steel sheets installed in emplacement drifts may be conservatively assumed to behave like a flat plate, rigidly fixed on its edges, and subjected to a uniform load over its entire area, as stated in *Ground Control for Emplacement Drifts for LA* (BSC 2003, Section 6.4.3). The maximum stress at the center of the plate under a uniform load can be estimated using the following expression (Young 1989, p. 464, Case No. 8, Loading Case No. 8a):

$$\sigma = \frac{\beta w l^2}{t^2} \qquad \text{(Eq. F-3)}$$

where t is the thickness of the steel sheet (3 mm) and β is a constant, equal to 0.1386 for the case considered.

Stress in the stainless steel sheets is estimated to be approximately 370 MPa with the base dimension l as 2 m, corresponding to the factor of safety of 1.67 based on a tensile strength of 620 MPa for stainless steel (BSC 2003, Table 3-6). The factor of safety is calculated against the stress associated with peak elastic strain in the steel (i.e., the stress state at the onset of inelastic hardening). However, it is not the rupture condition since this sheet will have considerable inelastic strain prior to rupture. The combination of the rock bolt and steel sheets is, therefore, considered adequate even for an extreme scenario with rotated blocks (shown in Figure F-11).

F.4.5 Conclusions

The sensitivity and uncertainty analyses for fracture patterns using the site-specific ground motion history with the discontinuum model are summarized in Sections F.4.3 and F.4.4. The design basis rock blocks have been generated from these analyses for evaluation of waste packages. The uncoupled ground support analysis shows that the ground support system is adequate with a relatively large margin of safety with consideration to sensitivity and uncertainty of the fracture patterns.

F.5 REFERENCES

F.5.1 Documents Cited

BSC (Bechtel SAIC Company) 2003. *Ground Control for Emplacement Drifts for LA.* 800-K0C-TEG0-00100-000-00A. Las Vegas, Nevada: Bechtel SAIC Company. ACC: ENG.20031016.0001

BSC 2004a. *Evaluation of Emplacement Drift Stability for KTI Resolutions.* 800-KMC-SSE0-00200-000-00A. Las Vegas, NV: Bechtel SAIC Company. ACC: MOL.20040510.0199.

BSC 2004b. *Drift Degradation Analysis*. ANL-EBS-MD-000027 REV 03. Las Vegas, NV: Bechtel SAIC Company. ACC: MOL.20040513.0081.

BSC 2004c. *Development of Earthquake Ground Motion Input for Preclosure Seismic Design and Postclosure Performance Assessment of a Geologic Repository at Yucca Mountain, NV.* MDL-MGR-GS-000003 REV 00, with errata. Las Vegas, Nevada: Bechtel SAIC Company. ACC: DOC.20031201.0001; DOC.20040401.0004.

CRWMS M&O (Civilian Radioactive Waste Management System Management and Operating Contractor) 2000. *Ground Control for Emplacement Drifts for SR.* ANL-EBS-GE-000002 REV 00. Las Vegas, Nevada: CRWMS M&O. ACC: MOL.20000414.0875.

Itasca Consulting Group 2002. *Itasca Software–Cutting Edge Tools for Computational Mechanics*. Minneapolis, Minnesota: Itasca Consulting Group. TIC: 252592.

NRC (U.S. Nuclear Regulatory Commission) 2002. *Integrated Issue Resolution Status Report.* NUREG-1762. Washington, D.C.: U.S. Nuclear Regulatory Commission, Office of Nuclear Material Safety and Safeguards. TIC: 253064.

Reamer, C.W. and Williams, D.R. 2001. Summary Highlights of NRC/DOE Technical Exchange and Management Meeting on Repository Design and Thermal-Mechanical Effects. Meeting held February 6-8, 2001, Las Vegas, Nevada. Washington, D.C.: U.S. Nuclear Regulatory Commission. ACC: MOL.20010307.0511 through MOL.20010307.0521.

Young, W.C. 1989. *Roark's Formulas for Stress and Strain.* 6th Edition. New York, New York: McGraw-Hill. TIC: 10191.

F.5.2 Data, Listed by Data Tracking Number

MO0306SDSAVDTH.000. Seismic Design Spectra and Acceleration, Velocity, and Displacement Time Histories for the Emplacement Level at 10-4 Annual Exceedance Frequency. Submittal date: 06/26/2003.

APPENDIX G

ANALYSIS OF ROCK MOVEMENT IN INVERT (RESPONSE TO RDTME 3.09)

Note Regarding the Status of Supporting Technical Information

This document was prepared using the most current information available at the time of its development. This Technical Basis Document and its appendices providing Key Technical Issue Agreement responses that were prepared using preliminary or draft information reflect the status of the Yucca Mountain Project's scientific and design bases at the time of submittal. In some cases this involved the use of draft Analysis and Model Reports (AMRs) and other draft references whose contents may change with time. Information that evolves through subsequent revisions of the AMRs and other references will be reflected in the License Application (LA) as the approved analyses of record at the time of LA submittal. Consequently, the Project will not routinely update either this Technical Basis Document or its Key Technical Issue Agreement appendices to reflect changes in the supporting references prior to submittal of the LA.

APPENDIX G

ANALYSIS OF ROCK MOVEMENT IN INVERT (RESPONSE TO RDTME 3.09)

This appendix provides a response for Key Technical Issue (KTI) agreement Repository Design and Thermal-Mechanical Effects (RDTME) 3.09. This agreement relates to concerns regarding the rock movement in the invert during the repository preclosure period.

G.1 KEY TECHNICAL ISSUE AGREEMENT

G.1.1 RDTME 3.09

Agreement RDTME 3.09 was reached during the U.S. Nuclear Regulatory Commission (NRC)/U.S. Department of Energy (DOE) Technical Exchange and Management Meeting on Repository and Design Thermal-Mechanical Effects held February 6 to 8, 2001, in Las Vegas, Nevada (Reamer and Williams 2001). There has been no submittal to the NRC related to this KTI agreement.

The wording of this agreement is as follows:

RDTME 3.09

> Provide appropriate analysis that shows that rock movements in the invert are either controlled or otherwise remain within the range acceptable to provide for retrieval and other necessary operations within the disposal drifts. DOE will provide appropriate analysis that shows rock movements in the floor of the emplacement drift are within the range acceptable for preclosure operations. The analysis results will be provided in a revision to the Ground Control for Emplacement Drifts for SR, ANL-EBS-GE-000002 (or other document) supporting any potential license application. This is expected to be available to NRC in FY 2003.

The agreement focuses on a concern regarding the rock movement in the invert during the repository preclosure period. Due to waste emplacement, emplacement drifts will experience elevated temperatures. Similar to the rock mass near the crown and the wall of an emplacement drift, the rock in the invert may also move inward due to displacement induced by thermal expansion. Excessive rock movement may complicate or preclude retrieval and other operations addressed in 10 CFR Part 63.

G.1.2 Related Key Technical Issue Agreements

Agreements RDTME 3.02 (Appendix D), RDTME 3.05 (Appendix A), RDTME 3.10 (Appendix D), and RDTME 3.13 (Appendix D) are related to RDTME 3.09.

- RDTME 3.02 addresses critical combination of in situ, thermal, and seismic stresses for ground support design. The loading combinations, based on the study described in resolution of RDTME 3.02 (Appendix D) are used for resolution of RDTME 3.09.

- RDTME 3.05 addresses rock mass mechanical properties of lithophysal rock. The rock mass properties estimate, based on the approach described in resolution of RDTME 3.05 (Appendix A), is used for resolution of RDTME 3.09.

- RDTME 3.10 addresses justification for use of two-dimensional modeling for emplacement drifts. The two-dimensional models, based on the study described in resolution of RDTME 3.10 (Appendix D), are used for resolution of RDTME 3.09.

- RDTME 3.13 addresses justification for boundary conditions used in modeling for emplacement drifts. The boundary conditions, based on the study described in resolution of RDTME 3.13 (Appendix D), are used for resolution of RDTME 3.09.

G.2 RELEVANCE TO REPOSITORY PERFORMANCE

The preclosure safety analysis is to be used to demonstrate the safety of the proposed design and operations in the geologic repository operations area with regard to the overall preclosure performance objectives through a systematic examination of the site, design, potential hazards, initiating events and their resulting event sequences, and the potential radiological exposures to workers and the public (10 CFR 63.112). The emplacement drifts are an array of horizontal tunnels trending at 72° azimuth. Each drift will have a diameter of 5.5 m and will be separated from the adjacent drifts by a center-to-center distance of 81 m (BSC 2003; Williams 2002). The emplacement drifts provide the subsurface access and openings for the structures, systems, and components required for emplacement and retrieval operations. The emplacement area host rock provides shielding for the rest of the underground facilities from radiation emanating from the waste packages.

The rock mass surrounding the emplacement drifts, including the invert, is subjected to loads induced by in situ stress, thermal loading, and seismic ground motions. Using the anticipated load conditions, the rock mass movement around the emplacement drifts during the preclosure period is analyzed to evaluate the drift stability and the potential need for invert ground control. The rock movement is evaluated to ensure that the retrieval operations are maintained. This appendix addresses the movement of the rock mass in the invert during the preclosure period only and does not evaluate or discuss rock movement in the postclosure period.

G.3 RESPONSE

To respond to agreement RDTME 3.09, an analysis was performed that shows that the rock movements in the invert of the emplacement drifts are within acceptable ranges for preclosure operations. A summary discussion of the analysis is provided within this appendix, with the detailed information covered in *Evaluation of Emplacement Drift Stability for KTI Resolutions* (BSC 2004a).

The items covered in this appendix to respond to RDTME 3.09 include:

- Acceptable range of rock deformation in the invert
  - The maximum allowable rock displacements considered in the design of the invert

  - Design tolerances for gantry rails, which are related to retrieval operations

- Methods for the prediction of rock deformation in the invert

- Predicted rock deformation in the invert

  - Results of the predictions, including the rock deformations in the vertical, lateral, and longitudinal directions

- Comparison of the predicted rock deformations and the design tolerances.

The conclusions from the analysis (BSC 2004a), which utilizes a two-dimensional numerical method to predict the rock deformation in the invert, are:

- Thermally induced rock expansion is the primary induced force regarding the rock deformation in the invert.

- Preclosure seismically-induced ground motions have insignificant effect on the invert rock deformation.

- Rock movement due to in situ stress release occurring from excavation will be equilibrated prior to the installation of the invert structures or gantry rails and will have no effect on repository operations.

- The invert structure (i.e., the ballast material and ground support system) is not designed to control the rock deformation in the invert.

- The predicted rock deformation in the invert is small compared to the design tolerances listed in Table G-1.

Table G-1. Summary of Design Tolerances for Rock Deformation in Invert

Components	Design Tolerance (mm)
Lateral[a]	28.6 (6.4)
Vertical[b]	6.4
Longitudinal[c]	12.7

Source: BSC 2004a, Section 6.4.1.

NOTE: [a]The numbers in parentheses are the lateral relative displacements per 6 m of drift.
[b]The numbers are the vertical relative displacements per 6 m of drift.
[c]The numbers are the longitudinal relative displacements per 12 m of drift.

These design tolerances are based on acceptable clearance ranges and rail/gantry crane alignment to maintain proper emplacement equipment operations.

The information in this report is responsive to agreement RDTME 3.09 made between the DOE and NRC. This report contains the information that the DOE considers necessary for NRC review for closure of this agreement.

G.4 BASIS FOR THE RESPONSE

The acceptable range of rock deformations in the invert was determined based on the information from the design of invert steel structure and gantry rails (BSC 2004b, pp. 69 and 70; CMAA 70-2000, Section 1.4.2 and Table 1.4.2-1). The analysis for predicting the rock deformation in the invert is a two-dimensional model, as discussed in Section G.4.2, with the primary loading condition caused by the thermally induced rock movement in the invert after waste emplacement.

G.4.1 Acceptable Range of Rock Deformation in Invert

Rock deformation in the invert, specifically in the lateral, vertical, and longitudinal directions, is one of the criteria considered in the design of the invert structure and gantry rails and is reflected in the range of specified design tolerances.

From the invert structure design perspective, the relative lateral and longitudinal displacements in the invert need to be predicted in order to appropriately define the design tolerances for the invert structure, or steel beams (BSC 2004b, Section 2). The steel invert structure will provide a framework, consisting of a series of steel beams bolted to the invert rock mass, that supports the emplacement pallets, waste packages, and the drip shields. It will also provide the support for the rails that support the gantry crane rails for emplacement and retrieval of waste packages and installation of the drip shield. The design tolerances for the steel invert structure are specified as follows (BSC 2004b, pp. 69 and 70):

- Lateral displacement: 28.6 mm (1.13 in.)
- Axial (drift) displacement: 12.7 mm (0.5 in.) every 12 m (39 ft) of steel beams.

From the gantry rail design perspective, the predicted relative lateral and vertical displacements in the invert are also used to check or define the design tolerances. According to the *Specifications for Top Running Bridge and Gantry Type Multiple Girder Electric Overhead Traveling Cranes* (CMAA 70-2000, Section 1.4.2 and Table 1.4.2-1), the design tolerances for the gantry rails installed in emplacement drifts are specified as follows:

- Lateral displacement: ±6.4 mm (±0.25 in.) every 6 m (20 ft) of rails
- Vertical displacement: ±6.4 mm (±0.25 in.) every 6 m (20 ft) of rails.

G.4.2 Methods for Prediction of Rock Deformation in Invert

Figure G-1 shows the distributions of time-dependent drift wall temperatures along the emplacement drift (BSC 2004a, Figure 6.4-1). The temperatures were developed by the *Ventilation Model and Analysis Report* (BSC 2004c, DTN: MO0306MWDALAFV.000) using a continuous, preclosure forced ventilation airflow rate of 15 m^3/s. The temperature distributions are nearly linear along the drift with respect to time. The maximum temperature difference over a 600-m-long drift is about 42°C, occurring at 2 years after waste emplacement completion. Due

to the confinement provided by the rock mass, thermally induced deformation in the longitudinal direction will likely be minimal. Using a conservative assumption of a plane strain condition in estimating the lateral and vertical deformations in the invert, a two-dimensional approach, in which the longitudinal strain is assumed to be zero, is appropriate to predict the rock deformation in the invert.

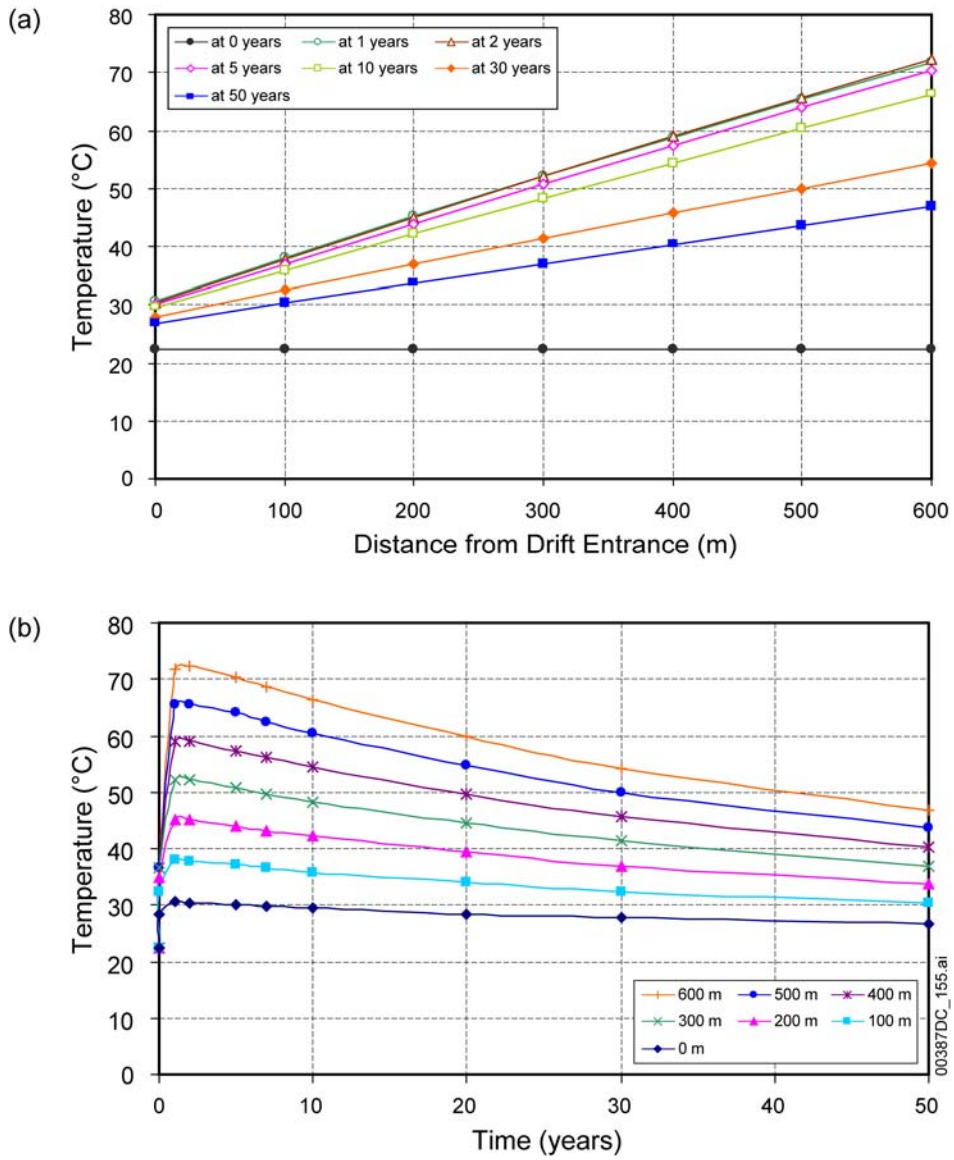

Source: BSC 2004a, Figure 6.4-1.

Figure G-1. Distributions of Time-Dependent Drift Wall Temperatures along Emplacement Drift: (a) as a Function of Location from the Drift Fresh Air Inlet; (b) as a Function of Time

The 600-m-long emplacement drift is represented by seven cross-sectional planes, each with a thickness of 1 unit (meter) located at distances measured from the drift entrance: 0 m, 100 m, 200 m, ···, 600 m. The behavior of these cross-sectional planes are assumed to be independent of each other and can be analyzed independently based on the rationale that: (1) two adjacent

locations are separated by a distance of 100 m, and thermally induced deformations in the rock mass at one location will have limited impact on the behavior of the other location; and (2) the maximum difference in temperatures between two adjacent locations is only about 7°C, as shown in Figure G-1, and this small thermal gradient is unlikely to significantly affect the behavior of each location. The thermal-mechanical response at locations between two adjacent stations (planes) is predicted using linear interpolation.

Both in situ and seismic loading conditions are assumed to be the same for each of these cross-sectional planes with the thermal loading condition unique for each plane. The in situ loading condition is the geostatic state of stress existing prior to excavation and is related to the overburden thickness and horizontal stress ratios described in Section 2.3.3 of this technical basis document. Along an emplacement drift, the change of the overburden depth, and, therefore, the resulting change of the in situ stress state is assumed to be small. Use of the bounding in situ load in the analysis (BSC 2004a, Section 6.1.1.1) addresses the potential uncertainty associated with the variation in the in situ loading condition. At a drift or repository scale, seismically induced ground motions will have similar effect on the rock movement at different locations along an emplacement drift as long as the ground conditions at these locations are similar.

Seven two-dimensional analyses were performed, each given an identical in situ or seismic condition but a unique temperature boundary condition that is associated with the specific location of the analysis. Since the seismic ground motions and temperature changes expected in the emplacement drifts are time-dependent, these two-dimensional analyses were assumed to be quasi-steady state and conducted using the FLAC computer code. The model configurations and boundary conditions used in these analyses are shown in Figure G-2. The rock mass mechanical properties considered are for lithophysal rock strength Categories 1 and 5, as listed in *Evaluation of Emplacement Drift Stability for KTI Resolutions* (BSC 2004a, Table 4-5a). The Category 1 rock mass represents the weakest rock anticipated, whereas the Category 5 rock mass is for the strongest lithophysal rock. Detailed discussions on the rock mass strength categories and associated mechanical properties are provided in Sections 3.2, 4.2, and 5.3 and Appendix A of this document.

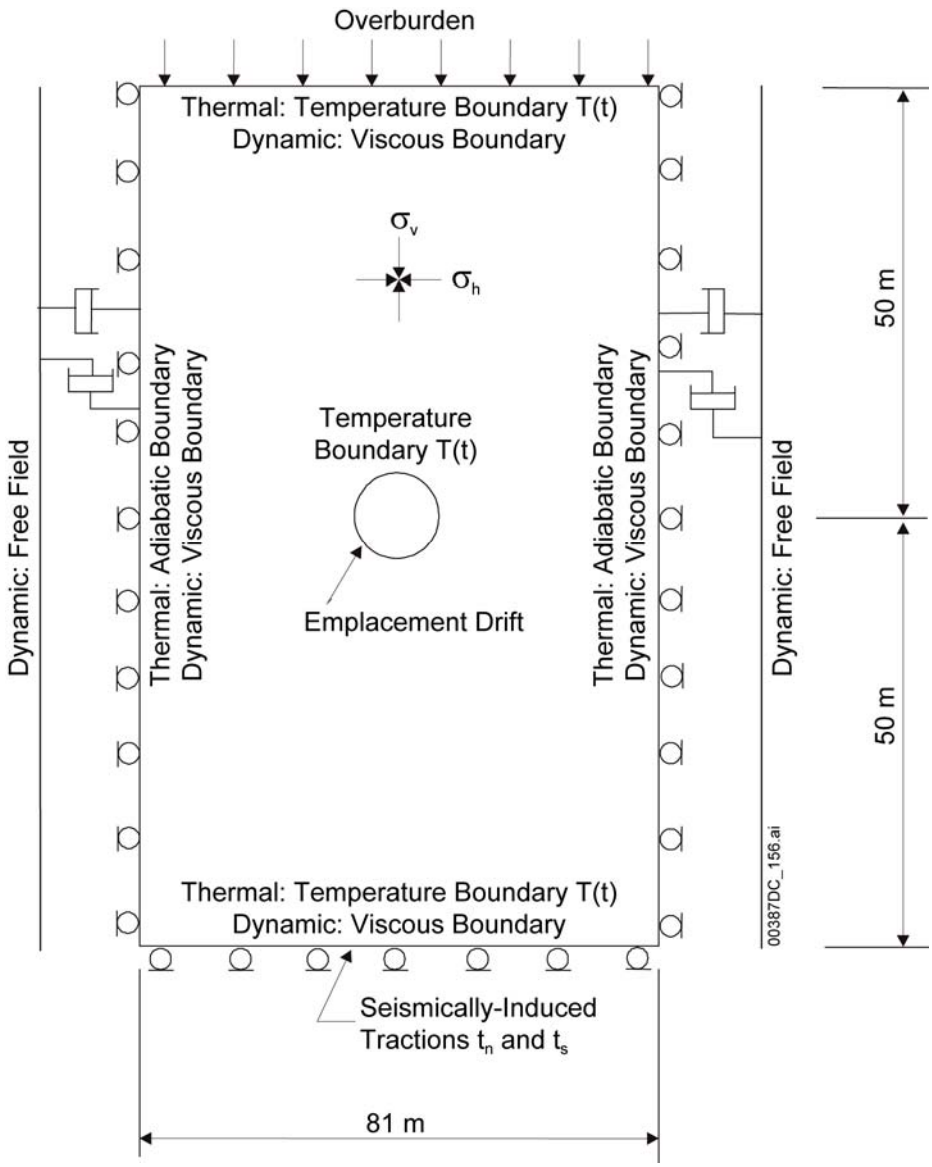

Source: BSC 2004a, Figure 6.1-4.

Figure G-2. Geometry and Boundary Conditions for a Typical Two-Dimensional Model

The two-dimensional analyses are limited to predicting the lateral and vertical deformations in the invert (the longitudinal deformation was assumed to be zero). The upper bound for total invert longitudinal displacement can be determined using an approach where an emplacement drift is modeled as a column that can expand freely in the longitudinal direction when subject to elevated temperatures. The total thermal expansion or elongation can then be estimated from the following equation:

$$\Delta L = \alpha \Delta T L \qquad \text{(Eq. G-1)}$$

where ΔL = thermally induced elongation, in meters
α = coefficient of thermal expansion, per degree Celsius
ΔT = increase in temperature, in degrees Celsius
L = length of drift, in meters.

G.4.3 Predicted Rock Deformation in the Invert

From the perspective of the steel invert structure and gantry rail design, only the effects of thermal and seismic loading conditions on the rock deformation in the invert are important. The deformation induced by in situ loading condition is inconsequential because the deformation of the entire drift wall, including the invert region, has already occurred and equilibrated prior to the installation of the invert structure and rails. Consequently, the excavation-induced rock deformation will not have any effect on the installed invert structure or rails or the emplaced waste packages. Any offset in the invert structure or the gantry rails caused by the rock movement in the invert will be due primarily to either thermally induced expansion or seismic ground motions. Since in situ load is considered in every model, its effect on the rock deformation is excluded by subtracting the rock displacements induced by the in situ load from the total displacements caused by the other combined loads.

Seven plane-strain FLAC analyses were completed for each ground condition or rock type and initial stress state (K_0 value[1]), representing seven locations with different temperature conditions along an emplacement drift. With two bounding rock mass categories and two initial stress conditions, a total of 28 FLAC runs were performed. Detailed results from these runs assessing the impact on rock deformations induced by elevated temperatures in the invert are provided in *Evaluation of Emplacement Drift Stability for KTI Resolutions* (BSC 2004a, Section 6.4.3). A summary of the results is presented below.

Vertical Displacement–The vertical relative displacements at the invert are illustrated in Figure G-3. These values are estimated between any location along the drift and the entrance (Station 0) from the predicted total vertical displacements under combined in situ and thermal loads. These vertical relative displacements are relevant to the criterion specified for the gantry rail design (see Section G.4.1). The maximum vertical relative displacement over a distance of 600 m (between Station 6 and Station 0) is predicted to be about 4 mm and not sensitive to either the rock mass categories or the initial stress conditions (K_0 values). Also, the vertical relative displacements vary linearly along the drift, indicating that a linear interpolation can be used to

[1] K_0 is the ratio of horizontal to vertical stress. The vertical stress is the major principal stress component, with K_0 values ranging from 0.36 to 0.62 (Section 2.3.3 of this technical basis document). The K_0 values are conservatively assumed to vary from 0.3 to 1.0 in these analyses.

estimate the relative displacement between any two locations. The vertical relative displacements in the invert over a distance of 6 m for various rock mass categories and initial stress conditions are then estimated and listed in Table G-2.

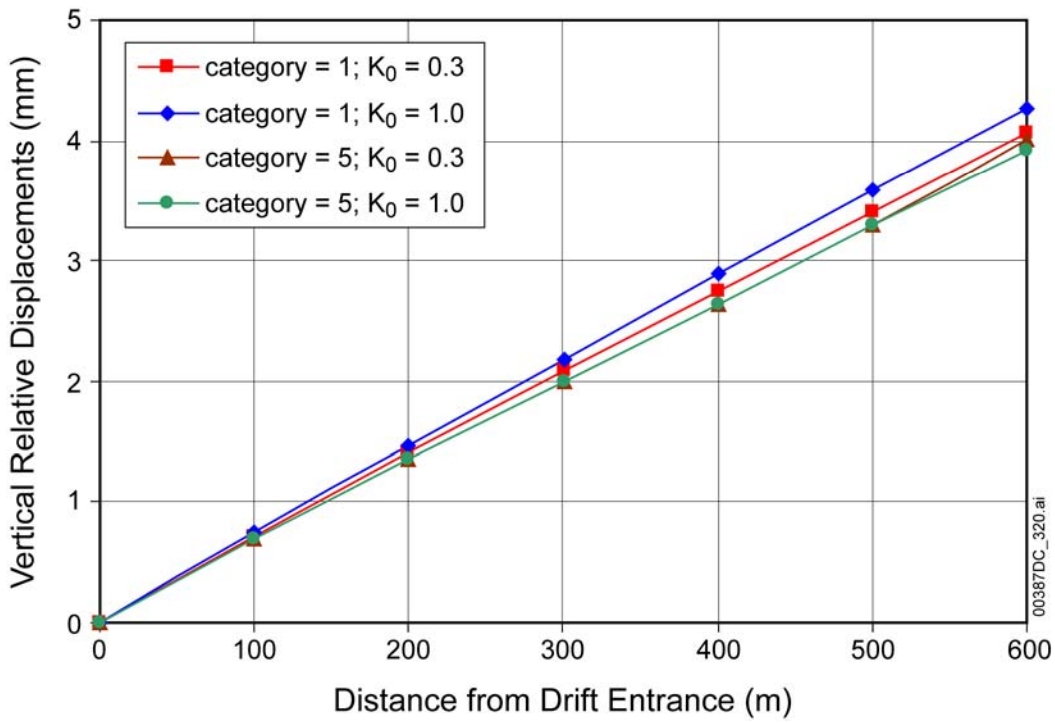

Source: BSC 2004a, Figures 6.4-2b, 6.4-5b, 6.4-8b, and 6.4-11b.

Figure G-3. Vertical Relative Displacements in Invert as a Function of Location along Emplacement Drift

Table G-2. Summary of Predicted Rock Vertical Relative Displacements in Invert under Thermal and Seismic Loading Conditions

Rock Type and Initial Stress Condition	Relative Displacements under Thermal Loading[a] (mm)	Relative Displacements under Seismic Loading (mm)	Total Relative Displacements (mm)
Category 1 and K_0 = 0.3	0.04	0.0	0.04
Category 1 and K_0 = 1.0	0.04	0.0	0.04
Category 5 and K_0 = 0.3	0.04	0.0	0.04
Category 5 and K_0 = 1.0	0.04	0.0	0.04

Source: BSC 2004a, Table 6.4-1.

NOTE: [a]The numbers are the vertical relative displacements per 6 m of drift.

The preexisting conditions, whether a drift is heated or not, have practically no effect on the rock vertical relative displacements during seismic ground motions (BSC 2004a, Figures 6.1-6, 6.1-11, 6.1-16, and 6.1-21). The invert of the entire drift, even with a thermal gradient, will move in translational mode like a rigid body during seismic ground motions. This observation indicates that the vertical relative displacements between any two locations along a drift during seismic ground motions are close to zero. The values are listed in Table G-2.

Lateral Displacement–Due to the thermal symmetry during heating, the maximum horizontal relative displacements within a drift occur between the walls at the springline. These relative displacements are defined as the drift horizontal closures (BSC 2004a, Section 6.1.4). A positive drift closure indicates a reduction in drift diameter. Use of the drift horizontal closures considered in the analyses to estimate the lateral displacements in the invert is very conservative.

The predicted drift horizontal closures induced by heating are shown in Figure G-4. The maximum values are associated with Station 6 (600 m), and predicted to be about 2 mm. Horizontal displacements are only slightly sensitive to the rock mass strength categories. A summary of these values is provided in Table G-3.

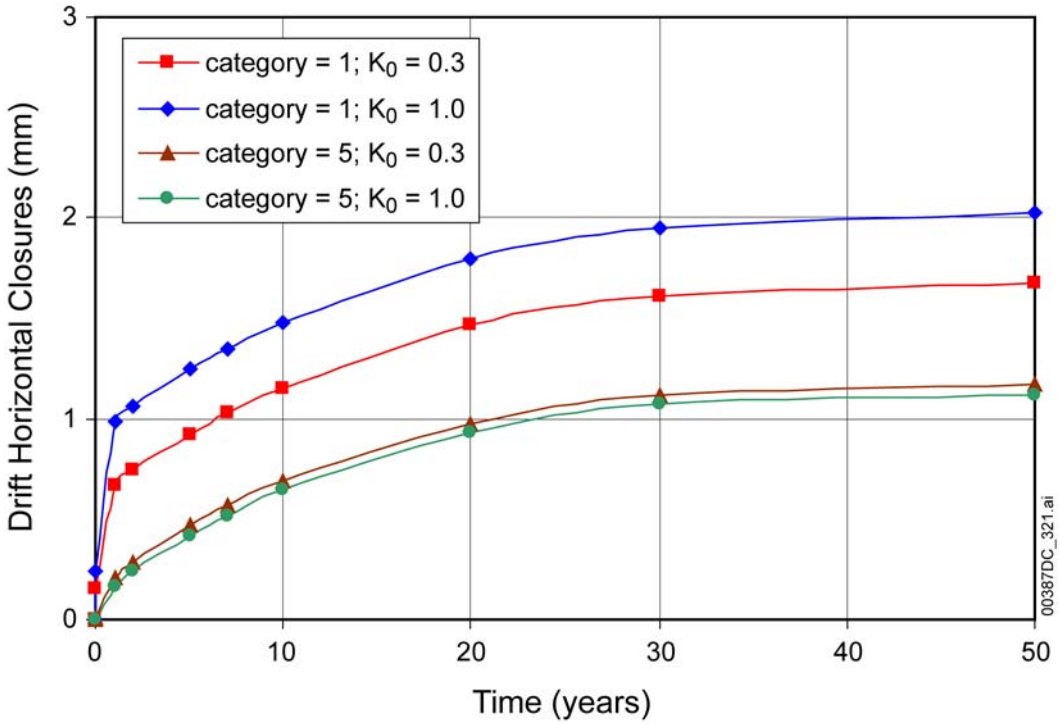

Source: BSC 2004a, Figures 6.4-3b, 6.4-6b, 6.4-9b, and 6.4-12b.

Figure G-4. Time-Dependent Drift Horizontal Closures along Emplacement Drift Induced by Heating

Table G-3. Summary of Predicted Drift Total Horizontal Closures under Thermal and Seismic Loading Conditions

Rock Type and Initial Stress Condition	Relative Displacements under Thermal Loading[a] (mm)	Relative Displacements under Preclosure (10^{-4}) Seismic Loading (mm)	Total Maximum Relative Displacements[a] (mm)
Category 1 and $K_0 = 0.3$	1.68 (0.01)	1.48	3.16 (0.01)
Category 1 and $K_0 = 1.0$	2.02 (0.02)	1.64	3.66 (0.02)
Category 5 and $K_0 = 0.3$	1.17 (0.01)	0.14	1.31 (0.01)
Category 5 and $K_0 = 1.0$	1.12 (0.01)	0.14	1.26 (0.01)

Source: BSC 2004a, Table 6.4-2.

NOTE: The numbers in this table are the horizontal closures and are conservatively used as the lateral displacements.
[a] The numbers in parentheses are the lateral relative displacements per 6 m of drift.

The horizontal relative closures between any station along the drift and Station 0 are shown in Figure G-5. They vary linearly along the drift, indicating that the linear interpolation can also be used for estimating the horizontal relative closure between any two locations. The difference in the horizontal closures between two locations separated by a distance of 6 m is then estimated, as listed in Table G-3. The difference in the horizontal closures between two locations separated by a distance of 6 m is practically negligible.

Table G-3 also lists the horizontal closures induced by seismic ground motions. It can be seen that they are generally less than 2 mm, and sensitive to the rock mass modulus but not to the temperature conditions existing prior to shaking.

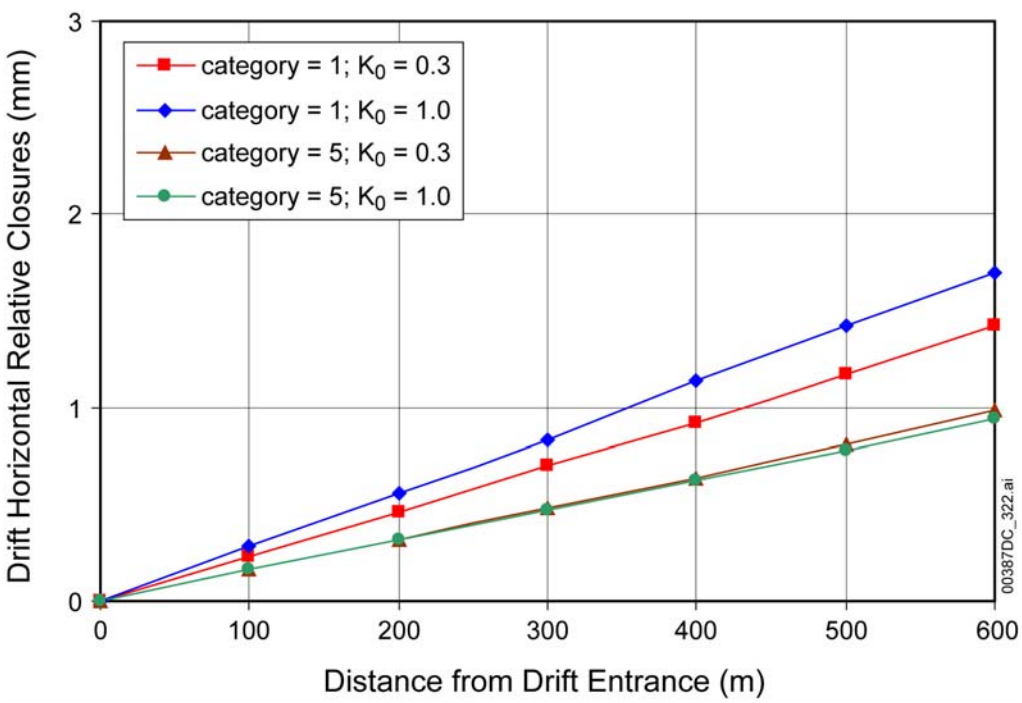

Source: BSC 2004a, Figures 6.4-4b, 6.4-7b, 6.4-10b, and 6.4-13b.

Figure G-5. Horizontal Relative Closures along Emplacement Drift Induced by Heating

Longitudinal Displacement–The thermal expansion in the longitudinal direction is about 4.0 mm over a distance of 12 m, which for a typical drift length of 600 m would be equal to 0.2 m in total. This was estimated based on Equation G-1, using the maximum temperature difference of 42°C over the 600-m-long drift (BSC 2004a, Table 4-1a) and a coefficient of thermal expansion of 8.02×10^{-6} per degree Celsius (BSC 2004a, Table 4-3).

Comparison of the Predicted Rock Deformation and the Design Tolerances–A summary of the predicted maximum relative displacements under thermal and seismic loading conditions is presented in Table G-4. It is evident that these relative displacements are well within the acceptable ranges of design tolerances for the steel invert structure and the gantry rails. Therefore, the rock movement in the invert during the repository preclosure period is not a concern from the perspectives of the steel invert structure performance and the retrieval operation.

Table G-4. Summary of Predicted Maximum Rock Relative Displacements in Invert under Thermal and Seismic Loading Conditions

Components	Total Maximum Relative Displacements (mm)	Design Tolerance (mm)	Acceptance
Lateral[a]	3.66 (0.02)	28.6 (±6.4)	Satisfied
Vertical[b]	0.06	±6.4	Satisfied
Longitudinal[c]	4.0[d]	12.7	Satisfied

Source: BSC 2004a, Table 6.4-3.

NOTE: [a] The numbers in parentheses are the lateral relative displacements per 6 m of drift.
[b] The numbers are the vertical relative displacements per 6 m of drift.
[c] The numbers are the longitudinal relative displacements per 12 m of drift.
[d] The number is estimated based on free expansion at 2 years per 12 m of drift.

G.4.4 Summary and Conclusions

The rock movement in the invert of the emplacement drift is predicted to remain within the acceptable limits of design tolerances for the steel invert structure and the gantry rails. Both the invert structure performance and the retrieval operation during the preclosure period are expected to remain unaffected by the rock movement in the invert.

G.5 REFERENCES

G.5.1 Documents Cited

BSC (Bechtel SAIC Company) 2003. *Underground Layout Configuration*. 800-P0C-MGR0-00100-000-00E. Las Vegas, Nevada: Bechtel SAIC Company. ACC: ENG.20031002.0007.

BSC 2004a. *Evaluation of Emplacement Drift Stability for KTI Resolutions*. 800-KMC-SSE0-00200-000-00A. Las Vegas, NV: Bechtel SAIC Company. ACC: MOL.20040510.0199.

BSC 2004b. *Steel Invert Structure-Emplacement Drifts*. 800-SSC-SSE0-00100-000-00A. Las Vegas, Nevada: Bechtel SAIC Company. ACC: ENG.20040119.0012.

BSC 2004c. *Ventilation Model and Analysis Report*. ANL-EBS-MD-000030 REV 03 ICN 03, with errata. Las Vegas, Nevada: Bechtel SAIC Company. ACC: DOC.20031216.0002; DOC.20040202.0004; DOC.20040325.0003.

Reamer, C.W. and Williams, D.R. 2001. Summary Highlights of NRC/DOE Technical Exchange and Management Meeting on Repository Design and Thermal-Mechanical Effects. Meeting held February 6-8, 2001, Las Vegas, Nevada. Washington, D.C.: U.S. Nuclear Regulatory Commission. ACC: MOL.20010307.0511 through MOL.20010307.0521.

Williams, N.H. 2002. "Thermal Inputs for Evaluations Supporting TSPA-LA." Interoffice memorandum from N.H. Williams (BSC) to Distribution, September 16, 2002, 0911024159, with enclosures. ACC: MOL.20021008.0141.

G.5.2 Codes, Standards, and Regulations

10 CFR Part 63. *Energy: Disposal of High-Level Radioactive Wastes in a Geologic Repository at Yucca Mountain, Nevada*. Readily available.

CMAA 70-2000. *Specifications for Top Running Bridge and Gantry Type Multiple Girder Electric Overhead Traveling Cranes.* Charlotte, North Carolina: Crane Manufacturers Association of America. TIC: 249445.

G.5.3 Data, Listed by Data Tracking Number

MO0306MWDALAFV.000. ANSYS-La-Fine Ventilation. Submittal date: 06/23/2003.

INTENTIONALLY LEFT BLANK

APPENDIX H

CONTINUUM AND DISCONTINUUM ANALYSES OF GROUND SUPPORT SYSTEM PERFORMANCE (RESPONSE TO RDTME 3.11)

Note Regarding the Status of Supporting Technical Information

This document was prepared using the most current information available at the time of its development. This Technical Basis Document and its appendices providing Key Technical Issue Agreement responses that were prepared using preliminary or draft information reflect the status of the Yucca Mountain Project's scientific and design bases at the time of submittal. In some cases this involved the use of draft Analysis and Model Reports (AMRs) and other draft references whose contents may change with time. Information that evolves through subsequent revisions of the AMRs and other references will be reflected in the License Application (LA) as the approved analyses of record at the time of LA submittal. Consequently, the Project will not routinely update either this Technical Basis Document or its Key Technical Issue Agreement appendices to reflect changes in the supporting references prior to submittal of the LA.

APPENDIX H

CONTINUUM AND DISCONTINUUM ANALYSES OF GROUND SUPPORT SYSTEM PERFORMANCE (RESPONSE TO RDTME 3.11)

This appendix provides a response to Key Technical Issue (KTI) agreement Repository Design and Thermal-Mechanical Effects (RDTME) 3.11. The agreement relates to concerns regarding the continuum and discontinuum analyses of the ground support system performance that take into account long-term (preclosure period) degradation of the rock mass, joint-strength properties, and ground support components.

H.1 KEY TECHNICAL ISSUE AGREEMENT

H.1.1 RDTME 3.11

Agreement RDTME 3.11 was reached during the U.S. Nuclear Regulatory Commission (NRC)/U.S. Department of Energy (DOE) Technical Exchange and Management Meeting on Repository and Design Thermal-Mechanical Effects held February 6 to 8, 2001, in Las Vegas, Nevada (Reamer and Williams 2001). There has been no submittal related to this KTI agreement to the NRC.

The wording of this agreement is as follows:

RDTME 3.11

> Provide continuum and discontinuum analyses of ground support system performance that take into account long-term degradation of rock mass and joint-strength properties. The DOE will justify the preclosure ground support system design (including the effects of long term degradation of rock mass and joint strength properties) in a revision to the Ground Control for Emplacement Drifts for SR, ANL-EBS-GE-000002 (or other document) supporting any potential license application. This is expected to be available to NRC in FY 2003.

The agreement focuses on the time-dependent performance of the ground support system, taking into account the time-dependent degradation of rock mass and joint strength during preclosure. The role of ground support is to: (1) provide for personnel safety during construction and operation, (2) provide for operational clearances for equipment to facilitate repository operations during the preclosure period, (3) ensure that the regulatory requirement for waste retrievability is maintained, and (4) provide operational conditions facilitating installation of the drip shield at closure.

The ground support is not introduced to protect waste packages from rockfall because the size and shape of the drift and potential rockfall particle sizes are small (see Appendix F for discussion of preclosure rockfall prediction). Ground support is considered to be not important to safety because the preclosure rockfall masses and velocities do not result in a credible scenario for breach of the waste package (BSC 2004a). Although ground support could remain functional for some additional period of time after closure, its functionality during the postclosure period is

not considered in analyses of the postclosure performance of the repository. Analyses and the repository performance assessment during the postclosure period do not assign any credit to the installed ground control system, and the stability of the rock mass during that period is evaluated without considering ground control measures.

The NRC concerns (NRC 2002, Section 2.1.7, p. 19) regarding the KTI agreement are as follows:

- Time-dependent degradation of the repository host rock during preclosure, although not discussed in the DOE thermal-mechanical analyses for site recommendation (BSC 2001), is potentially important because an operational life up to 100 years may be expected for the ground-support system (Wisenburg 2003).

- A DOE expert panel on drift stability (Brekke et al. 1999) indicated that time-dependent degradation of the rock mass can be expected because of coupled thermal-hydrologic-mechanical processes operating over a long period of time (100 years). Thermal, water-pressure, and rock-stress gradients occurring in the rock mass after nuclear waste emplacement would drive processes such as thermally induced fracture propagation, rock loosening, and cyclical evaporation and condensation of water. Such processes can be expected to cause degradation of the rock mass and ground support components.

H.1.2 Related Key Technical Issue Agreements

RDTME 3.04–This KTI agreement involves providing a geotechnical parameters report that includes rock-mass property estimates of the lithophysal rocks of the Topopah Spring Tuff. RDTME 3.11 deals specifically with providing time-dependent characterization of the nonlithophysal and lithophysal rock-mass properties (Sections 3 and 4 of this technical basis document). Thus, the work performed to resolve RDTME 3.11 also forms a portion of the geotechnical parameters report that is used to resolve RDTME 3.04.

RDTME 3.05–This KTI agreement involves providing a methodology to account for the effect of lithophysae on ground control quality. The technical basis document discusses these load combinations in Section 4.2.3.

RDTME 3.06–This KTI agreement focuses on providing the design sensitivity and uncertainty analyses of the emplacement drift stability. The technical basis document discusses these load combinations in Section 5.

TSPAI 2.02, Items 58 and 62–TSPAI 2.02 Items 58 and 62 relate to the inclusion of rockfall and its potential mechanical impacts on engineered barriers (Item 58) and on the thermal-mechanical impacts of long-term rock-mass degradation on engineered barriers and potential hydrologic changes in the rock mass. RDTME 3.11 deals specifically with time-dependent rock-mass property estimates of the Topopah Spring Tuff nonlithophysal and lithophysal rocks and the development of rock-mass material and numerical models for representing rock damage, fracture development and propagation, and long-term degradation. The estimates feed long-term degradation and change of opening shape performance assessment

studies of the engineered barriers. Section 4.2 of the technical basis document describes this integration in more detail.

H.2 RELEVANCE TO REPOSITORY PERFORMANCE

As planned, the repository excavations will be developed in two major types of lithostratigraphic volcanic tuff: the blocky nonlithophysal units (the middle nonlithophysal unit (Tptpmn) and the lower nonlithophysal unit (Tptpln)) and the lithophysal units (the upper lithophysal unit (Tptpul) and the lower lithophysal unit (Tptpll)). The lithophysal rock units constitute approximately 85% of the repository emplacement area, whereas the nonlithophysal units (particularly the Tptpmn) make up the remaining 15% of emplacement area (see Section 2.2 of this technical basis document). Section 2.3 of the technical basis document describes the rock mass structural characteristics of the nonlithophysal and lithophysal units that control the rock mass mechanical properties. Section 3 of this technical basis document provides a description of the resulting rock mass and fracture properties of these units, while Section 4 describes the development of modeling capabilities to represent their mechanical response. Characterization of time-dependent effects for these two different rock types requires an application of numerical methods capable of accounting for the different structures that control mechanical response. Analyses involve the use of numerical models representing the rock strata as either an equivalent continuum or discontinuum media (see Section 4 of this technical basis document). A demonstration of the appropriateness of using these approaches for characterizing the tuff strata performance, considering in particular the long-term degradation of rock and ground support system, was described in Section 5 of this technical basis document.

Estimates of rock mass mechanical properties (including time-dependent strength properties) are used as direct input to numerical models that predict the emplacement drift behavior when subjected to in situ, thermal, and seismic loading, as well as evaluating time-dependent changes in mechanical properties of rock (see Section 5 of this technical basis document). The results from these calculations are used to evaluate the impact that long-term change of rock strength may have on the stability and functionality of emplacement drifts during the preclosure period.

H.3 RESPONSE

Summary–The approach to analyzing the ground support system considering continuum and discontinuum analyses of nonlithophysal and lithophysal tuff units and long-term degradation are summarized in this appendix.

A considerable effort was extended to evaluate appropriateness of utilizing continuous and discontinuous numerical models for representing lithophysal and nonlithophysal rock. In general, the three-dimensional discontinuum approach is considered appropriate for analyzing degradation and rockfall in the hard, jointed, and blocky nonlithophysal tuff units. A two-dimensional discontinuum approach was considered more applicable for analyzing degradation and rockfall in the lithophysal tuff units, where the tuff behavior is governed by the distribution and dimensions of lithophysae (voids) in the rock mass structure (see Sections 4.1 and 4.2 of this technical basis document). Stability of the drifts in the preclosure time frame have been examined using parametric studies based on a continuum based modeling approach, in which rock mass properties have been derived from large-scale laboratory testing (lithophysal

rock) and empirically-estimated rock mass mechanical properties (nonlithophysal rock). These analyses are reviewed in Appendix B.

The response to RDTME 3.11 is derived from the following analyses:

- Three-dimensional 3DEC modeling of drift degradation and rockfall in nonlithophysal rocks associated with in situ, thermal, and seismic loading, as described in Sections 5.3.1 and 5.3.2.1 of this technical basis document, was performed. The fracture geometries in the 3DEC model were derived from a stochastically-defined fracture network developed from the FracMan program, and were based on field mapping of fractures in the ESF and ECRB (Section 4.1.1).

- Two-dimensional UDEC modeling of drift degradation and rockfall in lithophysal rocks associated with in situ, thermal, and seismic loading were completed, as described in Sections 5.3.1 and 5.3.2.2.

- Two-dimensional UDEC modeling of long-term, time-dependent degradation of emplacement drifts in lithophysal rocks is based on the use of a stress corrosion model for representing time-dependent strength loss. The static fatigue laboratory data and time-related strength loss algorithm is described in Section 5.3.2.2.4.

- Ground support techniques and materials have been chosen to ensure longevity through the preclosure time frame (BSC 2003a).

The results of these analyses are described below:

- A bounding analysis of potential effects of long-term degradation of fracture properties was conducted for nonlithophysal rock using the 3DEC program. It is assumed that the ultimate impact of long-term degradation of fracture properties would occur by shearing off surface asperities, leaving a smooth and cohesionless surface whose friction angle would equal the assumed residual friction angle of 30° (Section 5.3.2.1.8). These analyses indicate stable, unsupported emplacement drifts during the preclosure period. This analysis is very conservative in that shearing of fracture surfaces under the low preclosure stress conditions is not expected to result in time-dependent shearing of asperities.

- The two-dimensional UDEC model of emplacement drifts in lithophysal rock was used to examine drift stability for bounding ranges of rock mass mechanical and thermal properties, as well as loading from in situ, thermal, and seismic stresses. Additionally, time-dependent strength degradation modeling was performed by reduction of the rock mass shear strength (cohesion) and tensile strength based on extrapolations from static fatigue testing. These analyses all indicate that unsupported drifts in the lithophysal rock are expected to be stable during the preclosure period.

- Ground support methods, consisting of rock bolts and thin perforated steel sheeting over the entire exposed periphery of the emplacement drifts, were developed to allow air circulation to the rock surface, while minimizing any potential loosening or raveling of

small rock fragments from the tunnel surface. Ground support materials are to be constructed from stainless steel to provide certainty of preclosure longevity.

The above summary indicates a high degree of conservatism in the analysis of preclosure time-dependency and in the ground support methods developed to ensure their function over the preclosure period.

The information in this report is responsive to agreement RDTME 3.11 made between the DOE and NRC. This report contains the information that DOE considers necessary for NRC review for closure of this agreement.

H.4 BASIS FOR THE RESPONSE

This section describes the strategy, technical basis, and approach for resolving agreement RDTME 3.11.

H.4.1 Overview of Resolution Strategy

As a general approach for resolving the geomechanical issues related to the RDTME KTIs and addressing the associated NRC and DOE agreements, a resolution strategy was outlined in *Resolution Strategy for Geomechanically-Related Repository Design and Thermal-Mechanical Effects (RDTME)* (Board 2003), as discussed in Section 6.1. Documents that include analyses of aspects associated with issues required for the resolution of the RDTME 3.11 are listed below.

H.4.2 Basis for Resolution of RDTME 3.11

The emphasis of this agreement is to determine the adequacy of the DOE approach to applying continuum and discontinuum analyses of ground support system performance that take into account long-term degradation of rock mass and joint-strength properties.

H.4.3 Underground Environment

Excavation of the repository drifts will result in concentration of the in situ stress around the openings (Section 1.2.2.1). The magnitude of in situ stresses at the repository horizon, considering the upper bound case of 400-m depth (Section 2.3.3) (BSC 2003b, Section 4.1) is equal to 9.2 MPa and is low in comparison to the uniaxial strength of tuff, whether nonlithophysal or lithophysal (BSC 2003c, Figure 8-22). Because the in situ stresses are relatively small in comparison to the rock mass strength, little, if any, yield of the rock mass is expected, even for the case of unsupported openings. Thus, the openings will undergo primarily elastic deformation, which equilibrates within a short distance (about two tunnel diameters) behind the advancing tunnel boring machine. Because permanent ground support is placed after the emplacement drift is completed and the tunnel boring machine withdrawn, it will be subjected only to deformation and loading that may occur from transient effects, such as thermal and seismic loading (Section 1.2.2.1 of this technical basis document).

During the preclosure period, approximately 100 years from initial excavation of the emplacement drifts, forced ventilation will be used to remove approximately 90% of the heat generated by the waste packages (BSC 2004b). This heat removal will keep drift wall

temperatures below about 75°C for 600-m drifts and 85°C for 800-m drifts (Section 1.2.2.1) (BSC 2004b, Figure 6.6) and will result in small thermally related rock mass stress changes. These temperature ranges are also too low to cause significant impact on the ground support hardware. As discussed in Section 5 and Appendix B, little yielding is expected in either lithophysal or nonlithophysal rock due to preclosure loading.

H.4.4 Ground Support System

The role of ground support in nonlithophysal and lithophysal tuff is somewhat different. However, the element of providing confinement to the surface of tunnel walls and preventing loosening that would lead to detachment of blocks of nonlithophysal tuff or raveling of lithophysal tuff is common to both units. The ground support will be installed in two steps: (1) initial support, installed immediately behind the advancing tunnel boring machine for safety and personnel protection, and (2) the permanent support installed after the excavation is completed.

During the preclosure period, the emplacement drifts will be supported by rock bolts and slotted stainless steel sheeting (BSC 2003a, Section 7.4), thus, minimizing, if not eliminating, mechanical degradation of the excavations. In particular, ground support consists of 3-m-long friction rock bolts placed on a square pattern on 1.25-m spacing and 3-mm-thick (approximately) perforated stainless steel sheets installed in a 270° arc around the drift periphery. Analyses, presented in Appendix B, indicate stability of the openings, even without ground support. Rock bolts and sheeting are expected to perform satisfactorily with acceptable factors of safety (BSC 2003b, Section 7).

As pointed out in *Ground Control for Emplacement Drifts for LA* (BSC 2003b), the ground support methods are selected based on the requirements of function, performance, and service life of the ground support system. The stability analyses described in this report employ the two-dimensional (FLAC) and three-dimensional (FLAC3D) programs, where rock mass is modeled as a continuum medium and is used to represent both nonlithophysal and lithophysal rock via input of different rock mass properties. Performance of the rock strata is assessed considering the opening response to thermal and seismic loads. The stability of emplacement drifts is assessed in two stages. Stage 1 provides assessment of unsupported drifts. Stage 2 includes evaluation of emplacement drifts with ground support installed.

Analysis of ground reinforcement performance in discontinuous strata is also reported in *Evaluation of Emplacement Drift Stability for KTI Resolution* (BSC 2004c, Section 6.3.5). The uncoupled ground support calculation (see Appendix F) represents the ground reinforcement installation identical to the one discussed above for fractured nonlithophysal rock. Rock strata represented within the three-dimensional discontinuum code, 3DEC, contain a network of joints subjected to in situ, thermal, and seismic loading. The performance of the ground support system subjected to dynamic loads is tested for the most severe case of preclosure in situ, thermal, and seismic loads. The modeling results indicate that the ground support performs well with an ample factor of safety for the extreme scenario assuming occurrence of unfavorable block orientations (BSC 2004c, Section 6.3.6, Appendix F).

The performance of ground support during preclosure is also determined by the ability of its materials and components to remain functional without excessive deterioration. *Longevity of Emplacement Drift Ground Support Materials for LA* (BSC 2003a) reports on a range of factors potentially affecting the performance of ground support under preclosure environment in emplacement drifts. These factors include temperature and humidity within the drifts and rock bolt holes. Various forms of corrosion were examined, leading to the choice of stainless steel for ground support materials. Conclusions indicate that under these conditions the recommended materials and ground support hardware will perform satisfactorily for the preclosure period, taken to be nominally 100 years (BSC 2003a, Sections 7.3 and 7.4).

H.4.5 Long-Term Degradation of Nonlithophysal Tuff

Extensive work has been performed to enhance the understanding of the behavior and long-term performance of the hard, blocky, fractured nonlithophysal tuff. A three-dimensional discontinuum model (3DEC) for nonlithophysal rocks that accounts for joint structure and formation of the wedge-type blocks has been developed. Extensive discussion on this subject is presented in *Drift Degradation Analysis* (BSC 2004d) and Section 5.3.2.1 of this technical basis document. Appendices C and F provide a summary on the approach to the analysis of seismic, thermal, and time-dependent effects on rockfall and drift degradation.

H.4.6 Long-Term Degradation of Fractures

Fractures are an integral part of nonlithophysal tuff structure. Fracture surfaces have some degree of roughness due to undulations and asperities. When the fracture is subjected to shearing stress, as is typical around an excavation, the asperities will become points of stress concentration. These asperities may eventually yield due to stress corrosion cracking,[1] with the resulting effect of shearing off the surface roughness. The ultimate (and extremely conservative) time-degradation effect of long-term loading of fracture surfaces would, therefore, be to shear all surface roughness, resulting in no cohesion or dilation of the surfaces, and with friction angle reduced to its residual value, taken to be approximately 30° (Section 5.3.2.1.8). Analyses of the impact of long-term joint deterioration, conducted using the 3DEC program, conservatively assume that the fractures have no cohesive strength, no dilation, and are at their residual angle of friction. The procedure used to determine the magnitude and range of stress conditions applied in the process of examining impact of long-term deterioration of joints is discussed in *Drift Degradation Analysis* (BSC 2004d, Section 6.3.1.5) and are summarized in Appendix C, Section C.4.5, Part 3d. Analyses performed using these parameters are presented in *Evaluation of Emplacement Drift Stability for KTI Resolution* (BSC 2004c, Section 6.3).

H.4.7 Long-Term Degradation of Lithophysal Tuff

The time-dependent change in strength of lithophysal rock is discussed at length in Section 5.3.2.2.4 of this technical basis document, in *Drift Degradation Analysis* (BSC 2004d, Appendix S), and in *Subsurface Geotechnical Parameters Report* (BSC 2003c, Section 9). Static fatigue laboratory experiments (essentially, creep testing of hard rock) have been conducted on nonlithophysal tuff to determine the time-to-failure of samples as a function of the ratio of

[1] A description of stress corrosion cracking as a mechanism for time-dependency in tuff is given in Section 5.3.2.2.4 of this technical basis document.

applied stress to the unconfined compressive strength. The PFC model was calibrated to reproduce the time-dependency of the nonlithophysal rock. The model was then used to examine the impact of lithophysal porosity on the time-to-failure. The result of these analyses is a relationship of time-dependency for lithophysal tuff as a function of lithophysal porosity. An engineering model was developed in which the strength of the lithophysal rock (in terms of cohesion) as a function of time for given levels of applied stress was developed. This abstraction provides a means of directly incorporating time-dependency into the UDEC discontinuum model that has been developed for examination of rockfall in lithophysal rock. This model has been used to examine the combined effect of in situ, thermal, and seismic loading, in addition to time-dependent strength degradation, on drift stability and collapse in lithophysal rocks. It was found that significant time-dependency during the postclosure period was restricted to the lowest strength category for the lithophysal rock, and little time-dependent strength loss is expected for the mean strength categories that represent the majority of the Tptpll. Based on these results, little time-dependent failure response is expected in the lithophysal rock over the preclosure time frame. Therefore, the existing ground support design for the preclosure period need not consider time-dependency in the lithophysal rock mass.

H.4.8 Modeling of Time-Dependent Deterioration of Lithophysal and Nonlithophysal Rock–Summary

Time-dependent analysis of emplacement drifts in lithophysal and nonlithophysal rock is reviewed in *Drift Degradation Analysis* (BSC 2004d) and Section 5 of this technical basis document. The approach taken to time-dependency is as follows:

- **Nonlithophysal Rock**–Time-dependent effects are assumed to take the form of stress-corrosion failure of stress asperities on joint surfaces, with the ultimate result of joints achieving their residual strength condition with 0 cohesive strength, 0 dilation, and residual angle of friction (assumed to be 30°). Even with these very conservative assumptions, 3DEC discontinuum analysis of stability of the emplacement drifts indicates stable conditions in the preclosure for unsupported tunnels (see Section 5.3.2.1.8). A minor amount of rockfall is predicted for unsupported tunnels in the event of seismic shaking.

- **Lithophysal Rock**–As described above, time-dependent strength properties of the lithophysal rock mass were developed based on laboratory static fatigue testing of nonlithophysal rock and extrapolation using the PFC2D program. Use of the resulting time-dependent strength properties within two-dimensional discontinuum modeling (see Section 5.3.2.2.4) shows that little time-dependent degradation of the emplacement drifts is predicted over the postclosure time frame, with little or no time-dependency expected during the preclosure time period of 100 years (Figures 5-41 to 5-47 of this technical basis document).

Based on these discontinuum numerical analyses, preclosure time-dependency effects are estimated to be minimal, and the ground support, consisting of rock bolts and slotted steel surface sheeting, is considered to be sufficient to maintain drift stability.

H.4.9 Conclusions

The current approach to assessing ground support system performance employs routinely numerical codes in which rock strata are represented as continuum or discontinuum. These two-dimensional and three-dimensional codes are used to analyze ground support performance considering the time-dependent properties of rock and ground support under a range of loading conditions, which satisfies the requirements of RDTME 3.11.

H.5 REFERENCES

Board, M. 2003. *Resolution Strategy for Geomechanically-Related Repository Design and Thermal-Mechanical Effects (RDTME).* REV 00. Las Vegas, Nevada: Bechtel SAIC Company. ACC: MOL.20030708.0153.

Brekke, T.L.; Cording, E.J.; Daemen, J.; Hart, R.D.; Hudson, J.A.; Kaiser, P.K.; and Pelizza, S. 1999. *Panel Report on the Drift Stability Workshop, Las Vegas, Nevada, December 9-11, 1998.* Las Vegas, Nevada: Management and Technical Support Services. ACC: MOL.19990331.0102.

BSC (Bechtel SAIC Company) 2001. *Ground Control for Emplacement Drifts for SR.* ANL-EBS-GE-000002 REV 00 ICN 01. Las Vegas, Nevada: Bechtel SAIC Company. ACC: MOL.20010627.0028.

BSC 2003a. *Longevity of Emplacement Drift Ground Support Materials for LA.* 800-K0C-TEG0-01200-000-00A. Las Vegas, Nevada: Bechtel SAIC Company. ACC: ENG.20030922.0004.

BSC 2003b. *Ground Control for Emplacement Drifts for LA.* 800-K0C-TEG0-00100-000-00A. Las Vegas, Nevada: Bechtel SAIC Company. ACC: ENG.20031016.0001.

BSC 2003c. *Subsurface Geotechnical Parameters Report.* 800-K0C-WIS0-00400-000-00A. Las Vegas, Nevada: Bechtel SAIC Company. ACC: ENG.20040108.0001.

BSC 2004a. *Bounding Characteristics of Credible Rockfalls of Preclosure Period.* 800-00C-MGR0-00200-000-00A. Las Vegas, Nevada: Bechtel SAIC Company. ACC: ENG.20040315.0009.

BSC 2004b. *Ventilation Model and Analysis Report.* ANL-EBS-MD-000030 REV 03 ICN 03, with errata. Las Vegas, Nevada: Bechtel SAIC Company. ACC: DOC.20031216.0002; DOC.20040202.0004; DOC.20040325.0003.

BSC 2004c. *Evaluation of Emplacement Drift Stability for KTI Resolution*. 800-KMC-SSE0-00200-000-00A. Las Vegas, Nevada. Bechtel SAIC Company. ACC: MOL.20040510.0199.

BSC 2004d. *Drift Degradation Analysis*. ANL-EBS-MD-000027 REV 03A. Las Vegas, Nevada. Bechtel SAIC Company. ACC: MOL.20040513.0081.

NRC (U.S. Nuclear Regulatory Commission) 2002. *Integrated Issue Resolution Status Report*. NUREG-1762. Washington, D.C.: U.S. Nuclear Regulatory Commission, Office of Nuclear Material Safety and Safeguards. TIC: 253064.

Reamer, C.W. and Williams, D.R. 2001. Summary Highlights of NRC/DOE Technical Exchange and Management Meeting on Repository Design and Thermal-Mechanical Effects. Meeting held February 6-8, 2001, Las Vegas, Nevada. Washington, D.C.: U.S. Nuclear Regulatory Commission. ACC: MOL.20010307.0511 through MOL.20010307.0521.

Wisenburg, M. 2003. "Licensing Position on Duration of the Preclosure Period." E-mail from M. Wisenburg to T. Dunn and M. Board, July 1, 2003, with attachment. ACC: MOL.20030922.0234.

APPENDIX I

THE EFFECT OF SUSTAINED LOADING ON INTACT ROCK STRENGTH (RESPONSE TO RDTME 3.07)

Note Regarding the Status of Supporting Technical Information

This document was prepared using the most current information available at the time of its development. This Technical Basis Document and its appendices providing Key Technical Issue Agreement responses that were prepared using preliminary or draft information reflect the status of the Yucca Mountain Project's scientific and design bases at the time of submittal. In some cases this involved the use of draft Analysis and Model Reports (AMRs) and other draft references whose contents may change with time. Information that evolves through subsequent revisions of the AMRs and other references will be reflected in the License Application (LA) as the approved analyses of record at the time of LA submittal. Consequently, the Project will not routinely update either this Technical Basis Document or its Key Technical Issue Agreement appendices to reflect changes in the supporting references prior to submittal of the LA.

APPENDIX I

THE EFFECT OF SUSTAINED LOADING ON INTACT ROCK STRENGTH (RESPONSE TO RDTME 3.07)

This appendix provides a response to Key Technical Issue (KTI) agreement Repository Design and Thermal-Mechanical Effects (RDTME) 3.07. The agreement relates to the impact of potential long-term strength changes of the repository host horizon on stability of emplacement drifts. The drifts will be subjected to sustained in situ and thermal stress, and related time dependency of rock strength could result in drift degradation over time.

I.1 KEY TECHNICAL ISSUE AGREEMENT

I.1.1 RDTME 3.07

Agreement RDTME 3.07 was reached during the U.S. Nuclear Regulatory Commission (NRC)/U.S. Department of Energy (DOE) Technical Exchange and Management Meeting on Repository Design Thermal-Mechanical Effects held February 6 to 8, 2001, in Las Vegas, Nevada (Reamer and Williams 2001). This KTI agreement response is Appendix I of *Technical Basis Document No. 4: Mechanical Degradation and Seismic Effects*, Revision 1. The technical basis document, including Appendices A to H, was previously submitted to the NRC on June 17, 2004.

The wording of the agreement is as follows:

RDTME 3.07

> The DOE should account for the effect of sustained loading on intact rock strength or provide justification for not accounting for it. The DOE will assess the effects of sustained loading on intact rock strength. The DOE will provide the results of this assessment in a design parameters analysis report (or other document), expected to be available to NRC in FY 2002.

The agreement is concerned with the estimation of the impacts of time-dependent strength changes in repository host rocks due to sustained stresses from in situ and thermal loading and from environmental influences, such as wetting and drying. The impact of these strength changes on emplacement drift stability needs to be accounted for in the assessment of postclosure performance. The concern is further elaborated in *Integrated Issue Resolution Status Report* (NRC 2002, Section 2.1.7.3.3.2, pp. 2.1.7-19 and 2.1.7-20). The NRC concerns are paraphrased as follows:

- Emplacement drift degradation over time can be expected due to coupled thermal-hydrologic-mechanical processes (Brekke et al. 1999) and needs to be accounted for in analysis of time-dependent degradation modes. Thermally induced fracturing, rock loosening, and cyclical evaporation and condensation of water may drive degradation mechanisms.

- Geochemical alteration of the rock mass resulting from elevated temperatures in the presence of saturated rock conditions could impact mineral chemical stability, driving rock weathering alteration processes that could lead to degradation. This effect could be most pronounced for fracture and lithophysae coatings, affecting the shear strength of joints or strength of the lithophysal rock mass.

I.1.2 Related Key Technical Issue Agreements

RDTME 3.02–This KTI agreement response was submitted to the NRC on June 17, 2004, as Appendix D to *Technical Basis Document No. 4: Mechanical Degradation and Seismic Effects*. This KTI agreement requires that drift degradation and ground support analyses be conducted for critical combinations of in situ, thermal, and seismic stresses.

RDTME 3.04–This KTI agreement response was submitted to the NRC on June 17, 2004, as Appendix E to *Technical Basis Document No. 4: Mechanical Degradation and Seismic Effects*. This KTI agreement involves providing a geotechnical parameters report that includes rock-mass property estimates of the subunits of the Topopah Spring Formation. RDTME 3.07 deals specifically with providing estimates of time-dependent strength changes of repository host horizon rocks, which is included in the geotechnical parameters report.

RDTME 3.05–This KTI agreement response was submitted to the NRC on June 17, 2004, as Appendix A to *Technical Basis Document No. 4: Mechanical Degradation and Seismic Effects*. This KTI agreement requires that the methodology for estimation of rock mass properties for lithophysal rock be described.

RDTME 3.10–This KTI agreement response was submitted to the NRC on June 17, 2004, as Appendix D to *Technical Basis Document No. 4: Mechanical Degradation and Seismic Effects*. This KTI agreement requires verification of the adequacy of the use of two-dimensional models for analysis of drift degradation. Sections 4.2.2.2 and 5.2.3.1.2 of this technical basis document discuss the use of two- and three-dimensional models for drift degradation analysis.

RDTME 3.11–This KTI agreement response was submitted to the NRC on June 17, 2004, as Appendix H to *Technical Basis Document No. 4: Mechanical Degradation and Seismic Effects*. This KTI agreement requires examination of the long-term degradation of the rock mass in lithophysal and nonlithophysal rocks, particularly as it affects ground support. Section 5.2.3.2.4 of the technical basis document summarizes the specific approach to accounting for long-term strength degradation of material properties via use of static fatigue testing of tuffs.

RDTME 3.12–This KTI agreement response was submitted to the NRC on June 17, 2004, as Appendix F to *Technical Basis Document No. 4: Mechanical Degradation and Seismic Effects*. This KTI agreement requires a dynamic analysis of ground support systems during the preclosure phase using site-specific ground motions and discontinuum numerical modeling. The technical basis document centers on the postclosure dynamic analysis of lithophysal and nonlithophysal rocks using discontinuum methods.

RDTME 3.13–This KTI agreement response was submitted to the NRC on June 17, 2004, as Appendix D to *Technical Basis Document No. 4: Mechanical Degradation and Seismic Effects*.

This KTI agreement requires technical justification for boundary conditions for models used in drift degradation and ground support analyses. Section 5 of this technical basis document discusses static and dynamic mechanical and thermal boundary and initial conditions.

TSPAI 2.02, Items 58 and 62–TSPAI 2.02, Items 58 and 62 are related to the inclusion of rockfall and its potential mechanical impacts on engineered barriers and on the thermal-mechanical impacts of long-term rock-mass degradation on engineered barriers and potential hydrologic changes in the rock mass. RDTME 3.07 deals specifically with the estimation of time-dependent degradation of emplacement drifts subjected to in situ and thermal loading. The estimates made for long-term degradation and change of opening shape feed performance assessment studies of the engineered barriers. Section 1 of this technical basis document describes this integration in more detail.

I.2 RELEVANCE TO REPOSITORY PERFORMANCE

Agreement RDTME 3.07 deals with examination of time-dependent effects on emplacement drift degradation. Time-dependent degradation, as opposed to possible drift instability induced by a seismic event, is envisioned to be a relatively slow process involving sequential dislodging of blocks from the excavation periphery, which then fall into the drift and build up around the drip shield. This process is referred to as a raveling mode of rock failure. The root causes of time-related degradation are either changes in loading conditions around the drifts, geochemical alteration of the rock matrix or fracture fillings, or time-dependent changes in rock or fracture strength resulting from coupled thermal-hydraulic-mechanical effects.

Time-dependent degradation of emplacement drifts may have an important impact on repository performance. Appendix H (the response to RDTME 3.11) addresses the issue of the effect of time-dependent degradation in the preclosure (i.e., 100 year) time frame and the impact this could have on ground support. It was concluded that time dependency in fracture or rock-mass strength is insignificant in the preclosure period, and that ground support is properly designed to account for potential rock-mass loosening and raveling mechanisms and uses materials that have sufficient longevity to function over this time period. In the postclosure period, ground support will eventually degrade, leaving unsupported drifts. The impact of drift degradation modes, which could lead to partial or complete drift collapse, could be important to performance in the following areas:

1. Partial or complete drift collapse would result in rubble within the drift, which could create an insulating blanket surrounding the drip shield and waste package. This could, in turn, affect in-drift temperature and humidity conditions. The importance of this effect is dependent to some extent on the timing of the degradation (i.e., the number of years after waste emplacement). If it happens more than a few hundred years after closure, drift collapse has a relatively small effect on waste package peak temperature. Drift collapse is also accompanied by a decrease in drift relative humidity as a result of the enlargement of the emplacement drift, the overall temperature rise in the drift, and the increased temperature gradient from the waste package to the solid drift wall.

2. Drift degradation could result in an enlargement of the emplacement drift over time. Change in drift footprint (i.e., plan view dimension), shape, and the presence of rubble could impact seepage to the drift in the postboiling time frame.

3. Rubble accumulation in the drift will result in static loading to the drip shield. These potential loads are required as input to the evaluation of drip shield performance.

This appendix summarizes the results of analyses of time-related drift degradation in the nonlithophysal and lithophysal rocks that comprise the repository host horizon. A detailed description of the analyses can be found in Section 5.3 of this technical basis document and in *Drift Degradation Analysis* (BSC 2004a, Appendix S). Drift degradation resulting from seismic events is also described in Section 5.3 of this technical basis document.

I.3 RESPONSE

Long-term response of excavations depends on a number of factors, including:

1. Degradation due to time-dependent fracture development in the rock matrix or along joint (or existing fracture) surfaces in the presence of water vapor and driven by mechanical and thermal stresses. Large-span excavations initially created with low factor of safety against collapse and using poorly controlled excavation methods increase degradation potential.

2. Degradation due to time-dependent alteration of rock matrix or joint-filling materials due to rock mass thermal and moisture conditions. Water sensitive minerals, such as clays, increase degradation potential.

General understanding of the time dependency of tunnels in hard rocks is subject to a high degree of uncertainty because most engineered excavations are designed for a relatively short life-span or are typically heavily supported to provide safe access for personnel. Although it is well known that many unsupported mining excavations deteriorate within years of initial excavation, there are also many examples of man-made excavations and natural underground openings hundreds to millions of years in age that have suffered little deterioration. A detailed database of the long-term stability of unsupported man-made excavations and natural underground openings is not readily available. Therefore, it is difficult to develop general rules for time-dependent degradation based purely on empirical observations. The approach used here for estimation of time-dependent degradation effects is based on development of a mechanistic understanding of the time dependency of strength change of Yucca Mountain site-specific rocks. The approach is based on development of a database of laboratory test results defining time-related strength changes of tuff, followed by application of these data within numerical models of drift stability. This analysis accounts for the site-specific, time-evolving stress conditions over the postclosure time period, as well as environmental effects on rock strength change. Uncertainty in the rock mass properties is accounted for through use of appropriate ranges of estimated rock mass strength and time-dependent variability.

Due to the general lack of water-sensitive in-filling materials on natural fractures or within the rock matrix, the impact of environmental effects on rock strength as a function of time is expected to be inconsequential. The primary driving mechanism for time dependency is

expected to be strength loss of the matrix material due to subcritical microcrack growth resulting from a stress corrosion mechanism (e.g., Potyondy and Cundall 2001). This mechanism results in time-dependent crack growth due to stress, temperature, and the partial pressure of water at the tips of microcracks. These microcracks may begin as flaws in the rock or grain-boundary contacts. A crack grows either through grains or along grain boundaries due to the hydration and breaking of silicon–oxygen bonds at the tip of the crack. The rate at which the crack grows is controlled by the diffusion of water to the crack tip, which is, in turn, dependent on the crack geometry, which is stress-dependent. The overall impact of these factors is a logarithmic form of crack growth as a function of time and stress. This mechanism is commonly termed stress corrosion cracking. Experimental data on single crystals of quartz, as well as in rocks, have validated these mechanisms (e.g., Martin 1972; Kranz 1979). Laboratory testing has been performed to define the rate at which this stress corrosion mechanism occurs in Yucca Mountain tuff under saturated and heated conditions (Martin et al. 1997; DTN: SN0406L0212303.002). The results of this testing have been used to develop a time-dependent strength model that has been implemented within a drift-scale stability model. This model was then used to examine time-dependent drift degradation for the postclosure in situ and thermal stress history.

The analyses described in the technical basis document (Section 5.3.2.2.4), and summarized here, indicate that in situ and thermal stressing result in only minor damage and degradation around the tunnels and that time-dependency of the strength change in tuff provides a more important mechanism, particularly in high porosity lithophysal rock. A range in drift degradation conditions is expected to occur in lithophysal rocks as a result of variability of rock porosity, which, in turn, affects rock-mass strength. In general, the analyses indicated that:

- A small percentage of emplacement drifts—those located in the highest porosity/lowest quality areas of the Tptpll—are expected to show significant degradation over time. These constitute less than about 10% of the emplacement drift length based on the mapped lithophysal cavity data described in Section 4.2.2.1.

- In the average quality rock conditions, little drift deterioration is expected from time-dependent effects.

- Analysis of drip shield stability, based on a conservative assumption of rubble loading from complete collapse of the emplacement drifts, indicates that the drip shield is structurally stable.

- Analysis of the effects of drift degradation on in-drift temperature and relative humidity conditions shows that little impact on maximum waste package temperatures are expected for partial or complete collapse, if it occurs more than a few hundred years after repository closure. Significant decrease in drift humidity can occur as a result of collapse due to the enlargement of the emplacement drift, the overall temperature rise in the drift, and the increased temperature gradient from the waste package to the solid drift wall.

- Collapse and accompanying increase in drift plan-view footprint can result in impact to seepage flux into the tunnel.

Finally, evidence from observations of drift collapse in mining is used to verify that emplacement drifts in lithophysal and nonlithophysal rocks have dimensions that are well below those known to induce collapse. The field observations are obtained from experience in caving mines in which the span of excavations is increased to induce collapse. Additionally, the emplacement drift tunnels are developed with a stable circular shape and are driven using a non—rock-damaging mining technique using tunnel boring machines. Observations of tunnels in the existing ESF and ECRB Cross-Drift show stable conditions with no observed time-related damage in the repository host horizon units. Evidence of large, unsupported tunnels in similar rock at Hoover Dam is presented. These tunnels, which have been in continuous service for worker access for over 70 years, are stable and have shown little deterioration.

The information in this report is responsive to agreement RDTME 3.07 made between DOE and NRC. This report contains the information that DOE considers necessary for NRC review for closure of this agreement.

I.4 BASIS FOR THE RESPONSE

I.4.1 Introduction

As demonstrated by the ESF and ECRB Cross-Drift, excavations in the repository host horizon are currently stable under the existing conditions of in situ stresses and rock mass strength with only light[1] ground support. However, it is expected that the ground support will completely lose its integrity during the 10,000-year regulatory period and, to some extent, drift degradation will occur due to increased stress from thermal loading and due to strength decay of the rock mass. Drift degradation is an important issue for repository design and performance because drifts must remain stable during the preclosure operational period and, eventually, rubble resulting from degradation could impact in-drift environmental conditions, seepage, and the integrity and performance of the drip shields. Estimation of the rate of drift degradation for the duration of the 10,000-year regulatory period is, therefore, required.

I.4.2 Empirical Observations of Degradation and Collapse of Excavations

I.4.2.1 Unsupported Excavation Spans and Stand-Up Time

There is currently no accepted methodology for estimating the time-dependent degradation behavior of tunnels in hard rocks. However, a number of empirical correlations have been developed for providing a means of estimating maximum stable spans of unsupported excavations and the length of time that an unsupported excavation may remain open and still provide a safe working environment[2] (termed stand-up time) (Bieniawski 1989). Because these correlations are often used in estimating the time of instability of excavations and could be used for estimation of long-term degradation response, this appendix discusses their applicability to the postclosure stability of emplacement drifts at Yucca Mountain.

---

[1] Current ground support in 5 m and 7.62 m diameter tunnels in the repository host horizon includes friction rock bolts on nominal 1.25 m centers and light wire mesh on the crown of the excavations. In some locations, bolting and meshing of the sidewalls was also performed.

[2] A safe working environment here means that there is minimal danger of rockfall from loose pieces of surface rock created by blast damage or unstable blocks formed by fracture planes.

Emplacement Drifts Act As Isolated Excavations–Emplacement drifts for the repository, 5.5 m in diameter, are separated from one another by a center-to-center distance of 81 m and are located at a nominal depth of 300 m below ground surface. The large ratio of drift diameter to spacing and diameter to depth means that the emplacement drifts are mechanically isolated from one another and from the effects of the ground surface. There is, eventually, thermal interaction between tunnels, but the local mechanical effects related to isolated tunnels is of greatest importance to stability. As discussed in Section I.4.2.2, the span of the emplacement drifts is well below the critical span for collapse of unsupported excavations as observed in mining practice.

Empirical Correlations for Unsupported Spans and Standup Time—As the span of an excavation is made larger, there eventually comes a point when instability and unsafe working conditions result. Empirical correlations (e.g., Hoek and Brown 1980, p. 287) of the maximum safe unsupported span and the time that this span may remain unsupported have been developed to assist tunneling engineers in planning excavations that provide a safe working environment for tunnel construction workers. These correlations, which are typically based on some measure of rock mass quality, are inherently conservative in nature due to their primary purpose, which is to ensure the safety of construction personnel from rockfall hazard (not necessarily from general collapse). It is important to note that these correlations are not based on case histories of actual collapse.

Stand-up time curves (e.g., Hoek and Brown 1980, Figure 6) provide an estimate for potential of safe unsupported tunnels and are expressed in terms of span versus stand-up time for various rock-mass qualities (as determined by a geotechnical rock mass quality rating). For a given span of a tunnel, the stand-up time decreases as the quality of the rock mass becomes poorer. The stand-up time is a crude measure of unsupported span stability in that it does not account for opening shape, tunneling method, or, most importantly, the stress state around an excavation (e.g., depth of the excavation). For excavations whose span is well below the critical collapse span, the ratio of the stress concentration around the excavation to the short-term strength of the rock mass is one of the most important factors controlling stability and its evolution as a function of time. Stand-up time curves were developed based on empirical evidence of instability of excavations in particular stress conditions (e.g., deep South African mines), and their application to completely different conditions is questionable.

Stand-up time is typically projected to be on the order of hours or days, even for good quality rock masses and may be only on the order of years. The long-term stability of existing lightly-supported or unsupported tunnels in mechanically-similar tuffs and rhyolite at the Yucca Mountain site and Hoover Dam (described in Section I.4.2.3) is evidence that stand-up time is a worker-safety-related indicator and is not relevant to predictions of degradation or true collapse time. These remarks indicate that construction-related span and stand-up time correlations have only limited application to postclosure predictions of drift degradation at the Yucca Mountain site. Therefore, as described in Section I.4.3.1, an analytical approach, based on the mechanics of time-dependent fracture growth in brittle rocks, is used for estimation of long-term degradation response rather than reliance on existing empirical estimations.

I.4.2.2 Evidence of Maximum Unsupported Span from Mining Case Examples

The mining industry, on the other hand, routinely drives unsupported excavations to large spans with the express purpose of inducing collapse for caving of ore bodies. Therefore, empirical evidence of maximum unsupported spans from mining case examples is more relevant to the estimation of the actual spans of excavations that induce degradation and ultimate collapse. The span of an excavation required to induce caving and collapse has been the topic of extensive study in the mining industry because certain types of mining methods (e.g., block and panel caving) are predicated to induce caving when a rock mass is undercut. Brown (2003) provides a summary of worldwide caving operations and the spans of excavations necessary to induce collapse as a function of the rock mass quality (i.e., strength). Figure I-1 provides a summary of worldwide experience in excavation span and collapse potential for cave mining. The plot provides an experience-based correlation between rock mass quality rating (in terms of rock mass rating) and the ratio of the plan view area of the excavation to its perimeter (A/P)[3] for excavations that produce: (1) stable spans, (2) transitional excavations in which instability may begin but caving is not yet occurring, and (3) caving. As the rock mass quality rating decreases, the spans at which collapse occurs also decrease. To apply these data to emplacement tunnels at Yucca Mountain, an estimate of the rock mass quality is required. The case of lithophysal rock is presented here because it is the weakest of the host horizon units. As described in *Subsurface Geotechnical Parameters Report* (BSC 2003, Section 9.2.5), the estimated rock mass quality rating in terms of Geologic Strength Index or Rock Mass Rating (GSI or RMR) for the lithophysal rocks at Yucca Mountain is in the range of approximately 50 to 60. For this range of RMR, the hydraulic radius of a flat-roofed excavation required for caving is in the range of approximately 25 to 35 m. A transitional zone between stable excavations and caving for the lithophysal rock RMR range occurs for A/P ratios of 15 to 20 m. For the proposed 5.5-m diameter emplacement drifts, the hydraulic radius is simply equal to the radius (2.75 m). Therefore, field practice indicates that the stable to transitional caving–stable state is characterized by a hydraulic radius for lithophysal tuff in the range of 15 to 20 m. The boundary between transitional stable/caving to a caving state is characterized by an A/P ratio in the range of approximately 25 to 35 m. Note that the typical mining undercut has a flat roof, which promotes instability, while the shape of the emplacement drifts is circular, which promotes stability. The emplacement drift A/P ratio is, therefore, approximately 5 to 7 times below what would be considered to be a transitional state between stable and caving conditions. Based on field experience in caving, the A/P ratio of the emplacement drifts is well below the level of the A/P ratio estimated to be in a transitional state of collapse and even further below the level for assurance of complete collapse. Therefore, it is not surprising that the existing ESF and ECRB Cross-Drift (7.62 and 5 m diameter, respectively) are stable and show no evidence of degradation nearly a decade after excavation, even though the ground support is minimal.

[3] The plan view area of an excavation divided by its perimeter is termed hydraulic radius in the mining industry, and is typically used as a parameter for estimation of caving potential or roof instability because it takes into account the span and shape of excavation. This term is not to be confused with the hydraulic diameter, which typically is used in fluid mechanics calculations and is 4 times the cross-sectional area of a conduit divided by the perimeter. For a long tunnel of constant cross section, such as an emplacement drift, the hydraulic radius is simply equal to the tunnel radius.

I.4.2.3 Observations of Yucca Mountain Tunnels and Excavations at Hoover Dam

Unsupported or lightly supported tunnels (although perhaps not considered safe from a personnel standpoint) can stand in a stable condition for long time periods, particularly in good quality rock masses. For example, the ESF (7.62 m diameter) and ECRB Cross-Drift (5 m diameter) tunnels at the Yucca Mountain site were constructed in 1995 to 1997 and in 1998, respectively. Although the ESF main loop is located largely in the Tptpmn, the ECRB Cross-Drift cuts through and exposes all of the repository host horizon units. The tunnels are, in general, lightly supported with friction rock bolts and light wire mesh in the tunnel roof, with occasional friction bolts in the tunnel walls. There is no evidence of significant deterioration or degradation of the rock mass, and no significant episodes of rockfall have occurred.

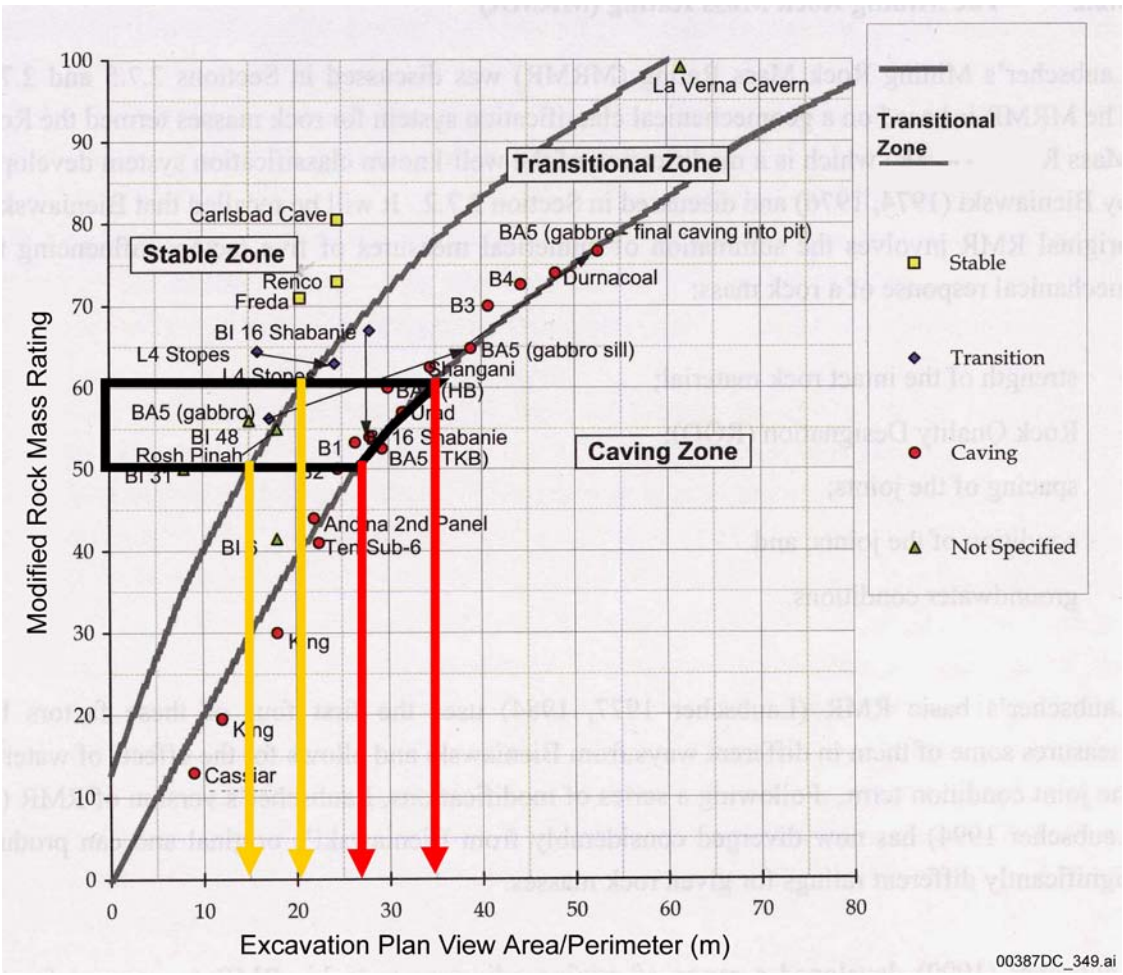

Source: Brown 2003.

NOTE: Caving potential is expressed in terms of the modified rock mass rating and the ratio of the excavation's plan view area to its perimeter. Modified rock mass rating is equivalent to rock mass rating in the case of Yucca Mountain excavations. Stable and caving regions are separated by a transition zone.

Figure I-1. Excavation Dimensions Required for Caving Gained from Field Experience in Block and Panel Caving Mines

An external review panel convened to examine Yucca Mountain drift stability (Brekke et al. 1999) found that excavations of the north ramp through the upper lithophysal zone and the ECRB Cross-Drift through the lower lithophysal zone show that both zones have properties that are favorable for stability with minimum ground support. The panel also found that rock conditions in the lower lithophysal zone in the ECRB Cross-Drift were similar to those observed in the upper lithophysal zone in the north ramp; that continuous joints were not apparent, and there was almost no overbreak or loosening of the slabs or blocks; and that zones with more frequent short fractures were present and could be described as fracture zones, but even in these areas, overbreak and block loosening were largely absent. Tunnel deformation measurements have been regularly monitored since excavation, showing stable conditions. The conclusion is that the tunnels in both the lithophysal and nonlithophysal rock masses are obviously in a stable and self-supporting mode with no obvious deterioration in 5 to 8 years. Additionally, the Drift Scale Test involved heating a representative repository-scale tunnel in the nonlithophysal rock mass, first, to postclosure temperature distributions, followed by a thermal overdrive experiment to test rock strength limits. The experiment, now well into its cooldown phase, showed stable and predictable conditions at expected repository peak temperature conditions. Overdrive to approximately 200°C drift-wall temperatures showed predictable, minor spalling of a small portion of the center of the crown of the drift (BSC 2004a, Section 7.7.7.5.3). Cooldown has showed no observable loosening or instability of the tunnel. This experiment confirmed modeling estimates of stable drift conditions for expected repository temperature and combined in situ and thermal stress conditions.

The Hoover Dam, with abutments excavated in Tertiary pyroclastic flows, was completed by the Bureau of Reclamation in 1936. Along with the construction of the dam itself are a series of tunnels and adits (Figure I-2) that were excavated to accommodate the various penstocks, valves, access ways, spillways, and river bypasses. With the exception of the visitor center elevator shaft (completed in the 1990s), all the excavations were completed with simple drill and blast methods ("simple" meaning here that no smooth-wall blasting techniques were used). Some of the larger openings, generally those more than 6 m (20 ft) high, were excavated using heading-and-bench methods (i.e., the tunnel is mined in two passes with the upper portion excavated first, followed by bench blasting of the lower portion) to develop the full size of the openings. Many of the tunnels and adits were excavated to greater than 12 m (40 ft) in diameter. While some of the penstock and spillway tunnels were lined with concrete, many of the adits[4] and access ways remain unlined.

The rock at the site is the tuff of Hoover Dam, a fairly localized unit composed of andesitic to dacitic pyroclastic flows and breccias. At the dam, the volcanics are slightly to densely welded, and slightly weathered to unweathered. At the penstock adits, the rock is moderately hard to hard and contains abundant lithic fragments and occasional corroded pumice fragments. The rock is slightly to moderately fractured, with most fractures devoid of fracture filling. Many of the discontinuities exposed in the adits are frequently shears and small faults displaying distinct

[4] An adit is a term for a tunnel with one end that daylights.

slickensides[5]. Where the adits extend below the phreatic surface, occasional calcium carbonate precipitate is present adjacent to active or old seeps.

The adits were excavated downstream of the power plant to allow insertion of large, steel penstock sections into tunnels that paralleled the canyon walls. The adits are still in use, housing the sewage treatment system and other support utilities necessary to the function of the dam. The adits are approximately 40 ft (12 m) high by 35 ft (10.7 m) wide (Figure I-3) becoming slightly taller with depth. After the drill and blast excavation, the adits were left unlined and unsupported, and continue to be unsupported to the present time. Rock fall in the adits has been limited to very occasional centimeter-size fragments, even without ground support.

[5] A slickenside is a striated, polished fracture surface resulting from shear displacement. Typically, the slickensided surface has low friction angle.

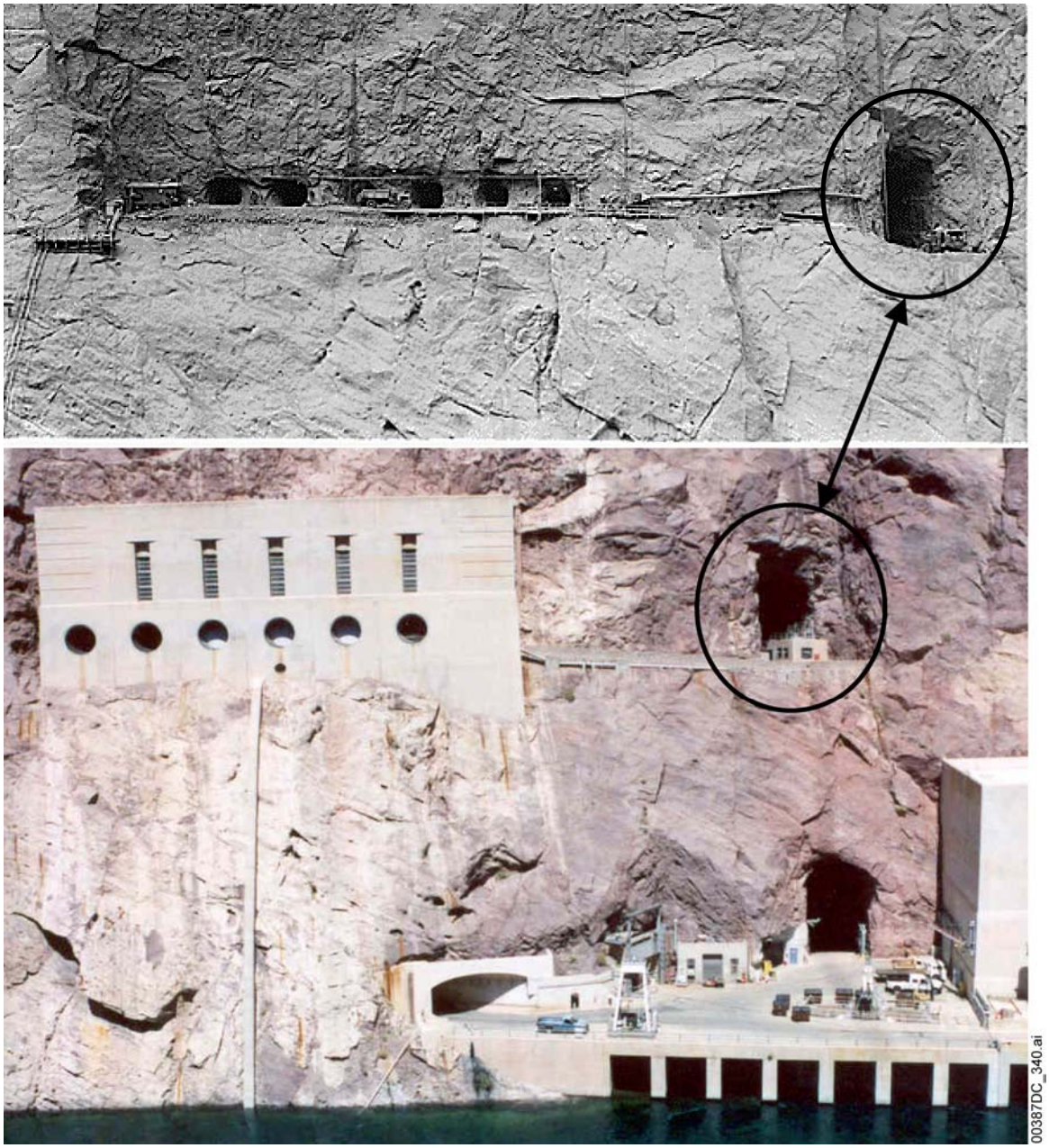

NOTE: Construction adit, shown at right, is approximately 40 ft high.

Figure I-2. Excavation for Nevada Canyon Wall Outlet Works (Top) Showing Construction Adit in 1933 and (Bottom) in 2004

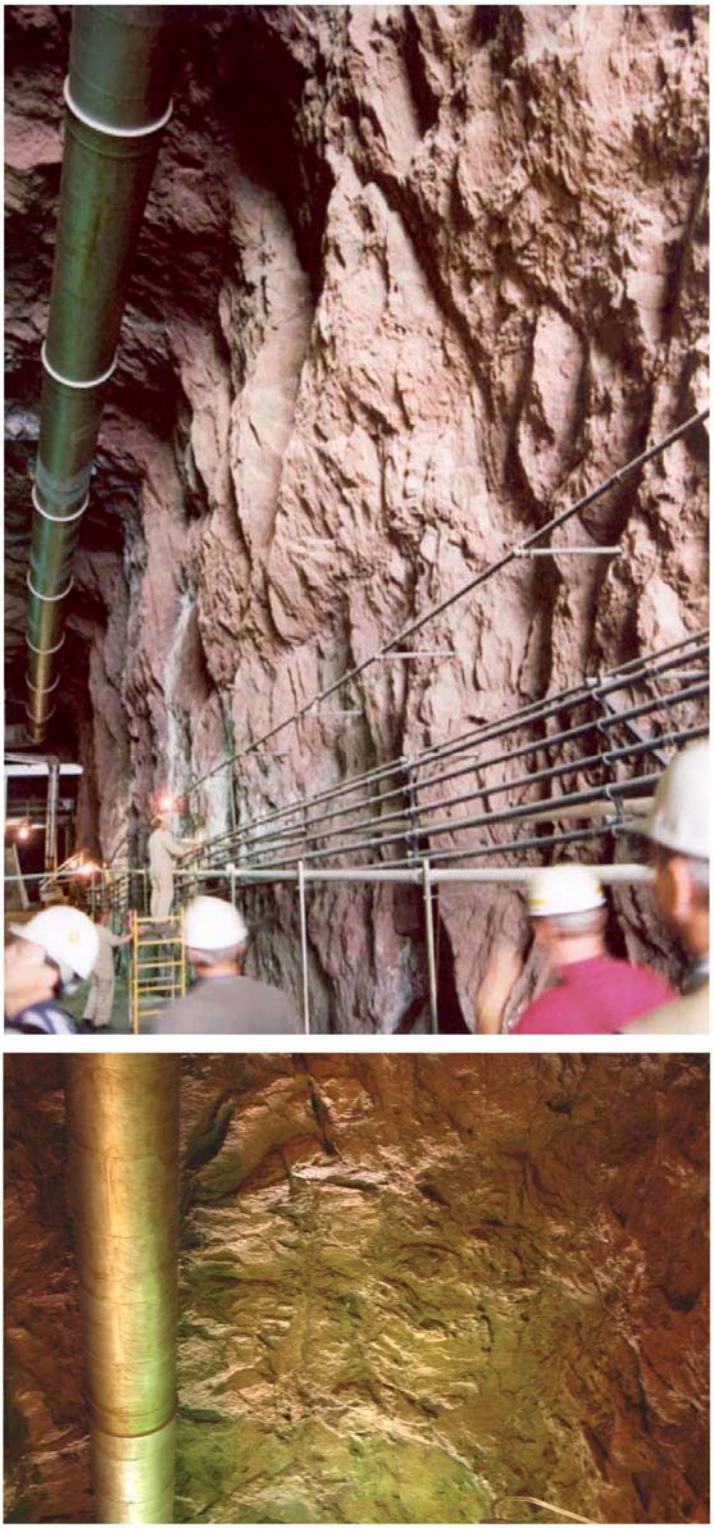

NOTE: Irregular tunnel walls resulting from drill-and-blast excavations (top) and close-up view of the tunnel crown showing evidence of drill half-barrels (bottom).

Figure I-3. 2004 Photographs of Unsupported Construction Adit at Hoover Dam, Excavated in 1931

Additionally, there are numerous access ways throughout the lower canyon walls in and around the Hoover Dam power plant. These smaller tunnels, 6 to 15 ft (1.8 to 4.6 m) in diameter, allow access by personnel and tourists to various areas of the power plant and penstocks. Few of these tunnels are supported either by rock bolts or mesh. No steel supports are visible in the Hoover excavations. As with the adits, rock in the access ways and tunnels has been limited to rare centimeter-size fragments that are removed by the janitorial staff.

I.4.2.4 Summary of Empirical Observations

The safety-related empirical correlations for maximum unsupported span and stand-up time of excavations developed for the tunneling industry are not relevant for prediction of long-term response of repository excavations. The span of the emplacement drifts is significantly less than that required to initiate collapse, as indicated by practice in the mining industry. The excavations will be developed using nonblasting methods (i.e., using a tunnel boring machine) and with a circular shape that minimizes overbreak and promotes stability. Observations of existing tunnels in the repository host horizon at the Yucca Mountain site as well as in similar rock at Hoover Dam show stable conditions with minimal or no ground support.

I.4.3 Potential Mechanisms of Time-Related Degradation of Emplacement Drifts

During the postclosure period, the following mechanisms (excluding seismic events) of time-dependent degradation could be important:

1. Degradation due to time-dependent fracture development in the rock matrix or along joint surfaces in the presence of water vapor and driven by mechanical and thermal stresses. Large-span excavations, initially created with a low factor of safety against collapse using poorly controlled excavation methods, increase degradation potential.

2. Degradation due to time-dependent alteration of rock matrix or joint filling materials due to rock mass thermal and moisture conditions. Water sensitive minerals, such as clays, increase degradation potential.

Each of these issues is addressed below.

I.4.3.1 Degradation Due to In Situ, Thermal, and Thermal-Hydraulic Stress Conditions and Time-Dependent Fracture Development

I.4.3.1.1 Emplacement Drift Degradation from In Situ and Thermal Stress Change

The nominal preclosure time period is assumed to be 100 years and will be followed by closure of the facility. Closure of the repository will involve emplacement of drip shield structures over the waste packages, cessation of forced ventilation of emplacement drifts, and backfilling of the ramps, shafts, access mains, and exhaust mains with crushed tuff. With the cessation of forced ventilation, the emplacement drifts and surrounding rock mass temperature will rise, as shown nominally in Figure I-4 (BSC 2004b). Here, the average drift wall and waste package temperature is shown as a function of time for a range of waste package types that spans the temperature range for locations within an emplacement drift in the lower lithophysal unit (designated Tptpll) emplacement area. The drift temperature rapidly rises, resulting in a peak

21-PWR waste package temperature of approximately 170°C approximately 30 years after cessation of forced ventilation. The temperature then undergoes a slow cooling over time, with the waste package surface remaining above the boiling point for approximately 1,000 years. In this nominal scenario, it is assumed that forced ventilation of the waste packages has occurred for 50 years.

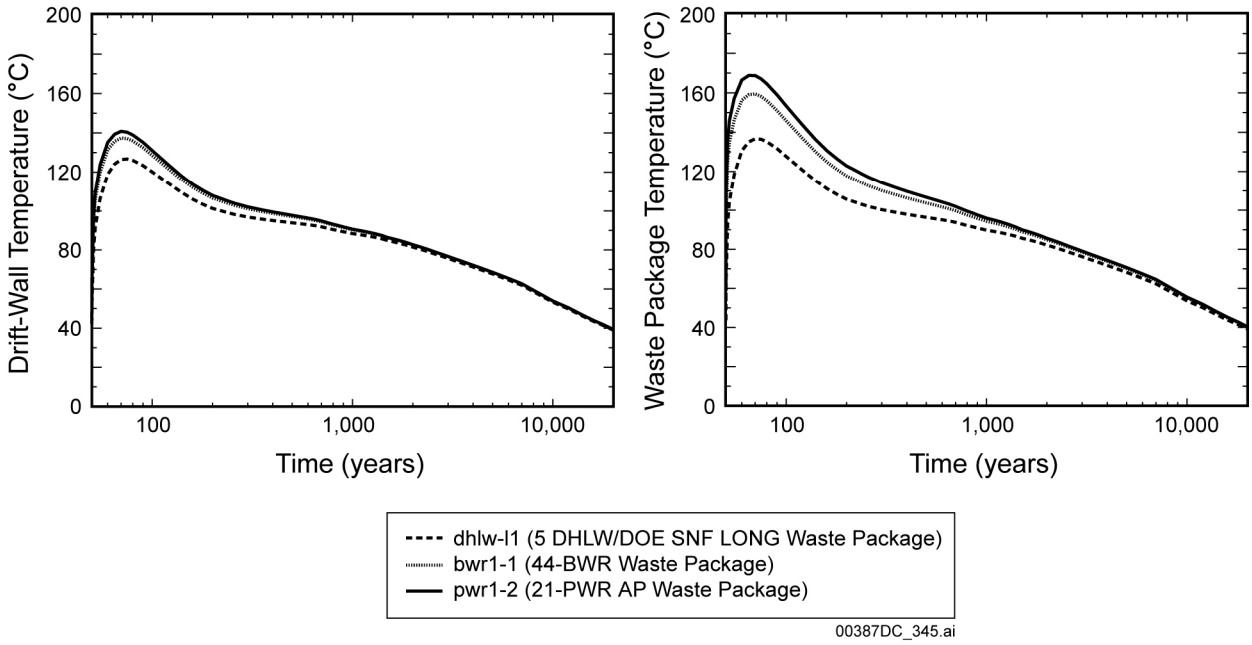

Source: BSC 2004b, Figure 6.3-14.

NOTE: These waste packages bracket the range of temperature within a centrally located emplacement drift.

Figure I-4. Drift-Wall Temperature (a) and Waste Package Temperature (b) as a Function of Time for Three Waste Package Types, Emplacement Drift in the Tptpll, Mean Seepage Infiltration Case

This temperature history will result in transient, thermally induced stresses in the emplacement drift walls that are superimposed on the preexisting excavation-induced stresses to obtain the total wall stress. A complete discussion of the transient, thermally induced stresses around emplacement drifts in nonlithophysal and lithophysal rocks is given in *Drift Degradation Analysis* (BSC 2004a, Sections 6.3.1.3 and 6.4.2.3). The combined in situ and thermally induced stresses result in no predicted yield in the stronger, nonlithophysal rock mass (in agreement with observations from the Drift Scale Test) and result in only minor yield at the springline (sidewalls) of emplacement drifts in lithophysal rock. Figure I-5 shows that less than 0.5 m of the immediate springline area of the drift is expected to yield in any rock mechanical properties quality category[6] of the lithophysal rock mass. The predicted sidewall shear failure would be observed as spalling of the sidewalls of the tunnels. In summary, parametric analyses of the

[6] A discussion of the rock mass mechanical property ranges for lithophysal rocks can be found in Section 4.2.2 of this technical basis document or in Appendix A. The lithophysal rock mechanical properties have been subdivided into a series of five strength categories that span the range of expected in situ porosity conditions, with category 1 being the lowest quality, highest porosity case, and category 5 being the highest quality, lowest porosity condition.

effect of combined in situ and thermally induced stresses (in the absence of time-dependent effects on material properties) are predicted to result in only minor drift degradation.

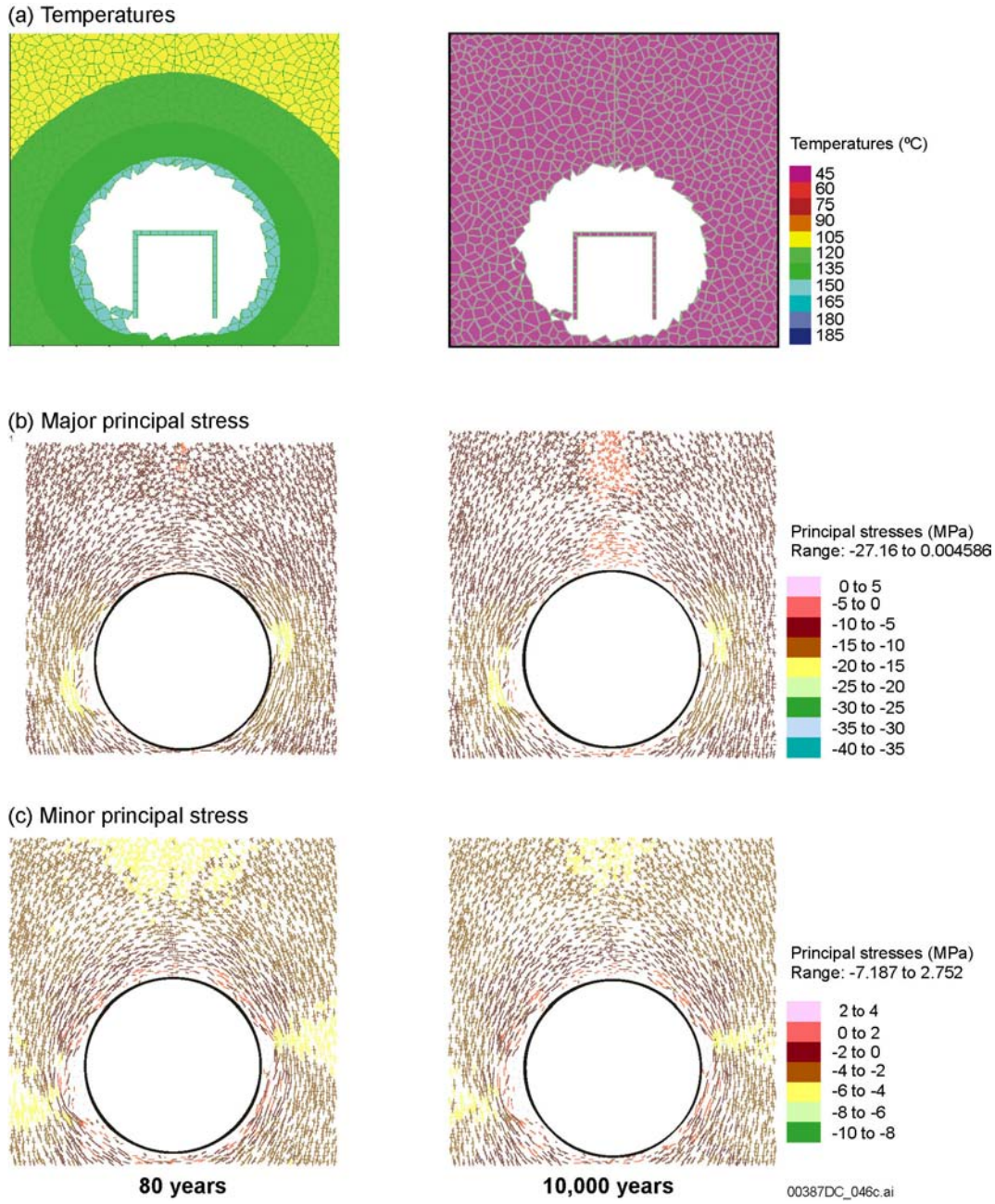

Source: BSC 2004a, Figure 6-142.

NOTE: 80 years (i.e., 30 years after cessation of nominal 50 years of forced ventilation) is the time of maximum drift wall temperature and thermally induced stress. Yield at springline can be seen (c) as that region that has failed and unloaded (destressed) due to shear fracture development.

Figure I-5. Thermally Induced Rockfall and Stresses after 80 and 10,000 Years of Heating in Rock Mass for Poorest Quality Tptpll Strength

I.4.3.1.2 Impact of Thermal-Hydrologic Effects on Emplacement Drift Degradation

Estimates of the coupled thermal-hydrologic behavior of the rock mass in the near vicinity of the drifts is examined in *Multiscale Thermohydrologic Model* (BSC 2004b). Numerical parameter analyses of the impact of waste heating on fluid pressures on fractures and infiltration into the emplacement drifts were conducted using the multiscale thermal-hydrologic model. For the range of hydrologic properties of the four host-rock units, the fracture permeability is sufficiently large and fractures are sufficiently well connected to allow gravity-driven drainage of water to occur in an unrestricted fashion. Thus, percolation flux, not fracture permeability, is the rate-limiting quantity governing the magnitude of gravity-driven liquid-phase flow to the boiling–dryout zone. Additionally, the analyses show that potential pressure buildup along fractures due to vapor pressure from boiling of water is also negligible due to the free-draining nature of the fractured rock mass. From a mechanical stability standpoint, this means that fluid pressure on fractures during the drying and rewetting phases of the postclosure period has a negligible effect on drift stability. These predictions are borne out by the Drift Scale Test in which no mechanical drift instabilities occurred for thermal conditions representative of repository postclosure conditions.

In summary, the conjecture in the Drift Stability Panel Report that postclosure temperature coupled with hydrologic effects in fractures will inevitably lead to collapse of some of the drifts (Brekke et al. 1999, p. 3-13) is not supported by either the results of the Drift Scale Test or the coupled thermal-hydrologic or coupled thermal-mechanical analyses.

I.4.3.2 Degradation Due to Time-Dependent Fracture Development in the Rock Matrix in the Presence of Water Vapor and Driven by In Situ and Thermal Stresses

As stated in Section I.3, time-dependent strength loss in the rock mass was examined using a mechanics-based approach in which laboratory testing is combined with numerical model extrapolations for prediction of the drift stability. The following section summarizes this work. A detailed description can be found in *Drift Degradation Analysis* (BSC 2004a, Appendix S).

I.4.3.2.1 Background on Time Dependent Characteristics of Brittle Rocks

One of the most striking characteristics of brittle rocks is that at temperatures well below the melting point, a rock subjected to a constant load exhibits a continuous increase in strain with time. This time-dependent deformation is termed creep. Studies on creep indicate that the observed strain depends upon the applied stress, the temperature, the partial pressure of water, and the confining pressure (e.g., Martin 1972). Moreover, the same mechanism responsible for the strain of brittle rocks in constant strain-rate tests is also operative in creep. That is, cracking, both along grain boundaries and through individual grains, produces the observed strain (e.g., Brace et al. 1966). Above approximately one half to two-thirds of the compressive strength, the dominant mode of deformation for brittle rocks is the opening and growth of cracks parallel to the major principal stress direction or axial orientation in unconfined compression. It is typically assumed that the strain rate of hard rocks in creep is related to the time-dependent growth of these cracks.

Verification of the relationship between time-dependent crack growth and creep strain rate in brittle rock is performed through laboratory testing. Experimental results indicate that stable time-dependent crack growth at a constant compressive load or at a constant stress intensity factor occurs in quartz and glass in the presence of water vapor. Moreover, the rate of crack growth depends on the applied stress, the temperature, and the partial pressure of water in the atmosphere surrounding the crack. The relative weakening of quartz or silicate glass, reflected by an increase in the rate of crack growth with an increase in any of the three variables, is consistent with the general theory of stress corrosion in silicates proposed by Charles (1959). He postulated that the velocity of a slowly propagating crack with a high tensile stress at the crack tip is proportional to the rate of the hydration reaction at the crack tip. The following equation (Martin 1972) quantifies the general relationship for environment-sensitive crack growth.

$$\nu = \nu_0 \beta P^n \exp\left(\frac{\Delta F - V^* \sigma}{RT} + \frac{\gamma V_m}{\rho RT} \right) \qquad \text{(Eq. I-1)}$$

where ν is the rate of crack growth, ν_0 is the initial flaw size, P is the partial pressure of water, ΔF is the activation energy for the process, T is temperature, R is the universal gas constant, V^* is the activation volume, σ is stress, γ is the surface energy of the solid, V_m is the molar volume of the solid, ρ is the radius of curvature of the crack tip, and β and n are constants.

If the partial pressure of water, the temperature, and the applied stress are constant, a constant crack propagation velocity will be observed. When any one of the thermodynamic variables is increased, the crack velocity increases. This expression has been verified with experimental studies (Wiederhorn 1968; Martin 1972; Scholz 1972).

The validation of Equation I-1 is extremely important. First, it establishes a rate-dependent process for the propagation of cracks in quartz and silicate glass. If the same behavior is observed in rocks then it implies that time can be scaled from very short times to extremely long times in the absence of other competing mechanisms. Specifically, if moisture-assisted stable crack growth is the primary mechanism of creep in brittle rocks, measurements made at laboratory scales of up to 10^6 seconds can be extrapolated to much longer scales on the order of 10^{11} to 10^{14} seconds. Presently there are no other independent data that suggest other competing mechanisms for time dependent deformation in brittle rocks at temperatures below 300°C. Based on these results, there is confidence that Equation I-1 accurately represents the behavior of the rate of crack growth at the crack tip for brittle silicate materials at temperatures below 300°C.

Next, the behavior of brittle rocks can be examined during creep and compared to the observations of stable, time-dependent crack growth gained from tests on quartz and glass. A creep test is conducted by rapid application of uniaxial or triaxial load to a rock sample to a given differential stress, followed by holding the load constant while monitoring the longitudinal and lateral strains. Typically, creep is reported in terms of three distinct phases: (1) primary or transient creep, (2) secondary or steady-state creep, and (3) tertiary or accelerating creep (Figure I-6).

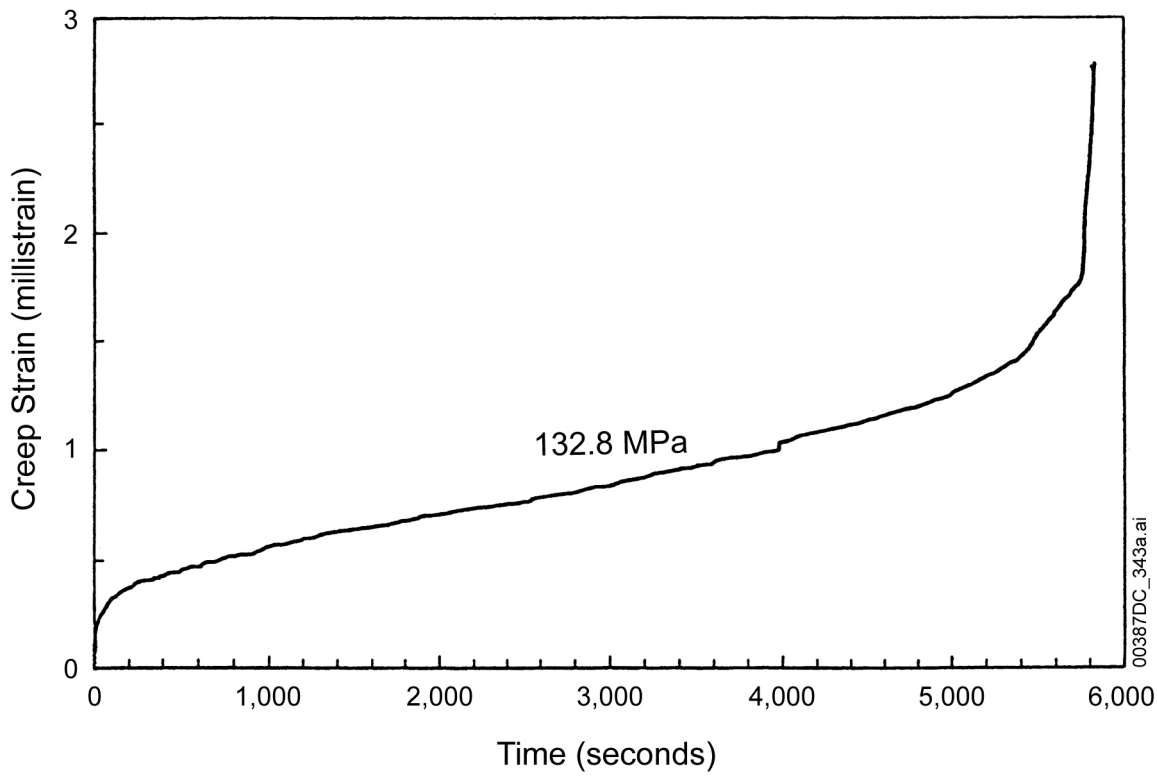

Source: Martin et al. 1997, Figure 4.

NOTE: Specimen failed at tertiary creep phase.

Figure I-6. Example of Creep Strain Plotted as a Function of Time for a Static Fatigue Test Conducted on a Sample of Topopah Spring Tuff at a Constant Differential Stress of 132.8 MPa, a Confining Pressure of 5.0 MPa, a Pore Pressure of 1 MPa, and a Temperature of 150°C.

Transient creep has been reported for a variety of rock types over a wide range of temperatures and pressures. The strain in this region decelerates rapidly under static load and is often reported as proportional to the logarithm of time. Moreover, both the lateral and the longitudinal strains exhibit this logarithmic time dependence.

At low stresses, transient creep may account for the observed strain. However, at high stresses, secondary creep is often observed. Generally, in secondary creep, often called steady-state creep, the strain is proportional to time. The total strain caused by both primary and secondary creep is often represented by an equation of the form

$$\varepsilon = A + B \log t + Ct \qquad \text{(Eq. I-2)}$$

where ε is strain, t is time, and A, B, and C are constants.

If secondary creep is allowed to continue, eventually the strain rate increases (tertiary creep) and the rock fails. All three stages of creep have been observed in granite, quartzite, and tuff (Martin 1972; Martin et al. 1997). A typical creep curve for a specimen of welded tuff from the middle nonlithophysal unit of the Topopah Spring (Tptpmn) is shown in Figure I-6. All three stages of creep are clearly evident.

Stable crack growth in quartz reported by Martin (1972) and Martin and Durham (1975), illustrated specific characteristics that are related to creep deformation. In these studies, the specimens were loaded to a fixed compressive stress and the growth of a crack parallel to the applied load was observed. Each specimen was tested in a controlled environment and the change in crack length was noted as a function of time. A typical data set obtained on a single specimen of quartz tested at a temperature of 241°C and a partial pressure of water of 4.5×10^{-2} kPa is shown in Figure I-7. The test specimen geometry is shown in the upper left portion of the graph. At a stress of 66 MPa, the change in crack length with time is very similar to that observed in the creep of brittle crystalline rocks. The crack exhibits an initial period of rapidly decelerating growth followed by a quasi-linear or secondary segment. After 6.3×10^4 seconds, the stress was increased to 74 MPa. Immediately, the rate of crack growth increased. The same characteristics observed at the lower stress were exhibited for the 74 MPa segment. There was a strong transient followed by a secondary or quasi-linear crack growth segment. At approximately 8×10^4 seconds, the stress was increased to 83 MPa. The rate of crack growth increased dramatically; and the experiment was terminated when the crack length reached 3.7 mm. These data are consistent with Equation I-1; that is, the rate of crack growth increased with increasing stress and nearly vanishes at low stresses. Additional experiments showed that increasing either the partial pressure of water surrounding the crack or the temperature also results in an increase in the rate of crack growth.

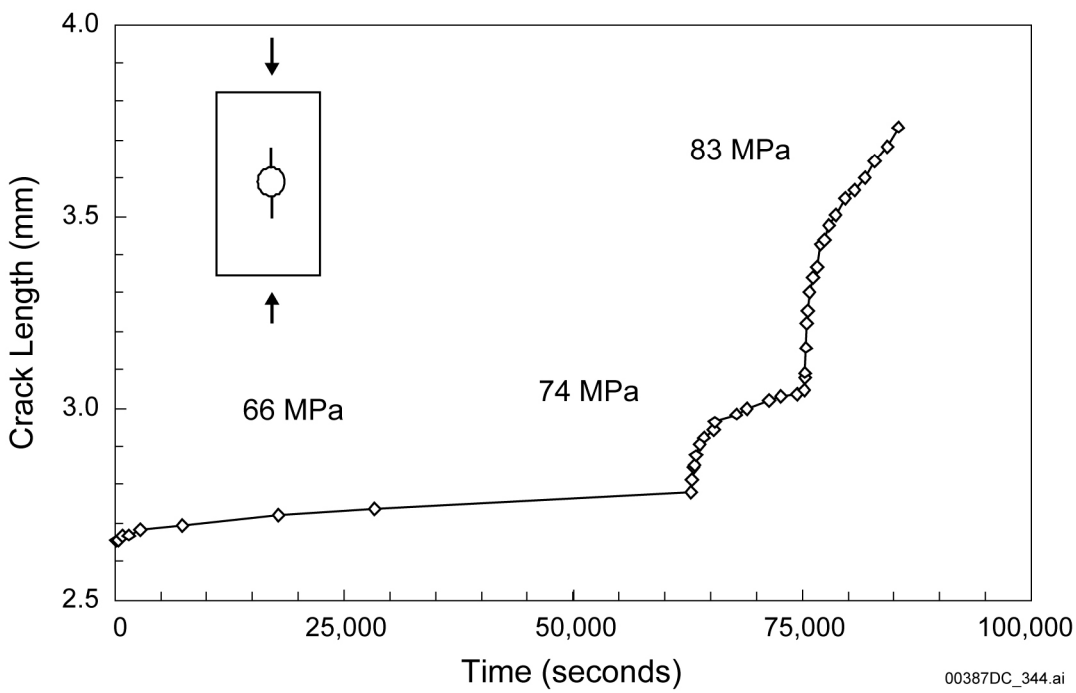

Source: Martin et. al. 1997, Figure 1.

NOTE: The experiment was conducted at 241°C and a partial pressure of water of 4.05×10^{-2} kPa.

Figure I-7. Crack Length as a Function of Time for an Axial Crack Growth Experiment in Single Crystal Quartz

The above discussion points out that creep experiments with complex, silicate rocks display the same basic time-dependent response as demonstrated by crack-growth studies in single crystals of quartz and glass. From a practical standpoint, it is advantageous to define the ultimate time-to-failure in terms of the stress, temperature and partial pressure of water, rather than in terms of crack growth. Time-to-failure is typically defined using the creep test to determine the static fatigue of a material. Static fatigue refers to the failure time of a rock or single crystal at constant stress, temperature, confining pressure, and partial pressure of water without regard to the strain history. Scholz (1972) conducted a series of static fatigue tests in compression on single crystal quartz. He observed that the mean time to failure, $\langle t \rangle$, depended on the partial pressure of water, P, stress, σ; the activation energy, F; and temperature, T, according to:

$$\langle t \rangle = t_0 P^{-a} \exp\left(\frac{\Delta F}{RT} - K' \sigma \right) \qquad \text{(Eq. I-3)}$$

where a and K' are constants.

The foregoing discussion demonstrates that:

- The strength of brittle silicate rocks such as tuff is not a single-valued function of any parameter, but is a complex continuum that depends on the state of stress, the saturation (pore pressure), the temperature, and the time (including strain rate).

- Studies of the basic growth of single fractures and the creep strain resulting from microcrack growth in complex silicate rocks demonstrate that the same basic stress corrosion mechanism is responsible for time-dependent crack growth and the ultimate time-to-failure of the material.

- The stress corrosion mechanism gives rise to a logarithmic relationship of time-to-failure as a function of the state of stress, the temperature, and the pore pressure.

- As a result of the basic understanding of the static fatigue mechanism in brittle rocks, it is possible to extrapolate long-term failure response from relatively short-term static fatigue experiments in the laboratory.

Since the effects of time-dependent fracture development on weakening of tuff and its impact on drift degradation may be important in the postclosure repository environment, creep experiments on tuff samples have been conducted to determine its static fatigue response under appropriate environmental conditions.

I.4.3.2.2 Static Fatigue Testing to Define Time-Dependent Behavior of Welded Tuff

The typical way to define the time-dependent strength of rock is to establish the time required for failure of heated, saturated rock samples that are subjected to an applied constant axial stress. Creep test experiments are conducted to determine the static fatigue strength of the rock associated with tertiary creep rupture. These tests, typically conducted in uniaxial or triaxial compression, involve rapidly increasing the applied axial stress to a given percentage of the estimated compressive strength of the same size rock samples. The stress is then held constant

until the sample spontaneously fails due to time-dependent rupture. A plot of the logarithm of the time-to-failure versus the ratio of the applied stress to the unconfined compressive strength is developed. The plot is typically linear, reflecting the basic mechanisms of stress corrosion as described above. Rock samples subjected to stress levels that are small in comparison to the compressive strength (i.e., below about 50% to 60%) result in excessively long times to failure and cannot be tested practically in the lab due to the long test duration. However, these loading conditions are not of interest for drift stability in the postclosure time frame of hundreds to thousands of years. The loading conditions of interest to time-dependent degradation at Yucca Mountain are those in which the applied stresses from in situ and thermal loading in the drift wall periphery are a high percentage of the rock strength (e.g., greater than approximately 60% to 70%). Here, the time to failure may result in significant degradation in hundreds to thousands of years. In this case, relatively short-term laboratory experiments (on the order of days to weeks) can supply time constants capable of describing the stress corrosion process.

A series of triaxial static fatigue experiments were conducted on heated and saturated nonlithophysal cores from the Tptpmn in 1997 (Martin et al. 1997) and in 2004 (DTN: SN0406L0212303.002). Triaxial experiments on 50.8 mm diameter cores with a confining pressure of 5 MPa and pore water pressure of 4.5 MPa were conducted so that pore water of the saturated samples would remain in a liquid state as the temperatures were increased over boiling (125°C and 150°C). The resulting effective stress (the confining pressure minus the pore water pressure) was approximately 0.5 MPa, or essentially a state of uniaxial compression. This procedure was used to ensure a conservative state in which saturated samples were maintained at postclosure rock temperatures. Figure I-8 shows a typical specimen ready for testing.

Figure I-8. Triaxial Static Fatigue Experimental Setup and Posttest Sample for Heated, Saturated, 50.8 mm Diameter Samples of Tptpmn

The results of the testing on nonlithophysal cores of Tptpmn, as well as those from similar testing of Lac du Bonnet granite performed for the Canadian high-level radioactive waste

program (Schmidtke and Lajtai 1985; Lau et al. 2000) are given in Figure I-9. Granite results are included as a means of comparing the effects of rock type and for demonstrating the similarity in the general nature of the time-to-failure data for different rock types. Scatter in the data is due to sample heterogeneity, as well as the fact that the driving stress ratio (the horizontal axis) uses an estimated value for the unconfined compressive strength (adjusted for sample porosity) for normalizing the applied stress level.

Since there is significant variability in the unconfined compressive strength of each sample, there will be a scatter in the resulting plot of time-to-failure versus driving stress ratio. As seen in Figure I-7, the welded tuff has a significantly slower time static fatigue failure than granite, as evidenced by the steeper slope of the linear fit to the data. This slower time-to-failure is presumably a result of the relatively homogeneous, fine-grained, high silica content nature of the tuff, as opposed to the heterogeneous nature of the grain structure of granite.

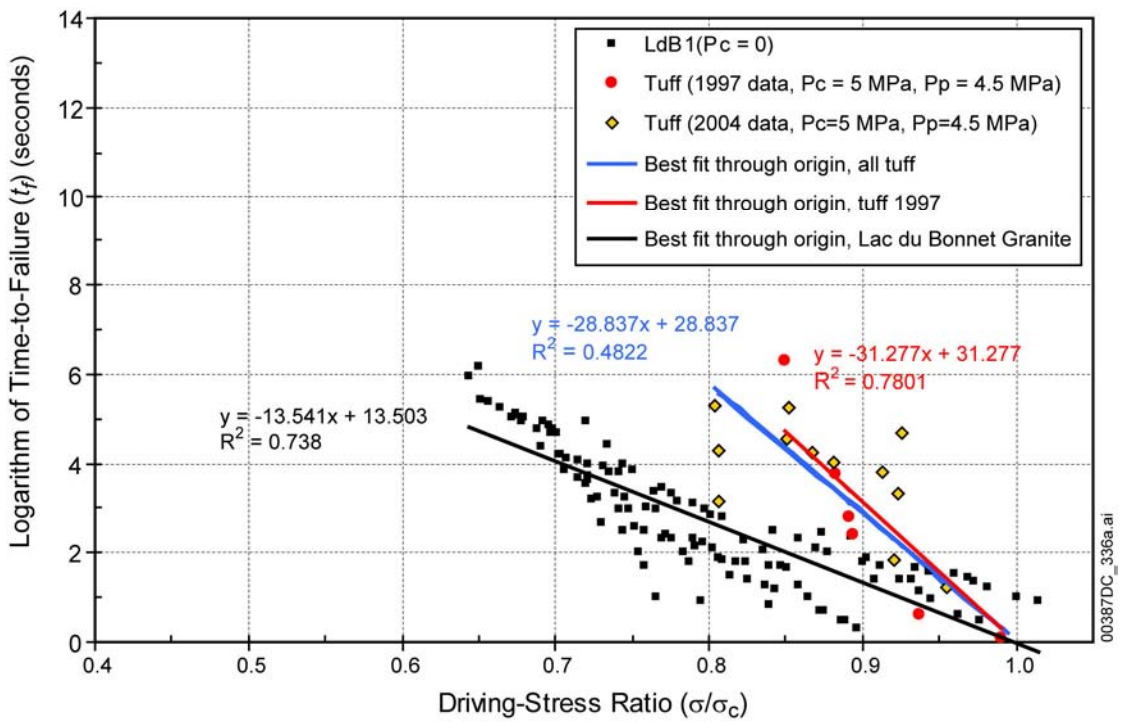

Source: BSC 2004a, Figure S-1 (Lac du Bonnet data); Martin et al. 1997 (tuff 1997 data); DTN: SN0406L0212303.002 (tuff 2004 data).

NOTE: Tests of Lac du Bonnet granite were conducted at 25°C. The driving stress ratio is defined as the ratio of applied constant test stress to the estimated unconfined compressive strength. 1997 tuff tests were conducted at 150°C, 2004 tuff tests were conducted at 125°C. LdB = Lac du Bonnet. Linear fits to 1997 Lac du Bonnet only and 1997 and 2004 tuff tests are shown. Samples that did not fail are also shown but not used in developing linear fits to data.

Figure I-9. Static-Fatigue Data for Unconfined and Triaxial Compression of Heated, Saturated Welded Tuff and Lac du Bonnet Granite

Linear fits to the unconfined compression data of Lac du Bonnet granite and to the 1997 only and to all (1997 and 2004) welded tuff data are given. The fits to both sets of welded tuff data are given because the analysis of drift degradation presented in the following section was conducted based on fits to only the 1997 data. After these analyses were completed, the

additional 2004 data were collected. The linear fits to the data sets show the general consistency of the overall slope of the fits, although there is considerably more scatter in the 2004 test results. Due to data uncertainty, a lower bound for the slope of the time-to-failure curve based on the Lac du Bonnet data, was also used in numerical modeling estimates. The static fatigue testing was performed on saturated tuff cores at elevated temperature, ensuring that the impact of water on time-dependent yielding was accounted for in the estimation of time-dependent effects on drift stability.

I.4.3.2.3 Development of a Mechanical Model for Simulating Time-Dependency in Nonlithophysal and Lithophysal Rock

After an estimate of the relationship of stress level to time-to-failure for nonlithophysal tuff has been defined through testing, it is necessary to establish the impact of lithophysal porosity on the time dependence and to generalize the results into a time-dependent strength model that can be used to estimate drift stability. The methodology for development of a mechanical model for representing time-dependent degradation effects in welded tuff is described below.

The particle flow code (PFC2D (BSC 2002a) and PFC3D (BSC 2002b)) discontinuum numerical modeling tools were used for understanding the impact of lithophysal porosity on time-to-failure as a function of applied stress. The particle flow code represents rock as a packed assemblage of small, rigid, grains that are bonded together at their contact points with shear and tensile strength. Porosity is developed naturally in the model by control of the shape and size of void space between chains of bonded grains. The macroscopic deformability of the assemblage is governed by the normal and shear stiffness at the contact points. Shear or tensile fracture between grains can form in a physically realistic manner as dictated by applied stresses, resulting in deformation and fracture of the rock mass. Quasi-static or dynamic stresses may be applied to the simulated rock for the solution of general boundary value problems. Details on the mechanics of the particle flow code program are provided in *Itasca Software–Cutting Edge Tools for Computational Mechanics* (Itasca Consulting Group 2002). A modification to the basic particle flow code program was developed for simulation of time-dependent, stress corrosion cracking of rock. This model, termed the particle flow code stress corrosion model, was used for simulating time-dependent tunnel fracturing of Lac du Bonnet granite for the Canadian waste disposal research program. In this model, time-dependent intergranular bond fracture strength was developed based on the general concept of a stress corrosion mechanism. The long-term behavior is controlled by three particle flow code stress corrosion model parameters, β_1, β_2, and σ_a. The terms β_1 and β_2 (rate constants) and σ_a (microactivation stress) do not affect short-term material properties. These material parameters are derived from calibration against the time-to-failure data supplied by static fatigue testing (e.g., Figure I-9). The particle flow code stress corrosion model has been extensively documented and calibrated against static fatigue testing of Lac du Bonnet granite and validated against time-dependent tunnel breakout observed at the Underground Research Laboratory in Manitoba, Canada (Potyondy and Cundall 2001). Details of the stress corrosion model in particle flow code and its calibration can be found in *Drift Degradation Analysis* (BSC 2004a).

Prior to representing time dependency, it was necessary to demonstrate that the particle flow code model can reproduce the basic, non-time-dependent mechanical behavior of nonlithophysal and lithophysal tuff. The calibration of the model against laboratory compression data from

small cores of nonlithophysal tuff and from large cores of lithophysal tuff from the Tptpul and Tptpll was described in Section 4.2.2.3 of the technical basis document and in Appendix A. The same basic particle flow code model, incorporating a time-dependent particle bonding strength, was then calibrated to reproduce the time-to-failure dependent response of nonlithophysal tuff determined from the static fatigue testing. The calibration of the model is carried out by conducting simulated creep tests on nonlithophysal samples in exactly the same way they are performed in the laboratory. Figure I-10 presents a typical simulated creep test in which axial load is applied to the particle flow code sample and held constant at 80% of its unconfined compressive strength. Tensile fractures (cracks) develop spontaneously in the model as a function of time based on the time-dependent bond strength of the constituent grains. The plot shows the development of a network of tensile stress corrosion cracks that accumulate and propagate within the sample until a macroscopic shear failure mechanism develops with resulting brittle rupture during the tertiary creep stage. The simulated creep test shows all three stages of creep: transient, secondary and tertiary, and reproduces the typical response of creep experiments in tuff (e.g., Figure I-6).

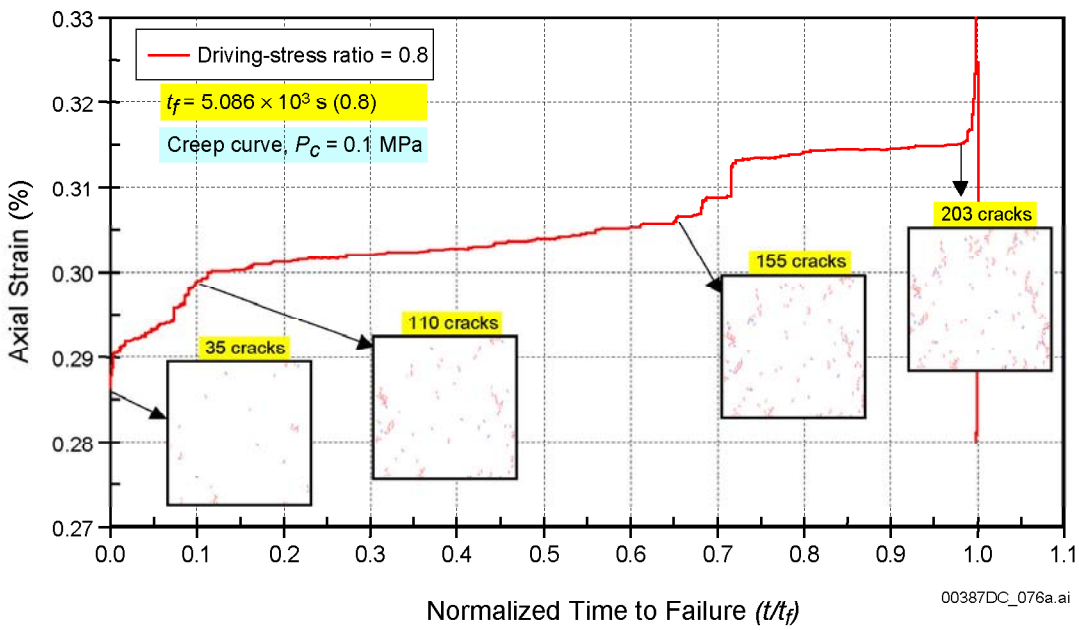

Source: BSC 2004a, Figure S-12.

NOTE: Numerical simulation of creep test run by holding applied axial stress constant at 0.8 times the unconfined compressive strength. The damage, in terms of new crack growth, is displayed at various times along the creep curve. Brittle failure of the sample occurs when sufficient time-dependent crack growth results in failure mechanism.

Figure I-10. Example of Simulated Creep Curve and Brittle Rupture Calibration for Nonlithophysal Tuff, (in This Case, Providing a Lower-Bound Estimate by Using Lac du Bonnet Granite Time-to-Failure Curve) Static-Fatigue Test at Driving-Stress Ratio (Ratio of Applied Stress to Unconfined Compression Strength) of 0.8

A large number of particle flow code simulations of static fatigue tests of nonlithophysal rock was run at a wide range of driving stress ratios, and two particle flow code stress corrosion parameters were calibrated, so that the model was able to reproduce the basic time-to-failure fits

shown in Figure I-9 for tuff and granite. The third stress corrosion parameter, the activation stress, was conservatively assumed to be 0. The consequence of this assumption is that the long-term strength of the particle flow code synthetic material is 0. It is well known that real rocks have long-term (true) strength that is on the order of 50% of the short-term strength. In other words, if the load is less than long-term strength, the rock will never fail, irrespective of duration of the load. The model was then used to investigate the impact of lithophysal porosity on the rate of time dependence. It is assumed that time-dependent behavior of the matrix is the same for both lithophysal and nonlithophysal rocks. A series of simulated creep experiments for lithophysal porosities of 11% and 20% were conducted, resulting in the generation of a set of time-to-failure versus driving stress ratio plots for various levels of lithophysal porosity (Figure I-11).

I.4.3.2.4 Drift-Scale Model for Simulation of Time-Degradation of Emplacement Drifts

The particle flow code model for time dependency of lithophysal rock, shown in Figure I-11, is computationally very large and is difficult to apply on the scale of a complete emplacement drift. To overcome these computational limitations, a drift-scale model using the UDEC discontinuum program was developed for investigation of non-time-dependent drift degradation analyses in lithophysal rocks (see Section 4.2.7 of the technical basis document). The UDEC model is described below. The same model is used for time-dependent drift-scale analyses with the exception that the strength properties of the model are adjusted as a function of time. The relationships for time-to-failure as a function of lithophysal porosity developed from the laboratory testing and particle flow code extrapolations are used to define time-dependent strength properties for the drift-scale UDEC model. The approach to definition of time-dependent effects on strength in UDEC is simplistic in that it relates rock mass damage resulting from stress corrosion cracking directly to a loss of cohesion and tensile strength of the rock mass. The degree of strength loss was determined by (1) conducting a series of particle flow code numerical creep tests at different values of driving stress ratio and (2) interrupting the particle flow code creep test simulations at various times during a simulated test and conducting numerical compression and tensile strength tests on the damaged sample. For example, Figure I-10 shows four “snapshots” of the crack-damaged state of a simulated rock sample at various times along the creep curve. The strength properties of these damaged states were determined, and the resulting cohesion and tensile strength defined as a function of time for a given driving stress ratio. The strength loss was generalized into a damage coefficient that varies from 0 to 1 (0 indicates no strength loss, while 1 is complete strength loss). The cohesion and tensile strength of the rock is multiplied by this coefficient to derive the strength properties of the rock mass as a function of time. Essentially, this approach relates the reduction in strength properties (shear and tensile strength) to the increase in fracture density or damage to the rock mass. Figure I-12a shows the form of the damage coefficient as a function of time for various driving stress ratios as derived from the particle flow code stress corrosion model for a nonlithophysal simulation. As seen in this plot, damage occurs in a brittle fashion with abrupt failure near the peak strength. The amount of damage accumulated prior to the abrupt failure (as shown by the damage coefficient) is less than 10% for high driving stress ratios (e.g., greater than 0.6), whereas damage accumulation is significantly larger for low driving stress ratios (e.g., less than 0.6). A simplified representation of the damage coefficient evolution in terms of time is shown in Figure I-12b.

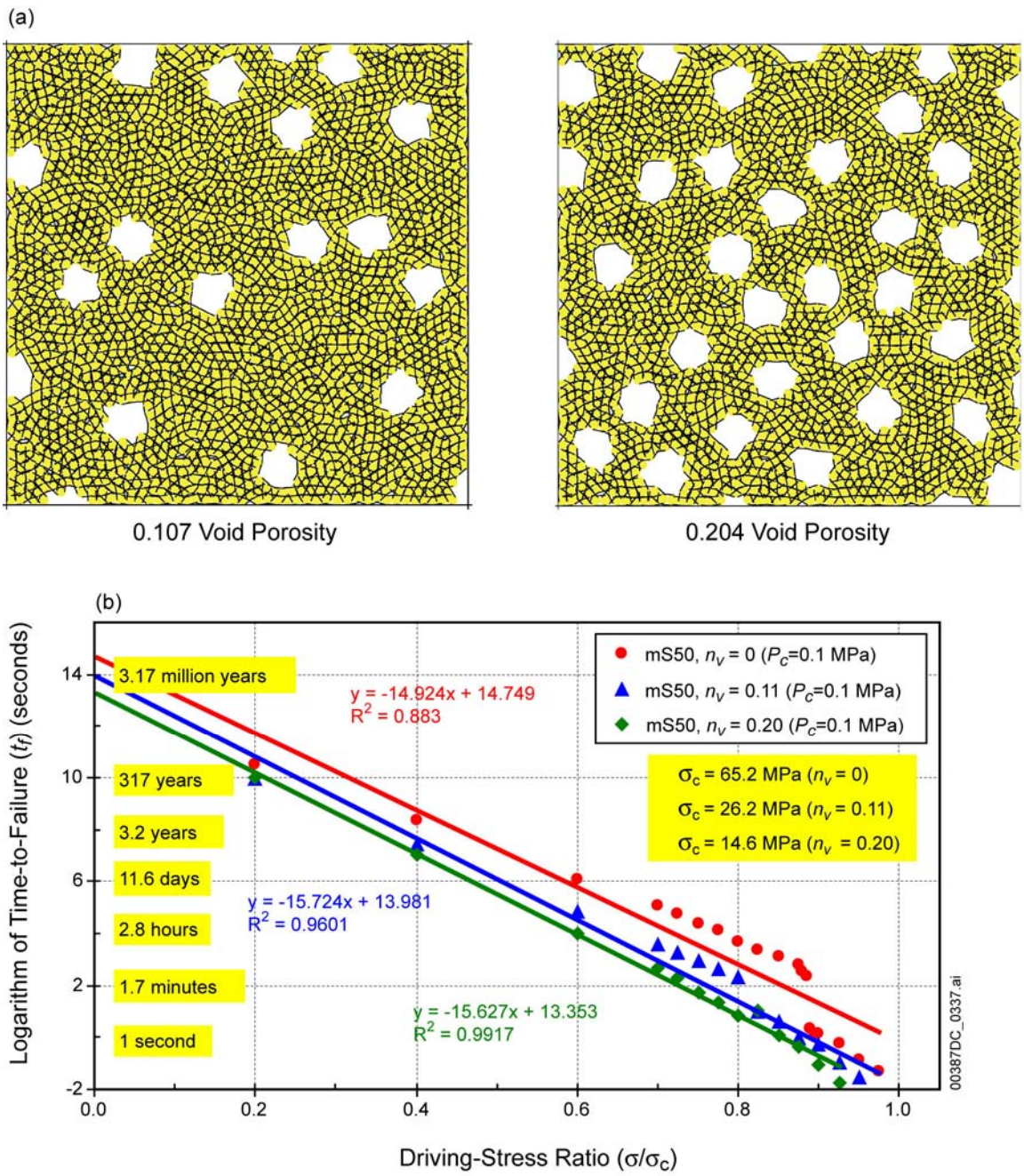

Source: BSC 2004a, Figures S-5 and S-16.

NOTE: The time dependency has approximately the same slope for all void porosities for the straight-line fit. Lithophysae are simulated as circles with a diameter of 90 mm. MS50 is the designation for the material properties of the matrix derived from nonlithophysal calibrations.

Figure I-11. (a) Example Particle Flow Code Specimens with Void Porosities of 0.107 and 0.204 and, (b) Effect of Void Porosity on Time-to-Failure Response for Lithophysal Tuff Material (0% to 20% Void Porosity, n_v)

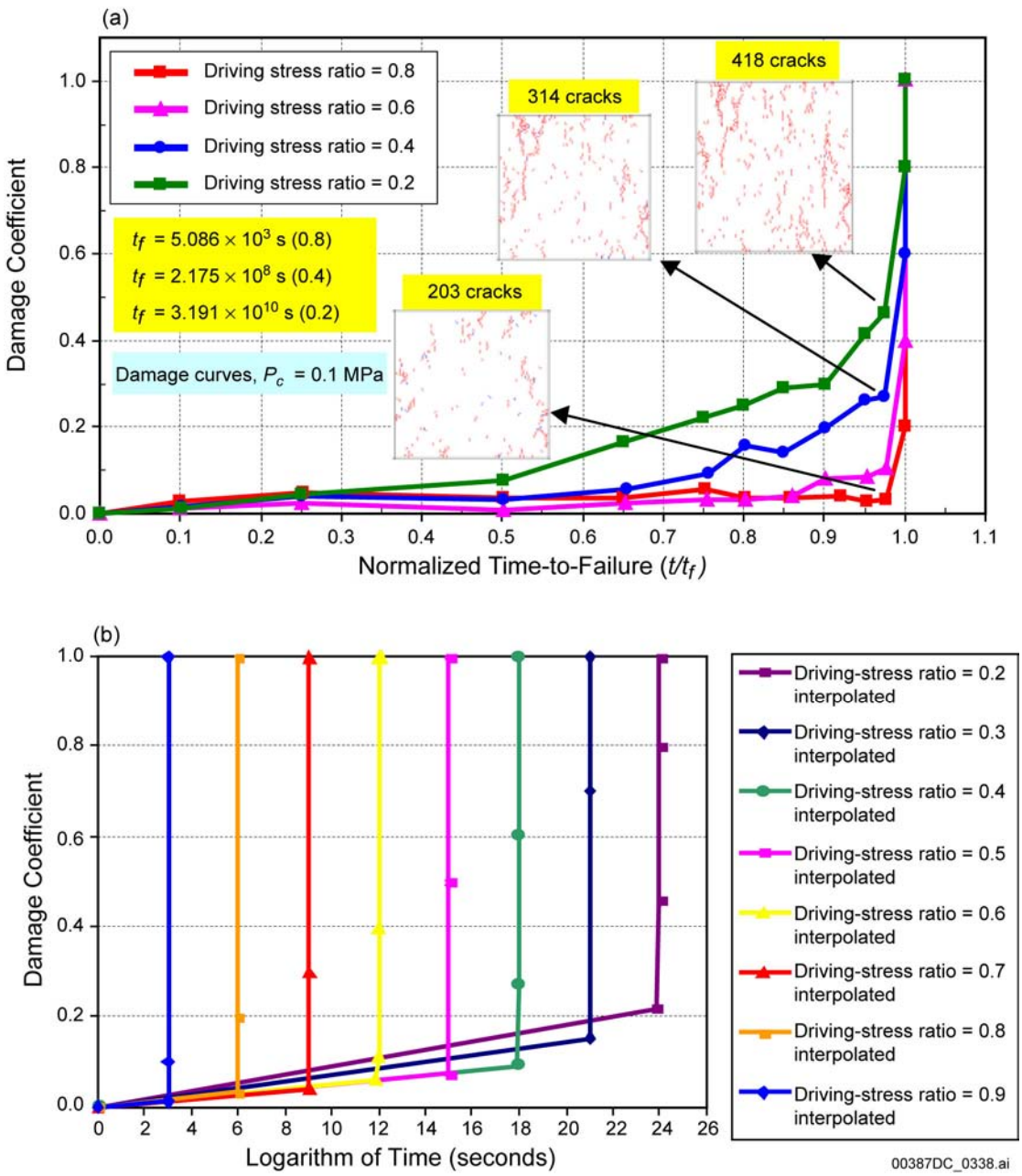

Source: BSC 2004a, Figures S-21 and S-28.

NOTE: Each curve has a vertical asymptote at a time-to-failure for a given driving-stress ratio, which is provided by the best fit to tuff given in Figure I-7.

Figure I-12. Time Evolution of Damage Due to Strength Degradation Coefficient for Nonlithophysal Tuff Material during Static-Fatigue Tests at Driving-Stress Ratios Ranging from 0.2 to 0.8 (a) and Idealized Damage Coefficient as a Function of Time for a Range of Applied Stress Conditions (b)

As discussed in Section 4.2.7 of the technical basis document, the UDEC drift-scale model is composed of many small elastic blocks that are bonded across incipient,[7] ubiquitous fractures with shear and tensile strength components (Figure I-13). While the non-time-dependent UDEC drift-scale model assumes constant strength properties for the incipient fractures, the time-dependent damage model is transient in nature and assigns cohesion and tensile strength based on the damage coefficient as a function of time after excavation (i.e., Figure I-12b).

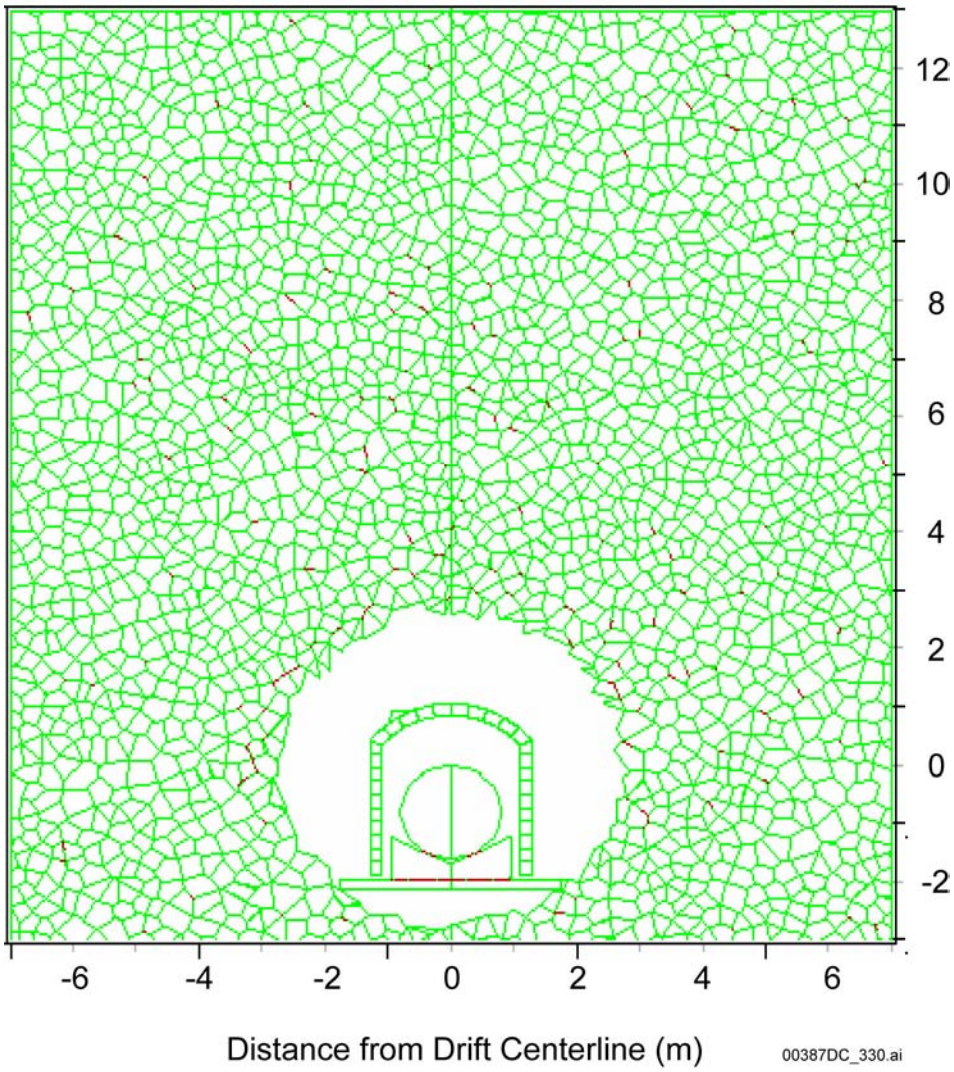

NOTE: Model composed of irregular blocks joined across ubiquitous, incipient fractures. Blocks are bonded by shear and tensile strengths calibrated to rock mass strength estimates. These shear and tensile strengths are dependent on time based on the damage coefficients given in Figure I-12.

Figure I-13. UDEC Model of Emplacement Drift in Lithophysal Rock Mass

[7] The term incipient here refers to the fact that the contact planes between blocks are initially bonded with the deformability and strength properties of the rock mass, and, thus, prior to failure, the rock mass acts as a continuum. If forces dictate, shear or tensile failure may occur along any of the incipient fractures, with the result of propagation along the incipient fracture network. The random nature of the incipient fracture network allows directional freedom of fracture growth.

I.4.3.2.5 Time-Dependent Drift Degradation Analyses

I.4.3.2.5.1 Effect of In Situ Stress Only in Lithophysal Rocks

A series of parametric drift degradation simulations were conducted for the range of potential lithophysal rock mass strength categories in the Tptpll. The response to RDTME 3.05 (Appendix A of this technical basis document) describes the subdivision of the expected range of mechanical properties of the lithophysal rock into five mechanical properties categories, each characterized by a Young's Modulus and unconfined compressive strength. Each of these categories was related to the degree of lithophysal porosity, which, in turn, can be related to the level of abundance of that porosity in the Tptpll. Figure I-14 provides a histogram of approximate abundance of lithophysal porosity in the Tptpll obtained from geologic mapping in the ECRB Cross-Drift (BSC 2004a, Appendix O). An approximate relationship between lithophysal porosity and the rock mass mechanical properties category (1 is the weakest rock, highest porosity and 5 is the strongest rock, lowest porosity) is also given in this figure.

Thermal-mechanical, time-dependent drift degradation analyses for the postclosure time frame were conducted for each of these strength categories as follows. Each of the incipient fractures in the drift-scale model (Figure I-13) is assigned stiffness, cohesion, tensile strength, and a friction angle corresponding to a particular rock mass mechanical properties category. Calibration of the model shows that these properties provide the proper overall rock mass deformability and strength properties corresponding to the particular mechanical properties category. When performing a time-dependent drift degradation analysis, the cohesion and tensile strength at each incipient fracture location is adjusted as a function of time, with yield assumed to occur in a brittle fashion when the time-to-failure is reached (Figure I-12). Thus, as the drift is excavated and as transient thermal stresses develop, time-dependent yield and fracture can occur around the excavation, resulting in redistribution of stress and possible propagation of drift breakout, collapse, and rockfall.

The model was run by first excavating the emplacement drift under in situ stresses only, followed by application of the transient rock mass temperature conditions. The time-dependent fracture state and drift stability was examined at 1, 5, 10, 100, 1,000, and 10,000 years during the heating and cooling phases of the postclosure period. Additional analyses were conducted to examine the effect of seismic loading with the application of the 10^{-4} annual exceedance level ground motion time histories (approx. 0.5 m/s peak ground velocity; see Section 5.3.2.1.3 of this technical basis document). This ground motion was applied to the time-degraded model at the time of peak thermal stress (approximately 30 years after closure), at 1,000 years, and at 10,000 years. The 10^{-4} event was chosen to determine if the added seismic stress and shaking would be sufficient to dislodge time-degraded, fractured, and loosened rock that may still be in place on tunnel walls.

Figures I-15 to I-18 show the resulting time-dependent drift degradation estimates for mechanical property categories 1, 2, 3, and 5 for loading by in situ stresses only for 1 to 10,000 years. As seen in these plots, the results for the lowest rock qualities (categories 1 and 2) show significant deterioration of the drifts would be expected soon after excavation as a result of in situ stress loading only. Observations in the ECRB Cross-Drift and the ESF, which have been excavated for 6 or more years, show no progressive raveling or overbreak (e.g., Brekke et al.

1999, p. 2-5). This observation holds even in those areas of high lithophysal porosity found near the top of the Tptpll (see Section 2.3.2 of this technical basis document). Categories 3 and 5 show little time-dependent effect from in situ stressing only. These results point out that the best estimate of tuff time dependence, coupled with the assumptions of brittle rock failure and constant, homogeneous properties within a given model cross section produces conservative damage estimates. Category 3 is considered to represent an average condition of lithophysal porosity for the Tptpll and shows little overbreak with time. Analyses presented in *Drift Degradation Analysis* (BSC 2004a, Appendix S) examine the impact of spatially variable rock properties within a given model section based on the mapped variability of lithophysal porosity in the ECRB Cross-Drift. The spatially variable model has a range of rock categories distributed throughout the cross section, and results of analyses show time-dependent drift degradation response similar to that shown for category 3 mechanical properties. An important conclusion from these initial in-situ-stress-only analyses is that best estimate time-dependent fracture growth within the tuff matrix is not expected to lead to collapse modes and significant drift degradation.

I.4.3.2.5.2 Combined Thermal and Time-Dependent Effect in Lithophysal Units

Throughout the regulatory period of 10,000 years, the emplacement drifts and surrounding rock mass will be subject to a heating cycle. Time-dependent strength degradation will happen concurrently with transient, thermally induced stress changes. Increased stresses around the excavation will accelerate the process of strength degradation. The results of numerical simulation of drift degradation as a result of these two processes are shown in Figures I-19 to I-21. Time-dependent strength degradation is assessed using the tuff best-fit static-fatigue line. As expected, most rockfall occurs in category 2 rock mass, as shown in Figure I-19. Initially, most of the rockfall comes from the walls, which are loaded almost to a yielding state for this rock mass category under in situ stress conditions only. Strength degradation combined with a temperature increase, which at early times increases the hoop stress in the walls (not only in the roof), results in some rockfall from the wall at 5 and 10 years after emplacement of the waste. The large increase in the temperature and, consequently, in the stresses after the forced ventilation stops causes additional rockfall (at 80 years). At this stage, stress increase is predominantly in the roof. Therefore, some rockfall comes from the roof. It is counterintuitive that more rockfall is predicted in category 5 (Figure I-21) than in category 3 (Figure I-20). However, a large stiffness of category 5 lithophysal rock mass causes a large (larger than in category 3) increase in the hoop stress and yielding in the roof, even assuming the short-term yield strength of the rock mass.

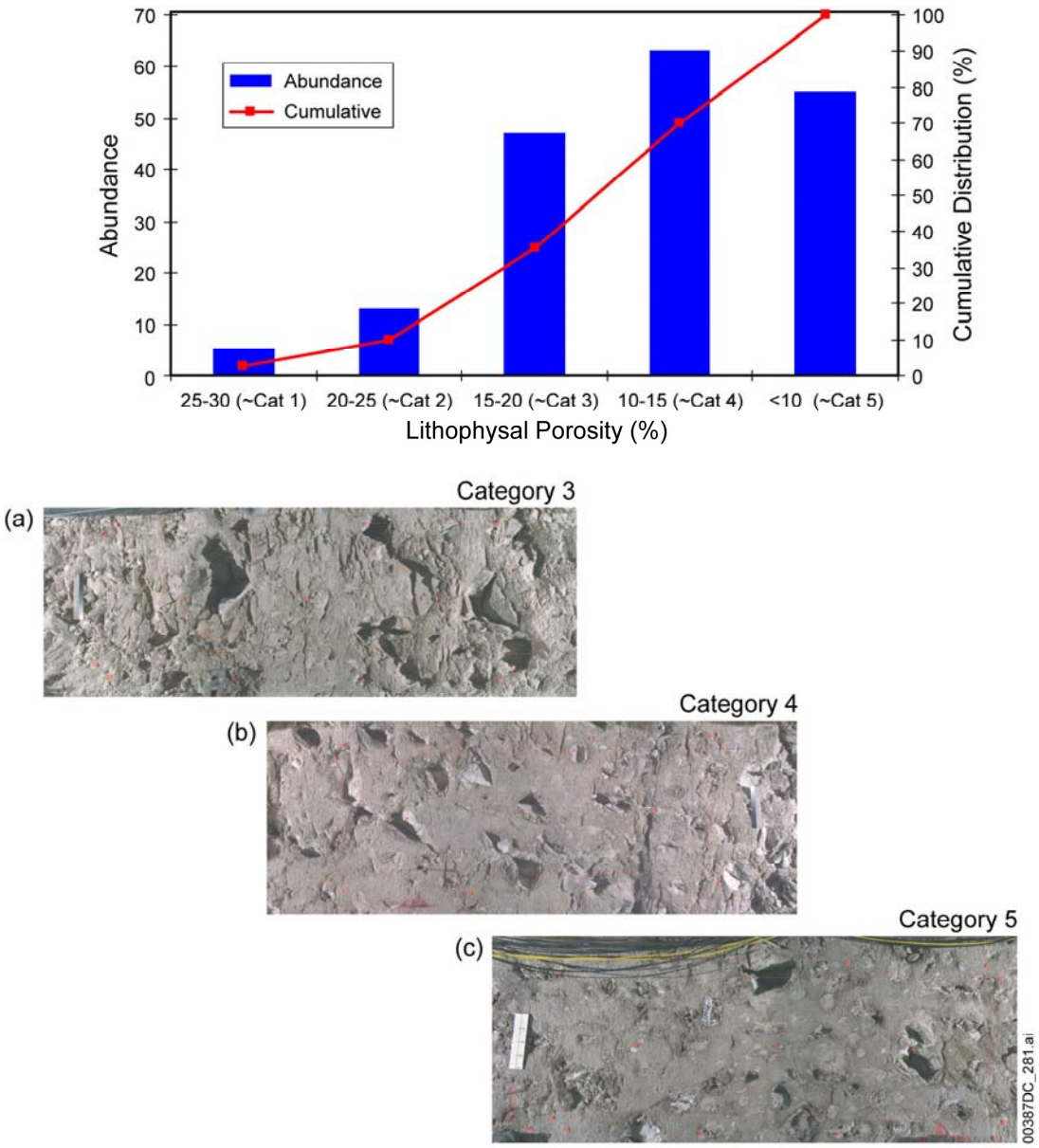

Source: BSC 2004a, Figures E-9 and E-10.

NOTE: Lithophysal porosity data are from ECRB Cross-Drift station 14+44 to 23+26. Examples of approximate rock strength category levels taken from 1 by 3 m panel maps: (a) Category 3 with lithophysal porosity of approximately 19%; (b) Category 4 with lithophysal porosity of 13.3%; and (c) Category 5 with lithophysal porosity of 8.5%.

Figure I-14. Distribution of Lithophysal Porosity and Estimated Rock Properties Categories for the Tptpll in the ECRB Cross-Drift

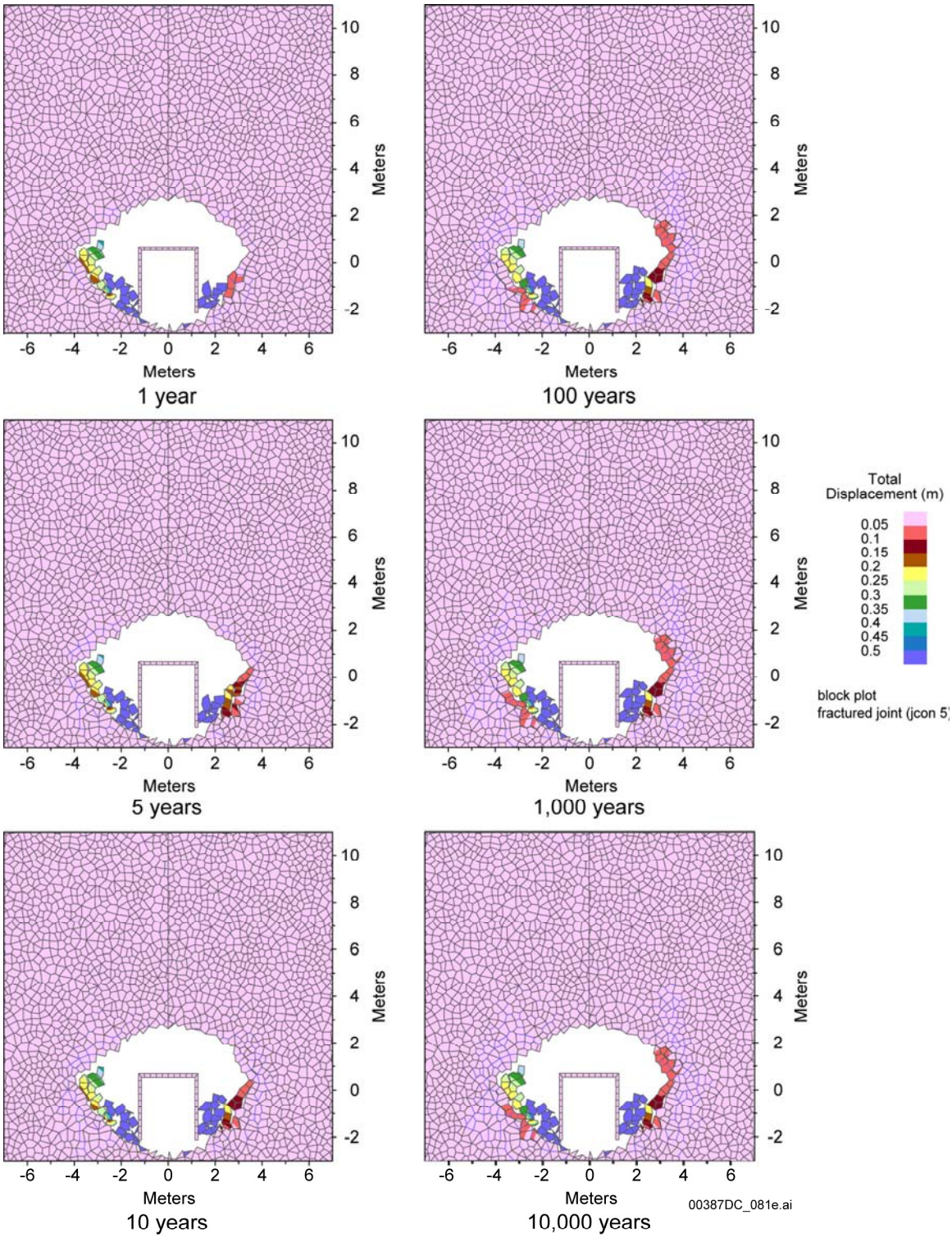

Source: BSC 2004a, Figure S-36.

NOTE: Block colors correspond to their displacement (in meters) as shown in scale at right. Block color helps visualize those blocks that have moved.

Figure I-15. Predicted Evolution of Damage Due to Strength Degradation for Category 1–Tuff Best-Fit Static-Fatigue Curve, Applied In Situ Stress Only

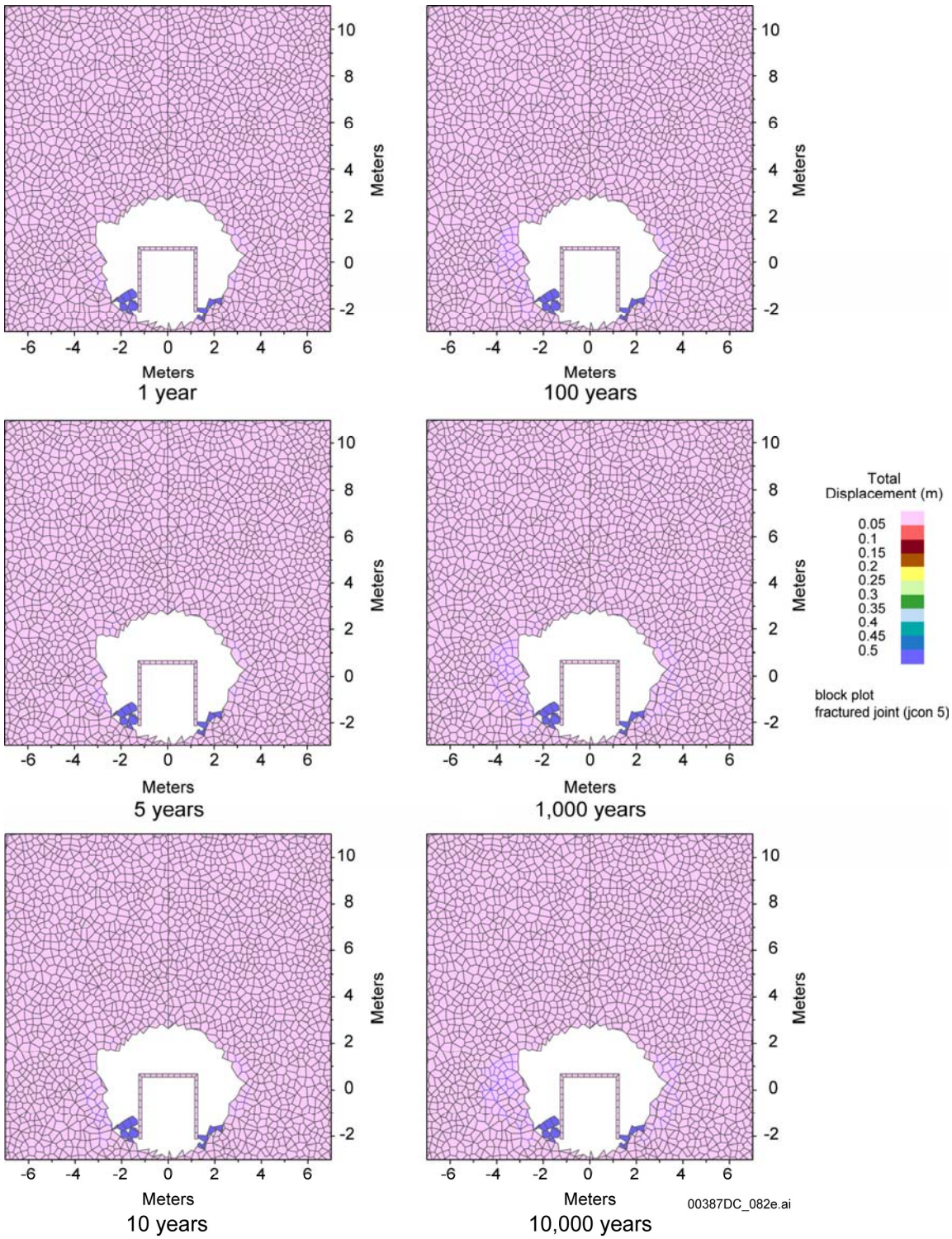

Source: BSC 2004a, Figure S-37.

NOTE: Block colors correspond to their displacement (in meters) as shown in scale at right. Block color helps visualize those blocks that have moved.

Figure I-16. Predicted Evolution of Damage Due to Strength Degradation for Category 2–Tuff Best-Fit Static-Fatigue Curve, Applied In Situ Stress Only

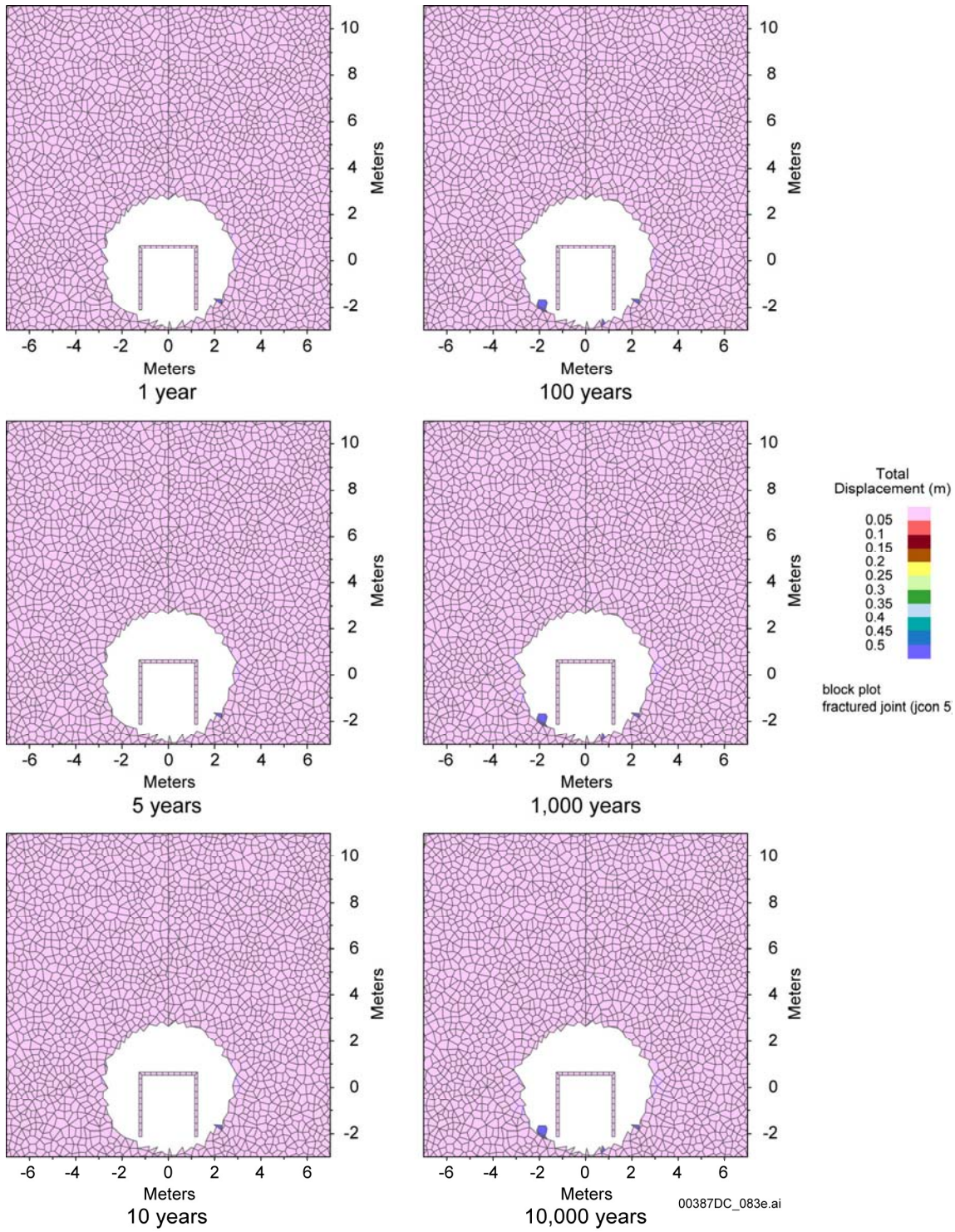

Source: BSC 2004a, Figure S-38.

NOTE: Block colors correspond to their displacement (in meters) as shown in scale at right. Block color helps visualize those blocks that have moved.

Figure I-17. Predicted Evolution of Damage Due to Strength Degradation for Category 3–Tuff Best-Fit Static-Fatigue Curve, Applied In Situ Stress Only

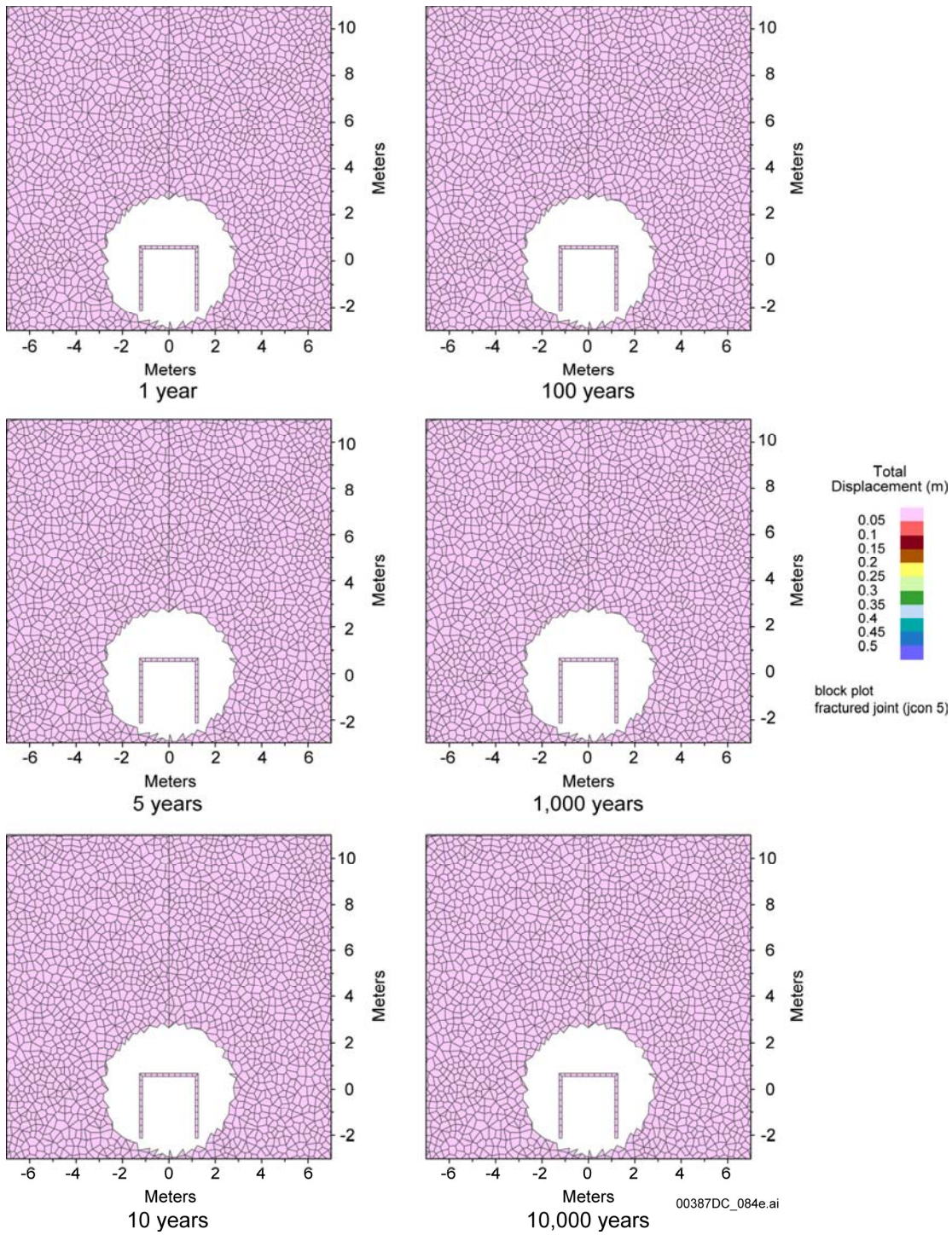

Source: BSC 2004a, Figure S-39.

NOTE: Block colors correspond to their displacement (in meters) as shown in scale at right. Block color helps visualize those blocks that have moved.

Figure I-18. Predicted Evolution of Damage Due to Strength Degradation for Category 5–Tuff Best-Fit Static-Fatigue Curve, Applied In Situ Stress Only

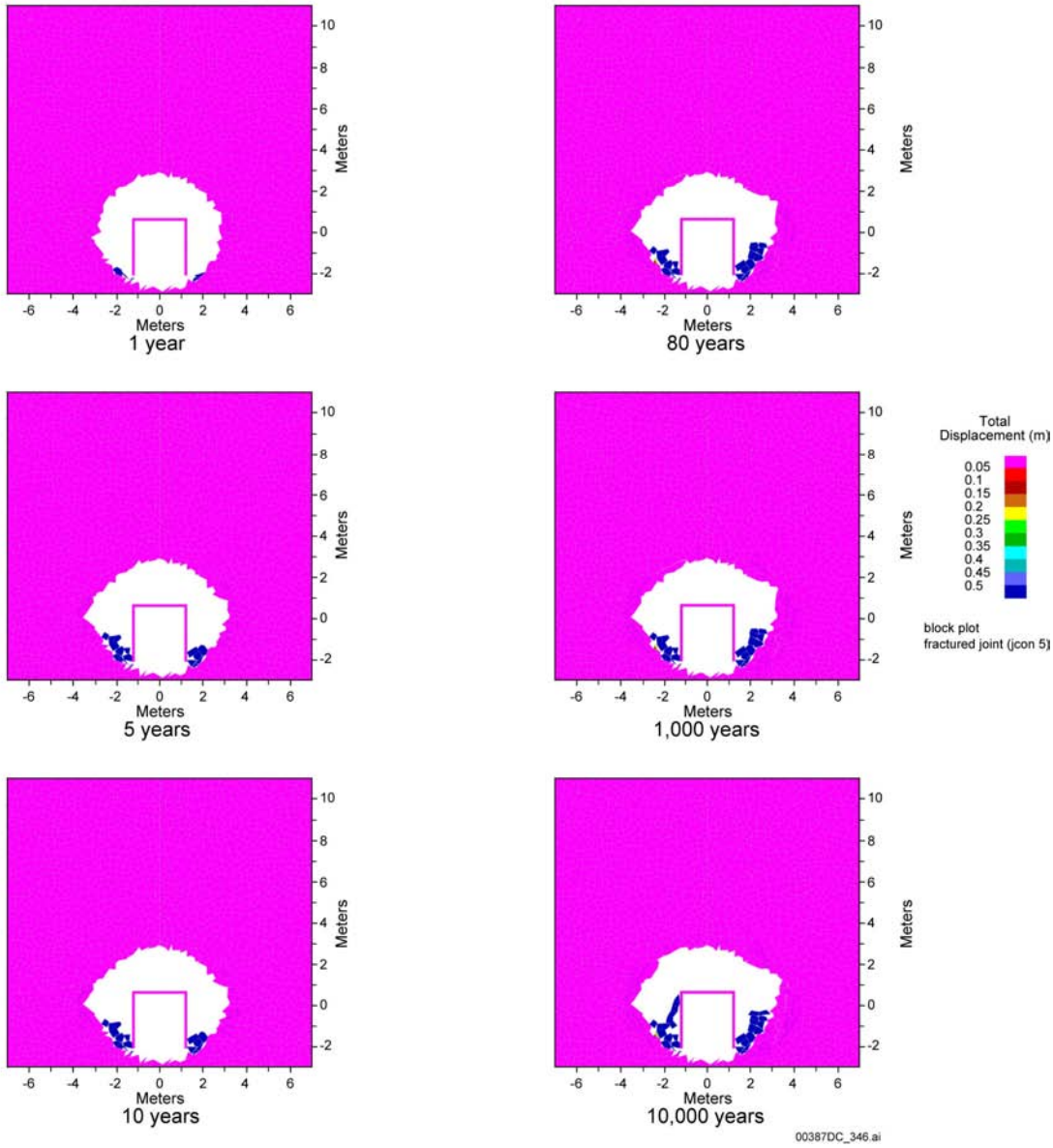

Source: BSC 2004a, Figure S-41.

NOTE: Block colors correspond to their displacement (meters).

Figure I-19. Evolution of Damage Due to Strength Degradation Resulting from In Situ and Thermal Load for Category 2 – Tuff Best-Fit Static-Fatigue Curve

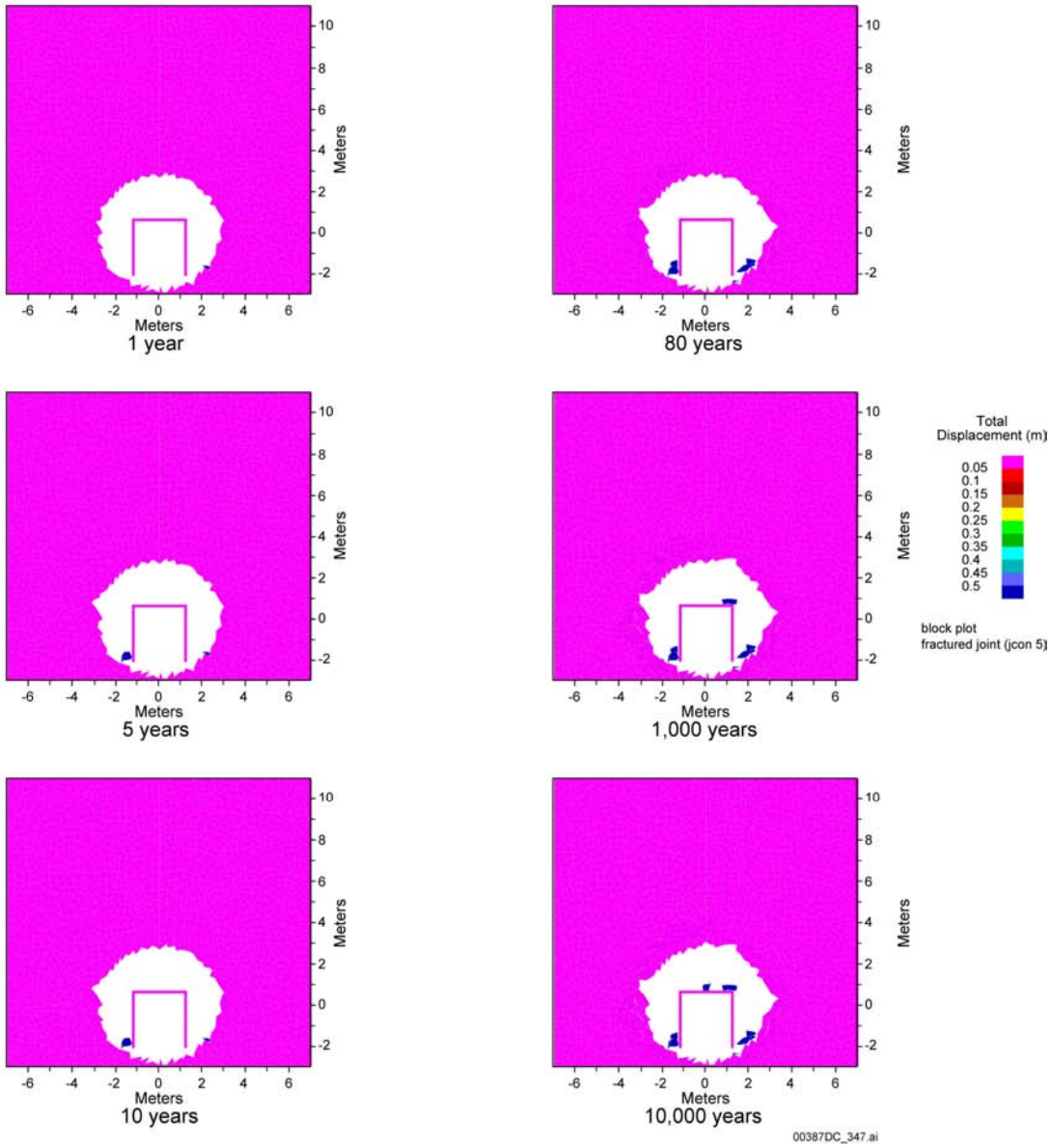

Source: BSC 2004a, Figure S-42.

NOTE: Block colors correspond to their displacement (meters).

Figure I-20. Evolution of Damage Due to Strength Degradation Resulting from In Situ and Thermal Load for Category 3 – Tuff Best-Fit Static-Fatigue Curve

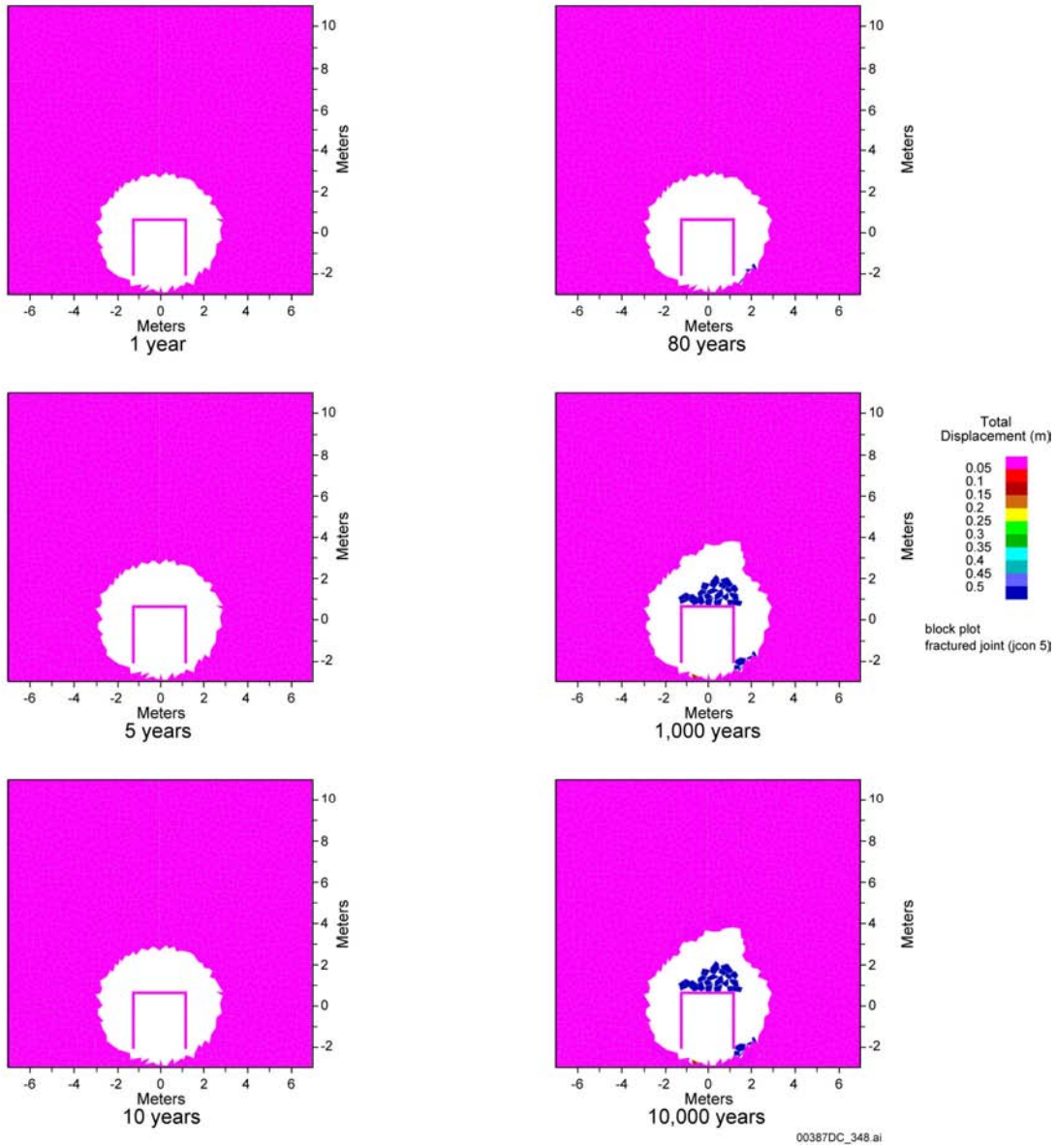

Source: BSC 2004a, Figure S-43.

NOTE: Block colors correspond to their displacement (meters).

Figure I-21. Evolution of Damage Due to Strength Degradation Resulting from In Situ and Thermal Load for Category 5 – Tuff Best-Fit Static-Fatigue Curve

It should be noted that static-fatigue curves are temperature dependent. This dependence is not explicitly included in the analysis. However, the tuff data are obtained from tests conducted at 150°C, which is higher than the maximum temperature of the rock mass anticipated throughout the repository for postclosure. Consequently, the results obtained in this analysis, although for isothermal static-fatigue curves, are conservative.

I.4.3.2.5.3 Combined Seismic, Thermal, and Time-Dependent Effect in Lithophysal Units

The 10^{-4} ground motion was applied to category 2 and 5 rock mechanical property cases at two time periods: (1) at the time of the peak thermal stress state (nominally at 80 years after emplacement, or 30 years after cessation of 50 years of forced ventilation) and (2) at 10,000 years at the completion of the postclosure heating and cooling cycle. Figures I-22 and I-23 show the resulting predicted degraded drift states for these cases. Essentially, the application of the 10^{-4} ground motion (peak ground velocity of approximately 0.5 m/s) dislodges any fractured and loosened rock created by the thermal stress and time dependency. As seen in these figures, the impact of time dependency of strength properties is to widen the diameter of the emplacement drifts in the lower quality (category 2) rock due to progressive shear failure at the sidewalls. In the highest quality (category 5) rock, additional progressive yield of the roof is evident. Roof yield in higher quality rock is due to the higher modulus of the rock mass and, thus, higher roof-parallel thermally induced stresses during the heating cycle. This is similar to the roof crown spalling effect observed in the Drift Scale Test.

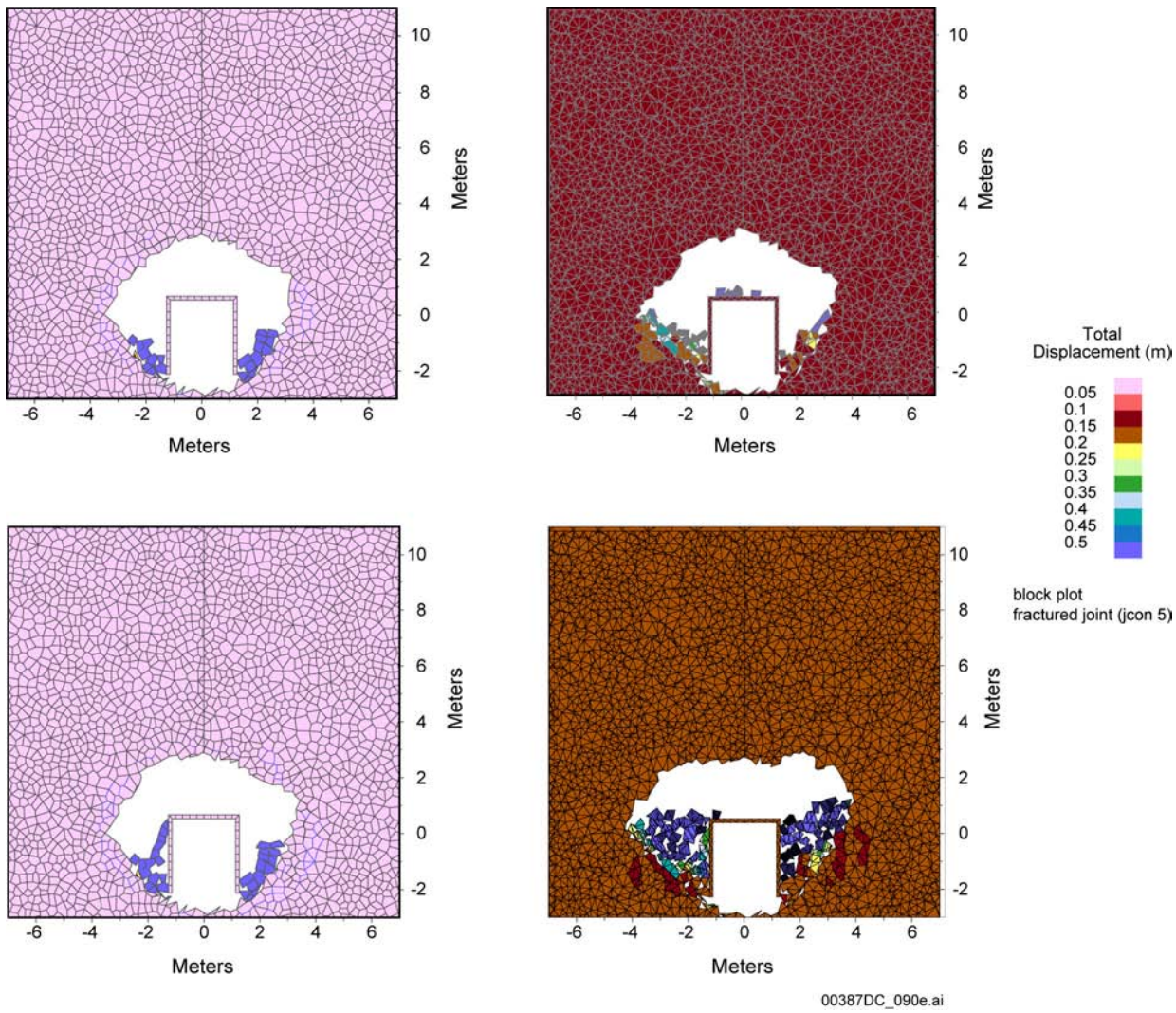

Source: BSC 2004a, Figures S-44 and S-46.

NOTE: Left figure shows state for in situ plus thermal stress; right figure shows state for in situ plus thermal plus seismic stress. Blocks colored by total displacement to allow visual recognition of blocks detached from surrounding intact mass. Block colors correspond to their displacement (meters) as shown in scale at right.

Figure I-22. Effect of 10^{-4} Ground Motion after (Top) 80 Years and (Bottom) 10,000 Years of the Heating and Cooling Cycle in Category 2 Rock Mass

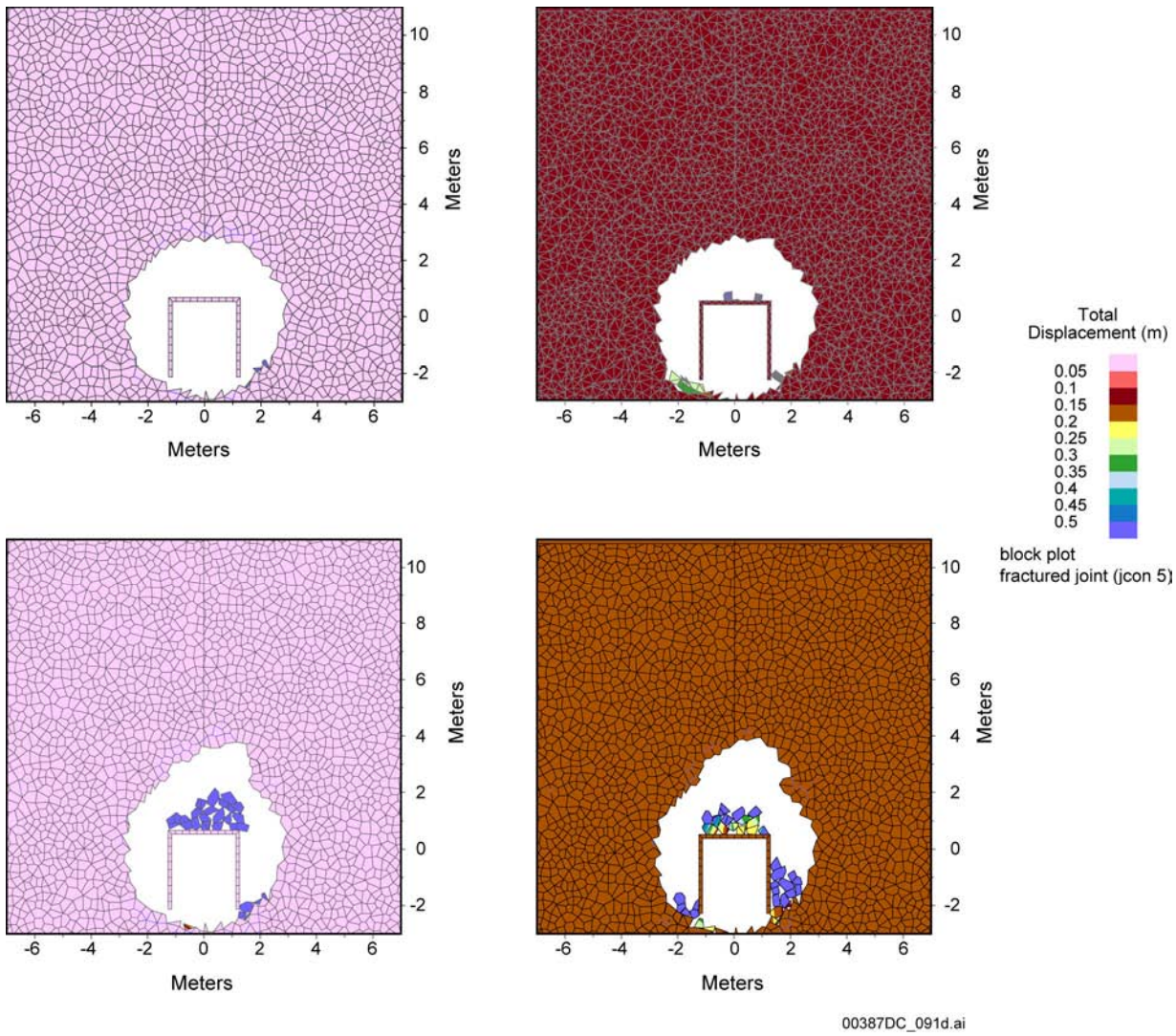

Source: BSC 2004a, Figures S-45 and S-47.

NOTE: Left figure shows state for in situ plus thermal stress; right figure shows state for in situ plus thermal plus seismic stress. Blocks colored by total displacement to allow visual recognition of blocks detached from surrounding intact mass. Block colors correspond to their displacement (meters) as shown in scale at right.

Figure I-23. Effect of 10^{-4} Ground Motion after (Top) 80 Years and (Bottom) 10,000 Years of the Heating and Cooling Cycle in Category 5 Rock Mass

I.4.3.2.5.4 Time-Dependent Degradation of Nonlithophysal Rock

The time-to-failure for intact nonlithophysal rock blocks shows significantly less time dependency than for the lithophysal rock described in the previous section (see Figure I-11). Therefore, insignificant time-related fracture growth is expected in the intact rock blocks. However, the potential exists for time-dependent yield of roughness (asperities) on fracture surfaces subjected to long-term shear stress. As described in Section 5.3.2.1 of this technical basis document, natural fractures in the nonlithophysal rock tend to control the drift stability response. There are four sets of fractures in the nonlithophysal rock: two subvertical cooling fracture sets, and one set of low dip-angle vapor phase partings and one set of random fractures

with dip averaging around 45° (see Section 4.1.2). The vertical cooling fractures are smooth and planar with low cohesion, friction, and dilation angle, while the vapor phase partings are rough and filled with vapor phase mineralization. The vertical cooling fractures consequently have higher cohesion, friction, and dilation angles (see Table 3-5). Stability of the emplacement drifts in the nonlithophysal rock has been examined for applied in situ, thermal, and seismic stressing (summarized in Section 5.3.2 of this technical basis document). The potential effect of time-dependent degradation of the fracture surfaces was examined in an impact study described in Section 5.3.2.1.8. A conservative approach to accounting for time-dependent effects was taken by assuming that:

- The fractures were smooth, with roughness completely sheared off. Surface properties were set to a dilation angle of 0 and a residual friction angle of 30°. The reduced friction angle is a typical value for a smooth joint reported by Goodman (1980, p. 158) and is consistent with the direct shear test results described in Section 3.2.4.1 of this technical basis document (DTN: GS030283114222.001).

- The fractures have no cohesion.

Stress analyses under in situ, thermal, and seismic stressing show that these highly conservative assumptions result in only a minor change in drift degradation. Increased thermal loading tends to increase stability of the fractured rock mass as thermally induced tangential stress around the excavation tends to increase the clamping forces on fractures. It is concluded that fracture geometry and the potential for formation of kinematically unstable blocks is the greatest influence on drift stability.

I.4.3.2.6 Summary of Time-Dependent Strength Degradation Effects

A mechanics-based model of time-dependent degradation of nonlithophysal and lithophysal tuff was developed using time-to-failure data generated from laboratory triaxial compression of heated, saturated samples of the Tptpmn. Using a similar approach to that developed for the Canadian high-level radioactive waste storage program, the laboratory data were used to calibrate a time-dependent fracture model for nonlithophysal rock within the particle flow code discontinuum numerical model. Lithophysal voids were added to the particle flow code model to estimate the impact of lithophysal porosity on the creep and time-to-failure response of tuff. This behavior was then embedded into the strength properties for the drift-scale model of emplacement drift stability in lithophysal rocks. In turn, this model was used for conducting parametric studies of drift stability subjected to in situ, thermal, and seismic stressing over the postclosure time period. The results indicate that some drift sidewall failure and breakout can be expected for the lowest mechanical property categories of lithophysal tuff (i.e., categories 1 and 2) that represent approximately 10% of the rock mass. For the average and highest mechanical property categories (i.e., categories 3, 4, and 5), representing approximately 90% of the lithophysal rock mass, little time-dependent degradation is expected. Time-related degradation effects in fractured nonlithophysal rock were examined through three-dimensional discontinuum stress analyses in which the surface roughness and cohesion were assumed to be completely destroyed. Even with these highly conservative assumptions, it was found that fracture geometry, not surface properties, control the degree of degradation of the tunnels in nonlithophysal rock.

I.4.3.2.7 Bounding Case of Drift Degradation Using Lac du Bonnet Granite Time-to-Failure Data

The analyses presented in Section I.4.3.2.6 were performed assuming the slope of the best fit time-to-failure data for tuff. As shown in Figure I-9, the slope of the time-to-failure data fit obtained for Lac du Bonnet granite provides a lower bounding case to that for Topopah Spring Tuff. In other words, the granite exhibits significantly greater time dependency and strength loss than tuff. A series of time-dependent drift degradation analyses similar to those summarized in Figures I-15 to I-18 were performed for lithophysal rock categories 1, 2, and 5 but using the slope of the time-to-failure best fit for Lac du Bonnet granite in unconfined compression as shown in Figure I-9. These analyses are performed to investigate drift degradation extent as a function of time for a bounding case of time-dependent properties. The results, described in detail in *Drift Degradation Analysis* (BSC 2004a, Appendix S), show:

- Using the granite time-dependency behavior for Tptpll strength category 1 (represents local conditions of less than about 5% of the Tptpll) shows significant drift breakouts at the sidewalls of the tunnel within 1 year of excavation and complete drift collapse in hundreds to thousands years. The conservatism in these properties is obvious because it would indicate extensive drift damage at early times, which is not observed in existing ECRB Cross-Drift and ESF tunnels.

- Using the granite time-dependency behavior for Tptpll strength category 2 (represents local conditions, combined with category 1 that account for less than 10% of the Tptpll) results in breakouts at the sidewalls of the drift and rubble accumulation that does not cover the drip shield after thousands of years. Again, these analyses show significant early (1 to 5 years after excavation) breakouts on drift sidewalls not observed in existing tunnels at the site.

- Using the granite time-dependency behavior for Tptpll strength category 5 results in minor breakouts at the springlines of the drift with little rubble accumulation.

The above analyses use a highly conservative rate of time dependency evidenced by predictions of breakout at drift sidewalls and significant raveling at early times for the lower mechanical property categories 1 and 2. As discussed previously, there are no observations in either the 7.62-m-diameter ESF or 5-m-diameter ECRB Cross-Drift that support such observations. However, even with these conservative calculations, significant breakout and raveling is restricted to those categories representing local conditions of high lithophysal porosity and less than about 10% of the Tptpll. Therefore, the overall conclusion that drift degradation resulting from time-dependent fracture and strength loss based on calculations using the best-fit, site-specific time-to-failure data for Topopah Spring Tuff is reasonable and represents typical conditions to be expected in the Tptpll.

I.4.4 Degradation Due to Time-Dependent Alteration of Rock Matrix or Joint Filling Materials from Postclosure Thermal and Moisture Conditions

One of the mechanical degradation issues raised in *Integrated Issue Resolution Status Report* (NRC 2002, Section 2.1.7.3.3.2, pp. 2.1.7-19 and 2.1.7-20) is the potential for geochemical

alteration of the rock mass resulting from elevated temperatures in the presence of saturated rock conditions. The concern is that alteration of minerals in the postclosure environment, either along or filling rock fractures or within the rock matrix, could impact rock or fracture strength and lead to enhanced degradation processes. Time-related degradation of tunnels due to wetting and drying cycles is an important factor for drift stability in some rock types. These rock types are typically those in which highly-altered rock, or rock with significant swelling clay along fracture planes occurs. In the case of the host repository horizon at Yucca Mountain, these issues are not particularly important. Clay is not a common mineral in the crystallized rocks of the repository host horizon, nor are clay minerals a volumetrically significant fracture-coating material. Four types of data support this observation:

A number of detailed geologic studies have been conducted at the Yucca Mountain site to define the basic mineralogy of the rocks and the petrologic and geochemical processes that occurred during the formation of the Topopah Spring Tuff and have continued from that time. These studies included a detailed description of the mineralogy of the repository host horizon from samples and observations developed from surface-based core holes through the repository block, as well as from the ESF and ECRB Cross-Drift. From the standpoint of mechanical degradation of the rock mass, these studies show:

- The Topopah Spring Tuff is largely composed of fine-grained feldspars and silicate-based rocks that formed during the cooling of the rock mass shortly after deposition. Clay-forming minerals were typically not formed during the petrogenesis of the repository host horizon.

- Clays typically do not form significant fracture-fill materials in the crystallized rocks of the Topopah Spring Tuff.

- There are limitations on the environmental conditions needed to form clays and indicate the minimum likelihood that clays might form along fractures in the near field of a repository. Therefore, mineral alteration during the postclosure period is considered negligible.

The following discussion summarizes the data obtained from a number of studies that support the above points.

1. **Mineralization in the Repository Host Horizon**–The Topopah Spring Tuff is a compositionally zoned pyroclastic flow deposit. High-silica rhyolite forms approximately the lower two-thirds of the deposit, and trachyte (or quartz latite) forms the upper one-third of the deposit. The crystallized rocks that formed during the cooling of the deposit consist primarily of very fine-grained intergrowths of feldspar and silica polymorphs of quartz and cristobalite. These minerals typically crystallized from volcanic glass at temperatures of approximately 800°C. X-ray diffraction analyses of 444 core samples from 13 boreholes that penetrate 3.5 km of the crystallized Topopah Spring Tuff indicate that there are different ratios of feldspar and silica polymorphs in the crystal-rich rocks (DTNs LADB831321AN98.002, LADV831321AQ97.001, LADV831321AQ99.001, LA000000000086.002). In the crystal-rich member, 93 samples have mean percentages of feldspar (69.1%), quartz

(2.4%), cristobalite (13.3%), and tridymite (11.2%), and in the crystal-poor member, 351 samples have mean percentages of feldspar (55.7%), quartz (15.8%), cristobalite (19.3%), and tridymite (5.1%). The total of the percentages cited for these two members do not sum to 100% because there are minor amounts of other minerals in many of these rocks. Smectite values vary from trace amounts to 15% with a mean value of 3.1%. These compositions of rocks form the walls of fractures where the minerals are very fine-grained and form various textures; however, the minerals are relatively uniformly distributed at scales of millimeters to centimeters. These data indicate that concentrations of smectite minerals along fractures do not occur as a result of crystallization during cooling.

2. **Clay Infillings Are Rarely Observed along Fractures in the ESF and ECRB Cross-Drift–**Detailed line survey data collected in the ECRB Cross-Drift indicate that of the 1,816 fractures in the 2.66-km-long tunnel, only 10 (or 0.4%) of the discontinuities, such as fractures, shears, and faults, have some amount of clay (DTNs: GS990408314224.001, GS990408314224.002). These 10 discontinuities are filled (or partially filled) with clay and broken or crushed rock or sand. Detailed studies of the clast textures, structures, and architectures of the broken or crushed rock or sand fill materials have not been completed, but general observations indicate many of these features do not show evidence of mechanical degradation and shear. Buesch and Lung (2003) describe volcaniclastic tuffaceous sandstone and claystone as fracture-fill material in the crystallized rocks of the Tiva Canyon and Topopah Spring Tuff. They proposed that volcanic glass particles settled by gravity along open fractures from the superjacent nonwelded bedded tuffs, and the clay formed in place (possibly millions of years later) by water seeping along the fractures and reacting with the glass. This mechanism is entirely consistent with occurrences of clays in the ECRB Cross-Drift detailed line survey data. Detailed line survey data from the crystallized Topopah Spring Tuff in the ESF main drift have not been recently reexamined, but only 4% of the fractures recorded have clay as filling material.

Integrated Issue Resolution Status Report (NRC 2002) specifically discussed the work by Carlos et al. (1995) in regard to fracture fillings:

> Mineral-alteration products currently occur at Yucca Mountain mostly as fracture coating and as lithophysal-cavity deposits (Carlos, et al., 1995). The mineralogy, thickness, and amount and uniformity of coverage of fracture coatings are highly variable and uncertain (Thoma, et al., 1992). The coatings consist mainly of zeolites, manganese oxide minerals, silica phases, carbonates (mostly calcite), and clay minerals (mostly smectite but occasionally illite). Smectite is fairly ubiquitous in fractures throughout the volcanic sequence (Carlos, et al., 1995).

Carlos et al. (1995) described the qualitative amount of materials in the fractures only, but typically they did not describe the amount or thickness of the mineral coatings. For example, if a mineral, such as clay (smectite), is listed as having major abundance, then greater than 20% of the minerals in the fractures are clay. However, the mineral coating might be less than 1 mm thick. Only for mordenite in the crystallized

Topopah Spring Tuff did Carlos et al. (1995) describe about 1% of the fractures with this mineral and the amount increased with depth to more than 20% (and more than 50% in some boreholes). The relevant point for this discussion is that selective fractures were sampled, and the intention was not to quantify the relative proportion of fractures with specific minerals or to quantify the thickness or continuity of the mineral coatings. However, there is one detailed study of mineral coatings on fracture walls in core with descriptions of the percentages of the amount of mineral coatings and thickness of the coatings (DTN: LA9912SL831151.001). Borehole ESF-HD-TEMP-2 is a 60 m (200 ft) long, horizontal borehole in the Drift Scale Test, and the rocks are in the middle nonlithophysal (Tptpmn) zone of the Topopah Spring Tuff. Only fractures in two 1.3 m (4.3 ft) long segments of core were described (7.6 to 8.9 m (25.0 to 29.3 ft) and 18.9 to 20.3 m (62.15 to 66.45 ft)). Clay forms localized deposits on the fracture surfaces that typically are less than 5% of the fracture surface area with thickness typically about 0.1 mm and a few deposits as much as 0.5 mm thick. These descriptions demonstrate that clay does not form continuous coatings on fracture walls and that the coats are very thin.

3. **Alteration of Repository Host Rocks Is Not Expected in the Repository Environment**–Conditions such as temperature, chemistry of water, and amount of water needed for the alteration of feldspars in the crystallized host rock to form clay and other sheet silicate minerals (sericite) are not considered to have been present within the Topopah Spring Tuff since its formation. Sericite is a general term for very fine-grained sheet silicates (illites) that form with other alteration products in hydrothermal systems at temperatures near or above 400°C, typically in acidic aqueous solutions (Jackson 1997). As pointed out by the predicted temperature conditions expected in the repository environment (e.g., Figure I-24), these conditions are not anticipated in the near-field environment of the repository. Even in samples from the Drift Scale Test boreholes, the clays on fractures appeared to have been there prior to the test and were not affected by the experimental conditions.

In summary, these petrologic and empirical relations indicate that clays typically do not form significant fracture-fill materials in the crystallized rocks of the Topopah Spring Tuff. They also indicate that the expected repository environmental conditions are not conducive to formation of clays during the postclosure period. Therefore, the impact of geochemical alteration within the postclosure environment is expected to have a negligible impact on drift degradation processes.

I.4.5 Effect of Drift Collapse on the In-Drift Environment

A parameter study was conducted to examine the impact of drift collapse on in-drift thermal-hydrologic parameters (BSC 2004b). The multiscale thermal-hydrologic model was used to examine the effect of a rubble-filled drift on waste package and invert temperature and relative humidity at the waste package and invert. The drift is assumed to collapse (instantaneously) to twice the initial diameter (i.e., 11 m collapsed diameter) and is filled with rubble with a bulking factor of 0.231. The thermal conductivity of the rubble (K_{th}) is defined as the intact rock thermal conductivity of the Tptpll multiplied by the factor (1/(1 + bulking factor)). Two thermal conductivity values (a high case calculated as defined above for a bulking factor of 0.231, and a

low case, which is taken to be one-half the high case value) of the dry and wet rubble thermal conductivity were used in the analyses, as shown in Table I-1.

Table I-1. Thermal Conductivity of Rubble

Property	Intact Host-Rock Property Value	Host-Rock Rubble Property Value	Basis for Rubble Property Value
Bulk dry thermal conductivity	1.28 W/m·K	1 W/m·K (High-K_{th} case)[a] 0.5 W/m·K (Low-K_{th} case)	Intact Value × 1/(1 + BF) (High-K_{th} rubble value)/2
Bulk wet thermal conductivity	1.89 W/m·K	1.515 W/m·K (High-K_{th} case)[b] 0.7575 W/m·K (Low-K_{th} case)	Intact Value × 1/(1 + BF) (High-K_{th} rubble value)/2

Source: BSC 2004b, Table 6.2-3.

NOTE: [a]This value is rounded down slightly
[b]Value is close to, but slightly less than, the value obtained from the Intact Value x 1/(1 + BF), in order to be consistent with the slight reduction made to the dry K_{th} value, which was rounded down.

Figure I-24 shows the in-drift thermal-hydrologic parameters as functions of time from repository closure for the case of the hottest waste package, which is the 21-PWR Absorber Plate waste package. These plots show three cases: (1) an open, noncollapsed drift, (2) a collapsed, rubble-filled drift with high K_{th} for the rubble, and (3) a collapsed, rubble-filled drift with low K_{th}. The temperature (or any of the other environmental parameters plotted) will follow the intact drift curve until the assumed time of collapse. At that point, the temperature (or other parameters) will translate vertically to one of the other curves, depending on the assumed thermal conductivity of the rubble.

Examination of the waste package temperature curve (Figure I-24a) shows that significant impact to peak waste package temperature results only if drift collapse occurs within the first 100 to 200 years after closure. After that time, the waste package temperature will always be below the peak temperature for the intact drift case, which occurs within about 20 to 30 years after closure. The total time at which the waste package surface remains above boiling for the hottest waste package case is approximately 1,000 years for the intact drift, 1,500 years for the high K_{th} case, and 2,000 years for the low K_{th} case. The relative humidity at the waste package decreases significantly for collapsed cases.

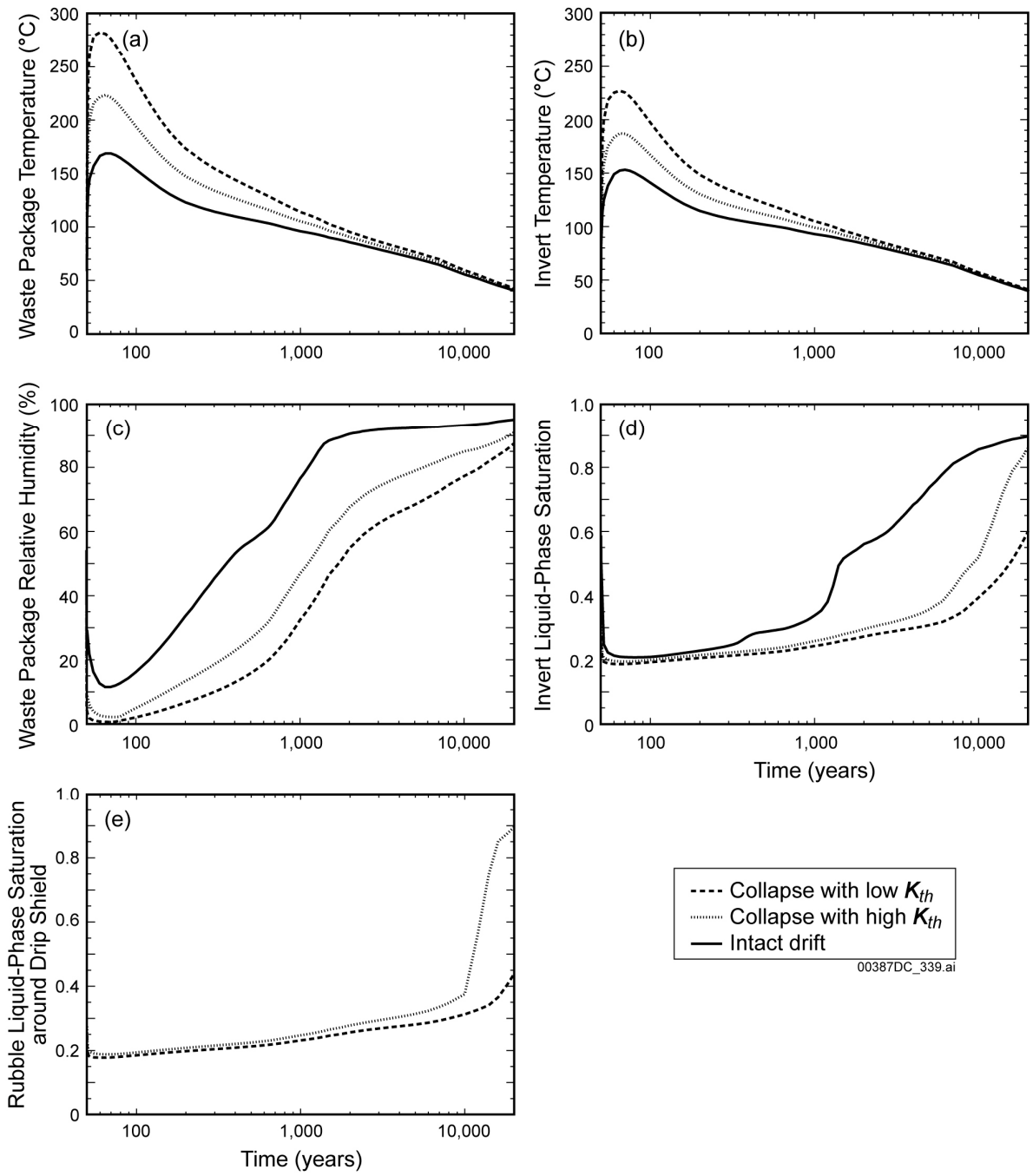

Source: BSC 2004b, Figure 6.3-1.

NOTE: The cases are: (1) intact-drift (nominal) case, (2) low-probability-seismic collapsed drift with high-K_{th} host-rock rubble, and (3) low-probability-seismic collapsed drift with low-K_{th} rubble. The plotted variables are (a) waste package temperature, (b) invert temperature, (c) waste package relative humidity, (d) invert liquid-phase saturation, and (e) matrix liquid-phase saturation of the rubble surrounding the drip shield.

Figure I-24. Thermal-Hydrologic Variables for the "Hottest" Waste Package (21-PWR Absorber Plate Waste Package) at the P2WR5C10 Location in the Tptpll (tsw35) Unit for the Mean Infiltration Flux Case

I.4.6 Effect of Drift Collapse on Drip Shield Stability

The drip shield design was developed to withstand the static load supplied by the weight of the collapsed drift. The methodology for estimating the rubble loading to the drip shield was described in detail in Section 5.3.2.3 of this technical basis document. The UDEC drift-scale model shown in Figure I-13 was used for determination of rubble loading. Six realizations of randomly shaped, 0.2 m side-length bonded blocks are used to describe the initial state of the rock mass. The shear and tensile strength of the rock mass was reduced from the initial calibrated rock mass strength until collapse was induced and was allowed to continue until the bulked rubble provided a back-pressure to the surrounding intact rock and effectively stopped further collapse (Figure I-25). The bulking factor of the rubble ranges from about 18% to 25%, depending on the particular realization (see Figure 5-58 of the technical basis document), and drift diameter expands to roughly 1.5 to 2 times its original size.

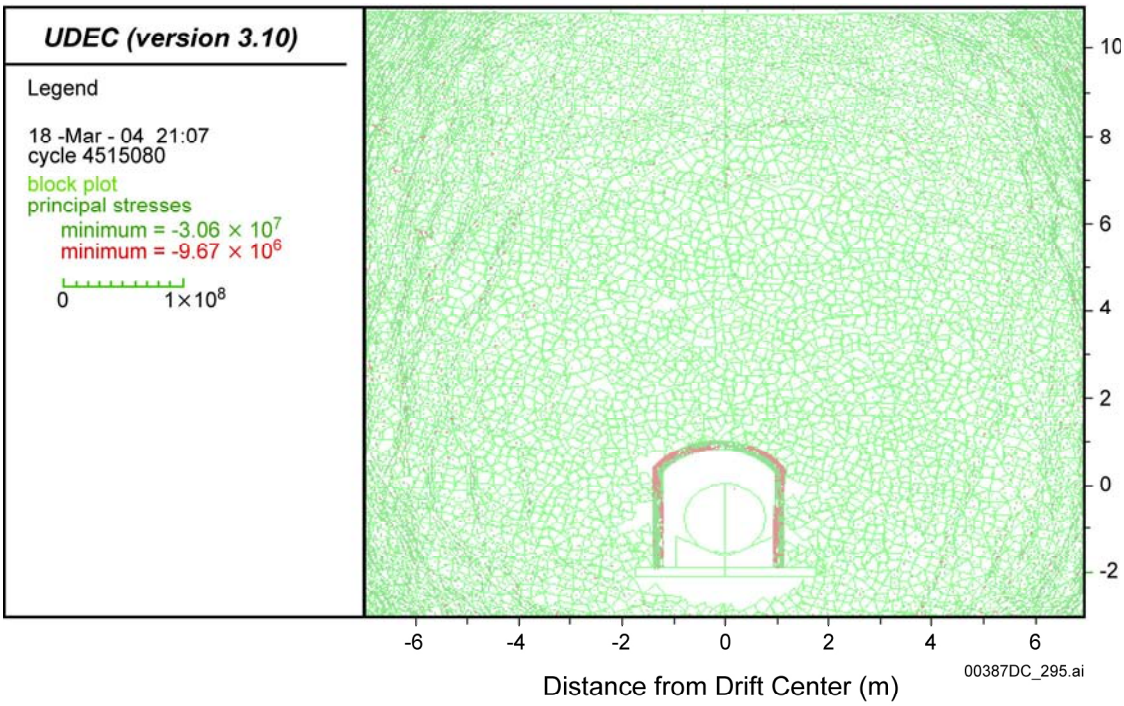

Source: BSC 2004a, Appendix V, Figure V-6.

Figure I-25. Quasi-Static Drift Degradation, 0.2 m Block Size: Equilibrium State for Deformable Drip Shield with Arched Top, Footings Free to Slide or Detach from the Invert

The resulting pressure distribution around the drip shield was determined for each of the six realizations. The results show a highly nonuniform load distribution around the drip shield due to point load contacts when the small blocks become wedged against the drip shield (Figure I-26).

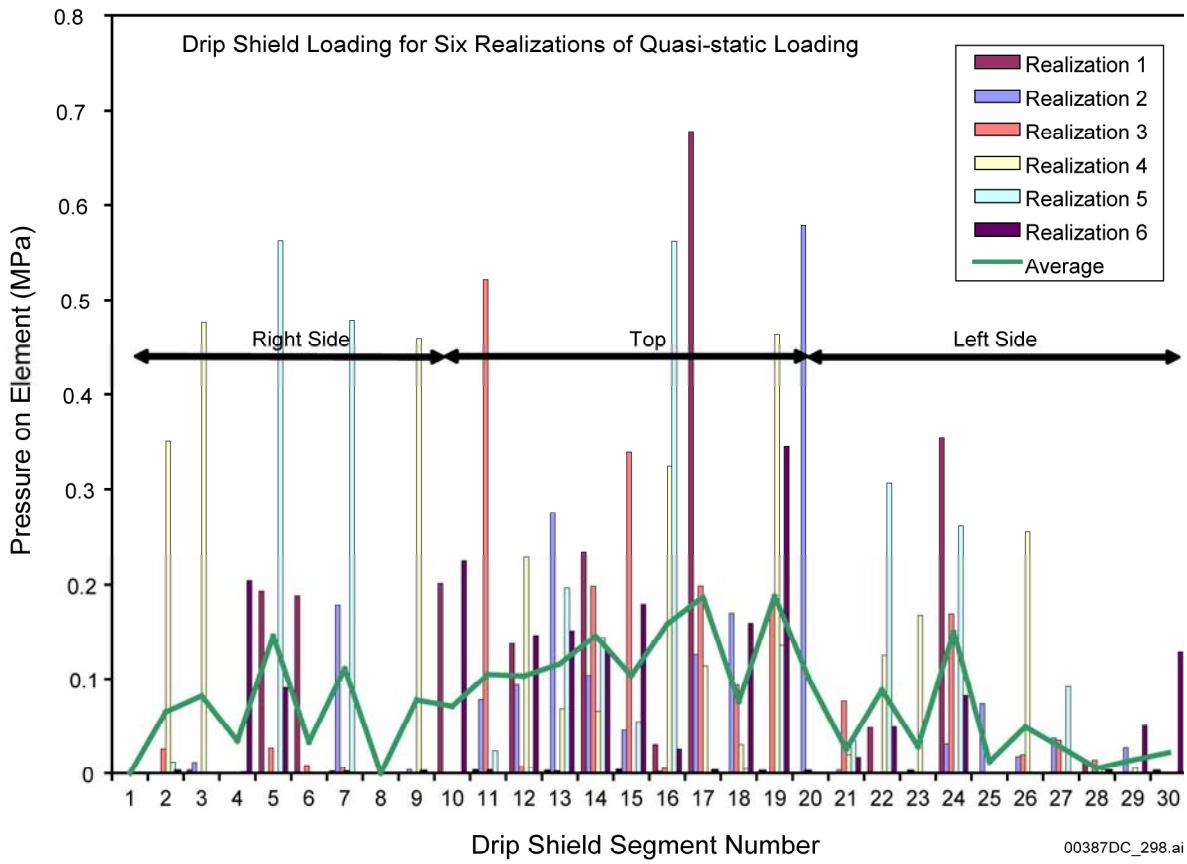

Source: BSC 2004a, Figure 6-166.

NOTE: Average pressure on each segment is shown for all six realizations. Segment numbering starts at 1 at the right footing and continues counterclockwise to the left footing. Those elements on the right, top, and left sides of the drip shield are shown.

Figure I-26. Quasi-Static Pressure on Drip Shield Segments for Six Realizations for Random, 0.2-m Block Geometries

The pressure distribution for each realization was used as input to a three-dimensional, nonlinear finite element structural analysis of the drip shield (BSC 2004c). The nonuniform pressure distribution was applied to the structure, followed by solution of the stress state and deformation. The analysis examines all of the potential failure modes including excessive deformation of the surface plates or load-bearing structure, development of yielded areas due to stress corrosion crack development, and potential buckling of the legs. It was found that the drip shield is stable under all quasi-static loading distributions.

I.4.7 Conclusions

RDTME 3.07 deals with the time-dependent degradation of emplacement drifts. This appendix presented discussion on five potential mechanisms or factors that could be associated with time-dependent degradation of the rock mass. These factors are listed below, with a summary of the conclusions.

Degradation due to the in situ stress state combined with the transient thermal and hydrologic stress conditions:

- Numerical analyses were performed to examine the effects of the combined in situ and thermally induced stresses on the stability of the excavations for both nonlithophysal and lithophysal rock. A range of fracture geometries and mechanical properties spanning the expected range of conditions in the repository host horizon provided the basis for these analyses. The analyses show that yielding of the rock mass surrounding the excavations due to these sources of loading is minor for the entire postclosure period.

- The potential impact of fluid vapor pressures along fractures in destabilizing the rock mass around the tunnel was investigated using the multiscale thermal-hydrologic model. The conclusion is that the fracture permeability is great enough that fluid or vapor pressure change is negligible during the entire heating and cooling cycle of the postclosure period.

Degradation due to time-dependent fracture development in the rock matrix in the presence of water vapor and driven by mechanical and thermal stresses:

- Time-dependent fracture development in the matrix in the presence of water vapor and in situ and thermal stresses was examined using discontinuum numerical modeling approaches. Laboratory creep experiments were conducted to define the static fatigue strength and rate of strength loss of Topopah Spring Tuff. Tests were conducted using water-saturated samples at temperatures at 125°C or 150°C. The samples were confined to prevent drying of the samples through boiling of water, thus ensuring water vapor was present to promote stress corrosion crack growth. Time-dependent results for granite determined for the Canadian high-level waste program were used as a means of comparison to the tuff data.

- A mechanics-based, discontinuum model (particle flow code) was developed to simulate time-dependent fracture development in tuff. The model was calibrated to reproduce the time-to-failure behavior of tuff for varying applied constant stress levels. This model was then used to simulate the effect of lithophysal porosity on time-to-failure.

- The UDEC drift-scale discontinuum model, which is used for drift stability simulation in lithophysal rocks, was then used to examine drift degradation due to time-dependent fracturing. The time-to-failure response generated from the laboratory testing of nonlithophysal rocks and the extrapolations for lithophysal rock was embedded into the drift-scale model through adjustment of rock properties.

- Analyses of drift stability for the expected range of lithophysal rock mechanical properties variability indicate that relatively minor levels of time-dependent drift degradation are expected over the postclosure regulatory time frame.

Degradation due to time-dependent fracture development and yield of asperities (roughness) on fracture surfaces:

- Potential time-dependent degradation of surface roughness and cohesion was conservatively represented in three-dimensional discontinuum stability models by setting the cohesion and dilation angle to 0. In other words, a bounding case was assumed in which all surface roughness was assumed to have been destroyed due to time-dependent failure of the asperities.

- Analyses of drift stability show that this assumption leads to only minor changes in rockfall because the stability of nonlithophysal rock is controlled primarily by fracture geometry.

Degradation due to time-dependent alteration of rock matrix or joint filling materials due to rock mass thermal and moisture conditions:

- The rock joints and rock matrix in the repository host horizon units are composed of minerals that will not undergo chemical alteration over postclosure temperature, moisture, and time frames. Fractures are characterized by rock wall contact with only minor amounts of clay minerals.

- Time-dependent chemical alteration of rock joints or matrix has a minor impact on drift degradation.

Degradation due to large excavation dimensions, unfavorable tunnel shape, and construction methods:

- Repository excavations at Yucca Mountain have small dimensions in comparison to unsupported spans known to result in collapse from practice in the mining industry.

- Emplacement drifts are to be excavated with a circular cross section using tunnel boring machines. The circular shape and nonexplosive excavation method are favorable to stability.

I.5 REFERENCES

I.5.1 Documents Cited

Bieniawski, Z.T. 1989. *Engineering Rock Mass Classifications.* New York, New York: John Wiley & Sons. TIC: 226350.

Brace, W.F.; Paulding, B.W., Jr.; and Scholz, C.H. 1966. "Dilatancy in the Fracture of Crystalline Rocks." *Journal of Geophysical Research, 71,* (16), 3939–3953. Washington, D.C.: American Geophysical Union. TIC: 226778.

Brekke, T.L.; Cording, E.J.; Daemen, J.; Hart, R.D.; Hudson, J.A.; Kaiser, P.K.; and Pelizza, S. 1999. *Panel Report on the Drift Stability Workshop, Las Vegas, Nevada, December 9-11, 1998.* Las Vegas, Nevada: Management and Technical Support Services. ACC: MOL.19990331.0102.

Brown, E.T. 2003. *Block Caving Geomechanics.* JKMRC Monograph Series in Mining and Mineral Processing, 3. Indooroopilly, Queensland, Australia: Julius Kruttschnitt Mineral Research Centre. TIC: 256115.

BSC (Bechtel SAIC Company) 2002a. *Software Code: PFC2D*. V2.0. PC WINDOWS 2000/NT 4.0. 10828-2.0-00.

BSC 2002b. *Software Code: PFC3D*. V.2.0. PC. 10830-2.0-00.

BSC 2003. *Subsurface Geotechnical Parameters Report*. 800-K0C-WIS0-00400-000-00A. Las Vegas, Nevada: Bechtel SAIC Company. ACC: ENG.20040108.0001.

BSC 2004a. *Drift Degradation Analysis*. ANL-EBS-MD-000027 REV 03A. Las Vegas, Nevada: Bechtel SAIC Company. ACC: MOL.20040513.0081.

BSC 2004b. *Multiscale Thermohydrologic Model*. ANL-EBS-MD-000049 REV 02 DRAFT A. Las Vegas, Nevada: Bechtel SAIC Company. ACC: MOL.20040630.0537.

BSC 2004c. *Mechanical Assessment of the Drip Shield Subject to Vibratory Motion and Dynamic and Static Rock Loading.* CAL-WIS-AC-000002 REV 00. Las Vegas, Nevada: Bechtel SAIC Company. ACC: MOL.20040630.0540.

Buesch, D.C. and Lung, R.C. 2003. "Tephrostratigraphic Relations and the Timing and Locations of Faulting near Exile Hill at Yucca Mountain, Nevada." *Proceedings of the 10th International High-Level Radioactive Waste Management Conference (IHLRWM), March 30–April 2, 2003, Las Vegas, Nevada.* Pages 388–397. La Grange Park, Illinois: American Nuclear Society. TIC: 254559.

Carlos, B.A.; Chipera, S.J.; and Bish, D.L. 1995. *Distribution and Chemistry of Fracture-Lining Minerals at Yucca Mountain, Nevada.* LA-12977-MS. Los Alamos, New Mexico: Los Alamos National Laboratory. ACC: MOL.19960306.0564.

Charles, R.J. 1959. "The Strength of Silicate Glasses and Some Crystalline Oxides." *Fracture: Proceedings of an International Conference on the Atomic Mechanisms of Fracture, Swampscott, Massachusetts, April 12-16, 1959*. Pages 225–249. Averback, B.L.; Felbeck, D.K.; Jahn, G.T.; and Thomas, D.A., eds. New York, New York: John Wiley & Sons. TIC: 236240.

Goodman, R.E. 1980. *Introduction to Rock Mechanics.* New York, New York: John Wiley & Sons. TIC: 218828.

Hoek, E. and Brown, E.T. 1980. *Underground Excavations in Rock*. London, England: Institution of Mining and Metallurgy. TIC: 217420.

Itasca Consulting Group 2002. *Itasca Software–Cutting Edge Tools for Computational Mechanics*. Minneapolis, Minnesota: Itasca Consulting Group. TIC: 252592.

Jackson, J.A., ed. 1997. *Glossary of Geology*. 4th Edition. Alexandria, Virginia: American Geological Institute. TIC: 236393.

Kranz, R.L. 1979. "Crack Growth and Development During Creep of Barre Granite." *International Journal of Rock Mechanics, Mining Sciences & Geomechanical Abstracts, 16,* 23–35. New York, New York: Pergamon. TIC: 255955.

Lau, J.S.O.; Gorski, B.; Conlon, B.; and Anderson, T. 2000. *Long-Term Loading Tests on Saturated Granite and Granodiorite.* Report No. 06819-REP-01300-10016 R00. Toronto, Ontario, Canada: Ontario Power Generation, Nuclear Waste Management Division. TIC: 254970.

Martin, R.J., III. 1972. "Time-Dependent Crack Growth in Quartz and its Application to the Creep of Rocks." *Journal of Geophysical Research, 77,* (8), 1406–1419. Washington, D.C.: American Geophysical Union. TIC: 224770.

Martin R.J. and Durham W.B. 1975. "Mechanisms of Crack Growth in Quartz." *Journal of Geophysical Research, 80,* 4837–4844. Washington, D.C.: American Geophysical Union. TIC: 224771.

Martin, R.J.; Noel, J.S.; Boyd, P.J.; and Price, R.H. 1997. "Creep and Static Fatigue of Welded Tuff from Yucca Mountain, Nevada." *International Journal of Rock Mechanics and Mining Sciences, 34,* (3/4), 287–298. New York, New York: Elsevier. TIC: 255040.

NRC (U.S. Nuclear Regulatory Commission) 2002. *Integrated Issue Resolution Status Report*. NUREG-1762. Washington, D.C.: U.S. Nuclear Regulatory Commission, Office of Nuclear Material Safety and Safeguards. TIC: 253064.

Potyondy, D. and Cundall, P. 2001. *The PFC Model for Rock: Predicting Rock-Mass Damage at the Underground Research Laboratory.* Report No. 06819-REP-01200-10061-R00. Toronto, Ontario, Canada: Ontario Power Generation, Nuclear Waste Management Division. TIC: 253569.

Reamer, C.W. and Williams, D.R. 2001. Summary Highlights of NRC/DOE Technical Exchange and Management Meeting on Repository Design and Thermal-Mechanical Effects. Meeting held February 6-8, 2001, Las Vegas, Nevada. Washington, D.C.: U.S. Nuclear Regulatory Commission. ACC: MOL.20010307.0511 through MOL.20010307.0521.

Schmidtke, R.H. and Lajtai, E.Z. 1985. "The Long-Term Strength of Lac du Bonnet Granite." *International Journal of Rock Mechanics and Mining Science & Geomechanics Abstracts, 22,* (6), 461–465. New York, New York: Pergamon. TIC: 254874.

Scholz, C.H. 1972. "Static Fatigue of Quartz." *Journal of Geophysical Research, 77,* (11), 2104–2114. Washington, D.C.: American Geophysical Union. TIC: 224772.

Wiederhorn, S.M. 1968. "Moisture Assisted Crack Growth in Ceramics." *International Journal of Fracture Mechanics, 4*, (2), 171–177. Groningen, Netherlands: Wolters-Noordhoff. TIC: 256161.

I.5.2 Data, Listed by Data Tracking Number

GS030283114222.001. Direct Shear Data from Selected Samples of the Topopah Spring Tuff. Submittal date: 02/20/2003.

GS990408314224.001. Detailed Line Survey Data for Stations 00+00.89 to 14+95.18, ECRB Cross Drift. Submittal date: 09/09/1999.

GS990408314224.002. Detailed Line Survey Data for Stations 15+00.85 to 26+63.85, ECRB Cross Drift. Submittal date: 09/09/1999.

LA000000000086.002. Mineralogic Variation in Drill Core UE-25 UZ#16 Yucca Mountain, Nevada. Submittal date: 03/28/1995.

LA9912SL831151.001. Fracture Mineralogy of Drill Core ESF-HD-TEMP-2. Submittal date: 01/05/2000.

LADB831321AN98.002. Revised Mineralogic Summary of Yucca Mountain, Nevada. Submittal date: 05/26/1998.

LADV831321AQ97.001. Mineralogic Variation in Drill Holes. Submittal date: 05/28/1997.

LADV831321AQ99.001. Quantitative XRD Results for the USW SD-6 and USW WT-24 Drill Core Samples. Submittal date: 04/16/1999.

SN0406L0212303.002. Static Fatigue Data from New England Research (NER) (Test Dates: 1/2/2004 through 2/25/2004). Submittal date: 06/08/2004.